UNIVERSITY OF OXFORD



Investigating the role of the *Crh* gene family in *Magnaporthe oryzae* on cell wall integrity and fungal virulence

Sarena Che Omar

St Hugh's College

Thesis submitted for the degree of

Doctor of Philosophy

Hilary 2015

Abstract

"Investigating the role of the *Crh* gene family in *Magnaporthe oryzae* on cell wall integrity and fungal virulence"

The rice blast disease caused by the fungus *Magnaporthe oryzae* causes significant annual crop losses of up to 30%. The fungal specific cell wall is a potential antifungal target due to the external location and importance to fungal survival and morphogenesis. The skeletal framework of the cell wall is made from glucan chains cross-linked with chitin, facilitated by the Congo Red Hypersensitivity (Crh) enzyme. In *Saccharomyces cerevisiae,* Δ*Crh1/*Δ*Utr2* mutants exhibit reduced wall integrity and the same is observed in *Candida albicans*, with reduced virulence in a mammalian host. Little is known about the cell wall in fungal plant pathogens and nothing of the *Crh* orthologs.

Bioinformatics revealed five *M. oryzae Crh-like* genes lying in two clades. Gene expression analyses revealed up to four-fold elevated expression of *MGG_Crh2* and *MGG_Utr2* when grown under cell wall stress. Consistently, the corresponding deletant strains showed hypersensitivity towards cell wall perturbants and was attributed to a loss in cell wall rigidity. Cell wall analysis of the mutant ΔΔ*MGG_Crh2_Utr2* revealed changes in the cell wall composition consistent with the reduction of Crhp activity and activation of cell wall compensatory mechanism often observed in a compromised cell wall. Furthermore, eGFP-tagged MGG_Crh2p showed localisation to the lateral cell wall with high accumulation at septum and polarised growth sites, consistent with sites of chitin accumulation. These mutants are, however, able to form normal infective structures and are fully pathogenic on susceptible rice cultivars.

In conclusion, the *Crh* gene family in *M. oryzae* is important for cell wall integrity by the cross-linking of chitin to glucan, but dispensable for virulence. Future work should explore the compensatory mechanism of other cell wall proteins in the ΔΔ*MGG_Crh2_Utr2* as this could shed light on the potential for targeting multiple cell wall components in a synergistic approach to confer effective disease control.

Thesis submitted for the degree of Doctor of Philosophy in Plant Sciences
Hilary Term 2015

Acknowledgements

Heartfelt gratitude to my three supervisors, Prof Dr S. Gurr, Dr G. Preston and Dr S. Kelly for their superb supervisory role, commitment, and helpful inputs. I would also like to extend my appreciation to Khazanah Nasional for generously supporting this D.Phil program without which this could not have been possible, via the Merdeka Scholarship Award.

Special thanks to collaborators and contributors of this thesis, Dr G. Morieri and Mr. M. Bentley for their input in the quantitative real-time PCR work, Mr J. Baker for his assistance in photographing fungal images, Ms S. Rodgers and Ms C. O'Brien for their efficient technical support in the laboratory and for the preparation of Electron Microscopy samples. Also thank you to Dr V. Bulone and Dr H. Melida from KTH Biotechnology Sweden for conducting the cell wall analysis, Dr S. Myhra from the Department of Materials, the University of Oxford for providing training in Atomic Force Microscopy and Dr Molly for her input on fungal extracellular matrix.

Big thanks to colleagues from the Gurr and Preston group. Not to forget departmental friends, especially Mr J. Baker, Mr. I. Geoghagen, Dr K. Au, Dr M. Kalde, Dr S. Mcraw, Dr A. Hoerje, and Mr. M. Bentley for their support and cheerfulness, making this D.Phil such an enjoyable journey. Special thanks to Prof Dr P. Jarvis, my undergraduate lecturer from Lincoln University (New Zealand) for helping to proof-read this thesis all on his own good will. Thank you Peter.

Appreciation and much love goes to mak and ayah for believing in me and likewise to the rest of the Omar and Ismail family. Most importantly, thank you to my loving and supportive husband Mr. Kalif Ismail. My D.Phil journey was made that much more meaningful, fun, and easier with you by my side.

Table of Contents

Abstract.....

Acknowledgements..... ii

Table of Contents..... iii

List of Figures xiv

List of Tables..... xx

1 CHAPTER 1 1

1.1 Introduction Overview 2

1.2 Global Rice Production & Rice Blast Disease..... 2

1.3 Rice Blast Disease..... 4

1.4 Fungal Cell Wall..... 7

1.4.1 Cell Wall Structure..... 8

1.4.2 Cell Wall Components & Biosynthesis 11

1.4.2.1 Carbohydrates: Alkaline Insoluble Fraction 11

1.4.2.1.1 Beta-Glucan 13

1.4.2.1.2 Chitin 15

1.4.2.2 Carbohydrates: Alkaline Soluble Fraction 17

1.4.2.2.1 Mannan & Short Glucan Chains..... 18

1.4.3 Cell Wall Proteins (CWP) 19

1.4.3.1 Cell Wall Remodelling Protein: Mechanism & Genetics 20

1.4.3.1.1 Congo Red Hypersensitivity Protein Family (Crhp) 21

1.5 Hypothesis & Thesis Aims 28

2 CHAPTER 2 29

2.1 Materials 30

2.1.1 Solutions & Media 30

2.1.2 Manufacturer's Details 32
2.1.3 Fungal Strains 35
2.2 Routine Methods 36
2.2.1 Fungal Growth & Tissue Preparation 36
2.2.1.1 Growth on Agar & Stock Maintenance 36
2.2.1.2 Spore Harvesting 36
2.2.1.3 Germling Preparation on Artificial surface 37
2.2.1.4 Germling Preparation on Onion Peel 37
2.2.1.5 Vegetative Growth in Liquid Media 38
2.2.1.6 Mycelial Tissue Preparation for Microscopy Work 38
2.2.2 Molecular Methods 39
2.2.2.1 Ethanol Precipitation of DNA 39
2.2.2.2 Quick Genomic DNA Extraction 39
2.2.2.3 RNA Extraction, Quantity & Quality Test 40
2.2.2.4 Complementary DNA (cDNA) Preparation 40
2.2.2.5 Routine quantitative Real Time PCR (qRT-PCR) 41
2.2.2.6 Primer Design 41
2.2.2.7 Low-Fidelity PCR Amplification 42
2.2.2.8 High-Fidelity PCR Amplification 43
2.2.2.9 DNA sequencing 44
2.2.2.10 Size Separation by Gel Electrophoresis 44
3 CHAPTER 3 45
3.1 Chapter Introduction 46
3.1.1 Fungal Phylogeny & Classification 46

3.1.2 Glycosyl Hydrolase 16 Family of Enzymes 48
3.1.3 Characteristics of Cell Wall Proteins 52
3.1.4 Fungal Gene Expression & Regulation 53
3.1.4.1 CWP Regulation by External Stressors 53
3.1.4.1.1 Hyperosmotic Stress Pathway 55
3.1.4.1.2 Fungal Cell Wall Integrity Pathway 57
3.1.4.2 CWP Regulation by Cell Cycle Progression 62
3.1.4.3 Measuring Expression of CWPs 63
3.1.5 Introduction Summary 65
3.2 Aims & Objectives 65
3.2.1 Bioinformatics Section 66
3.2.2 Gene Expression Analyses 66
3.2.2.1 Reference Gene Selection for qRT-PCR 66
3.2.2.2 Gene Expression of Genes of Interest (GOI) 66
3.3 Materials & Methods 66
3.3.1 Bioinformatic Work 66
3.3.1.1 *Saccharomyces cerevisiae Crh1, Utr2 & Crr1* Orthologues 66
3.3.1.2 Transcription Factor DNA Binding Site Prediction 68
3.3.1.3 Modular Structures of *Crh-like* Genes in *M. oryzae* 69
3.3.1.4 Signal Peptide Cleavage Site Prediction 69
3.3.1.5 GPI-Anchor Prediction 69
3.3.1.6 Phylogenetic Tree Description 70
3.3.2 Gene Expression Analyses 72
3.3.2.1 Fungal Strains & Growth Conditions 72

3.3.2.2 Tissue Preparation for RNA Extraction 72
3.3.2.2.1 Mycelial Tissue Grown Under Various Stressors 72
3.3.2.2.2 Dormant Spores 73
3.3.2.2.3 Germling Tissues 73
3.3.2.2.4 Perithecia 74
3.3.2.3 RNA Extraction, Quantity & Quality Test 74
3.3.2.4 Complementary DNA (cDNA) Preparation 74
3.3.2.5 Primer Design, Specificity & Efficiency 74
3.3.2.6 Quantitative Real Time PCR (qRT-PCR) 76
3.3.2.7 Cycle Threshold Criteria 76
3.3.2.8 Evaluation of Reference Gene Expression Stability 76
3.3.2.9 Data Analysis – Expression Profile of *Crh-like* Genes 78
3.3.2.9.1 Preliminary Analysis 78
3.3.2.9.2 Gene Expression Analysis 78
3.4 Results & Discussion 80
3.4.1 Bioinformatic Analyses 80
3.4.1.1 *Saccharomyces cerevisiae Crh1, Utr2 & Crr1* Orthologues 80
3.4.1.2 Transcription Factor DNA Binding Site Prediction 81
3.4.1.3 Modular Structures of Crh-like Proteins 84
3.4.1.4 GPI-Anchor Prediction 87
3.4.1.5 Maximum Likelihood GH16 Phylogenetic Tree 88
3.4.1.6 Crh1 Clade and Crr1/Utr2 Clade 93
3.4.2 Gene Expression Analysis 98

3.4.2.1 Gene Info, Primer Design, Specificity, and Efficiency 98

3.4.2.2 RNA and cDNA Quality & Quantity 101

3.4.2.3 Quantitative Real Time – PCR Data Analysis 101

3.4.2.3.1 Control Assays 101

3.4.2.3.2 Preliminary Sample Cycle Threshold Evaluation 101

3.4.2.3.3 Expression Stability of Candidate Reference Genes 105

3.4.2.3.4 Expression Profile: Data Quality & Calculation 109

3.4.2.3.5 Expression Profile: Infective Stage 112

3.4.2.3.6 Expression Profile: Vegetative & Global Stage 115

3.5 Chapter Summary & Conclusion 124

4 CHAPTER 4 128

4.1 Chapter Introduction 129

4.1.1 Functional Gene Studies in Fungi by Reverse Genetics 130

4.1.2 Reverse Genetics: Knockdown or Knock-out? 130

4.1.3 Targeted Transformation by Homologous Recombination 131

4.2 Experimental Aims & Objectives 133

4.3 Materials & Methods 134

4.3.1 Generation of Deletant Strains 134

4.3.1.1 Media, Solutions & Chemical Reagents Used 134

4.3.1.2 Primers Used in the Generation of Deletant Mutants. 135

4.3.1.3 Generation of Transformation PCR Cassettes 136

4.3.1.4 Fungal Transformation 137

4.3.1.4.1 Protoplast Generation 137

4.3.1.4.2 PEG-Mediated Protoplast Transformation 139

4.3.1.4.3 Candidate Mutant Confirmation 140

4.3.1.4.4 Absence of Transcript Validation by qRT-PCR in Mutants 146

4.3.2 Generation of Revertant Strains 148

4.3.2.1 Genotypes and Strains Used 148

4.3.2.2 Native Vectors Used: 149

4.3.2.3 Cloning: Vector Amplification & Extraction 150

4.3.2.4 Insert Design & Preparation 151

4.3.2.5 Insert & Vector Restriction Digest & Ligation 154

4.3.2.6 Preparation of Stock *E. coli* DH5α Super Competent Cells 156

4.3.2.7 *E. coli* DH5α Supercompetent Transformation by Heat-shock 156

4.3.2.8 Confirmation of Ligation 157

4.3.2.9 Line Screening for Phenotype Recovery 158

4.4 Results & Discussion 159

4.4.1 Generation of Deletant Strains 159

4.4.1.1 Generation of Deletant Strains 159

4.4.1.1.1 Construction of Deletion Cassettes 159

4.4.1.1.2 Confirmation of Transformed Mutants 162

4.4.1.2 Absence of Transcript: Validation by qRT-PCR 173

4.4.2 Generation of Revertant Strains 177

4.4.2.1 Construction of Revertant Plasmids 177

4.4.2.1.1 Cloning Work 179

4.4.2.2 Fungal Line Transformation Confirmation & Imaging 187

4.5 Chapter Summary & Conclusion 190

5 CHAPTER 5 191

5.1 Chapter Introduction 192
5.1.1 Chapter Overview 192
5.1.2 Cell Wall Integrity: Growth Assays 192
5.1.2.1 Cell Wall Stress & Osmo-stabiliser 193
5.1.2.2 Cell Wall Stress Caused by Caffeine 195
5.1.2.3 Other External Stressors 196
5.1.3 Fungal Morphology and Cell Wall Structure 196
5.1.4 *Magnaporthe oryzae* Pathogenicity 198
5.2 Aims & Objectives 200
5.3 Materials & Methods 201
5.3.1 Plate Assay: Fungal Growth & Sensitivity Test 201
5.3.1.1 Strains Used 201
5.3.1.2 Preparation of Inoculating Agar Plug 201
5.3.1.3 Preparation of Various Treatment Plates 202
5.3.1.4 Data Analysis 205
5.3.2 Liquid Biomass Assay 206
5.3.3 Cell Wall Structure: Fluorescence Staining 207
5.3.4 Cell Wall Structure: Transmission Electron Microscopy (TEM) 207
5.3.4.1 Spore Tissue Preparation 207
5.3.4.2 Vegetative Mycelium Tissue Preparation 208
5.3.4.3 Sample Fixing & Image Visualisation 208
5.3.5 Germling Morphology (Artificial surface) 209
5.3.6 Penetration Assay (Onion peel) 210
5.3.7 Virulence Assay (Cut leaves) 210
5.3.7.1 Barley leaf preparation 210

5.3.7.2 Rice leaf preparation 211

5.3.7.3 Infection strategy 211

5.4 Results & Discussion 213

5.4.1 Vegetative Growth: Plate Assay 213

5.4.1.1 Selection for the Appropriate Concentration of Reagents 213

5.4.1.2 Growth Assay: Control (CM), Starvation (MM) and Membrane Stress (SDS) 214

5.4.1.3 Growth Assay: Cell Wall Stress 218

5.4.1.3.1 Cell Wall Stress by Congo Red 218

5.4.1.3.2 Cell Wall Stress by Caffeine 224

5.4.1.4 Plate Growth Assay: Discussion of Results 228

5.4.2 Vegetative Growth: Liquid Biomass Assay 230

5.4.3 Cell Wall Structure: Fluorescent Staining 231

5.4.4 Cell Wall Structure: Transmission Electron Microscopy 235

5.4.5 Germling Morphology, Fitness & Virulence 239

5.4.5.1 Germling Morphology 239

5.4.5.2 Germling Fitness 241

5.4.5.3 Early Infection on Host 243

5.4.5.4 Virulence Assay 245

5.5 Chapter 5 Summary & Conclusions 248

6 CHAPTER 6 249

6.1 Chapter Introduction 250

6.1.1 Introduction to Atomic Force Microscopy 251

6.1.1.1 AFM Topographic Imaging 251

6.1.1.2 Force Spectroscopy (Elasticity) 252

6.1.1.3 Measuring Fungal Cell Wall Mechanical Properties by AFM ... 255
6.1.2 Introduction to Fungal Cell Wall Composition ... 257
6.2 Aims & Objectives ... 261
6.3 Materials & Methods ... 262
6.3.1 Cell Wall Topography & Elasticity ... 262
6.3.1.1 Tissue Preparation ... 262
6.3.1.1.1 Vegetative Hyphae ... 262
6.3.1.1.2 Germling ... 262
6.3.1.1.3 AFM Analysis ... 263
6.3.2 Cell Wall Analysis ... 266
6.3.2.1 Tissue Preparation ... 266
6.3.2.2 Cell Wall Preparation ... 266
6.3.2.3 Monosaccharide Analysis ... 266
6.4 Results & Discussion ... 268
6.4.1 Surface Topography & Elasticity ... 268
6.4.1.1 Surface Topography by Tapping Mode ... 268
6.4.1.2 Surface Elasticity by Contact Mode ... 279
6.4.2 Cell Wall Analysis ... 286
6.4.2.1 Total Cell Wall Composition ... 288
6.4.2.1.1 WT Alkaline Insoluble Fraction ... 290
6.4.2.1.2 WT Alkaline Soluble Fraction ... 294
6.4.2.2 Mutant Cell Wall Analysis ... 300
6.4.2.2.1 Single Gene Knockout Mutant *ΔMGG_Crh1* ... 300
6.4.2.2.2 Double Gene Deletion Mutant *ΔΔMGG_Crh2_Utr2* ... 300

6.4.2.2.3 Discussion of Results for Mutant Cell Wall Analysis 306

6.5 Chapter Summary & Conclusion 309

7 CHAPTER 7 310

7.1 Chapter Introduction 311

7.1.1 Gene Redundancy & Compensation 311

7.1.2 Protein Localisation 314

7.2 Aims & Objectives 316

7.3 Materials & Methods 317

7.3.1 Gene Compensation Analysis 317

7.3.1.1 Tissue Preparation 317

7.3.1.2 RNA Extraction, Quantity & Quality Assessment 317

7.3.1.3 Primer Quality Assessment 318

7.3.1.4 Complementary DNA Synthesis & qRT-PCR Analysis 318

7.3.1.5 Data Analysis 318

7.3.2 Protein Localisation 320

7.3.2.1 Protein Visualisation in Fungal Tissues 320

7.3.2.2 Sample Visualisation by Confocal Microscopy 320

7.4 Results & Discussion 321

7.4.1 Gene Compensation Analysis 321

7.4.1.1 Sample and Primer Quality Assessment 321

7.4.1.2 Quantitative Real-Time PCR Results Analysis 322

7.4.2 Protein Localisation 330

7.4.2.1 Protein Localisation of eGFP tagged MGG_Crh2p 330

7.4.2.2 Protein Localisation: mCherry tagged MGG_Utr2p 338

7.5 Chapter Summary & Conclusion 341

8 CHAPTER 8 342

8.1 Key Findings 343

8.2 Thesis Summary, Conclusion & Future Work 345

Reference List 355

Abbreviations 385

Appendices 386

List of Figures

Chapter 1

Figure 1.1. *Magnaporthe oryzae* Causes Rice Blast Disease. 4
Figure 1.2. Life Cycle of *Magnaporthe oryzae*..... 5
Figure 1.3. Polysaccharides of the Cell Wall of *Aspergillus fumigatus* and *Saccharomyces cerevisiae*..... 9
Figure 1.4. Fungal Cell Wall of *Candida albicans*..... 9
Figure 1.5. Sequential Events in the Biosynthesis of Cell Wall Polysaccharides. 12
Figure 1.6. Molecular Structure of Beta(1-3/1,6/1,4)-Glucan..... 13
Figure 1.7. Putative Functions of GPI-anchored Proteins During the Construction of the Fungal Cell Wall. 20
Figure 1.8. Localisation of *Saccharomyces cerevisiae* Crh1-HA and Crh2-HA in the WT strain GRA007. 23
Figure 1.9. Predicted Structure of Crh1 Protein. 24
Figure 1.10. Residues Within the Catalytic Site of Crh1p are Essential for the Transglycosylase Activity of This Protein *In Vivo*. 25

Chapter 3

Figure 3.1. The Phylogeny and Classification of the Kingdom Fungi. 47
Figure 3.2. List of the Sub-Domains Found in Glycosyl Hydrolase 16 Family of Enzymes. 48
Figure 3.3. An Illustration for the Origins of the Various GH16 Sub-Groups from a Common Ancestor and Protein Structures. 49
Figure 3.4. Putative Functions of GPI-Anchored Proteins During the Construction of the Fungal Cell Wall. 52
Figure 3.5. MAPK Pathways in Fungal Pathogens..... 55
Figure 3.6. High Osmolarity Glycerol (Hog) MAPK Pathway..... 56
Figure 3.7. Cell Wall Integrity MAPK Pathway. 57
Figure 3.8. Modular Structure of *Crh-like* Genes in Four Fungal Species. 86
Figure 3.9. Glycosyl Hydrolase 16 Maximum Likelihood Phylogenetic Tree. ... 90
Figure 3.10. Maximum Likelihood *Crh-like* Phylogenetic Tree. 94

Figure 3.11. Ranking of Nine Candidate Reference Genes According to the Calculated Average Expression Stability (M). 106
Figure 3.12. Determination of the Optimal Number of Reference Genes for Accurate Normalisation. 107
Figure 3.13. *MGG_40s* Amplification Plot. 110
Figure 3.14. Expression Profile for *MGG_Utr2* Gene across the Infective Life Stage of *Magnaporthe oryzae.* 113
Figure 3.15. Expression Profile for *MGG_Crh1* Gene across the Infective Life Stage of *Magnaporthe oryzae*. 113
Figure 3.16. Expression Profile for *MGG_Crh2* Gene across the Infective Life Stage of *Magnaporthe oryzae.* 114
Figure 3.17. Expression Profile of *Magnaporthe oryzae MGG_Utr2* Grown Vegetatively Under Various Growth Conditions. 117
Figure 3.18. Expression Profile of *Magnaporthe oryzae MGG_Crh1* Grown Vegetatively Under Various Growth Conditions. 118
Figure 3.19. Expression Profile of *Magnaporthe oryzae MGG_Crh2* Grown Vegetatively Under Various Growth Conditions. 119
Figure 3.20. Expression Profile of *Magnaporthe oryzae MGG_Crh2* across Major Stages of the Life Cycle. 123

Chapter 4

Figure 4.1. An Illustration of the Designed Deletion Cassette. 137
Figure 4.2. Flow Chart Describing PEG-Mediated Protoplast Transformation Steps. 140
Figure 4.3. An Illustration of a Restriction Digest Strategy. 141
Figure 4.4. An Illustration for the Construction of a Capillary Transfer Tower. 144
Figure 4.5. Visual Illustration of the Components and Restriction Enzyme Sites of pUCAP Vectors (1-1) and (3-2). 150
Figure 4.6. Genes *MGG_Utr2* and *MGG_Crh2* Insert Design by Overlapping PCR..... 152
Figure 4.7 A Description for the Construction of Utr2_Hyg Deletion Cassette by Overlapping PCR. 161
Figure 4.8. PCR Integration and Southern Blot Confirmation for the Replacement of *MGG_Utr2* Gene with Utr2_Hyg Deletion Cassette. 164

Figure 4.9. Targeted Transformation Using the Utr2_Hyg Deletion Cassette and *MGG_Utr2* Gene Absence Confirmation. 165
Figure 4.10. PCR Integration and Southern Blot Confirmation for the Replacement of *MGG_Crh1* Gene with Crh1_Hyg Deletion Cassette. 167
Figure 4.11.Targeted Transformation Using the Crh1_Hyg Deletion Cassette and *MGG_Crh1* Gene Absence Confirmation. 168
Figure 4.12. PCR Integration and Southern Blot Confirmation for the Replacement of *MGG_Crh2* Gene with Crh2_Hyg Deletion Cassette. 169
Figure 4.13. Targeted Transformation Using the Crh2_Hyg Deletion Cassette and *MGG_Crh2* Gene Absence Confirmation. 170
Figure 4.14. PCR Integration and Southern Blot Confirmation for the Replacement of *MGG_Utr2* Gene with Utr2_BAR Deletion Cassette. 171
Figure 4.15. Targeted Transformation using the Crh2_Hyg Deletion Cassette and *MGG_Crh2* Gene Absence Confirmation. 172
Figure 4.16. Vector Check by Restriction Enzyme Digestion. 181
Figure 4.17. Polymerase Chain Reaction Product Quality Check by Gel Electrophoresis. 184
Figure 4.18. An Illustration for the Confirmation of Vector 13c and 13c_2ci by Sequencing and Restriction Enzyme Double Digest. 185
Figure 4.19. Confirmation of Vector Ligation by Restriction Enzyme for the Construction of Vector 13c and 13c_2ci. 185
Figure 4.20. A Visual Illustration for the Confirmation of *MGG_Utr2* Insert Ligation to Vector (3-2) by Sequencing and Restriction Enzyme Double Digest. 186
Figure 4.21. Confirmation of Vector Ligation by Restriction Enzyme for the Construction of Vector #5 and #5_9a. 186
Figure 4.22. Confirmation by PCR for the Presence of Linearized Plasmids in Revertant Strains. 188

Chapter 5

Figure 5.1. Sensitivities to Congo red and Calcofluor White of *Crh-like* Deletant Strains in *Saccharomyces cerevisiae.* 193
Figure 5.2. The Chemical Structures of Calcofluor White (a) and Congo Red (b). 194

Figure 5.3. Congo Red Hypersensitivity Assay for *Arl* Deletant Strains in *Saccharomyces cerevisiae*..... 195
Figure 5.4. Electron Micrographs of *Saccharomyces cerevisiae* Wild-Type and *crr1*Δ mutants..... 198
Figure 5.5. An Illustration of the Measurement of Colony Growth. 205
Figure 5.6. Plate Growth Assay of WT Strain Guy11 Grown on a Range of Sodium Dodecyl Sulphate (SDS) Concentrations. 213
Figure 5.7. *Magnaporthe oryzae* Fungal Strains Grown Under Optimal Conditions in Complete Medium Agar..... 215
Figure 5.8. *Magnaporthe oryzae* WT Guy11 and Mutant Strains Grown Under Starvation..... 216
Figure 5.9. *Magnaporthe oryzae* Strains Grown Under Cell Membrane Stress. 217
Figure 5.10. *Magnaporthe oryzae* Strains Grown Under Cell Wall Stress (Congo Red). 221
Figure 5.11. *Magnaporthe oryzae* Strains Grown in CM Agar Buffered with Hepes at pH 7.0..... 222
Figure 5.12. *Magnaporthe orzyae* Fungal Strains Grown Under Osmotic Stress. 223
Figure 5.13. *Magnaporthe oryzae* Strains Grown Under Caffeine Stress (2.5 mM)..... 226
Figure 5.14. Liquid Biomass Assay Showing the Total Dry Weight of Fungal Mycelia..... 231
Figure 5.15. Cell Wall Staining (Calcofluor White) of Vegetative Mycelium in Five *Magnaporthe oryzae* strains..... 233
Figure 5.16. Germling Cell Wall Staining (Calcofluor White) of Five *Magnaporthe oryzae* Strains Inoculated onto an Artificial Hydrophobic Surface. 234
Figure 5.17. Transmission Electron Micrographs of *Magnaporthe oryzae* Vegetative Mycelium Cultured in CM. 237
Figure 5.18. Transmission Electron Micrographs of *Magnaporthe oryzae* Dormant Spores Mycelium Cultured in CM. 238
Figure 5.19. Morphology of Mutants During Germling Development..... 240
Figure 5.20. Germination Rate of Mutant Spores..... 242
Figure 5.21. Germling Penetration Assay on Onion Sheath..... 244

Figure 5.22. Mutant Strain Virulence Assay on Barley and Rice Cut Leaves. 246

Chapter 6

Figure 6.1. An Illustration of an AFM Apparatus. 251
Figure 6.2. A Schematic Diagram Describing the Principles of Force Spectroscopy. 253
Figure 6.3. An Illustration for the Location of Indentations Made for The Force-Distance Curve Analysis on a Vegetative Hypha. 265
Figure 6.4. Magnified Imaging of the Surface Structures of Fungal Vegetative Mycelium. 269
Figure 6.5. Contour Line Analysis on Strain Guy11 Fungal Structures. 270
Figure 6.6. *Magnaporthe oryzae* WT Vegetative Hypha Imaged by AFM. 271
Figure 6.7. *Magnaporthe oryzae* WT Germlings Imaged by AFM. 273
Figure 6.8. Pilot Force Versus Distance Curves of WT and Mutant Strain. 280
Figure 6.9. Force Versus Distance Curves of WT and Mutant Strain. 281
Figure 6.10. Contribution (% mol) of the Alkali Soluble/Insoluble Fractions to the Total Cell Wall in *Magnaporthe oryzae* Strains. 288
Figure 6.11. Total Sugar Composition of the Alkaline Insoluble Fraction of WT Cell Wall. 291
Figure 6.12. Linkage Composition of the Alkaline Insoluble Fraction of WT Cell Wall. 292
Figure 6.13. WT Guy11 Fungal Cell Wall Composition in the Alkaline Soluble Fraction. 295
Figure 6.14. Linkage Composition of the Alkaline Soluble Fraction of WT Cell Wall. 296
Figure 6.15. A Schematic Representation of *Magnaporthe oryzae* WT Cell Wall Composition in Vegetative Mycelium. 299
Figure 6.16. Sugar Composition of the Alkaline Insoluble Fraction of Mutant Cell Wall. 302
Figure 6.17. Linkage Composition of the Alkaline Insoluble Fraction of Mutant Cell Wall. 303
Figure 6.18. Alkaline Soluble Fraction of WT Guy11 Fungal Cell Wall Composition. 304

Figure 6.19. Linkage Composition of the Alkaline Soluble Fraction of Mutant Cell Wall. 305

Chapter 7

Figure 7.1. Expression of *Crh-like* Genes in Five *Magnaporthe oryzae* Genotypes Grown Under Optimal Conditions by qRT-PCR. 324
Figure 7.2. Expression of *Crh-like* Genes in Five *Magnaporthe oryzae* Genotypes Grown Under Cell Wall Stress by qRT-PCR. 325
Figure 7.3. Expression of *Crh-like* Genes in Five *Magnaporthe oryzae* Genotypes Grown Under Oxidative Stress by qRT-PCR. 326
Figure 7.4. The Expression Profile of *MGG_Crh3* and *MGG_Crh4* Grown Under Oxidative Stress Relative to Growth Under Optimal Conditions by qRT-PCR. 327
Figure 7.5. Visualization of MGG_Crh2p Localization in the Vegetative Structures of *Magnaporthe oryzae* Expressing eGFP. 332
Figure 7.6. Visualization of MGG_Crh2p Localization in the Early Stage of Germling Development in *Magnaporthe oryzae* Expressing eGFP. 334
Figure 7.7. Visualization of MGG_Crh2p Localization in the Late Stage of Germling Development in *Magnaporthe oryzae* Expressing eGFP. 335
Figure 7.8. Visualization of MGG_Crh2p Localization *In Planta* in *Magnaporthe oryzae* Expressing eGFP. 336
Figure 7.9. Visualization of MGG_Utr2p Localization *In Planta* in *Magnaporthe oryzae* Expressing mCherry. 339

List of Tables

Chapter 2

Table 2.1. List of Reagents and Solutions Routinely Used..... 30
Table 2.2. List of Equipments and Suppliers. 32
Table 2.3. Kits and Enzymes Routinely Used and the Corresponding Supplier33
Table 2.4. Suppliers of Consumable Products Routinely Used 33
Table 2.5. List of Softwares and the Manufacturers. 34
Table 2.6. List of Bioinformatics Websites Routinely Visited 34
Table 2.7 List of *Magnaporthe oryzae* Strains Used 35
Table 2.8. *Taq DNA Polymerase* PCR Reagents..... 42
Table 2.9*. Taq DNA Polymerase* Chain PCR Thermal Cycling Conditions 42
Table 2.10. *Herculase* II PCR Reagents 43
Table 2.11. *Herculase* II PCR Thermal Cycling Conditions..... 43

Chapter 3

Table 3.1. Matinspector Transcription Factor DNA Binding Site Prediction..... 82
Table 3.2. List of Genes Used for the qRT-PCR Gene Expression Analysis.... 99
Table 3.3. Raw Cycle Threshold (ct) Values of Five *Crh-like* Genes Amplified from Pooled Infective Stage cDNA. 102
Table 3.4. Raw Cycle Threshold (ct) Values of Five *Crh-like* Genes Amplified from Mycelial cDNA. 103

Chapter 4

Table 4.1. List of Media, Solutions and Reagents Used in Routine *Magnaporthe oryzae* Transformation 134
Table 4.2. List of Primers Designed for the Amplification of Deletion Cassette and Mutant Confirmation by PCR Integration. 135
Table 4.3. List of Reagents and Solutions Used for Cloning Work. 148
Table 4.4. Reagents Used for Restriction Enzyme Digest (Vector Validation). 150
Table 4.5. Reagents Used for Routine Restriction Enzyme Digestion. 154
Table 4.6. Reagents Used for Routine Restriction Enzyme Ligation Reaction155
Table 4.7. Averaged Cycle Threshold of *Crh-like* Genes in Five Strains..... 175

Table 4.8. Primers Designed for the Amplification of PCR Inserts and Vector Validation 182
Table 4.9. List of New Vectors Designed in This Study Coding for genes *MGG_Crh2* and *MGG_Utr2*..... 187
Table 4.10. List of *Magnaporthe oryzae* Deletant and Revertant Strains Generated in This Study..... 190

Chapter 5

Table 5.1. List of Medium and Reagents Used For Plate Growth Assay..... 204
Table 5.2 Transmission Electron Microscopy Reagents for Sample Fixing.... 209
Table 5.3. Growth Ratio of Mutants Relative to WT Strain Guy11 for Seven Treatment Types. 227
Table 5.4. Average Number of Lesions per Unit Area. 247

Chapter 6

Table 6.1. Comparative* Summary of Fungal Cell Wall Components n *S. cerevisiae, C. albicans*, *A. fumigatus* and *N. crassa*. 257
Table 6.2. Averaged Slopes of Force Versus Distance Curves in Three Assays. 282
Table 6.3. *Magnaporthe oryzae* Total Cell Wall Carbohydrate Composition.. 289

Chapter 7

Table 7.1. Cycle Threshold Values for Gene *MGG_Crh3* Generated by qRT-PCR..... 327

CHAPTER 1

Introduction

1.1 Introduction Overview

The primary aim of this study is to expand on the limited understanding of the cell wall of *M. oryzae* through characterizing the function and importance of the Crh-like protein family in maintaining cell wall integrity and fungal virulence. As such, this Chapter aims to provide an introduction to this research topic, beginning with a justification for choosing *M. oryzae* as the model organism. This is followed by an overview of current understanding of the fungal cell wall structure, composition, biosynthesis and subsequent applications to disease control in the medical field. The chapter will then focus on the well-studied Crh-like family of cell wall remodelling protein in other fungal species. Finally, after exploring the potential of Crh-like proteins as an antifungal target in phytopathogen disease control, this Chapter will end by outlining the aims and hypotheses that have driven this work.

1.2 Global Rice Production & Rice Blast Disease

Rice (*Oryza sativa*) is a staple diet for more than half of the world's population. In 2011, the global population stood at 7 billion, with the biggest proportion found in developing countries in Asia (Gerland *et al.* 2014). These developing countries also happen to be the world's biggest rice consumers, with Asia consuming 90% of the world's rice in 2008 (Zeigler and Barclay 2008). From the perspective of developing nations, current rice supply and demand is roughly in balance (Skamnioti and Gurr 2009). However the world population is projected to rise to an estimated 10 billion by 2050, and in under-developed nations, demand exceeds supply. Food security-related issues is expected to affect up to 4.5 billion people (Brinkman *et al.* 2010). To ensure the maintenance of a

sustainable increase in global food supply and interest towards rice research and the development of crop protection strategies is imperative.

Worldwide rice cultivation is vulnerable to pests and diseases, especially in developing countries. Provided effective protection strategies and resistant cultivars are used, about 38% of attainable rice production can be safeguarded from diseases (Oerke and Dehne 2004). Unfortunately, effective plant pest management (PPM) systems are not always readily applied, afforded or taught to poor local farmers in developing nations. With the absence of effective PPM practices, it was estimated that Rice Blast (caused by *Magnaporthe* oryzae) can cause between 5% and 30% loss in yield (Skamnioti and Gurr 2009, Zeigler and Savary 2010). The estimated losses incurred by rice blast disease could feed for a year, up to 10.6% of the world's population at 2000 calories per day (Fisher *et al.* 2012). Recorded in over 85 countries, the rice blast pathogen is regarded as a serious problem not only due to its impact on rice yield, but also its widespread distribution, which may be attributable to it having spread alongside the expansion of rice cultivation (Couch and Kohn 2002, Couch *et al.* 2005, Khush 2005, Nandy *et al.* 2010, Molina *et al.* 2011).

More disconcerting is the recent outbreak of rice blast despite the application of PPM systems. In regions where rice agriculture is thought to be advanced, severe rice blast epidemics have occurred. In China, between 2001-2005, 5.7 million hectares of rice were destroyed (Wilson and Talbot 2009). In the Southern United States, the 'Banks' rice cultivar containing the resistance (R) gene *Pi-Ta* was resistant to rice blast for 14 years until it was overcome in 2005 by the virulent strain IE-1k of the blast pathogen (Lee *et al.* 2009). This phenomenon suggests that additional and continuous studies need to be

undertaken in developing better crop protection strategies. A potential approach is to combine factors that counter the fast-evolving fungal avirulent (*AVR*) genes with antifungals that target more conserved genes governing fungal viability. Enzymes responsible for the remodelling of fungal cell walls were shown to be highly conserved and are fungal-specific, hence, an ideal anti-fungal target to be explored in *M. oryzae* (Coronado *et al.* 2007, Xie and Lipke 2010).

1.3 Rice Blast Disease

Rice blast disease is caused by the ascomycete filamentous fungus *Magnaporthe oryzae* (previously known as *Magnaporthe grisea*). Recent multilocus genealogy separated *Magnaporthe* sp. into two separate groups: *Magnaporthe grisea* group infecting *Digitaria* sp (crabgrass) and *M. oryzae*, capable of infecting rice, millet, oats and other grasses (Couch and Kohn 2002). This fungus is a hemibiotrophic pathogen, capable of infecting all aerial parts of the host plant. Symptomatic plants exhibit neck rot, node and leaf blast (Figure 1.1). The life cycle of this pathogen is well studied (Figure 1.2).

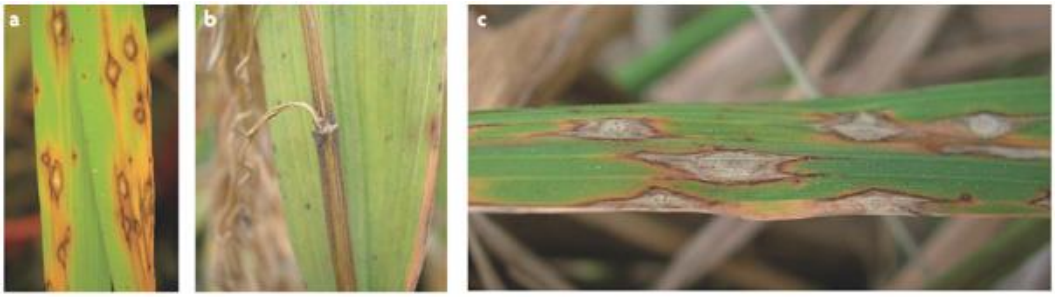

Figure 1.1. *Magnaporthe oryzae* Causes Rice Blast Disease. Panel (a) Symptoms characterized by large, spreading lesions with a necrotic centre and a chlorotic margin. **Panel (b)** In the field, neck, and panicle blast are the major causes of rice yield losses. The fungus sporulates profusely at nodes on the rice stem and rots the neck of the mature rice plant, either causing the panicle to be lost or preventing grain filling and maturation. **Panel (c)** Large rice blast lesions, which can be more than 1 cm in length, on a mature rice plant. Image (a)–(c) are from a rice blast outbreak in Hunan Province, China, in October 2007. Figure and captions edited from Wilson and Talbot (2009).

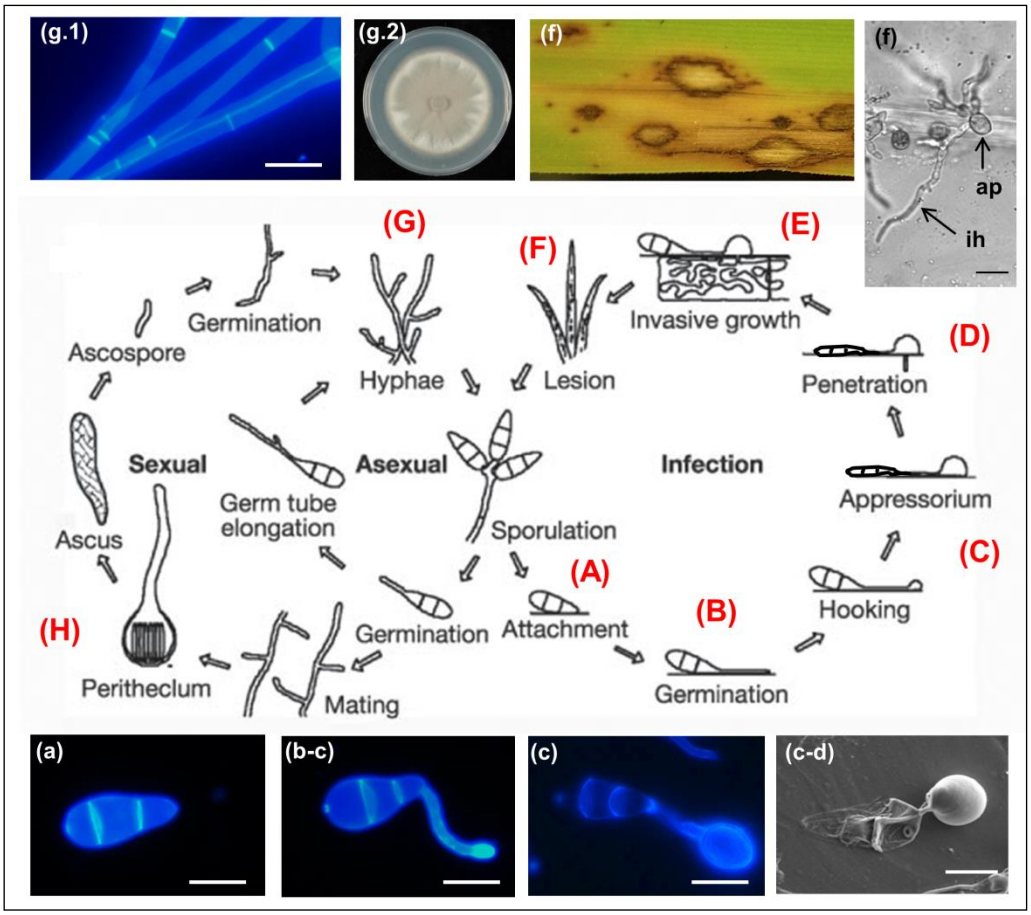

Figure 1.2. Life Cycle of *Magnaporthe oryzae*. (A) When there is sufficient moisture, spores attach tightly to the hydrophobic leaf surface. Fluorescence image (a) shows a three-celled, tear-drop shaped spore with the cell wall stained with Calcofluor White (CFW). **(B)** By 1-4 hours post inoculation (hpi), the spore germinates at the tapered end and produces a germ tube that eventually swells. Fluorescence image (b-c) shows a CFW stained germling with a swollen tip. **(C)** Between 12-24 hpi, the swollen tip differentiates into an appressorium whereby upon maturation (melanisation), the spore collapses. Fluorescent image (c) shows a CFW stained germling with the formation of an immature appressorium. **(D)** Between 24-48 hpi, a mature appressorium produces sufficient turgor pressure to penetrate the host using narrow penetration pegs. Electron micrograph (c-d) shows a germling with a collapsed spore and mature appressorium. **(E)** Between 24-48 hpi, upon successful host penetration, the fungus develops thick invasive hypha that colonise host cells for nutrient accumulation. Light microscopy image (f) show infective hyphae (ih) developing in onion cells, growing from the melanised appressorium (ap). **(F)** After 72-96 hpi, a disease lesion is evident on the leaf surface, and provided there be sufficient humidity (>80%), aerial conidiophores emerge and spores are dispersed through rain or dewdrop splash. Image (f) shows lesions emerging on a rice leaf infected with *M. oryzae.* **(G)** In the absence of a hydrophobic surface or host, and in the presence of sufficient moisture and nutrients, spores germinate to form vegetative hyphae and subsequent conidiation. **(H)** When the fungi encounter a suitable mating type, sexual reproduction occurs. Image (g.1) show CFW stained vegetative hyphae and image (g.2) shows *M. oryzae* grown vegetatively on Complete Medium agar. Scale bars represent 10 µm except for image (f) in which the bar represents 20 µm. Image of life cycle edited from Dean *et al.* (2005), image (d) electron micrograph taken from Skamnioti *et al.* (2007), image (f) taken from Wilson and Talbot (2009) and remaining images were taken from this work.

Apart from understanding the biology and mechanism of infection in *M. oryzae*, recent years have seen *M. oryzae* frequently used as a model organism for other phytopathogen-related studies. This pathogen is not an obligate parasite and thus, can continue to grow vegetatively in the absence of a plant host, such as in the soil (although less frequent in nature) and can be cultured in the laboratory. This makes *M. oryzae* an ideal model for appressorium forming fungi which are mostly obligate phytopathogens such as *Blumeria graminis* (powdery mildew), *Puccinia graminis* (wheat rust) *Ustilago maydis* (corn smut) and *Puccinia triticina* (wheat leaf blight) (Thomas *et al.* 2001, Both *et al.* 2005, Bolton *et al.* 2008, Fehser and Moerschbacher 2011, Freitag *et al.* 2011). Due to this, laboratory cultivation and cross-species comparison is possible.

Advances in genome sequencing have contributed significantly in the genetic study of this organism. This is because the availability of fully sequenced genomes of both *M. oryzae* (Dean et al. 2005) and its host, *Oryzae sativa*, made host-pathogen genetic studies more accessible (Itoh *et al.* 2007). Also, this pathogen is an ideal model organism for forward genetics due to its' small genome size (~40 Mb), therefore taking a genomics and transcriptomics approach in studying expression changes under various conditions, is made possible. Furthermore, high rates of ectopic insertion make forward genetics and generation of complemented strains relatively straight forward. For example, Balhadere *et al.* (1999) managed to generate up to 20,000 mutants using *Agrobacterium*-mediated transformations. Albeit at a lower rate, the occurrence of homologous recombination DNA repair and the application of targeted gene replacement, have contributed towards the success of a plethora of gene functional studies (Talbot and Foster 2001).The economic and health threat of

this plant pathogen to the global population, coupled with ease of genetic manipulation, lead to the use of this species in this work to explore the importance of fungal cell wall in maintaining normal function and towards virulence.

1.4 Fungal Cell Wall

The fungal cell wall is a multifunctional, dynamic cell structure. Not only is the cell wall needed for rigidity and mechanical support, but it is also required to maintain plasticity, enabling cell cycle progression, growth, infection and the sensing of changes to the external environment (Gow and Gadd 1995, Bowman and Free 2006, Klis *et al.* 2006). For example, the cell wall is rich with sensory proteins such as Mid2, Wsc1, Wsc2 and Wsc3, shown to be important for sensing changes to cell wall or temperature stress, leading to a cascade of signal transduction and cellular response mechanisms (Ketela *et al.* 1999, Lommel *et al.* 2004, Jendretzki *et al.* 2011). In another example, the cell wall of the human pathogen *Histoplasma capsulatum* is remodelled during infection to contain the polysaccharide α-glucan (1,3) at the outer layers of the cell wall (Rappleye *et al.* 2007). This 'masks' the pathogen and prevents the host immune system from pathogen recognition.

In addition to the importance of the cell wall to the fungi, it is an external structure unique to the fungal kingdom. This makes the cell wall an ideal target for the development of new antifungal treatments and disease management systems (Georgopapadakou and Tkacz 1995). Unfortunately, while the structure is thoroughly studied in the yeast *S. cerevisiae* and the human fungal pathogen *C. albicans,* little is known of this structure in fungal plant pathogens. Given the suitability of *M. oryzae* as a model organism and as the recently ranked number

1 (Dean *et al.* 2012) most destructive fungal phytopathogen, it is apt that this study attempted at unravelling and understanding *M. oryzae* cell wall in this study, in hopes of elucidating new methods of disease control.

1.4.1 Cell Wall Structure

The fungal cell wall is comprised of polysaccharides and proteins. It is estimated that ~90% of the cell wall is made from both long and short chained polysaccharides, while the remainder percentage are cell wall proteins (CWP) decorating the sugar polymers (Latgé 2010). The wall component can be simplistically separated to two layers or fractions: the alkaline insoluble fraction (AIF) and the alkaline soluble fraction (ASF) (Figure 1.3). The inner layer of AIF is often shown as electron transparent in Transmission Electron Microscopy (TEM) images, and is comprised of a fibrillar network of long β-glucan and chitin chains cross-linked to provide mechanical strength and rigidity to the cell wall (Sandula *et al.* 1995, Orlean 2012). In contrast, the ASF comprises both the outer amorphous layer, seen as a hair-like electron dense area (Figure 1.4), and dispersed within the AIF as short newly synthesised glucan chains (before it is cross-linked). The ASF is made of (1,2/1,6)-mannans, short β(1,6/1,3)-glucans, α(1,2)-glucans and glycoproteins (Kapteyn *et al.* 1999b, Hardison and Brown 2012).

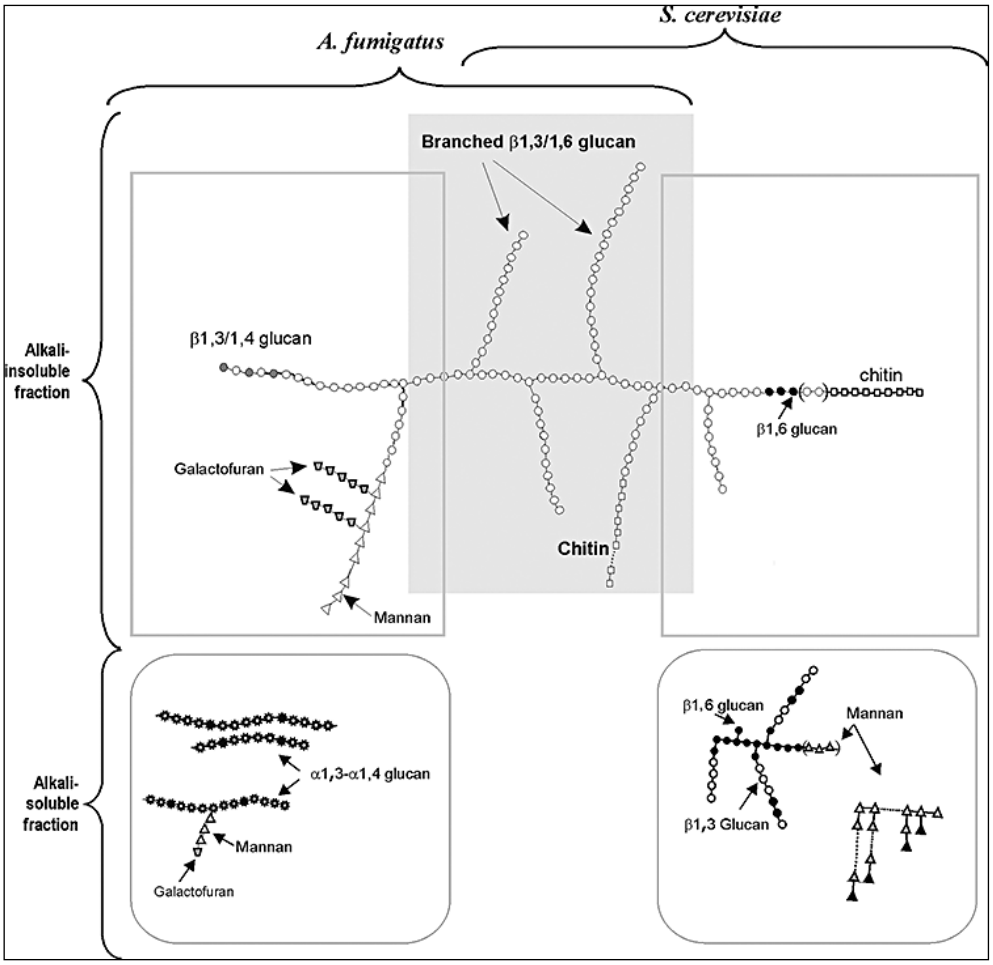

Figure 1.3. Polysaccharides of the Cell Wall of *Aspergillus fumigatus* and *Saccharomyces cerevisiae*. Components of the alkali-insoluble and alkali-soluble fractions. The grey area represents shared components for both species. Figure and captions edited from Latgé (2007).

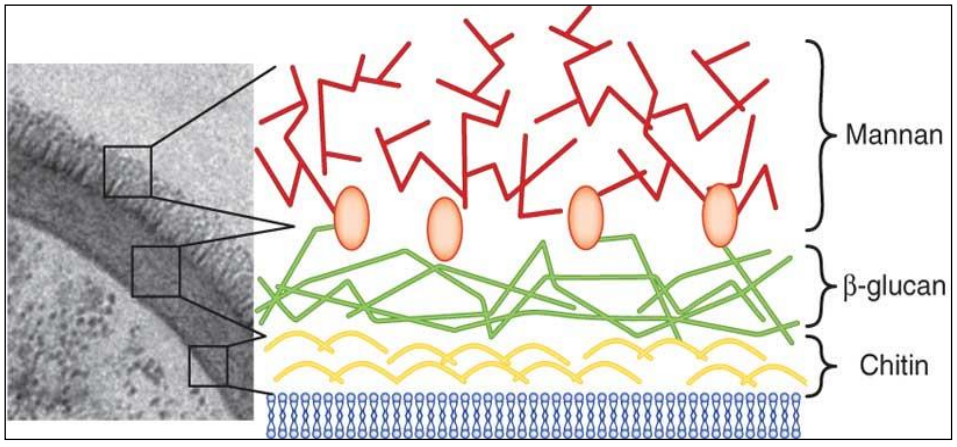

Figure 1.4. Fungal Cell Wall of *Candida albicans*. The electron micrograph shows the carbohydrate-rich layers of the fungal cell wall highlighted: mannan (and mannosylated proteins), β-glucan (and glucan-linked proteins) and chitin. The figure and caption were edited from Hardison and Brown (2012).

The composition of fungal cell wall varies significantly within (eg. stage of life cycle and growth conditions) and between species (Gow and Gadd 1995, Chaffin 2008, Fujikawa *et al.* 2009). For example, the outer layer of the spore wall of a filamentous fungus differs greatly from the cell wall in vegetative hyphae. Using Atomic Force Microscopy (AFM) surface imaging and 2-D cross-sectional images by TEM, it was shown that spores of *Aspergillus fumigatus* have an outer layer of melanin-covered by hydrophobic rodlets, while an amorphous layer is seen on vegetative hyphae for the latter (Dague *et al.* 2008, Latgé and Beauvais 2014). In another example, during infection, the phytopathogen *Puccinia graminis* re-constructed the cell wall of their infectious hyphae to contain a layer of chitosan, protecting the fungi from plant chitinases (El Gueddari *et al.* 2002). Differences in the cell wall composition are also seen across different fungal species. For example, *Aspergillus fumigatus* has ~10 times more chitin content compared to *S. cerevisiae,* while the yeast *Schizosaccharomyces pombe* have no chitin in the cell wall (Roelofsen and Hoette 1951, Bernard and Latgé 2001).

Except the model organism *S. cerevisiae* and the human fungal pathogens *A. fumigatus* and *C. albicans*, limited knowledge is available regarding cell wall composition in fungal phytopathogens. With this consideration, subsequent descriptions of the various cell wall components will use *S. cerevisiae* as it is a widely studied, model fungus and whenever possible, comparisons will be made to other studied filamentous fungi. However, given the diversity of the fungal cell wall described above, comparisons must be regarded with caution. This limitation in available knowledge and the variations seen across species, emphasise the importance of investigating the specific composition and structure of *M. oryzae*

cell wall at various stages of the life cycle if an effective new disease control strategy is hoped to develop.

1.4.2 Cell Wall Components & Biosynthesis

1.4.2.1 Carbohydrates: Alkaline Insoluble Fraction

As mentioned previously, the cell wall of fungi comprises of carbohydrates and proteins and these can be found in both the alkaline soluble or alkaline insoluble fraction of the wall. The synthesis of this large extracellular structure poses both physical and thermodynamic problems. It is impossible to synthesise the matrix intracellularly followed by secretion due to the physical barrier of the plasma membrane, while any restructuring that needs to be performed on the extracellular cell wall experiences the scarcity of free energy abundant in the cytoplasm (such as ATP) (Cabib *et al.* 2008). Over the course of evolution, however, these problems have been addressed elegantly.

The synthesis of the cell wall carbohydrates can be divided into two parts as suggested by Latge and Beauvais (2014). The largest structures of the cell wall: β-glucan and chitin polymers are first synthesised vectorially in short chains, into the external environment at the plasma membrane (Figure 1.5). Both energy (UDP) and glucose/chitin monomers are derived from the cytoplasm and monomers linked into chains by glucan and chitin synthase complexes (Free 2013). Once extruded, these polymers are further remodelled by specialised glycosyl transferase (GST) enzymes (Figure 1.5) designed to bypass the thermodynamic problem by harnessing energy from the hydrolysis of glycosidic linkages, and using the energy to form new bonds (Cabib *et al.* 2008). These GST or cell wall remodelling enzymes are found covalently linked to wall

polymers or anchored to the plasma membrane by GPI-anchoring to ensure close proximity to substrates (Kapteyn *et al.* 1999b). By controlling the amount and types of GSTs decorating the cell wall, the fungi effectively controls the remodelling of the cell wall based on needs in response to intracellular developmental changes, or in response to external stimuli.

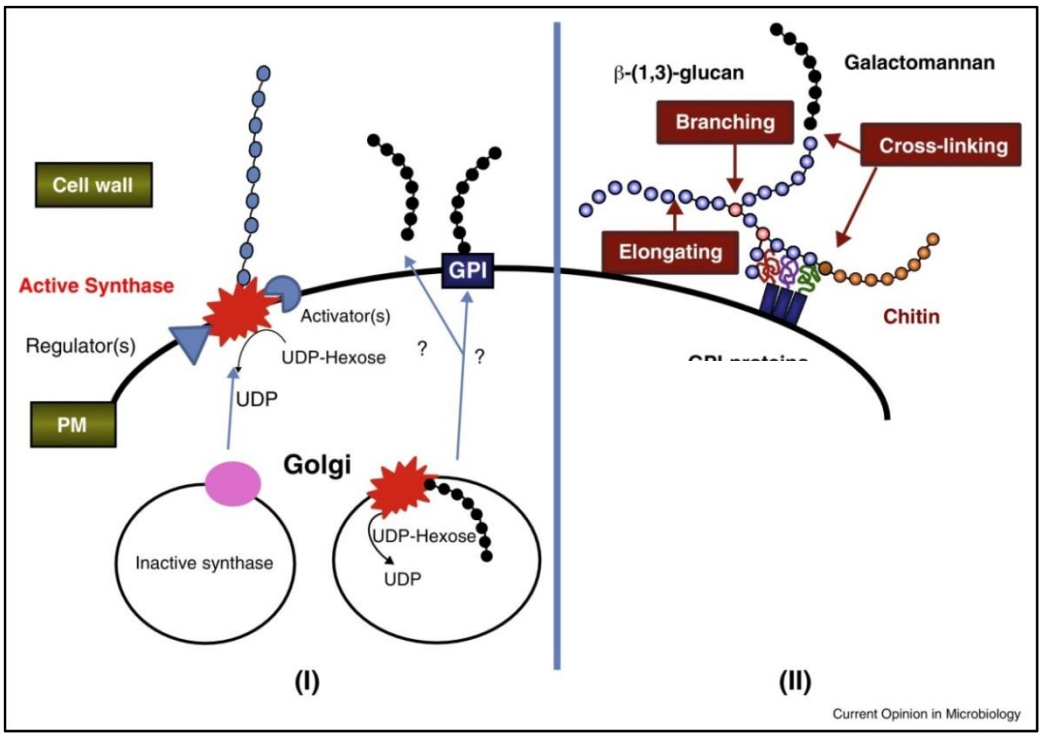

Figure 1.5. Sequential Events in the Biosynthesis of Cell Wall Polysaccharides. Part I Vectorial synthesis of linear glucan and chitin polymers by transmembrane polysaccharide synthases. Some of the synthases such as chitin and β(1,3)-glucan synthases are synthesised and transported inactive to the plasma membrane where they become part of a multiprotein complex comprising activator and regulator proteins; regarding galacto-mannan (α 1,2/1,6 mannan) synthesis, the synthase is located and active in the Golgi where biosynthesis takes place. **Part II** Remodelling of neosynthesised polysaccharides to construct the three-dimensional network of cell wall polysaccharides. Glycosyl Phosphatidyl inositol (GPI) proteins are hypothesised to play a major role in the elongation, branching and crosslinking of the major polysaccharides of the structural core. The synthesised proteins are transported by an unknown mechanism through the PM to the cell wall where they are either covalently linked to the polymers or anchored by GPI-anchoring to the PM. Figure and caption edited from Latgé and Beauvais (2014).

1.4.2.1.1 Beta-Glucan

Beta-glucan polymers are the biggest component of the cell wall and the Alkaline Insoluble Fraction, forming the primary 'skeleton' in fungal cell walls. Located near the plasma membrane, they are long polymers of D-glucose molecules linked at carbon 1 and 3, forming β-(1,3) glycosidic linkages (Figure 1.6) (Bowman and Free 2006, Latgé 2007). It is estimated that between 65% and 90% of cell wall glucan is β-(1,3) glucans, with the remaining existing as β-(1,3) mixed with (1,4) or β-(1,3) mixed with (1,6) glucans in *A. fumigatus* and *C. albicans* (Bernard and Latgé 2001, Klis *et al.* 2001).

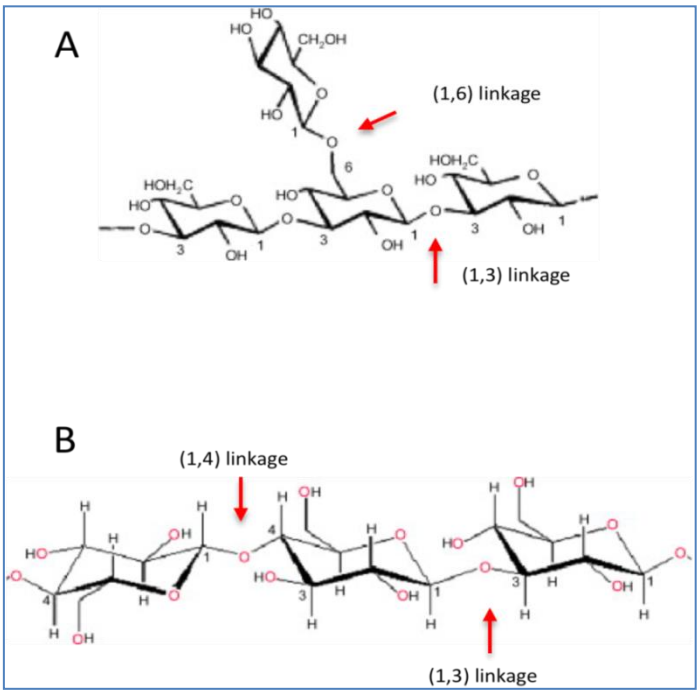

Figure 1.6. Molecular Structure of Beta(1-3/1,6/1,4)-Glucan. Panel A A chain of D-glucose linked at carbon 1 and 3 forming linear β-(1,3) linkages, and branching forming at carbon 6 (red arrow). **Panel B** β-(1,3/1,4) glucan chain with D-glucose linked at carbon 1 to carbon 3 or 4. Figure modified from Mantovani *et al.* (2008).

Beta glucan is vectorially synthesised at the plasma membrane through a glucan-synthesizing protein complex. The protein complex comprises of catalytic glucan synthases and a regulatory unit (Douglas 2001, Smits *et al.* 2001a) that uses intracellular UDP-glucose as the donor and GTP as the energy source, yielding glucan chains each with 60-80 glucose monomers (Shematek *et al.* 1980, Kang and Cabib 1986). Once these short polymers are synthesised *de novo*, these chains do not remain linear nor short, but are further elongated by up to 1500 glucose monomers (Fleet 1985) and remodelled, acting as scaffolds for other cell wall constituents forming cross-links and branching with proteins, chitins, and other glucans. Genes encoding glucan synthases were first identified in *S. cerevisiae* as genes *Fks1* to *Fks3*, regulated by Rho1p (Smits *et al.* 2001a, Lesage *et al.* 2004, Bowman and Free 2006, Ishihara *et al.* 2007, Okada *et al.* 2010). Since glucan synthase is essential for the construction of the cell wall, studies searching for antifungals affecting the biosynthesis of glucan have been very successful in human pathogens.

Antifungal drugs targeting the glucan synthase complex have already been administered in humans. Echinocandins are a class of antifungal drugs belonging to the fungal specific lipopeptide group targeting β-glucan synthase (Kurtz and Douglas 1997). *In vivo* studies showed echinocandin is fungicidal to *Candida* spp. and growth inhibiting to *Aspergillus* spp. (Denning 2003). It is commercially sold as caspofungin (Cancidas: Merck), micafungin (Mycamine: Astellas) and anidulafungin (Reaxis: Pfizer) (Walker *et al.* 2011). Unfortunately within the last five years, there are reports of echinochandin resistant *C. albicans* strains with mutations in the *Fks* functional domain (Kurtz and Douglas 1997). Consequently, a study in 2011 explored the impact of combining the loss

mannosyl transferase (Mnnp) cell wall remodelling enzyme and chitin synthase (Chsp) with echinochandin treatment (Ueno *et al.* 2011). They showed that the double-mutant Δ*Chs3A* and *ΔMnn10* in *Candida glabrata* exhibited synergistic stress sensitization and echinochandin hypersensitivity.

The enfolding scenario above indicates that while there is potential to find antifungals acting on glucan synthases in plant pathogens, it is evident that cell wall remodelling enzymes warrant a strong emphasis and have the potential to be used synergistically with other fungal inhibitors. There is no available literature exploring the orthologues of *S. cerevisiae Fks* genes in *M. oryzae*, further highlighting the dearth of cell wall related knowledge in this fungal species

1.4.2.1.2 Chitin

Chitin is a linear homopolymer chain of β-(1,4) linked N-acetylglucosamine. In yeasts such as *S. cerevisiae* and *C. albicans*, chitin accounts for only 1-2% of the yeast cell wall, but up to 15% in filamentous fungi such as *Neurospora crassa* and *A. fumigatus* (Nobel *et al.* 2000, Gastebois *et al.* 2009, Maddi and Free 2010). Although comprising such a small fraction of the cell wall, these chitin polymers have tremendous tensile strength and significantly contribute to wall rigidity (Free 2013).

Similar to glucan, chitin is vectorially synthesised at the plasma membrane, catalysed by the chitin synthase complex and UDP-*N*-acetylglucosamine as substrates (Bowman and Free 2006, Latgé 2007). The nascent chitin chain is then immediately remodelled by forming cross-links with 1,3 and/or 1,6-beta glucans (Marian *et al.* 2013) as matured chitin with mutually

associated hydrogen bonds are impervious to enzymatic attack (Cabib *et al.* 2008).

In *S. cerevisiae*, chitin synthase enzymes form a chitin-synthesizing protein complex at the cell membrane where chitin is synthesised. The synthase enzyme Chs3p synthesises the bulk of chitin biosynthesis (80-90%), while Chs2p is associated with septal synthesis and Chs1p acts as a repair enzyme during cell division (Klis *et al.* 2006). Other fungi also have orthologous *Chs* genes, and comparative ascomycete studies classified *Chs* genes into seven classes (Choquer *et al.* 2004). In *M. oryzae,* seven chitin synthases have been characterised (Vidal-Cros and Boccara 1998, Kong *et al.* 2012). The gene *Chs3* was found to be most highly and stably expressed throughout the life cycle of *M. oryzae* (Vidal-Cros and Boccara 1998), while the single gene knockout of *Chs1, Chs6* and *Chs7* were shown to affect pathogen virulence (Kong *et al.* 2012). Due to the structural integrity that chitin provides and the role of chitin synthases to pathogen virulence, it is an ideal target for anti-fungal agents with significant interest in both animal and plant fungal pathogens.

Antifungal agents targeting chitin synthase biosynthesis have been applied in the clinical sector, while those in plants are still at the research stage. Nikkomycin is a naturally occurring human drug that competes with the chitin synthase substrate, UDP-*N*-acetylglucosamine. However Nikkomycin has only proved effective when used with other treatments (Li *et al.* 2011). In plant pathogen studies, there is an increase in the interest of *Chs* genes as an antifungal target. Despite variations in morphology, almost all phytopathogen species studied (*Ustilago maydis, Fusarium verticillioides, Botrytis cineria, Fusarium asiaticum* and *M.oryzae*) have at least one class of *Chs* gene important

for virulence (Odenbach *et al.* 2009, Arbelet *et al.* 2010, Treitschke *et al.* 2010, Xu *et al.* 2010, Larson *et al.* 2011). The incidence of antifungal resistant strains in animals and the promising reverse genetics research in plant pathogens emphasises the need to study and incorporate synergistic antifungal compounds to be used simultaneously, each drug having different targets.

1.4.2.2 **Carbohydrates: Alkaline Soluble Fraction**

In contrast to the AIF, polysaccharides in the ASF are less characterised and vary significantly between species. These ASF carbohydrates include (1,2/1,6) mannans, short chains of α(1,3)-glucans, glycoproteins as well as short β(1,3/1,6)-glucans (Latgé 2010). The outer amorphous layer important for specific cell-cell recognition and sensing of environmental changes, is rich in mannoprotein and glycoproteins and as such, its composition is unique to each species and stage of the life cycle (Hardison and Brown 2012). Additionally, newly synthesised β(1,3/1,6)-glucan chains located near the plasma membrane that are not (or due to be) linked to chitin, could also be eluted in hot alkali. Therefore, it is imperative to note that the ASF is dispersed throughout the cell wall and not restricted to the amorphous layer. Little is understood in relation to the synthesis of the carbohydrate components of the ASF. It is possible that these components are synthesised in the golgi and secreted to the cell wall (Latgé 2007). However such generalisation is open to debate as each component may have its' own unique synthesis pathway and instead each component will be discussed in greater detail in the following sections.

1.4.2.2.1 Mannan & Short Glucan Chains

Mannans are polymers of the sugar mannose, found as short chains and mostly in the amorphous layer of the cell wall with the primary function of tethering proteins (mannoproteins). In *S. cerevisiae*, mannans can be found as α(1,6)-mannan branched to other ASF components, both carbohydrates or proteins (Gómez-Miranda *et al.* 2003, Latgé 2010). It is proposed that mannan chains, due to their short nature (less than 200 monomers) are synthesised at the Golgi and secreted to the extracellular region (Latgé 2007, Engel *et al.* 2012).

An additional, less-understood cell wall component is β(1,6)-glucan. In *S. cerevisiae,* these are short, highly branched polymers of D-glucose with an average size of 350 glucose monomers (Kollár *et al.* 1997). The biosynthetic pathway of β(1,6)-glucan shares similarity with the mannan counterpart, with *Kre* genes associated with the synthesis of this carbohydrate (Meaden *et al.* 1990). This fungal-specific polymer is an important 'linker' between components of the wall, such as the attachment of mannoproteins to β(1,3)-glucan chains, and as such, is found mostly in the amorphous layer (Aimanianda *et al.* 2009). To a smaller extent, β(1,6)-glucan has also been found interconnecting chitin to β(1,3)-glucan (Kapteyn *et al.* 1997, Kollár *et al.* 1997).

Another component of the ASF is α(1,3)-glucan. In pathogens, this carbohydrate has been shown to be produced only during infection and used to 'mask' the pathogen from host recognition. This remodelling of the cell wall to include a 'mask' of α(1,3)-glucans and its importance for virulence, have been noted in *Histoplasma capsulatum* (Klimpel and Goldman 1988), *Cryptococcus neoformans* (Reese *et al.* 2007) *Blastomyces dermatitidis* (Hogan and Klein 1994) and recently, even in *M. oryzae* (Fujikawa et al. 2009). Interestingly, in *A.*

fumigatus, α(1,3)-glucans account for up to 35% of total wall carbohydrate (Beauvais *et al.* 2007) and the gene *Ags3* was found to be responsible for α(1,3)-glucan synthesis (Maubon *et al.* 2006). Unfortunately, similar to other ASF components, the detailed biosynthetic pathway of this glucan chain is poorly understood.

1.4.3 Cell Wall Proteins (CWP)

Cell wall proteins (CWP) make up the remaining ~10% of the fungal cell wall. They are primarily anchored to the plasma membrane through glycosylphosphatidyl (GPI) anchors, covalently bound to alkaline insoluble polysaccharides or to short chains of mannans and glucans in the ASF (Kapteyn *et al.* 1999b). In *S. cerevisiae* and *C. albicans*, proteins account for up to 30-50% of the cell wall dry weight, but it is less in filamentous fungi (20-30%) (Bowman and Free 2006, Bowman *et al.* 2006). Most of the proteins in the ASF can be found at the amorphous layer and function mainly as sensory proteins. For example, some species such as *S. cerevisiae* and *C. albicans* contain mannoproteins (attached to mannan chains) while filamentous fungi such as *Neurospora crassa* and *Aspergillus fumigatus* have proteins with galactomannan attached.

Cell wall proteins found in the inner cell wall are specialised cell wall remodelling enzymes (GST) and can be covalently linked to polysaccharides, or anchored to the plasma membrane via a glycosylphosphatidyl (GPI) moiety (Figure 1.7). These GSTs play an important role in cell wall remodelling and as such, warrant further discussion.

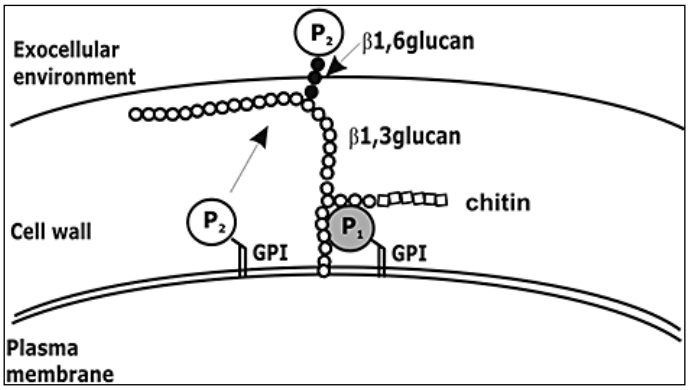

Figure 1.7. Putative Functions of GPI-anchored Proteins During the Construction of the Fungal Cell Wall. (i) GPI-anchored proteins (P1) that remain attached at the plasma membrane remodel cell wall polysaccharides (examples are Gel/Gas or Crh proteins). (ii) GPI-anchored proteins (P2) become covalently bound to β1,3 glucans through β1,6 glucans. This is a way for protein P2 to remain at the cell surface to fulfill its biological function, for example, in cell-to-cell interactions. Legend: β(1,3)-glucan (○);β(1,6)-glucan(●); chitin (□). Figure and caption obtained from (Latgé 2007).

1.4.3.1 Cell Wall Remodelling Protein: Mechanism & Genetics

As described by Latge and Beauvais (2014), GSTs play an important role in the second part of cell wall synthesis: cell wall remodelling. Out of 30 CWPs identified to date (Cappellaro *et al.* 1998, Molina *et al.* 2000, Yin *et al.* 2005), several proteins have been characterised as GSTs. These include glucan elongating glucanosyltransferase, Gas1p (Nuoffer et al. 1991), Defective cell wall protein Dcw5p (Kitagaki *et al.* 2002c), beta glucanase Bgl2p (Goldman *et al.* 1995), as well as the *Crh*-like family (Rodriguez-Pena *et al.* 2000). The *Gelp* genes, first described in *S. cerevisiae* and later *C. albicans* (Fonzi 1999) specifically remodel the cell wall by β(1,3)-glucan elongation and branching to other glucans (Popolo and Vai 1999). Little is known regarding the function of the transglycosylase protein Dcw5p apart from the observation that mutant lines showed increased sensitivity to the cell wall degrading enzyme Zymolyase (Kitagaki *et al.* 2002c). The GST protein Bgl2p has been implicated in the cross-linking of laminaribiose and glucan polymers (Goldman *et al.* 1995), with mutants

in *C. albicans* showing reduced virulence in mouse models (Sarthy *et al.* 1997). Last but not least, are the Crh-like family of enzymes responsible for the cross-linking of chitin to glucan polymers (Rodriguez-Pena *et al.* 2000), which have since attained considerable interest in the model yeast *S. cerevisiae* as well as in the human pathogen *C. albicans* for justifiable reasons.

1.4.3.1.1 Congo Red Hypersensitivity Protein Family (Crhp)

Three *Crh*-like cell wall remodelling genes were first identified in *S. cerevisiae* as *Crh1, Utr2* (syn *Crh2*) and *Crr1* respectively (Rodriguez-Pena *et al.* 2000). According to the NCBI Conserved Domain database, *Crh*-like genes belong to the Glycosyl Hydrolase 16 (GH16) family of Carbohydrate Active Enzymes (CaZy) and are classified within the fungal-specific 'GH16_fungal_CRH1_transglycosylase' sub-group (cd02183) (Marchler-Bauer 2011). In addition to the GH16 functional domain, all proteins in this family share several structural features such as an N-terminus signal peptide, a Ser/Thr rich region, GPI-anchorage at the C-terminus and a jellyroll β-sandwich structure (Hamada *et al.* 1998). Crh-like protein function, cellular localisation and catalytic mechanisms, have been well studied in the yeast *S. cerevisiae* by two research teams in Spain and Maryland USA, led by Arroyo and Cabib respectively.

Through mutagenic, *in vivo* and *in vitro* studies, the functions of these Crh protein families were associated with the catalysis of the cross-linking of chitin to glucan polymers. When Rodriguez-Pena *et al.* (2000) first characterised the *Crh* gene, the authors noted that *Δcrh1Δcrh2/utr2* mutants had twice the level of alkali-soluble glucan fraction than the Wild Type, suggesting that less glucan was linked to chitin (Rodriguez-Pena *et al.* 2000). This change in cell wall composition was later confirmed by Cabib and colleagues (Cabib *et al.* 2007, Cabib 2009)

using an *in situ* chitin deacetylation technique. Here the authors showed that all chitin in *Δcrh1Δutr2* double mutants was free (unbound), compared with the Wild Type which had 31% free chitin, 44% chitin bound to β–(1,3)-glucan and 25% to β-(1,6)-glucan. Finally, using a more sophisticated *in vitro* approach, Mazan *et al.* (2013) used fluorescently labelled sulfordamine-linked laminari- and pustule-oligosaccharides (1,6-glucan, 1,3-glucan and chitin) as artificial acceptors. The authors showed that *S. cerevisiae* Crh-like proteins heterologously expressed in *Pichia pastoris,* could use soluble chitin derivates (eg. glycol-chitin) as donors. These enzymes were then able to join the reducing end of the donor chitin chain to a non-reducing end of the fluorescently labelled acceptors (with a minimal length of 2 monomers).

Immunolabelling as well as fluorescent protein tagging studies revealed that these Crh-like proteins are located at polarised growth sites. For example, a recent study by Blanco *et al.* (2015) introduced Hemagglutinin (HA)-tagged proteins to complement the *Crh-like* gene deletant strains. The authors showed that both *Crh1* and *Utr2* can be found distributed at the lateral cell wall and accumulate most at sites of polarised growth sites and bud scars (Figure 1.8). In an earlier study, Rodriguez-Pena *et al.* (2000) generated green fluorescent protein (GFP)-tagged *Crh1* and *Utr2* strains, with an identical outcome to the localisation of both *Crh1* and *Utr2* in *S. cerevisiae* cells. Not surprisingly, these sites of accumulation corresponded to sites of chitin accumulation. In fact, it was showed that it is the cross-linking of chitin to glucan that determines yeast morphogenesis at the bud neck, as opposed to the mere presence of the chitin ring (Blanco *et al.* 2012, Cabib and Arroyo 2013).

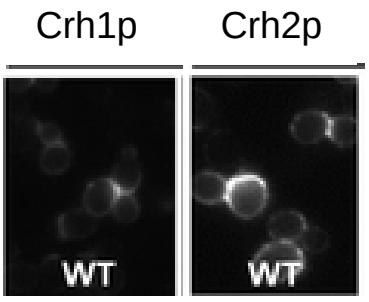

Figure 1.8. Localisation of *Saccharomyces cerevisiae* Crh1-HA and Crh2-HA in the WT strain GRA007. Crh1-HA and Crh2-HA were immune-detected by overnight incubation with anti-HA monoclonal antibody 16B12. Figure and captions edited from Blanco *et al.* (2015).

In contrast to the functional and regulatory information described above, there was a dearth of information pertaining to the structure and mechanistic aspects of Crh-like protein, until recently addressed by Blanco *et al.* (2015). Here, the authors generated a 3D-structure of *S. cerevisiae Crh1* (Figure 1.9) by homology modelling with a known crystal structure of bacterial lichenase (GH16). It was predicted that residues E134 and E138 of *Crh1* as well as E166 and E170 of *Utr2* correspond to the donor (nucleophile) and acceptor (acid/base) respectively. To confirm this prediction, Blanco *et al.* (2015) performed site-directed mutagenesis in a Δ*crh1*Δ*crh2* background strain and showed that these regions are important for transglycosylase activity (Figure 1.10).

The authors deduced that the retaining transglycosylase mechanism of the Crh1 protein can be described in two steps. In the glycosylation step, carboxylate (enzyme derived) at residue E138 of Crh1 protein acts as a nucleophile that attacks C1 carbon from the non-reducing end of a chitin polymer. This reaction is assisted by simultaneous proton transfer from the general acid residue E134 to the glycosidic oxygen, producing a covalent glycosyl-enzyme intermediate. In de-glycosylation, E134 then functions as a general base and activates the +1 O4 hydroxyl group from the non-reducing end of a nearby glucan

polymer (donor), thereby hydrolysing the covalent-glycosyl enzyme intermediate. This facilitates the coupling between donor nascent chitin and the glucan acceptor. Thus far, only the Crh family of proteins catalyse this cross-linking of chitin to glucan, a crucial step needed to maintain cell wall rigidity and strength.

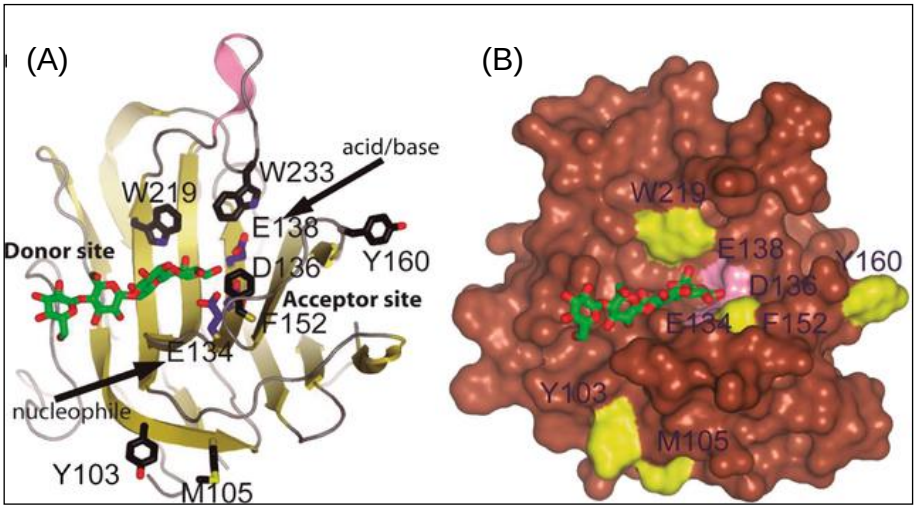

Figure 1.9. Predicted Structure of Crh1 Protein. Panel A Schematic ribbon diagram of Crh1 model showing a β-jelly roll arrangement that is common in GH16 family. By comparison with bacterial 1,3-1,4-β-d-glucanase crystal structures, the catalytic machinery is shown as blue sticks, whereas potential residues involved in sugar binding are shown in black. Residues Y103 and M105, with their side chains pointing outside of the sugar binding cleft and used as controls in site-directed mutagenesis experiments are also shown. A tetrasaccharide based on the superimposition of Crh1p with lichenase in complex with β-1,4-tetrasaccharide is shown as green sticks to indicate the donor and acceptor sites of Crh1p. **Panel B** Surface representation of the active site. Mutated residues of the catalytic machinery are shown in pink and other mutated residues are shown in yellow. Figure and captions edited from Blanco *et al.* (2015).

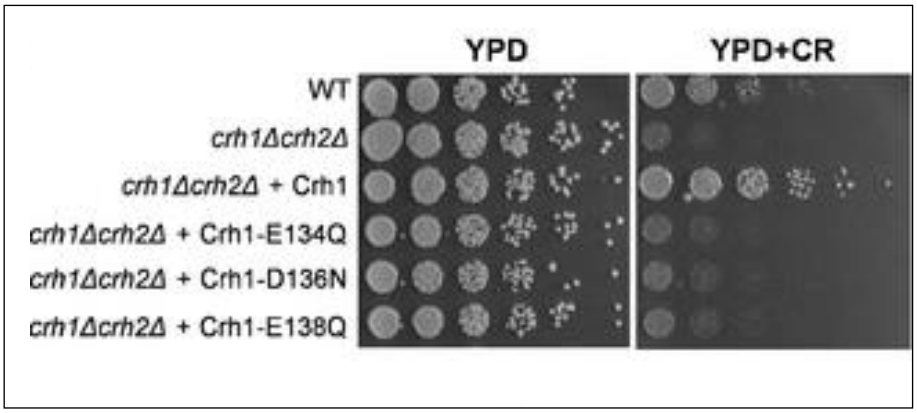

Figure 1.10. Residues Within the Catalytic Site of Crh1p are Essential for the Transglycosylase Activity of This Protein *In Vivo*. Yeast strains were exponentially grown and 1:5 dilution series were spotted onto YPD plates containing 100 $\mu g \cdot ml^{-1}$ of Congo Red (CR). Image show sensitivity assay to Congo red of six yeast strains including WT, double deletant strain Δ*crh1*Δ*crh2,* partial revertant with the addition of gene *Crh1* as well as three strains in which the *Crh1* gene was re-introduced with site-directed mutations at the respective locations: E134, D136 and E138. Figure and caption edited from Blanco *et al.* (2015).

Given the highly specialised function described above, *Crh*-like genes in model fungi were shown to be important for maintaining cell wall integrity. In *S. cerevisiae, C. albicans* and *Yarrowia lipolytica*, *Crh* deletant mutants exhibited increased sensitivity to cell wall perturbing compounds such as Congo Red and Calcofluor White (Rodriguez-Pena *et al.* 2000, Hwang *et al.* 2006, Pardini *et al.* 2006). In another study, the rigidity of the *S. cerevisiae* cell wall in *Δcrh1Δutr2* double mutant was dramatically affected relative to Wild Type (Dague *et al.* 2010). It is thought that in these mutants, the cell wall is no longer rigid, and therefore cannot prevent hyphal tip swelling and bursting caused by cell wall perturbants such as Congo Red (Pancaldi *et al.* 1984, Guerriero *et al.* 2013). This compromise in the normal functioning of the cell wall, begins to suggest that inhibition of *Crh*-like enzymes could then, lead to reduced pathogen fitness and virulence.

In agreement to the above, *Crh-like* enzymes are fast becoming prime candidates as antifungal targets against human fungal pathogens. In addition to affecting cell wall integrity, *C. albicans ΔUtr2* was less virulent and unable to colonise mice organs (Alberti-Segui *et al.* 2004). Furthermore, Pardini *et al.* (2006) then developed a triple mutant which was fully non-pathogenic even when mice were infected at a lethal dose. Results from the studies above are an important indication that targeting *Crh*-like genes has the potential to impair a pathogen's viability, subsequently affecting its ability to infect and/or colonise a host.

Perhaps owing to the external cellular localisation of Crh-like proteins, an interesting association between *Crh-like* genes in *C. albians* and host sensing has been observed. Work by Zelante *et al.* (2012) showed that the mammalian IL-17A protein produced by T-cells binds strongly to fungal hyphal tips. Pre-exposure of fungal cells to IL-17A resulted in increased virulence through an increase in gut inflammation of intragastrically infected mice. To investigate which fungal structure IL-17A specifically binds to, researchers purified fungal CWP and fungal cell wall polysaccharides and conducted an enzyme-linked immunosorbent assay. It was discovered that IL-17A specifically binds to Crh11p, and not Crh12 nor Utr2p. This observation was further confirmed by a co-immunoprecipitation assay of fungal Crh11p and murine IL-17A proteins. The study concluded that fungal sensing of mammalian IL-17A via Crh11p affects fungal growth and morphology.

The apparent Crhp trigger of host immune responses leads to studies in disease control via the vaccination route. In mice, the injection of serum containing Crf1p antigen from *A. fumigatus* (orthologue of *S. cerevisae* Crh1p) conferred resistance to infection by *A. fumigatus* and cross-protective immunity to *C. albicans* (Stuehler *et al.* 2011b). It is highly unlikely that plant pattern recognition receptors (PRRs) are orthologous to animal PRRs or other host animal immune recognition systems. Despite this, it seems probable that some domains sharing an ancient ancestor may have independently formed similar mechanisms for detecting pathogen-associated molecular patterns (PAMPs), (Zipfel 2008). Given the success described above in animal systems, spraying of Crh1p may induce resistance to susceptible crops. Spraying of fungal derived β-glucans has already been shown to be successful against *Plasmopara viticola* in grapevines and *Septoria tritici* in wheat (Trouvelot *et al.* 2008, Shetty *et al.* 2009). These studies show that there is indeed a strong correlation between Crhp and fungal disease control, which is worth exploring in the agriculture industry where other means of control are fast being exhausted.

1.5 Hypothesis & Thesis Aims

About the literature review above, it is hypothesised that proteins from the Crh family in *M. oryzae* play an important role in the maintenance of cell wall integrity, thereby affecting morphogenesis, growth as well as pathogenicity.

The above hypothesis was addressed by executing the following experimental aims:

1. Identify *M. oryzae Crh-like* genes from the orthologues in *S. cerevisiae* followed by gene expression analyses at various stages of the life cycle and under various growth conditions (Chapter 3)

2. Perform single and double gene knockout by targeted homologous recombination and generation of the revertant strains (Chapter 4)

3. Perform various experimental tests to analyse the phenotype of the generated mutants relative to the Wild Type (WT) strain Guy11 (Chapters 5 and 6).

4. To elucidate the cell wall composition of *M. oryzae* WT during vegetative growth, and to then compare with the mutant counterpart (Chapter 6)

5. To conduct homologous gene compensation analyses on the remaining *Crh-like* genes in the mutant background (Chapter 7)

6. Finally, to study the localisation of the Crh-like protein during vegetative and infective growth and to compare the localisation to chitin deposition (Chapter 7)

CHAPTER 2

General Materials

&

Methods

2.1 Materials

In this chapter, the materials and methods used in this thesis relevant to all chapters are described in detail. This includes information on instrument settings, reagent manufacturers, reagents, recipes for solutions as well as routine laboratory methods.

2.1.1 Solutions & Media

Water used throughout this work was de-mineralised (de-min) or further purified via passage through PURELAB Ultra (Elga) for ultra-pure water (designated MilliQ-H_2O onwards). Both de-min and MilliQ-H_2O were autoclaved before usage.

Below lists all routine solutions made and used in this thesis work. Unless otherwise stated, all chemicals in this study were bought from Sigma-Aldrich and when mentioned, autoclaved at 121^oC 151b.sq.in^{-}1 for 20-30 minutes using PriorClave 40 (Midas).

Table 2.1. List of Reagents and Solutions Routinely Used

Solution	Composition
Complete medium	In 800 ml ddH_2O: 1 x nitrate salts, 0.1 % (w/v) trace elements, 0.1 % vitamin solution, 1 % D-glucose, 0.2% Peptone (BD), 0.1 % Yeast extract (BD), 0.1 % Casamino acids (BD). pH adjusted to 6.5 with NaOH, made up to 1 litre with MilliQ-H_2O . For solid media, 1.5 % agar was added. Autoclaved.
Minimal medium	1x nitrate salts, 1% D-glucose, 0.1% ml trace elements solution, 0.1 % thiamine solution, 0.05% biotin solution. Made up to 1 l with MilliQ-H_2O. For solid media, 1.5 % agar was added. Autoclaved
Water agar	1.5% (w/v) agar in 1 l ddH_2O. Autoclaved
Genomic DNA Extraction Buffer	200 mM Tris-HCL pH 7.5, 250 mM NaCl, 25 mM EDTA, 0.5 % SDS stock, filled up to 100 ml with MilliQ-H_2O water. Autoclaved.
20 x nitrate salts	1.4 M $NaNO_3$, 140 mM KCl, 36 mM $MgSO_4.7H_2O$, 223 mM KH_2PO_4. MilliQ-H_2O to 1 litre. Autoclaved. Stored at 4 °C.
1000 x trace elements	80 ml MilliQ-H_2O, 77 mM $ZnSO_4.7H_2O$, 178 mM H_3BO_3, 25.3 mM $MnCl_2.4H_2O$, 18 mM $FeSO_4.7H_2O$, 7.1 mM $CoCl_2.6H_2O$, 6.4 mM $CuSO_4.5H_2O$, 6.2 mM $Na_2MoO_4.2H_2O$, 171 mM

	EDTA. Components were added and solution boiled for 30 minutes then cooled to 60 °C. The pH was adjusted to 6.5 with KOH, the solution was cooled to 20 °C and the volume adjusted to 100 ml with MilliQ-H_2O.
1000 x vitamin solution	100 ml MilliQ-H_2O, 0.01 % Biotin, 0.01 % Pyridoxin, 0.01 % Thiamine, 0.01 % Riboflavin, 0.01 % p-aminobenzoic acid, 0.01 % Nicotinic acid. Stored at 4°C.
50X stock TAE Buffer	242 g Tris, 57.1 ml glacial acetic acid, 100 ml 0.5 M EDTA pH 8.0. Made up to 1 l with MilliQ-H_2O.
1X TE Buffer	10 mM Tris (pH 8.0 with HCl), 1 mM EDTA pH 8.0, filled up to 100 ml with sterile MilliQ-H_2O.
1M Tris Buffer	60.55 g Tris, 400 ml MilliQ-H_2O. The pH was adjusted to the desired value with concentrated HCl, and the volume was made up to 500 ml with MilliQ-H_2O.
Sodium acetate (NaOAc)	3 M, pH 5.2
1% Congo Red	1% (w/v) of Congo Red (Sigma-Aldrich) was diluted in sterile MilliQ-H_2O in a falcon tube wrapped with aluminum foil. Solution was vortexed vigorously and filter sterilised before use
1% Calcofluor White	1% (w/v) of Calcofluor White, syn. Fluorescent Brightener 23 (Sigma-Aldrich) was diluted in sterile MilliQ-H_2O in a falcon tube wrapped with aluminum foil. Solution was vortexed vigorously and filter sterilised before use

2.1.2 Manufacturer's Details

This section lists all the relevant manufacturers, developers, and companies used in this thesis. It includes a full list of machines and equipment (Table 2.2), the various laboratory kits and enzymes purchased (Table 2.3) as well as laboratory consumables such as pipette tips, falcon tubes, microtubes and petri dishes (Table 2.4). Included in this section are download and online-based software or tools frequently used (Table 2.5) and websites frequently visited (Table 2.6) throughout this research.

Table 2.2. List of Equipment and Suppliers.

Equipment (Model)	Supplier
Nanodrop	**NanoDrop model ND-1000** by Thermo Scientific**.**
Table-top Centrifuge (Heraeus Pico)	**Biofuge** by Thermo Scientific.
Large Centrifuge	**Model Allegra X-15R** by Beckman Coulter
Bioanalyzer	**Bioanalyzer model 2100** by Agilent.
Thermal Cycler	**Model PTC -100** by Bio-rad.
37°C incubators (cloning work)	1. **Multipurpose Shaker Model 10X 400** by Weiss-Gallenkamp. 2. **Incubator model SI 50** by Stuart Scientific.
37°C non-shaking incubator (cloning work)	**Keison Incubator**, manufacturer unknown
25°C shaking incubator (*M. oryzae* growth chamber)	**Model Innova 4230** by New Brunswick Scientific.
25°C non-shaking (*M. oryzae* growth chamber)	**Incubator 1: Model MLR 350** by Sanyo. **Incubator 2: Model MLR 352H** by Panasonic.
Plant growth chamber (Barley and rice plants)	**Model: Fi-totron PG660 Plant Growth Chamber** by Weiss-Gallenkamp.
Quantitative Real Time – Polymerase Chain Reaction Instrument	**Model: Real-Time PCR System AB 7000** by Life Technologies.
Autoclaving Instrument	**Model: PriorClave 40** Priorclave Ltd.
Olympus Microscope	**KeyMed House**
Gel Tank	**GeneFlow Ltd.**
Gel Imaging	**Model G:Box** by SynGene.
Vortex Shaker	**Vortex Shaker** by Ningbo Kingstic Trading & Industrial Co., Ltd.

Table 2.3. Kits and Enzymes Routinely Used and the Corresponding Supplier

Product	Supplier
QIAquick Gel Extraction Kit QIAprep Spin Miniprep Kit QIAquick PCR Purification Kit Rneasy Mini Kit & on-column Rnase-Free Dnase Set Dneasy Plant Mini Kit	Qiagen
RNA 6000 nano kit	Agilent Technologies, Inc.
All restriction enzymes, bovine serum albumin (BSA) and T4 DNA Ligase.	New England Biolabs (NEB),
GeneRuler 1kb DNA Ladder GeneRuler 100bp DNA Ladder GeneRuler Ultra Low Range DNA Ladder 10 to 300 bp 6x DNA Loading Dye Maxima First strand cDNA synthesis kit SYBR® Green PCR Master Mix	Thermo-Fisher Scientific UK,

Table 2.4. Suppliers of Consumable Products Routinely Used

Consumables	Manufacturer
Labware	Fischer Scientific
Menzel slides	Menzel
Glassware	VWR International Ltd.
Eppendorf tubes and pipettes	Eppendorf
Whatman filter paper	Whatman
Labware	GE Healthcare Life Sciences
Mira-cloth	Merck Chemicals
Instruments and labware	Thermo Scientific
Chemicals	Sigma-Aldrich
Growth media	BD

Table 2.5. List of Softwares and the Manufacturers.

Software (Version)	Supplier
QI Imaging (QCapture Pro 7)	QI Imaging Corporation
Endnote (X2)	Thomson Reuters,
LSM Imaging (5)	Carl Zeiss Ltd.
GeneSnap (7.12)	SynGene Ltd
2100 Agilent (B.02.08)	Agilent Technologies Ltd
Image J (1.48v)	Wayne Rasband

Table 2.6. List of Bioinformatics Websites Routinely Visited

Description	Web site/page name and URL
M. oryzae fully sequenced genome	**MIT Broad Institute Database** Website: www.broadinstitute.org
Primer design	**AutoDimer (Vallone and Butler 2004)** Website: yellow.nist.gov
Sequence blast, homology search and GH16 Protein Database	**NCBI Blast and Conserved Domain Database (CDD)** Website**:** blast.ncbi.nlm.nih.gov
GPI anchor predictor	**1. Big-Pi Predictor (Eisenhaber *et al.* 2004)** Website: mendel.imp.ac.at **2. GPI-SOM (Fankhauser and Mäser 2005)** Website: gpi.unibe.ch
Signal Peptide, cleavage site prediction	**1. SignalP 4.1. (Petersen *et al.* 2011)** Website: www.cbs.dtu.dk
Reverse Complement	**Reverse complement** Website: www.bioinformatics.org
DNA sequence to amino acid	**ExPASy Translate** Website: web.expasy.org

2.1.3 Fungal Strains

Following are fourteen *M. oryzae* strains used throughout this work (Table 2.7). These are the Wild Type (WT) strains Guy11 and the mating strain TH3, eight deletant mutants and four revertant strains. Unless otherwise stated, all WT strain mentioned the following chapters refer to the Guy11 strain.

Table 2.7 List of *Magnaporthe oryzae* Strains Used

Strain	Background Strain	Source	Resistance Marker*	Description
Guy11 (MAT1-2)	N/A	Prof. N. Talbot, University of Exeter	None	Wild type strain
TH3 (MAT1-1)	N/A	Prof. N. Talbot, University of Exeter	None	Wild type strain, mating strain to Guy11
Δ*MGG_Utr2:* Line 1 Line 2	Guy11	This study	HYG	Targeted *MGG_Utr2* knockout
Δ*MGG_Crh1*: Line 36 Line 43	Guy11	This study	HYG	Targeted *MGG_Crh1* knockout
Δ*MGG_Crh2*: Line 37 Line 39	Guy11	This study	HYG	Targeted *MGG_Crh2* knockout
ΔΔ*Crh2_Utr2:* Line 25 Line 27	Δ*MGG_Crh2* Line 39	This study	BAR & HYG	Targeted double *MGG_Crh2* and MGG_*Utr2* gene knockout
13c_2ci_6	Δ*MGG_Crh2* Line 39	This study	BAR & HYG	Ectopic insertion of eGFP tagged MGG_Crh2p
13c_2	Δ*MGG_Crh2* Line 39	This study	BAR & HYG	Ectopic insertion of MGG_Crh2p
#5_6	Δ*MGG_Utr2* Line 2	This study	BAR & HYG	Ectopic insertion of MGG_Utr2p
#5_9a_14	Δ*MGG_Utr2* Line 2	This study	BAR & HYG	Ectopic insertion of mCherry tagged MGG_Utr2p

* Hygromycin (HYG), Bialaphos (BAR)

2.2 Routine Methods

Unless otherwise stated, all centrifugation were conducted using a table-top centrifuge (Heraeus Pico by Thermo Scientific) at room temperature.

2.2.1 Fungal Growth & Tissue Preparation

2.2.1.1 Growth on Agar & Stock Maintenance

A dried filter paper carrying spores and mycelium of the relevant *M. oryzae* strains were inoculated onto a complete medium (CM) agar. The plate culture was incubated at 25°C with a 14/10 hour light/dark photoperiod for 10 days in a designated *M. oryzae* growth chamber (Incubator 1/Incubator 2). Unless otherwise stated, routine fungal growth on solid media used standard petri dishes (10 cm diameter) sealed with micropore tape and opened only in sterile flow-hoods.

For propagation and long-term storage, sterile filter papers were arranged onto the surface of a CM agar plate and the fungal strain allowed to grow over the sterile 0.5 cm x 0.5 cm cut filter papers (Whatman Plc) for up to 12 days until all filter papers were fully grown over. These filter papers were harvested and dried in a dehumidifying chamber containing silica gel for two weeks, followed by storage at -20°C.

2.2.1.2 Spore Harvesting

Spores were harvested by scraping the surface of a 10 day-old *M. oryzae* fungal strain grown on CM plate, with 5 ml de-min. water. The spore suspension was filtered through triple-layered sterile Mira cloth (Merck Chemicals Ltd) into a Sterilin tube, to remove any debris (fragments of mycelium and agar), and centrifuged at room temperature for 5 minutes at 3,000 rpm (2,095*g*) using a

large centrifuge (Allegra X-15R by Beckman Coulter). The supernatant was removed and the pellet re-suspended in 1 ml de-min. water. Spore concentration was then determined using a haemocytometer and adjusted to the appropriate concentration.

2.2.1.3 Germling Preparation on Artificial surface

Spores were harvested as per 2.2.1.2 with spore concentration adjusted to 15-20 x10^4 spores/ml, and 80 µl of the suspension was placed onto a hydrophobic cover slip (Menzel) placed onto a glass slide. The inoculated glass slide was kept in a plastic box containing wet filter papers to provide a nearly saturated humidity. This was then kept at 25°C for various lengths of time, corresponding to the various infective stages: 0 hpi (dormant spore), 2 hpi (germ tube), 4 hpi (immature appressoria), 24 hpi (mature melanised appressoria).

2.2.1.4 Germling Preparation on Onion Peel

Onions (*Allium cepa*) were cut into half and the outermost layer removed. Between the outer and inner layers, a thin single-celled layer was carefully removed and placed onto a 1.5% (w/v) water agar plate with the shiny (hydrophobic) side up. The onion peel was cut into a rectangular shape with an estimated size of 2.0 cm x 5.0 cm. Peels were kept from curling by placing two sterile glass slides at opposite edges of the peel. A spore suspension containing the appropriate fungal strain, at a concentration of 20 x 10^4 spores/ml, was prepared as per 2.2.1.2. The spore suspension (80 µl) was placed onto the onion peel as a droplet and incubated for 24 hr at 24°C with a 14/10 hour light/dark photoperiod at 60% humidity.

2.2.1.5 Vegetative Growth in Liquid Media

Two hundred µl of 20 x 10^4 spores/ml of fungal spore suspension was added to 50 ml of liquid CM containing a concentration of 100 µg/ml Penicillin and 100 µg/ml Streptomycin in a 100 ml sterile conical flask (VWR). Inoculated culture was incubated at 25°C for three days in the dark, under continuous shaking (150 rpm) using a designated *M. oryzae* shaking incubator (Innova 4230 by New Brunswick Scientific). Mycelia were harvested by filtering through sterile double-layered Mira-cloth (Merck Chemicals Ltd), dried using paper towels and 0.1 g mycelia was either stored in -80°C or used immediately in downstream procedures.

2.2.1.6 Mycelial Tissue Preparation for Microscopy Work

A small coverslip (0.5 cm x 0.5 cm) was sterilised by washing in 70% ethanol, followed by two washes in sterile MilliQ-H_2O and air dried in a sterile flow hood with UV exposure of 20 minutes. Still under aseptic conditions, the cover slip was carefully placed at the growing edge of an eight day old fungal colony growing on CM agar. After 24 hours, slides containing overgrown mycelium were carefully lifted from the agar and placed onto a glass slide and between 40-50 µl sterile MilliQ-H_2O were dispensed onto the sample. A cover slip was carefully placed over of the small coverslip containing overgrown mycelia. About ten drops of MilliQ water or immersion oil (Sigma-Aldrich) were dispensed onto the coverslip using a 1.5 ml plastic pipette depending on the type of lense and magnification required.

2.2.2 Molecular Methods

2.2.2.1 Ethanol Precipitation of DNA

This procedure was conducted when a higher concentration of DNA is needed. Depending on the total volume of DNA solution, 1/10 volume of 3M Sodium acetate (NaOAc) pH 5.2 was added, followed by the addition of 100% (v/v) cold ethanol at 2x the total volume of DNA solution with NaOAc. The sample was kept for a minimum of 30 minutes at -20°C before centrifugation at 13,000 rpm (16,060*g*), for 1 hour at 4°C. The supernatant was removed carefully, and the pellet washed with 70% cold ethanol. The sample was spun again at 13,000 rpm (16,060*g*), for 30 minutes at 4°C, then supernatant decanted and tube centrifuged briefly to collect remaining 70% ethanol. This was pipetted out and the pellet air-dried for no longer than 5 minutes followed by elution in 15 µl sterile ddH_2O water and storage at -20°C.

2.2.2.2 Quick Genomic DNA Extraction

A sterile scalpel was used to cut 1 cm x 1 cm size thin CM agar containing 10 day old fungal mycelial grown over the surface of the medium. Using a sterile plastic pestle, the sample was powdered in a 1.5 ml Eppendorf tube for 15 seconds, followed by the addition of 400 µl extraction buffer and immediately vortexed for 5 seconds. Samples were incubated for 1 hour at room temperature, then centrifuged (5 min, 13, 000 rpm or 16,060*g*) and 300 µl supernatant transferred to a new Eppendorf tube. An equal volume of isopropanol was added and samples were incubated for two mins at room temperature followed by centrifugation (5 min 13, 000 rpm or 16,060*g*). The supernatant was removed,

and the pellet air-dried no more than 30 minutes. The DNA pellet was then eluted in 50 µl TE buffer and stored at 4ºC for up to 3 weeks.

2.2.2.3 RNA Extraction, Quantity & Quality Test

Tissues were extracted with TRIzol® Reagent (Ambion®) using the manufacturers' instructions, followed by the addition of 50% volume isopropanol, with 5 minutes incubation at room temperature. Samples were loaded into an RNA Quick Spin column (Qiagen RNeasy Minikit) for on-column DNAse digestion and subsequent elution in RNase-free water. RNA sample concentration was determined using the Thermo Scientific 'NanoDrop® ND-1000' spectrophotometer. Samples were normalised to the same concentration of 1000 ng/µl (±100ng). RNA quality and RIN number for each sample were tested using the 'Agilent 2100 Bioanalyzer Instrument' as per the manufacturer's instructions to ensure minimal RNA degradation. Sample RNA was discarded if the RIN value was below 7.5 for samples containing only fungal RNA, and if the RIN value was below 6.0 for samples containing a mix of plant leaf and fungal pathogen RNA.

2.2.2.4 Complementary DNA (cDNA) Preparation

A Qiagen 'Maxima First Strand cDNA Synthesis Kit for RT-qPCR' kit was used as per the manufacturer's instructions. The same concentration (1000 ng/**µ**l) and volume (1 µl) of template RNA were added per 20 µl reactions for each tissue sample. Three controls were prepared: Non-template control (NTC), minus Reverse Transcriptase (-RT) and control RNA from barley leaf only (BL). The reaction mix was incubated for 10 min at 25°C, followed by 30 min at 50°C, and the reaction terminated by heating at 85°C for 5 min. Products were retained at -20ºC and used within two weeks.

2.2.2.5 Routine quantitative Real Time PCR (qRT-PCR)

Quantitative Real-time Polymerase Chain Reaction (qRT-PCR) was conducted using the ABI 7300 apparatus (Applied Biosystems). All reactions were conducted in 96-well plates (MicroAmp® Optical 96-Well Reaction Plate cat N8010560). 'Power SYBR® Green PCR Master Mix' assay (Applied Biosystems) was used in a total volume of 25 μl per well/reaction. Each 25 μl reaction contained 2.0 μl cDNA, 8.5 μl water, 1.0 μl (10 μM) forward primer, 1.0 μl (10 μM) reverse primer and 12.5 μl 'Power SYBR® Green PCR Master Mix'. All qRT-PCR plate amplifications followed the thermal cycler steps: 50°C for 2 minutes followed by 95°C for 10 minutes; 95°C 15 seconds, followed by 60°C annealing temperature for 1 minute, repeating this final step for 40 cycles. Fluorescence of the 'SYBR Green I' dye was calibrated against ROX™. At the end of each reaction, a dissociation curve analysis was performed, with the following thermal profile: 95°C for 15 seconds; 60°C for 30 seconds followed by 95°C for 15 seconds.

2.2.2.6 Primer Design

Routine primer design described below was used for all PCR-based applications with the exception to quantitative Real Time PCR (qRT-PCR) which required more stringent primer design requirements.

Genomic sequence DNA obtained from the fully sequenced genome of *M. oryzae* (70-15) (Broad Institute) were used to design 18-22 bp long primer sequences. Primer pairs were checked for the formation of secondary structures and primer dimers using the online tool 'Autodimer' (Vallone and Butler 2004). Those with such structures at a Gibbs free energy smaller (more negative) than -2.0 kCal/mol

at 37ºC, were discarded. The specificity of primers designed was queried through the blastn tool against the *M. oryzae* genome (70-15) provided in the Broad Institute Blast Similarity Search (www.broadinstitute.org). Search results giving sequences with e-values greater than $1e^{-3}$ were not included in this analysis. Where possible, primer pairs were designed to have less than 5ºC difference in melting temperature. Primers were synthesised by Sigma-Aldrich.

2.2.2.7 Low-Fidelity PCR Amplification

Routine PCR amplification was conducted using *Taq DNA Polymerase* (Thermo Scientific) and according to the manufacturer's instructions. All PCR amplification was conducted using a thermal cycler (PTC-100 by Bio-Rad) with the following recipe and cycling conditions:

Table 2.8. *Taq DNA Polymerase* PCR Reagents

Reagent	Amount (µl)
Forward Primer (10 µM)	0.5
Reverse Primer (10 µM)	0.5
Template (100 ng – 1000 ng)	2.0
MilliQ-H_2O	16.25
dNTP mix (25 mM each dATP, dTTP, dCTP, dGTP)	0.25
X10 Taq Buffer	0.50
Taq DNA Polymerase	1.0
TOTAL	25.0

Table 2.9*. Taq DNA Polymerase* Chain PCR Thermal Cycling Conditions

Step	Process	Temperature (ºC)	Time	Repeats
Step 1	Denaturation	94ºC	0:03:00	1
Step 2	Denaturation	94ºC	0:00:30	x35
Step 3	Annealing	55ºC-65ºC	0:00:30	
Step 4	Elongation	72 ºC	0:01:00/kb	
Step 5	Final elongation	72 ºC	0:10:00	1
Step 6	Cooling	4 ºC	∞	1

2.2.2.8 High-Fidelity PCR Amplification

When it is necessary to obtain amplified PCR products where sequence accuracy is crucial, high-fidelity PCR was performed. In these circumstances, the proofreading *Herculase* II *Fusion DNA Polymerase enzyme* (Agilent Technologies) was used. This includes work in producing PCR cassettes for targeted homologous recombination mutant generation and DNA inserts for vectors in constructing complemented mutant strains, as well as probe amplification for Southern Blot analysis. All amplification reactions were conducted using thermal cycler (PTC-100 by Bio-Rad) with the following recipe and cycling conditions:

Table 2.10. *Herculase* II PCR Reagents

Reagent	Amount (µl)
Forward Primer (10 µM)	1.25
Reverse Primer (10 µM)	1.25
Template (100 ng – 1000 ng)	1.0
MilliQ-H_2O	
dNTP mix (250 µM each dATP, dTTP, dCTP, dGTP)	1.0
X5 Herculase II Reaction Buffer	10.0
MilliQ-H_2O	34.5
Herculase II Fusion DNA Polymerase	1.0
TOTAL	**50.0**

Table 2.11. *Herculase* II PCR Thermal Cycling Conditions

Step	Process	Temperature (ºC)	Time	Repeats
Step 1	Denaturation	95ºC	0:02:00	1
Step 2	Denaturation	95ºC	0:00:20	x30
Step 3	Annealing	55ºC-65ºC	0:00:20	
Step 4	Elongation	72 ºC	0:00:30/kb	
Step 5	Final elongation	72 ºC	0:03:00	1
Step 6	Cooling	4 ºC	∞	1

2.2.2.9 DNA sequencing

Vector and PCR products were sent to Source BioScience (Department of Biochemistry, University of Oxford) for Sanger sequencing using the Applied Biosystems ABI3730 apparatus (by Thermo Fisher Scientific Inc). Sequences obtained were aligned with the gDNA sequence sourced from MIT Broad Institute (MG8) to ensure no nucleotide changes. To ascertain the quality of the sequencing products, peaks for each nucleotide sequenced was viewed using FinchTv Version 1.4.0 (free software). A single sharp peak with the colour corresponding to a single nucleotide was preferred as opposed to multiple broad peaks.

2.2.2.10 Size Separation by Gel Electrophoresis

Agarose (Sigma-Aldrich) at a percentage of 1% (w/v) was added to 1x TAE buffer and heated to dissolve the agarose. Ethidium bromide was added to the molten agar to a final concentration of 0.5 µg/ml and allowed to set in a gel tray with a comb inserted. The tray with the hardened agar was then placed into a gel tank containing 1XTAE buffer. Sample DNA was pre-mixed with 6x loading dye and loaded into the wells together with an appropriate DNA ladder. A voltage of 80 V was applied for 0.5-1 hour to separate the DNA fragments according to size. The gel was then imaged under UV using the G:Box (SynGene) apparatus and image analysed using the software provided by SynGene, ‘GeneSnap’

CHAPTER 3

Bioinformatics

&

Gene Expression

3.1 Chapter Introduction

The following introduction section will provide an overview regarding fungal phylogeny and current classification system that will be used throughout this work. This is followed by a detailed look at the evolution of the structure and function of the Glycosyl Hydrolase 16 (GH16) family of enzymes and a short description regarding the characteristics of a cell wall protein (CWP) structure. A literature overview concerning current understanding of CWP regulatory mechanism, focusing on the Mitogen Activated Protein Kinase signal transduction together with the various tools used to capture CWP expressions, is also included here.

3.1.1 Fungal Phylogeny & Classification

The Kingdom Fungi is a major group of Eukaryotes (Woese and Fox 1977, Moore 1980). There are about 80 000 named species of fungi, though it is estimated that there could be up to 5.1 million different species (Hawksworth 2001, O'Brien *et al.* 2005, Blackwell 2011). Until recently, fungal classification and evolutionary diversity were solely based on species amenable to growth in cultures, such as the yeasts and filamentous fungi. With the use of environmental DNA analyses, a new, highly diverse clade of fungi named Cryptomycota was discovered, falling into the same clade as *Rozella* (Jones *et al.* 2011). The authors noted that these newly identified, previously un-culturable fungal species now constitute almost half of all fungal species. As a consequence of these technological advancements, there have been several recent revisions of fungal taxonomic classification. Due to this, the version presented by Hibbett *et al.* (2007) and updated accordingly as shown in Figure 3.1 below, is referred to in all seven Chapters of this thesis.

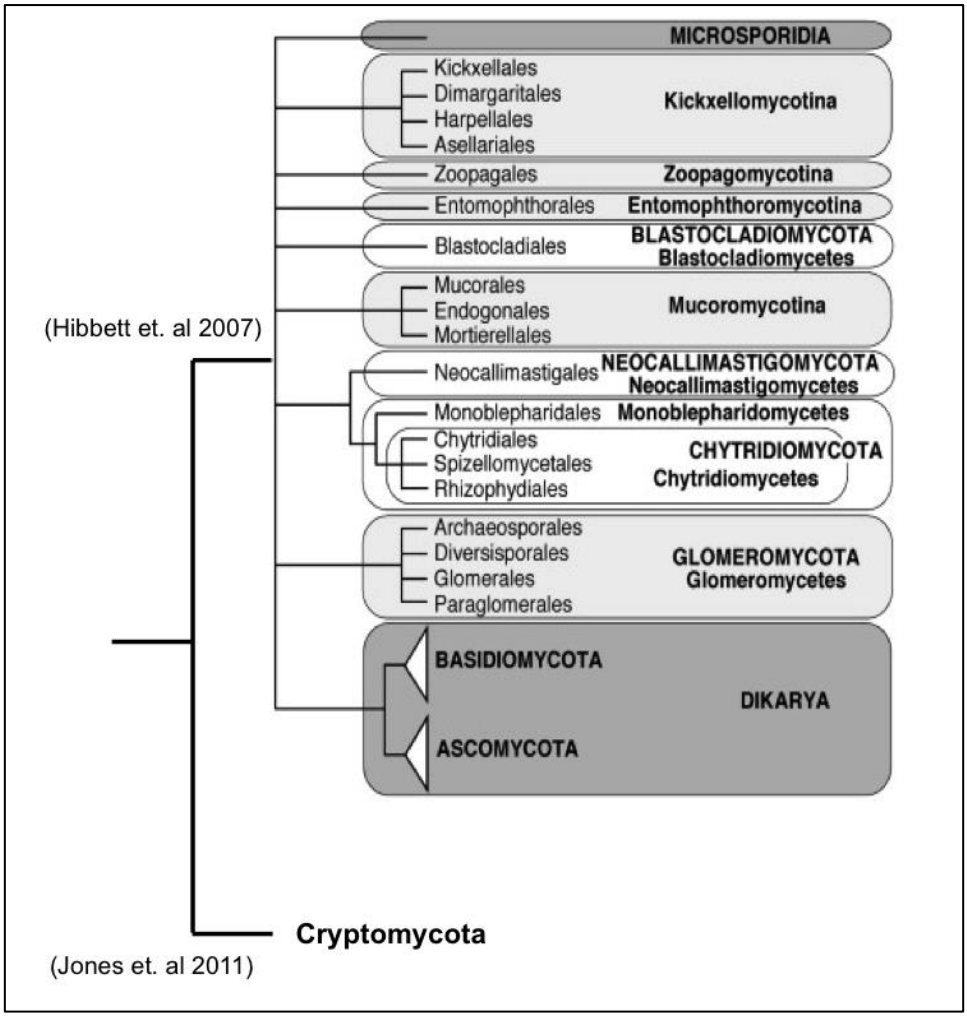

Figure 3.1. The Phylogeny and Classification of the Kingdom Fungi. Note that the branch lengths shown are not proportional to genetic distances. Figure modified from Hibbett *et al.* (2007) with reference to Jones *et a*l. (2011).

The subkingdom Dikarya containing the phyla Basidiomycota and Ascomycota is where the majority of the named fungal species lie. The phylum Ascomycota contained an estimated 100,000 genera and 1,600,000 species (Hawksworth 1991). These ascomycetes are characterised by the production of ascospores in sacs, and can be single-celled (e.g. *Saccharomyces cerevisiae*), dimorphic (eg.*Candida albicans*) or filamentous (*Neurospora crassa*) (Eriksson 2009). It is also here within the Phylum Ascomycota, Class Sordariomycetes, Order Magnaporthales and Family Magnaporthaceae, where the fungal species for this research work, *Magnaporthe oryzae*, belongs.

3.1.2 Glycosyl Hydrolase 16 Family of Enzymes

Enzymes belonging to the superfamily glycosyl hydrolases (GH) catalyse the hydrolysis of glycosidic bonds between carbohydrates or between a carbohydrate and a non-carbohydrate structure. Enzymes categorised as belonging to the GH16 group catalyze the breakage of β-1,3 and/or β-1,4 glycosidic bonds in glucans and galactans (Baumann *et al.* 2007). Glycosyl Hydrolase 16 enzymes have a β-jelly roll 3D structure and share the common ancestor β-glucanase (Barbeyron *et al.* 1998). Over the course of molecular evolution, enzymes within this group diverged, became specialised, and are now mostly Kingdom-specific (Figure 3.2 and Figure 3.3).

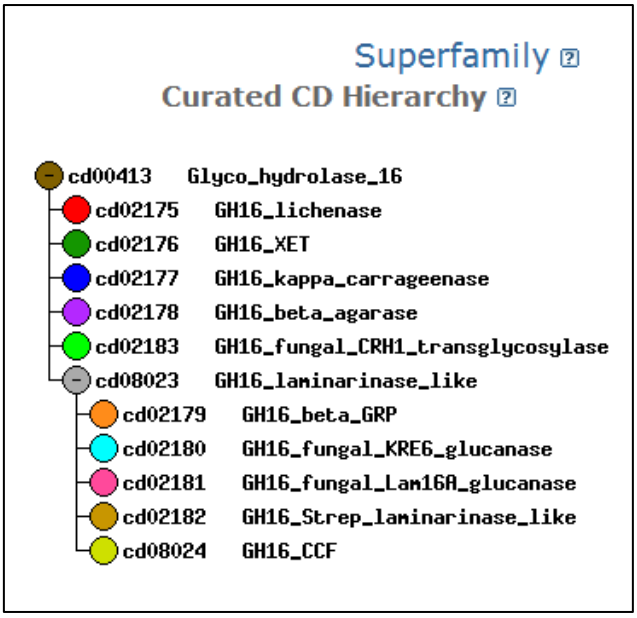

Figure 3.2. List of the Sub-Domains Found in Glycosyl Hydrolase 16 Family of Enzymes. Enzymes belonging to this GH16 family can be identified into six broad groups, with multiple sub-groups on the GH16_laminarinase_like group of GH16 enzymes. Image taken from the NCBI Conserved Domain Database GH16 website (Marchler-Bauer 2011).

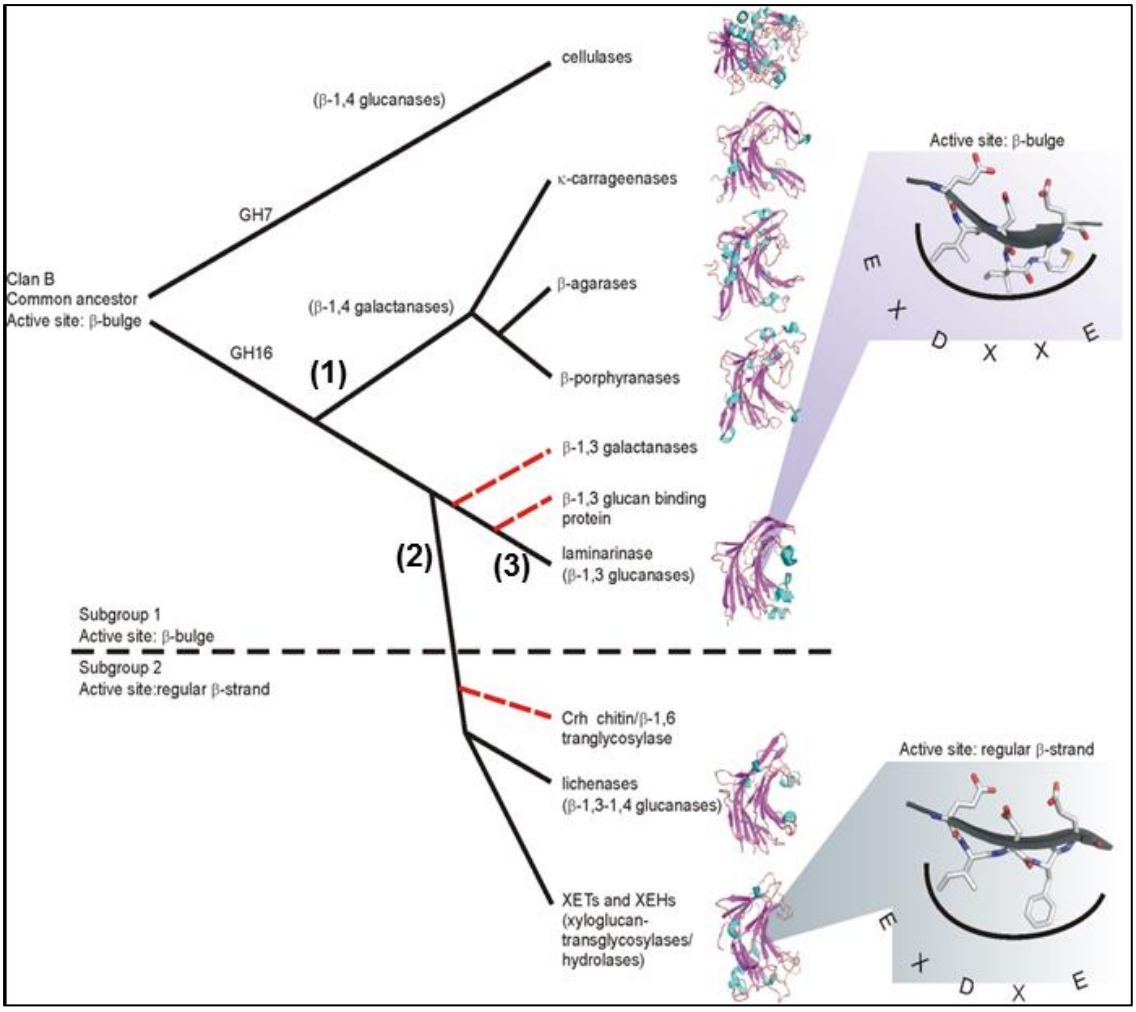

Figure 3.3. An Illustration for the Origins of the Various GH16 Sub-Groups from a Common Ancestor and Protein Structures. Both GH16 and GH7 families share the β-jellyroll fold with the different sub-groups and specificities of GH16 proteins were thought to have evolved from an ancestral β-1,3-glucanase (Barbeyron *et al.* 1998). First, branching **(1)** lead to the evolution of k-carrageenans and β-agarases, followed by a branching event **(2)** leading to lichenases, Crhs and XETs (Michel *et al.* 2001) with the remaining laminarinase-like branch **(3)** as consisting of the β-1,3 galactanases, β-1,3 glucan binding protein and laminarinase. Structural based studies suggest that GH16 active site residues are on one beta-strand with the signature motive EXDXXE (beta-bulge motive) or EXDXE (regular beta-strand). The large occurrence of the beta-bulge motive and similarity to GH7 lead Michel *et al.* to propose that the ancestral enzyme is indeed a beta-bulge with a recent evolve by deletion of one amino acid, into the regular beta-strand common in XETs, Lichenases and Crhs. Red-dotted lines indicate recently added information by a CaZypedia user however the author failed to cite linked publications. Figure taken and edited from CaZypedia (Cantarel *et al.* 2009).

The first GH16 enzymes to branch off and specialise were the agarases, followed by the recent (in evolutionary time) branching of β-(1,3;1,4;1,6) glucanases from the rest of the laminariase-like GH16 enzymes. Strohmeier *et al.* (2004) then showed through protein alignment and phylogenetic analysis, the recent branching of the β-(1,3;1,4;1,6) glucanases forming xyloglucan endotransglucosylase/hydrolase (XET syn. XTH), lichenases and fungal Crh proteins leaving the rest of the GH16 enzymes within the main branch of laminarinases.

The GH16 group of Laminarinase-like enzymes [cdd08023 in Figure 3.2 and branch (3) in figure 3.3] belong to various kingdoms with diverse functions. For example, the GH_16_beta_GRP and closely related group GH16 coelomic cytolytic factor (CCF) are limited to invertebrates and associated with the immune response against pathogens. The three remaining GH16_Laminarinase-like sub domains are fungal- specific. These are enzymes with the GH16_fungal_KRE6_glucanase, GH16_fungal_Lam16A_glucanase and GH16_Strep_laminarinase_like domains. The KRE6 protein was first identified in *S. cerevisiae* and shown to have a crucial role in fungal cell wall β,(1-6)-glucan synthesis (Roemer *et al.* 1994), while Lam16A is important for the hydrolysis of laminarin as a source of carbon in *Phanerochaete chrysosporium* (Vasur *et al.* 2009). There is no refereed literature about the biological role of *Streptomyces* Laminarinase-like proteins in fungi. The only location where this is mentioned is at the National Center for Biotechnology Information (NCBI) Conserved Domain Database GH16 page. Here, it is stated that these are fungal proteins similar to beta-1,3-glucanase and laminarinase found in *Streptomyces sioyaensis*.

Perhaps the most well-studied GH16 group of enzymes are the ones with a regular bulge active site, having recently branched off from the rest of the GH 16 family. This includes the plant-specific xyloglucan endotransglucosylase/hydrolases (XETs cdd02176), fungal Crhp and Lichenases (Figure 3.3 branch 2). Plant XETs are specialised plant enzymes that remodel the synthesised xyloglucan chain, a hemicellulose found in plant cell wall, which forms bonds with cellulose microfibrils (Nishitani 1997, Strohmeier *et al.* 2004). While XETs are plant-specific, the closely-related enzyme "type", Lichenase (GH16 Lichenase cdd00413) is found in bacteria colonizing in the gut of ruminants. These enzymes hydrolyze β-1,3 and β-1,4 glycosidic bonds of lichenin, a polysaccharide found in lichens (Cunningham and Manners 1964). The third sub-group of enzymes in branch 2 of Figure 3.3 is the fungal Congo Red Hypersensitivity (Crhp) family of glycosyl transferases (GSTs).

The fungal specific Crh-like group of proteins has received more attention of late, all sharing the GH16_Fungal_CRH1_Transglycosylase (cdd02183) functional domain. These enzymes are functionally redundant but vary in regulation, with the specific activity of cleaving β-1,4 glycosidic linkages in chitin and transferring the molecule to β-1,3-glucan or β-1,6 glucan polymers (Blanco *et al.* 2015). Due to the specialised role and an external site of reaction, CWPs such as GH16 fungal Crh proteins require unique characteristics to enable efficient functionality in response to a complex network of regulatory mechanisms. This poses a strong platform to justify the potential of using this protein as an anti-fungal target in the war against rice blast disease.

3.1.3 Characteristics of Cell Wall Proteins

Hitherto, more than 30 proteins have been identified as CWPs. Almost all of these CWPs are Glycosylphosphatidylinositol (GPI) anchored except PIRs (Proteins with Internal Repeats) - which are directly covalently bound to β-(1,3) glucan through the proposed O-glycosidic linkage (Kapteyn *et al.* 1999a, Mrša and Tanner 1999, De Groot *et al.* 2005). The GPI anchor is a post-transcriptional modification at the C-terminus of a protein that functions in fixing the protein to the cell membrane or cell wall (Caro *et al.* 1997). This is a crucial feature for post-synthesis cell wall remodelling enzymes such as Glucan elongation protein (Gas1p) and Crhp protein families (Figure 3.4). The GPI anchoring of CWPs enables close proximity to target site of cell wall polymers without leading to external secretion into the environment (Arroyo *et al.* 2007, Latgé 2007). Indeed, the Crhp of *S. cerevisiae* and orthologues in *Aspergillus fumigatus* and *C. albicans* all showed the presence of a GPI-anchor (Rodriguez-Pena *et al.* 2000, Arroyo *et al.* 2007).

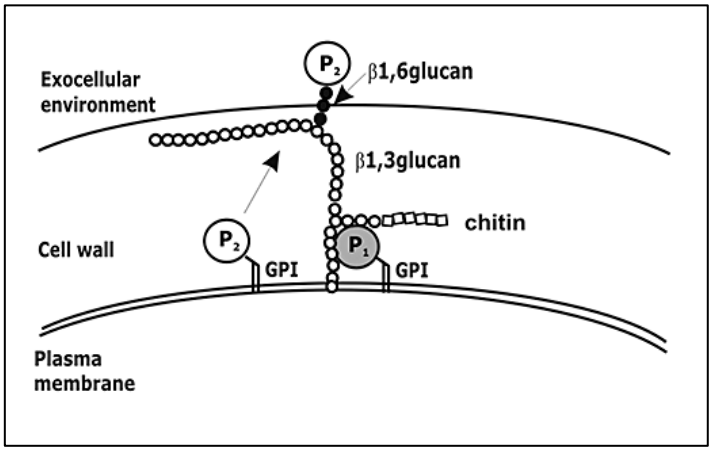

Figure 3.4. Putative Functions of GPI-Anchored Proteins During the Construction of the Fungal Cell Wall. GPI-anchored proteins (P1) that remain attached at the plasma membrane remodel cell wall polysaccharides (examples are Gel/Gas1 or Crh proteins). GPI-anchored proteins (P2) can also become covalently bound to β-(1,3) glucans through β-(1,6) glucans. This is a way for protein P2 to remain at the cell surface to fulfil its biological function, for example, in cell-to-cell interactions. Image and caption were taken from Latgé J.P (2007).

Kapteyn *et al.* (1999b) recorded that GPI-anchored CWPs all carry a distinctive hydrophobic N-terminal signal peptide and Serine/Threonine (Ser/Thr) rich proteins between the functional domain and the C-terminal GPI-anchor site. It has long been known that the N-terminal signal peptide is crucial to channel newly synthesised proteins into the secretory pathway towards the cell membrane (Blobel and Dobberstein 1975). However, the role of the C-terminal Ser/Thr region remained elusive until recently. Boisramé *et al.* (2011) showed that the Serine/Threonine region of GPI anchored IFF (not an acronym) proteins in *C. albicans* play a role in forming disulphide and NaOH bonds to β-(1,3) glucan polymers. It is possible that the Ser/Thr rich region enhances attachment to the cell wall via additional linkages.

3.1.4 Fungal Gene Expression & Regulation

The fungal cell wall is a dynamic structure constantly being remodelled as part of a compensatory response to external stressors as well as part of the cell cycle progression, enabling morphological changes. The plasticity of the cell wall is made possible through the coordination and regulation of CWP expression (Igual *et al.* 1996, Cabib *et al.* 2001, Smits *et al.* 2001b). The expression and regulation of CWPs warrants a full Chapter by itself, however for purposes of this thesis, it has been simplified and described in the following section.

3.1.4.1 CWP Regulation by External Stressors

The external living environment of organisms is unpredictable and hostile. As a result of this, having an efficient detection and response mechanism is crucial for the survival of these organisms. In Eukaryotes, the key mechanism governing external detection and subsequent cellular response are signal

transduction pathways such as mitogen-activated protein kinases (MAPKs) (Alonso 2009). For simplicity, the MAPK pathways can be segmented into three generic sections: cell surface sensory proteins acting as stress sensors, core MAPKs (MAPK, MAPK Kinase, and MAPK Kinase Kinase) that phosphorylate sequentially and finally, specific transcription factors (TF). These TF will, in turn, bind to transcription factor DNA binding sites (TFDBS) in the promoter region and regulate the expression of targeted genes relevant to the type of external stress experienced.

In *S. cerevisiae* where this mechanism is most understood, five MAPK pathways have been characterised. These pathways regulate mating, invasive growth, cell wall integrity (CWI), hyperosmoregulation (Hog1) and ascospore formation (Gustin *et al.* 1998, Zhao *et al.* 2007). These MAPK pathways are found across all Eukaryotes with phylogenetic studies showed high conservation of the three core MAPKs but with high divergence in both upstream sensors and downstream TF regulators (Kültz 1998, Alonso-Monge *et al.* 2009, Nikolaou *et al.* 2009, Rispail *et al.* 2009). It was hypothesised that these divergences reflect the need to accommodate different environmental niche and living conditions. As such, while it is useful to use *S. cerevisiae* MAPK model as a proto-typical MAPK cascade, it is worth bearing in mind the possibility of a varied MAPK signal transduction route or transcriptional response in the fungal phytopathogen, *M. oryzae.*

In *M. oryzae,* three mitogen-activated protein kinases are present, as opposed to five in *S. cerevisiae* (Dean *et al.* 2005). Comparison between the five MAPKs in *S. cerevisiae* and the orthologues in *M. oryzae* is presented in detail in Figure 3.5**.** One of the pathways is the Pmk1 MAPK leading to the activation

Mst12 transcription factor, an orthologue of *S. cerevisiae Kss1* MAPK and Ste12 transcription factor (Hamel *et al.* 2012). Both have been implicated in starvation, filamentation, invasive hyphal growth as well as roles in appressorium development upon sensing the host plant surface through cyclic AMP (Lee and Dean 1993, Xu and Hamer 1996). The other two pathways, the hyperosmotic and cell wall stress response, are described in greater detail below due to their association with regulation of CWPs.

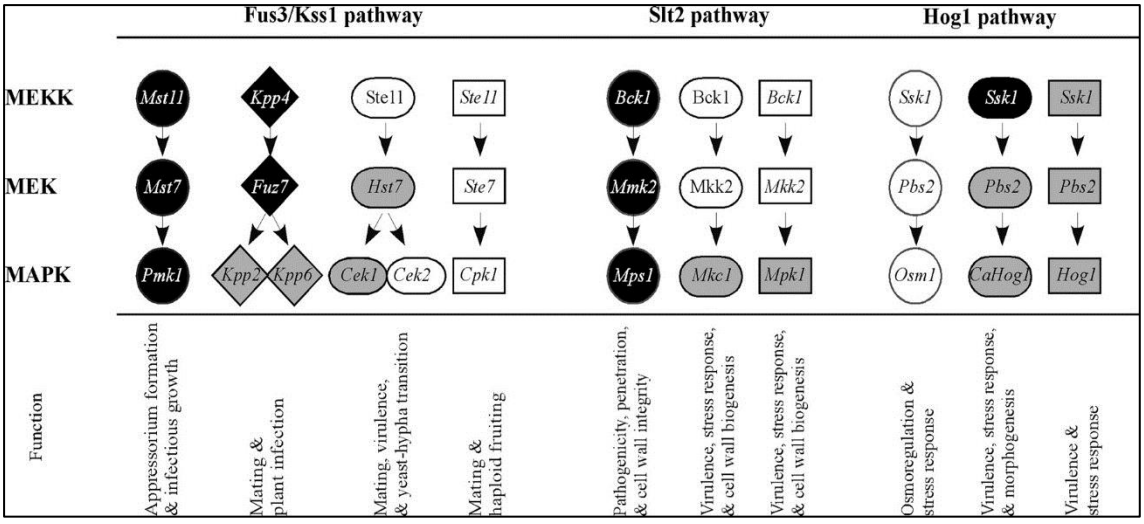

Figure 3.5. MAPK Pathways in Fungal Pathogens. The core components of three MAPK signal pathways in four selected fungal pathogens are in circles for *M. oryzae*, squares for *Ustilago maydis*, ovals for *C. albicans*, and rectangles for *Cryptococcus neoformans*. Components that have been functionally characterised are in italics. The roles of these genes in fungal pathogenesis are shaded in black for essential, grey for important but not essential, and white for dispensable. Figure and caption obtained from Zhao *et al.* (2007).

3.1.4.1.1 Hyperosmotic Stress Pathway

Under conditions of osmotic stress, the High Osmolarity Glycerol (Hog1) MAPK pathway in *S. cerevisiae* is activated (Gustin *et al.* 1998, Hohmann 2002). Sensory proteins (Figure 3.6) detect hyperosmotic stress and start a series of downstream MAPK phosphorylation leading to the regulation of transcription factors Msn2, Msn4, Smp1 and Sko1 targeting specific genes for an osmo-protective response (Krantz *et al.* 2006).

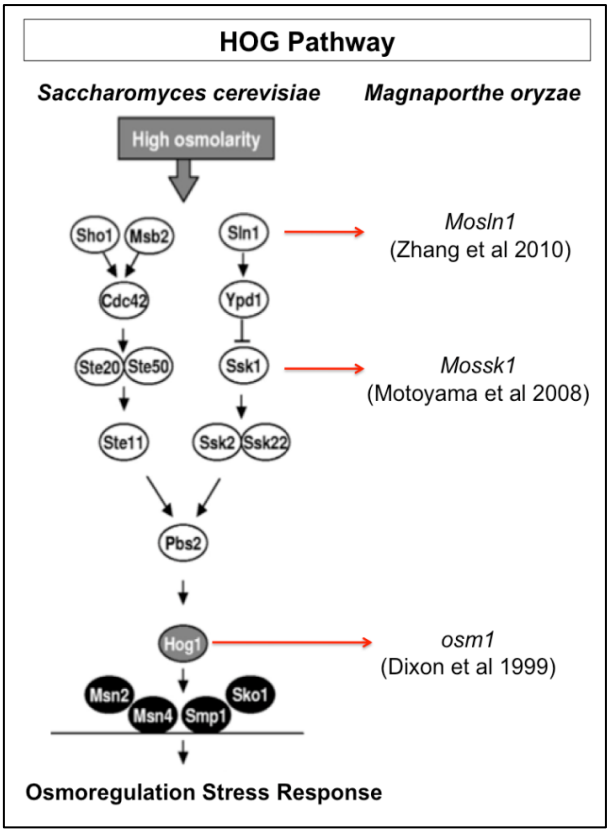

Figure 3.6. High Osmolarity Glycerol (Hog) MAPK Pathway. Shown above the prototypical HOG pathway in *S. cerevisiae* and published orthologues in *M. oryzae*. Figure edited from Zhao *et al.* (2007).

In the plant pathogen *M. oryzae*, the highly conserved Hog1 pathway is important for osmoregulation and components within this pathway were found to be important for virulence (Dixon *et al.* 1999, Motoyama *et al.* 2008, Zhang *et al.* 2010, Zhang *et al.* 2014). The deletion of *MoSln1* (orthologue of *S. cerevisiae Sln1*) (Zhang *et al.* 2010), the downstream response regulator gene *Mossk1* (orthologue of *S. cerevisiae Ssk1*) (Motoyama *et al.* 2008), and *MoMsn2* (orthologue of *S. cerevisiae* Msn2p) (Zhang *et al.* 2014), resulted in hypersensitivity to osmotic, oxidative and cell wall stress. Additionally, all three deletant strains *MoSln1*, *Mossk1* and *MoMsn2* mutants showed significantly ($p<0.01$) reduced virulence when inoculated onto rice cut leaves (cv. CO39 and Nihonbare). By contrast, while the *Osm1* (orthologue of *S. cerevisiae Hog1*) nulled mutant in *M. oryzae* was more sensitive to osmotic stress relative to WT,

mutants were however, fully pathogenic on rice leaves (cv CO39) (Dixon *et al.* 1999).

Currently, there is no knowledge on the regulation and importance of *M. oryzae* cell wall remodelling enzymes, such as *S. cerevisiae* orthologues of *Gas1, Pir* or *Crh-like* genes, against hyperosmotic stress and subsequent effect on pathogenicity.

3.1.4.1.2 Fungal Cell Wall Integrity Pathway

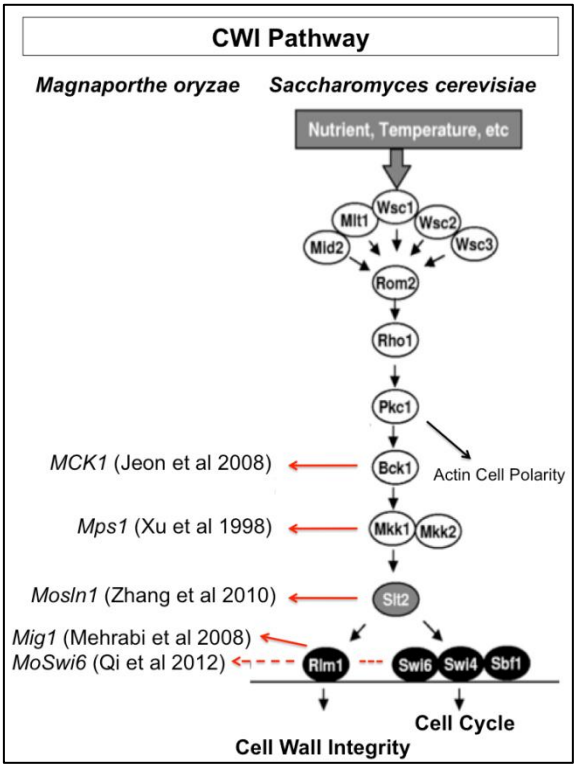

Figure 3.7. Cell Wall Integrity MAPK Pathway. The prototypical CWI pathway in *S. cerevisiae* and published orthologues in *M. oryzae*. Figure edited from Zhao *et al.* (2007)

Due to the importance of the cell wall to fungal survival, stress conditions that compromise the cell wall will lead to the activation of the cell wall integrity pathway (Popolo *et al.* 2001, Levin 2005). These external stress conditions include hypo-osmotic shock, heat shock as well as cell wall perturbants such as Congo Red (Ketela *et al.* 1999, de Nobel *et al.* 2000). The CWI pathway is best understood in the model yeast *S. cerevisiae* (Figure 3.7). Here, stress sensing

proteins Mid2 and Wsc1 (Verna *et al.* 1997, Ketela *et al.* 1999) detect cell wall damage and lead to a series of downstream phosphorylation of MAPKs. The phosphorylated protein kinase Slt2 will, in turn, activate the two cell wall integrity transcription factors: Rlm1 (MADS-box transcription factor) (Watanabe *et al.* 1997) and a heterodimeric SBF Complex comprising Swi4 and Swi6 (Baetz *et al.* 2001).

Stressed or weakened CWP mutants also constitutively activate the CWI pathway. For example, the CWI pathway was shown to be constitutively activated in the mutants ***fks1Δ*** and ***gas1Δ*** in *S. cerevisiae* (de Groot *et al.* 2001b, Lagorce *et al.* 2003). It is understood that these CWP mutants experienced stressed cell wall, whereby the activation of the CWI pathway leads to a compensatory mechanism by an upregulation of other CWPs (Garcia *et al.* 2004). This is noted through changes to total chitin content of the cell wall as well as changes to the branching of the chitin-glucan meshwork leading to adjustments in cell wall elasticity.

Through MAPK Slt2, the MADS-box transcription factor Rlm1 activates a specific group of CWPs. In a DNA microarray transcriptional study (Garcia *et al.* 2004), *S. cerevisiae* cells were grown under cell wall stress (30 µg/ml of Congo Red) and the expression of 6,306 open reading frames (ORFs) were measured from 0 hour to 6 hour post exposure to Congo Red relative to untreated controls. A total of 132 genes were induced and, according to the YPD/SGD classification, the main functional group of some 34 up-regulated genes belongs to the cell wall synthesis, organisation, and metabolism, including the GPI-anchored *Crh1* gene, (up-regulated by three fold). The authors showed that the expression of *Crh1* in the background mutant strains *slt2* and *rlm1* exposed to Congo Red did not

change (Garcia *et al.* 2004), implicating the role of Slt2p and specifically, Rlm1p in Crh1 regulation in yeast under cell wall stress.

The second *Slt2*-activated transcription factor is the SBF (Swi4p/Swi6p) dimeric complex, a cell-cycle regulator involved in the activation of genes at the end of G_1 phase (Koch *et al.* 1993, Breeden 2003). In a Chromatin immuno-precipitation (ChIP) experiment, phosphorylated Mpk1p of the CWI pathway formed a complex with Swi4 (Kim *et al.* 2008) and subsequently, the trimeric Mpk1-Swi4-Swi6 through Swi4. This trimeric complex was shown to bind to a seven-nucleotide sequence on the promoter region of genes, with Swi6 recruiting RNA Pol II, resulting in the transcription of targeted genes (Kim and Levin 2011). Recent work suggests that the SBF complex regulates gene expression through the CWI pathway (Kim *et al.* 2008, Truman *et al.* 2009, Kim and Levin 2011, Levin 2011). The yeast glucan synthases *Fks1* and *Fks2* are examples of CWPs regulated by the SBF complex. In *Swi4* deletant mutants, the expression of a *Fks1* promoter (-712 to -82 upstream) *lacZ* reporter construct was found to be four-fold lower than in WT (Igual *et al.* 1996).

The relationship between the CWI pathway and virulence in the rice blast fungus has provoked much interest. The *Mps1* (orthologue of *Slt2* in *S. cerevisiae*) (Xu *et al.* 1998), *Mck1* (orthologue of *Bck1* in *S. cerevisiae*) (Jeon *et al.* 2008) and *Mig1* (orthologue of *Rlm1* in *S. cerevisiae*) (Mehrabi *et al.* 2008) deletion mutants are all non-pathogenic with deletion mutants *Mps1* and *Mck1* showing increased sensitivity to cell wall digesting enzymes. The MoSwi6p transcription factor was shown to interact with MoMps1p in a yeast two-hybrid assay and is required for germling morphogenesis, hyphal growth, and pathogenicity (Qi *et al.* 2012). Furthermore, *MoSwi6* deletant strains were

hypersensitive to sodium dodecyl sulphate (SDS), hydrolysing enzymes, Calcofluor White and sorbitol (osmotic stress) (Qi *et al.* 2012).

These studies suggest that the regulation of cell wall in response to external cues is not only important for fitness and survival, but also for virulence. The co-occurrence of a compromised cell wall along with non-virulence is not surprising as the CWI pathway has been shown to play an important role in pathogen resistance against oxidative stress exerted by the host as described in the next section.

Oxidative Stress Regulatory Response

Oxidative stress due to exposure to UV, aerobic conditions, host-derived reactive oxygen species (ROS) or hydrogen peroxide (H_2O_2) all compromise a fungus' first line of defence: the cell wall (Fuchs and Mylonakis 2009). As a result of this, the compensatory reaction lies in a complex network of cross-talks between MAPK pathways such as the activation of the Sln1p-Ssk1p branch of the Hog1 pathway (Singh 2000, Alonso-Monge *et al.* 2003, Arana *et al.* 2005) and downstream Rom2 CWI pathway (Navarro-García *et al.* 2005, Vilella *et al.* 2005). In *S. cerevisiae*, CWI sensors Mid2 and Wsc1 are not required for Rom2 activation of the CWI pathway in cells exposed to H_2O_2, suggesting an alternative sensory mechanism possibly via Hog1 sensory proteins. Similarly, Mkc1of the Cell Wall Integrity pathway (orthologue of *Slt2* in *S. cerevisiae*) in *C. albicans* (Navarro-García *et al.* 2005) is also activated under oxidative stress, and is dependent on *Pbs2* and *Hog1*, pointing again to cross-talk with other MAPK pathways (Arana *et al.* 2005).

Four transcription factors have been shown to be crucial in response and regulation of genes against oxidative stress in *S. cerevisiae* and *Candida glabrata*. These are Skn7, Yap1 and Msn2 and Msn4 and TFs from the HOG pathway (Kuge and Jones 1994, Martinez-Pastor *et al.* 1996, Morgan *et al.* 1997, Cuéllar-Cruz *et al.* 2008). Due to the phytopathogen nature of *M. oryzae*, it is expected that exposure to high levels of oxidative stress mean that most CWPs are directly or indirectly regulated by the aforementioned transcription factors, and are worth noting during CWP prediction and characterization. The orthologue of *Yap1* in *M. oryzae*, *MoAp1* was shown to be highly expressed in conidia and invasive hyphae by up to twelve-fold higher compared with vegetative mycelium in a qRT-PCR assay (Guo *et al.* 2011). Additionally, *MoAp1* deletant strains were sensitive to H_2O_2 (2.5 mM), leading to 19% less growth compared with WT. Guo *et al.* (2011) also found that the CWP *MoChs2* predicted to contain the *MoAP1* binding region in the promoter, was up-regulated in *MoAp1* deletant strains. More importantly, the deletant strain *MoSwi6*, an orthologue of *S. cerevisiae Swi6*, was hypersensitive to oxidative stress in as low as two mM H_2O_2 (Qi *et al.* 2012). The MoSwi6p was also shown, in a yeast two-hybrid assay, to interact with MoMps1p (orthologue of *S. cerevisiae* Slt2p) in the same study. Given that these *in vitro* studies directly linked oxidative stress resistance in *M. oryzae* to the MAPK cell wall integrity pathway and regulation of cell wall biosynthesis, it is worth exploring further the regulation of *M. oryzae* cell wall remodelling proteins such as the *Crh-like* genes under oxidative stress and the importance of these genes in conferring added resistance against plant ROS.

No studies have yet investigated the importance of cell wall remodelling genes in oxidative resistance and regulatory response mechanisms under

oxidative stress. An *M. oryzae* transcriptomic approach showed that the group of genes most up-regulated under oxidative stress was those associated with nutrient starvation (Mathioni *et al.* 2011). However, it can be argued that transcriptomic technology such as the microarray analyses used by Mathioni *et al.* (2011) may not be able to capture small yet significant fold changes, which are characteristic of the CWP expression profile, due to the lack of sensitivity of these technologies (see section 3.1.4.3). Utilising the highly sensitive qRT-PCR tool to measure the expression profile of *M. oryzae Crh-like* genes under oxidative stress could provide a glimpse towards using CWPs as potential antifungal targets. A compromised cell wall could increase the sensitivity of the pathogen against host ROS and confer the crop enhanced resistance against rice blast disease.

3.1.4.2 CWP Regulation by Cell Cycle Progression

The remodelling of the cell wall is not only important as a compensatory reaction to external environmental stressors, but also to enable the fungi to progress through various morphological changes (Smits *et al.* 2001b). In *S. cerevisiae, Crh-like* genes showed differential cell-cycle regulation, with *Crr1* expression up three-fold (Northern Blot) at the G_2/M stage of the cell cycle. Contrary, *Crh1* showed a peak in the early G_1 phase of unbudded yeast cells and another peak at the later stage of G_2 with large buds in cells while *Crh2* expression remained constant throughout the cycle (Rodriguez-Pena *et al.* 2000). The SBF complex (Swi4/swi6) has been shown to play a key role in the cell-cycle regulation of these CWPs through the activation of Rho1p (Madden *et al.* 1997, Eriksson *et al.* 2011). This points to the importance of the CWI pathway in regulating CWP via a complex interplay with other regulatory components.

In the context of the fungal phytopathogen *M. oryzae*, this is especially crucial in germling morphological changes. The germling morphological changes require precise control of CWP expression according to internal cues. Despite this, little is known regarding the dynamics of *M. oryzae* cell wall remodelling and CWP regulation across the life cycle. A study conducted by Fujikawa *et al.* (2009) gave insightful findings. Here, the authors used fluorophore-labelled antibodies and showed that the cell wall of an *M. oryzae* infective hyphae at 48 hpi *in-planta* was remodelled to contain an outer layer of 'mask' made of α-1,3-glucan, thereby preventing the host from detecting the presence of fungal chitin or β-1,3-glucan. This is supported by the significant ($p<0.001$) up-regulation of *MgAgs1,* an α-1,3-glucan synthase, at 48 hpi ($p<0.001$) relative to 24 hpi. In contrast, the expression of β-1,3-glucan synthase gene, *MgFks1* was significantly lowered ($p<0.001$) at 48 hpi relative to 24 hpi. The study further showed that the expression of *MgAgs1* is regulated by *Mps1* MAP Kinase in the cell wall integrity pathway. *Magnaporthe oryzae* deletion mutant *Mps1* mutant failed to form infectious hyphae, α-1,3-glucan was not detected on germlings and consistent with this, the expression of *MgAgs1* was suppressed during germling formation (Fujikawa *et al.* 2009). These findings opened a promising door towards the study of cell wall remodelling in *M. oryzae* and given the importance of *Crh-like* genes in other fungal species, warrants an interest in the regulation of this gene in *M. oryzae* genome across various stages of the life cycle as well as under various external conditions.

3.1.4.3 **Measuring Expression of CWPs**

Capturing the expression profile of candidate *Crh-like* genes in *M. oryzae* is the second step in characterizing *M. oryzae Crh-like* genes (orthologues of *Crh1* and *Utr2* in *S. cerevisiae*) after phylogenetic work. However, there are

several experimental challenges including small fold changes and small quantities of pathogen RNA in a background of host RNA (often <0.1%), emphasizing the need for a highly sensitive measuring technique. Fold changes in gene expression of CWPs are often small but biologically important. For example in yeast, the temporal expression of *Crh1* increases only two-fold upon entering the budding phase of the life-cycle, while under cell wall stress (Congo Red, Calcofluor White or Zymolyase), the expression increases by only two to four-fold relative to control conditions (Boorsma *et al.* 2004, Garcia *et al.* 2004). Despite the small fold change, yeast *Crh* mutants exhibit hypersensitivity to these cell wall perturbing compounds as well as altered cell surface plasticity (Dague *et al.* 2010).

A multitude of publications attest to the usefulness of both individual and genome-wide gene expression studies in *M. oryzae.* However, whilst large-scale transcript analyses with microarrays and /or High Throughput-SuperSAGE have captured gross fold-changes over several thousand genes (Kawahara *et al.* 2012, Park *et al.* 2013), such analyses are not sensitive enough to detect small changes in low abundance genes. Moreover, they are overly challenging or, indeed, impossible to perform with minute samples of tissue-specific RNA. Quantitative Real-Time PCR (qRT-PCR) provides a low throughput (*ie* a restricted number of genes) but highly sensitive technique (Broad Institute , Bustin 2002). Indeed, it has been shown to be 5-fold more sensitive than microarray data (Czechowski *et al.* 2004).

The expression of a gene of interest generated by qRT-PCR is essentially calculated as a relative value. The gene of interest (GOI) expression in a treated/target tissue sample is measured as a relative against the internal

reference gene in the same tissue and then compared to the GOI ratio in a control tissue sample. Due to this, any technical errors could result in inaccurate expression values. Thus to obtain reliable data, qRT-PCR requires stringent preparation strategies (Gutierrez *et al.* 2008, Bustin *et al.* 2009, Guenin *et al.* 2009). Justifiably, given the sensitivity of the qRT-PCR, this technique was deemed most suitable for measuring *M. oryzae Crh-like* gene expression and as such, the stringent preparations were meticulously adhered to.

3.1.5 Introduction Summary

Based on the literature reviewed above, it is hypothesised that putative *Crh-like* genes would have the conserved GH16_fungal_CRH1_transglycosylase (cd02183) domain belonging to the Glycosyl Hydrolase 16 family. These putative proteins would also be GPI-anchored, contain a Ser/Thr rich region as well as the signal peptide cleavage site. Furthermore, promoter analysis would reveal similar regulatory mechanism as most CWPs.The putative *M. oryzae Crh-like* genes would show a regulatory response when exposed to cell wall, osmotic and oxidative stress. Given the importance of the cell wall during infection, it is hypothesised that *M. oryzae Crh-like* genes may exhibit a regulatory pattern during infection.

3.2 Aims & Objectives

The objective of Chapter 3 is to generate bioinformatic data and gene expression profile to better characterise the *Crh-like* genes in *M. oryzae* and to use the results to assist in choosing candidate *Crh-like* genes for subsequent generation of deletant strains (Chapter 4). This is achieved by performing several aims as described below.

3.2.1 Bioinformatics Section

1. To reliably predict *S. cerevisiae Crh*-like gene orthologues in *M. oryzae* using mutlple toos: reciprocal BLASTp search, prediction of various CWP characteristic structures and transcription factor DNA binding site prediction were included.

2. Generation of GH 16 and *Crh-like* gene phylogenetic tree construction to provide visual distribution of putative *Crh*-like *M*. *oryzae* genes against other orthologous genes of various species and between the different GH 16 sub-domains.

3.2.2 Gene Expression Analyses

3.2.2.1 Reference Gene Selection for qRT-PCR

1. To identify and validate stably expressed internal reference genes under various growth conditions

3.2.2.2 Gene Expression of Genes of Interest (GOI)

1. To capture the expression pattern of *M. oryzae Crh*-like genes identified in section 3.3.1 in the bioinformatics section, under various types of tissue samples.

3.3 Materials & Methods

3.3.1 Bioinformatic Work

3.3.1.1 *Saccharomyces cerevisiae Crh1, Utr2 & Crr1* Orthologues

Three *Crh-like* genes *Utr2, Crh1* and *Crr1* were first identified in the model yeast *S. cerevisiae* (Rodriguez-Pena *et al.* 2000). As a result of this, the protein sequence from each of these genes was obtained from the *Saccharomyces* Genome Database (www.yeastgenome.org) (Cherry *et al.* 2011). The

corresponding orthologue for each gene in *M. oryzae* was obtained from "*Magnaporthe comparative* Sequencing Project", Broad Institute of Harvard and MIT" (Broad Institute) using the BLASTp search tool (Altschul *et al.* 1990). Here, the yeast *Crh1, Utr2* and *Crr1* protein sequences was queried against proteins predicted to be encoded by the *M. oryzae* 70-15 (MG8) sequenced genome. The best hit gene and successive gene hits were recorded with a cut-off value of e^{-10}. A reciprocal BLASTp (Altschul *et al.* 1990) was then conducted for the *M oryzae* best hit gene against *S. cerevisiae* genome in the NCBI database (www.ncbi.nlm.nih.gov).

The putative orthologues of yeast *Crh1, Utr2* and *Crr1* was also searched in other fungal species. The Saccharomycotina sub-phylum, including two closely-related yeast species *Saccharomyces mikatae* and *Saccharomyces paradoxus* were included, as well as *Candida glabrata* and *Kluyveromyces lactis*. Also included were several pathogenic species such as plant pathogens *Fusarium graminaeurum* and *U. maydis* as well as human pathogens *A. fumigatus and C. albicans*. Finally, the well-studied model organism *Aspergillus nidulans* and *N. crassa,* a closely related species to *M. oryzae,* were also included. Sources of the amino acid sequences used for this chapter are described in results section. These putative orthologues were obtained using the freely-available online tool 'Fungal Orthogroup Repository' (Broad Institute 2009) or by querying the three *S. cerevisiae Crh-like* genes against BLASTp tool provided in these webpages: Candida Genome Database (CGD) (Inglis *et al.* 2012) (www.candidagenome.org), Pombase (Wood *et al.* 2011) (www.pombase.org), Broad Fungal Genome Initiative (www.broadinstitute.org) (Broad Institute 2015), Genolevures (Sherman *et al.* 2009) (http://www.genolevures.org/) and

*Aspergill*us Genome Database (AspGD) (Cerqueira *et al.* 2013) (www.aspergillusgenome.org). Protein BLASTp search (Altschul *et al*. 1997) results greater than e-value of e^{-10} were discarded. Remaining genetic data were obtained from the NCBI Conserved Domain Database Search (http://www.ncbi.nlm.nih.gov/Structure/cdd/cdd.shtml), Cazypedia (www.cazypedia.org) and Carbohydrate-Active enZYmes Database (www.cazy.org) as listed in Table 3.1 in the results section.

3.3.1.2 Transcription Factor DNA Binding Site Prediction

Seven upstream nucleotide promoter sequences (1000 bp upstream from translation START codon) from *S. cerevisiae Crh1, Utr2* and the orthologues in *M. oryzae Crh-like* genes predicted above were subjected to transcription factor DNA binding site (TFDBS) prediction. This was achieved using the MatInspector (Quandt K *et al.* 1995, Cartharius *et al.* 2005) online-based tool by Genomatix. The tool locates matches between available matrix library and the seven queried FASTA sequences for TFDBS prediction. Results were given a score using the matrix similarity algorithm that takes into account similarity of both the core conserved region and less conversed regions of the matrix, relative to the queried sequence. A matrix of '1' is when the candidate sequence matches 100% to each nucleotide in the matrix. Mismatches in the core region decreases the matrix similarity score more than mismatches in less conserved regions. According to the manufacturer's recommendation (Genomatix), a matrix similarity of >0.8 is usually a "good" match but not as an absolute cut-off value. Results for TFDBS prediction for key MAPK transcription factors were tabulated with a cut-off value of 0.75.

3.3.1.3 Modular Structures of *Crh-like* Genes in *M. oryzae*

Five putative *M. oryzae Crh-like* genes were queried for the presence of conserved functional domains. For comparison purposes, the corresponding orthologues in *S. cerevisiae* and the dimorphic fungus *C. albicans* were added because domain architecture is publicly available for these genes (Rodriguez-Pena *et al.* 2000, Pardini *et al.* 2006, Blanco *et al.* 2014). The closely-related species to *M. oryzae*, the filamentous fungus *N. crassa* was also studied to see if any similarity/differences observed could be associated with genetic similarity. This sums to a total of 15 amino acid sequences sourced from various databases as described above and in results section. Each sequence was queried in NCBI BLASTp (Altschul *et al.* 1990) and the predicted conserved domains noted along with the Conserved Domain Database (cdd) identity number (Marchler-Bauer *et al.* 2012).

3.3.1.4 Signal Peptide Cleavage Site Prediction

The freely available online tool Signal IP 4.1 Server (Petersen *et al.* 2011) was used to predict the signal peptide cleavage site (www.cbs.dtu.dk/services/SignalP). In the webpage, 15 amino acid sequences were uploaded in FASTA format using the default settings and generated results recorded.

3.3.1.5 GPI-Anchor Prediction

Two GPI predictive programs were selected based on the recommendation by Sernova V. P (2006). These were GPI-SOM (Fankhauser and Mäser 2005) and BIG-PI Fungal Predictor (Eisenhaber *et al.* 2004), both freely available at gpi.unibe.ch and mendel.imp.ac.at/gpi/fungi_server.html respectively. All 15

FASTA amino acid sequences were queried against both programs and results compared.

3.3.1.6 Phylogenetic Tree Description

A total of 63 amino acid sequences belonging to the GH 16 family were used in this analysis. These sequences were taken from thirteen fungal species, three bacteria, 2 plants and 2 invertebrates. Forty five of these amino acid sequences belong to the fungal-specific GH16_fungal_CRH1_transglycosylase (cd02183) domain. Twelve amino acid sequences belonged to other GH16 known subdomains, obtained from the NCBI Conserved Domain Database (Marchler-Bauer *et al.* 2012) GH16 subdomain sequences. Five *M. oryzae* GH16 genes with unspecified GH16 subdomains were also added, sourced from the Broad Institute's '*Magnaporthe comparative* Sequencing Project' (Broad Institute) database of genes categorised by PFAM domain.

All sequences obtained from above were aligned using the MAFFT Version 7.0 Multiple Alignment Program (mafft.cbrc.jp/alignment/server) designed by Katoh *et al.*(2013). BLOSUM62 and L-INS-I (Katoh *et al.* 2005) were used as the scoring matrix and protein alignment respectively. The MAFFT Version 7.0 aligned data was exported into FASTA format and Phylip 3.2. The latter was used as a query against ProtTest software to select for the best-fit model of protein evolution (Abascal *et al.* 2005). The MAFFT version 7.0 aligned protein in FASTA format was uploaded into MEGA 6.0 (Tamura *et al.* 2013). Further deletion of gaps and un-aligned sections at both N and C-terminal ends were conducted manually. Using the MEGA 6.0 software, a Maximum Likelihood tree was constructed using the ProtTest-recommended protein evolution model, with 500 bootstrap values and rooted to a GH7 sequence. To check for tree robust-ness, Neighbour-Joining

(NJ) and Maximum Likelihood (ML) trees were constructed using the same parameters (500 Bootstrap and rooted) but with different protein evolution models.

3.3.2 Gene Expression Analyses

3.3.2.1 Fungal Strains & Growth Conditions

The Rice blast fungus *Magnaporthe oryzae* (*M. grisea* (T.T. Herbert) M.E. Barr) wild type strain Guy11 (WT) were used as routine culture growth on complete medium (CM) as described in Chapter 2 (Section 2.2.1.1).

3.3.2.2 Tissue Preparation for RNA Extraction

3.3.2.2.1 Mycelial Tissue Grown Under Various Stressors

Routine fungal growth in liquid media was performed as described in Chapter 2 (Section 2.2.1.5), with the various stressors added as described in the next paragraph. Harvested mycelium (0.1 g) was stored at -80°C until ready for RNA extraction. The process was repeated to gather three biological replicates for each condition assayed.

For control vegetative growth under optimal conditions, the WT strain was cultured in Complete Medium (CM). The starvation condition (MM) was achieved by replacing CM with Minimal Medium (MM), and for extreme starvation, glucose was omitted from the standard Minimal Medium preparation (MM-glucose). For cell wall stress, the cell wall perturbant Congo Red was filter-sterilised and added to liquid CM buffered with 50 mM HEPES (pH 7.0) at a concentration of 100 µg/ml. Stress by caffeine was induced by adding 2.5 mM filter-sterilised caffeine to liquid CM (pH 6.5). To achieve osmotic stress, 1 M Sorbitol was added to liquid CM (pH 6.5) prior to autoclaving. For oxidative stress, 2.5 mM of filter sterilised H_2O_2 (30% w/v) was added to each 2 day-old culture grown in liquid CM, prepared as above.

3.3.2.2.2 Dormant Spores

Magnaporthe oryzae strain Guy11 spores were harvested as described in Chapter 2 (Section 2.2.1.2), with 25 plates per biological replicate (three biological replicates harvested separately). Once centrifuged, the supernatant was removed and the pellet containing spores from 25 CM plates was snap frozen in liquid nitrogen and stored at -80°C until ready for RNA extraction.

3.3.2.2.3 Germling Tissues

Barley seeds (*Hordeum vulgare* L.) cv. Golden Promise were grown in a 50:50 (w/w) mixture of Erin Multipurpose Compost and John Innes No. 2 soil-based compost, for 7 days at 25°C, 12/12 light, 70% humidity. Seven-day-old barley leaves were cut and placed onto 1.5% (w/v) water agar and inoculated with harvested spores (6-7 x 10^{6} spores/ml) and re-suspended in 0.4% (w/v) gelatine. The inoculation procedure: for each time point, used 2.5 ml spore suspension sprayed uniformly onto 24 leaves, which were then covered to maintain high humidity and incubated at 25°C for 2, 8, 12, 24 or 48 hours post inoculation. The hours post inoculations (hpi) correspond to the various infective stages: 2 hpi (germ tube emergence), 8 hpi (immature appressorium), 12 hpi (mature appressorium), 24 hpi (penetration and early invasive growth) and 48 hpi (*in planta* growth). Prior to harvest, one leaf was selected, at random, and its surface viewed by light microscopy to monitor germling development and formation of appressoria. Approximately 0.1 g of leaf material was then snap frozen in liquid nitrogen and stored at -80°C until ready for RNA extraction. The process was repeated, harvesting three biological replicates. Control samples (BL) containing only 0.2% gelatine sprayed onto barley leaves was also prepared.

3.3.2.2.4 Perithecia

Perithecia were produced by crossing WT strain Guy 11 with the opposite mating type strain TH3; CM agar plug inoculum of the 2 strains was placed 4 cm apart on oatmeal agar at 10% (w/v) and incubated under constant fluorescent light at 18°C for 29 days. Perithecia were then harvested using a dissecting microscope and 0.1 g was snap-frozen in liquid nitrogen stored at -80°C prior to RNA extraction. Three biological replicates were harvested independently.

3.3.2.3 RNA Extraction, Quantity & Quality Test

Details of RNA extraction and determination of RNA quality and quantity as described in Chapter 2 (section 2.2.2.3).

3.3.2.4 Complementary DNA (cDNA) Preparation

Preparation of fourty two cDNA samples from a total of fourty two RNA samples (fourteen sample types, each with three biological replicates) were prepared as described in Chapter 2 (Section 2.2.2.4).

3.3.2.5 Primer Design, Specificity & Efficiency

Candidate reference genes were selected on the basis of being (a) previously used in *M. oryzae* gene expression studies (Chen *et al.* 2008, Oh *et al.* 2008, Haiyan *et al.* 2012), and (b) from several essential functional groups (protein translation, glycolysis pathway, cytoskeleton). These genes were then cross-checked with the publicly available COGEME high throughput-superSAGE transcript profile *M. oryzae* database (Soanes *et al.* 2012), for an estimation of stability. Ratios were calculated using the given base mean values between samples of the same growth stage (example: CM against MM, or 4 hpi against 16 hpi). Genes with a ratio of less than 10 were selected for further analysis.

Sequences for the respective genes were obtained from the 8th annotation (MG8) *Magnaporthe oryzae* strain 70-15 sequenced by Broad Institute (Broad Institute). Primer pairs were synthesised by Sigma-Aldrich and designed according to the following specifications: annealing Tm 60ºC (±2ºC); G-C content 50-60%; no non-specific product amplification; no primer-dimer or secondary structures; amplicon of 60-100 bp; primer efficiency 80-110%, r^2 value 0.98-0.99; either Forward or Reverse primer to span exon/exon boundary (transcript-specific). Primer specificity: primers were deemed acceptable if the targeted gene showed an e-value less of than 10^{-3} in NCBI Blast search. In addition, primer pairs were shown to be pathogen-specific by conducting qRT-PCR using only host barley leaf cDNA as a negative control (BL). Primers were tested for non-specific product/s by amplicon separation on gel electrophoresis using 2% (w/v) Agarose Gel (Sigma-Aldrich) and 10-300 bp GeneRuler Ultra Low Range DNA Ladder (Thermo Scientific).

Complementary DNA (cDNA) from all samples was pooled, diluted 5-fold and used as templates. Each primer pair was amplified using the five-fold cDNA serial dilution and cycle threshold (ct) values were analysed as follows: the primer efficiency (E) was calculated from the four point slope of the plotted dilution row, using the formula $E=5^{\wedge(1/S)}$ whereby S is the slope of the regression line. Primer pairs with slope $r^2<0.99$, $E<1.8$ or dissociation curve and gel electrophoresis runs showing non-specific product/s, were rejected and re-designed, prior to gene stability analysis. Quality control: samples with technical replicates showing more than 0.8 difference, non-template and host-only control (CTRL BL) with ct values less than 35, were rejected. Once the appropriate set of reference genes were

selected, the same quality control process as above was repeated for primer design involving genes of interest.

3.3.2.6 Quantitative Real Time PCR (qRT-PCR)

Real time PCR was conducted using the ABI 7300 apparatus (Applied Biosystems) as described in Chapter 2 (Section 2.2.2.1).

3.3.2.7 Cycle Threshold Criteria

The qRT-PCR technology is an extremely sensitive assay, being able to amplify the most minute amount of template and often due to this, it is impossible to achieve complete absence of contamination during routine qRT-PCR reactions. While subject to heated debate, it is emphasised that the decision to determine a cutting line between an acceptable sample amplification, an amplification due to contamination and a negligible amplification in qRT-PCR reactions varies between assays and is based on recommendations by Bustin & Nolan (2004). In this work, if there is amplification in the non-template control (NTC) but it is 10 cycles higher than the corresponding reaction with the template, the minute contamination in NTC is considered negligible. Additionally, when run together, genes giving ct values similar to housekeeping genes (below 20) can be considered to be highly expressed, while those giving readable amplification above 25 cycles are considered lowly expressed.

3.3.2.8 Evaluation of Reference Gene Expression Stability

Analysis of raw ct data for candidate reference genes was performed using ‘qBase+ Basic’ licensed software (Biogazelle). The most stably expressed genes for each tissue type (infective, vegetative and global) was identified. This means that measuring the expression of genes from tissues derived from the asexual

infective cycle or from the asexual vegetative cycle will have their own recommended “best set” of normalizing reference genes. In addition, this work included the most stably expressed genes to use if samples originated from a mix of both asexual and sexual life cycle i.e a global expression profile analyses.

For the analysis of most stable genes, each tissue group (Infective, Vegetative and Global) was analysed separately. The Infective Group included tissues from dormant spores (0 hpi) as the control sample, together with germ tube (2 hpi), immature appressoria (8 hpi), mature appressoria (12 hpi), penetration peg and infective hyphae (24 hpi), and *in planta* growth (48 hpi). The Vegetative Group included fungal mycelia harvested from various environmental stresses such as starvation (MM+glucose), extreme starvation (MM-glucose), osmotic stress (Sorbitol), cell wall stress (Congo Red), caffeine stress and control samples grown under optimal condition (CM). The Global Group included a mixture of the above: dormant spores, immature appressoria, CM, MM+glucose and also included of Perithecia (sexual reproductive stage).

For each group (Infective, Vegetative or Global), raw ct values were converted to relative expression values using the Pfaffl Method (Pfaffl 2001). An inter-run calibration was performed to correct for run-to-run variation (Hellemans *et al.* 2007). The GeNorm algorithm (Vandesompele *et al.* 2002) in ‘qBase+ Basic’ licence software version 2.5 (Biogazelle) was used to calculate the average expression stability score (M) for each reference gene, and the pairwise variability score (V) for sequential normalisation factors, resulting from stepwise inclusion of additional reference genes. Expression stability values were used to identify the most stably-expressed reference genes at each stage, whilst pairwise

variability scores were used to determine the most appropriate number of reference genes to use as the normalisation factor.

3.3.2.9 Data Analysis – Expression Profile of *Crh-like* Genes

3.3.2.9.1 Preliminary Analysis

An initial investigation to look at the raw expression of these candidate genes was conducted. This was done to give a general impression of the relative amount of cDNA between five candidate *M. oryzae* genes. Raw ct values from each gene, amplified from the same pool of WT cDNA vegetative mycelium and on the same qRT-PCR plate, was averaged (two technical replicates per sample per gene), standard deviation calculated and data tabulated.

3.3.2.9.2 Gene Expression Analysis

The expression patterns during infection of three genes, *MGG_Utr2, MGG_Crh1* and *MGG_Crh2* in WT were measured using qRT-PCR. Tissues analysed included dormant spores (0 hpi) as the control sample, germ tube stage germlings (2 hpi), immature appressorium stage (8 hpi), mature appressorium stage (12 hpi), mature appressorium and penetration peg (24 hpi) and invasive *in planta* growth (48 hpi).

The expression profile of these three *Crh-like* genes were also captured when grown vegetatively under various stressors, including cell wall stress by Congo Red (100 µg/ml), caffeine stress (2.5 mM), osmotic stress by Sorbitol (1 M), starvation (MM+glucose), extreme starvation (MM-glucose) and oxidative stress (H_2O_2) with vegetative samples grown under optimal conditions (CM) used as the control sample.

Additionally, *MGG_Crh2* expression was also compared across the fungal life cycle. In this assay, samples were taken from across the fungal life-cycle, including appressorium formation (8 hpi), *in planta* growth (48 hpi), sexual stage (Perithecia), vegetative growth under nutrient rich (CM), in starvation (MM+glucose) and with dormant spores (0 hpi) as the control sample.

Two technical replicates were used per reaction. When possible, the plate design carried all three biological replicates for target and control sample respectively, on the same plate; and, for each sample analysed, the gene of interest and two validated reference genes were deposited onto the same plate. For expression analysis involving more than 1x 96-well plate, comparison of samples across different plates were achieved by incorporating inter-run calibration (IRC) wells for each gene, on the same well number within each 96-well plate. The generated ct values for samples from multiple runs were imported into MxPro QPCR Software or 'qBase-Plus Basic Version 2.5' for IRC calibration (Hellemans *et al.* 2007) . The calibrated values from multiple runs and raw cycle threshold values from one well, were exported into a Microsoft Excel file and analysed separately according to the recommendations by Wilhelms et al (Willems *et al.* 2008) with the use of Pfall's equation (2001), log transformation, mean centring and autoscaling for subsequent statistical analysis at 95% Confidence Interval.

3.4 Results & Discussion

3.4.1 Bioinformatic Analyses

3.4.1.1 *Saccharomyces cerevisiae Crh1, Utr2 & Crr1* Orthologues

All three *S. cerevisiae Crh-like* genes (*Utr2, Crh1* and *Crr1*) were queried using the Broad Institute Magnaporthe Comparative Project (Broad Institute) BLASTp tool against the *M. oryzae* genome (Taxid: 242507). Best hit results for each gene were then BLASTp back against *S. cerevisiae* (taxid: 4932). Note that for this work, a putative homologue is when BLASTp search of query gene (*S. cerevisiae Crh-like* genes) against genome of other fungal species, gives hits with an e-value lower than $1x10^{-4}$. A pair of orthologous genes is when BLASTp of one gene gives the other gene as the best hit, and *vice versa*.

The reciprocal BLASTp search revealed no *S. cerevisiae Crr1* orthologue in *M. oryzae*, a single copy of *S. cerevisiae Utr2* orthologue designated *MGG_Utr2* and four *M. oryzae* orthologoues of *S. cerevisiae Crh1* (designated *MGG_Crh1* to *MGG_Crh4*). Lower hits revealed a combination of these genes as well as other un-identified GH16 *M. oryzae* genes. The best hit gene, as well as other hits are shown in detail in Appendix A.1. To confidently identify these genes belonging to the *Crh-like* gene family, subsequent promoter, GPI anchor prediction, modular structures as well as phylogenetic analysis were conducted.

3.4.1.2 Transcription Factor DNA Binding Site Prediction

A total of seven *Crh-like* homologous genes from *S. cerevisiae* and *M. oryzae* were analysed for transcription factor DNA binding site prediction by submitting 1000 bp upstream of each gene into Matinspector (Quandt K *et al.* 1995, Cartharius *et al.* 2005), an online-based tool (www.genomatix.de).

Results from the Matinspector analysis generated a total of 120 transcription factor DNA binding site matrices for all seven genes queried. For each gene, the prediction tool provided a list of results. However for the purpose of this work, data in Table 3.1 showed results relevant to cell wall protein regulation. Complete list of matrices, description of each matrix and the conserved sequence, can be found in Appendix A.2 and A.3. Matrix similarity is an algorithm that measures similarity of the matrix sequence in the library relative to the queried sequence. Therefore a cut-off value with a low matrix will result in false-positives while a cut-off of 1 would result in missing real homologues matrices in other fungal species. A cut-off value at 0.75 was deemed most appropriate for this work as recommended by Cartharius *et al.* (2005).

Table 3.1. Matinspector Transcription Factor DNA Binding Site Prediction. Two *S. cerevisiae Crh-like* genes *Crh1* and *Utr2* and the orthologues in *M. oryzae* were queried against the Matinspector database of matrix sequences for transcription factor DNA binding site prediction in the promoter region of each gene.

Gene	Matrix ID (Transcription Factor) *motif*		
	RLM1.01 (Rlm1) *TCTA*	**SWI4.01 (Swi4) *CGAA***	**MSN2.01 (Msn2) *GGGG***
SC_Crh1	2	2	0
MGG_Crh1	0	1	1
MGG_Crh2	1	0	4
MGG_Crh3	2	2	1
MGG_Crh4	0	1	4
SC_Utr2	1	2	2
MGG_Utr2	0	1	5

*Only matrices with a matrix similarity result above 0.75 are listed

All seven *Crh-like* genes showed the presence of transcription factor DNA binding sites related to the regulatory mechanism shared by genes responding to cell wall stress (Garcia *et al.* 2004), such as Rlm1p, SBF (Swi4p/Swi6/) and Msn2p/Msn4p (Table 3.1). Using a DNA binding motif program RSAT (Van Helden 2003), Garcia *et al.* (2004) investigated 800 bp upstream of genes up-regulated under cell wall stress and concluded that the highest occurrence of transcription factor (TF), shared by most genes, included Rlm1p, SBF (Swi4p/Swi6p), Msn2p/Msn4p and Crz1p among others. This suggests that a complex inter-regulatory mechanism involving other MAPK pathways is expected in a cell wall compensatory mechanism and justifies the need to examine the expression of *M. oryzae Crh-like* genes under various conditions, particularly when under cell wall, oxidative and osmotic stress as this could provide more information regarding the function of these genes.

In *S. cerevisiae,* both *Crh1* and *Utr2* have the transcription factor DNA binding site for cell wall integrity regulation: Rlm1 and SBF complex (Swi4/Swi6). However, in *M. oryzae*, in exception to *MGG_Crh3*, all other genes have either one of the MAPK cell wall integrity TF DNA binding motifs. For example, *MGG_Crh2* only has one predicted Rlm1 DNA binding motif. The Rlm1p transcription factor of the cell wall integrity pathway (Figure 3.7) has been shown to be associated with cell wall stress response caused by Congo Red (Garcia *et al.* 2004). On the contrary, *MGG_Utr2* did not have Rlm1 but contains the DNA binding motif for Swi4, which has been associated with cell-cycle regulation and caffeine stress (Madden *et al.* 1997, Truman *et al.* 2009). This begins to suggest that *Crh-like* homologues in *M. oryzae* may be differentially regulated and warrants further experimental confirmation. It is also worth pointing out that the prediction results showed that *M. oryzae* genes seem to have an increase in motifs or matrixes matrix related to oxidative and osmotic stress, particularly Msn2p and Yap1p.

Results from this analysis suggest that further experimental analyses are worthwhile to shed further light into the regulatory mechanism of these genes. Specifically, given the list of matrices found in the promoter region, changes in expression when the fungus is exposed to osmotic, oxidative as well as cell wall stress caused by Congo Red and caffeine is worth exploring further as later described in section 3.4.2 of this chapter.

3.4.1.3 Modular Structures of Crh-like Proteins

According to the NCBI Conserved Domain Database (cdd), the three *Crh*-like genes *Crh1, Utr2/Crh2* and *Crr1* from *S. cerevisiae* share one functional domain belonging to the Glycosyl Hydrolase 16 (GH16) family of carbohydrate active enzymes with the signature motif EXDXE (Rodriguez-Pena *et al.* 2000, Marchler-Bauer 2011). Specifically, these are the GH16_Fungal_CRH1_Transglycosylase GH16 sub-domain (cd02183) (Marchler-Bauer 2011). In addition to the GH16 domain, both *Utr2* and *Crr1* contain a chitin binding domain 1 (cd06923) at the N-terminus after the signal peptide sequence (Figure 3.8). Consistently, it was discovered during NCBI BLASTp and protein alignment that all other orthologues of *S. cerevisiae Utr2* and *Crr1* have the characteristic chitin binding domain 1 (cd06923). According to the NCBI Conserved Domain Database, chitin binding domain 1 co-occurs with GH 16 enzymes. It is possible that these domains confer an additional function related to improving the catalytic efficiency of the enzyme (Boraston *et al.* 2004, Hashimoto 2006). Recent work by Blanco *et al.* (2015) confirmed this hypothesis by generating strains with mutations at the amino acid G49 located within the chitin binding domain and showed that there was a reduction in the transglycosylase activity (hydrolysis of chitin chain and subsequent transfer to a glucan acceptor). Additionally, they conducted a protein modelling analysis and predicted that cysteines 33, 39 and 40 within the chitin binding domain form disulphide bridges and as such, are probably important for protein folding and stability.

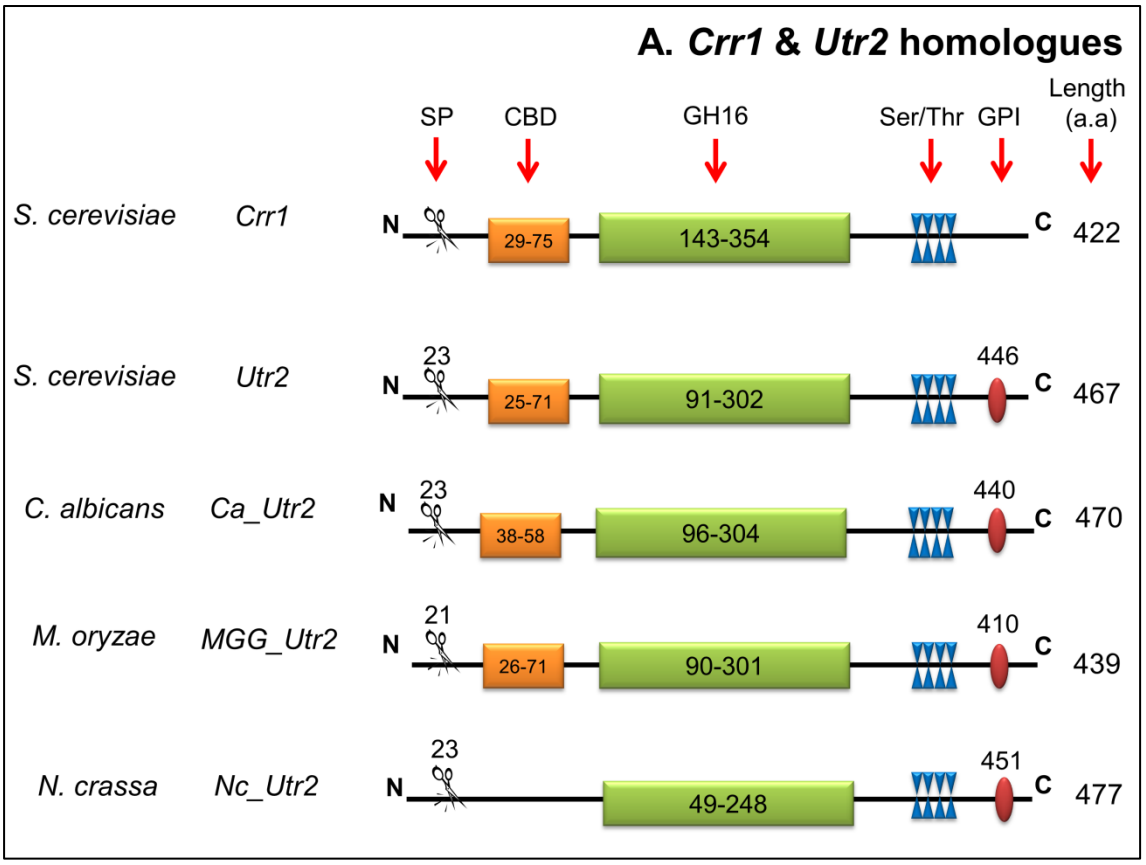
A. Crr1 & Utr2 homologues
SP
CBD
GH16
Ser/Thr
GPI
Length (a.a)
S. cerevisiae
Crr1
N
29-75
143-354
C
422
S. cerevisiae
Utr2
23
25-71
91-302
446
467
C. albicans
Ca_Utr2
23
38-58
96-304
440
470
M. oryzae
MGG_Utr2
21
26-71
90-301
410
439
N. crassa
Nc_Utr2
23
49-248
451
477

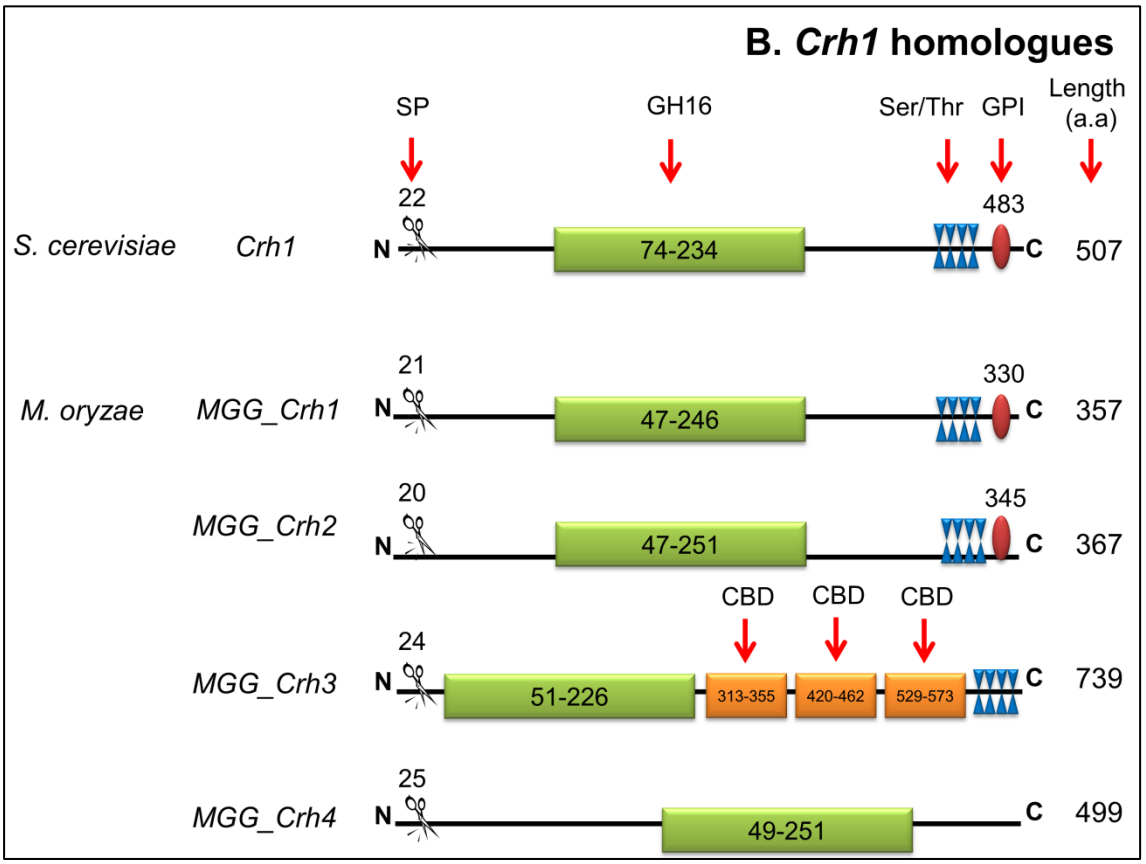
B. Crh1 homologues
SP
GH16
Ser/Thr
GPI
Length (a.a)
S. cerevisiae
Crh1
22
74-234
483
507
M. oryzae
MGG_Crh1
21
47-246
330
357
MGG_Crh2
20
47-251
345
367
CBD
CBD
CBD
MGG_Crh3
24
51-226
313-355
420-462
529-573
739
MGG_Crh4
25
49-251
499

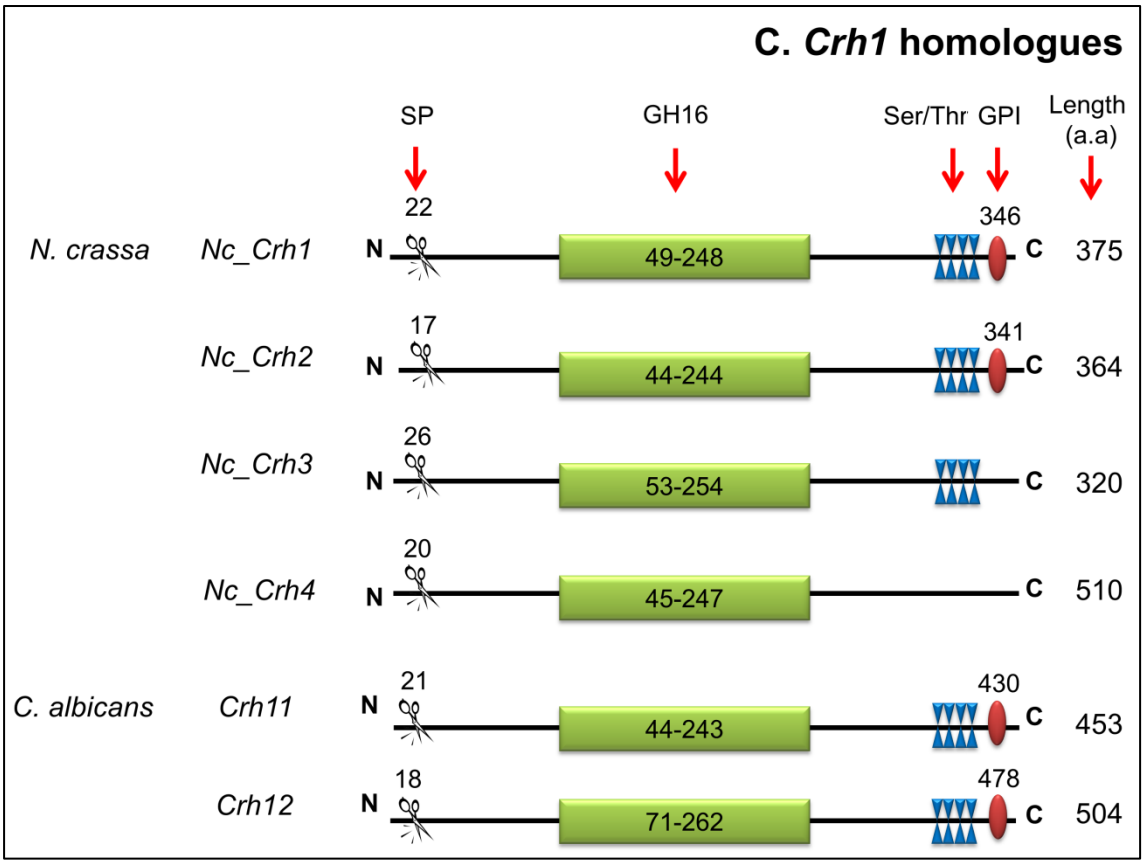

Figure 3.8. Modular Structure of *Crh-like* Genes in Four Fungal Species. Panel A *S. cerevisiae* Crr1p and Utr2p with the corresponding orthologues in *C. albicans, M. oryzae,* and *N. crassa*. **Panel B** *S. cerevisiae* Crh1p and four orthologues in *M. oryzae*. **Panel C** The orthologues of *S. cerevisiae* Crh1p in *C. albicans* and *N. crassa*. The signal peptide cleavage site (SP) was predicted using the Fungal big-PI Prediction Software (Eisenhaber *et al.* 2004).Chitin Binding Domain (CBD) and Glycosyl Hydrolase 16 Domain (GH16) were predicted using the Conserved Domain Database at NCBI (Marchler-Bauer 2011). Serine/Threonine (Ser/Thr) rich region was observed during visual inspection of protein alignment in MEGA 5.0 while the GPI-anchor site above was predicted using bigPI (Eisenhaber *et al.* 2004).

3.4.1.4 GPI-Anchor Prediction

A total of 16 amino acid sequences were queried against both GPI prediction softwares GPI-SOM (Fankhauser and Mäser 2005) and big-PI (Eisenhaber *et al.* 2004). Both tools were consistent in detecting the presence or absence of a GPI anchor. However, there were discrepancies in the specific location of the predicted GPI anchor site (Appendix A.4). To experimentally determine and validate the location of the predicted GPI anchor is beyond the scope of this study and as such, while the presence/absence of GPI can be confidently accepted, the precise location must be treated with caution for future work involving GPI-anchors.

Both prediction programs showed that the homologues of *S. cerevisiae Utr2* genes were all GPI-anchored. As expected, the *S. cerevisiae Crr1* gene is not GPI-anchored, consistent with the observation noted by Gómez-Esquer *et al.*(2004). On the contrary, not all homologues of the *S. cerevisiae Crh1* genes were predicted to be GPI-anchored. Out of four *M. oryzae* genes homologous to *S. cerevisiae Crh1*, only *MGG_00918* (syn *MGG_*Crh1) and *MGG_00592* (syn *MGG_Crh2*) have predicted GPI-anchors. Similarly for the closely related species *N. crassa,* only *Nc_Crh1* and *Nc_Crh2* are GPI-anchored. This result should be taken into consideration when selecting *M. oryzae* genes for further studies. This is because GPI-anchoring plays a crucial role in the activity of CWPs as it ensures the enzymes remain close to the cell wall, as opposed to being excreted externally (Klis *et al.* 2009). It is especially true if the orthologue (in this case *S. cerevisiae Crh1*) is GPI-anchored. Therefore, *M. oryzae* GPI-anchored *MGG_Crh1* and *MGG_Crh2* should be a likely candidate to be a functional CWP.

3.4.1.5 Maximum Likelihood GH16 Phylogenetic Tree

The objective of a GH16 phylogenetic tree construction is two-fold. Firstly, it is to visualise the distribution of five putative *Crh-like Magnaporthe oryzae* genes against other *Crh-like* genes from various fungal species. Secondly, to explore further the putative identity of five other *M. oryzae* GH16 genes to ensure that no *M. oryzae* GH16 were identified with the wrong sub-domain. This is because there are other fungal GH16 enzymes that break β-glucan chains but without the transglycosylase activity such as those found in Kre6p and Lam16p group of proteins (Chesters and Bull 1963, Roemer *et al.* 1994, Vasur *et al.* 2009).

A total of 63 amino acid sequences belonging to the GH 16 family were used in this analysis (Appendix A.5). Sequences were taken from thirteen fungal species, three bacteria, two plants and two invertebrates. Seventy-one percent of the sequences belong to the fungal-specific GH16_fungal_CRH1_transglycosylase (cd02183) domain. These homologous *Crh-like* genes were carefully chosen to include yeasts, dimorphic fungi, and filamentous fungi (plant pathogenic/non-pathogenic). Also, GH16 proteins with other functions and known to belong to other sub-domains were included, such as bacterial Laminarinases, plant XETs, and agarase. Since the phylogenetic distribution of these proteins are known (Barbeyron *et al.* 1998, Michel *et al.* 2001, Strohmeier *et al.* 2004), it was used as a positive control in determining the identity of five GH16 *M. oryzae* of unknown sub-domain (*MGG_02573, MGG_09861, MGG_09733, MGG_00374, and MGG_13777*).

Additional strategies were further employed to ensure the tree constructed is robust and reliable. Firstly a decision was made to use *A. nidulans* GH7 gene sequence as an outgroup, thereby forming a rooted tree with evolutionary information as opposed to only providing genetic distances. Evolutionary studies showed that GH7 and GH16 shared the same β-jellyroll fold and that both evolved from the same ancestor, β-1,3-glucanase (Barbeyron *et al.* 1998). Secondly, multiple protein models (JTT, WAG, LG) were used when constructing Neighbour Joining (NJ) and Maximum likelihood (ML) trees, at 500 bootstrap values. A very robust tree should have identical or highly similar gene groupings/clades across different models and types of trees constructed. This was the observation, and a representative tree is presented (Figure 3.9).

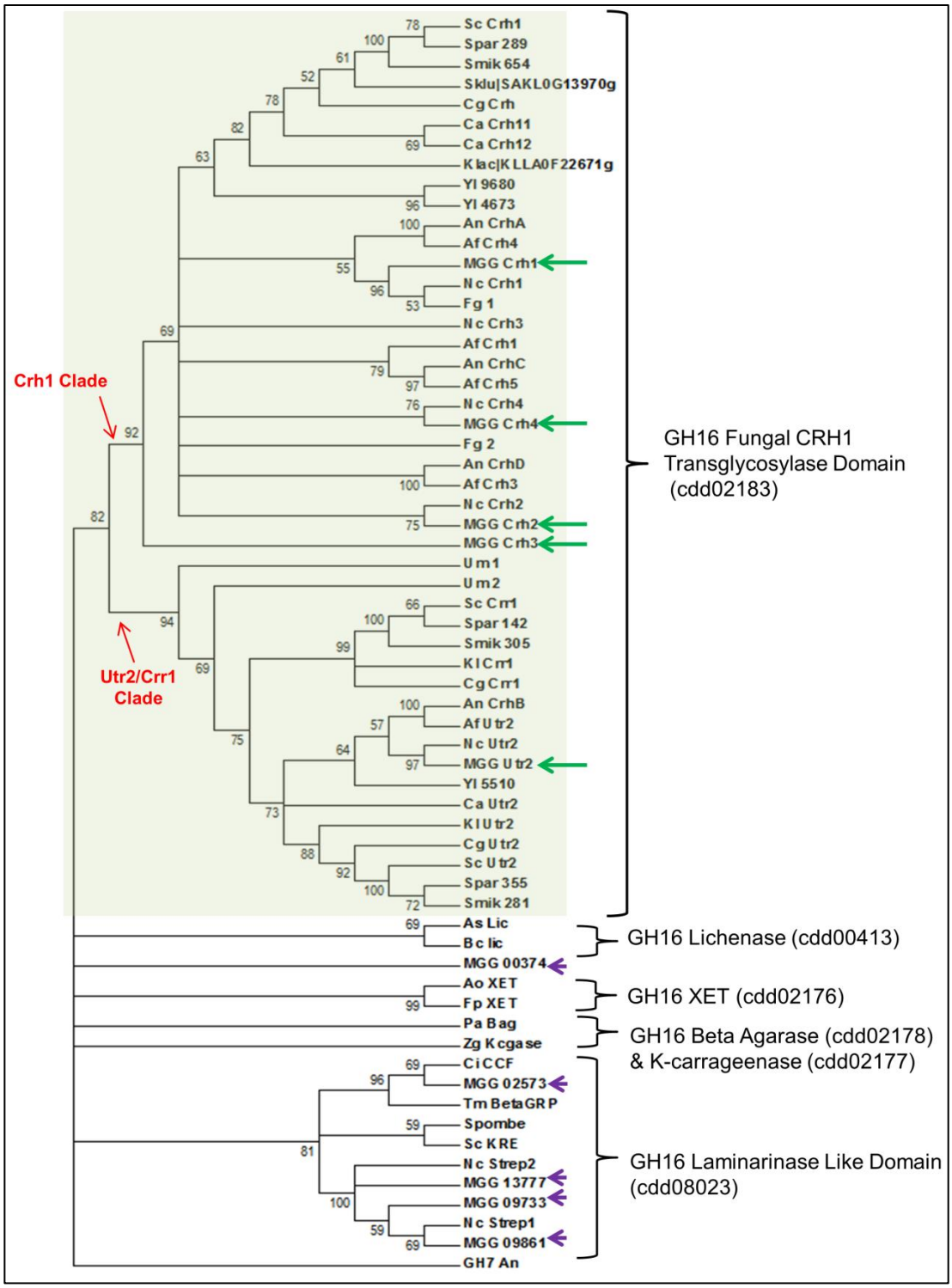

Figure 3.9. Glycosyl Hydrolase 16 Maximum Likelihood Phylogenetic Tree. The tree was build using the LG+F model of amino acid substitution, 500 bootstrap rooted at GH7_An. Tree is a consensus at 50% of 500 bootstrap, and constructed using the MEGA 7.0 Windows 7 Program (Tamura *et al.* 2013). Green arrows show the location of putative *M. oryzae Crh-like* genes clusters, purple arrows show the location of other previously un-identified GH16 *M. oryzae* genes and light green shading indicate the clade containing enzymes with the GH16_fungal_CRH1_transglycosylase domain.

The rooted phylogenetic tree construction from 63 amino acid sequences provided useful information regarding the GH16 family. All trees generated consistent branching pattern albeit variations in bootstrap values (data not shown). The phylogenetic tree shown in Figure 3.9 is a representative tree of maximum likelihood with the best bootstrap values. Shown in Figure 3.9, five *M. oryzae* genes clustered with other *Crh1/Utr2* homologues (green arrows), four GH16 *M. oryzae* genes of unknown sub-domain belonged to the GH16_Laminarinase-like sub-domain (purple arrows) with the sub-domain of one gene, *MGG_00374* remain undetermined.

Despite the independent construction of this phylogenetic tree, it closely resembles an unrooted maximum likelihood phylogenetic tree constructed by Strohmeier *et al.* (2004). The work by Strohmeier *et al.* used 260 proteins from the GH 16 family and subjected these proteins to sequence alignment, phylogenetic analysis and substrate specificity. The authors divided these GH 16 enzymes into three subfamilies, with GH16a containing all the agarases and laminarinase-like enzymes, GH16b for the XETs, Lichenases and Crhs and GH16c for non-attributable proteins. The phylogenetic tree generated in this chapter (Figure 3.9**)** showed two general separations between the GH16a and GH16b groups, which is consistent with the work of Strohmeier *et al.* (2004). Unfortunately, while the phylogenetic distribution of GH16a and GH16b is consistent with high bootstrap values, the branching pattern within GH16b (XETs, Lichenases and Crhs) proved problematic for this study.

There are observed inconsistent branching patterns for XET and Lichenase across all phylogenetic trees developed in this work with low bootstrap values. For every tree generated, the *M. oryzae* gene *MGG_00374* clustered to either XET or Lichenase genes, but never within the GH16 *Crh-like* branch. This is an unexpected outcome and further future work is needed to determine the true identity and function of this gene which seems to be more closely related to plant and bacterial GH16 than presently found fungal GH16 enzymes. The author proceeded to compare these data against other sources (Barbeyron *et al.* 1998, Strohmeier *et al.* 2004) and similarly, there are inconsistencies with the higher branching pattern splitting XET, Crh-like and Lichenase in the phylogenetic trees constructed. The evolutionary and branch position of Crh against XET and Lichenase is still debatable and requires more in-depth evolutionary studies.

3.4.1.6 Crh1 Clade and Crr1/Utr2 Clade

The representative phylogenetic tree (Figure 3.9) showed one main branch specific to *Crh-like* genes with two clades, Crh1 Clade and Utr2/Crr1 Clade each with high bootstrap values (>90). All four *M. oryzae Crh-like* genes orthologous to *S. cerevisiae Crh1* belonged to the Crh1 Clade but does not cluster together (Figure 3.9 green arrows). A maximum likelihood analyses was repeated (Figure 3.10) using only the 45 homologous *Crh-like* sequences, with the GH 7 enzyme as an outgroup.

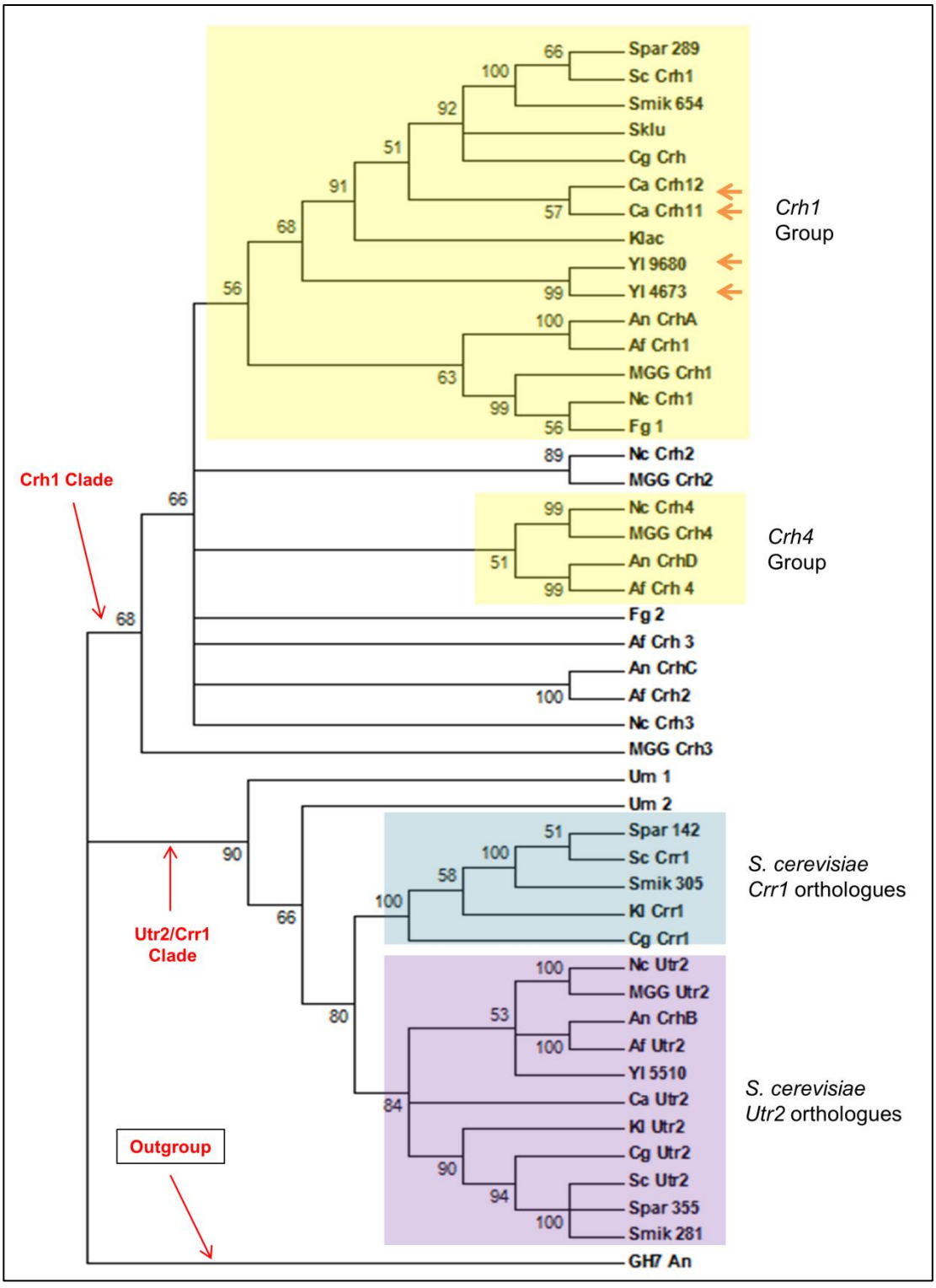

Figure 3.10. Maximum Likelihood *Crh-like* Phylogenetic Tree. The analysis above was constructed omitting sequences from other sub-domains, rooted to a GH7 protein, at 500 bootstrap and using LG protein evolution model. Orange arrows show the location of gene duplication in *C. albicans* and *Yarrowia lipolytica*. The yellow squares highlight clustering of *Crh* genes into distinct grouping of Crh1-group and Crh4-group.

Branching patterns of the phylogenetic trees constructed in Figure 3.9 were consistent with *Crh-like* genes separated into the two clades as in Figure 3.10. Careful inspection of Crh1 Clade in Figure 3.10 reveals a pattern reflective of the fungal Ascomycota Phylum, whereby species belonging to the Pezizomycota sub-phylum such as yeasts (*S. cerevisiae*) and the dimorphic fungi *C. albicans* are clustered together**.** As expected, *M. oryzae* genes (*MGG_Crh1* to *MGG_Crh4*) were clustered with genes from *N. crassa*, a closely related but non-phytopathogenic fungus. Similarly, *A. fumigatus* genes clustered closest to the non-pathogenic fungus *A. nidulans* due to genetic similarity. This suggests that *Crh* gene duplication occurred before speciation of both species. Contrary to the pattern seen in filamentous fungi, gene duplication seen in *C. albicans* and *Y. lipolytica* would have been recent and occurred after speciation, as both genes were found to be clustered within the same species.

Copies of homologous *Crh-like* genes from each species do not cluster together. On the contrary, these genes can be seen to cluster within a distinct group, the most obvious is *Crh*1 group and to a lesser extent, the *Crh4* group (Figure 3.10). It was discovered that at least one copy of a *Crh*-like gene from each species, falls into the same cluster with *S. cerevisiae Crh1,* supporting the finding that each gene was indeed the best hit gene when *S. cerevisiae Crh1* sequence was queried (BLASTp) against the respective fungal genomes. As such, genes within the *Crh1* group are the original orthologue of *Crh1*, while other genes may be the paralogues as a result of gene duplication seeming to occur only in filamentous fungi. This suggests that *MGG_Crh1*, clustered with *S. cerevisiae Crh1*, warrants further downstream experimental investigations.

The occurrence of *Crh-like* gene expansion in the filamentous group is not an isolated observation. With the development of full genome sequencing, the genomes of most filamentous fungi were found to be larger than in the yeast counterpart. For example, *N. crassa* and *M. oryzae* both have a genome size of 41 Mb relative to 12 Mb in *S. cerevisiae* and *S. pombe* respectively (Broad Institute). Perhaps the best explanation for this is the morphological and developmental complexity involving various stages of the life cycle in filamentous fungi relative to *S. cerevisiae* (Springer 1993).

It has been theorised that the expansion of genes seen in filamentous fungi allows complexity in the regulatory mechanism, which leads to functional innovation (Wapinski *et al.* 2007, Tirosh and Barkai 2008). This will then provide a fitness advantage in filamentous fungi to colonise diverse environmental conditions and develop complex life cycles. This work showed that both of the non-pathogenic fungi *N. crassa* and *A. nidulans* had the same copy number of *Crh* genes (four) as the pathogenic counterpart, *M. oryzae* and *A. fumigatus*. Thus, it is possible to conclude that the expansion of *Crh1* homologues seen in the phylogenetic tree is not attributable to a pathogenic lifestyle, but associated with the filamentous fungi lifestyle in general relative to unicellular yeasts.

Utr2/Crr1 Clade consists of two groups of genes belonging to the *S. cerevisiae Crr1* and *Utr2* orthologues. What is noted here is that both genes share the characteristic Chitin Binding Domain 1 (cd06923) not present in the Crh1 Clade (except *MGG_Crh3)*. It is observed that not all fungal species retain this gene (Figure 3.10). The gene *Crr1* seemed to be limited to certain species within the fungal class Saccharomycetes. This is because when *S. cerevisiae Crr1* amino acid sequence was queried in NCBI BLASTp, the best hit gene for all

filamentous fungi used in this analysis is the species' *Utr2* gene. Similarly, a *Crr1* orthologue is absent for the human pathogen *C. albicans*, suggesting that the absence of *Crr1* is not Class specific. In *S. cerevisiae, Crr1* was shown to have a specific role in spore formation (Gómez-Esquer *et al.* 2004). Gómez-Esquer *et al.* (2004) showed that *Crr1* is up-regulated during sporulation by up to seven-fold higher and green fluorescent protein (GFP) tagged Crr1p was found to be localised to the spore wall surrounding each ascospore. Since fungi used in this analysis all belong to the Ascomycota Phylum, it is theorised that the *Utr2* gene has now taken the role of *Crr1* in species where this gene is absent.

Another observation from the Utr2/Crr1clade is that gene copy per species seems to be limited to one gene, in contrary to the Crh1 Clade. Notably, both *Crr1* and *Utr2* homologous genes are singly represented from each species (contrary to *U. maydis*). This suggests that *Utr2* genes may have been evolutionarily conserved due to their importance for fungal survival in both yeasts and filamentous fungi. Considering the points mentioned above, *MGG_Utr2* (syn. MGG_01134) would be one of the key *Crh-like* genes to select for downstream studies and it warrants further investigation in the form of gene expression analysis and genetic manipulation.

In conclusion, phylogenetic analyses revealed the separation of *Crh-like* genes into two clades: Crh1 clade and the Utr2/Crr1 clade. Species of filamentous fungi in the Crh1 clade exhibited gene expansion and this is not correlated with pathogenicity, while genes in the Utr2/Crr1 clade were found to be strictly one gene copy per species.

3.4.2 Gene Expression Analysis

The bioinformatics data obtained above involving reciprocal blast search, site predictions (GPI-anchor, signal peptide cleavage, Ser/Thr), promoter region analysis and phylogenetic tree construction, identified five candidate *M. oryzae Crh-like* genes for subsequent gene expression analysis below.

Results from the transcription factor DNA-binding site prediction showed the presence of DNA binding sites for typical transcription factors associated with responses to cell wall stress, osmotic as well as oxidative stress. This information assisted in the downstream experimental design for the type of fungal tissues to analyse, which included WT strain Guy11 grown vegetatively under various conditions. The target here was to measure expression changes to the *M. oryzae Crh-like* genes identified in section 3.4.1, when under starvation (MM+Glucose), extreme starvation (MM-Glucose), cell wall stress (CR), osmotic (SORB), and oxidative stress (H_2O_2), relative to an optimal growth in complete medium (CM). Additionally, given that the literature review above showed a correlation between cell wall integrity and pathogenicity, the expression profile of candidate *M. oryzae Crh-like* genes were also studied on infective tissues at various stages of infection and during sexual development.

3.4.2.1 Gene Info, Primer Design, Specificity, and Efficiency

Before any qRT-PCR gene expression analysis, the most crucial step to producing reliable data is sample preparation, normalisation, and primer quality validation. A total of fourteen *M. oryzae* genes were used in this section, as listed in Table 3.2 along with the ascension number and gene symbol used throughout this work. Appendix A.6 lists all 14 primer pairs used, 13 of which were designed

in this study together with primer efficiency and amplicon size. Each primer pair has one primer that spans the exon/exon boundary, with an annealing temperature difference between primers to be less than 5°C.

Table 3.2. List of Genes Used for the qRT-PCR Gene Expression Analysis. Included are the generic gene names, gene ID, accession number and gene symbol designated for this study.

Gene name	Gene ID and accession num	Gene Symbol
Candidate Reference Genes		
β-Tubulin chain	MGG_00604 (XM_003718381)	*MGG_β-Tubulin*
Elongation factor 1-α	MGG_03641 (XM_003716200)	*MGG_Ef1*
Actin	MGG_03982 (XM_003719823)	*MGG_Actin*
Ubiquitin-conjugating enzyme	MGG_04081 (XM_003719709)	*MGG_Ubiq*
Glyceraldehyde-3-phosphate dehydrogenase	MGG_01084 (XM_003717805)	*MGG_Gapdh*
40S ribosomal protein subunit S27a	MGG_02872 (XM_003720814)	*MGG_40S*
40S ribosomal protein subunit S8	MGG_03251 (XM_003716675)	*MGG_S8*
FAD binding domain-containing protein	MGG_01605 (XM_003714541)	*MGG_Fad*
Nucleolar Protein	MGG_07008 (XM_003709718)	*MGG_Nuc*
Genes of Interest (GOI)		
Utr2 cell wall glucanase	MGG_01134 (XM_003717744)	*MGG_Utr2*
Hypothetical protein	MGG_09918 (XM_003709968)	*MGG_Crh1*
Crh2 cell wall *glycosyltransferase*gene	MGG_00592 (XM_003718400)	*MGG_Crh2*
Hypothetical protein	MGG_10432 (XM_003719403)	*MGG_Crh3*
Extracellular cell wall glucanase Crf1	MGG_12652 (XM_003721148)	*MGG_Crh4*

Primer specificity assays comprising of melt-curve analysis and size separation by gel electrophoresis yielded single amplicons of the expected size for all of the primer sets tested. Melt-curve analysis conducted at the end of a qRT-PCR run showed the presence of only one PCR product for all nine candidate reference genes and five candidate *M. oryzae Crh-like* genes (Appendix A.7 and A.8). Similarly, amplification of primer pairs using standard PCR and pooled cDNA from all RNA samples, produced a single product at the appropriate size when size was separated by gel electrophoresis (Appendix A.9 and A.10).

Calculation of primer efficiencies using five-fold dilution of pooled cDNA for all nine candidate reference genes and five *M. oryzae Crh-like* genes gave r^2>0.99 and 80-100% efficiency (E) values (Appendix A.11 and A.12). This showed that all primer pairs were specific and had similar amplification efficiencies between different sets of primers. Note that for gene *MGG_Crh3* (Appendix A.11), only three points instead of the recommended four-point were used for a regression line. This was because the native expression level of *MGG_Crh3* is already extremely low. Therefore the primer pair was unable to amplify the diluted cDNA template after x25 fold dilution as template concentration was too low.

3.4.2.2 RNA and cDNA Quality & Quantity

The RNA Integrity Number (RIN) values derived from pure fungal RNA samples (dormant spores, perithecia, and vegetatively-grown tissues) were >7.5, indicating good quality, undegraded RNA (Appendix A.13). Samples containing a mix of pathogen and host leaf tissues had RIN values >6.0. The lowered RIN values from plant-derived RNA (Appendix A.14) were attributable to the presence of both pathogen and host leaf RNA that contains both cytosolic and chloroplastic ribosomes, giving rise to additional multiple peaks during electrophoretic separation. Consequently, the slightly lowered RIN number is not due to actual nucleic acid degradation (RIN <6.0), but due to the presence of additional peaks, which increases the calculated total area below the electrophoretic graph, a measurement required for the RIN algorithm (Babujee and Gnanamanickam 2000, Krupp 2005).

3.4.2.3 Quantitative Real Time – PCR Data Analysis

3.4.2.3.1 Control Assays

There was no amplification, or amplification only at high ct values (>35 ct), for non-template control (NTC), minus reverse transcriptase (-RT) and the host-only control (BL). This showed that the reagents were free from contamination (including gDNA) and the absence of non-specific amplification of plant cDNA.

3.4.2.3.2 Preliminary Sample Cycle Threshold Evaluation

Initially, cycle threshold (ct) values from five *M. oryzae Crh*-like genes from the same cDNA stock of pooled template which were amplified on the same qRT-

PCR 96-well plate, were averaged from two technical replicates. This step gives a general indication regarding the relative amount of RNAs present in the organism for each *Crh-like* gene. Table 3.3 showed that using the template from pooled cDNA (RNA samples from various infective stages were converted to cDNA and pooled), gene *MGG_Crh2* is expressed at the highest amount, since it gives the lowest ct value, while *MGG_Crh3* is the lowest expressed gene among the five *Crh*-like genes. This explains why it was difficult to obtain an amplification of *MGG_Crh3* primers after x25 fold dilution in the primer efficiency assay.

Table 3.3. Raw Cycle Threshold (ct) Values of Five *Crh-like* Genes Amplified from Pooled Infective Stage cDNA. Data shown below are mean raw ct values from two technical replicates for each gene, obtained from one qRT-PCR plate, using pooled cDNA samples from fungal WT containing infective stage fungal tissues.

Gene Symbol	Mean (ct)	St. Dev
MGG_Utr2	13.76	0.11
MGG_Crh1	21.83	0.22
MGG_Crh2	12.40	0.34
MGG_Crh3	26.99	0.37
MGG_Crh4	20.05	0.08

In a second independent assay, only cDNA from vegetative mycelia were used and this time, a housekeeping gene known to be expressed highly (positive control) was also added. This was the Elongation factor 1-α designated *MGG*_Ef1 (Soanes *et al* 2012). This assay was conducted to obtain a better insight in the expression level during the vegetative stage and also as an alternative repeat to pooled cDNA as above. In Table 3.3, it is obvious that gene *MGG_Crh2* was again highly expressed. It was almost as high as the essential housekeeping gene *MGG_Ef1* as both were in the range of 14-15 ct values. Similarly, *MGG_Utr2* was the second highest, with *MGG_Crh3* giving the lowest

expression, consistent with the pattern seen in Table 3.4 Table 3.3 for pooled cDNA taken from RNA of infective tissues.

At first sight, the *MGG_Crh2* ct value in vegetative mycelium is lower than the raw ct in pooled infective cDNA, but it is important not to compare these raw ct values across separate assays. This is because both assays were generated independently on different 96-well plates with cDNA preparation varying temporally and differing in stock reagents used. It needs to be emphasised that this is preliminary data and further carefully designed qRT-PCR will need to be conducted to compare expression across different tissues.

Table 3.4. Raw Cycle Threshold (ct) Values of Five *Crh-like* Genes Amplified from Mycelial cDNA. Data are mean raw ct values from two technical replicates for each gene, obtained from one qRT-PCR plate, using cDNA from fungal WT vegetative mycelium

Gene Symbol	Mean (ct)	St. Dev
MGG_Utr2	18.14	0.10
MGG_Crh1	22.45	0.07
MGG_Crh2	14.69	0.13
MGG_Crh3	28.68	0.10
MGG_Crh4	22.42	0.06
MGG_Ef1 **(reference gene)**	15.03	0.06

The raw ct results complemented a published genome wide transcriptomic profile of WT during appressorium development using High-Throughput (HT) SuperSAGE (Soanes *et al.* 2012) (Appendix A.14). While the base mean cannot be compared directly to ct values, the ranking of expression level can be made. Data from Soanes *et al.* 2012 showed that *MGG_Crh2* is the most highly expressed gene with base mean values reaching up to 36,298 during the vegetative stage (CM) followed by *MGG_Utr2* at 208.1 base mean. Both genes *MGG_Crh1* and *MGG_Crh3* can be seen to be lowly expressed regulated, with

base means ranging 0-39. *MGG_Crh4* is not available in the SuperSAGE database developed by Soanes *et al.* (2012). It is important to point that while this tool is high throughput, it may not be able to resolve the expression profile of genes that are lowly expressed. Therefore, it is difficult to conclude from these data if *MGG_Crh1* and *MGG_Crh3* are expressed at all or if it is indeed the least expressed gene. This is where qRT-PCR is a more superior tool, and by comparing to data in this work (Table 3.3 and Table 3.4), it is clear that *MGG_Crh1* is actually expressed albeit with lowered expression and that *MGG_Crh3* is the least expressed gene.

Preliminary data gives a suggestion that *MGG_Crh3* with ct values close to 30, can be considered the gene with least priority for targeted homologous recombination transformation. On the contrary, preliminary analysis of the raw ct values showed that genes *MGG_Utr2* and *MGG_Crh2* warrant further gene expression analysis. Given that *MGG_Crh1* is in the same clade as *S. cerevisiae Crh1* (Section 3.3.1.6, Figure 3.10), it may be useful to include this gene in upcoming expression profile analysis. This is because it is emphasised here that at this stage, data obtained can only be used as preliminary information but certainly not enough for a definitive decision. More expression analysis as conducted henceforth will need to be conducted to obtain reliable expression profile data, involving various tissue types representative of the various stages of the life cycle and under various stress conditions.

It is concluded that three *M. oryzae Crh-like* genes will be chosen for subsequent qRT-PCR work: *MGG_Utr2, MGG_Crh1,* and *MGG_Crh2* on the basis of the relative level of transcripts observed by the ct values generated.

3.4.2.3.3 Expression Stability of Candidate Reference Genes

Prior to conducting qRT-PCR assay and data analysis on three genes of interest (*MGG_Utr2, MGG_Crh1,* and *MGG_Crh2*), the most appropriate set of internal reference genes were first determined. This is an essential step to ensure that during calculation of relative expression, a reliable and accurate normalisation against truly stable reference genes was used.

The ranking by gene expression stability (M) values of the nine candidate reference genes, assayed separately for each group of tissues (Vegetative, Infective, and Global), are shown in Figure 3.11. Candidate genes with the lowest M value were the most stably expressed, while genes with the highest M value were least stable. The minimum number of reference genes required for reliable and accurate normalisation for each Group was determined as two genes, with a "cut-off" value was set at 0.15 (Vandesompele *et al.* 2002) as shown in Figure 3.12. The gene stability (M) and pairwise variation (V) measurement data were used to identify the two best-performing reference genes for each group; *MGG_Ef1* and *MGG_40s* for the Vegetative Group; *MGG_40s* and *MGG_Actin* for the Infection Group, and *MGG_40s* and *MGG_S8* for the Global Group.

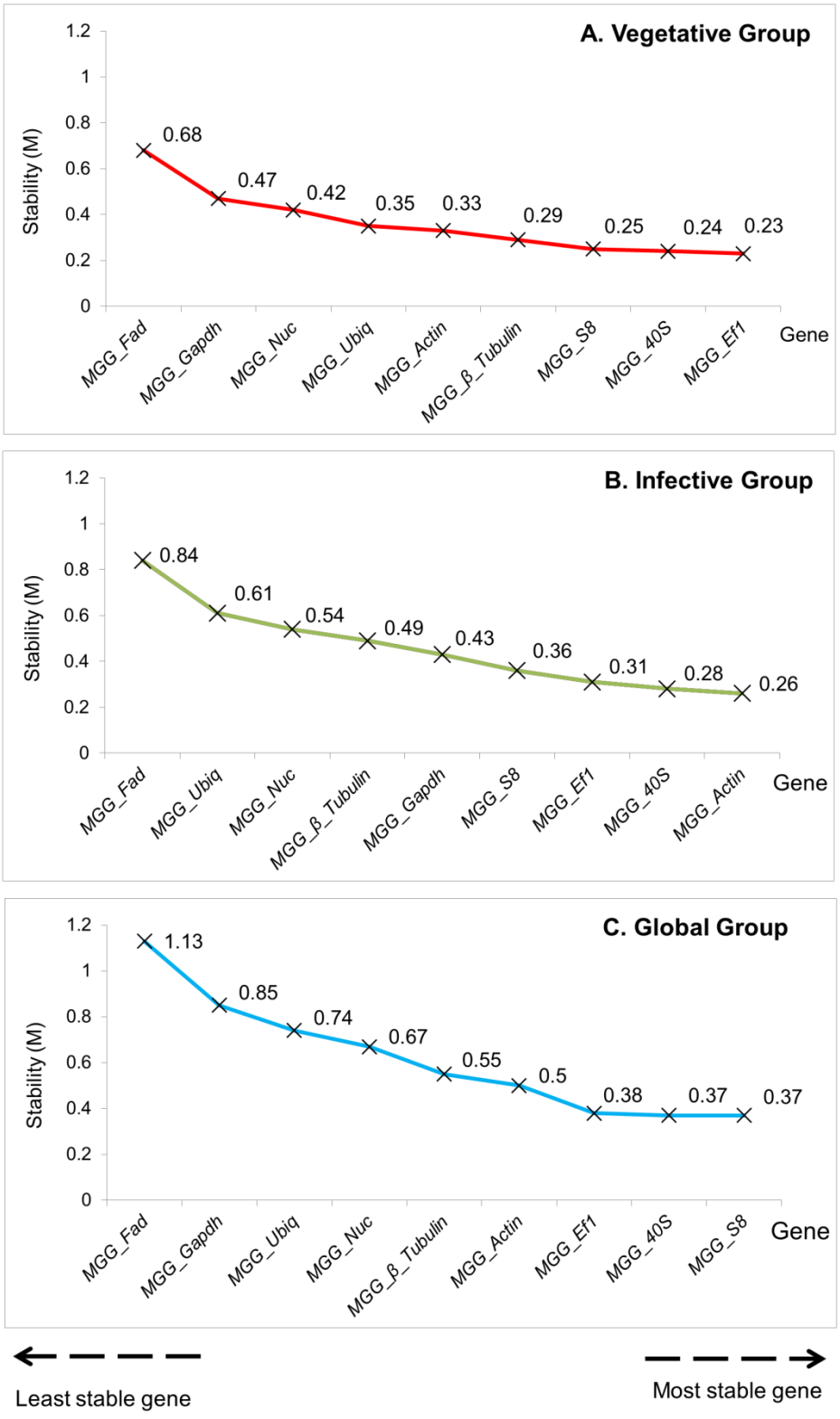

Figure 3.11. Ranking of Nine Candidate Reference Genes According to the Calculated Average Expression Stability (M). Sequential removal of the least stable reference gene improves average expression stability, indicated by lower values of M. The cut-off for an unstable gene was taken to be M ≥ 1. The analysis was repeated for three groups of tissues: A) Gene stability (M) values for genes in the Vegetative group; B) Gene stability (M) values for genes in the Infective group and; C) Gene stability (M) values for genes in the Global group.

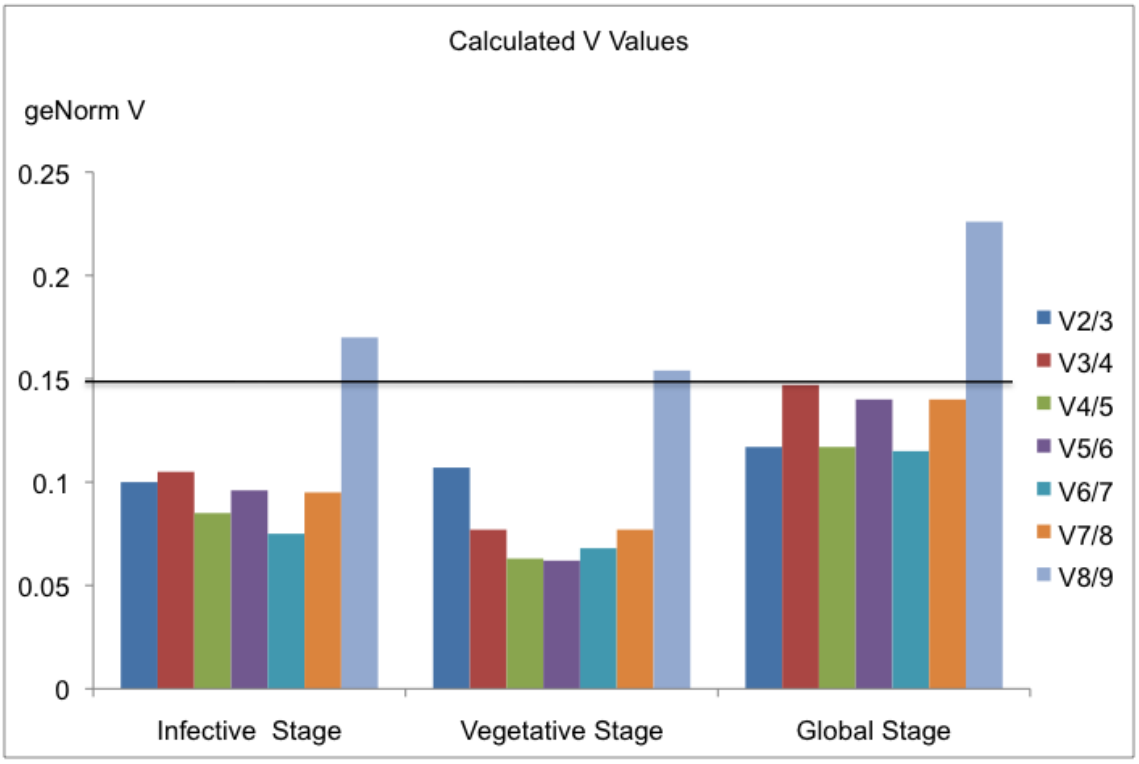

Figure 3.12. Determination of the Optimal Number of Reference Genes for Accurate Normalisation. Graphs show calculated pairwise variation, $V_{n/(n+1)}$ between normalisation factor NF_n and NF_{n+1} for a total of nine candidate reference genes. The optimal number of reference genes for accurate normalisation is taken to be the smallest number for which V is less than a cut-off of 0.15 (Vandesompele *et al.* 2002). The analysis was repeated for the three designated groups: A) Infective; B) Vegetative, and; C) Global.

The recommendations for use of the named reference genes for the given tissues are robust, but caution is advocated in extrapolation to untested experimental conditions, such as in the use of different exogenous stresses (eg pH or temperature stress). Moreover, inferred co-regulation is an important consideration in the choice of reference genes and one to avoid, if possible. Here, at least two candidate genes from key functional classes, that is, the glycolysis pathway (*MGG_Fad and MGG_Gadph*), protein synthesis (*MGG_Ef1*, *MGG_S8,* and *MGG_40s*), cytoskeleton assembly (*MGG_β-Tubulin* & *MGG_Actin*) and protein degradation (*MGG_Ubiq*) were selected. For the Infective Group, the two most stable genes, *MGG_40s,* and *MGG_Actin* belong to two distinct functional groups. However, for the Vegetative and Global Groups, genes belonging to the

protein synthesis pathway proved most robust in stability, being unaffected by changes to environmental stressors or fungal growth phases. In this case, it is more important to use a set of validated stable genes instead of prioritising genes from different biological pathways. Furthermore, for the Vegetative Group, the two most stable genes belonged to protein synthesis pathways with exclusive functions: *MGG_Ef1* and *MGG_40s,* therefore, have little risk of co-regulation (Sandbaken and Culbertson 1988, Planta and Mager 1998). In the Global Group, the most stable genes lie in the RNA synthesis pathway. As *MGG_40s* and *MGG_S8* both from one 40S functional subunit, it is recommended instead *MGG_Ef1* (M=0.38), used in conjunction with *MGG_40s* (M=0.37) or *MGG_S8* (M=0.37). Here, the M value differences are very small, suggesting that all three genes are similarly stable, and thus this will not significantly affect normalisation reliability.

Thus far, a single study has attempted identification and validation of *M. oryzae* reference genes for qRT-PCR (Park *et al.* 2013). In that study, Park *et al.* (2013) chose seven candidate genes, three of which are used herein and can, therefore, be compared directly: *MGG_β-Tubulin*, *MGG_Actin,* and *MGG_Gapdh*. Based on GeNorm analysis, Park *et al.* (2013) ranked their seven genes across tissue sample types that concur with Global Group, whereby *MGG_Gapdh* has lower stability (high M value), with *MGG_Actin* and *MGG_β-Tubulin* being more stably expressed (low M value). The combined findings also correspond for the Infective Group, whereby *MGG_Actin* is more stable than *MGG_Gapdh* and *MGG_β-Tubulin*. This consistency confirms the reproducibility and reliability of qRT-PCR when quality control practices were adhered to. In addition to the three genes shared by both studies, more importantly in this work,

a validated set of robust genes were introduced belonging to the protein synthesis pathway (*MGG_Ef1*, *MGG_40s,* and *MGG_S8*) that can be used for gene expression studies in *M. oryzae*. This study also demonstrates that for reliable normalisation in *M. oryzae* across all tissue groups (Infective, Vegetative, and Global), the optimal number of reference genes to use are two.

3.4.2.3.4 Expression Profile: Data Quality & Calculation

To summarise the calculation strategy, the raw expression of a GOI or reference gene (in ct values) is recorded by qRT-PCR amplification of a primer pair specific to the gene. Successful qRT-PCR amplification is when the amplification plot of the GOI or reference gene showed a typical PCR exponential graph (Figure 3.13), with the same threshold line crossing the exponential phase of all other amplification plots for the qRT-PCR reactions assayed in separate wells of the same 96-well plate. Each cycle represents a complete PCR cycle, with the doubling of primer products at each subsequent cycle.

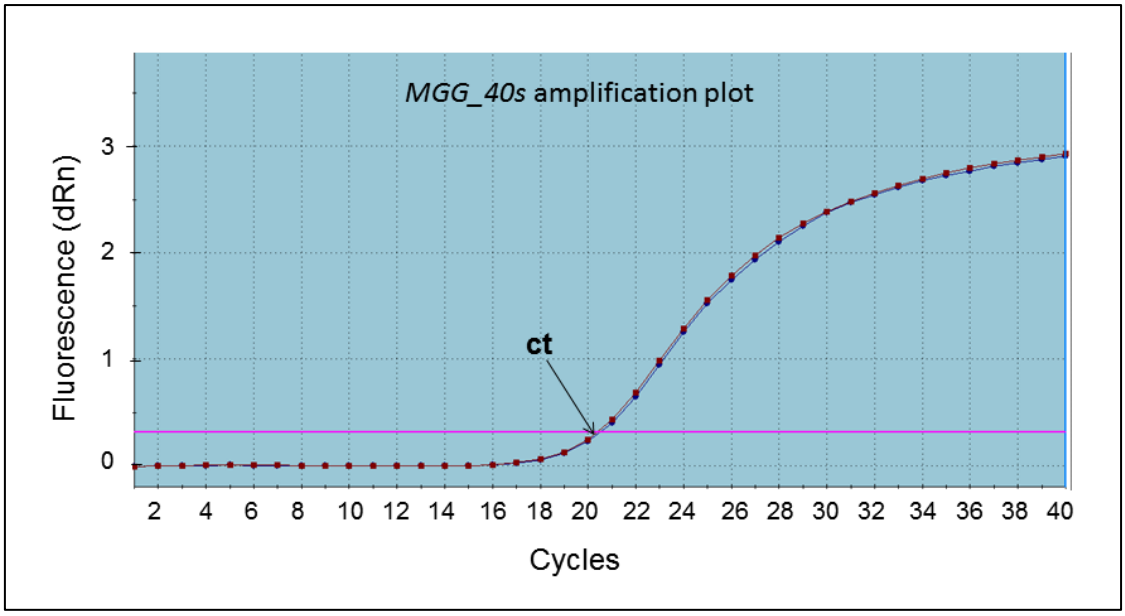

Figure 3.13. *MGG_40s* Amplification Plot. An example of a typical qRT-PCR amplification cycled 40 times. The dRN is the fluorescence of the reporter dye (SYBR® Green) divided over the passive dye (ROX^{TM}). Initially, the absence of fluorescence at low cycle number is because the fluorescence of SYBR® Green is less than that of ROX^{TM}. Once there are sufficiently high numbers of PCR products, SYBR® Green dye binds to the double-stranded DNA product and fluorescence. As the PCR products double at each successive cycle, fluorescence is seen to increase exponentially. As reagents are exhausted, a plateau phase towards the higher end of the cycle is seen. Two technical replicates were used in this amplification, the overlapping of two graphs indicate consistency in pipetting and minimal human error. The ct value is the threshold line determined that crosses the exponential phase for all reactions within the 96-well plate assayed.

The relative expression or fold change (NRQ_{GOI}) of a GOI was calculated as described in Pfaffl M.W (2001). Here, the relative expression of GOI was measured against a set of validated reference genes shown to be stably expressed across the tissue types sampled, with the Normalizing Factor ($2^{\Delta ct\ reference\ gene}$) adjusted to include the mean of two reference genes by using Geometric Mean.

$$\text{Fold Change (Pfall's equation)} = \frac{2^{\Delta ct\ GOI}}{2^{\Delta ct\ reference\ gene}}$$

$$\text{Fold Change } (NRQ_{GOI}) = \frac{2^{\Delta ct\ GOI}}{\text{GEO MEAN } (2^{\Delta ct\ reference\ gene1}),(2^{\Delta ct\ reference\ gene2})}$$

Where:

Δct GOI = Mean ct GOI in control sample – Mean ct GOI in target sample

Δct reference gene = Mean ct of reference gene in control sample – Mean ct reference gene in target sample.

Control sample is dormant spore or vegetative growth (CM)
Target sample is any other tissue type/sample

To allow comparison between plates with minimal technical variations between two or more 96-well plates, sample maximisation was adhered to as recommended by Hellemans *et al.* (2007). Each 96-well plate if possible is a stand-alone assay: three biological replicates for each control sample and target sample must be on the same plate. Each of these biological replicates must have a total of three sets of primers amplified separately with two technical replicates each: primer pair for reference gene 1, primer pair for reference gene 2 and primer pair for gene of interest. For each 96-well plate qRT-PCR amplification, ct data was collected and averaged from two technical replicates. The Normalised Relative Quantities (NRQ) for each biological replicate was calculated, followed by a series of sequential corrections including log transformation, mean centring, autoscaling and averaging of biological replicates as described by Wilhelms *et al.* (2008) to draw reliable conclusions from qRT-PCR data generated. Standard Error of Mean was measured and statistical analysis analysed using 95% confidence interval and shown in error bars.

3.4.2.3.5 Expression Profile: Infective Stage

The validated set of reference genes *MGG_Actin* and *MGG_40s* were used as the normalizing factor for qRT-PCR data calculation in measuring the relative expression of *MGG_Utr2, MGG_Crh1,* and *MGG_Crh2*.

The expression profile for *MGG_Utr2* from 2 hpi up to 48 hours *in planta* growth (Figure 3.14) showed a general pattern of successive reduction in expression relative to *MGG_Utr2* expression in dormant spores. In a technical qRT-PCR publication, Karlen *et al.* (2007) showed that a qRT-PCR assay can only provide reliable estimations of expression ratio from two-fold change or higher. As a result, for 2 hpi, 8 hpi and 12 hpi, the fold-change is less than 2. Therefore, it can be accepted that there is minimal or biologically insignificant change to expression. On the contrary, and as statistically supported at $p<0.05$, the expression of *MGG_Utr2* at 48 hpi is seen to be down-regulated by 0.8 to 2.5-fold less compared with the expression of *MGG_Utr2* in dormant spores. Analysis on *MGG_Crh1* showed a different expression pattern for the same set of tissue samples. As shown in Figure 3.15, the gene was up-regulated highest at 2 hpi and 8 hpi by up to four-fold change relative to dormant spores. The expression then dropped to being non-significantly different (12 hpi), or the fold change was less than 2. Similar to the expression profile of *MGG_Utr2,* the expression of *MGG_Crh2* was generally down-regulated during infection, relative to dormant spores (Figure 3.16).

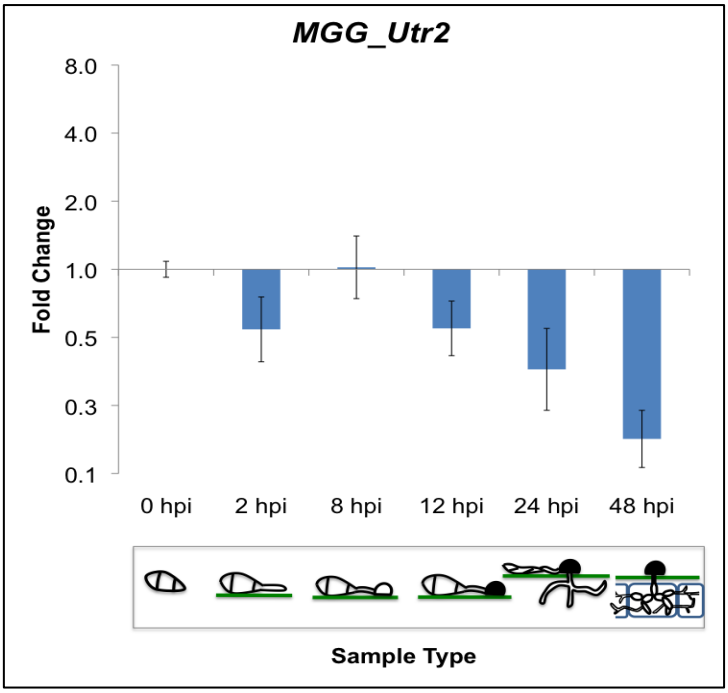

Figure 3.14. Expression Profile for *MGG_Utr2* Gene across the Infective Life Stage of *Magnaporthe oryzae.* Samples normalised against validated reference genes *MGG_Actin* and *MGG_40s* with dormant spore (0 hpi) used as the control sample. Each bar corresponds to three biological replicates of the same tissue. Error bars are at 95% confidence interval. Statistical calculations as according to the recommendations by Willems *et al.* (2008).

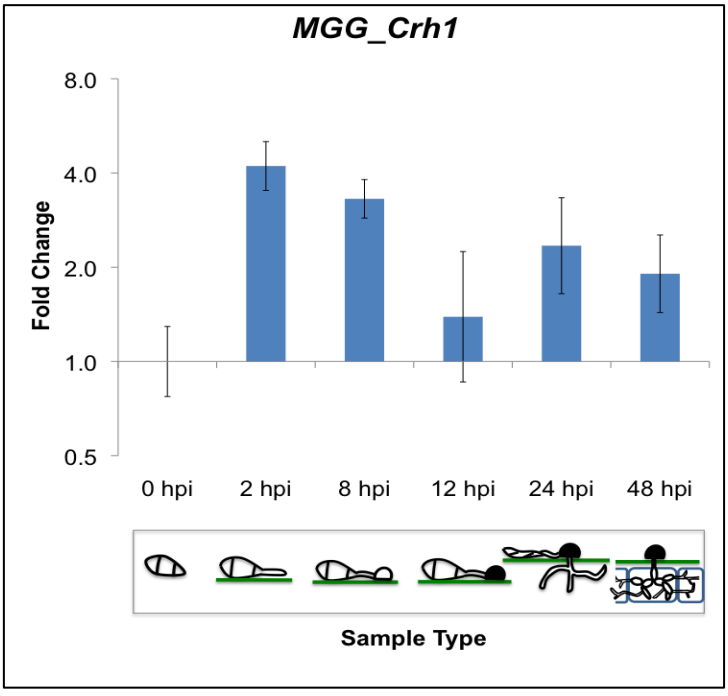

Figure 3.15. Expression Profile for *MGG_Crh1* Gene across the Infective Life Stage of *Magnaporthe oryzae*. Samples normalised against validated reference genes *MGG_Actin* and *MGG_40s* with dormant spore (0 hpi) used as the control sample. Each bar corresponds to three biological replicates of the same tissue. Error bars are at 95% confidence interval. Statistical calculations as according to the recommendations by Willems *et al.* (2008).

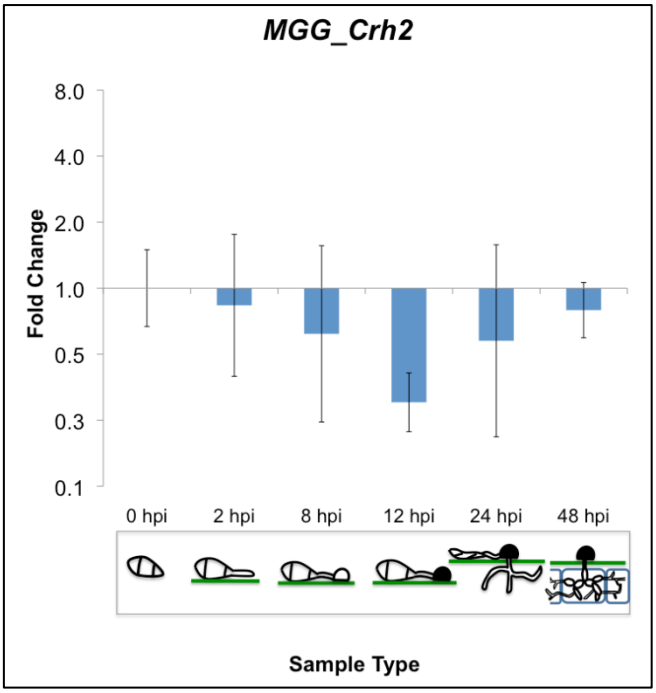

Figure 3.16. Expression Profile for *MGG_Crh2* Gene across the Infective Life Stage of *Magnaporthe oryzae.* Samples normalised against validated reference genes *MGG_Actin* and *MGG_40s* with dormant spore (0 hpi) used as the control sample. Each bar corresponds to three biological replicates of the same tissue. Error bars are at 95% confidence interval. Statistical calculations as according to the recommendations by Willems *et al.* (2008).

It can be deduced from Figure 3.16 that early infective stages (2 hpi to 12 hpi) required less *MGG_Crh2*, and that the need for these transglycosylase proteins increased as there was an increase in mycelial growth (see global assay in next section). Conversely, in extensive *in planta* growth, the expression of *MGG_Utr2* continued to be significantly ($p<0.05$) down-regulated.

This variation in expression of *Crh-like* profile at different stages of the life cycle is not limited to *M.* oryzae. Gene expressions (by Northern Blot) of *S. cerevisiae Crh1, Crh2* and *Crr1* showed that only *Crr1* was up-regulated by a ninefold higher level during the sporulation stage relative to vegetative growth (Rodriguez-Pena *et al.* 2000). On the contrary, the *Crh2* expression was not detected at all at this stage while *Crh1* showed no change in expression, leading the authors to conclude that while these genes may be functionally redundant,

they are clearly differently regulated. This variation in expression is also seen in *C. albicans Crh-like* genes with neo-functionalisation. In this species, three genes belong to the *Crh-like* gene family, *caUtr2, Crh11* and *Crh12* with a phylogenetic distribution in the GH 16 tree as described in section 3.4.1.5. Zelante *et al.* (2012) showed that apart from being cell-cycle regulated, the Crh11p have a specific affinity for the mammalian T-cell protein, IL-17A but this is not the case with Crh12p nor caUtr2p.Therefore, besides variation in expression, it is probable that these *M. oryzae Crh-like* genes may also begin to form neo-functionalisation, but more experimental work such as mutational work will need to be conducted to prove this hypothesis.

3.4.2.3.6 Expression Profile: Vegetative & Global Stage

The aim of this assay was to identify any changes to gene expression under various stressors, relative to the growth of WT under optimal vegetative conditions (in CM). This would give an indication of the signalling pathways responsible for regulating the expression of *M. oryzae Crh-like* genes. The validated pair of reference genes *MGG_Ef1* and *MGG_40s* were used as the normalizing factors to trace the expression profile of cell wall remodelling genes, *MGG_Utr2, MGG_Crh1* and *MGG_Crh2* during vegetative growth under various stressors.

The gene *MGG_Utr2* responded by an up-regulation of up to four-fold under cell wall stress caused by Congo Red (100 µg/ml) relative to optimal vegetative growth in Complete Medium as shown in Figure 3.17. Similarly, but to a lesser extent, under Caffeine (2.5 mM) stress and starvation (MM), *MGG_Utr2* was significantly ($p<0.05$) up-regulated up to three-fold and two-fold respectively, with no significant changes observed when under other types of stress. On the

contrary, the gene *MGG_Crh1* showed no significant changes to any of the six stress conditions (Figure 3.18). Interestingly, for gene *MGG_Crh2*, only cell wall stress caused by Congo Red resulted in a significant up-regulation ($p<0.05$) by two-fold (Figure 3.19) while oxidative stress and extreme starvation both caused a significant ($p<0.05$) down-regulation, 2.8 and 1.2-fold respectively.

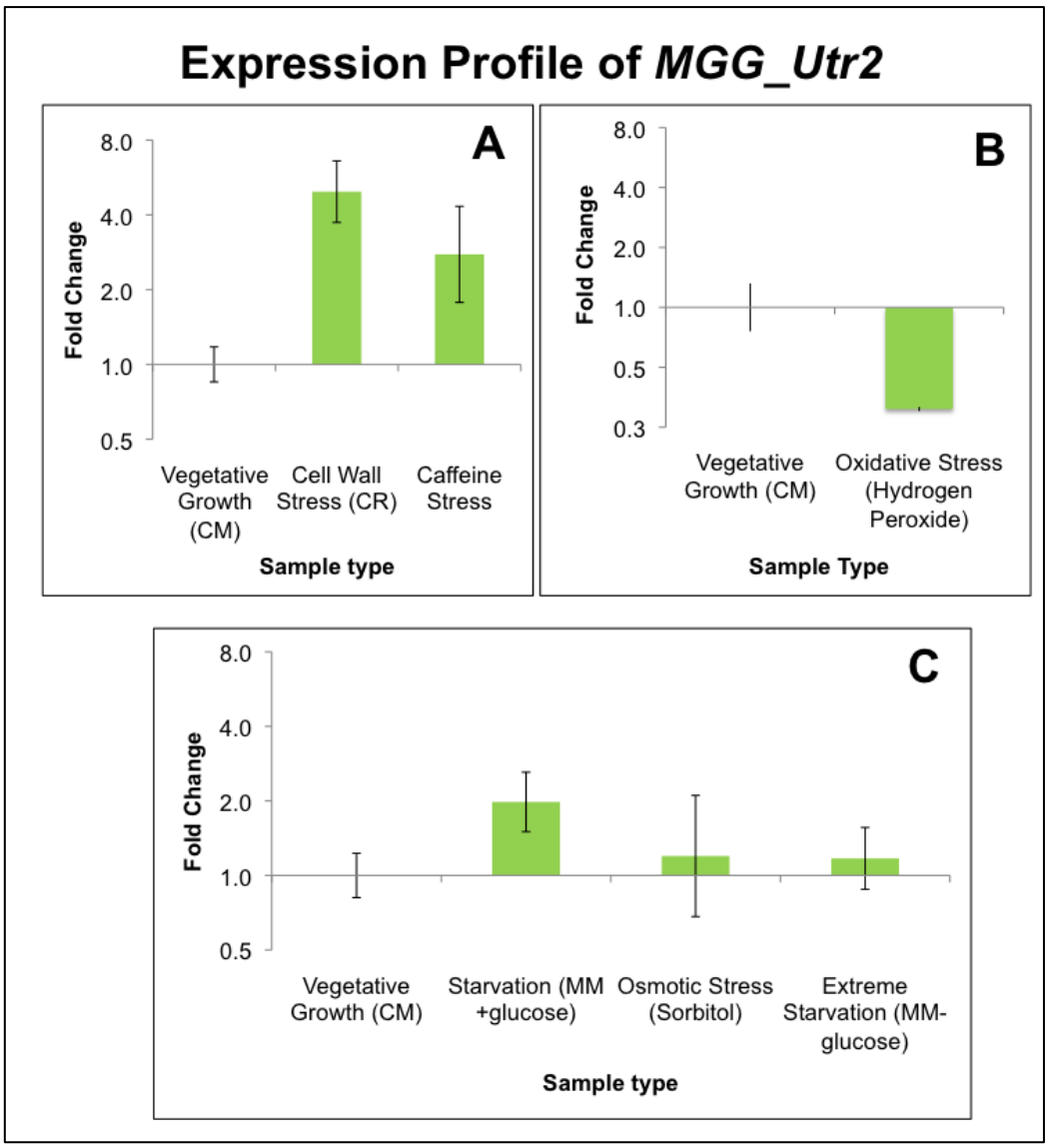

Figure 3.17. Expression Profile of *Magnaporthe oryzae MGG_Utr2* Grown Vegetatively Under Various Growth Conditions. Wild Type Guy11 strain was grown vegetatively for three days in nutrient rich liquid Complete Medium (CM) containing various stress-inducing compounds. The RNA was extracted from each sample type, and gene expression measured using qRT-PCR against a control sample, Vegetative Growth (CM) (designated a value of 1) and normalised against two validated reference genes, *MGG_40s,* and *MGG_Ef1.* **Panel A** Expression of *MGG_Utr2* grown under cell wall stress caused by Congo Red (100 µg/ml) and Caffeine stress (25 mM), relative to control (CM). **Panel B** Expression of *MGG_Utr2* grown under oxidative stress caused by H_2O_2 (2.5 mM) relative to control (CM). **Panel C** Expression of *MGG_Utr2* grown under starvation (MM+glucose), osmotic stress (Sorbitol 1M) and extreme starvation (MM-glucose) measured relative to control (CM). Fold-change values averaged from three biological replicates with error bars representing 95% confidence intervals. Statistical calculations as according to the recommendations by Willems *et al.* (2008).

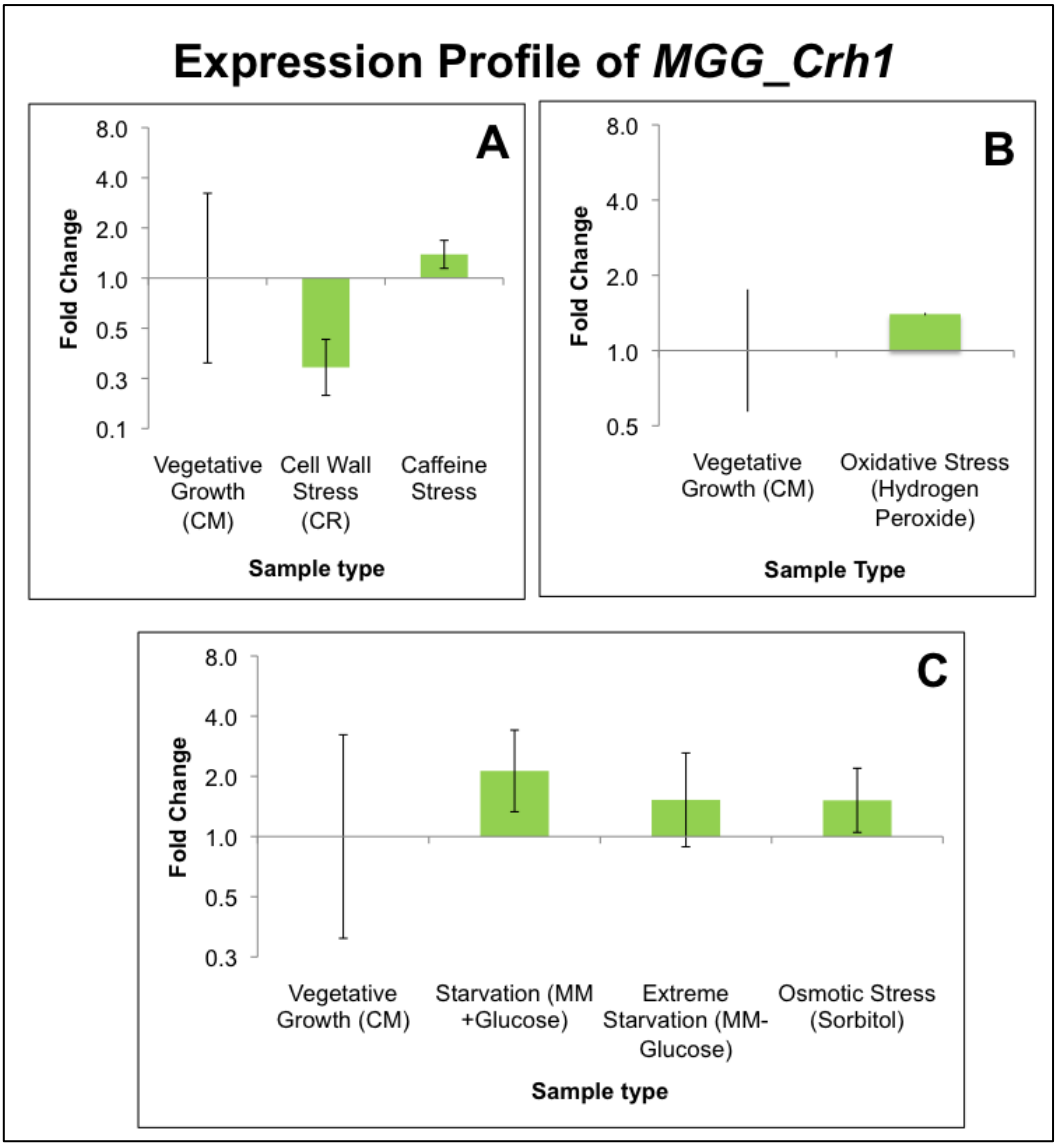

Figure 3.18. Expression Profile of *Magnaporthe oryzae MGG_Crh1* Grown Vegetatively Under Various Growth Conditions. Wild Type Guy11 strain was grown vegetatively for three days in nutrient rich liquid Complete Medium (CM) containing various stress-inducing compounds. The RNA was extracted from each sample type and gene expression measured using qRT-PCR against a control sample, Vegetative Growth (CM) (designated a value of 1) was normalised against two validated reference genes, *MGG_40s,* and *MGG_Ef1.* **Panel A** Expression of *MGG_Crh1* grown under cell wall stress caused by Congo Red (100 µg/ml) and Caffeine stress (25 mM), relative to control (CM). **Panel B** Expression of *MGG_Crh1* grown under oxidative stress caused by H_2O_2 (2.5 mM) relative to control (CM). **Panel C** Expression of *MGG_Crh1* grown under starvation (MM+glucose), extreme starvation (MM-glucose) and osmotic stress (Sorbitol 1M), measured relative to control (CM). Fold-change values averaged from three biological replicates with error bars representing 95% confidence interval. Statistical calculations as according to the recommendations by Willems *et al.* (2008).

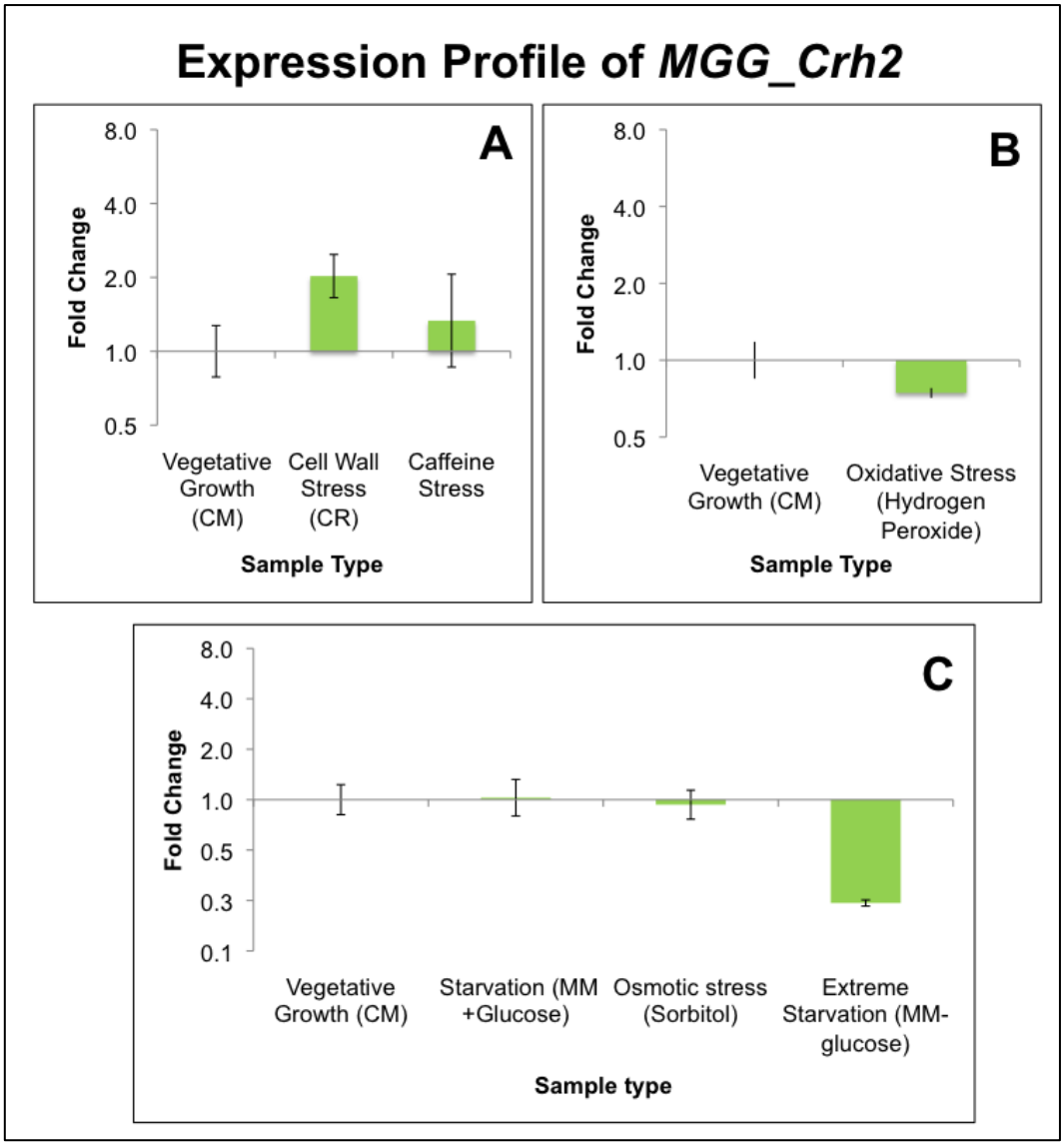

Figure 3.19. Expression Profile of *Magnaporthe oryzae MGG_Crh2* Grown Vegetatively Under Various Growth Conditions. Wild Type Guy11 strain was grown vegetatively for three days in nutrient rich liquid Complete Medium (CM) containing various stress-inducing compounds. The RNA was extracted from each sample type and gene expression measured using qRT-PCR against a control sample, Vegetative Growth (CM) (designated a value of 1) and normalised against two validated reference genes, *MGG_40s,* and *MGG_Ef1.* **Panel A** Expression of *MGG_Crh2* grown under cell wall stress caused by Congo Red (100 µg/ml) and Caffeine stress (25 mM), relative to control (CM). **Panel B** Expression of *MGG_Crh2* grown under oxidative stress caused by H_2O_2 (2.5 mM) relative to control (CM). **Panel C** Expression of *MGG_Crh2* grown under starvation (MM+glucose), osmotic stress (Sorbitol 1M) and extreme starvation (MM-glucose) measured relative to control (CM). Fold-change values averaged from three biological replicates with error bars representing 95% confidence interval. Statistical calculations as according to the recommendations by Willems *et al.* (2008).

Through the use of specific compounds known to activate certain MAPK signalling pathways, the vegetative assay above provided insights into the regulatory mechanism of *M. oryzae Crh-like* genes. The vegetative assay showed that both *MGG_Utr2* and *MGG_Crh2* responded to cell wall stress imposed by Congo Red, being elevated between two to four-fold. This confirms the expectation that *MGG_Crh2* and *MGG_Utr2* are regulated by the cell wall integrity pathway under conditions that stresses the cell wall. In *S. cerevisiae*, cell wall stress caused by Congo Red was shown to directly activate the cell wall integrity pathway via the phosphorylation of Rlm1 but not the SBF complex (Swi4/Swi6) (Garcia *et al.* 2004). When grown in Congo Red (from 2 hr to 6 hr exposure), *S. cerevisiae Crh1* was up-regulated 2-4 fold, with a weaker response by *Utr2* (Garcia *et al.* 2004). It is, therefore, possible that the *M. oryzae* Rlm1p orthologue, MOMig1 (Mehrabi *et al.* 2008) was phosphorylated under cell wall stress caused by Congo Red, which then directly increases the expression of *MGG_Crh2* (see results section 3.4.1.2) shown to have a DNA binding motif for Rlm1. The up-regulation of *MGG_Utr2* in Congo Red is an interesting observation, given that promoter analysis could not detect Rlm1p motif in *MGG_Utr2*, rather Swi4p was identified instead. This contradicts the study by Garcia *et al.* (2004) associating Congo Red to activating Rlm1 and not the SBF complex of the integrity pathway.

Contrary to the cell wall perturbant Congo Red, the presence of caffeine was found to activate the yeast cell wall integrity pathway independent of Rlm1 activation in a Tor1 dependant fashion (Kuranda *et al.* 2006). This compound was used to investigate if any of the *M. oryzae Crh-like* genes were activated independently from Rlm1. *Crh-like* genes analysed showed that only *MGG_Utr2*

responded to caffeine stress and nutrient limitation (MM+glucose). However, strangely, this gene was not up-regulated under extreme starvation (MM-glucose). While there may not be sufficient information to deduce the reason for differences in regulation under starvation, it can still be concluded *M. oryzae Crh-like* genes, especially between *MGG_Crh2* and *MGG_Utr2* are indeed differentially regulated.

Osmotic and oxidative stress caused by sorbitol and H_2O_2 respectively is known to induce the Hog1 MAPK signalling pathway (Posas and Saito 1997, Singh 2000, Alonso-Monge *et al.* 2003, Arana *et al.* 2005). Results obtained in this study showed that osmotic stress had no significant effect on the expression of all three *M. oryzae*, while expression is significantly down-regulated under oxidative stress for both *MGG_Utr2* and *MGG_Crh2.* This is contrary to the hypothesis given that promoter analysis (section 3.4.1.2) indicated multiple copies of Msn2/Msn4p TF binding motifs associated with osmotic and oxidative stress. Two possible explanation for this is presented: firstly, the prediction method may be too yielding, thereby mis-identifying some of the Hog1-related TFs. In the second theory, sorbitol (osmotic stress) and H_2O_2 (oxidative stress) may not cause an activation of Msn2/Msn4p TF destined for the regulation of *M. oryzae Crh-like* genes but may involve other TFs and possibly, an inter-network of other signalling pathways. The significant down-regulation of *Crh-like* genes under oxidative stress is an intriguing response and warrant consideration when discussing results from experiments in subsequent Chapters.

Results from both vegetative and infective assay confirmed the hypothesis put forward in section 3.4.1.2 whereby indeed *M. oryzae Crh-like* genes are regulated differentially at different stages of the life cycle and under different environmental conditions. Studies have shown that functional innovation often arises from variation in regulation as opposed to changes to the protein sequence and this is most evident in ascomycetes (Wapinski *et al.* 2007, Tirosh and Barkai 2008). Variations in the expression of *M. oryzae Crh-like* genes emphasises the need to follow up with mutational analysis especially in *MGG_Crh2* and *MGG_Utr2,* given that the variations also arise from these *genes* belonging to different clades (Clade Crh1 or Clade Crr1/Utr2), suggesting the possibility of different functions.

Preliminary expression data from both vegetative and infective tissues suggests that *MGG_Crh2* play a key role in the fitness and function of mycelial growth. This is because of the high levels of expression (low ct values), response pattern to cell wall stress during vegetative growth, and lack of up-regulation during infection. From here, a global expression assay was conducted (Figure 3.20) to provide an indication of the relative expression level across life cycles. In reference to Figure 3.20, the expression of *MGG_Crh2* in various tissues was measured against its expression in dormant spores (0 hpi). This gene was found to be up-regulated by up to three-fold during vegetative growth, two-fold higher in perithecia and least expressed during appressorium maturation (8 hpi) and in *in-planta* growth (48 hpi), relative to *MGG_Crh2* expression in dormant spores. The above expression analysis supports the theory that the primary role of *MGG_Crh2* is in maintaining fungal cell wall integrity during the vegetative stage

of the life cycle. Subsequent downstream experimental analysis (following chapters) will aim to confirm this.

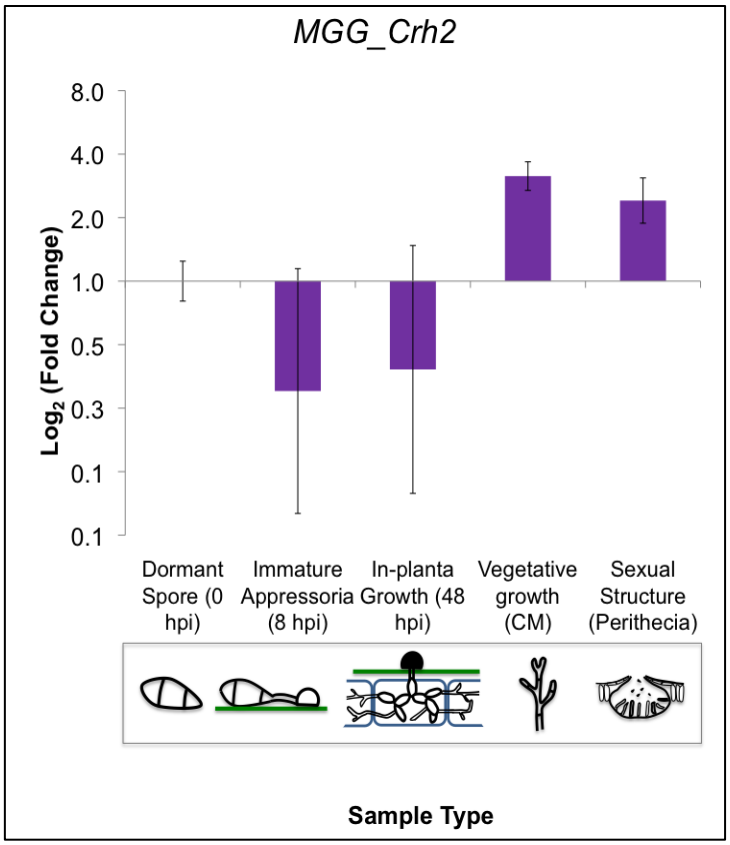

Figure 3.20. Expression Profile of *Magnaporthe oryzae MGG_Crh2* across Major Stages of the Life Cycle. Tissues of Wild Type Guy11 strain were harvested from dormant spores (0 hpi), immature appressoria and *in-planta* growth (8 hours and 48 hours post inoculation on cut barley leaves respectively), as well as perithecia developed by growing Guy11 strain with TH3 strain. The RNA was extracted from each tissue type and expression of *MGG_Crh2* measured using qRT-PCR, with tissues from dormant spore used as the control sample (designated a value of 1). Relative quantities normalised against two validated reference genes, *MGG_40s,* and *MGG_Ef1*. Fold-change values averaged from three biological replicates with error bars representing 95% confidence interval. Statistical calculations as according to the recommendations by Willems *et al.* (2008).

3.5 Chapter Summary & Conclusion

Bioinformatics section

Reciprocal blast search between three *S. cerevisiae Crh-like* genes (*Crh1, Utr2,* and *Crr1*) revealed five candidate *Crh-like* genes in *M. oryzae*. The orthologue of *S. cerevisiae Utr2* gene was found as a single copy in *M. oryzae,* named *MGG_Utr2*. Surprisingly, the orthologue of *S. cerevisiae Crr1* is not present in the genome of *M. oryzae*, while *S. cerevisiae Crh1* had four orthologues in *M. oryzae,* named *MGG_Crh1* to *MGG_Crh4.*

The amino acid sequence of these five candidate *Crh-like* genes were then subjected to a series of queries for the prediction of modular structures characteristic of a CWP. It was discovered that only *MGG_Utr2, MGG_Crh1,* and *MGG_Crh2* were GPI-anchored. All genes had a predicted signal peptide cleavage site and the Ser/Thr rich region. These results begin to suggest that *MGG_Crh3* and *MGG_Crh4* may not be a functional CWP. However more investigation such as gene expression analysis and phylogenetic analyses will need to be made before reaching to this conclusion.

Phylogenetic tree analysis of a set of 63 GH16 proteins from various species revealed that all *Crh-like* genes belonged to a fungal specific sub-group and within this, two distinct clades emerge: the Crh1 clade and the Utr2/Crr1 clade. The latter clade is exclusive for the orthologues of *S. cerevisiae Utr2* and *Crr1* genes, sharing an additional chitin binding domain at the N-terminus, and exist as a single copy per species. On the contrary, the former is exclusive to orthologues of the *S. cerevisiae Crh1* gene with gene expansion events leading to multiple copies of *Crh1* observed in the filamentous group of fungi.

Gene expression section

This work also identified an optimum set of internal reference genes for studying gene expression across the life-cycle of *M. oryzae* using qRT-PCR. Further work is required to expand this gene-set to cover a broader range of growth conditions. Notwithstanding, this robust approach sets a high standard of practice for qRT-PCR gene analysis which can only increase an understanding of this devastating rice pathogen.

Using these validated set of housekeeping genes, the expression profile of *M. oryzae Crh-like* genes was examined under various growth conditions and stages of the life cycle and resulted in a diversity of expression. *MGG_Crh2* and *MGG_Utr2* are the most highly expressed genes, both regulated by the cell wall integrity pathway and expression is highest during vegetative growth. *MGG_Utr2* is the only gene that responded to caffeine stress while *MGG_Crh1* showed no response to any of the stressors imposed and is variably regulated during infection.

Selection of putative M. oryzae Crh-like genes for downstream analysis

Characterizing each of the five putative genes through the generation of single and combinatory double knockout mutant lines, followed by phenotyping and the generation of re-integrated lines would prove too laborious and time consuming. As such, listed are putative *M. oryzae Crh-like* genes in order of priority for upcoming work in subsequent chapters

1. *MGG_Crh2* (syn. *MGG_00592)*

While reciprocal BLASTp of *S. cerevisiae Crh1* against *M. oryzae* genome did not give this gene as the best hit, it is shown to have all the characteristics of a CWP (GPI-anchored, Ser/Thr region and Signal Peptide site) suggesting that this may be a functional gene. Gene expression analysis showed this gene to be the most highly expressed with statistically significant regulatory response once the fungus is under cell wall stress. Results above indicate that this gene is likely to be the most important gene for cell wall integrity compared with the rest of the *Crh-like M. oryzae* genes. This gene warrants further characterization

2. *MGG_Utr2* (syn. *MGG_01134*)

Phylogenetic analysis suggests that this gene warrants further investigation given that it belongs to a separate clade, and only one copy of the *M. oryzae MGG_Utr2* gene lies within this clade. Furthermore, it also has all the characteristics of a functional CWP (GPI-anchored, Ser/Thr region and Signal Peptide site). Not surprisingly, gene expression analysis showed this gene to be the second most highly expressed after *MGG_Crh2*, with responses seen in both cell wall and caffeine stress. Given the above points, it is an obvious gene to prioritise for single knockout mutant generation and to explore the possibility of generating a

double knockout mutant with *MGG_Crh2*, along with further protein localisation studies.

3. *MGG_Crh1* (syn. *MGG_09918*)

Surprisingly, despite being the best hit for *S. cerevisiae Crh1* gene and having all the characteristics of a CWP, qRT-PCR expression analysis showed this gene to be poorly expressed with no response to any external stressors. While there may seem to be a temporal response during infection, the expression level captured by qRT-PCR is relatively low. Nonetheless, this gene will be included as a candidate for single knockout mutant transformation work

4. *MGG_Crh3* and *MGG_Crh4*

Both genes are the least important for subsequent analysis for three key reasons. Both are not predicted to be GPI-anchored, giving doubts as to whether these genes play a direct role at the cell wall. This suspicion is further supported by the doubling in amino acid size of the *MGG_Crh3* and the low expression levels (above 25 ct) when analysed by qRT-PCR in *MGG_Crh3* and absence of *MGG_Crh4* transcript in Soanes *et al.* (2012).

In conclusion, three *M. oryzae* genes were carefully selected and justified to be the most likely genes important for cell wall integrity. With this, a decision was made to choose *MGG_Utr2, MGG_Crh1,* and *MGG_Crh2* for further investigation, starting first with the generation of single and double gene knockout lines as described in the next Chapter

CHAPTER 4

Generation of Knockout

&

Revertant Strains

4.1 Chapter Introduction

In Chapter 3, five *M. oryzae Crh-like* genes were identified: *MGG_Utr2, MGG_Crh1, MGG_Crh2, MGG_Crh3,* and *MGG_Crh4* (orthologs of *S. cerevisiae Utr2* and *Crh1* genes). These genes were then subjected to various bioinformatics analyses as well as gene expression profiling. Based on the results obtained, three genes were chosen for subsequent generation of single and double gene knockout strains by targeted homologous recombination. These are genes *MGG_Crh1, MGG_Crh2,* and *MGG_Utr2*.

The use of molecular genetics to investigate gene function via mutation work is not complete without a revertant strain. Here, a strain that exhibits mutant phenotype with a mutant genotype requires reverse mutation through a second alteration of the mutant genome, resulting in a wild type phenotype (Michels 2002). This is achieved by re-introducing a functional gene that is nulled or deleted and is an important step to be able to confidently relate mutant phenotype to the function of the targeted gene.

This Chapter will describe in detail the methodology and strategy executed to generate mutant and revertant lines. This will include construction of PCR deletion cassette for transformation by targeted homologous recombination followed by methods used (PCR and Southern Blot) to confirm candidate knockout strains. Once nulled strains were generated, the chapter will proceed to describe the construction of plasmids containing native promoter and coding regions of the targeted gene with or without a fluorescently tagged protein. These will then be transformed ectopically into the genome of the single gene knockout strains, confirmed by PCR and phenotypic assays.

4.1.1 Functional Gene Studies in Fungi by Reverse Genetics

The rapid increase of sequenced fungal genomes, coupled with advances in gene silencing and genetic tractability, lead to an increase in the study of gene function by reverse genetics. In reverse genetics, the aim is to discover the role of a gene of known DNA sequence by manipulating the coded sequence and analysing the phenotypic effects as a result of these genetic alterations. There are multiple technologies available to achieve the absence or non-functioning of these targeted genes either directly (targeted gene knock-out), or indirectly by disrupting transcription and/or translation processes (knockdown) (Weld *et al.* 2006).

4.1.2 Reverse Genetics: Knockdown or Knock-out?

There are numerous technologies available to enable a reverse genetics approach to functional gene analysis. One such method is RNA Interference (RNAi), a downstream transcription application that can target and degrade transcribed mRNAs. This tool is particularly advantageous for genes with multiple copies as, providing they are identical, it can be used to target the degradation of all gene copies (Kadotani *et al.* 2003). There are however, several problematic issues including off-target effect and variation in silencing level (Nguyen *et al.* 2008, Nakayashi *et al.* 205). Perhaps the most important disadvantage of RNAi, is the inability to conduct strain recovery and attribute with confidence, the phenotype seen, to the gene silenced (Nakayashiki *et al.* 2005). This is where targeted gene knock-out is the preferred method not only because it will completely eliminate a locus specific gene and the expression, but also allow recovery of the phenotype by re-introduction of a functional gene to the mutant

genome. Any noted alterations in the organism's phenotype can then be attributed directly to the loss of function of the gene of interest.

In this study, for reasons described above, the use of targeted gene mutation through the introduction of an artificial construct by homologous recombination was deemed the more appropriate strategy for this project, as opposed to RNAi.

4.1.3 Targeted Transformation by Homologous Recombination

Homologous Recombination (HR) is the exchange of DNA between homologous sequences. It is an ubiquitous occurrence, conserved across multiple Kingdoms and play a crucial role in genetic diversity (meiotic chromosomal cross-over) and for DNA double-strand break (DSB) repair (Shinohara and Ogawa 1995). Given that this mechanism is highly conserved across Kingdoms, the yeast *S. cerevisiae* was the model organism used since the last decade to understand better the processes involved in homologous recombination in DNA repair. This led to the subsequent application in targeted gene knock-out mutation (Szostak *et al.* 1983, Pâques and Haber 1999, Pastink *et al.* 2001, Aylon and Kupiec 2004).

In targeted gene knock-out by homologous recombination, a specific gene within a specified location in the genome is replaced with the exogenous genetic material. This is achieved by designing a deletion cassette containing a selectable antibiotic marker flanked at both 3' and 5' end with sequences identical to regions flanking the targeted gene. The aim of this application is to 'trick' the cell to utilise the the DSB repair system to replace the endogenous gene with this introducted deletion cassette (Mortensen 2006). The deletion cassette can be a

linear PCR product or a linearised vector, inserted into the cell by various methods including electroporation, *Agrobacterium* sp. or direct PEG-mediated protoplast insertion (Lacroix *et al.* 2006, Meyer 2008). The specific mechanism involving this replacement is still not well-understood and can only be theorised that when the organism's DNA DSB mechanism recognises the flanking homologous segments at both ends, the whole cassette including the selectable marker is exchanged with the native functional gene through a double-cross over of homologous recombination.

In filamentous fungi, the DSB repair mechanism favors the non-homologous end-joining (NHEJ) pathway with HR occurring at a lower rate (Krappmann 2007). This means that this application will lead to lower success rate and higher false positives (ectopic insertions elsewhere) as opposed to the same technique in yeasts. Given the mentioned problem, the best strategy for this project is to compensate the low success rate by simply increasing the number of transformation conducted, and candidates screened. Large scale transformation will need to be conducted to compensate for the low success rate. Stringent mutant selection and confirmation involving both PCR and Southern Blot will need to be conducted to avoid choosing a false positive (i.e. mutants with non-targeted ectopic insertion of the deletion construct). This will ensure that any phenotype observed can be confidently attributed to the loss of *Crh*-like genes.

4.2 Experimental Aims & Objectives

Work described in this chapter aimed to:

(a) Generate three single deleted mutants with Wild Type strain Guy11 as the background genotype, for genes *MGG_Utr2*, *MGG_Crh1,* and *MGG_Crh2*.

(b) The generation of double gene knockout strain *MGG_Crh2_Utr2* using the generated single nulled gene mutant *ΔMGG_Crh2* as the background strain.

(c) Generation of revertant strains showing phenotype recovery for mutant lines *MGG_Crh2* line 39 and *MGG_Utr2* line 2 by:

1. Construction of two vectors each containing promoter and coding region for the functional protein Crh2p or Utr2p
2. Construction of two fluorescently tagged protein vectors for each gene *MGG_Utr2* and *MGG_Crh2*

4.3 Materials & Methods

4.3.1 Generation of Deletant Strains

4.3.1.1 Media, Solutions & Chemical Reagents Used

Listed in Table 4.1 below, all media, solutions, and compounds used for the PEG-mediated transformation of PCR knockout cassette into *M. oryzae* protoplast for the generation of single and double knockout mutant strains.

Table 4.1. List of Media, Solutions and Reagents Used in Routine *Magnaporthe oryzae* Transformation

Solution	Composition
Depurination solution	11 ml concentrated HCl, 989 ml ddH_2O. Autoclaved.
Denaturation solution	1.5 M NaCl, 0.5 M NaOH, 800 ml ddH_2O pH adjusted to 7.5 with concentrated HCl and made up to 1 litre with ddH_2O. Autoclaved.
Neutralisation buffer	1.5 M NaCl, 0.5 M Trizma® base, 800 ml ddH_2O, pH adjusted to 7.5 with concentrated HCl and made up to 1 litre with ddH_2O. Autoclaved.
20x SCC Buffer	3 M NaCl, 0.3 M Tri-Sodium citrate, pH 7.0 with NaOH, made up to 2 l with ddH_2O. Autoclaved.
OM lysis buffer	2.5 M $MgSO_4$, 1ml Na_2HPO_4 (1M), 1.3g Lysing Enzymes from *Trichoderma harzianum* (Sigma-Aldrich), pH 5.8 with NaH_2PO_4 and volume adjusted to 100ml with ddH_2O. Filter sterilised.
ST Buffer	0.6 M Sorbitol, 0.1 M Tris-HCl pH 7.0. in 1 litre ddH_2O. Autoclave.
STC Buffer	1.2 M Sorbitol, 10 mM Tris-HCl pH 7.5,10 mM $CaCl_2$ in 1 litre ddH_2O. Autoclaved.
PTC Buffer	60 g PEG 4000, 1 ml Tris-HCl (1 M) pH 7.5, 1 ml $CaCl_2$ (1 M), ddH_2O adjusted to 100 ml and then filter sterilised.
OCM bottom agar	273.84 g D-sucrose, 10% D-glucose, 2% Peptone, 1% yeast extract, 1% Casamino acids, 50 ml 20x Nitrate salts, 1.0 ml trace elements, 1.0 ml vitamin solution, pH 6.5 with 5 M NaOH, add ddH_2O to 1 litre, and finally 1.5% agar added. Autoclaved
Defined Complex Medium (DCM)	1.7% yeast nitrogen base without amino acids, 2% L-Asparagine, 1% Ammonium nitrate, 10% D-glucose, pH 6.0 with Na_2HPO_4 and dH_2O added up to 1 Litre with 1% agar added. Autoclaved.
Hygromycin B (Hygromycin) 450 units/mg	Calbiochem® Hygromycin B, purified from *Streptomyces* sp. Manufactured by EMD Millipore, Merck KgaA, Darmstadt, Germany, 2014. www.emdmillipore.com
Bialaphos (BAR) 10 mg/ml	Gold Biotechnology (GoldBio), USA. www.goldbio.com

dCTP, [α-32P]-3000Ci/mmol 10mCi/ml Lead	Perkin Elmer, 940 Winter Street, Waltham, Massachusetts 02451, USA.

4.3.1.2 Primers Used in the Generation of Deletant Mutants.

Primer design as described in Chapter 2 (Section 2.2.2.2). Name, sequence and resulting PCR product size used for the generation of deletion cassettes listed in Table 4.2. All primers synthesised by Sigma-Aldrich (United Kingdom).

Table 4.2. List of Primers Designed for the Amplification of Deletion Cassette and Mutant Confirmation by PCR Integration.

Primer	Sequence	Product size (kb)
1. Utr2_hyg deletion cassette		
#1_Utr2	TAAGTTGCTGAAGCAGGGTAG	1.44
#2_Utr2 (Hyg overhang underlined)	CTTCAATATCAGTTAACGTCGACGCAGGGCAGC AGCGCCTATCG	
#3_Hyg_F	GTCGACGTTAACTGATATTG	1.43
#4_Hyg_R	GTCGACGTTAACTGGTTCC	
#5_Utr2 (Hyg overhang underlined)	GACCGGGAACCAGTTAACGTCGACGCAGCGCT TTCGCCGTTG	0.98
#6_Utr2	CCTTCGTTTCTGGCCGTG	
Integration Utr2_i1.2F	CGACAGAAGACCGACAGAC	2.70
Integration Utr2_i1.2R	GTGCACCAAGCAGCAGATG	
Integration Utr2_i1.4F	GTCGGGCGTACACAAATC	1.52
Integration Utr2_i1.4R	GAATGGTACGGAAATGGAG	
Conf_Utr2_F	TGCTGTGGTCGTAAGTCTGC	0.79
Conf_Utr2_R	CTCCGACCTCTTCTTTGTGC	
2. Crh1_Hyg deletion cassette		
#1_Crh1	ATGCCAAACCCGTACATTTCC	1.13
#2_Crh1 (Hyg overhang underlined)	CTTCAATATCAGTTAACGTCGACAAGCACCCTC GCAATACACC	
#3_Hyg_F	-same as above-	
#4_Hyg_R	-same as above-	
#5_Crh1 (Hyg overhang underlined)	GACCGGGAACCAGTTAACGTCGACCGAGATTT GTATTCTTTGAGC	0.84
#6_Crh1	CTTCTGCGCACTCACTTCAGC	
Crh1_i1_F	GTTTGCGATGATTACAACG	1.51
Crh1_i1_R	GCCTGGACGACTAAACC	

Crh1_i2_F	GTCGGGCGTACACAAATC	1.08
Crh1_i2_R	TACACTTCGTCTCCTCTGC	
Conf_Crh1_F	ACGAGTGAGTTCACCCATCC	0.49
Conf_Crh1_R	CTTGTGAAATCCGTCCTGG	
3. Crh2_Hyg deletion cassette		
#1_Crh2	TGGCTTACCTGCGTTATG	1.21
#2_Crh2 (Hyg overhang underlined)	CTTCAATATCAGTTAACGTCGACATATAGCCGC CATTATATC	
#3_Hyg	-same as above-	1.43
#4_Hyg	-same as above-	
#5_Crh2 (Hyg overhang underlined)	GACCGGGAACCAGTTAACGTCGACCAGCAAAT CAATCAATCAAC	1.15
#6_Crh2	AGGCTCACACTTCTGCTC	
Crh2_i1_F	CCCTTCGCACATTATGGAG	1.28
Crh2_i1_R	GCACCAAGCAGCAGATG	
Crh2_i2_F	GTCGGGCGTACACAAATC	1.55
Crh2_i2_R	GAGGAGTCGGACAAGGATG	
Conf_Crh2_F	TGCGTGTCCAGAGCAACTAC	0.45
Conf_Crh2_R	ATCCTTGCTGCTGTTGTCC	
4. Utr2_BAR deletion cassette		
#1_Utr2_dko	CAGGGTAGCATAGGTAGTTAGGTTCG	1.41
#2_Utr2_dko (BAR overhang underlined)	CAATATCATCTTCTGTCGACCTTCATTATGAGTA TTGTGGTGG	
#3_Bar_F	GTCGACAGAAGATGATATTGAAGGAGC	0.95
#4_Bar_R	GTCGACCTAAATCTCGGTGACG	
#5_Utr2_dko (BAR overhang underlined)	GTCACCGAGATTTAGGTCGACGCAGCGCTTTC GCCGTTG	0.96
#6_Utr2_dko	CCTTCGTTTCTGGCCGTG	
Utr2_dko_i1.2_F	CGACAGAAGACCGACAGAC	2.48
Utr2_dko_i1.2_R	CCACTAGCTCCAGCCAAG	
Utr2_dko_i4_F	ATCGACCGTGTACGTCTC	1.66
Utr2_dko_i4_R	GAATGGTACGGAAATGGAG	
Conf_Utr2_F	-same as above-	0.79
Conf_Utr2_R	-same as above-	

4.3.1.3 Generation of Transformation PCR Cassettes

Transformation cassettes (deletion cassettes) were designed specific to the targeted genes, with WT gDNA as the template, constructed over a series of overlapping PCR using the high-fidelity enzyme *Herculase* II (refer Chapter 2 section 2.2.2.4). Each transformation cassette will have a selectable marker

(Hygromycin or Bialaphos) flanked by 0.5-2.0 kb long sequences identical to those flanking the targeted gene (Figure 4.1).

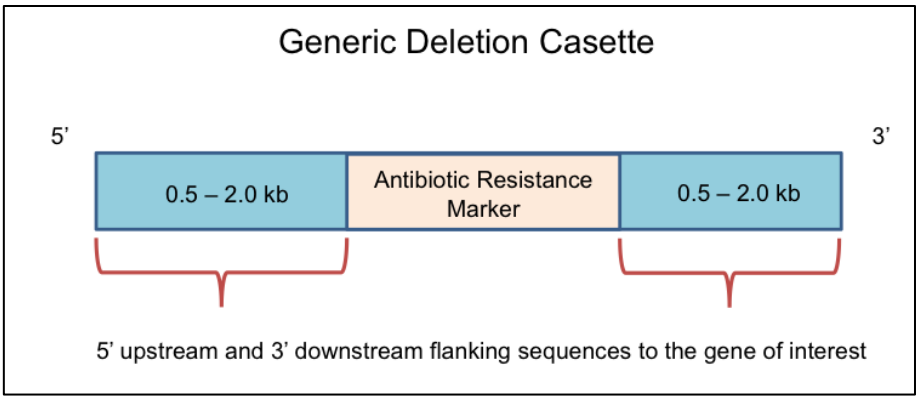

Figure 4.1. An Illustration of the Designed Deletion Cassette. Each deletion cassette comprises two flanking regions homologous to the upstream and downstream of targeted knockout gene with an antibiotic resistance marker in the middle. The flanking regions are typically between 0.5 kb to 2.0 kb depending on the distance of the next gene.

4.3.1.4 Fungal Transformation

4.3.1.4.1 Protoplast Generation

All centrifugation mentioned in this section were performed using Beckman-Coulter centrifuge at 4°C. The following procedure was conducted in a flow-hood under sterile conditions to prevent contamination of the fungal tissue prepared.

Spores were harvested as described in Chapter 2 (Section 2.2.1.2). Two hundred microliters of the spore suspension were pipetted into 300 ml sterile liquid CM in a 500 ml sterile conical flask. Three flasks were used per transformation. Streptomycin and Penicillin stock solution (50 µg/ml each) was added to the culture and incubated for 72 hours at 25°C, 150 rpm and in the dark to prevent bacterial cell growth and melanisation of mycelia.

Three-day-old un-melanised culture was collected by pouring all three conical flasks through a sterile funnel layered with sterile triple-layered Mira cloth (Merck) into a large flask. Mira cloth containing the mycelium was Blotted dry with sterile paper towels until most of the liquid CM was removed. With a sterile scalpel, the fungal tissue was divided into 3x50 ml falcon tubes. Fifty milliliters of filter sterilised OM buffer was then added to each falcon tube. The fungal tissue was carefully chopped into very small pieces in each of the falcon tube with a sterile scalpel, incubated for 4 hours at 30°C while shaking at 150 rpm. Once digested, the content from each falcon tube was split into 2x50 ml falcon tubes. Each falcon tube was gently overlayed with ice-cold ST buffer using sterile pipettes up to 50 ml mark and centrifuged for 5 minutes, 5000 rpm (5,588*g*). The thin, cream-colored band of protoplasts forming in the middle layer was carefully collected using sterile pipette into a new 50 ml falcon tube and gently overlayed with 10 ml ice-cold STC buffer. The falcon tube was subsequently centrifuged at 3,000 rpm (3,316*g*) for 10 minutes. Supernatant carefully decanted and protoplasts from 2 falcon tubes were combined and gently re-suspended in 10 ml ice-cold STC buffer and again centrifuged for 10 minutes at 3000 rpm (3,316*g*). The process was repeated once again, now combining protoplasts from remaining tubes into one 50 ml falcon tube with 10 ml cold STC buffer. The suspension was centrifuged at 3000 rpm (3,316*g*), for 10 minutes. Finally, the pelleted protoplasts were gently re-suspended in 5 ml ice-cold STC buffer. Protoplast concentration was determined using a haemocytometer (refer to Chapter 2) and diluted appropriately to a concentration of 50-100 x 10^4 protoplasts/ml.

4.3.1.4.2 PEG-Mediated Protoplast Transformation

In a sterile 1.5 ml Eppendorf tube, 150 µl of the protoplast suspension and 10 µl deletion cassette (5-10 µg DNA) were mixed and allowed to incubate to room temperature for a minimum 15 minutes, maximum 30 minutes (see illustration below in Figure 4.2). Filter-sterilised PEG solution was added at a quantity of 1 ml, followed by incubation for 15-20 minutes at room temperature. Following incubation, the PEG-protoplast suspension was added to 200 ml OCM agar (kept molten at 48°C) and poured thinly (1-3 mm thick) into 10 petri dishes (8.5 cm diameter). Plates were wrapped in aluminum foil and left for 16-24 hours at room temperature to allow protoplast regeneration before overlaying with 300 ml of MM agar (with 300 µg/ml Hygromycin B from Merck) or DCM agar (with 100 µg/ml Bialaphos from GoldBio). The type of antibiotic selectable marker used, depended on the resistance gene added into the deletion cassette. Plates were incubated in the dark (wrapped with aluminum foil) for 8-10 days at 24°C.

Fungal colonies that grew through the antibiotic-containing agar up to the surface, were selected for a second round of antibiotic selection. These selected colonies were inoculated onto small plates (5 cm diameter) containing MM (for Hygromycin) or DCM (for Bialaphos) with half the concentration of antibiotic marker used in the overlay. Wild Type Guy11 was used as the negative control for these plates. Colonies that grew (typically 30-60 colonies) on these plates, were then sub-cultured onto CM agar for 10 days for gDNA extraction and subsequent mutant confirmation by PCR and Southern Blot.

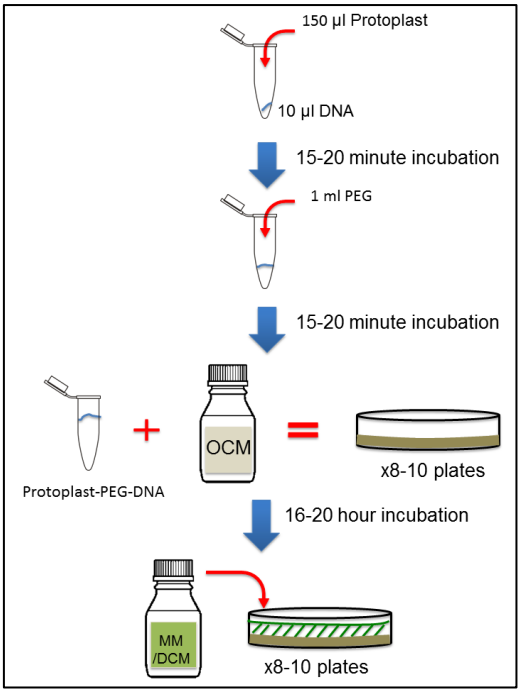

Figure 4.2. Flow Chart Describing PEG-Mediated Protoplast Transformation Steps. In the first step, DNA and protoplast were mixed and incubated in an Eppendorf tube for 15-20 minutes, followed by the addition of PEG with another 15-20 minutes incubation. This mixture was then pipetted into molten OCM agar, thoroughly mixed and poured into petri dishes (8.5 cm diameter sized plates). The OCM agar plates were then left at room temperature in the dark for 16 hours to allow protoplast regeneration, before overlaying with MM or DCM containing the appropriate selectable marker.Candidate Mutant Confirmation

Genomic DNA Isolation

Mycelium from 10 day old candidate mutant line grown on the surface of the CM agar was scraped with a sterile scalpel and immediately added into mortar filled with liquid nitrogen. The frozen sample was grounded into powder and without thawing, the sample was immediately transferred into liquid nitrogen dipped-Eppendorf tubes (1.5 ml). The protocol from Qiagen DNeasy Kit was subsequently followed. The sample was finally eluted in 50 µl sterile MilliQ-H_2O and concentration measured using the NanoDrop instrument (ND-1000). If gDNA concentration was less than 90-110 ng/µl, ethanol precipitation was conducted as described in Chapter 2 (section 2.2.2.1). If concentration was higher than the range indicated, it was diluted appropriately with ddH_2O.

Confirmation of Insert Location by PCR Integration

The appropriate primer pairs (see table 4.8) and the corresponding annealing temperature (Tm – 5°C) were used. Refer to Chapter 2 for routine PCR and product size separation by gel electrophoresis protocol (sections 2.2.2.3 and 2.2.2.6 respectively).

Confirmation for Absence of Non-target Insertion by Southern Blot

The freely available program pDraw 4.2 (www.acaclone.com) was used to predict restriction enzyme sites. Genomic DNA sequence containing the transformed target site and 1 kb region flanking both 5' and 3' of insert was uploaded into pDraw 4.2. One restriction enzyme was selected with cut sites flanking the inserted cassette (but not within the cassette) producing a fragment between 3-6 kb (Figure 4.3).

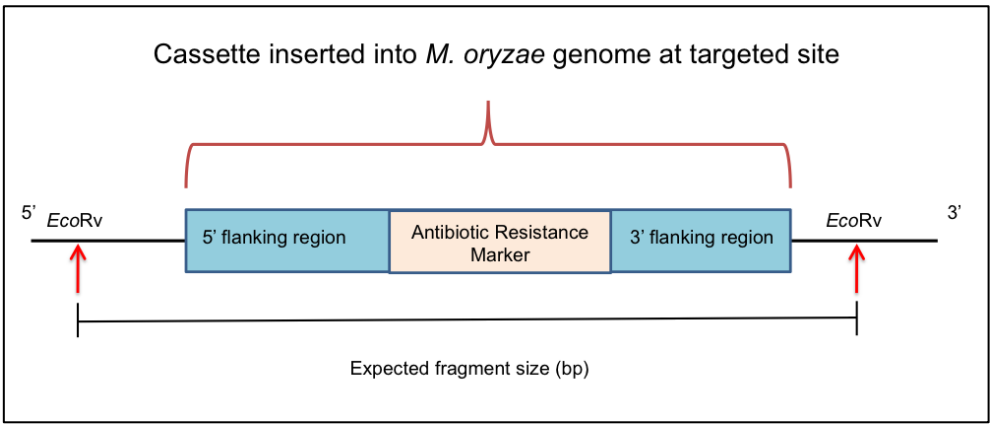

Figure 4.3. An Illustration of a Restriction Digest Strategy. This is an important step for subsequent reliable southern blot mutant confirmation.

The gDNA of candidate mutant lines were then digested with the selected restriction enzyme, with Wild Type Guy11 as the negative control. Digestion components were described on table below:

Reagent	Amount (µl)
gDNA	42.0 (giving 2-4 µg total DNA)
Restriction enzyme buffer	5.0
Restriction enzyme	3.0
Total	**50.0**

Samples were digested for 16 hours according to manufacturer's protocol and based on the type of enzyme used. All 50 µl of sample reaction was loaded with 5 µl loading dye, into a 0.8% agarose gel, including 12 µl of GeneRuler™ 1 kb DNA Ladder, pre-mixed with ethidium bromide (7:3). The gel was run for 10-16 hours at 20 mV. A gel picture was taken at this stage to show that DNA was successfully digested and size distributed along 2/3 of the gel. A ruler was added beside the well containing the GeneRuler™ 1 kb DNA Ladder, measuring from the bottom of the gel. This is to allow band size determination by measuring the distance of known band size when a film was later developed. The gel was then washed in a series of buffers while shaking (150 rpm) at room temperature, according to the table below:

Reagent	Time
1. Depurination buffer	20 mins
2. Denaturation buffer	30-60 mins (Loading dye turns yellow)
3. Neutralisation buffer	30-60 mins (Loading dye turns blue)

Southern Blot

Size distributed DNA in agarose gel was transferred onto a nylon Hybond N+ membrane (Amersham) by building a capillary transfer tower as shown in Figure 4.4 and described in Sambrook and Russell (2001). The tower was allowed to stand for a minimum of 12 hours to allow all Blot tissues to be fully soaked. The membrane was then UV cross-linked for 60 seconds using a cross-linker (Stratagene UV Stratalinker 2400). The membrane was then inserted into a 15 cm long hybridisation glass bottle (Wheaton by Thermo Fisher). Ten millilitres of 'Perfect Hyb^{TM} Plus Hybridisation Buffer' (Sigma-Aldrich) was slowly added into the glass bottle to ensure no air pockets forming between the membrane and wall of the glass bottle. The membrane was pre-hybridised for 1 hour at 65°C in a rotating oven.

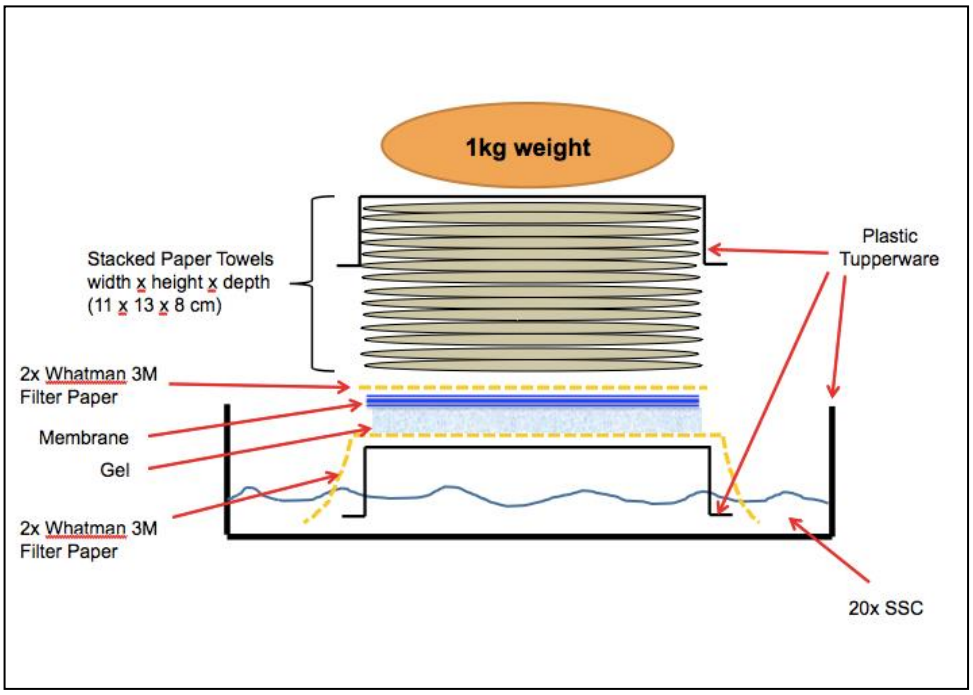

Figure 4.4. An Illustration for the Construction of a Capillary Transfer Tower. A double layered Whatman 3M filter paper was used as the wick, submerged in 20x SCC buffer. Gel placed upside down on the wick, and a nylon Hybond N+ membrane (Amersham) cut to the size of the gel was placed on top. This was followed by subsequent layers of Blot paper towels placed on top as shown in image.

Probe Labelling and Hybridisation

Depending on the type of selectable marker used in the deletion cassette, Hygromycin or Bialaphos probe was prepared by PCR amplification of the respective resistance marker gene using *Herculase* II enzyme according to the methods described in Chapter 2 (section 2.2.2.4). The PCR product was cleaned using QIAquick PCR Purification Kit (Qiagen) following the manufacturer's protocol and purity checked by gel electrophoresis. The concentration of probe DNA was measured using the NanoDrop instrument (ND-1000) and adjusted accordingly to 25-50 ng/µl. Purified probes were stored in -20°C and used within 1-3 days of product amplification.

'Amersham Readiprimer II DNA Labelling System' (GE Healthcare) probe labeling kit was used, and manufacturer's protocol followed. One microlitre of

probe DNA (Hygromycin or Bialaphos) prepared above was added to 44 µl TE Buffer in a 1.5 ml sterile Eppendorf tube and boiled for 10 minutes. The denatured probe was immediately cooled on ice for 5-10 minutes and centrifuged for 10 seconds using a conventional tabletop centrifuge at 3,500 rpm (1,164*g*) to collect any condensed moisture back to the bottom of the tube.

The following procedure was conducted behind a Perspex screen in a designated radiation work area. To one tube of 'Readiprime II' enzyme mix supplied by the manufacturer, 45 µl of the denatured probe and five µl α^{32}P dCTP (Perkin Elmer) was added and mixed by pipetting. The sample was incubated for 1 hour at 37°C in a heat block covered with a lead hat, followed by another quick spin at 3,500 rpm (1,164*g*) to collect any condensed moisture back to the bottom of the tube. The radio-labelled probe was then pre-mixed with 50 µl dextran blue (50 mg/ml) and purified from unincorporated nucleotides by size separation using the 'illustra NICK Columns' (GE Healthcare) according to the manufacturer's protocol. The column was first pre-washed with 3 ml TE buffer followed by the addition of 1 ml probe-dextran mixture and another gradual addition of 1-2 ml TE buffer into the middle of the column as the product is separating to ensure a continuous flow down the column. Only blue TE buffer (containing stained probe) was collected from the bottom of the column in a total volume of 1 ml. The collected probe was then boiled for 10 minutes at 100°C and flash cooled on ice for 5 minutes. The sample was briefly centrifuged for 10 seconds at 3,500 rpm (1,164*g*) and 1 ml pipetted into the hybridisation tube containing pre-hydridised membrane. Labelling was allowed to occur overnight (16 hours) in a rotating oven at 65°C. Following overnight hybridisation, the probe was discarded and the membrane was washed in a series of descending SSC concentrations as detailed in table:

Washing solutions (50 ml)	Time (minutes)
2x SSC with 0.1% SDS	30 minutes (repeat 2x)
1x SSC with 0.1% SDS	20 minutes
0.1x SSC with 0.1% SDS	20 minutes (repeat 2x)

Once washed, the membrane was air-dried and brought to a darkroom whereby it was placed into a lead cassette containing 'Amersham Hyperfilm MP' (Amersham) film. Using a black marker, the corners of the membrane were marked onto the film for later measurement. The cassette was left in -80°C for 24 hours. The film was developed in the dark using 'Carestream® Kodak® autoradiography GBX' developer and fixer (Sigma-Aldrich). A ruler was then placed at the bottom of the traced marker corresponding to the bottom part of the membrane, to allow band size determination when compared to the gel picture taken earlier with the same ruler.

4.3.1.4.4 Absence of Transcript Validation by qRT-PCR in Mutants

Tissue Sample Preparation

Five fungal strains, comprising of one WT and four knockout strains Δ*MGG_Crh1* (line 36)*,* Δ*MGG_Utr2* (line 2)*,* Δ*MGG_Crh2* (line 39) and ΔΔ*MGG_Crh2_Utr2* (line 25) were grown vegetatively in liquid CM as described in Chapter 6. The methodology for RNA extraction and cDNA synthesis are as described in Chapter 2 (section 2.2.2.3 and 2.2.2.4 respectively). Primers used in this section are as listed in Table 3.3 in Chapter 3 and the sequence, efficiency and amplicon size listed in Appendix A.6. The qRT-PCR reagent and thermal-cycling are as described in Chapter 2 (section 2.2.2.1).

qRT-PCR Experimental Design

The cDNA of five fungal samples, each amplifying six genes, could not fit into one 96-well plate (plate size of the qRT-PCR instrument used). Due to this, each 96-well plate was designed to be an independent assay, within which is sufficient to compare the expression of the target gene in the knockout strain, relative to the expression of the gene in WT(Illustration in Appendix B.1). Within each 96-well plate, the average cycle threshold (ct) value from two technical replicates was calculated for each gene, giving three sets (from three biological replicates) of ct values for each gene in each sample type (WT or knockout strain). A Student's t-test was conducted at $p<0.001$, by comparing the ct values of gene in WT against the knockout strain, data treated as a one-tailed distribution with two-sample of equal variance (homoscedastic).

4.3.2 Generation of Revertant Strains

All solutions used in this section were prepared as described in Table 4.3 below.

Table 4.3. List of Reagents and Solutions Used for Cloning Work.

Reagent	Composition
SOB Medium	2% (w/v) Tryptone, 5% (w/v) yeast extract, 10 mM NaCl (Mw: 58.44), 2.5 mM KCL (Mw: 74.55), pH 7.5 with 1 M NaOH, MilliQ-H_2O up to 1 Litre and autoclaved. Filter sterilised 1 M $MgCl_2$ was added to a final concentration of 10 mM.
SOC Broth	10 ml filter sterilised 2 M D-Glucose (Mw: 180.16), filled up to 1 Litre with the autoclaved SOB medium above. Broth preparation made under sterile conditions.
TB Solution	10 mM PIPES (Mw: 302.4), 15 mM $CaCl_2.H_2O$, 250 mM KCL (Mw: 74.55), pH 6.7 with 1M KOH. After pH was adjusted, 55 mM $MnCl_2.4H_2O$ (Mw: 197.91) was added and MilliQ-H_2O filled up to 1 Litre. Solution filter sterilised and stored at 4^oC indefinitely.
5M NaCl	29.2 g NaCl in 100 mL ddH_2O, autoclaved.
Luria-Bertani Broth (LB)	10 g NaCl, 10% (w/v) Bacto-tryptone, 5% (w/v) yeast extract, pH 7.0 with 1M NaOH, MilliQ-H_2O added up to 1 Litre and autoclaved.
Luria-Bertani Agar (LBA)	Same as above, with 1.5% agar (w/v)
Dimethyl Sulfoxide (DMSO)	Sigma-Aldrich (Mw: 78.13)

4.3.2.1 Genotypes and Strains Used

Magnaporthe oryzae strain Guy 11 (WT) gDNA was used as a template for PCR amplification of genes *MGG_Crh2* and *MGG_Utr2*. Vectors constructed were introduced into the genome of either *ΔMGG_CRH2* line 39 or *ΔMGG_Utr2* line 2 by ectopic insertion. Fungal strains were routinely grown as described in Chapter 2. For cloning work involving multiplication of plasmid vectors, *Escherichia coli* DH5α was used. These are super competent cells genotype FΦ80*lacZ*ΔM15, Δ(*lac*ZYA-*arg*F), U169, *rec*A1, *end*A1, *hsd*R17(R_k^-, m_k^+), *pho*A, *sup*E44, *thi*-1, *gyr*A96, *rel*A1, *ton*A originally developed by Woodcock *et al.*(1989)

4.3.2.2 Native Vectors Used:

Vector pUCAP (1-1) was obtained from a current member of the laboratory, Dr. Marketa Samalova. This vector contains the nucleotide sequence coding for Bialaphos (BAR) resistance gene, multiple cloning sites (MCS), ampicillin antibiotic resistance, poly A sequence and pUCAP (1-1) sequence. See Figure 4.5 for a visual description.

Vector pUCAP (3-2) has the same nucleotide sequences as vector (1-1) described above. However, the BAR resistance gene is reversed (Figure 4.5).

Before proceeding with cloning work, a series of restriction enzyme digestions were executed based on the nucleotide sequence of pUCAP. This is to ensure that the vector described have no unexpected additional fragments. In total, eight digestion reactions were conducted in separate reactions, for each vector. These were six single digests (*Asc*I, *Sbf*I, *Sal*I, *BamH*I, *Swa*I and *Pvu*II) and two double digests (*BamH*I with *Asc*I and *BamH*I with *Kpn*I). For the control, no enzyme was added to the reaction, resulting in undigested vectors. Each enzyme digestion was conducted according to the manufacturer's protocol (NEB) and using the reagents listed in table below.

Table 4.4. Reagents Used for Restriction Enzyme Digest (Vector Validation).

Reagent	Amount (µl)
Vector	2.5
Restriction enzyme buffer*	1.5
Restriction enzyme	0.35 each
Bovine Serum Albumin (BSA)	0.3
Water (H_2O)	Up to 15.0
Total volume	**15.0**

* Buffer used: Cutsmart, NEB 1, NEB 2 or NEB 3 depending on the enzyme used. If two different buffers were needed for a pair of enzymes, then a sequential digestion was conducted. Here, enzyme and buffer with the lower salt content was used first, followed by the addition of enzyme and buffer with higher salt content, as per manufacturer's instructions.

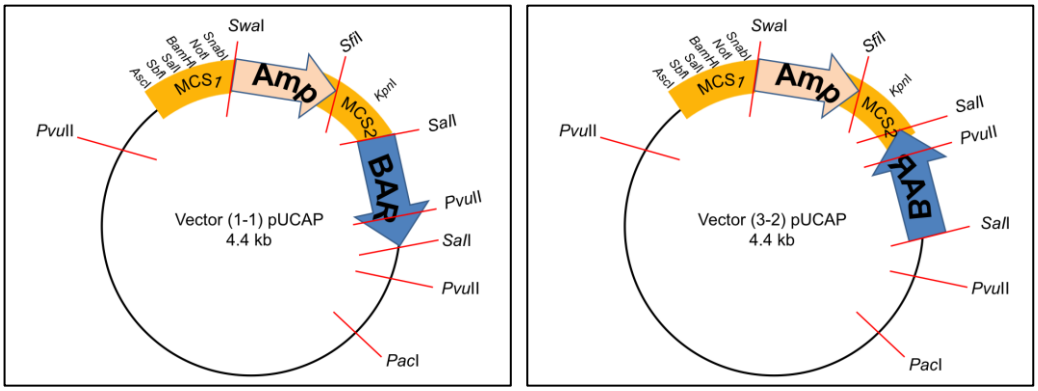

Figure 4.5. Visual Illustration of the Components and Restriction Enzyme Sites of pUCAP Vectors (1-1) and (3-2). Both vectors were used simultaneously for each cloning reaction, and depending on the ligation success rate, one vector with the correct insert were selected for downstream transformation into mutant *M. oryzae* lines.

4.3.2.3 Cloning: Vector Amplification & Extraction

A single *Escherichia coli* colony containing the desired vector was picked using a sterile toothpick, inoculated into 3 ml LB broth containing ampicillin (100 µg/ml ampicillin) and further incubated for 12-16 hr, at 37°C with shaking at 160 rpm. Cultures were centrifuged for 3 minutes at 4,500 rpm (4,974*g*) (Beckman-Coulter Centrifuge) at room temperature, the supernatant discarded and vector extracted from the pellet using Qiagen QIAprep Spin Miniprep Kit according to the manufacturer's protocols.

4.3.2.4 Insert Design & Preparation

A DNA insert containing both the promoter and coding region for *MGG_Crh2* was prepared by overlapping PCR from two fragments, with the introduction of a restriction enzyme *EcoR*V site after the predicted signal peptide cleavage site, and two restriction enzyme cut sites flanking each DNA insert (Figure 4.6). Similarly, a DNA insert for the *MGG_Utr2* gene was prepared as above. The signal peptide cleavage site was predicted for genes *MGG_Utr2* and *MGG_Crh2* as described in Chapter 3. The cleavage site for *MGG_Utr2* was predicted to be between amino acids 21 and 22, For *MGG_Crh2,* between amino acids 20 and 21. The enhanced Green Fluorescent Protein (eGFP) (Cinelli *et al.* 2000) and mCherry (Shaner *et al.* 2004) PCR fragments were amplified from previously designed plasmid from vector pUCAP (1-1) containing the gene sequence of either gene. Primer sequences were designed as described in next paragraph, to achieve an amplified eGFP and mCherry fragment with *EcoR*V sequence at both ends without the START and STOP codon sequence.

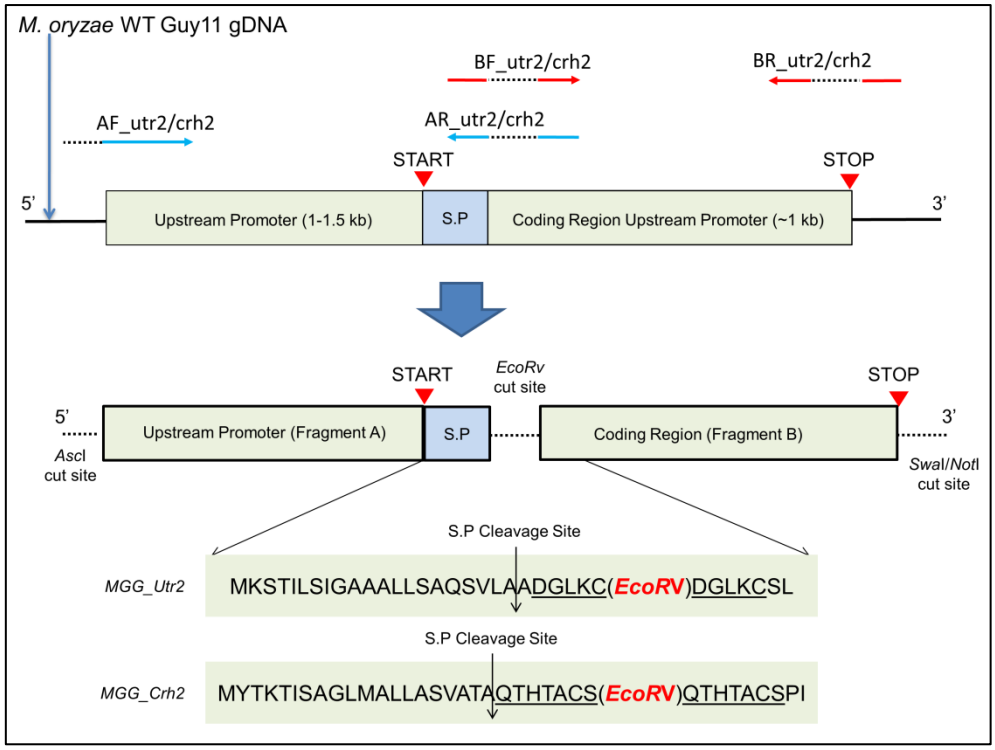

Figure 4.6. Genes *MGG_Utr2* and *MGG_Crh2* Insert Design by Overlapping PCR. Top image shows a theoretical location of genomic *M. oryzae* DNA where two sets of primers anneal and amplify two overlapping PCR fragments: a promoter region (Fragment A) and coding region (Fragment B) each sized between 1-1.5 kb with introduced restriction enzyme cut sites (dotted lines). Both fragments were then used as templates to generate one large PCR insert shown in the middle image. Here, the overlapping region contains an introduced *EcoR*V restriction enzyme cut site, and a restriction enzyme cut site (*Asc*I, *Swa*I or *Not*I) at both 5' and 3' ends. Bottom image show 34-36 amino acid sequence downstream from the START region for each PCR gene insert. Shown here the location where *EcoR*V cut site was introduced, which is 6 or 7 amino acid after the predicted signal peptide site for *MGG_Utr2* and *MGG_Crh2* PCR insert respectively, followed by repeating five to seven amino acid after the *EcoR*V site to ensure that the addition of this sequence causes not effect to protein function. Underlined amino acid sequence indicates the annealing site for overlapping primer pairs BF_Utr2 and AR_Utr2 as well as BF_Crh2 and AR_Crh2 respectively.

Each primer for the amplification of PCR promoter fragment A and PCR coding fragment B was designed containing 20-25 bp sequence complementary to the target insert at the 3' end of the primer sequence and the appropriate restriction enzyme sequence with four Adenines (AAAA) at the 5' end. The pDRAW32 tool (AcaClone software) freely downloaded from the website (www.acaclone.com) was used to select the appropriate restriction enzyme by checking for restriction

enzyme cut sites in both insert and vector sequences. The restriction enzymes chosen to flank the PCR gene insert (both Fragment A and B) for *MGG_Utr2* or *MGG_Crh2* is an enzyme with a restriction site found only in the Multiple Cloning Site 1 (MCS1) of vectors pUCAP (1-1) and (3-2) and not elsewhere in the insert fragment or vector. As such, these are *Asc*I and *Swa*I for *MGG_Utr2* PCR insert and *Asc*I and *Not*I for *MGG_Crh2* PCR insert. Restriction enzyme *EcoR*V cut sites flanking mCherry and eGFP were chosen on the basis that this enzyme does not cut elsewhere within the vector or gene insert.

PCR was conducted using the high fidelity enzyme *Herculase* II according to manufacturer's instructions and as described in Chapter 2 (section 2.2.2.4). The annealing temperature, cycling times and extension length were adjusted according to primer melting temperature and product length. Following amplification, product specificity was checked by gel electrophoresis, followed by DNA cleanup using the QIAquick PCR Purification Kit (Qiagen). If non-specific amplification occurred gel extraction was conducted using QIAquick Gel Extraction Kit (Qiagen) or PCR parameters adjusted until a single correct PCR product is obtained. Similarly, the DNA insert for *MGG_Utr2* was designed with the addition of an *Eco*RV site located after the predicted signal peptide cleavage site.

4.3.2.5 Insert & Vector Restriction Digest & Ligation

The following reaction conditions were used to digest vectors and DNA insert respectively before ligation. Restriction Enzyme buffers were used according to the manufacturer's protocol.

Table 4.5. Reagents Used for Routine Restriction Enzyme Digestion.

Reagent	Amount (µl)
DNA insert/Vector	40.0
Restriction enzyme buffer	10.0
Restriction enzyme	3.0
Bovine Serum Albumin (BSA)	2.0
Water (H_2O)	45.0
Total	**100.0**

Sample (a vector or DNA insert) was incubated for 10-16 hours at either 25°C or 37°C (depending on enzyme type), and heat-inactivated according to the manufacturer's protocol (New England Biolabs). If the sample was a vector, after digestion it was immediately de-phosphorylated to prevent re-ligation of digested ends, using Calf Intestinal Alkaline Phosphatase (CIP) by New England Biolabs and the below conditions:

Digested vector with sticky ends		
Step 1	37°C for 30 minutes	1.0 µl CIP
Step 2	37°C for 30 minutes	1.0 µl CIP
Digested vector with blunt ends		
Step 1	37°C for 15 minutes	1.0 µl CIP
Step 2	55°C for 45 minutes	1.0 µl CIP

Sample (digested DNA insert or vector) was then cleaned and precipitated using Phenol:Chloroform:Isoamyl Alcohol 25:24:1 saturated with 10 mM Tris (pH 8.0). This involved adding 100 µl sterile MilliQ-H_2O to 100 µl of sample reaction followed by the addition of 200 µl cold Phenol:Chloroform:Isoamyl Alcohol mixture. Samples were vortexed vigorously and centrifuged at 13,000 rpm (16,060*g*) for 2 minutes to separate the phases. The top aqueous phase was carefully pipetted (170 µl) into a new Eppendorf tube containing 30 µl sterile MilliQ-H_2O, being careful not to pipette the white mid-layer containing precipitates (proteins). Six microliters of NaCl (5 M) and 618 µl cold 100% ethanol were added to the aliquot and mixed. Samples were kept at -20^oC for a minimum of 4 hours before centrifugation at 4^oC, 13,000 rpm (16,060*g*) for 1 hour. The supernatant was removed, and the pellet washed carefully with cold 75% ethanol. Pellets were re-suspended in 15 µl sterile MilliQ-H_2O and run on gel electrophoresis to ascertain product purity and concentration before ligation. All ligation reactions (both blunt and sticky ends) incubated at 16^oC between 16-24 hours followed by heat inactivation at 75^oC for 5 minutes as per described in Table 4.6.

Table 4.6. Reagents Used for Routine Restriction Enzyme Ligation Reaction

Reagent	Amount (µl)
DNA*	1.0-2.0**
Vector*	1.0-2.0 (25-100ng)**
T4 Buffer	1.0
T4 Ligase Enzyme	2.0
Water (H_2O)	Up to 10.0
Total	**10.0**

*template DNA was pre-heated at 65^oC for 5 minutes to remove any secondary structures before ligation.

**The amount of insert DNA always equal or double the amount of vector used.

4.3.2.6 Preparation of Stock *E. coli* DH5α Super Competent Cells

A sterile inoculating loop was dipped into stock *E. coli* DH5α cells and streaked onto LB agar. The plate was incubated for 16 hours at 37ºC. One colony was picked and inoculated into 5 ml SOB broth and incubated for 16 hours at 37ºC and shaking (160 rpm). Under sterile conditions, 1 ml of the culture was added to 50 ml SOB broth in a 250 ml Erlenmeyer conical flask (VWR). Five flasks were prepared and incubated for 24 hours at 18ºC, 220 rpm until OD_{600} is 0.6, measured using a spectrophotometer (BioRad SmartSpec 3000). At OD_{600} 0.6, flasks were immediately placed on ice for 10 minutes. Each culture was transferred into 50 ml sterile Falcon tubes and centrifuged for 10 minutes at 3,000 rpm (3,316*g*), 4ºC in the Beckman-Coulter centrifuge. The supernatant was removed, and pellets from five tubes were gently re-suspended and combined into one 50 ml Falcon tube with 50 ml TB buffer. The cell suspension was centrifuged for 10 minutes at 3,000 rpm (3,316*g*), 4ºC using the Beckman-Coulter centrifuge. The supernatant was removed, and the pellet was gently re-suspended in 9.5 ml TB. Dimethyl Sulfoxide (DMSO) was added to a final concentration of 7%. Two hundred and fifty microlitre aliquots of the cell mixture were pipetted into a sterile 1.5 ml Eppendorf tube each and immediately frozen in dry-ice filled with 100% ethanol. Cells were stored at -80ºC until ready to use.

4.3.2.7 *E. coli* DH5α Supercompetent Transformation by Heat-shock

Cells were thawed and placed on ice. The ligation reaction was added to cold 1.5 ml Eppendorf tubes up to a maximum of 5 µl for every 50 µl *E.coli* DH5α cells aliquoted. For amplifying more vectors, 1 µl DNA vector was added to 50 µl cells. The cell mix was incubated on ice for 10 minutes before 30 seconds of heat shock at 42ºC without agitation. Tubes were immediately placed on ice for 2 minutes,

followed by the addition of 1 ml SOC broth and incubated for 1 hour at 37ºC shaking at 160 rpm. After incubation, cells were centrifuged slowly at 3500 rpm (1,164*g*) for 5 minutes, at room temperature. The supernatant was decanted, and pelleted cells carefully re-suspended in 200 µl SOC and spread evenly onto an LBA plate containing Ampicillin at a concentration of 100 µg/ml. Plates were incubated for 16 hr at 37ºC.

4.3.2.8 Confirmation of Ligation

Between 40-50 individual colonies were picked with a sterile toothpick and the procedure for vector amplification and extraction was followed as described. Each candidate vector was digested with restriction enzymes giving digested fragments of known sizes, according to the reaction conditions described in Table 4.5 for 1 hour and as recommended by the manufacturer (NEB). If it was a sequential digestion, the second enzyme, and corresponding buffer was added after 1 hour and left to incubate for another hour. Two control samples were always included: non-template control and empty vector without insert. Three microlitres of 6x Loading Dye were then added to each sample and loaded into 1% Agarose gel. Gels were run for 1.5 hours at 80 Volts and viewed using a gel-doc imaging system (G:Box by Syngene).

Following identification of candidate vectors containing the DNA insert, up to three were then sent for routine sequencing (refer to Chapter 2) to confirm the orientation of insertion and to ensure no changes to the genomic DNA sequence. Once confirmed, the vector was linearised with *Pac*I enzyme and ethanol precipitated. A total volume of 10 µl (concentration 1 µg/µl) was used to transform into the appropriate *M. oryzae* genotype, following the routine transformation protocol described in Chapter 4.

4.3.2.9 Line Screening for Phenotype Recovery

For each linearised vector transformation (plasmids 13c, 13c_2ci, #5, or #5_9a), between 40-50 independent colonies that were able to grow on DCM agar containing 50 µg/ml Bialaphos (GoldBio) were sub-cultured onto CM agar. The inoculated CM agar plates were then incubated for 10 days, followed by gDNA extraction for PCR vector insertion confirmation. Throughout the process, a negative control (background mutant line transformed with PEG only) was included. Routine culture preparation and gDNA extraction as described in Chapter 2 (section 2.2.2.2).

The primer pair (Conf_Crh2_F and Conf_Crh2_R) annealing to the gDNA coding region of *MGG_Crh2* designed in section 4.3.1.2 (Table 4.2) was used in this section to confirm the presence of ectopically inserted vector 13c or 2ci containing the *MGG_Crh2* promoter and coding region, within the genome of candidate transformed revertant strains obtained above. For this PCR reaction, gDNA of WT is the positive control, with a product size of 0.45 kb. Non-template control and gDNA of *ΔMGG_Crh2* line 39 is the negative control. The same was repeated for the presence of vector #5_6 using primer pairs (Conf_Utr2_F and Conf_Utr2_R) from Table 4.2 to amplify a section within the *MGG_Utr2* coding region with gene *MGG_Utr2* not present in the background mutant *ΔMGG_Utr2* line 2. A positive control using gDNA of WT was used to give the product size of 0.79 kb. To check for the presence of vector #5_9a in candidate transformants, the primer pair #1_utr 2_seq and R_Utr2 was designed (

Table 4.8) to amplify a 0.8 kb product spanning the region between *MGG_Utr2* promoter region and mCherry sequence, with *ΔMGG_Utr2* gDNA and non-template control used as the negative control.

4.4 Results & Discussion

4.4.1 Generation of Deletant Strains

The WT strain Guy11 was used as the background strain for the generation of single gene knock-out *ΔMGG_Utr2*, *ΔMGG_Crh1,* and *ΔMGG_Crh2*. The mutant *ΔMGG_Crh2* line 39 was then used as the background strain to generate a double gene knockout strain, *ΔΔMGG_Crh2_Utr2*.

4.4.1.1 Generation of Deletant Strains

4.4.1.1.1 Construction of Deletion Cassettes

A 3.85 kb transformation cassette containing a Hygromycin selectable marker was designed to replace the targeted *MGG_Utr2* gene on Chromosome 5 of the *M. oryzae* Guy11 genome. Within the 3.85 kb cassette, the resistance marker was flanked at both 3’ and 5’ ends with sequences identical to those flanking the targeted *MGG_Utr2*, allowing double cross-over by homologous recombination to take place. The Utr2_Hyg deletion cassette was designed in a series of overlapping PCR as shown in Figure 4.7 using primer pairs from Table 4.2.

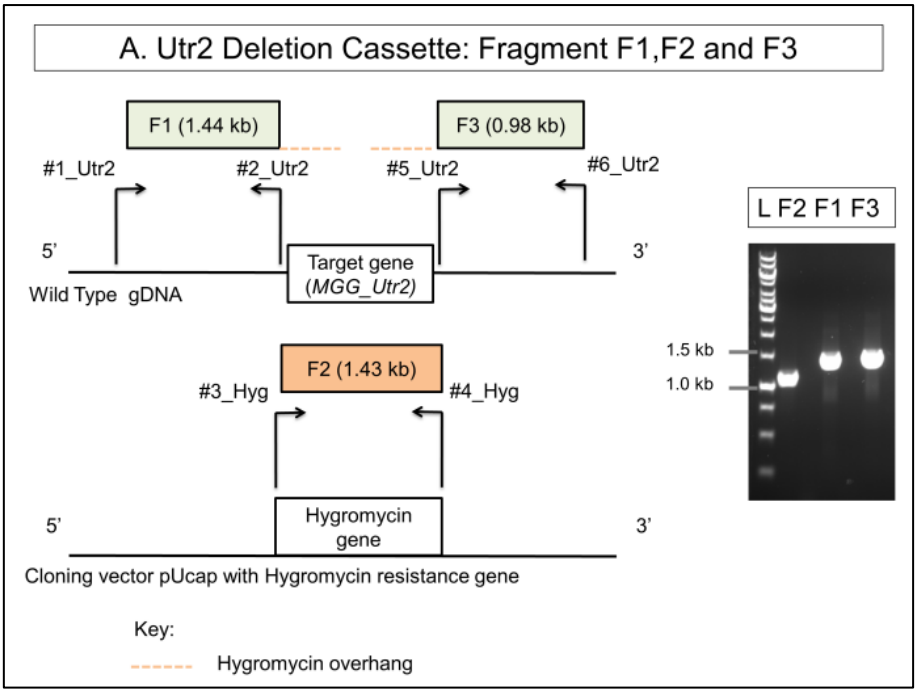
A. Utr2 Deletion Cassette: Fragment F1,F2 and F3
F1 (1.44 kb)
F3 (0.98 kb)
#1_Utr2
#2_Utr2
#5_Utr2
#6_Utr2
5'
3'
Target gene
(MGG_Utr2)
Wild Type gDNA
F2 (1.43 kb)
#3_Hyg
#4_Hyg
5'
3'
Hygromycin
gene
Cloning vector pUcap with Hygromycin resistance gene
Key:
Hygromycin overhang
L F2 F1 F3
1.5 kb
1.0 kb

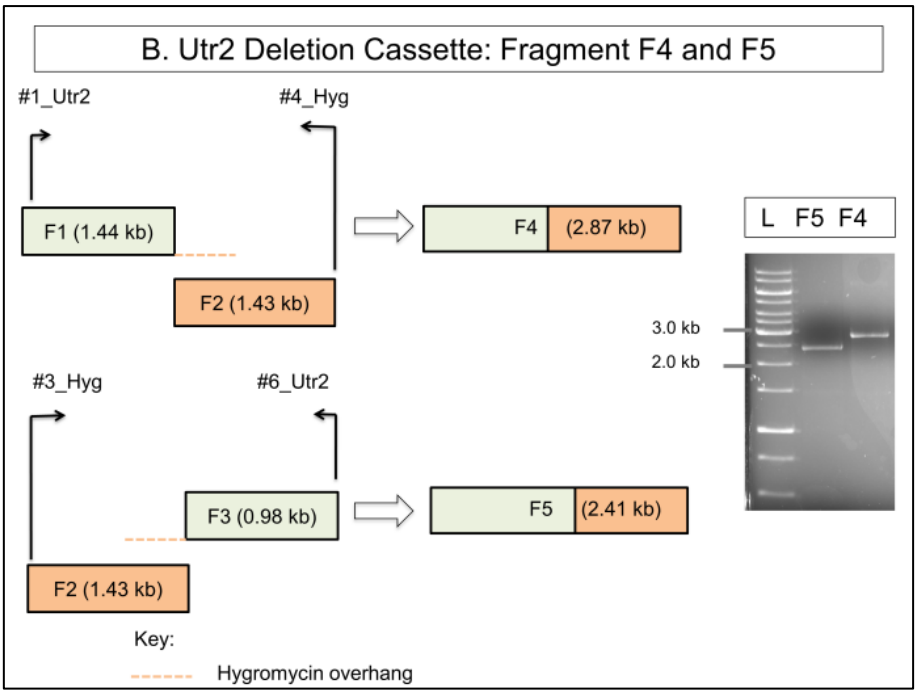
B. Utr2 Deletion Cassette: Fragment F4 and F5
#1_Utr2
#4_Hyg
F1 (1.44 kb)
F2 (1.43 kb)
F4
(2.87 kb)
#3_Hyg
#6_Utr2
F3 (0.98 kb)
F2 (1.43 kb)
F5
(2.41 kb)
Key:
Hygromycin overhang
L F5 F4
3.0 kb
2.0 kb

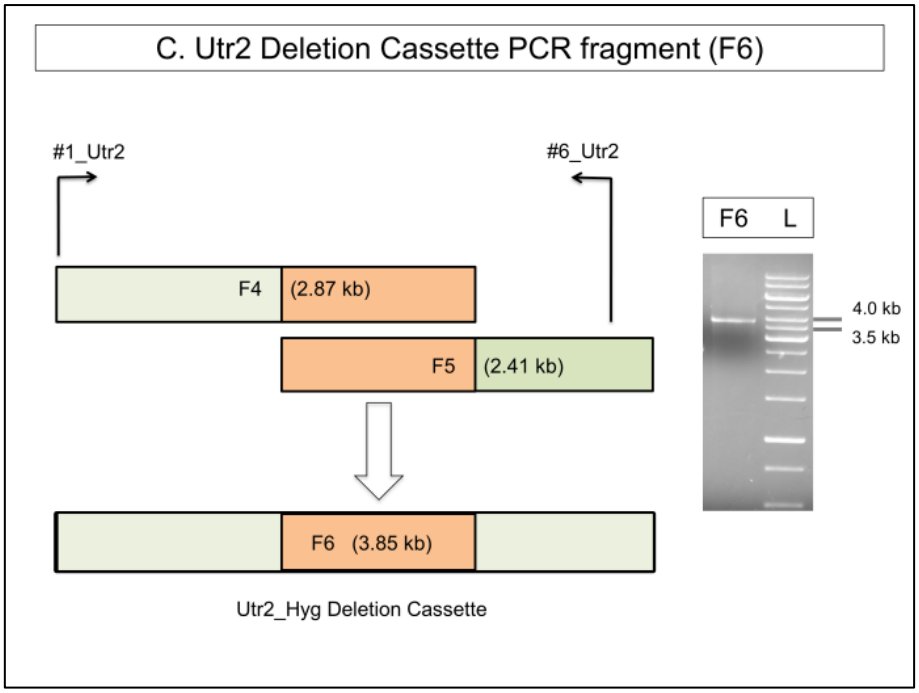

Figure 4.7 A Description for the Construction of Utr2_Hyg Deletion Cassette by Overlapping PCR. Panel A The design of three PCR fragments (F1, F2, and F3) and the corresponding PCR product on gel electrophoresis. **Panel B** Overlapping PCR for fragments F4 and F5 using F1, F2 and F3 as the template, with amplified products shown on gel electrophoresis. **Panel C** An illustration for the amplification of the final product, F6 using fragments F4 and F5 as template, with the final product shown on gel electrophoresis. GeneRuler™ 1 kb DNA Ladder was used as the molecular ladder (L) and all agarose gel prepared at 1%.

Similarly, deletion cassettes for genes *MGG_Crh1* and *MGG_Crh2* were designed using overlapping PCR, producing a final construct of 3.35 kb and 3.79 kb respectively with Hygromycin as the selectable marker. A 3.32 kb deletion cassette targeting the *MGG_Utr2* gene in the background genotype of mutant *ΔMGG_Crh2* line 39 was also constructed, with Bialaphos as the selectable marker. Refer to Appendix B.2, B.3 and B.4 for detailed illustrations of overlapping PCR construction for each deletion cassette.

4.4.1.1.2 Confirmation of Transformed Mutants

The gDNA of each candidate transformant (a total of 65 candidates) was tested for the presence of the introduced cassette at the targeted locus by integration PCR. This was achieved by designing a forward primer Utr2_i1.2F binding specifically to the native *M. oryzae* genomic sequence, and a reverse primer Utr2_i1.2 R binding specifically to a region within the introduced Hygromycin resistance gene (Figure 4.8). Similarly, another pair of primer was designed whereby the forward primer i1.4F binds specifically to the Hygromycin resistance gene, and the reverse primer Utr2_i1.4R binds specifically to a sequence found in the native *M. oryzae* genome close to the inserted cassette. An insertion at the right location will give PCR product sized 2.7 kb and 1.5 kb respectively. Additionally, a set of primers was designed to amplify a region in the targeted gene *MGG_Utr2.* In a successful transformation, no PCR amplification should occur as the *MGG_Utr2* gene is no longer present but replaced with the Utr2_Hyg deletion cassette (Figure 4.9). Contrary, a 0.79 kb PCR product size should be obtained from gDNA of the Wild Type Guy11. Ten candidate lines were shortlisted for subsequent confirmation by southern blot.

To confirm that only one deletion cassette was inserted at the targeted location with no additional copies of the deletion cassette inserted ectopically within the genome, Southern Blot was conducted. Here, gDNA of 10 candidate mutant lines shortlisted from PCR integration results obtained above was digested with *Hind*III enzyme. This enzyme was chosen as two cut sites were found to cut on regions flanking the inserted deletion cassette, giving a product size of 5.99 kb (Figure 4.8 Panel A and Panel C). Hygromycin probe was first amplified from a pUCAP vector, PCR-cleaned and product run on gel to show

product purity (Appendix B.5) before probe labelling and hybridisation to candidate DNA. Southern Blot results for candidate mutant *MGG_Utr2* lines 1 and 2 showed a single band almost at the same size as the 6 kb mark from the 1 kb ladder. In this film, a small amount of the radioactively labelled probe also hybridised to the ladder, omitting the need to use a ruler to measure band size.

Non-specific probe hybridisation to a molecular ladder is not a rare occurrence, particularly when the probe was amplified from a vector, as molecular ladders are made of repeating units derived from pUCAP vectors (www.NEB.com). It can also occur if small amounts of free-nucleotides were not completely removed during probe hybridisation preparation or too much molecular ladder was used. This does not affect the reliability of the band seen on mutant lines giving the expected size (5.99 kb) and brighter than the labelled molecular ladder, in addition to the control Wild Type Guy11 line showing the absence of band/s.

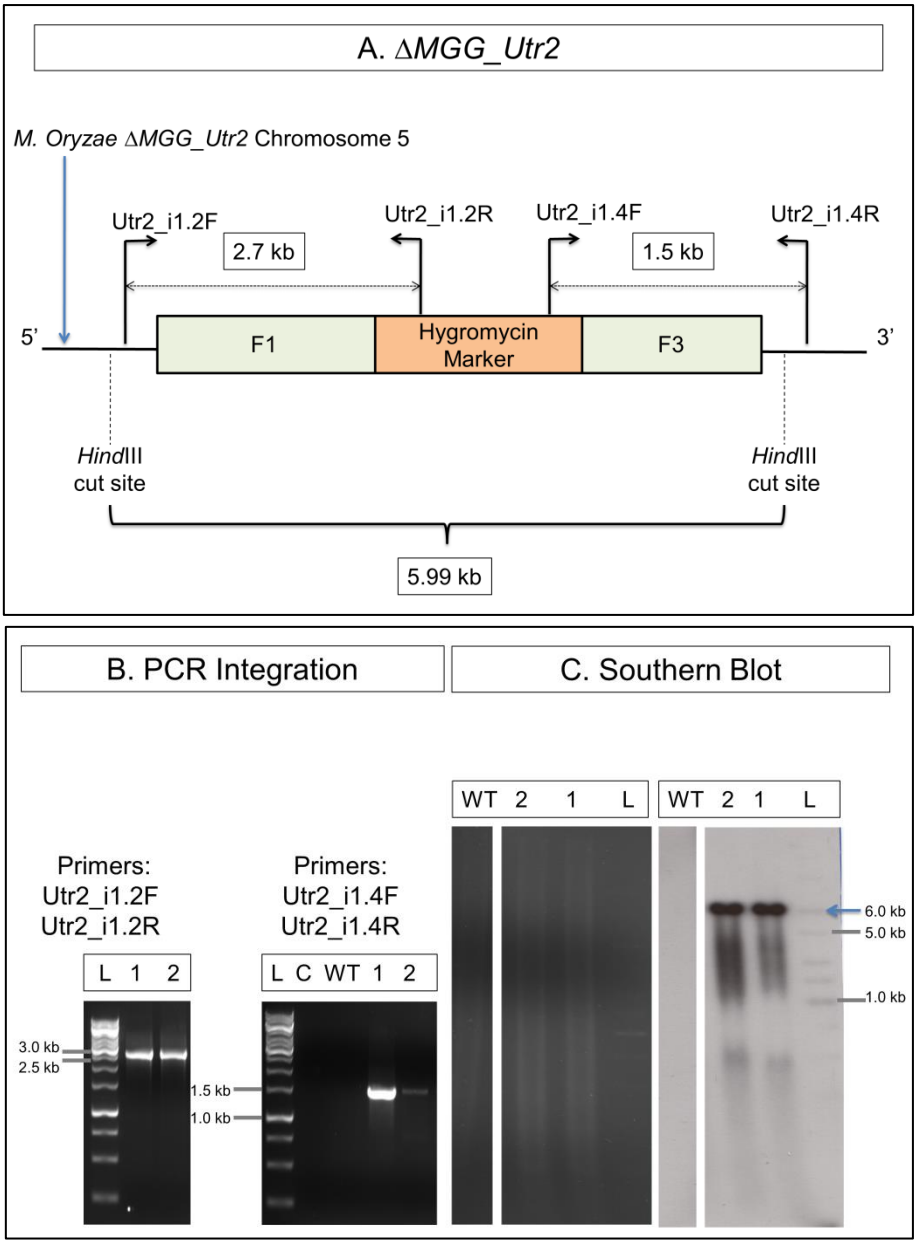

Figure 4.8. PCR Integration and Southern Blot Confirmation for the Replacement of *MGG_Utr2* Gene with Utr2_Hyg Deletion Cassette. Panel A. An illustration showing the use of two pairs of primers strategically designed to amplify a region spanning the border between the native genome and artificially inserted cassette. This illustration also showed the location of *Hind*III cut sites and subsequent expected southern blot size of 5.99 kb. **Panel B.** PCR integration analysis showing PCR products for candidate mutant Δ*MGG_Utr2* independent line 1 (1) and line 2 (2) at the expected sizes of 2.7 kb and 1.5 kb respectively. No amplification in the negative control Wild Type Guy11 (WT) and non-template control (C), indicating the presence of Utr2_Hyg cassette at the targeted location. **Panel C.** Picture left showed that gDNA was successfully digested by *Hind*III and size distributed alongside a 1 kb ladder (L) on an agarose gel. Picture right showed a Blot film with each Δ*MGG_Utr2* independent line 1 (1) and line 2 (2) having only 1 band at 5.99 kb and band absence in the negative control (WT). GeneRuler™ 1 kb DNA Ladder was used as the molecular ladder (L) and all agarose gel prepared at 1%.

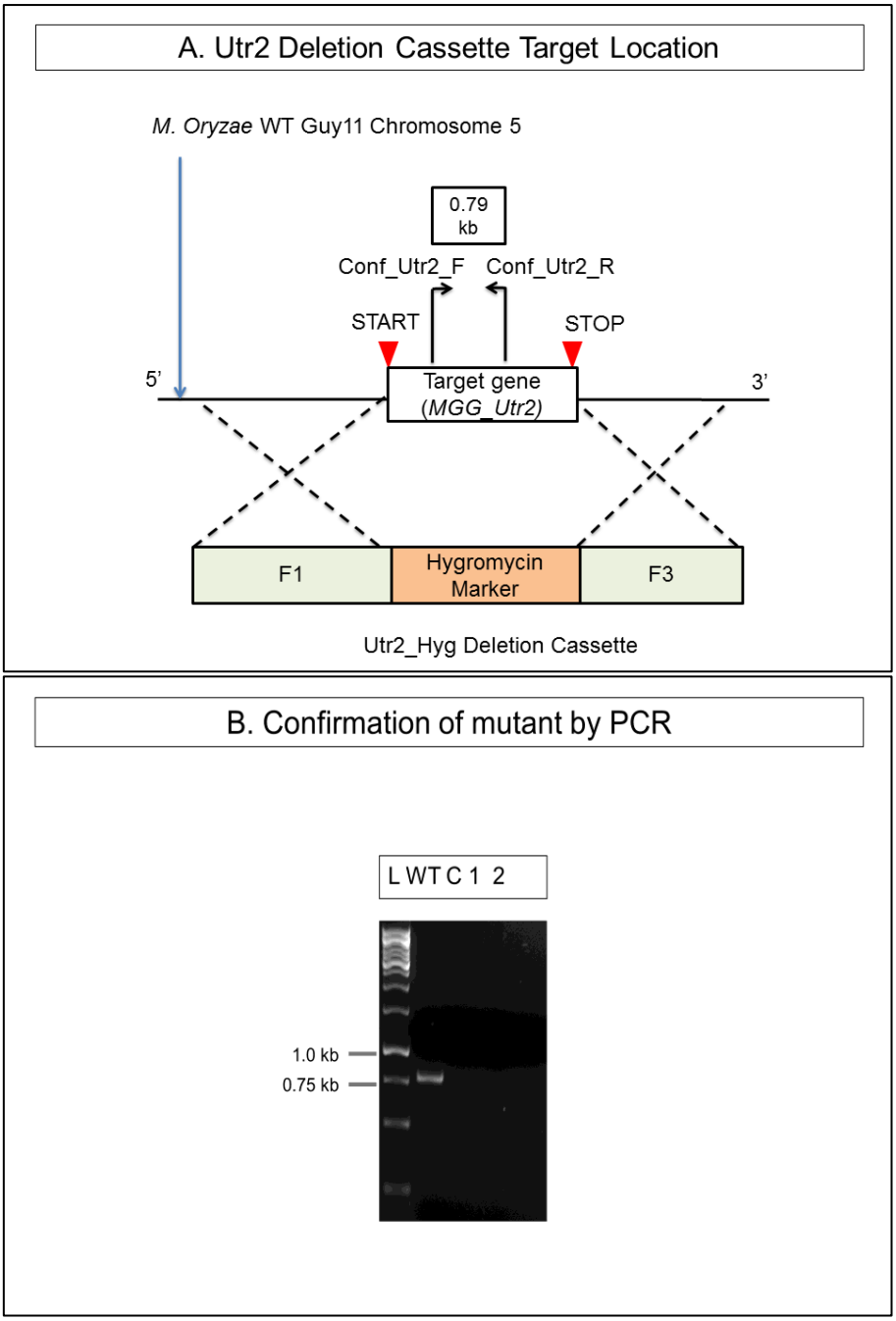

Figure 4.9. Targeted Transformation Using the Utr2_Hyg Deletion Cassette and *MGG_Utr2* Gene Absence Confirmation. Panel A. Illustration above showed location within the Wild Type Guy11 genome where the artificially introduced Utr2_Hyg deletion cassette must undergo double cross-over by homologous recombination for a successful transformation. If the native gene *MGG_Utr2* was not successfully replaced by the deletion cassette, then primer pairs Conf_Utr2_F and Conf_Utr2_R will amplify the stated region, giving a product size of 0.79 kb. **Panel B.** Gel picture showed the 0.79 kb product obtained from a Wild Type Guy11 gDNA (WT), but not from the candidate mutant *ΔMGG_Utr2* independent lines 1 (1) and line 2 (2. No amplification in the non-template control (C), indicating that the gene *MGG_Utr2* is no longer present on chromosome 5 within the genome of the candidate mutant lines 1 and 2. GeneRuler™ 1 kb DNA Ladder was used as the molecular ladder (L) and agarose gel prepared at 1%.

The same mutant confirmation strategy was practiced for the confirmation of candidate mutant lines *ΔMGG_Crh1* lines 36 and 43 and *ΔMGG_Crh2* lines 37 and 39 using Hygromycin as the hybridisation probe and Bialaphos for mutant *ΔΔMGG_Crh2_Utr2* lines 25 and 27. Figure 4.10 to Figure 4.15 showed confirmation by PCR integration and subsequent southern blot analysis for each of the candidate single and double gene knock-out independent lines.

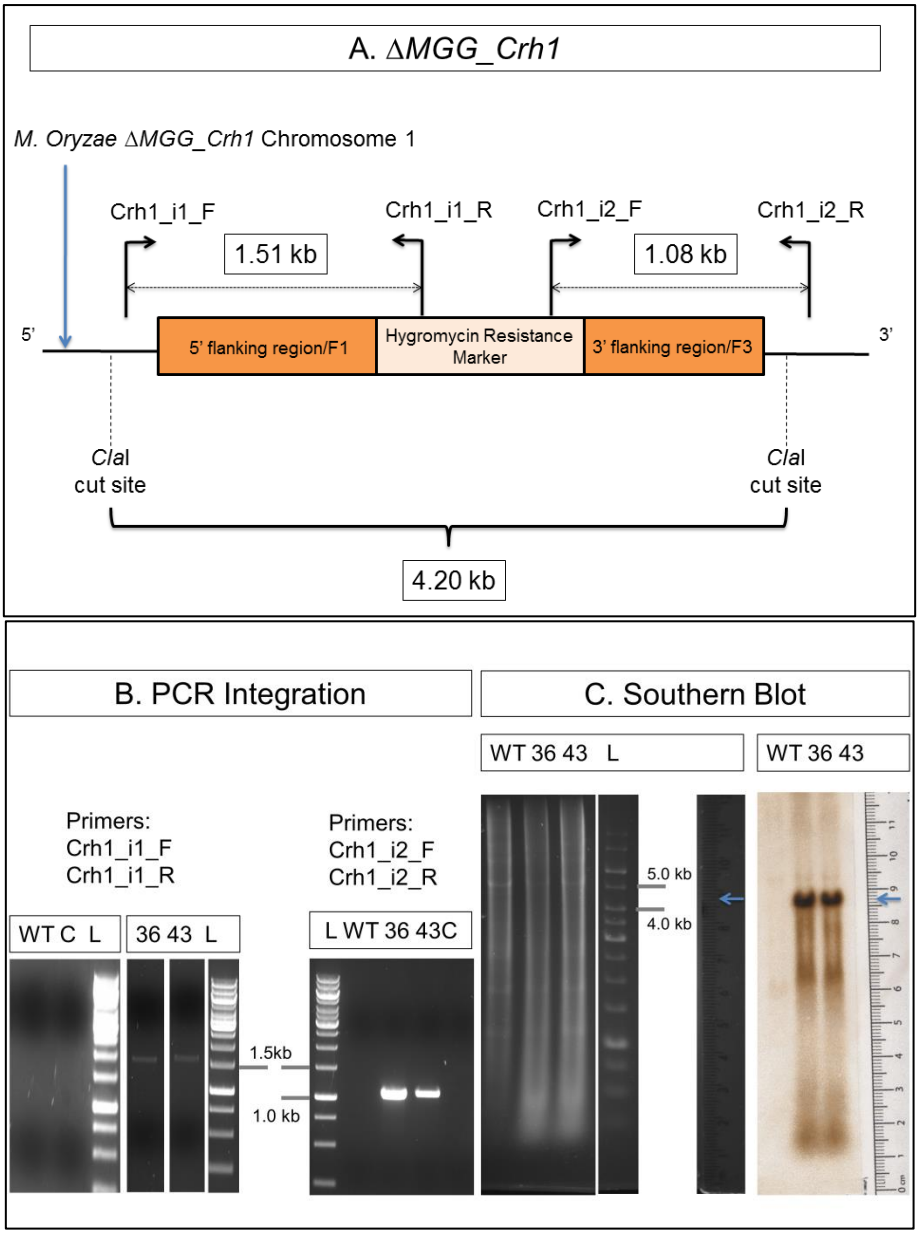

Figure 4.10. PCR Integration and Southern Blot Confirmation for the Replacement of *MGG_Crh1* Gene with Crh1_Hyg Deletion Cassette. Panel A An illustration showing the use of two pairs of primers strategically designed to amplify a region spanning the border between the native genome and artificially inserted cassette. This illustration also showed the location of *Cla*I cut sites and subsequent expected southern blot size of 4.20 kb **Panel B** PCR integration analysis showing PCR products for candidate mutant Δ*MGG_Crh1* independent line 36 (36) and line 43 (43) at the expected sizes of 1.51 kb and 1.08 kb respectively. No amplification in the negative control Wild Type Guy11 (WT) and non-template control (C), indicating the presence of Crh1_Hyg cassette at the targeted location. **Panel C** Picture left showed that gDNA was successfully digested by *Cla*I and size distributed alongside a 1 kb ladder (L) on an agarose gel. Picture right showed a Blot film with each Δ*MGG_Crh1* independent line 36 (36) and line 43 (43) having only 1 band at 5.99 kb and band absence in the negative control (WT). GeneRuler™ 1 kb DNA Ladder was used as the molecular ladder (L) and all agarose gel prepared at 1%.

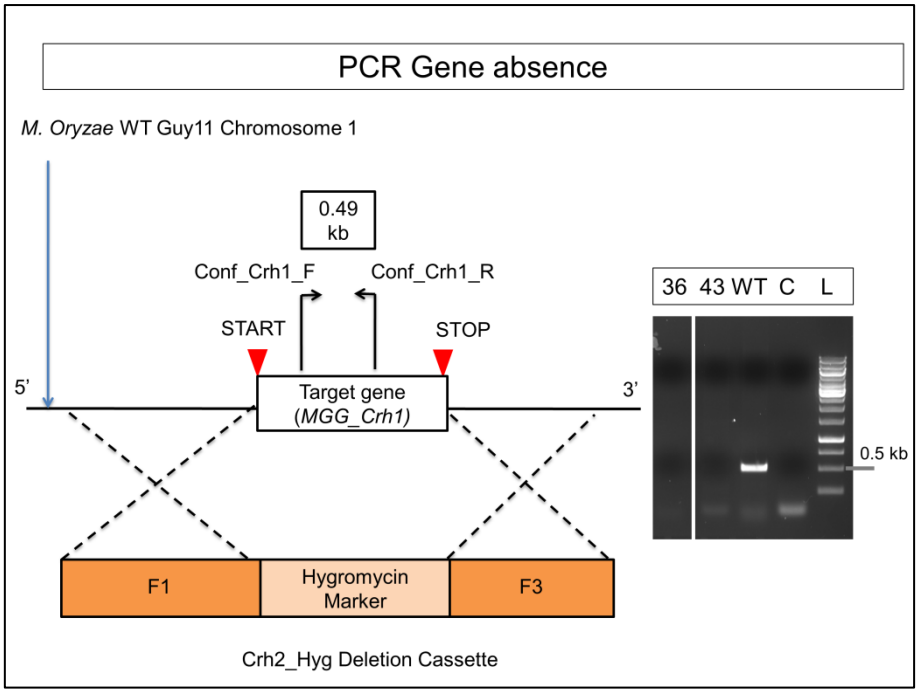

Figure 4.11.Targeted Transformation Using the Crh1_Hyg Deletion Cassette and *MGG_Crh1* Gene Absence Confirmation. Illustration above showed location within the Wild Type Guy11 genome where the artificially introduced Crh1_Hyg deletion cassette must undergo double cross-over by homologous recombination for a successful transformation. If the native gene *MGG_Crh1* was not successfully replaced by the deletion cassette, then primer pairs Conf_Crh1_F and Conf_Crh1_R will amplify the targeted region, giving a product size of 0.49 kb. Gel picture on the right showed the 0.79 kb product obtained from a Wild Type Guy11 gDNA (WT), but not from the candidate mutant *ΔMGG_Crh1* independent lines 36 (36) and line 43 (43). No amplification in the non-template control (C), indicating that the gene *MGG_Crh1* is no longer present on chromosome 1 within the genome of the candidate mutant lines 36 and 43. GeneRuler™ 1 kb DNA Ladder was used as the molecular ladder (L) and agarose gel prepared at 1%.

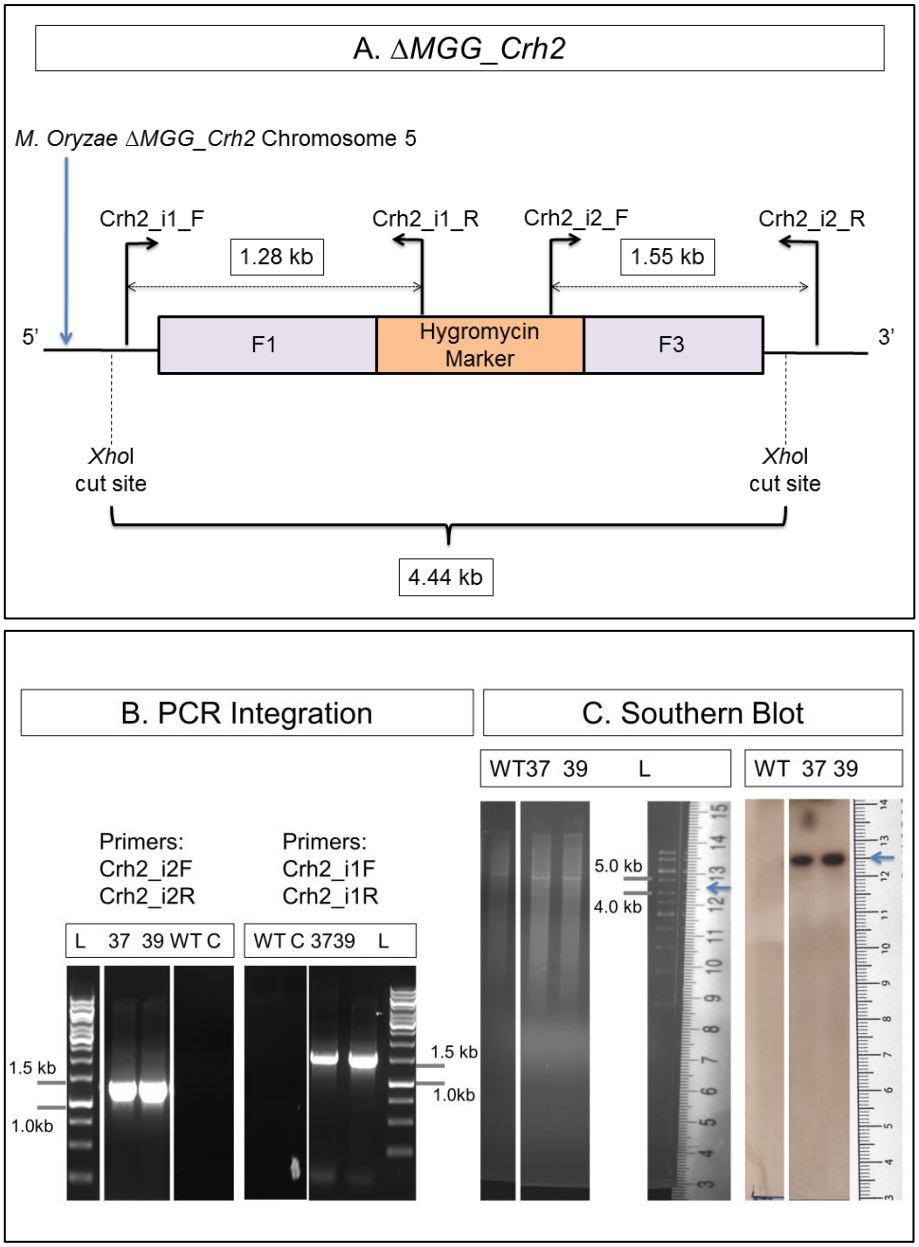

Figure 4.12. PCR Integration and Southern Blot Confirmation for the Replacement of *MGG_Crh2* Gene with Crh2_Hyg Deletion Cassette. Panel A An illustration showing the use of two pairs of primers strategically designed to amplify a region spanning the border between the native genome and artificially inserted cassette. This illustration also showed the location of *Xho*I cut sites and subsequent expected southern blot size of 4.44 kb. **Panel B** PCR integration analysis showing PCR products for candidate mutant Δ*MGG_Crh2* independent line 37 (37) and line 39 (39) at the expected sizes of 1.28 kb and 1.55 kb respectively. No amplification in the negative control Wild Type Guy11 (WT) and non-template control (C), indicating the presence of Crh2_Hyg cassette at the targeted location. **Panel C** Picture left showed that gDNA was successfully digested by *Xho*I and size distributed alongside a 1 kb ladder (L) on an agarose gel. Picture right showed a Blot film with each Δ*MGG_Crh2* independent line 37 (37) and line 39 (39) having only 1 band at 5.99 kb and band absence in the negative control (WT). GeneRuler™ 1 kb DNA Ladder was used as the molecular ladder (L) and all agarose gel prepared at 1%.

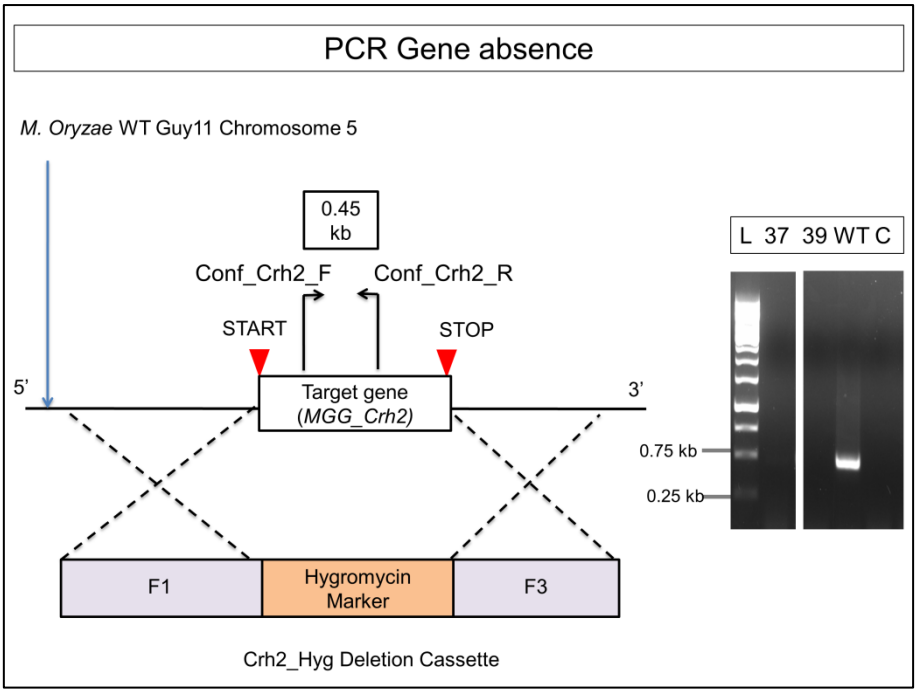

Figure 4.13. Targeted Transformation Using the Crh2_Hyg Deletion Cassette and *MGG_Crh2* Gene Absence Confirmation. Illustration above showed location within the Wild Type Guy11 genome where the artificially introduced Crh2_Hyg deletion cassette must undergo double cross-over by homologous recombination for a successful transformation. If the native gene *MGG_Crh2* was not successfully replaced by the deletion cassette, then primer pairs Conf_Crh2_F and Conf_Crh2_R will amplify the stated region, giving a product size of 0.45 kb. Gel picture on the right showed the 0.75 kb product obtained from a Wild Type Guy11 gDNA (WT), but not from the candidate mutant *ΔMGG_Crh2* independent lines 37 (37) and line 39 (39). No amplification in the non-template control (C), indicating that the gene *MGG_Crh1* is no longer present on chromosome 1 within the genome of the candidate mutant lines 37 and 39. GeneRuler™ 1 kb DNA Ladder was used as the molecular ladder (L) and agarose gel prepared at 1%.

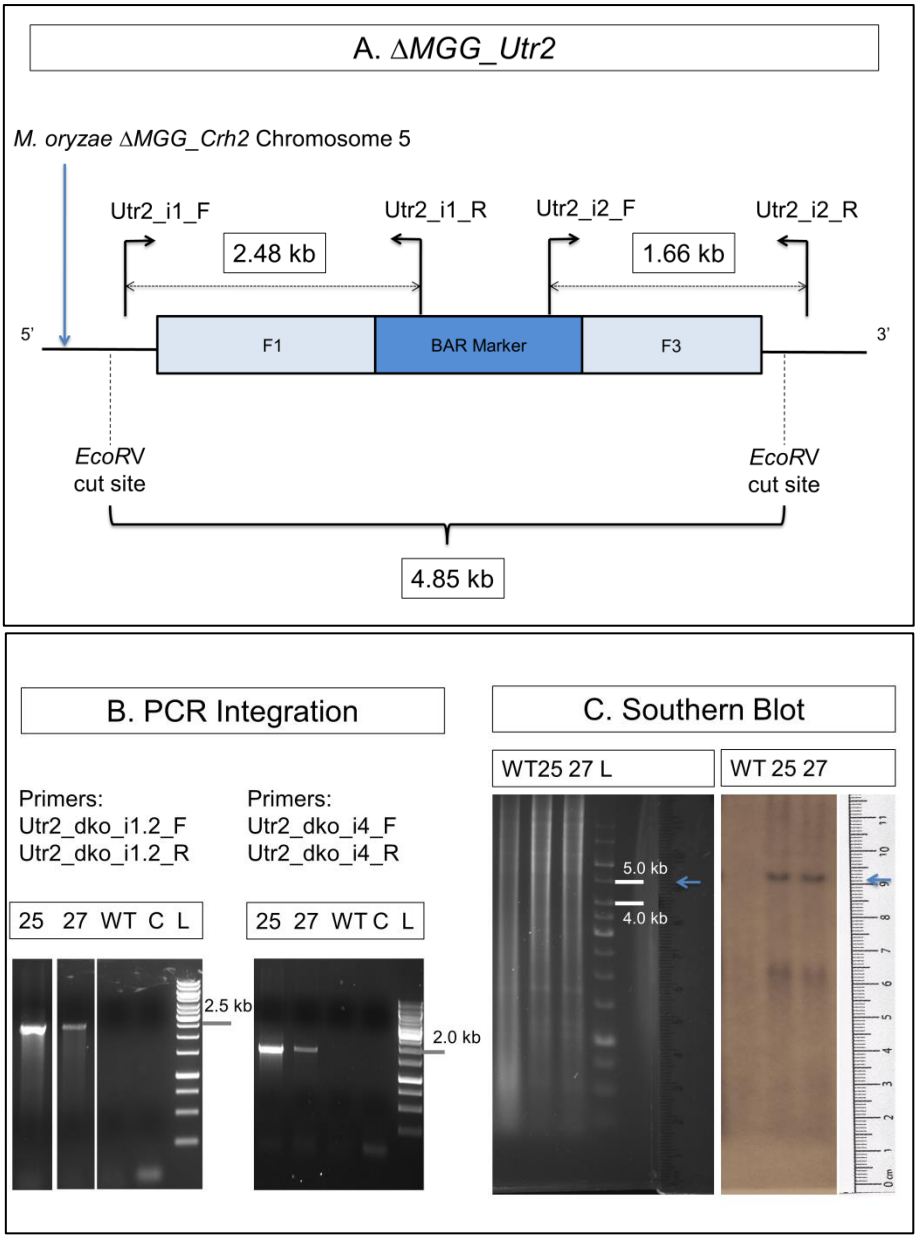

Figure 4.14. PCR Integration and Southern Blot Confirmation for the Replacement of *MGG_Utr2* Gene with Utr2_BAR Deletion Cassette. Panel A An illustration showing the use of two pairs of primers strategically designed to amplify a region spanning the border between the native genome and artificially inserted cassette. This illustration also showed the location of *EcoR*V cut sites and subsequent expected southern blot size of 4.85 kb **Panel B** PCR integration analysis showing PCR products for candidate mutant ΔΔ*MGG_Crh2_Utr2* independent line 25 (25) and line 27 (27) at the expected sizes of 2.48 kb and 1.66 kb respectively. No amplification in the negative control Wild Type Guy11 (WT) and non-template control (C), indicating the presence of Crh2_Hyg cassette at the targeted location. **Panel C** Picture left showed that gDNA was successfully digested by *Xho*I and size distributed alongside a 1 kb ladder (L) on an agarose gel. Picture right showed a Blot film with each Δ*MGG_Crh2* independent line 37 (37) and line 39 (39) having only 1 band at 5.99 kb and band absence in the negative control (WT). GeneRuler™ 1 kb DNA Ladder was used as the molecular ladder (L) and all agarose gel prepared at 1%.

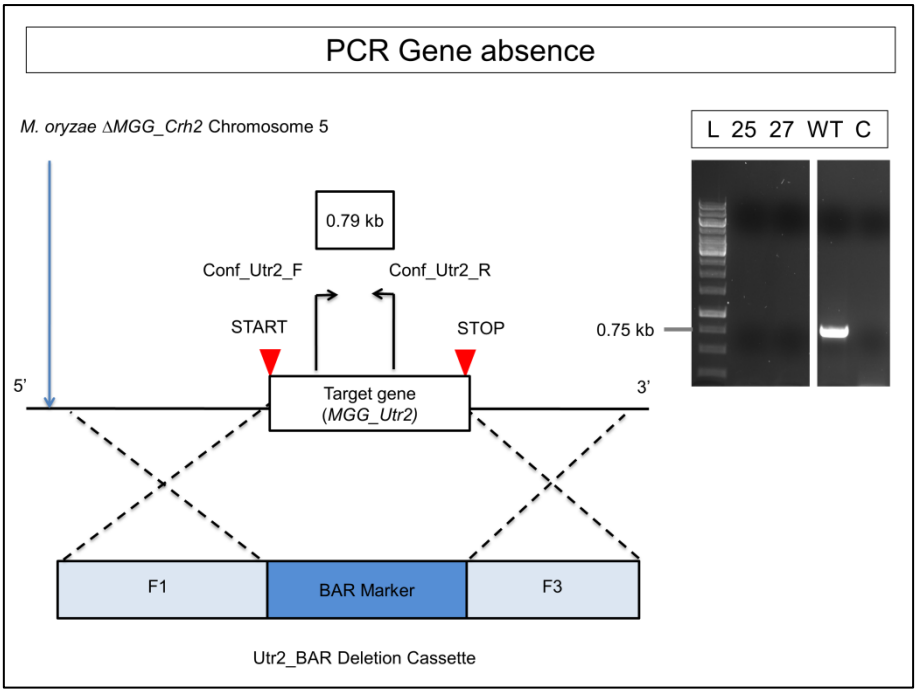

Figure 4.15. Targeted Transformation using the Crh2_Hyg Deletion Cassette and *MGG_Crh2* Gene Absence Confirmation. Illustration above showed location within the Wild Type Guy11 genome where the artificially introduced Crh2_Hyg deletion cassette must undergo double cross-over by homologous recombination for a successful transformation. If the native gene *MGG_Crh2* was not successfully replaced by the deletion cassette, then primer pairs Conf_Crh2_F and Conf_Crh2_R will amplify the stated region, giving a product size of 0.45 kb. Gel picture on the right showed the 0.75 kb product obtained from a Wild Type Guy11 gDNA (WT), but not from the candidate mutant *ΔMGG_Crh2* independent lines 37 (37) and line 39 (39). No amplification in the non-template control (C), indicating that the gene *MGG_Crh1* is no longer present on chromosome 1 within the genome of the candidate mutant lines 37 and 39. GeneRuler™ 1 kb DNA Ladder was used as the molecular ladder (L) and agarose gel prepared at 1%.

To summarise, section 4.4.1 generated in total four mutant strains, each with two independent lines. Table below summarises the mutant strain and background genotype used.

Deletion Cassette	Background strain	Mutant strain
Utr2_Hyg	WT	1. Δ*MGG_Utr2 Line 1* 2. Δ*MGG_Utr2 Line 2*
Crh1_Hyg	WT	1. Δ*MGG_Crh1 Line 36* 2. Δ*MGG_Crh1 Line 43*
Crh2_Hyg	WT	1. Δ*MGG_Crh2 Line 37* 2. Δ*MGG_Crh2 Line 39*
Utr2_Bar	Δ*MGG_Crh2 Line 39*	1. Δ*MGG_Crh2_Utr2* Line 25 2. Δ*MGG_Crh2*_Utr2 Line 27

4.4.1.2 Absence of Transcript: Validation by qRT-PCR

To show that the targeted gene is no longer expressed in the knockout strain, a qRT-PCR experiment was conducted to compare the amplification of the target gene in the cDNA of WT relative to the cDNA of the knockout strain.

The RNA for vegetative mycelium grown in liquid CM for each strain used in this section was obtained from section 6.4.2. All five *M. oryzae Crh-like* genes were amplified in each strain: WT, Δ*MGG_Crh1* (line 36), Δ*MGG_Utr2* (line 2), Δ*MGG_Crh2* (line 39) and ΔΔ*MGG_Crh2_Utr2* (line 25). Table 4.7 show the averaged cycle threshold (ct) values obtained for each gene from three biological replicates, in each fungal strain analyzed. Note that each 96-well plate was assayed independently; therefore ct values should only be compared and analyzed within each plate. A knockout strain is no longer expressing the gene if the ct value is above 35 or 10 ct higher than in WT (see Chapter 3 section 3.4.2.2.1 paragraph 5 for detailed explanation pertaining low/nil expression in qRT-PCR). Additionally, a Student's t-test must show that the ct value in the knockout strain as significantly different from ct value recorded in WT. A control

using the validated stably expressed gene *MGG_40s* (Chapter 3) was included to show that no differences in expression is seen between the fungal strains. Thus, any differences detected from the gene of interest is due to changes in the expression of the gene and not due to other external factors (such as differences in RNA quality or quantity).

Table 4.7. Average Cycle Threshold of *Crh-like* Genes in Five Strains. Mycelial RNA was prepared from the inoculation of spore suspension in liquid CM and cultured vegetatively for three days before harvesting. Each ct data averaged from three biological replicates each with two technical replicates (standard deviation in brackets). Differences in mean ct between WT and mutant calculated using Student's t-test at p<0.001 (double asterisk). The validated stably expressed gene *MGG_40s* were used as a negative control.

Gene	Strain				
	WT	Δ*MGG_Crh1*	Δ*MGG_Utr2*	Δ*MGG_Crh2*	ΔΔ*MGG_Crh2_Utr2*
96-Well Plate 1					
MGG_Utr2	19.40 (±0.17)	19.15 (±0.05)	-	19.21 (±0.04)	-
MGG_Crh1	26.12 (±0.44)	33.65** (±0.81)	-	25.15 (±0.26)	-
MGG_Crh2	16.42 (±0.17)	16.72 (±0.03)	-	35.06** (±0.47)	-
MGG_Crh3	-	-	-	-	-
MGG_Crh4	-	-	-	-	-
MGG_40S	20.60 (±0.31)	20.46 (±0.41)	-	19.55 (±0.12)	-
96-Well Plate 2					
MGG_Utr2	19.16 (±0.09)	-	36.13** (±1.05)	-	36.59** (±1.53)
MGG_Crh1	25.77 (±0.39)	-	25.93 (±0.08)	-	24.73 (±0.46)
MGG_Crh2	16.21 (±0.19)	-	16.57 (±0.12)	-	33.13** (±1.46)
MGG_Crh3	-	-	-	-	-
MGG_Crh4	-	-	-	-	-
MGG_40S	20.26 (±0.35)	-	20.16 (±0.03)	-	19.88 (±0.14)
96-Well Plate 3					
MGG_Utr2	-	-	-	-	-
MGG_Crh1	-	-	-	-	-
MGG_Crh2	-	-	-	-	-
MGG_Crh3	31.27 (±0.20)	31.35 (±0.78)	-	30.48 (±0.44)	-
MGG_Crh4	25.00 (±0.46)	24.56 (±0.41)	-	24.84 (±0.42)	-
MGG_40S	18.48 (±0.26)	18.61 (±0.34)	-	17.47 (±0.10)	-
96-Well Plate 4					
MGG_Utr2	-	-	-	-	-
MGG_Crh1	-	-	-	-	-
MGG_Crh2	-	-	-	-	-
MGG_Crh3	31.60 (±0.24)	-	30.64 (±0.38)	-	30.45 (±0.48)
MGG_Crh4	24.98 (±0.18)	-	24.95 (±0.40)	-	25.19 (±0.35)
MGG_40S	18.64 (±0.31)	-	18.34 (±0.22)	-	17.91 (±0.56)

Within plate one (Table 4.7), the expression of *MGG_Crh1* in the background strain Δ*MGG_Crh1* line 36 were very significantly different ($p<0.001$) relative to the expression in WT. However in this knockout strain, the ct is only slightly below 35 (between 32.84 ct to 34.46 ct) with only 7.5 ct less than in WT. A second strain, Δ*MGG_Crh2* line 39, also showed a very significant ($p<0.001$) difference in the expression of *MGG_Crh2* relative to WT with a difference of 18.64 ct. Similarly in plate 2, the expression of gene *MGG_Utr2* is very significant ($p<0.001$) in the knockout strain Δ*MGG_Utr2* line 2 and ΔΔ*MGG_Crh2_Utr2* line 25, relative to WT, both with a ct difference of 16.97 and 17.43 respectively. The gene *MGG_Crh2* was also found to be very significantly different ($p<0.001$) in the double knockout strain ΔΔ*MGG_Crh2_Utr2* line 25 relative to the expression in WT. No difference is seen for the remaining gene *MGG_Crh3, MGG_Crh4,* and the control gene *MGG_40s* in any of the knockout strain, relative to WT.

Results from this analysis confirmed the absence of transcript for the targeted gene deletion in the respective strains: Δ*MGG_Utr2,* Δ*MGG_Crh2,* and ΔΔ*MGG_Crh2_Utr2*. For strain Δ*MGG_Crh1*, the expression of *MGG_Crh1* was detected below 35 ct and less than 10 ct difference to WT. This is possibly due to the already low expression level of gene *MGG_Crh1* at 26.12 ct in WT.

4.4.2 Generation of Revertant Strains

Preliminary phenotypic analyses by plate growth assay indicate that the single gene knockout strains Δ*MGG_Utr2* and Δ*MGG_Crh2* exhibit mutant phenotype with a reduction in fungal growth under cell wall stress conferred by Congo Red and Caffeine. This lead to the construction of revertant plasmids and subsequent transformation into both these mutant lines. Additionally, this section also described the generation of two revertant strains each with a fluorescently tagged MGG_Utr2p or MGG_Crh2p with the aim to contribute towards knowledge in the localisation of MGG_Utr2p and MGG_Crh2p.

4.4.2.1 Construction of Revertant Plasmids

Previous bioinformatics work (Chapter 3 section 3.4.1.3 and 3.4.1.4) showed that *M. oryzae MGG_Utr2* and *MGG_Crh2* also contain a signal peptide and GPI-anchoring at both N and C terminus. Therefore, similar to *Crh-like* genes in *S. cerevisiae* and *C. albicans* described above, the insertion location of the fluorescent protein (FP) requires careful consideration. Unfortunately, unlike *S. cerevisiae Crh-like* genes, the orthologs in *M. oryzae* do not have an in-frame *SpeI* site nor is the GPI-anchor site experimentally validated as opposed to *Crh-like* genes in *C. albicans.* GPI-anchor prediction alone for *M. oryzae* is insufficient to confidently locate the true location of GPI-anchor site, especially with the conflicting results given by two softwares, GPI-Som and Big-pi (Chapter 3 Table 3.3). Therefore with current information, both N and C-terminal fusion may prove problematic. In a review written by Snapp (2005), the author noted that it is possible to conduct 'internal' fusion between two to ten amino acids downstream of the predicted signal peptide if N and C-terminal fusion is deemed inappropriate

(Appendix B.6). In agreement to this, it is proposed as the best strategy to fluorescently tag *M. oryzae* Crh-like proteins.

In this section, the main priority was to obtain transformed lines that complemented the phenotype of mutants *MGG_Utr2* and *MGG_Crh2*. Due to this, two vectors namely #5 and 13c, were developed through cloning work containing the native promoter and coding sequence for genes *MGG_Utr2* and *MGG_Crh2* respectively. The second priority is protein localisation of the most highly expressed gene, *MGG_Crh2*. This gene was identified as the gene to prioritise based on gene expression (Chapter 3) and mutant phenotype work in this Chapter. From these studies, it was evident that relative to four other *M. oryzae Crh-like* genes, *MGG_Crh2* is most highly expressed and most important for cell wall integrity. As such, the vector 13c_2ci containing eGFP tagged *MGG_*Crh2 was developed. The last and additional aim of this section was to tag MGG_Utr2p with a suitable fluorophore, with the intention that the vector #5_9a will provide not only localisation information of this protein, but also knowledge on co-localisation with eGFP tagged MGG_Crh2.

The fluorophore eGFP was chosen as a primary candidate to tag MGG_Crh2p due to various reasons. The reasons include the ability to visualise these proteins in living fungal tissues, it is pH stable (enable imaging of living cultures on various types of surfaces and media), and shown to be successfully tagged GPI-anchored Crh-like proteins in *S. cerevisiae* and *C. albicans* (Rodriguez-Pena *et al.* 2000, Pardini *et al.* 2006). The mCherry was the second fluorophore used as it was developed from mRFP1 (Shaner *et al.* 2004) but is more photostable than the mRFP1 counterpart. This is an ideal fluorophore to use in multi-fluorescent imaging and co-localisation work between eGFP tagged

MGG_Crh2 protein and mCherry tagged MGG_utr2 protein. This is due to the wide separation between the excitation and emission peaks of both fluorophores, thus allowing the use of distinct channels during imaging. This will minimise any 'bleeding' effect, whereby one channel begins to detect fluorescence from another channel.

4.4.2.1.1 Cloning Work

Vector Check

The PCR gene insert containing both promoter and coding region for *MGG_Utr2* and *MGG_Crh2* respectively, along with the fluorophores, were inserted into pUCAP vectors (1-1) or (3-2) in a series of restriction enzyme digestion, ligation and cloning work. However before this, both native vectors (1-1) and (3-2) were subjected to a thorough vector digestion check to ensure that it is the correct vector with all the listed coding sequences. With this, eight restriction enzyme digestion reactions were conducted for each vector.

According to the nucleotide sequence given, each digestion should produce digested fragment/s of known size. Shown in Figure 4.16, a size separation gel (1% agarose) with the various digested fragments. Both vector (1-1) and (3-2) were linearised when digested with *Asc*I, *BamH*I, *Swa*I, *Sbf*1 as these vectors only have one restriction enzyme cut site for each enzyme, thus giving a single band at 4.4 kb. The restriction enzyme *Sal*I cuts at three sites flanking the BAR sequence, on both (1-1) and (3-2), thus releasing the BAR fragment (0.93 kb) and remaining fragments of the vector (2.67 kb and 0.83 kb). The restriction enzyme *Pvu*II cuts each vector at three sites (refer to the illustration in Figure 4.5). One of the sites is found within the BAR sequence towards the 3' end. As such, since vector (3-2) contains BAR sequence in

reverse, each vector will give a different set of fragment sizes. Vector (1-1) will release three fragments sized 2.3 kb, 1.9 kb and 0.17 kb upon digestion with *Pvu*II. While vector (3-2) when digested with the same enzyme, will release three fragments sized 2.3 kb, 1.09 kb, and 0.98 kb. The double digestion of vector (1-1) and (3-2) respectively with *BamH*I and *Kpn*I resulted in the release of the ampicillin resistance sequence (0.8 kb) and the remaining vector fragment (3.6 kb).

To validate that there is no additional fragment within the multiple cloning sites (MCS1), a double digest of *BamH*I with *Asc*I was conducted and as expected, no fragments were released. Instead, both vectors were linearised to the vector size of 4.4 kb. In Figure 4.16, control (C) in this assay is undigested vector (1-1) or (3-2). The circular plasmid can exist as various conformations: supercoiled, linear or relaxed. This explains the presence of multiple bands for both undigested (1-1) and (3-2). In conclusion, the components of both vectors accurately reflect the nucleotide sequence given and subsequent cloning work can be conducted with confidence.

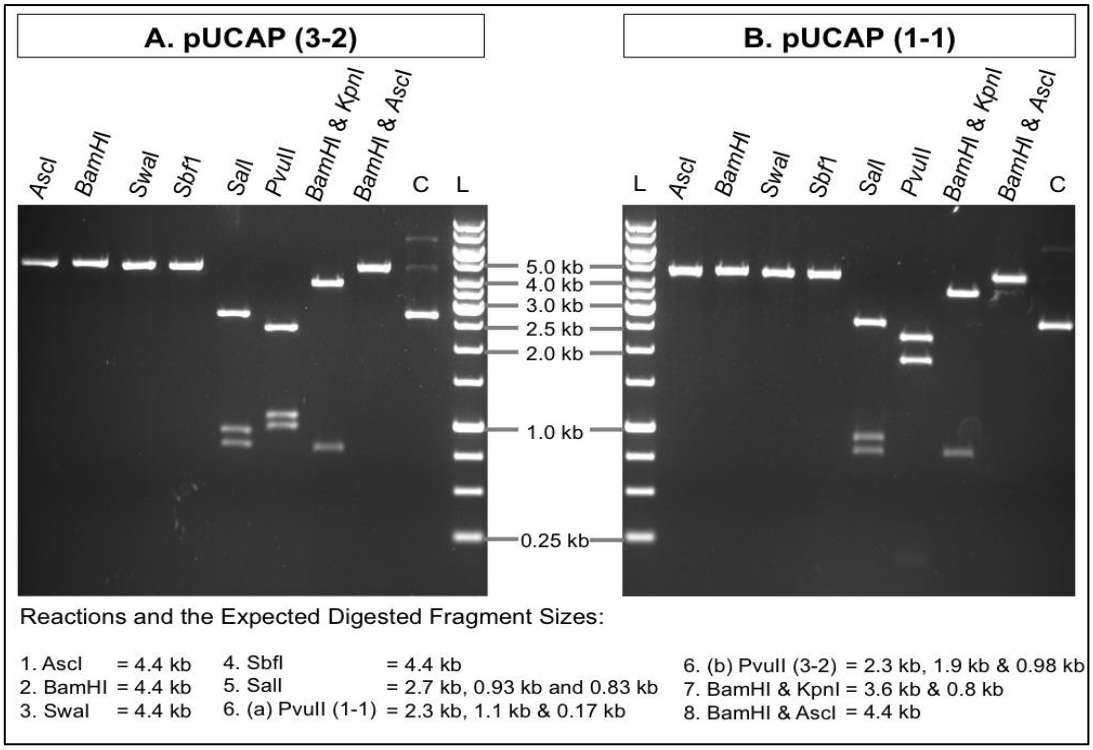

Figure 4.16. Vector Check by Restriction Enzyme Digestion. Vectors (1-1) and (3-2) were digested eight times respectively, each reaction using different combinations of restriction enzymes as listed above along with the expected digested fragment size. **Panel A.** Size-separated fragments of digested vector (3-2). Each lane loaded with digests using enzymes as per labeled lanes from left: *Asc*I, *BamH*I, *Swa*I, *Sbf*I, *Sal*I, *Pvu*II, *BamH*I & *Kpn*I, *BamH*I & *Asc*I, non-template control (C) and 1 kb molecular ladder (L). **Panel B.** Size-separated fragments of digested vector (3-2). Each lane loaded with digests using enzymes as per labeled lanes from left: 1 kb molecular ladder (L), *Asc*I, *BamH*I, *Swa*I, *Sbf*I, *Sal*I, *Pvu*II, *BamH*I & *Kpn*I, *BamH*I & *Asc*I and non-template control (C). Both size separation gel electrophoresis run used GeneRuler™ 1 kb DNA Ladder as the molecular ladder (L) and 1% Agarose gel.

Insert Design & Ligation to Vectors

Polymerase Chain Reaction (PCR) inserts containing sequences for genes of interest and fluorophores were amplified from genomic WT Guy11 DNA or existing vectors, using primers listed in Table 4.8.

Table 4.8. Primers Designed for the Amplification of PCR Inserts and Vector Validation

Insert	Primer sequence		Fragment size (kb)
eGFP	F: AAAA**GATATC**GTGAGCAAGGGCGAGGAGC (***EcoRV*** site) R: AAAA**GATATC**CTTGTACAGCTCGTCCATGC (***EcoRV*** site)		0.72
mCherry	F: AAAAAGATATCGTGAGCAAGGGCGAGGAGGATAAC R: AAAAAGATATCCTTGTACAGCTCGTCCATGCCG		0.71
MGG_Crh2 Insert	Fragment A (Promoter)	AF_crh2: AAAAA**GGCGCGCC**ACCTGGAGAAGGACAAGAC (***AscI*** site)	1.44
		AR_crh2: GATGGGGCTGCAGGCAGTGTGAGTCTG**GATATC**GCAGGCAGTGTGAGTCTG (***EcoRV*** site)	
	Fragment B (Coding Region)	BF_crh2: CAGACTCACACTGCCTGC**GATATC**CAGACTCACACTGCCTGCAGCCCCATC (***EcoRV*** site)	1.19
		BR_crh2: AAAAA**GCGGCCGC**TTACAGCATGAAGTAACCCAG (***NotI*** site)	
	Sequencing check	#1_crh2_seq: same as above #2_crh2_seq: ACAAGTGCCAACAACATGGTC #3_crh2_seq: GAGTTAGTAGGGCGTCACG #4_crh2_seq: ACCATCTTCTTCAAGGACGAC #5_crh2_seq: ATACATCTTCGGAGGCAAGG #6_crh2_seq: AAGGACCAGCTCCAGTGG #7_crh2_seq: AGGCCAGCAACGGTACTG	
MGG_Utr2 Insert	Fragment A (Promoter region)	AF_utr2: AAAA**GGCGCGCC**TCGTGGTTGTAAAGAC (**AscI** site)	1.2

		AR_utr2: AGTGAGCACTTGAGACCGTC**GAT ATC**GCACTTGAGACCGTCGGCAG C (**EcoRV** site)	
	Fragment B (Coding Region)	BF_utr2: TGCCGACGGTCTCAAGTGC**GATA TC**GACGGTCTCAAGTGCTCACTC (**EcoRV** site) BR_utr2: AAAA**ATTTAAAT**TCATAGCATGAC TAGTCC (**SwaI** Site)	1.5
	Sequencing check	#1_utr 2_seq AACACGGTGCACACACTC #2_utr 2_seq: TCCACCACAATACTCATAATG #3_utr 2_seq: AAGGCCAAGAAGCCCGTG #4_utr 2_seq: AGCCTCTCTTCTCGAATGG #5_utr2_seq: ATCCTCTCGTCGTTGCAGG	
	Utr2 PCR Check	F: same as #1_utr 2_seq: R_Utr2: GTTCATGTACGGCTCCAAG	0.8

Shown in Figure 4.17, four PCR fragment inserts product size and purity check prior to restriction enzyme digestion. Once ligated, candidate vectors were checked for the presence of the insert by double digestion. Shown in Figure 4.18 the location of restriction enzyme cut site for *Asc*I, *Not*I, and *EcoR*V in vectors 13c and 13c_2ci. Therefore in a successful ligation such as in clone 13c (Figure 4.19), an insert with the fragment size 2.6 kb and another fragment corresponding to linearised vector at 4.4 kb is seen. Subsequent 13c digestion with *EcoR*V and ligation to *EcoR*V-digested eGFP further yielded vector 2ci, as shown in Figure 4.19. Similarly, once the *MGG_Utr2* and mCherry inserts were ligated to vector (3-2) and #5 respectively, double digestion was conducted to check for the presence of insert. Figure 4.20 illustrates the location of the double digest enzyme used, *Asc*I and *Swa*I and the expected fragment sizes. Figure 4.21

showed results of the double digestion, confirming the presence of *MGG_Utr2* insert and *MGG_Utr2* containing the *EcoR*V-ligated mCherry. Once confirmed by restriction digests, vectors were further checked for orientation of insert and coding sequence by DNA sequencing, and each nucleotide was found to be identical to the native sequence. Table 4.9 summarises the list of vectors prepared in this study.

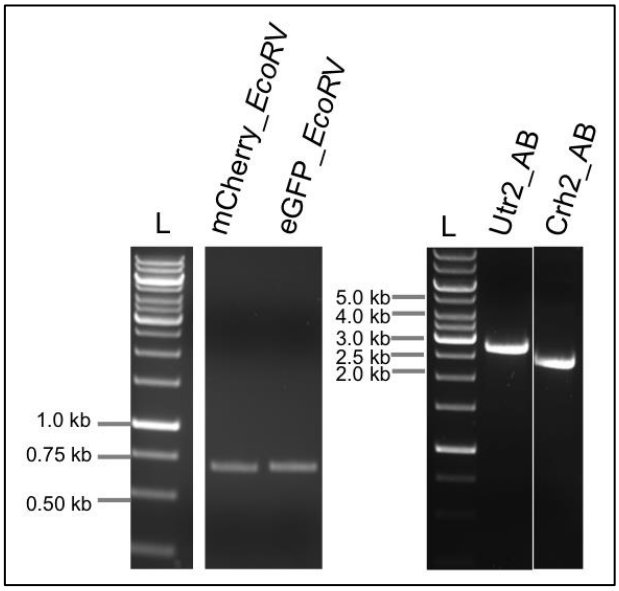

Figure 4.17. Polymerase Chain Reaction Product Quality Check by Gel Electrophoresis. Shown above a size separation gel electrophoresis run for four cloning inserts prepared by PCR to check for product size and purity. Lanes from left: GeneRuler™ 1 kb DNA Ladder (L), mCherry PCR product with *EcoR*V cut sites at both ends (0.71 kb), eGFP PCR product with *EcoR*V cut sites at both ends (0.72 kb), *MGG_Utr2* Insert (Utr2_AB) at 2.7 kb and *MGG_Crh2* Insert (Crh2_AB) at 2.3 kb. Gel electrophoresis run used 1% Agarose.

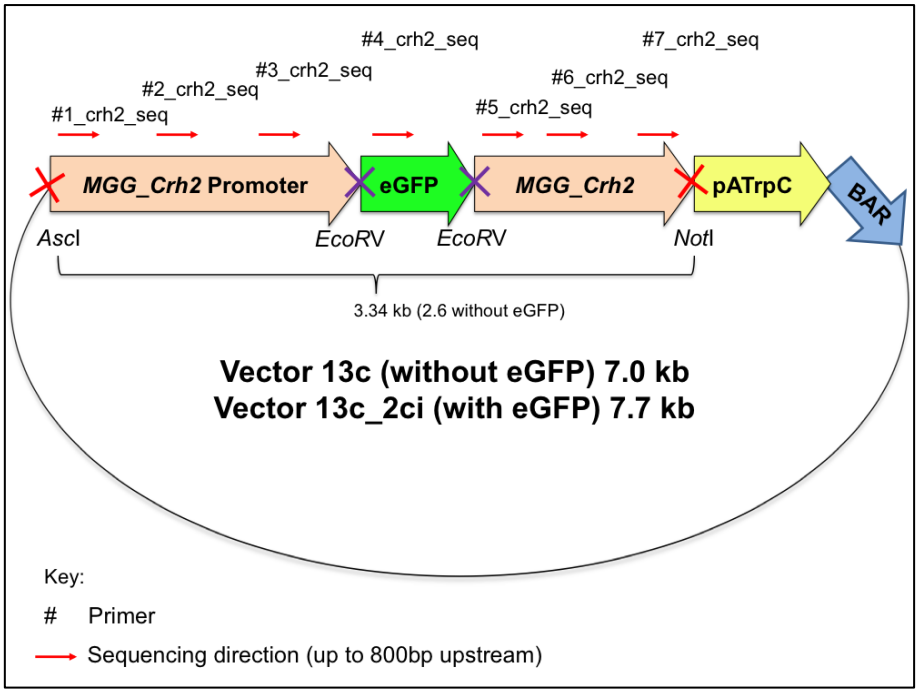

Figure 4.18. An Illustration for the Confirmation of Vector 13c and 13c_2ci by Sequencing and Restriction Enzyme Double Digest. Image above is an illustration for the location of seven primer sequences used for DNA sequencing. Each primer is estimated to sequence between 600 to 800 bp downstream. Thus, these primers were designed in an overlapping manner. Included in the image above are the location of restriction enzyme cut sites for *Asc*I and *Not*I (red crosses) where the insert was ligated to linearised vector (1-1) and *EcoR*V cut site (purple crosses) where it was ligated to *EcoR*V-linearised vector 13c.

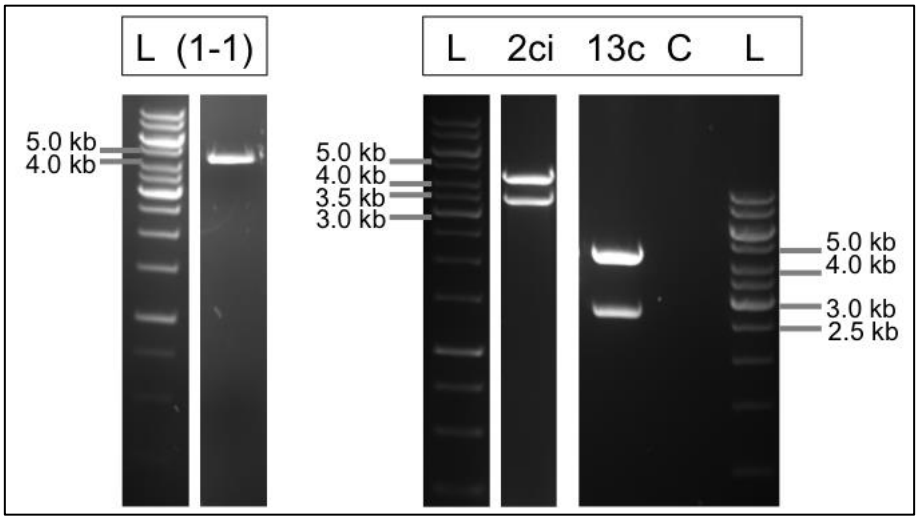

Figure 4.19. Confirmation of Vector Ligation by Restriction Enzyme for the Construction of Vector 13c and 13c_2ci. Gel run above shows *Asc*I and *Not*I digested vector 13c, 13c_2ci and the positive control vector (1-1). From left: GeneRuler™ 1 kb DNA Ladder (L), empty vector (1-1) linearised to give one fragment at 4.4 kb, clone 2ci releasing 2 fragments, namely the vector (4.4 kb) and *MGG_Crh2* insert containing eGFP (3.3 kb), clone13c, releasing 2 fragments, the vector at 4.4 kb and the *MGG_Crh2* insert (2.7 kb), non-template control (C) and GeneRuler™ 1 kb DNA Ladder (L). All size separation by gel electrophoresis used 1% Agarose.

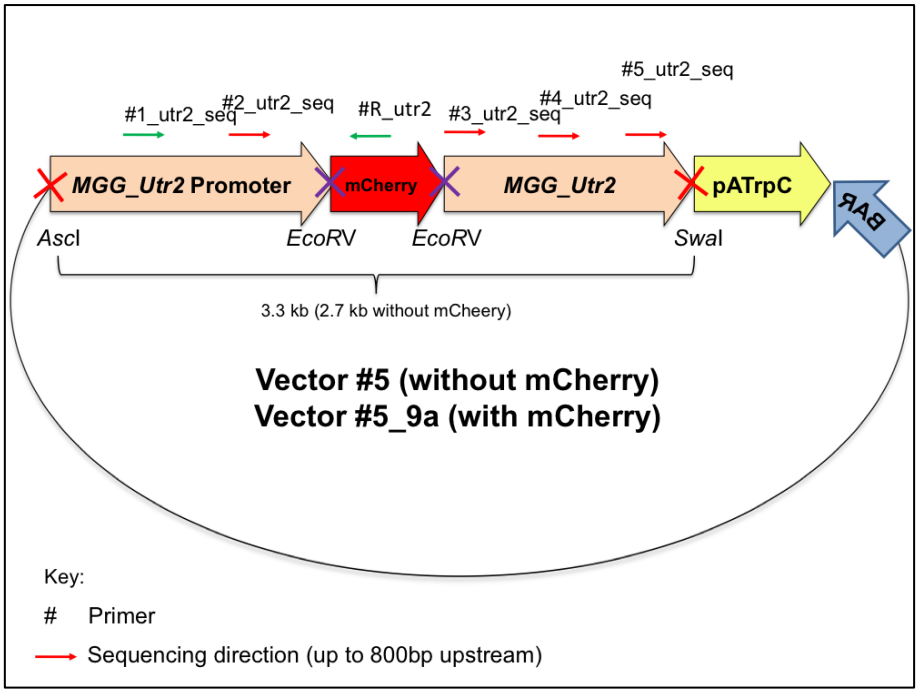

Figure 4.20. A Visual Illustration for the Confirmation of *MGG_Utr2* Insert Ligation to Vector (3-2) by Sequencing and Restriction Enzyme Double Digest. Image above is an illustration for the annealing location of five primer sequences used in DNA sequencing. Each primer is estimated to sequence reliably between 600 to 800 bp downstream. Thus, these primers were designed in an overlapping manner. Included in the image above are location of restriction enzymes *Asc*I and *Swa*I (red crosses) where the insert was ligated to *Asc*I-*Swa*I linearised vector (3-2) and location of the *EcoR*V ligation (purple crosses).

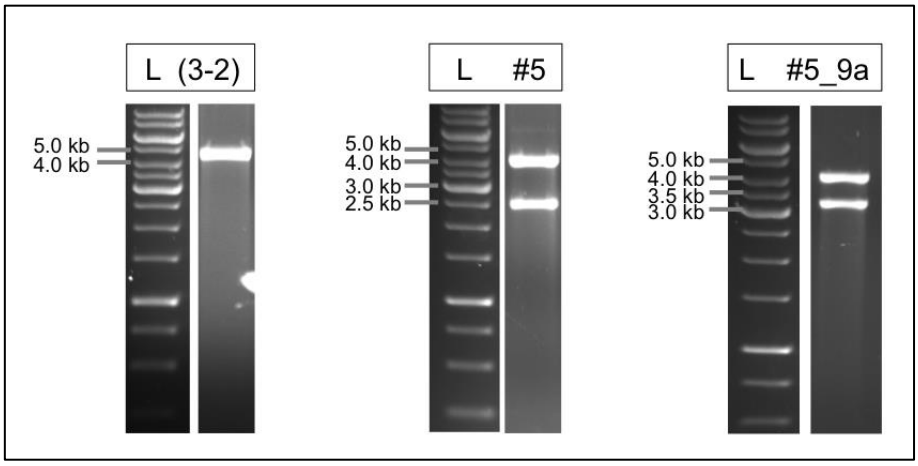

Figure 4.21. Confirmation of Vector Ligation by Restriction Enzyme for the Construction of Vector #5 and #5_9a. Vector #5 and #5_9a were digested with *Asc*I and *Swa*I using the empty vector (3-2) as the negative control. Gel on the left showed the presence of a linearised vector (3-2) at 4.4 kb with no insert present. Middle gel showed the release of insert *MGG_Utr2* sized 2.7 kb and the remaining vector at 4.4 kb. Gel on the most right showed that with the same set of enzymes, a larger insert fragment (3.3 kb) made from mCherry ligated internally within the *MGG_Utr2* PCR insert as well as the 4.4 kb vector fragment. All size separation by gel electrophoresis used 1% Agarose.

Table 4.9. List of New Vectors Designed in This Study Coding for genes *MGG_Crh2* and *MGG_Utr2*.

Vector name	Contents
13c	pUCAP (1-1), BAR, *MGG_Crh2* PCR fragment, ampicillin
13c_2ci	pUCAP (1-1), BAR, **eGFP** *MGG_Crh2* PCR fragment, ampicillin
#5	pUCAP (3-2), BAR, *MGG_Utr2* PCR fragment,
#5_9a	pUCAP (3-2), BAR, **mCherry**, *MGG_Utr2* PCR fragment,

4.4.2.2 Fungal Line Transformation Confirmation & Imaging

Once each vector was constructed and insert checked by both restriction enzyme digest and DNA sequencing, it was then transformed into the corresponding mutant lines for phenotype complementation and protein localisation.

Candidate transformed lines that grew on plates containing Bialaphos were first checked for the presence of the vector inserted ectopically by PEG-mediated transformation. Here, gDNA of candidate complemented lines, WT (positive control) and mutant lines *ΔMGG_Crh2* Line 39 and *ΔMGG_Utr2* Line 2 as negative controls, were extracted and used as templates in subsequent PCR reactions. For the confirmation of the presence of *MGG_Crh2* gene in candidate revertant strains, primer pairs (Conf_Crh2_F and Conf_Crh2_R) designed to amplify a genomic region no longer present in the nulled mutant *ΔMGG_Crh2* Line 39, would now give a product size of 0.45 kb (Table 4.2). Image left in Figure 4.22 showed the presence of gene *MGG_Crh2* in complemented line 2ci_6 (with eGFP), 13c_2 (no eGFP) and WT but not present in gDNA of *ΔMGG_Crh2* Line 39 and the non-template control.

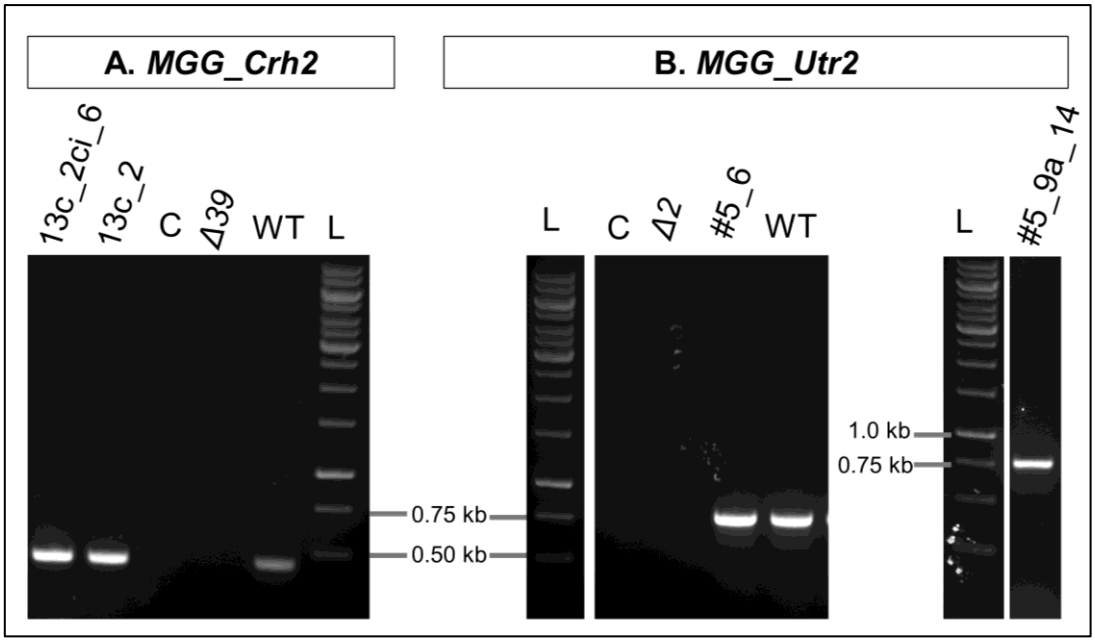

Figure 4.22. Confirmation by PCR for the Presence of Linearised Plasmids in Revertant Strains. The genome of two mutant lines were ectopically inserted with linearised revertant plasmids by PEG-mediated transformation. Mutant line Δ*MGG_Crh2* line 39 was transformed with plasmid 13c or 13c_2ci while Δ*MGG_Utr2* line 2 with plasmid #5 or #5_9a. Primers were designed to specifically amplify a target gene coding region found only in the introduced plasmid. **Panel A.** PCR product size separation by gel electrophoresis, using primer pairs designed to amplify a 0.45 kb sized product from within the coding sequence of *MGG_Crh2*. Lane from left: complemented line 2ci_6 (with eGFP), complemented line 13c_2 (without eGFP), Non-template control (C), negative control (Δ39) using gDNA from *ΔMGG_Crh2* line 39 as template, positive control (WT) using gDNA of WT as template and GeneRuler™ 1 kb DNA Ladder (L), **Panel B.** Left image show PCR product size separation by gel electrophoresis, using primer pairs that amplify a 0.45 kb product size from the coding sequence of *MGG_Utr2*. Lanes from left: GeneRuler™ 1 kb DNA Ladder (L), Non-template control (C), negative control (Δ2) using gDNA from *ΔMGG_Utr2* line 2 as template, complemented line #5_6 (without mCherry) and positive control (WT) using gDNA from WT strain as template. Gel image on the most right is a transformed line showing the presence of both *MGG_Utr2* insert and mCherry by the primers that amplify a region spanning both *MGG_Utr2* promoter region and mCherry giving a product size of 0.8 kb. All size separation by gel electrophoresis used 1% Agarose.

Similarly, for the confirmation of candidate complemented line #5_6, primer pairs (Conf_Utr2_F and Conf_Utr2_R) were designed as shown in table 4.2, to amplify a coding region within *MGG_Utr2* giving a product size of 0.79 kb. For the complemented line containing mCherry-tagged *MGG_Utr2,* a set of primers annealing to a region bordering the mCherry and *MGG_Utr2* promoter sequence was designed (Table 4.8), giving a product size of 0.8 kb. Shown in Figure 4.22, PCR product gel run in the middle image showed the presence of product sized 0.79 kb in transformed line #5_6 and in the positive control, WT, but absent in the negative control using gDNA of *ΔMGG_Utr2* Line 2 as a template. Similarly, a product sized 0.8 kb is seen in transformed line #5_9a_6 in the gel on the right in Figure 4.22. In conclusion, both negative controls *ΔMGG_Crh2* Line 39 and *ΔMGG_Utr2* Line 2 confirmed in PCR amplification check, that genes *MGG_Crh2* and *MGG_Utr2* are no longer present while still present in the gDNA of the positive control, WT. All four revertant lines showed the presence of the respective gene inserted back into the genome of previously nulled mutants.

4.5 Chapter Summary & Conclusion

In summary, work in this Chapter produced four knockout mutants each with two independent transformant lines. These are three single gene knockouts (Δ*MGG_Utr2,* Δ*MGG_Crh1,* and Δ*MGG_Crh2*) and one double gene knockout strain (ΔΔ*MGG_Crh2*_Utr2). This was followed by the generation of four revertant strains for Δ*MGG_Utr2* and Δ*MGG_Crh2*, each expressing a functional gene with/without a fluorescently tagged protein. These mutant and revertant lines were then phenotypically assayed with the WT strain in the next chapter.

Table 4.10. List of *Magnaporthe oryzae* Deletant and Revertant Strains Generated in This Study.

Deletion Cassette/ Revertant Plasmid	Background strain	Mutant strain
A. Generation of Mutant Lines		
Utr2_Hyg	WT	1. Δ*MGG_Utr2 Line 1* 2. Δ*MGG_Utr2 Line 2*
Crh1_Hyg	WT	1. Δ*MGG_Crh1 Line 36* 2. Δ*MGG_Crh1 Line 43*
Crh2_Hyg	WT	1. Δ*MGG_Crh2 Line 37* 2. Δ*MGG_Crh2 Line 39*
Utr2_Bar	Δ*MGG_Crh2 Line 39*	1. Δ*MGG_Crh2_Utr2* Line 25 2. Δ*MGG_Crh2*_Utr2 Line 27
B. Generation of Revertant Strains		
13c	Δ*MGG_Crh2 Line 39*	Line 13c_2
13c_2ci	Δ*MGG_Crh2 Line 39*	Line 13c_2ci_6
#5	Δ*MGG_Utr2 Line 2*	Line #5_6
#5_9a	Δ*MGG_Utr2 Line 2*	Line #5_9a_14

CHAPTER 5

Mutant Phenotyping- Growth, Morphology, & Pathogenicity

5.1 Chapter Introduction

5.1.1 Chapter Overview

The primary objective of Chapter 5 is to then study and compare the growth, morphology and pathogenicity of the deletant strains generated in Chapter 4 with Wild Type (WT) strain Guy11.

Phenotyping work of mutant strains in this chapter includes various assays covering both vegetative and infective life cycle of the fungus. Under vegetative growth, strains were exposed to various growth conditions known to cause stress and activate specific stress response pathways using plate and liquid biomass assays. In addition to this, cell wall structure was visualised by Transmission Electron Microscopy (TEM) and fluorescent staining with Calcofluor White (CFW). In the infective life cycle, strains were evaluated for germling fitness and morphology on artificial hydrophobic surfaces. Finally, deletant strains were tested for virulence and by inoculation on host plants.

5.1.2 Cell Wall Integrity: Growth Assays

A characteristic trait that most cell wall protein deletant strains exhibit is hypersensitivity to external stressors that exaggerate the stress on the already compromised cell wall, especially cell wall perturbants such as Congo Red and Calcofluor White. For example in *S. cerevisiae*, single and triple mutant lines for genes *Crh1, Crh2* (syn. *Utr2*) and *Crr1* grown on plates were hypersensitive to Congo Red (100 µg/ml), and Calcofluor White (20 µg/ml) (Figure 5.1). Similarly in *C. albicans* single and triple deletant strain *utr2*∆crh11∆crh12 showed pronounced sensitivity to Congo Red (100 µg/ml), SDS (0.06%) as well as to Calcium (500 mM).

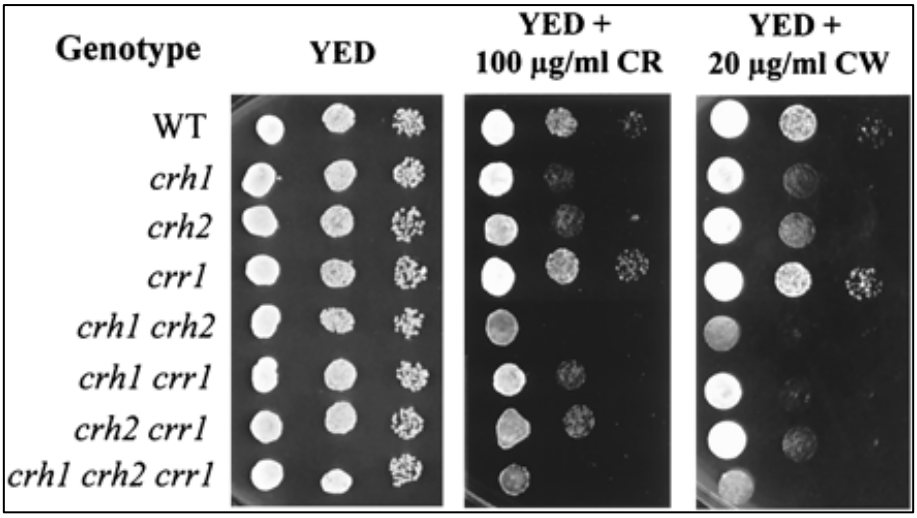

Figure 5.1. Sensitivities to Congo red and Calcofluor White of *Crh-like* Deletant Strains in *Saccharomyces cerevisiae.* Strains include all the possible combinations of deletions of the *Crh1*, *Crh2*, and *Crr1* genes were grown in YED, and 1/10 dilution series of each strain were spotted onto YED plates containing the indicated amounts of Congo red and Calcofluor white. Figure and caption were taken from Rodriguez *et al.* (2000) where this gene was first identified and studied.

5.1.2.1 Cell Wall Stress & Osmo-stabiliser

The most commonly used chemical compound to test for a compromised cell wall is Congo Red (Ram and Klis 2006). This cell wall perturbant is a secondary diazo dye and is the sodium salt of 3,3'-([1,1'-biphenyl]-4,4'-diyl)bis(4-aminonaphthalene-1-sulfonic acid) with the molecular formula $C_{32}H_{22}N_6Na_2O_6S_2$ and a molecular structure as shown in Figure 5.2. It is a water-soluble fluorescent dye with an excitation peak at 514 nm (Matsuoka *et al.* 1995). The dye interacts with various polysaccharides, with an especially strong affinity for *β*-glucan by the formation of hydrogen bonds with the latter (Wood 1980, Roncero and Duran 1985). This strong affinity for glucan polymers prevents the normal formation of microfibrils and chitin aggregation, resulting in a loss of cell wall rigidity (Kopecká and Gabriel 1992). In the 1990's, little is known regarding Crhp and the transglycosylase activity, however, recent literature enabled the presumption that it is likely Congo Red competes with the activity of Crh-like proteins from forming

cross-links between chitin and glucan polymers, thus the observation in the literature pertaining loss of microfibrils and cell wall rigidity.

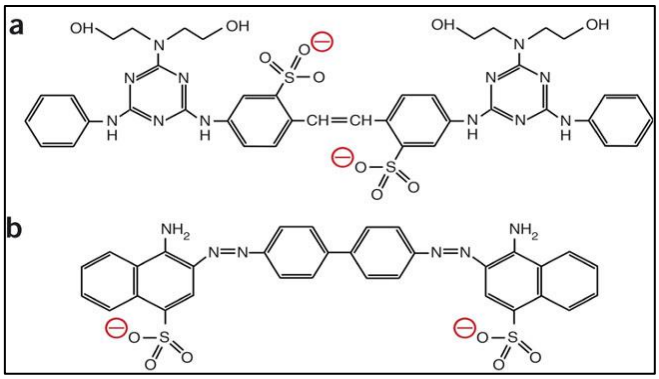

Figure 5.2. The Chemical Structures of Calcofluor White (a) and Congo Red (b). The presence of negatively charged sulfonic-acid groups on both compounds are only present at pH 5.5 and above. Thus to prevent protonation and subsequent lack of chemical function, pH of medium must be buffered above pH 5.5. Figure was taken from Ram and Klis (2006).

The loss of cell wall rigidity due to exposure to Congo Red results in deformed hyphae and reduction in fungal growth. In both *A. nidulans* and *A. niger,* exposure to 100-150 μg/ml of Congo Red leads to hyphae swellings and subsequent bursting due to the inability of the weakened cell wall to withstand internal hydrostatic pressures (Pancaldi *et al.* 1984, Guerriero *et al.* 2013). Given these facts, any compromise in the cell wall of mutant strains will result in added hypersensitivity to Congo Red. These swellings caused by Congo Red can be prevented with the addition of an osmotic stabiliser such as Sorbitol, as shown in Figure 5.3 by Lui *et al.* (2006). With this, hypersensitivity to Congo Red in a mutant strain can be confidently attributed to defects in cell wall strength by the occurrence of osmo-remedial traits. This coupled with the up-regulation of two *M. oryzae Crh-like* genes when grown in Congo Red, justify the relevance of testing the growth of mutants generated in Chapter 4, with this compound.

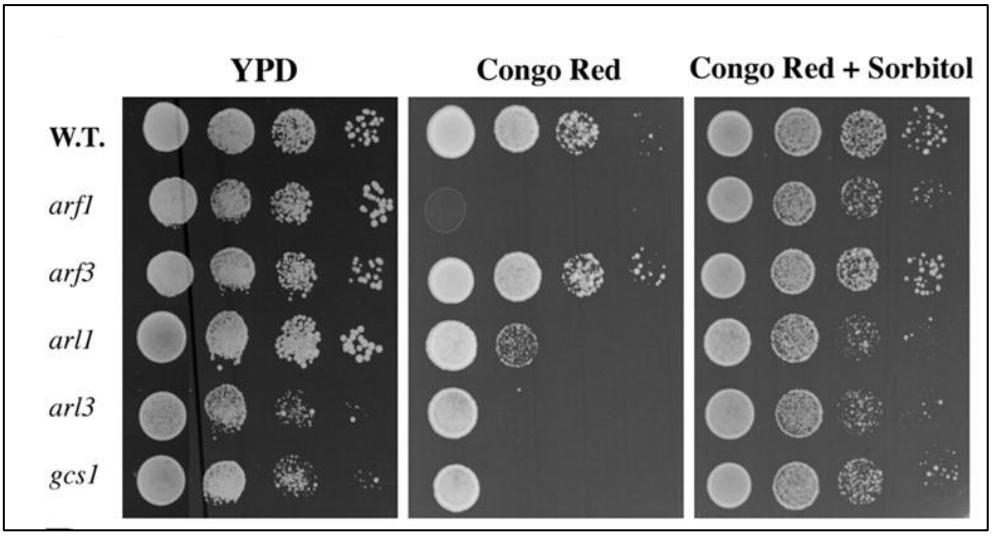

Figure 5.3. Congo Red Hypersensitivity Assay for *Arl* Deletant Strains in *Saccharomyces cerevisiae*. Yeast strains were serially diluted ten-fold as indicated and spotted on plates of yeast potato dextrose (YPD) agar, Congo Red (100 µg/ml) and Congo Red (100 µg/ml) with 1.2 M sorbitol to analyse their sensitivity to cell-wall interference. Figure and caption obtained from Liu *et al.* (2006) showing the occurrence of mutant hypersensitivity to Congo Red and subsequent osmo-redial by Sorbitol.

5.1.2.2 Cell Wall Stress Caused by Caffeine

Caffeine (1, 3, 7-trimethylxanthine), an analogue of purine bases, is a pleiotropic mutagen that causes fungal cell wall stress, although the specific mechanism is still unknown (Kuranda *et al.* 2006). While the Target of Rapamycin Complex (Torc1) may be the primary target of caffeine (Reinke *et al.* 2006, Wanke *et al.* 2008), recent studies suggest additional targets. Caffeine was shown to phosphorylate Mpk1p at an atypical site, thereby preventing the downstream binding of Mpk1p with Swi4p and subsequent formation of an SBF complex (Truman *et al.* 2009). The SBF complex is associated with the cell wall integrity (CWI) pathway (Kim and Levin 2011, Levin 2011) and cell-cycle regulation (Koch *et al.* 1993, Breeden 2003). This then explains the mutagenic effect of caffeine and the use in assessing for cell wall defects in mutant strains (Verna *et al.* 1997, Gerik *et al.* 2005, Ram and Klis 2006). For the purpose of this study, caffeine is deemed a suitable growth perturbant compound given the

alternative mode of causing cell wall stress and the observed variation in regulation under caffeine stress (Chapter 3).

5.1.2.3 Other External Stressors

Oher compounds routinely used in growth assays include Sodium Dodecyl Sulphate (SDS). Sodium Dodecyl Sulphate ($CH_3(CH_2)_{11}OSO_3Na$) is an anionic surfactant that specifically disrupts the plasma membrane and causes cell lysis and therefore mutants with a cell membrane defect will show added hypersensitivity (de Groot *et al.* 2001a, Carbó and Pérez-Martín 2010). While plasma membrane damage is unlikely for mutants associated with cell wall proteins such as *Crh-like* genes, it is a good assay as an indicator of general fungal fitness and detecting additional defects in cell wall mutants.

5.1.3 Fungal Morphology and Cell Wall Structure

The morphology and structure of the cell wall can be viewed in living tissues by staining with Calcofluor White (CFW), syn: Fluorescent Brightener 28 (Sigma-Aldrich). This water-soluble compound is a fluorescent dye with the excitation wavelength of 347 nm when exposed to UV. In the early 1940s, it is a common compound used in the textile industry as an optical brightener/whitener (Hoch *et al.* 2005). It is now commonly used in fungal staining due to the high affinity for chitin polymers (Elorza *et al.* 1983) and is used in clinical laboratory for pathogenic fungal detection in host tissues (Monheit *et al.* 1984, Lynch and Gibson 1987, Rasconi *et al.* 2009), as well as fungal cell wall staining work (Apoga and Jansson 2000, Santos and Snyder 2000). This compound is now a routine visualisation tool for studying fungal cell wall mutant lines, including the study of *Crh-like* genes in *C. albicans* (Pardini *et al*. 2006) and is deemed useful

in visualising living tissues of *M. oryzae* mutant lines with possible morphological defects.

Alternatively, the structure of the cell wall especially the septum and melanised layers, can be viewed under higher resolution in fixed cells, using the Transmission Electron Microscopy (TEM) technique. The fundamental concept of TEM is the channelling of electron beams across a thinly sliced specimen (cut with a diamond cutter). The specific pattern of electrons scattered by hitting the specimen is recorded by a CCD (charge-coupled device) camera. The use of electron instead of a light beam made this microscopic tool able to achievee far higher resolving power (picometre) as opposed to light microscopy (nanometre) (Erni *et al.* 2009). Due to the high level of magnification and resolution, the study of fungal cell wall structure by TEM is commonly used. For example, Gómez-Esquer *et al.* (2004) used TEM to visualise defects in the septum of a *S. cerevisiae Crr1* mutant line (Figure 5.4). From the *S. cerevisiae* study, it is hypothesised that *M. oryzae Crh-like* deletant strains exhibit cell wall defect, possibly at the septum area. However, there are caveats to this technique. Firstly, it is imaging a non-living specimen that has undergone a significant amount of washings and treatments. This technique, is particularly good in generating 2-D images, however, performs poorly in giving spatial information, especially surface topography. In these cases, imaging by Atomic Force Microscopy would complement well the information generated by TEM and is discussed in detail in the next Chapter.

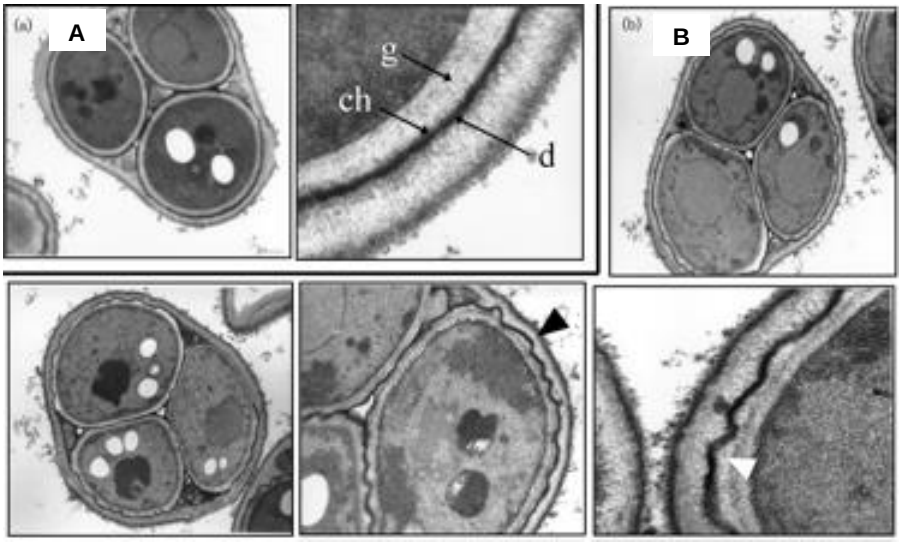

Figure 5.4. Electron Micrographs of *Saccharomyces cerevisiae* Wild-Type and *crr1*Δ mutants. Panel A Single asci of wild-type strain FY1679 at low (left) and high (right) magnifications, showing a perfectly organised spore wall: the inner electron-transparent glucan layer (*g*), followed by the chitin/chitosan layer (*ch*) and the dityrosine outermost layer (d); both of the latter appear as electron-dense layers. Old vegetative cell walls surround these structures. **Panel B** Low (first three panels) and higher (remaining panel) magnifications of mutant *crr1*Δ spores. The outermost chitosan and dityrosine layers are aberrantly assembled over the glucan/mannoprotein layer, appearing as ruffled layers (marked with arrowheads). In most of the spores, the dark electron-dense layer (the chitosan/dityrosine layer) is completely detached from the inner layer (denoted with arrows in the pictures). In some cases, discontinuities in the chitosan layer are even found (marked with an asterisk). Figure and obtained edited from Gómez-Esquer *et al.* (2004).

5.1.4 *Magnaporthe oryzae* Pathogenicity

The importance of cell wall integrity in *M. oryzae* virulence was proven many times with the deletion of key components associated with the synthesis of the cell wall or the cell wall integrity (CWI) pathway. For example, out of seven chitin synthase genes (*Chs*) in *M. oryzae*, *Chs1, Chs6* and *Chs7* were shown to be important for pathogenicity (Kong *et al.* 2012). Furthermore, deletant strains of genes linked to the CWI pathway such as the *Mps1* (Xu *et al.* 1998), *Mck1* (Jeon *et al.* 2008), *Mig1* (Mehrabi *et al.* 2008) and *MoSwi6* (Qi *et al.* 2012), which are orthologs of *Slt2, Bck1, Rlm1* and *Swi6* in *S. cerevisiae* respectively, all showed reduced or are non-pathogenic when inoculated onto a susceptible host. Hence, it can be concluded from these studies that indeed integrity of the cell

wall is important for *M. oryzae* virulence. While genes responsible for cell wall synthesis and CWI response pathway were thoroughly explored, no studies have yet confirmed the importance of cell wall remodelling proteins such as the Crhp and Gelp family of proteins in the virulence of *M. oryzae*.

In human fungal pathogens, *Crh-like* genes have been implicated with virulence and host immune response (described in detail in Chapter 1). However, the equivalent studies in fungal phytopathogens have never been explored. It is hypothesised that in *M. oryzae,* the *Crh-like* deletant strains with a weakened cell wall will result in reduced or inability to successfully infect and colonise a plant host. This section aims to confirm this hypothesis by studying the morphology of mutants during germling development, germling fitness as well as quantification methods to assess mutant pathogenicity against susceptible hosts.

5.2 Aims & Objectives

The primary aim of this chapter is to identify any phenotypic differences between Wild Type (WT) strain Guy11 and the mutant strains generated in Chapter 4. This is achieved by the following list of techniques and experimental aims:

1. Growth assays:

- To observe and quantify the vegetative growth of mutants under various stressors;
- To show that any phenotype observed is consistent between independent lines; and
- Complemented strains were added to show that a phenotype seen in the mutant lines can be reversed to WT with the re-introduction of the disrupted gene in the background mutant.

2. Microscopic techniques

- To visualise the cell wall structure of vegetative mycelium and germlings by fluorescent staining;
- To observe morphological changes and quantify germling fitness; and
- To observe the cross section (nanometre scale) of the fungal cell wall during vegetative growth and dormant spores.

(d) Infection on Host Leaf

- To visualise and quantify infective lesions of mutant strains after six days post inoculation on two species of hosts (barley and rice).

5.3 Materials & Methods

5.3.1 Plate Assay: Fungal Growth & Sensitivity Test

5.3.1.1 Strains Used

Single gene knockout lines, the corresponding complemented lines as well as double gene knockout lines described in Chapter 4, were all used in this phenotypic assay and are listed below:

(a) *ΔMGG_Utr2* lines 1 and 2

(b) *ΔMGG_Crh1* lines 37 and 43

(c) *ΔMGG_Crh2* lines 37 and 39

(d) ΔΔ*MGG_Utr2_Crh2* lines 25 and 27

(e) *MGG_Utr2* revertant strains #5_6 and #5_9a_14

(f) *MGG_Crh2* revertant strains 13c_2 and 13c_2ci_6

5.3.1.2 Preparation of Inoculating Agar Plug

The procedure described below was performed under aseptic conditions. A 50 ml falcon tube was used to measure and pour 35 ml molten agar (prepared as described below) per petri dish with a 10 cm diameter. A stock filter paper containing the respective *M*. *oryzae* genotype was placed in the middle of the agar plate and inoculated for 10 days at 25°C 14/10 hour light/dark photoperiod at 60% humidity. Circular agar plugs (1 cm diameter) were made at the growing edge of the 10 day old colony using a sterile cork borer.

5.3.1.3 Preparation of Various Treatment Plates

The vegetative growth of mutant lines relative to WT strain was compared under nine different growing conditions. These were selected by covering common types of stressors as well as the activation of various fungal MAPK signalling pathways. Osmotic stress and the activation of the high osmolarity glycerol (Hog1) pathway were achieved by adding Sorbitol to the routinely used Complete Medium (CM). For cell wall stress and the activation of the CWI pathway, the cell wall perturbing compound Congo Red (CR) was added to CM buffered with Hepes at pH 7.0. Sodium dodecyl sulphate (SDS) was added to CM to achieve cell membrane stress. Also, caffeine was added not only as a mutagenic-pleiotropic stressor, but it has also shown to activate the CWI pathway through a specific downstream phosphorylation route different from the CWI pathway activated by Congo Red. Minimal medium (MM) was used to achieve starvation, while an optimal growth condition (Control) was achieved by growing fungus on CM only. An additional control was used whereby all genotypes were grown on CM with 50 mM Hepes buffered at pH 7.0. This is because the sulfonic acid groups in Congo Red are only present at pH above 5.5 (Ram and Klis 2006). Therefore, this control was added to show that any differences in the phenotype seen, is due to the genotype and not because of the addition of HEPES (50 mM) or media buffered to pH 7.0.

The appropriate concentration of compound to use was first determined by growing WT agar plugs onto 35 ml agar plates containing a gradient of concentration. The concentration range chosen on the basis of the concentrations used in published fungal studies (Rodriguez-Pena *et al.* 2000, Pardini *et al.* 2006, Zhang *et al.* 2010, Zhang *et al.* 2011). The range used

includes 1-3 M for Sorbitol, 50 – 200 µg/mL for Congo Red, 0.005 – 0.05% for Sodium Dodecyl Sulphate and 2 – 5 mM for Caffeine. The appropriate concentration was selected when it caused a 30-50% reduction in growth of WT relative to the same strain grown on CM only plate (data not shown, as only a visual selection was conducted).

Each type of stress factor and concentration used was prepared according to Table 5.1. Using sterile 50 ml falcon tubes, 35 ml of the respective molten agar was poured into a sterile petri dish. A circular agar plug containing 10 day old *M. oryzae* genotype (prepared in section 5.3.1.2) was placed onto the middle of the plate and incubated in the dark (wrapped in aluminium foil) at 25°C. Colony diameter measured at five day old by drawing two lines across the middle section of the colony and marked with a marker pen where the furthest grown mycelium ends. After another three days, a line was marked again where the furthest mycelium ends (Figure 5.5). The difference in distance was measured in centimetres. A picture of the fungal colony was taken at 10 day old using a digital camera (Nikon D7000). A pilot assay was first conducted for each growth condition and each genotype (data not shown). This was then repeated comprising three biological replicates (three separate 10 day old CM agar plates for each genotype), and two technical replicates per biological replicate.

Table 5.1. List of Medium and Reagents Used For Plate Growth Assay.

Medium	Concentration	Preparation Method
Complete Medium (CM) Agar	n/a	Refer to Chapter 2 Table 2.1
CM agar buffered with Hepes (pH 7.0)	n/a	Complete medium (same as above) buffered with 50 mM Hepes, pH adjusted to 7.0 with NaOH (1M), 1.5% agar added and autoclaved.
CM (pH 7.0) with Congo Red (CR)	100 µg/ml Congo Red	The appropriate amount of 1% stock CR (Chapter 2 Table 2.1) was added to sterile molten CM agar buffered with Hepes (50 mM, pH 7.0). Plates prepared in flow hood without lights and used immediately.
Sorbitol	1 M	Complete medium prepared with 1 M Sorbitol (Sigma-Aldrich), 1.5% agar added and autoclaved.
Caffeine	2.5 mM	Complete medium prepared, 1.5% agar added and autoclaved. Filter sterilised stock caffeine (100 mM) added to sterile molten agar to give a final concentration of 2.5 mM Stock caffeine (100 mM): Caffeine prepared with hot Milliq_H_2O, mixed thoroughly to a concentration of 100 mM. Solution filter sterilised.
Sodium Dodecyl Sulphate (SDS)	0.005%	1% SDS (Sigma-Aldrich) diluted in Milliq_H_2O. Filter sterilised stock SDS (1%) then added to autoclaved CM to a final concentration of 0.005%.
Minimal Media	n/a	Refer to Chapter 2 Table 2.1
Congo Red with Sorbitol	100 µg/ml Congo Red and 1 M Sorbitol	The appropriate amount of 1% stock CR was added to sterile molten CM agar containing 1 M Sorbitol, buffered with HEPES (50 mM, pH 7.0).

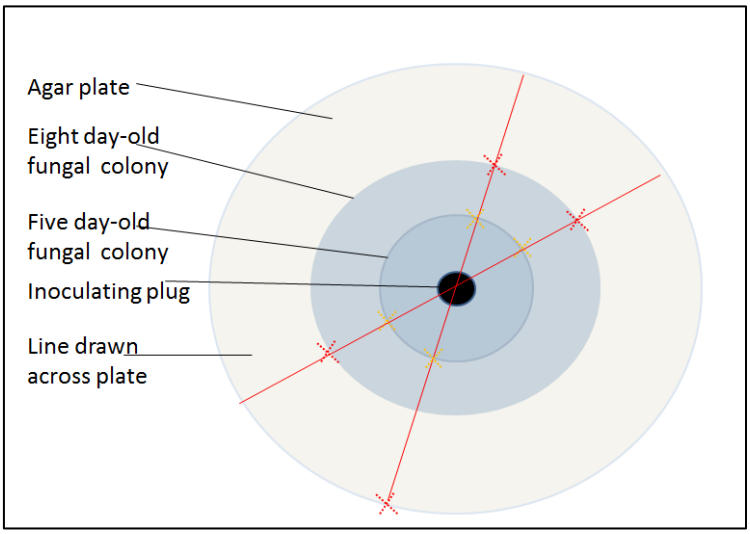

Figure 5.5. An Illustration of the Measurement of Colony Growth. Method used to measure colony growth by marking the edge of colony growth at five and eight-day old at two lines drawn randomly across the colony, giving rise to four technical replicates for each fungal colony.

5.3.1.4 Data Analysis

The difference in colony diameter (cm) between five day old and eight day old was recorded for each line. Averaged colony growth (cm over three days) for each biological replicate was calculated from the two lines. All growth treatments used the above measurement procedure, except for osmo-remedial (Congo Red with Sorbitol) whereby colony diameter was measured *in silico* using ImageJ and data analysed as per below.

For statistical analysis, a Student's t-test was used to compare the growths (three biological replicates per strain) of mutant strains, against the WT. Data was presented in the form of a ratio, whereby the averaged colony growth (cm) over three days for each genotype was measured against the corresponding WT for each assay type.

5.3.2 Liquid Biomass Assay

Liquid media used the same ingredients as described in Chapter 2 (Table 2.1) and above, omitting the 1.5% agar. For control medium (CTRL), CM was prepared with 50 mM HEPES buffered at pH 7.0. For cell wall stress medium (CR), the same was prepared, with the addition of 100 µg/ml Congo Red (1% filter sterilised).

Vegetative CM liquid culture conditions are as described in Chapter 2 (Section 2.2.1.5). After five days (instead of three days), total mycelium from each flask was harvested using a Buchner funnel and mycelium collected using a pre-dried (weighted) Whatman filter paper. The total amount of tissues at three days post inoculation were not sufficient for effective quantification. Therefore, samples had to be incubated longer. Mycelium was washed with 20 ml sterile MilliQ-H_2O and dried using a Buchner funnel until all liquid had been removed. The filter paper containing mycelium from each flask was loosely wrapped with aluminium foil and oven dried for 5 hours at 60°C. The dried sample (with filter paper) was weighted and dry weight of mycelium calculated [Mycelium dry weight = (Weight filter paper + Mycelium) – Weight of filter paper]. Data analysed using Student's t-test. For each assay (CR or CTRL media), three biological replicates were used per genotype, with three technical replicates for each. Genotypes chosen for this study includes WT strain Guy11 and two independent lines of the double mutant ΔΔ*MGG_Utr2_Crh2* (Line 25 and line 27) as these lines showed reduced growth under CR relative to WT in the plate growth assay.

5.3.3 Cell Wall Structure: Fluorescence Staining

Sample mycelium for microscopic visualisation was prepared on a cover slip (1cm x 1 cm) as described in Chapter 2. Coverslip containing overgrown mycelium was placed onto a clean glass slide with 40 µl of sterile MilliQ-H_2O and 1.0 µl of 1% Calcofluor White and sample immediately covered with another cover slip. Vegetative mycelium was imaged immediately using the BX50 Olympus Light Microscope (Olympus Microscopy) and image captured using Q Image Retiga Exi digital camera (QI Imaging Corporation). The fluorescence of Calcofluor White (excitation wavelength at 347 nm) was captured by using UV light from a mercury lamp and Olympus WU Filter Cube. This procedure was repeated twice for each genotype, with WT strain Guy11 as the Control.

Visualisation of the cell wall of a germinated spore at 24 hpi was achieved by first preparing the sample on an artificial surface as described in Chapter 2 (Section 2.2.1.3). After 24 hours incubation, 1.0 µl of 1% Calcofluor White (Chapter 2, Table 2.1) was added to the droplet and covered with a coverslip. The germling was imaged immediately as described above. The procedure was repeated twice for each genotype, with WT Guy11 as the Control.

5.3.4 Cell Wall Structure: Transmission Electron Microscopy (TEM)

5.3.4.1 Spore Tissue Preparation

Two genotypes were used in this study, Wild Type strain Guy 11 as control, and the double mutant ΔΔ*MGG_Utr2_Crh2* Line 25. For each genotype, five CM plates containing 10 day old fungal colonies were used. Spores from these plates were harvested as described in Chapter 2 (Section 2.2.1.2). The spore

suspension was combined into one 0.2 g microtube and finally spinned using a conventional tabletop centrifuge at 13,000 r.p.m (16,060*g*) for 3 minutes. The resulting pellet was used immediately for subsequent fixing as described below.

The procedure was repeated for both genotypes grown for 10 days with Congo Red (100 µg/ml) added into CM (pH 7.0 buffered with 50 mM HEPES) agar plates as described in Table 5.2 below.

5.3.4.2 Vegetative Mycelium Tissue Preparation

Spores were harvested from the surface of 10 day old WT Guy11 (control) and double mutant ΔΔ*MGG_Utr2_Crh2* Line 25 CM plates as described in Chapter 2 (Section 2.2.1.2). Vegetative CM liquid culture conditions are as described in Chapter 2 (Section 2.2.1.5). For each genotype, three biological replicates from three independent plates were used. The harvested mycelium was blotted dry with paper towels and about 0.1 g collected into 0.2 g microtube and briefly spun to collect the pellets to the bottom of the tube.

For mycelium grown under cell wall stress, 100 µg/ml of Congo Red was added to 50 ml CM liquid (pH 7.0 buffered with 50 mM HEPES). Growth conditions and mycelium harvested in the same fashion as from strains grown in CM.

5.3.4.3 Sample Fixing & Image Visualisation

Pellets were fixed overnight with 2.5% Glutaraldehyde in phosphate buffer followed by 3 x 10 minute washes in 0.1 M phosphate buffer (pH 7.4). Samples were then incubated for 1 hour with 1% Osmium tetroxide in phosphate buffer (w/v) followed by another 3 x 10 minute washed in distilled water. Pellets were further incubated with a 2% solution of uranyl acetate (w/v) in distilled water for 1 hour and washed with distilled water 2 x 5 minutes. Pellets were dehydrated in

succession of with 70%, 80%, 90% and 100% ethanol for 15 minutes each. An additional 100% wash in ethanol was repeated twice before overnight incubation in a 50:50 solution of 100% ethanol: Spurr resin (w/v). Pellets then transferred to a fresh 100% Spurr resin compound and incubated overnight before finally embedded by heating overnight at 60°C in the oven. An ultramicrotome was used to prepare ultra-thin cut sections of the embedded material and collected on nickel grids (Agar Scientific, Parsonage Lane, Stanstead, Essex CM24 8GF) followed by staining with lead citrate as described by Reynolds *et al.*(1963).

The ultra-thin sections were viewed using a Jeol Electron Microscope (model JEM 1010, Tokyo, Japan) at the Department of Human, Anatomy, and Genetics, University of Oxford. Images were captured by the development of negatives with calibrated bars corresponding to the magnification level used.

Table 5.2 Transmission Electron Microscopy Reagents for Sample Fixing.

Solution	Composition
Spurr Resin (Agar Scientific)	3.5 g DER (flexibiliser), 13 g NSA (hardener), 5 g ERL 4206 VCD (resin) and 0.24 ml S-1 DMAE (accelerator)
0.1 M Sodium Phosphate buffer	400 ml sterile MilliQ-H_2O, 56.8 g Na_2HPO_4, 12 g NaH_2PO_4. Made up to 500 ml with sterile MilliQ-H_2O

5.3.5 Germling Morphology (Artificial surface)

Germling preparations are as described in Chapter 2 (Section 2.2.1.4), according to the respective hours post inoculation (hpi): 0 hpi (dormant spore), 2 hpi (germ tube), 4 hpi (immature appressoria), 24 hpi (mature melanised appressoria). At the appropriate times, structures were viewed using a BX50 Olympus Light Microscope (Olympus Microscopy) and the images were captured using Q Image Retiga Exi digital camera (QI Imaging Corporation). Germination percentage was calculated by taking an image at x40 magnification for each sample. The

measurement of germlings for each genotype was conducted with three biological replicates, each biological replicate had two technical replicates. Therefore, a total of 6 images containing an average of 100 spores per image were measured for each genotype and a student's t-test was performed at 95% confidence interval. The assay was repeated twice for each genotype.

5.3.6 Penetration Assay (Onion peel)

Sample preparation for each fungal genotype as described in Chapter 2 (Section 2.2.1.5). The onion peel was viewed under a light microscope (Olympus) by placing it onto glass slides with a drop of MilliQ-H_2O before covering with a cover slip. Observation for the early development of *in-planta* fungal structures growing into the onion cell was recorded and the procedure repeated twice for each genotype, each time with a WT as the control assay.

5.3.7 Virulence Assay (Cut leaves)

5.3.7.1 Barley leaf preparation

In each pot, thirty barley seeds (*Hordeum vulgare L*.) cv. Golden Promise was sown in a 1:1 (w/w) soil mixture of Erin Multipurpose Compost: John Innes No. 3. Pots were watered and kept for seven days in a plant growth chamber (Gallenkamp Fi-totron PG660) at 14/10 h light/dark photoperiod at 20°C and 84% humidity. The first leaf of each seedling was harvested using a single edge blade (Fischer Scientific) and immediately placed adaxial side up onto 1.5% water agar. Each agar plate (120 mm x120 mm WA Petri dish) contained six leaves arranged in parallel and weighted down at the tips and ends with sterile glass slides.

5.3.7.2 **Rice leaf preparation**

In each pot, 20 rice seeds (*Oryzae sativa* cv. CO-39) were sown in John Innes No. 3. Pots watered and kept for 21 days in a plant growth chamber (Gallenkamp Fi-totron PG660) at 14/10 h light/dark photoperiod at 25°C and 90% humidity. The second leaf of a 21 day old rice seedling was carefully harvested with a sterile blade and immediately immersed into sterile MilliQ-H_2O followed by 30 seconds gentle wash by agitation with 2.0 % sodium hypochlorite (bleach) solution and triple washings in sterile MilliQ-H_2O. Harvested leaves were then cut to 10 cm in length, and placed onto 1.5% water agar in a square agar plate (120 mm x 120 mm WA petri dish). Each of the square plate contained five rice leaves arranged in parallel and adaxial side up, weighted down at both ends (leaf tip and bottom end of the leaf) with sterile glass slides.

5.3.7.3 **Infection strategy**

Routine spore suspension was prepared according to the method described in Chapter 2 (Section 2.2.1.2) with concentration adjusted to 10 (±5) x 10^4 spores/ml for each of the respective genotypes used for both barley and rice leaf assay. Wild Type Guy11 genotype was used as a positive control, while 0.2% (w/v) gelatine only, was used as the negative control. One millilitre of the spore suspension was pipetted and mixed with 1 ml 0.4% (w/v) gelatine solution. The gelatine solution was used to facilitate uniform spore adhesion to the plant leaf surface. The spore solution was sprayed evenly onto one square agar plate containing the arranged barley or rice leaves as described above using an artist's airbrush and compressed air (Spraycraft Universal Airbrush Propellant). Between different genotypes, the airbrush was sterilised by spraying onto an empty surface using 70% ethanol followed by sterile MilliQ-H_2O. The sprayed agar plate

was then kept with the lid covered and incubated for five days at 24°C with a 14/10 hour light/dark photoperiod at 60% humidity before imaging with a digital camera (Nikon D700). Each genotype had three biological replicates prepared independently from three independent 10 day old fungal colonies grown on CM agar plates. The average number of lesion per unit area (cm^2) for each genotype and lesion area was counted and measured using the software ImageJ (Version 1.48) and data analysed using Student's t-test.

5.4 Results & Discussion

5.4.1 Vegetative Growth: Plate Assay

5.4.1.1 Selection for the Appropriate Concentration of Reagents

Before conducting a plate assay, the appropriate concentration of the perturbant used was first determined by growing WT on plates containing a range of concentrations. As shown in Figure 5.6 below, the most appropriate concentration of Sodium Dodecyl Sulphate to use was 0.005% (w/v). This was sufficient to give a reduction in growth (by 30-50% relative to control plate), but not too high as to stop growth almost completely as seen under a concentration of 0.02% (w/v). This is an important step, as screening for a phenotype under too high a concentration will result in all strains being unable to grow, while too low a concentration may mean that it is below the sensitivity threshold for mutants to exhibit a reduction in colony size. While no pictures are shown, the best concentration for Congo Red (100 µg/ml), Caffeine (2.5 mM) and Sorbitol (1M) were selected using the same selection criteria.

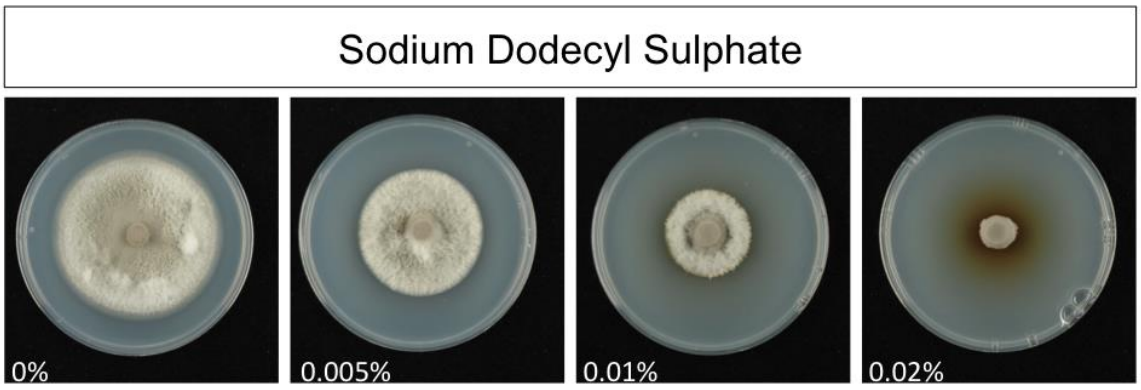

Figure 5.6. Plate Growth Assay of WT Strain Guy11 Grown on a Range of Sodium Dodecyl Sulphate (SDS) Concentrations. Fungal colonies were grown on CM agar plates for eight days under routine *M. oryzae* strain growth condition. The CM plates contained a range of concentrations of SDS from zero to 0.02% (w/v).

5.4.1.2 Growth Assay: Control (CM), Starvation (MM) and Membrane Stress (SDS)

A total of nine fungal genotypes were grown either under optimal conditions on Complete Medium (CM), starvation (MM) or under cell membrane stress (SDS) showed no significant ($p<0.01$) changes in colony growth. These include WT strain Guy11, three single nulled genes corresponding to genes *ΔMGG_Utr2, ΔMGG_Crh1* and *ΔMGG_Crh2* and one double nulled gene mutant *ΔΔMGG_Crh2_Utr2*, each having two independently transformed lines. Statistical analysis using Student's t-test showed no significant difference in colony growth for all mutant genotypes, against the WT for all three treatments (CM, MM, and SDS) mentioned above (Figure 5.7 to Figure 5.9 and Table 5.3).

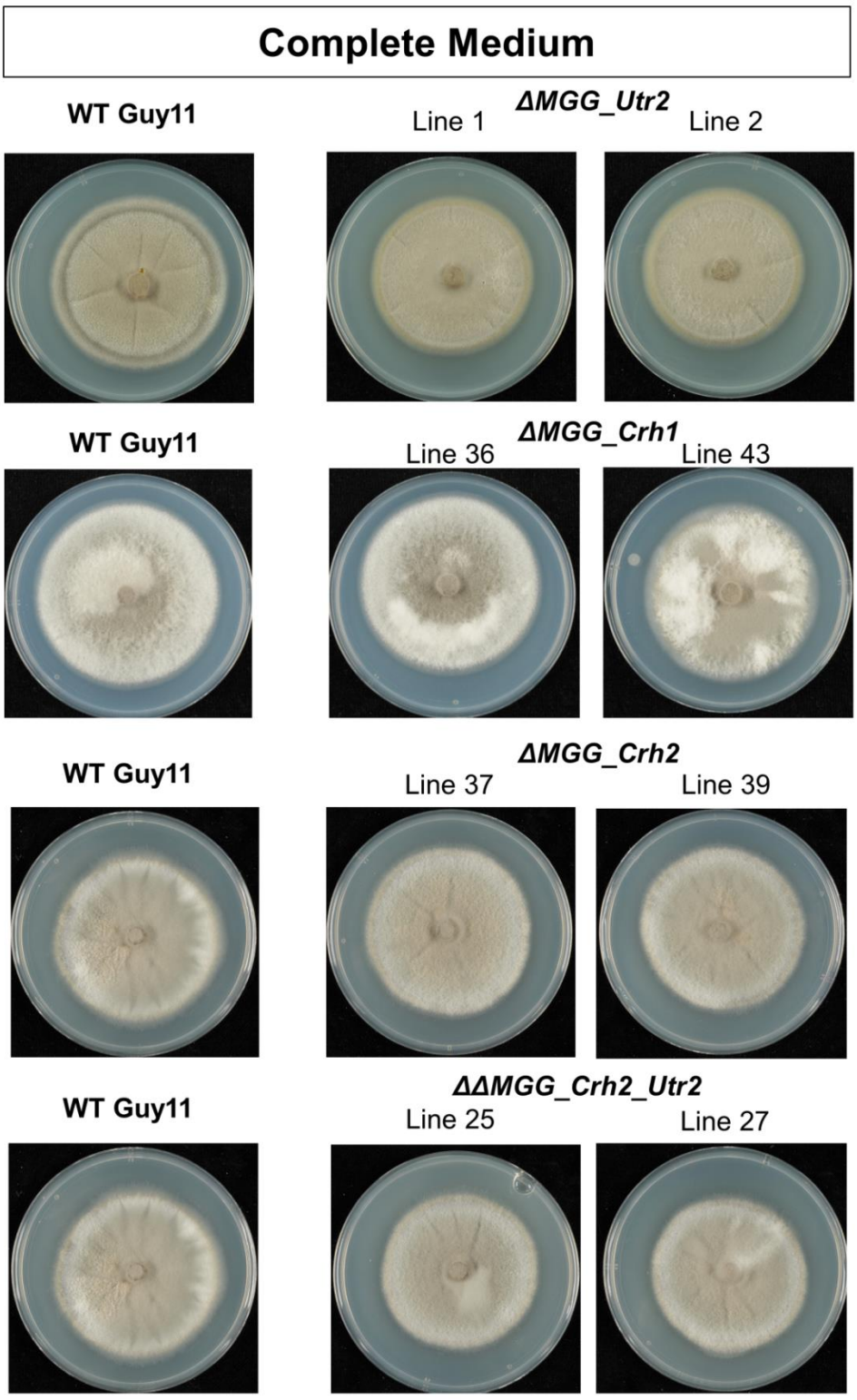

Figure 5.7. *Magnaporthe oryzae* Fungal Strains Grown Under Optimal Conditions in Complete Medium Agar. Fungal colonies were incubated for 10 days before imaging in CM agar. The WT (Control) was included in each assay (Left panel in each row), incubated together with two independent mutant lines (Middle and right panel in each row). Each genotype assayed had three biological replicates, each with two technical replicates. Data were statistically analysed using Student's t-test and assays repeated twice.

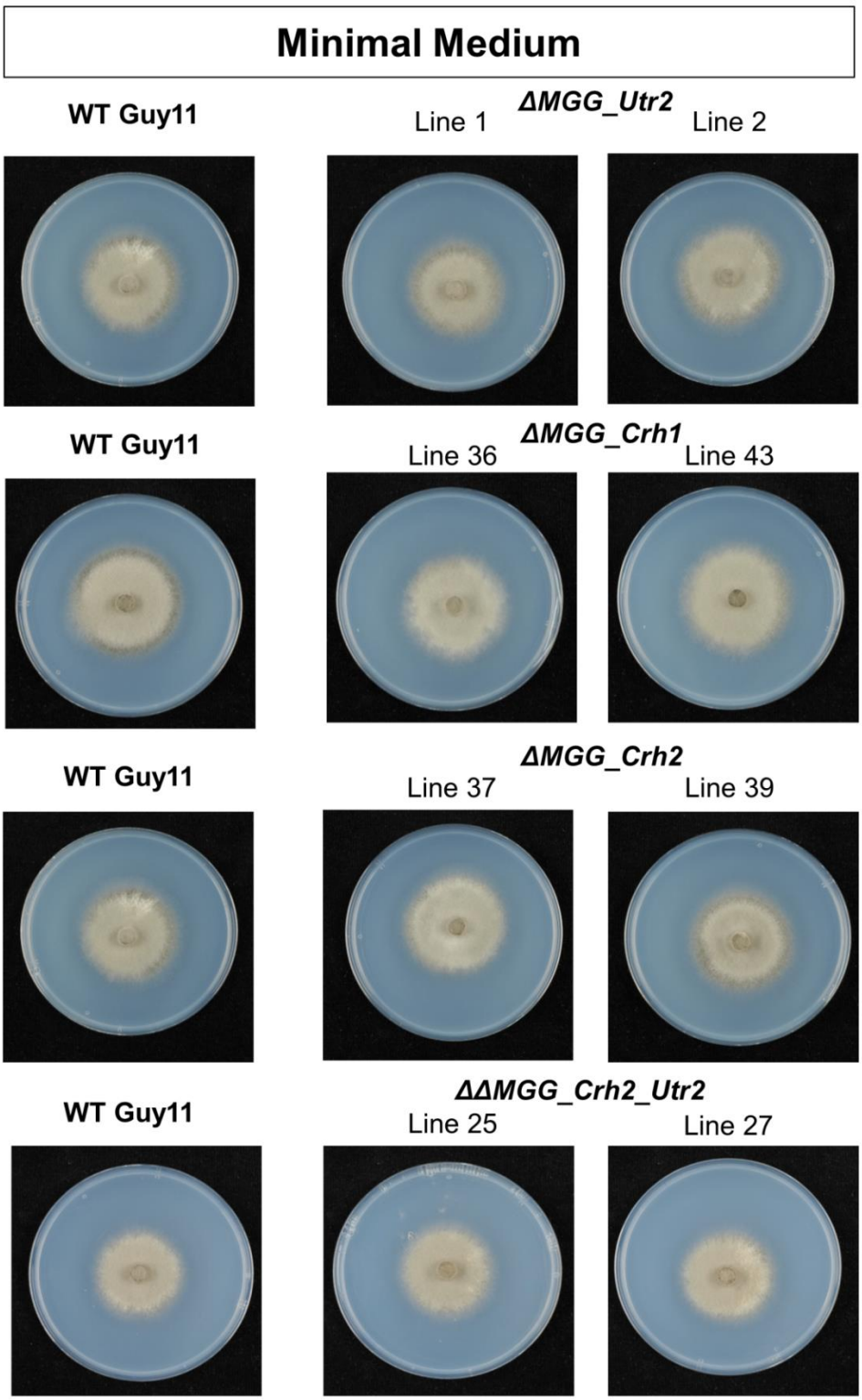

Figure 5.8. *Magnaporthe oryzae* WT Guy11 and Mutant Strains Grown Under Starvation. Fungal colonies were incubated for 10 days before imaging in MM agar. The WT (Control) was included in each assay (Left panel in each row), incubated together with two independent mutant lines (Middle and right panel in each row). Each genotype assayed had three biological replicates, each with two technical replicates. Data were statistically analysed using Student's t-test and assays repeated twice.

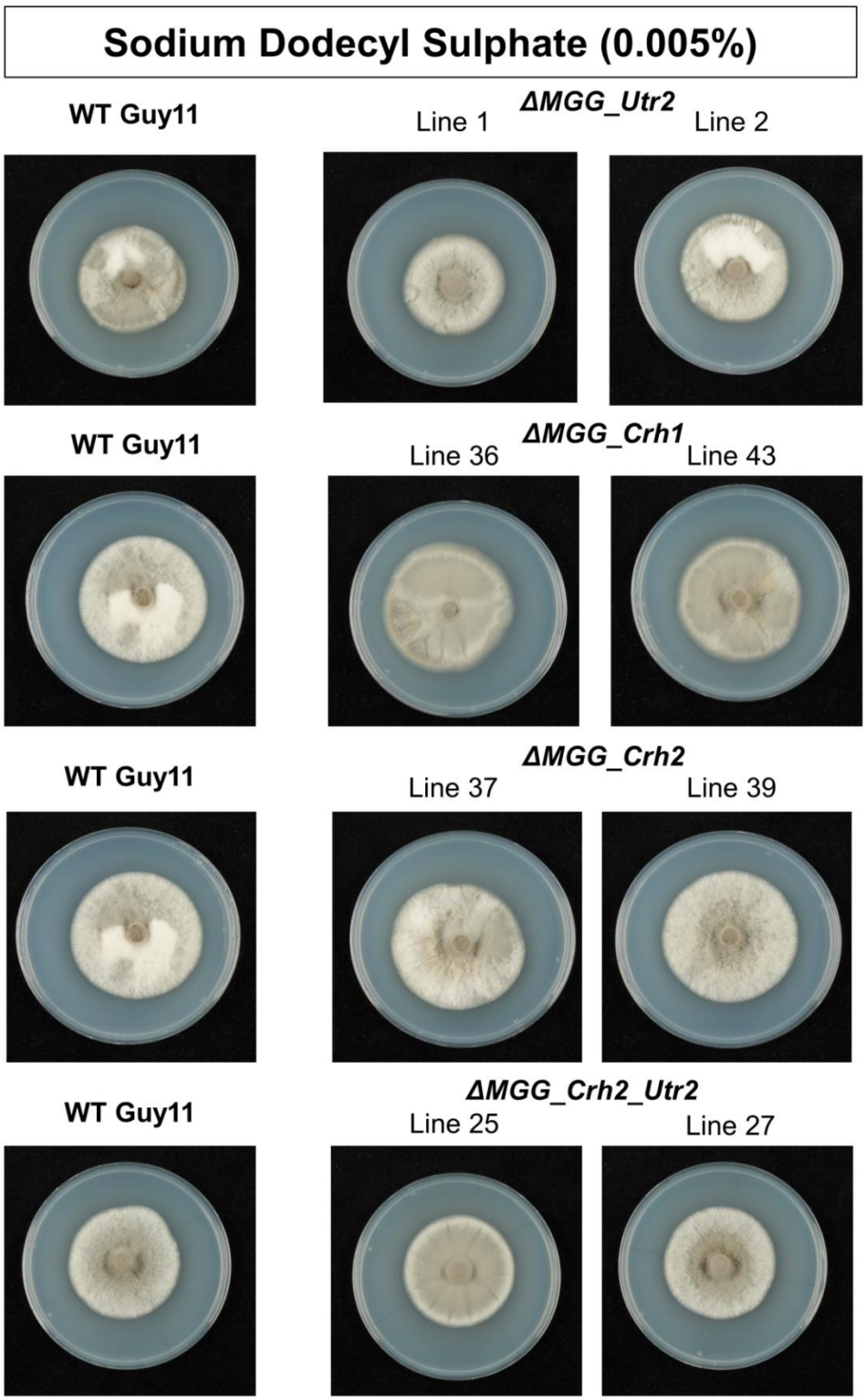

Figure 5.9. *Magnaporthe oryzae* Strains Grown Under Cell Membrane Stress. Fungal colonies were incubated for 10 days before imaging in CM agar containing sodium dodecyl sulphate (SDS) at 0.005%. The WT (Control) was included in each assay (Left panel in each row), incubated together with two independent mutant lines (Middle and right panel in each row). Each genotype assayed had three biological replicates, each with two technical replicates. Data were statistically analysed using Student's t-test and assays repeated twice

5.4.1.3 Growth Assay: Cell Wall Stress

5.4.1.3.1 Cell Wall Stress by Congo Red

In this treatment, eight mutant lines, two revertant strains and the control WT were grown under cell wall stress caused by the cell wall perturbing compound, Congo Red at a concentration of 100 µg/ml. Both independent lines for the single gene deletant *ΔMGG_Utr2* and *ΔMGG_Crh1* showed no significant reduction in growth, while the single gene deletant *ΔMGG_Crh2* independent lines 37 and 39 both showed up to a 30% significant reduction in growth ($p<0.01$) (Figure 5.10 Panel A and Table 5.3). The nulled double mutant *ΔΔMGG_Crh2_Utr2* independent lines 25 and 27 also showed a reduction in growth. However, it is at the same percentage reduction, 30% ($p<0.01$), as the single deletant strain, when measured against the control WT strain Guy11.

The growth of candidate complemented lines reverted to the WT phenotype. Revertant strains 13c_2 and 13c_2ci_6 were assayed together with the corresponding nulled gene mutant *ΔMGG_Crh2* line 39 and WT Guy11 in Congo Red (100 µg/ml). Results showed that both strains fully complemented the phenotype of *ΔMGG_Crh2* line 39 with the recovery of growth rate to be non-significantly different ($p>0.01$) to the growth of WT, but significantly higher than the deletant strain *ΔMGG_Crh2* line 39 ($p<0.01$) (Figure 5.10 Panel B).

To confirm that the phenotype seen is due to the compound Congo Red causing hypal tip swelling, three additional tests were assayed: Osmo-remedial of Congo Red with Sorbitol (1 M), osmotic stress (Sorbitol only) and a buffered CM assay (CM+Hepes pH 7.0). When osmo-remedial was conducted by maintaining the same Congo Red plate assay preparation but with the addition

of 1 M Sorbitol, partial reduction in growth 13-20% less, at $p<0.01$ was seen in the affected mutants *ΔMGG_Crh2* and *ΔΔMGG_Crh2_Utr2* for both independent lines (Figure 5.10 Panel C).

In the second control, to show that changes in phenotype in Congo Red osmo-remedial is not attributed to osmotic stress caused by Sorbitol, plate growth assay containing only Sorbitol at 1 M were also assayed (Figure 5.12). Results showed no significant changes in any of the mutant strains.

Routine optimal growth condition included growth on CM agar with pH adjusted to 6.5. However, the compound Congo Red requires a buffered medium with a pH of 7.0. Therefore, to show that the phenotype seen is not attributed to the addition of a buffer reagent (HEPES 50 mM) or due a pH of 7.0, a third control assay was conducted, containing only CM buffered with Hepes (pH 7.0) without Congo Red. Results showed that growth of all mutant colonies were non-significantly different from WT (Figure 5.11 and Table 5.3).

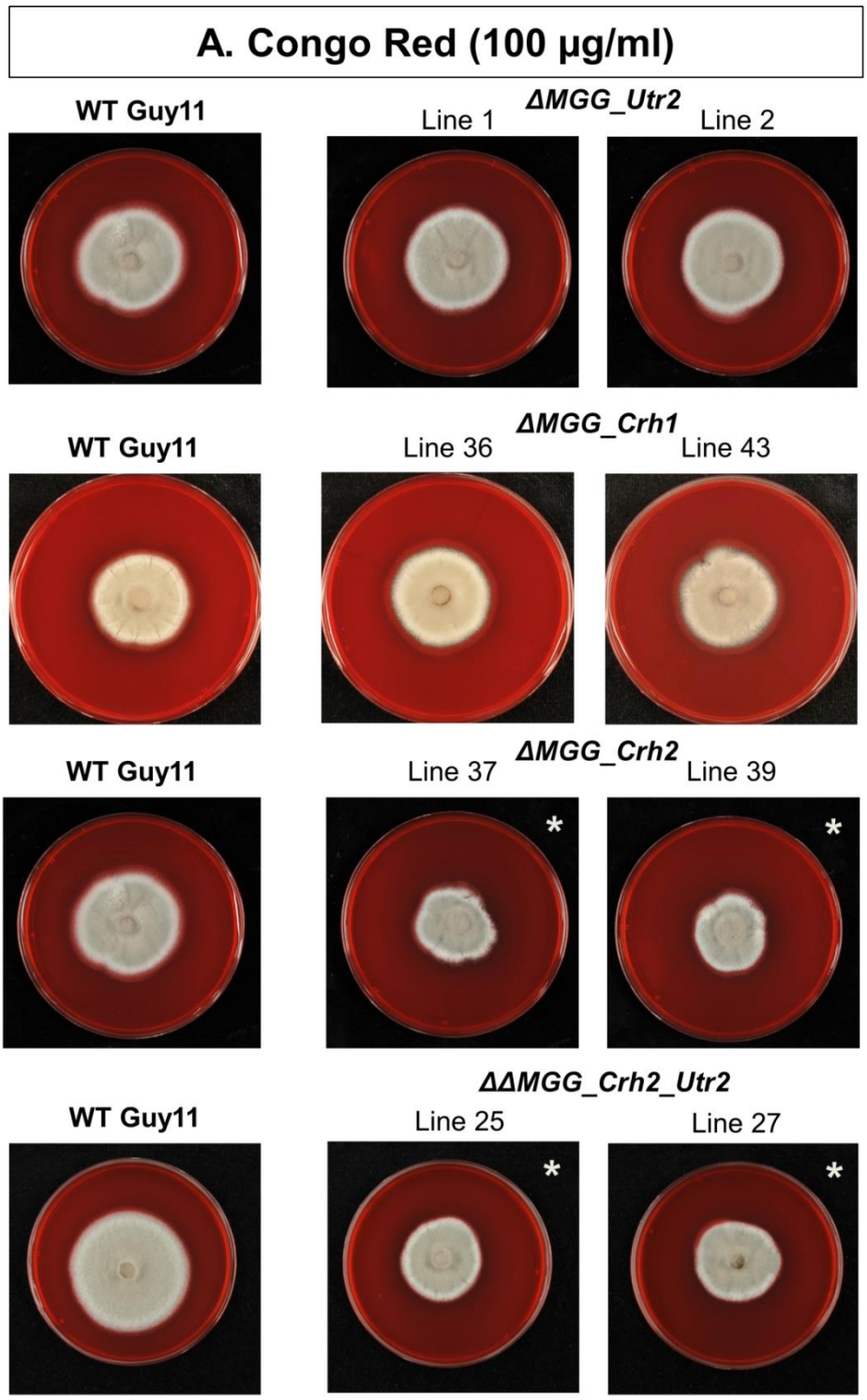
A. Congo Red (100 µg/ml)
WT Guy11
ΔMGG_Utr2
Line 1
Line 2
WT Guy11
ΔMGG_Crh1
Line 36
Line 43
WT Guy11
ΔMGG_Crh2
Line 37
Line 39
*
*
WT Guy11
ΔΔMGG_Crh2_Utr2
Line 25
Line 27
*
*

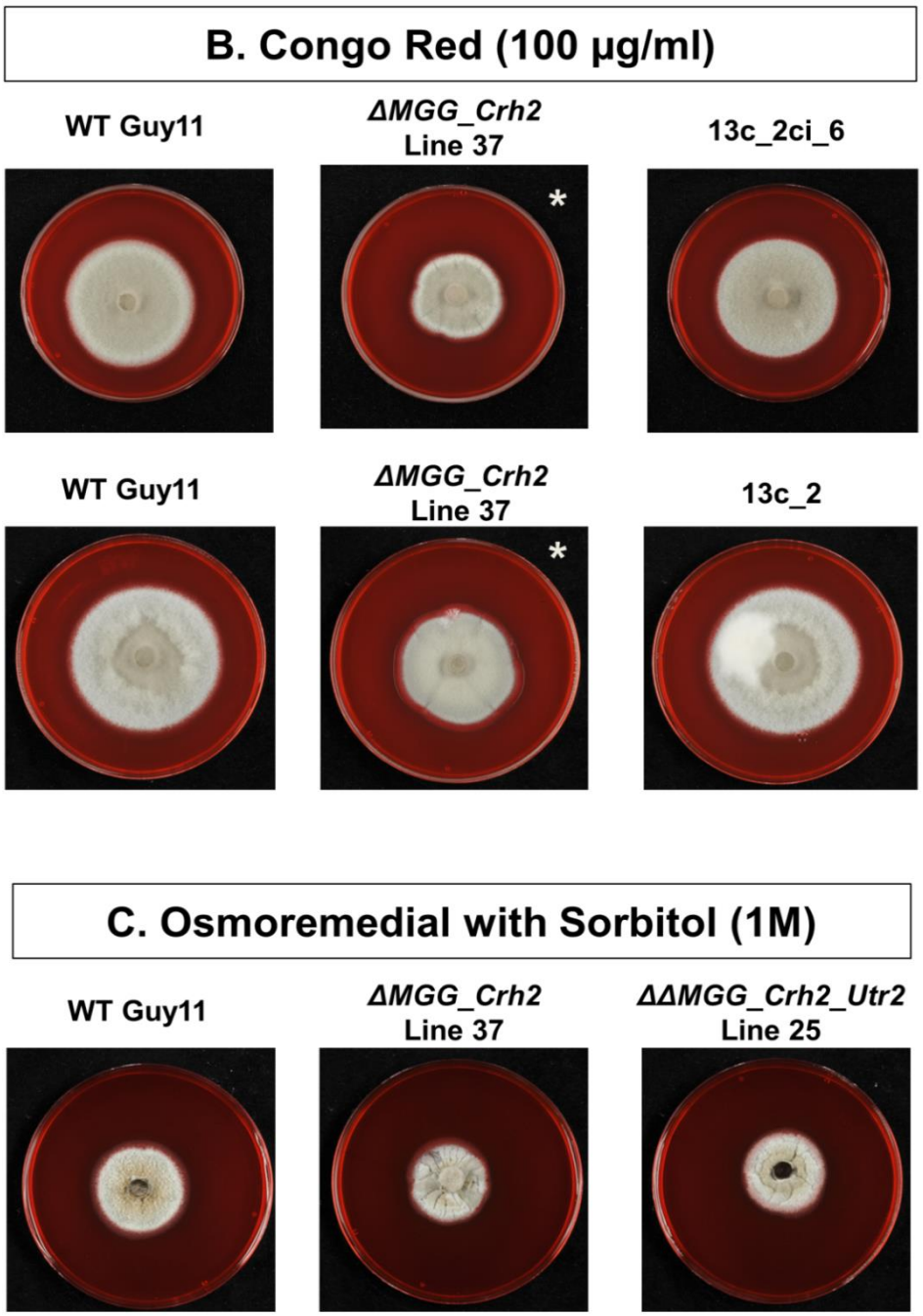

Figure 5.10. *Magnaporthe oryzae* Strains Grown Under Cell Wall Stress (Congo Red). Fungal colonies grown for 10 days in CM agar containing 100 µg/ml Congo Red buffered with 50 mM HEPES at pH 7.0 before imaging. **Panel A**. Each assay had WT as the control (Left image in each row), incubated together with two independent mutant lines (Middle and right images in each row). **Panel B**. Shown the control WT (Left image), negative control strain *ΔMGG_Crh2* Line 37 (Middle image) and the complemented line eGFP-tagged Crh2p strain 2ci_6 or Crh2p strain 13c_2. **Panel C.** Fungal colonies were grown in Congo Red as prepared in panels A and B, but with the addition of 1 M Sorbitol. The WT control (Left image), *ΔMGG_Crh2* Line 37 (Middle image) and *ΔΔMGG_Crh2_Utr2* Line 25 (Right image). Each genotype assayed above had three biological replicates, each with two technical replicates. Data were statistically analysed using Student's t-test with a white asterisk indicating a significant difference at $p<0.01$. All assays were repeated twice.

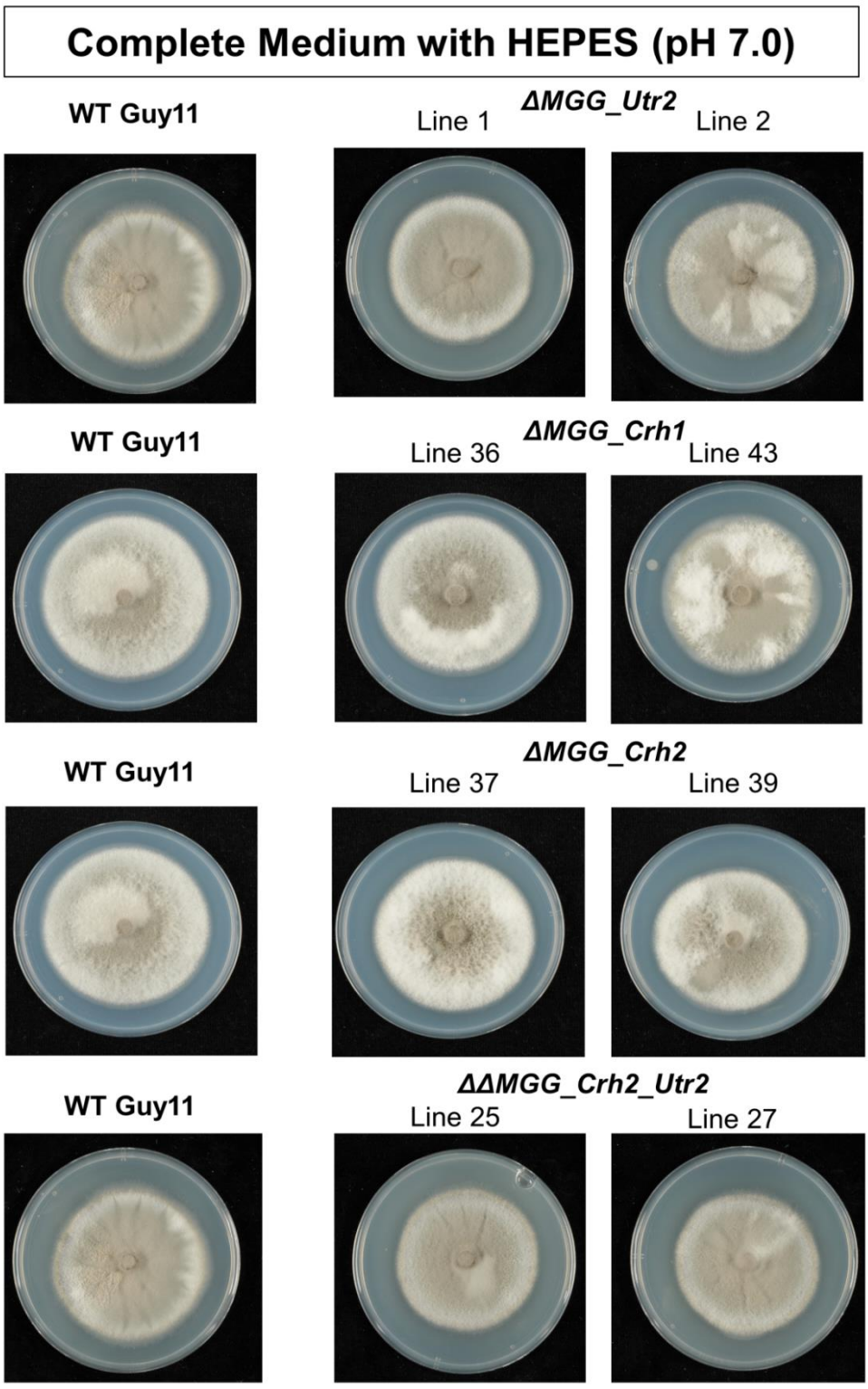

Figure 5.11. *Magnaporthe oryzae* Strains Grown in CM Agar Buffered with Hepes at pH 7.0. Fungal colonies were grown for 10 days before imaging. The assay above is a control for the Congo Red assay (Figure 5.16). Each assay had WT as the control (Left image in each row), assayed together with two independent mutant lines (Middle and right images in each row). Each genotype assayed had three biological replicates, each with two technical replicates. Data statistically analysed using Student's t-test. All assays repeated twice.

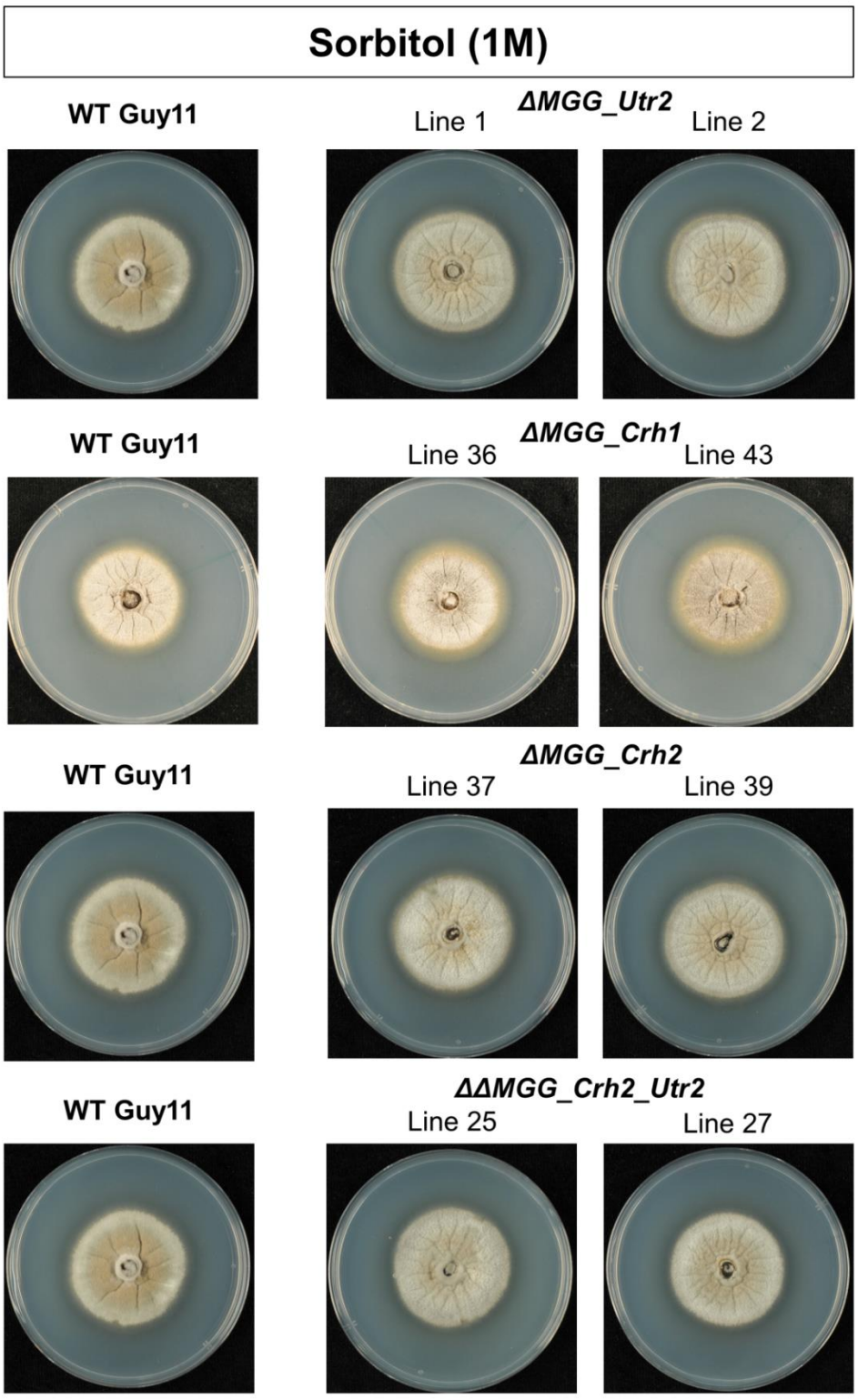

Figure 5.12. *Magnaporthe orzyae* Fungal Strains Grown Under Osmotic Stress. Fungal colonies were incubated for 10 days before imaging in CM agar with 1 M Sorbitol. The WT (Control) was included in each assay (Left panel in each row), incubated together with two independent mutant lines (Middle and right panel in each row). Each genotype assayed had three biological replicates, each with two technical replicates. Data were statistically analysed using Student's t-test and assays repeated twice.

5.4.1.3.2 Cell Wall Stress by Caffeine

Only mutants lacking *MGG_Utr2* showed hypersensitivity to Caffeine at 2.5 mM. This occurred in the mutant *ΔMGG_Utr2* independent lines 1 and 2, as well as the double deletant mutant *ΔΔMGG_Crh2_Utr2* independent lines 25 and 27, but not in the single deletant mutants *ΔMGG_Crh1* and *ΔMGG_Crh2*. In each of these mentioned strains, exposure to Caffeine (2.5 mM) caused up to 25-30% significant ($p<0.01$) reduction in colony growth relative to WT Guy11 without an additive effect in the double deletant mutant *ΔΔMGG_Crh2_Utr2* independent lines 25 and 27 (Figure 5.13 and Table 5.3). This absence of an additive effect is similar to the pattern seen under the Congo Red treatment.

The *MGG_Utr2* revertant line #5_6 complemented the phenotype of *ΔMGG_Utr2* line 2 when grown in Caffeine (2.5 mM) (Figure 5.13 Panel B) with growth rate non-significantly different ($p>0.01$) to WT but significantly different ($p<0.01$) from *ΔMGG_Utr2* Line 2 (Table 5.3**)**. However, the mCherry-tagged complemented line #5_6_14 did not complement the phenotype, with colony diameter similar to the mutant *ΔMGG_Utr2* line 2 (data not shown).

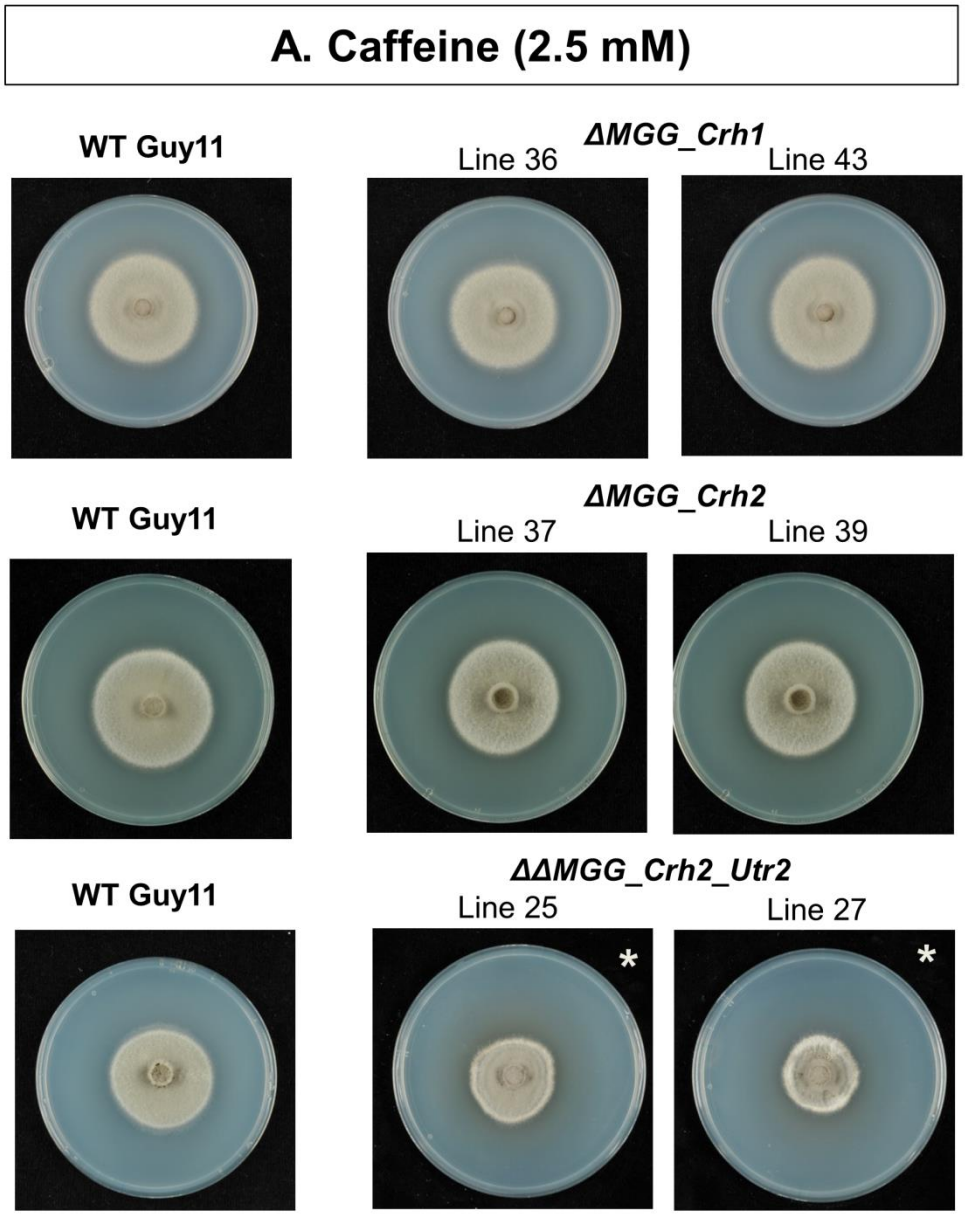
A. Caffeine (2.5 mM)
WT Guy11
ΔMGG_Crh1
Line 36
Line 43
WT Guy11
ΔMGG_Crh2
Line 37
Line 39
WT Guy11
ΔΔMGG_Crh2_Utr2
Line 25
Line 27
*
*

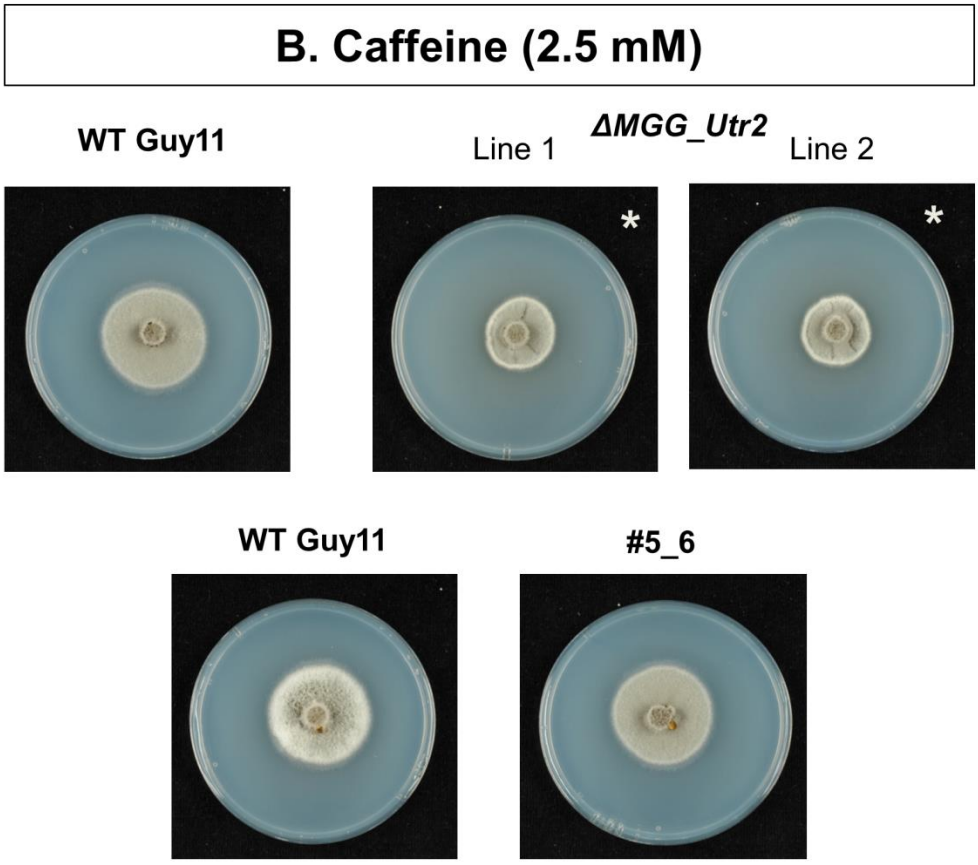

Figure 5.13. *Magnaporthe oryzae* Strains Grown Under Caffeine Stress (2.5 mM). Fungal colonies were grown for 10 days in CM agar containing 2.5 mM of Caffeine. **Panel A**. Wild Type Guy11 (control) was included in each assay (left panel of each row), incubated with two independent mutant lines (middle and right panel of each row). **Panel B**. In the top row are WT Guy11 control (top left) and two independent lines of the nulled *ΔMGG_Utr2* mutant line 1 and line 2 (middle and right images). Second and third row are the complemented strains from the background mutant *ΔMGG_Utr2* Line 2. Wild Type Guy11 as the control (left image) shown with a non-tagged Utr2p (strain #5_6). Each genotype assayed had three biological replicates, each with two technical replicates. Data were statistically analysed using Student's t-test with a white asterisk indicating a significant difference at $p<0.01$. All assays were repeated twice.

Table 5.3. Growth Ratio of Mutants Relative to WT Strain Guy11 for Seven Treatment Types. Given below, the calculated ratio of colony growth over three days (measured in cm) in each mutant line, against WT. Ratios with asterisks are those with a significantly ($p<0.01$) reduced growth rate, relative to WT with the percentage reduction in brackets. Ratio was calculated by averaging the mean from three biological replicates of each mutant line, over the WT strain. Statistical analyses conducted using Students t-test comparing the growth (cm) of three biological replicates in mutant lines, relative to WT.

Strain	Growth Ratio							
	CM	**CR (100 µg/ml)**	**SDS (0.005%)**	**Caffeine (25 mM)**	**Sorbitol (1 M)**	**MM**	**CM+H (pH 7.0)**	**CR+SORB**
***ΔMGG_Utr2* Line 1**	0.97	1.00	0.97	0.72* (28%)	0.98	0.93	0.97	n/a
***ΔMGG_Utr2* Line 2**	0.98	0.92	0.98	0.72* (28%)	1.01	0.95	0.96	n/a
***ΔMGG_Crh1* Line 36**	0.99	0.99	1.05	0.91	1.06	1.05	0.99	n/a
***ΔMGG_Crh1* Line 43**	1.05	0.97	1.05	1.48	1.02	1.06	1.00	n/a
***ΔMGG_Crh2* Line 37**	0.91	0.70* (30%)	0.96	0.98	0.98	0.95	0.94	0.86* (14%)
***ΔMGG_Crh2* Line 39**	0.99	0.78* (22%)	0.96	0.95	0.98	0.95	0.94	0.82* (18%)
ΔΔ*MGG_Utr2_Crh2* Line 25	0.92	0.70* (30%)	1.03	0.74* (26%)	0.98	1.01	1.01	8.87* (13%)
ΔΔ*MGG_Utr2_Crh2* Line 27	0.90	0.70* (30%)	1.03	0.71* (29%)	0.95	1.05	1.05	0.80* (20%)
13c_2ci_6 (revertant)	n/a	1.013	n/a	n/a	n/a	n/a	n/a	n/a
13c_2 (revertant)	n/a	0.933	n/a	n/a	n/a	n/a	n/a	n/a
#5_6 (revertant)	n/a	n/a	n/a	0.996	n/a	n/a	n/a	n/a

Abbreviations:

Complete Medium (CM), Congo Red (CR), Sodium Dodecyl Sulphate (SDS), Minimum Medium (MM), Complete Medium with Hepes (CM+H), Congo Red with Sorbitol (CR+SORB)

227

5.4.1.4 Plate Growth Assay: Discussion of Results

A total of twelve *M. oryzae* strains (including independent and revertant lines) were grown vegetatively under various conditions. All mutants generated in Chapter 4, showed consistent phenotypic variations between independent lines generated for each mutant, indicating that for subsequent assays or experiments, only one line for each mutant need be used. Also, the phenotype seen in both single deletant mutants Δ*MGG_Utr2* and Δ*MGG_Crh2* were complemented by the respective revertant strains. Therefore, it can be concluded with confidence that any phenotype seen, is attributed to the loss of the gene, as opposed to any other external factors.

From the plate assay results, it is evident that under optimal conditions (CM), starvation (MM), osmotic stress (Sorbitol) and cell membrane stress (SDS), no change in phenotype is seen. However, in agreement with the hypothesis, strains exhibited hypersensitivity to cell wall perturbants. Here, single deletant gene Δ*MGG_Crh2* exhibited hypersensitivity to cell wall stress caused by Congo Red but not by Caffeine. The opposite is seen in the deletant strain Δ*MGG_Utr2*, while the double deletion strain ΔΔ*MGG_Crh2_Utr2* showed a phenotype of both, without an additive effect. This is in contrary to *Crh-like* mutant studies in both *S. cerevisiae* and *C. albicans* whereby both double and triple mutant lines showed increased reduction in growth under cell wall stress relative to single deletant strains (Rodriguez-Pena *et al.* 2000, Pardini *et al.* 2006).

Both Congo Red and Caffeine causes cell wall stress but is associated with different MAPK response pathways. While Congo Red specifically activates the CWI pathway via Rlm1 (Garcia *et al.* 2004), caffeine is associated with responses through Tor1 (Reinke *et al.* 2006) and indirect phosphorylation of the Swi4/Swi6 complex (CWI) (Truman *et al.* 2009). Given that there was no additive effect in Congo Red or Caffeine hypersensitivity in the double gene deletant strain, coupled with the differences in fungal response pathway of both compounds, it suggests the presence of diversity in targeted function and regulation by *MGG_Crh2* and *MGG_Utr2* respectively.

The hypersensitivity to Congo Red, leading to a 30% reduction in growth experienced by mutants missing the *MGG_Crh2* gene, could be attributed to changes in cell wall elasticity. This is because as described earlier, the Congo Red compound has a high affinity for glucan polymers (Kopecká and Gabriel 1992), thus possibly competes with Crhp, reducing the number of linkages between chitin and glucan polymers. As a result, fungal cell wall becomes less rigid and susceptible to hyphal swellings (Pancaldi *et al.* 1984, Guerriero *et al.* 2013). Therefore, it is thought that in a mutant line where the activity of Crh-like proteins is compromised (i.e. ∆*MGG_Crh2* and ∆∆*MGG_Crh2_Utr2*), this situation is then exaggerated, which results in higher occurrence of hyphal swelling and bursting. To confirm that mutant hypersensitivity is due to hyphal swelling, osmo-remedial by the addition of 1 M of Sorbitol was performed. While 1 M of Sorbitol did not fully recover the phenotype, partial recovery suggests that Congo Red is indeed affecting the mutant lines by causing swelling of the hyphal tips, with 1M of Sorbitol partially counter-acting this symptom. A higher

concentration of Sorbitol may indeed confer full recovery to the WT phenotype, however, to repeat the assay under a higher concentration is no longer necessary.

From these results, it can be concluded that mutants missing the *MGG_Crh2* and/or *MGG_Utr2* gene experience changes in cell wall elasticity, while the removal of *MGG_Crh1* is insignificant. Confirmation of an alteration to surface elasticity can only be confirmed by direct measurement, made possible by the use of Atomic Force Microscopy, which is described in detail in Chapter 6.

5.4.2 Vegetative Growth: Liquid Biomass Assay

In addition to the plate growth assay, the total dry weight of a representative mutant line (ΔΔ*MGG_Crh2_Utr2*) was measured and compared to the dry weight of the WT strain Guy11. This assay was conducted to show that despite using a different system to measure growth (dry weight as opposed to colony diameter), a phenotype is still seen and consistent between two independent lines of ΔΔ*MGG_Crh2*_Utr2.

In the first assay, both strains were cultured in CM liquid buffered with HEPES (50 mM) for three days while in the second assay, the same liquid broth were prepared with Congo Red (100 µg/ml) and due to the slower growth rate, strains were cultured for five days. Oven dried mycelium were weighted and data presented in Figure 5.14. Student's t-test showed that both independent lines were non-significantly different ($p<0.01$) to each other and to WT, when grown under optimal conditions. On the contrary, when Congo Red was added to impart cell wall stress, there were 30-35% significantly ($p<0.01$) less growth in both independent mutant lines, compared to the WT.

These results showed that the observed phenotype in the plate assay for this mutant strain is reflected in the liquid biomass assay despite a very different approach to measure growth. Similar to the plate assay, no differences in growth is seen when strains were grown under optimal conditions, however once the cell wall is challenged, reduction in growth is seen. Additionally, this assay again showed that both independent lines were consistent and gave similar phenotype for the same genotype. For future phenotypic assays, results from only one independent line is presented (line 25) with the assumption that it is a true representation of the absence of both genes *MGG_Crh2* and *MGG_Utr2*.

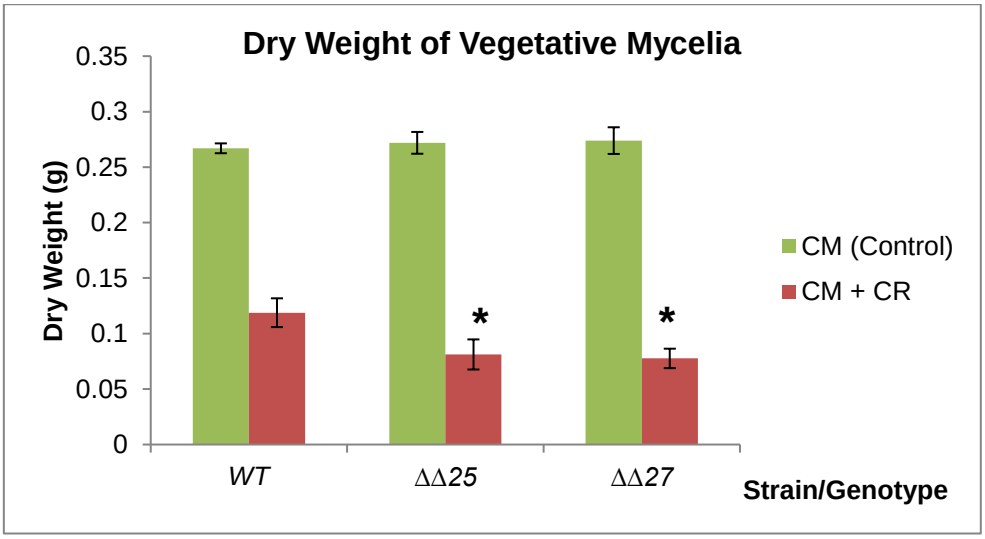

Figure 5.14. Liquid Biomass Assay Showing the Total Dry Weight of Fungal Mycelia. Three fungal strains were cultured in liquid CM (50 mM Hepes pH 7.0) with and without (Control) the addition of Congo Red (100 µg/ml). These strains are the WT strain Guy11 (WT), the double gene deletant strain ΔΔ*MGG_Crh2*_Utr2 independent line 25 *(*ΔΔ*25*) and independent line 27 (ΔΔ*27*). Harvested mycelia were oven dried overnight and total dry weight measured (g). Data presented as an average of three biological replicates. Assay repeated twice. Error bars represents 95% confidence interval. Asterisks represent calculated Student's t-test with a significant difference ($p<0.01$) in the dry weight compared to the WT.

5.4.3 Cell Wall Structure: Fluorescent Staining

Calcofluor white (CFW) was used to stain the cell wall of deletant strains, and WT strain Guy11 to observe any changes to the cell wall structure during

vegetative growth and germling development. All fungal strains showed staining at the hyphal cell wall with fluorescence brightest at the septae (Figure 5.15). A damaged or abnormal cell wall may exhibit irregularities in the septum, rough lines enveloping the cytoplasm or simply less/more brightness relative to the WT. However, as shown in Figure 5.15, all four fungal mycelia looked as normal as the WT. The same outcome is seen for the staining of germlings at 24 hpi on an artificial hydrophobic surface (Menzel slides). Here, CFW stained the spore wall, germ tube and melanised appressorium (Figure 5.16) with no observable differences between WT and the four deletant fungal strains.

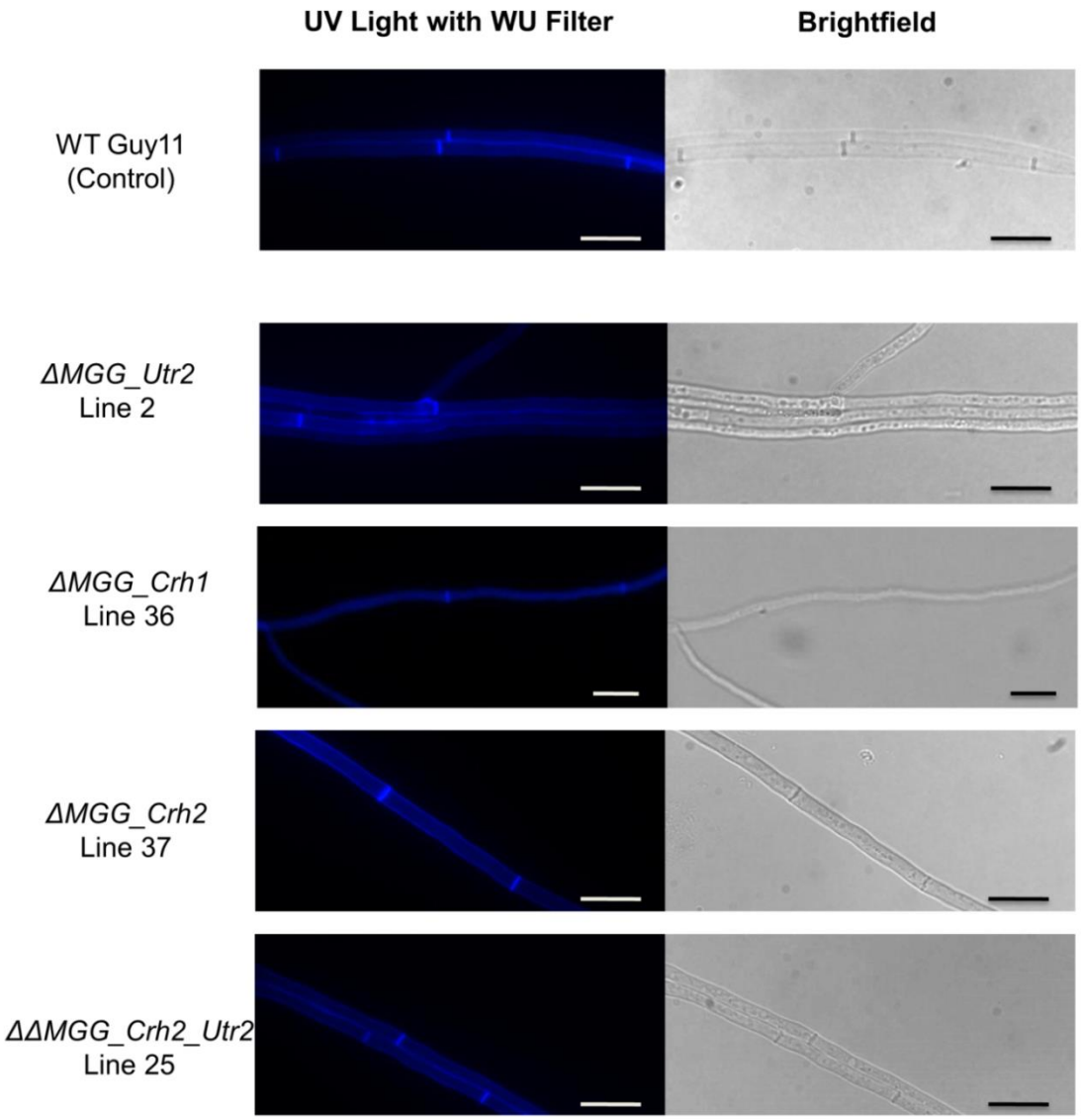

Figure 5.15. Cell Wall Staining (Calcofluor White) of Vegetative Mycelium in Five *Magnaporthe oryzae* strains. The vegetative mycelia were grown on CM agar for 10 days and allowed to overgrown onto a small microscope cover slip which was then removed from the agar surface and stained with 1 µl of 1% Calcofluor White. The sample was immediately imaged under UV light (mercury lamp, with WU filter) followed by an image under brightfield light using an Olympus Light Microscope (BX50). Scale bars represents 10 µm.

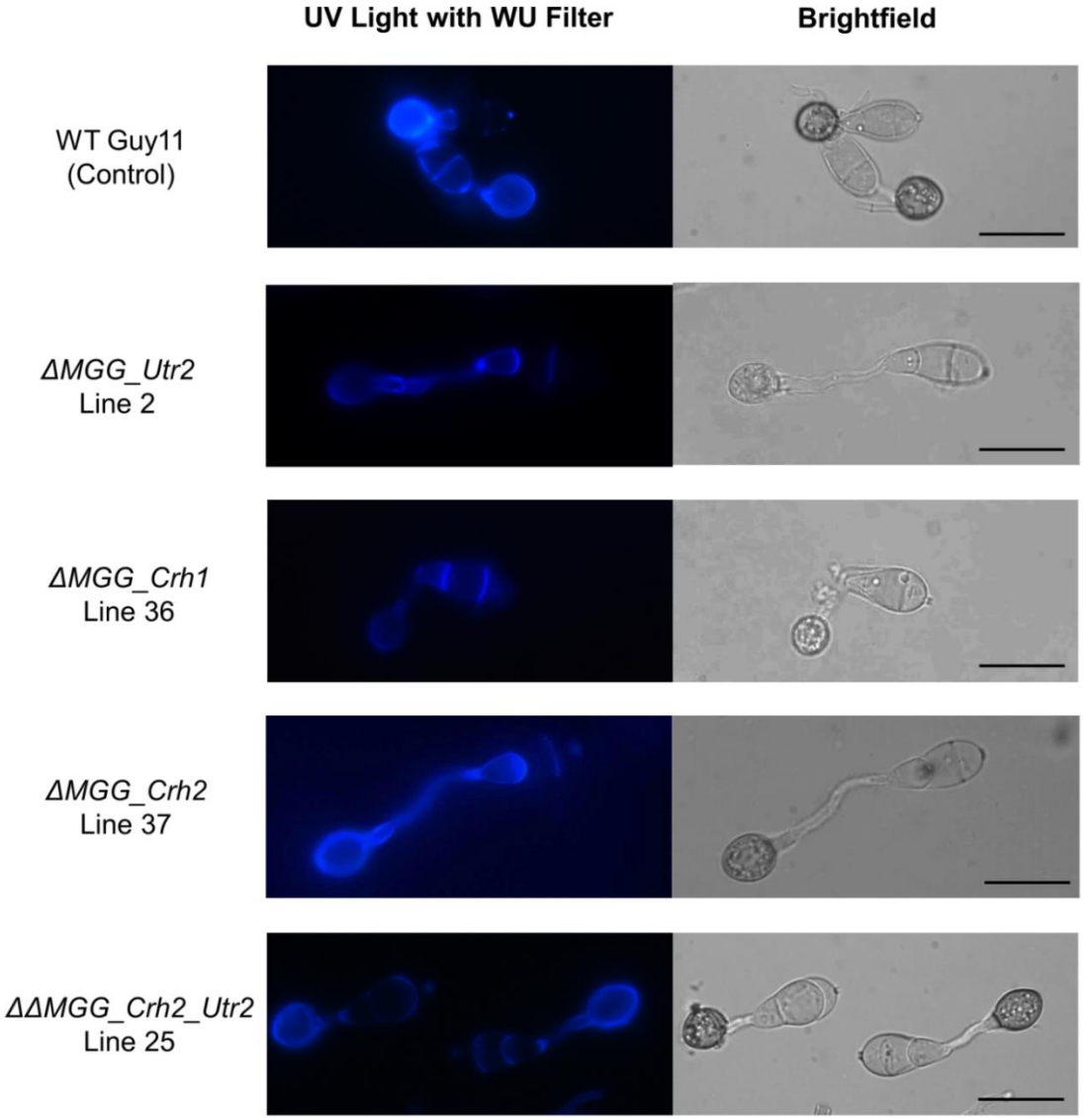

Figure 5.16. Germling Cell Wall Staining (Calcofluor White) of Five *Magnaporthe oryzae* Strains Inoculated onto an Artificial Hydrophobic Surface. The fungal infective structures were stained with 1 µl of 1% Calcofluor White and immediately imaged under UV light (mercury lamp, with WU filter) and another under brightfield light. Each image above showed the specific staining of Calcofluor White to the cell wall of spore, germ tube as well as appressorium, with no difference in shape and staining pattern between WT Guy11 against each mutant genotype observed. Scale bars represents 20 µm.

5.4.4 Cell Wall Structure: Transmission Electron Microscopy

Liquid biomass assay (Section 5.3.9) showed a 30% reduction in total dry weight of the double deletant strain ΔΔ*MGG_Crh2_*Utr2 line 25 relative to the WT when grown under cell wall stress. Therefore under the same culture conditions, the vegetative hyphae of both mutant and WT were then visualised by TEM to explore possible changes to the cell wall structure. In addition to this, dormant spores of both WT and the double deletant mutant strain were also included.

The aim of this section was to qualitatively compare the cross-sectional images of both strains during vegetative growth and in dormant spores, paying close attention to the distribution of melanin, continuity of the septum and cell wall (not disrupted or broken). In addition, these structures were compared when both strains in each growth stage mentioned above, were grown under cell wall stress caused by Congo Red (100 µg/ml) relative to the control (CM). This mutant strain was prioritised, given that it currently carries the strongest phenotype relative to the other single mutant lines. Only if a phenotype is seen, will the procedure be repeated for the single mutant lines.

Electron micrographs (Figure 5.17) of mutant vegetative hyphae grown in CM showed the formation of normal septum, uniform lateral cell wall with plasma membrane and a layer of ‘fluff’ suspected to be part of the amorphous layer (protein, glycoprotein rich, alkaline soluble) carpeting the cell wall matrix. Literature showed that the cross section of fungal cell walls in electron micrograph images revealed hair-like structures corresponding to the amorphous layer (Schoffelmeer *et al.* 1999, Hardison and Brown 2012). The absence of the hair-like structure in this study, but in replace are ‘fluff-like’ structures, could be

attributed to damages incurred to the outer layer during sample fixing. Similarly, even under cell wall stress caused by Congo Red, the mutant line was still able to form continuous cell wall and septum (Appendix C.2), without breaks or apparent structural deformities. However, it was observed that under the same fixing conditions (both WT and mutant samples prepared together), the mutant lines were stained strongly by the Spurr Resin, making mutant imaging more challenging, while under the same conditions, the WT strain was stained perfectly well. It is assumed that under cell wall stress, the mutant line experiences more hyphal tip damage and while this was not captured by TEM, disrupted hyphal tips meant that the stains were absorbed faster into the fungal tissues, as opposed to the WT strain.

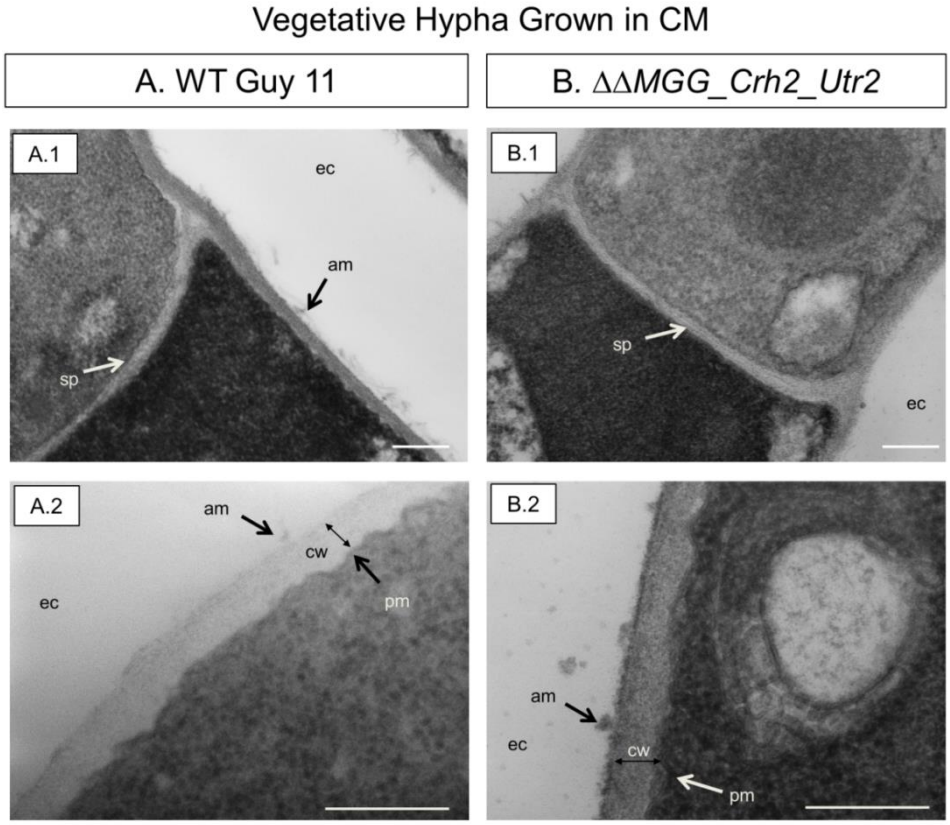

Figure 5.17. Transmission Electron Micrographs of *Magnaporthe oryzae* Vegetative Mycelium Cultured in CM. Samples were prepared by culturing fungal strains in CM liquid broth. **Panel A.1-A.3** WT strain Guy11 fungal hypha. **Panel B.1-B.3** Double gene deletant mutant strain Δ*MGG_Crh2*_Utr2 line 25 fungal hypha. Extracellular environment (em), cell wall (cw), septum (sp), plasma membrane (pm) and amorphous layer (am). Scale bars represents 200 nm.

Electron micrographs of mutant spores showed the formation of normal three-celled spores in both CM and Congo Red, relative to WT strain Guy11. Figure 5.18 of spores grown in CM showed the ability of the mutant strain to form septum, appropriately localised melanin and uniform cell wall distribution throughout the spore wall. Similarly is seen for spores of both genotypes grown in Congo Red (Appendix C.3). Given the thick layer of melanin and dormant form, mutant spores do not exhibit the same level of sensitivity to Congo Red relative to the vegetative counterpart and as such, the excessive staining issue is not seen here. Contrary, both WT and mutant lines were stained well and quality images were easily obtained.

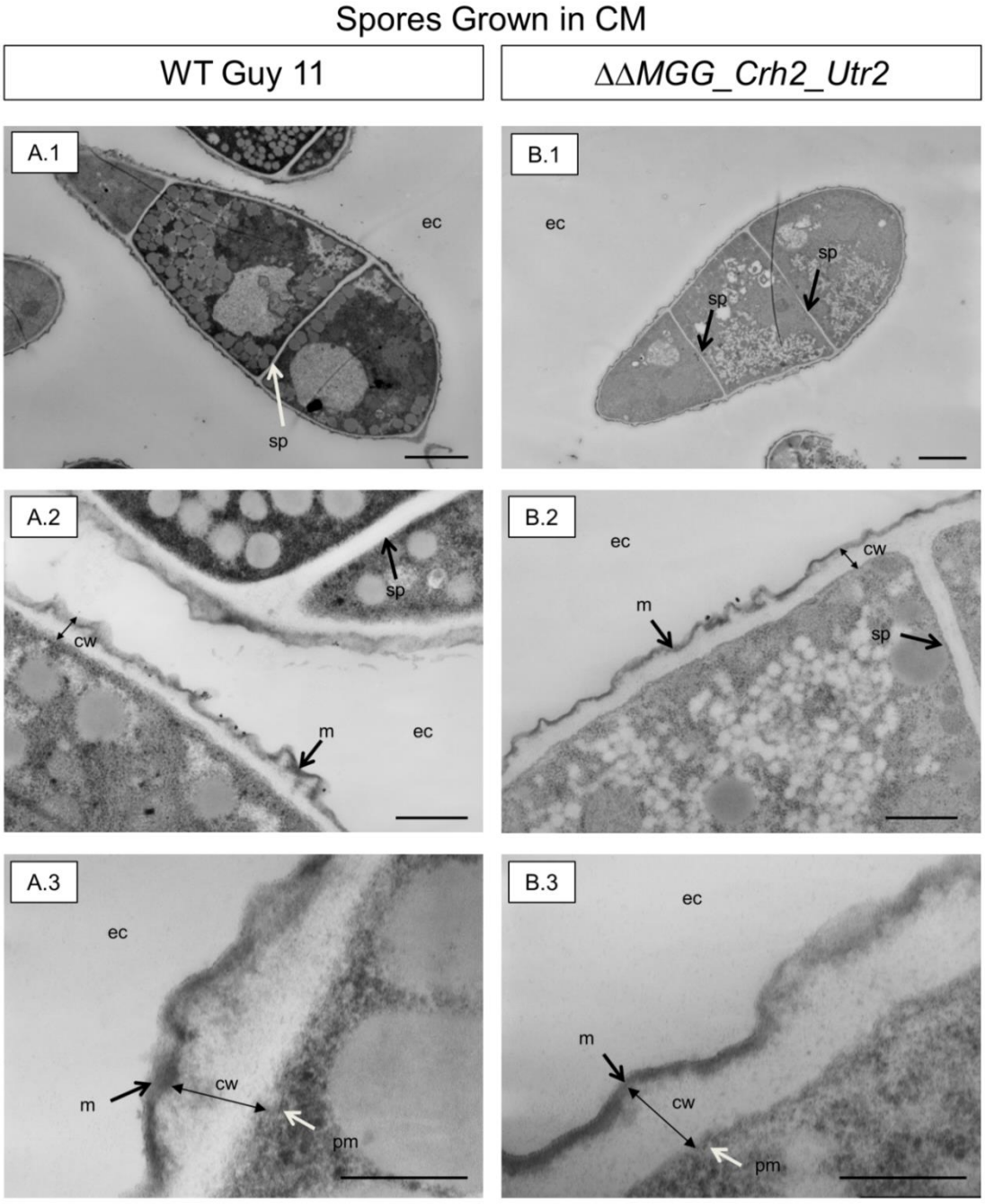

Figure 5.18. Transmission Electron Micrographs of *Magnaporthe oryzae* Dormant Spores Mycelium Cultured in CM. Samples were prepared by harvesting spores from 10 day old fungal colonies grown respectively on CM agar, followed by sample fixing. **Panels A.1-A.3.2** Dormant spores of WT strain Guy11 **Panels B.1-B.3** Dormant spores of Double gene deletant mutant strain Δ*MGG_Crh2*_Utr2 line 25. Extracellular environment (em), cell wall (cw), septum (sp), plasma membrane (pm) and melanin layer (m). Scale bars for Panels A1 and B1 represents 2 µm, scale bars for Panels A2, A3, B2 and B3 represents 200 nm.

In conclusion, the opposite is seen from the hypothesis presented in the introduction. Results showed that *M. oryzae Crh-like* mutants did not exhibit any visual deformities in the lateral cell wall or the septum in both vegetative hypha and dormant spores, either grown optimally or under cell wall stress. This is in contrary to TEM images of *Crh-like* mutants seen in *S. cerevisiae* (Figure 5.4) showing disrupted septum (Gómez-Esquer *et al.* 2004). It is possible to conclude that while *MGG_Crh2* and *MGG_Utr2* may be important for cell wall integrity and elasticity, it is not sufficient to cause a structural deformity observable by TEM imaging.

5.4.5 Germling Morphology, Fitness & Virulence

5.4.5.1 Germling Morphology

Spores harvested from four deletant strains and WT were inoculated onto artificial hydrophobic surfaces (Menzel slides) and immediately imaged (dormant spores at 0 hpi) or incubated for the respective hours of inoculation, before imaging. Time-points used correspond to the temporal development of WT infective structures, namely germ tube (2 hpi), immature appressoria (4 hpi) and mature melanised appressoria (24 hpi). Observation of the images showed that there were no obvious visual or size differences between the dormant spores and germlings of WT strain Guy11 and the four deletant strains Figure 5.19. All strains showed normal germ tube and development of appressoria.

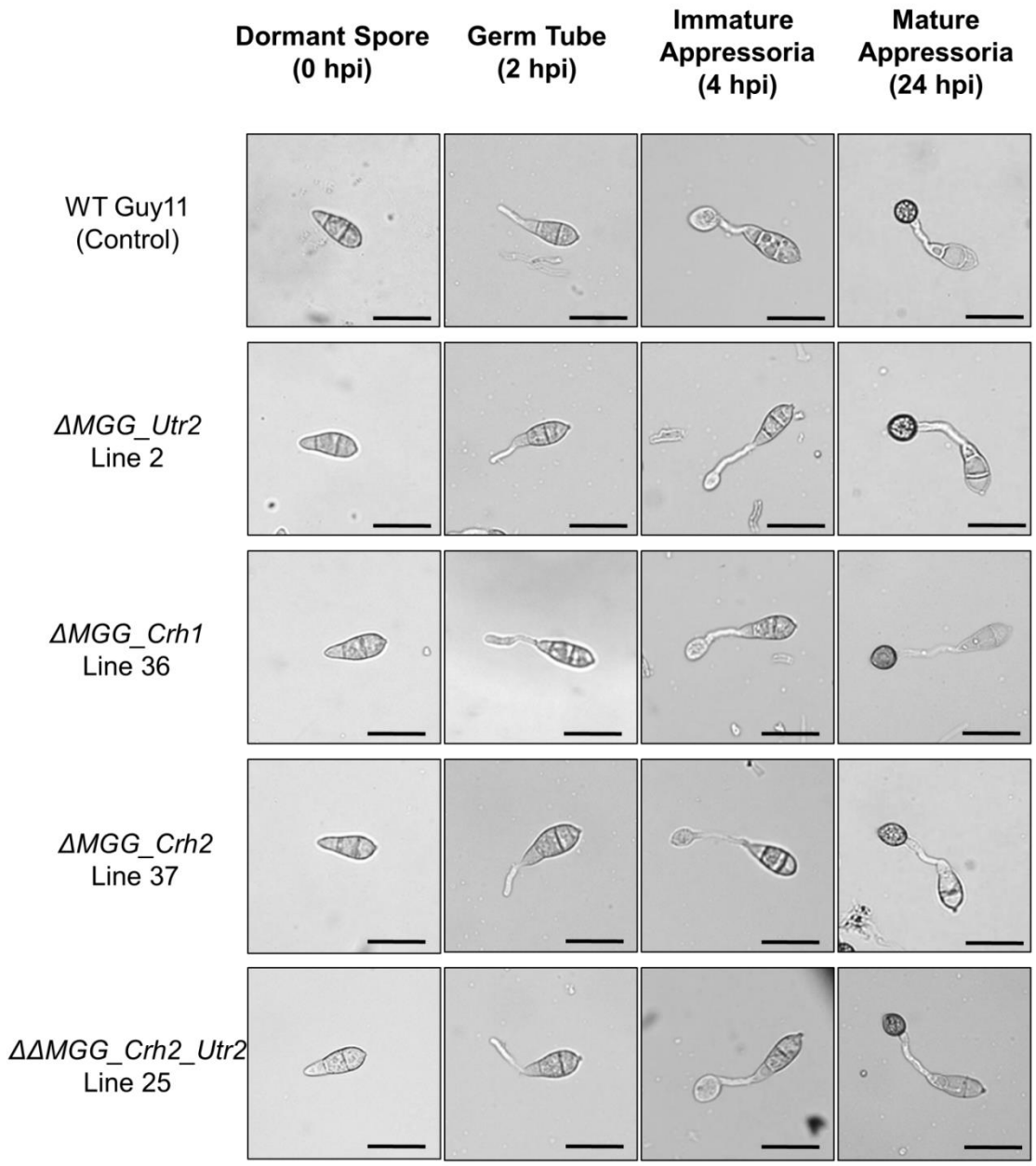

Figure 5.19. Morphology of Mutants During Germling Development. Dormant spores from each genotype was harvested from 10 day old cultures grown on CM agar and spore suspension deposited onto hydrophobic surface (Menzel slide). The dormant spores were allowed to germinate at the various times indicated, under high humidity. Images were taken at the dormant spore stage (0 hpi), germ tube production (2 hpi), formation of immature appressorium (8 hpi), and mature melanised appressorium (24 hpi). Shown above are brightfield images of WT Guy11 (Control) and four mutant strains. Germlings imaged within ± 5 minutes from the specified time points. Assay repeated 3 times. Scale bar is equivalent to 20 µm.

5.4.5.2 Germling Fitness

To validate for possible changes to fitness in spore germination, germlings from all five genotypes were imaged and germination rate for each time point was determined. Student's t-test analysis showed that there were no significant difference ($p>0.05$) between the germination rate of WT to any of the four deletant strains (Figure 5.20) at each time point assayed. At 2 hpi, 77% to 80% of all spores counted germinated into germ tubes in all five genotypes. By 4 hpi, most of these then formed appressoria with a percentage of 65% to 73%, with those remaining in germ-tube stage (13-27%) or as un-germinated spore (8% to 13%). As the time point proceeded to 24 hpi, as much as 90% to 95% of the spores formed melanised appressoria for all five genotypes, with less than 8% remaining as un-germinated spores and in the deletant strain *⊿MGG_Utr2* Line 2, about 2% still in the germ tube phase.

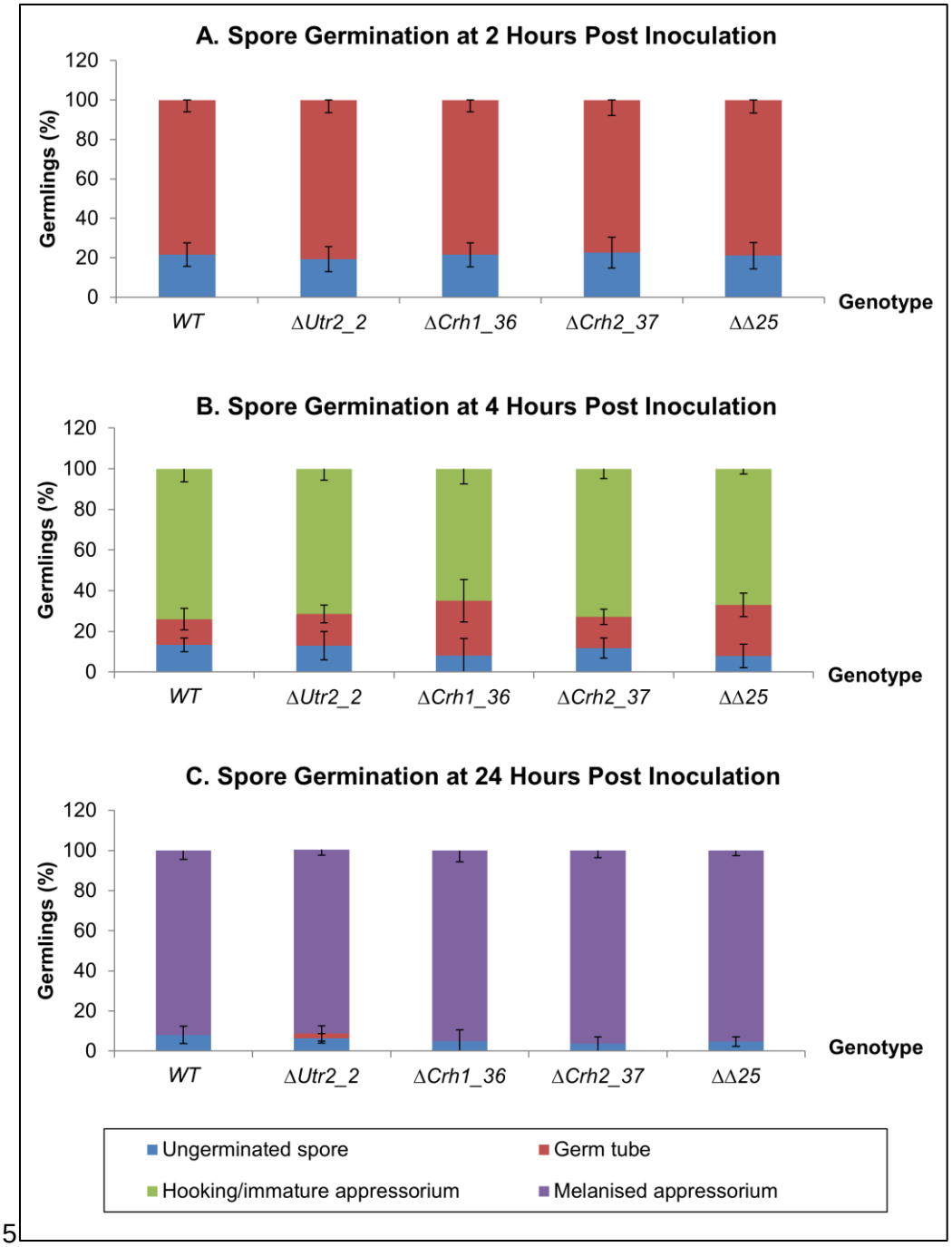

Figure 5.20. Germination Rate of Mutant Spores. Spores were harvested from 10 day old fungal colonies grown on CM and inoculated on a hydrophobic surface (Menzel slide) for 2, 4 or 24 hours. The five strains used were WT strain Guy11 (Control), and one independent transformant from each deletant strain generated: Δ*MGG_Utr2* Line 2 (Δ*Utr2)*, Δ*MGG_Crh1* Line 36 (Δ*Crh1*), Δ*MGG_Crh2* Line 39 (Δ*Crh2*) and ΔΔ*MGG_Crh2_Utr2* Line 25 (ΔΔ*25*). Germlings imaged within ± 5 minutes from the specified time points. Percentage germination rate (%) represents the percentage of germling (germ tube, immature appressoria or mature appressoria) compared with the total number of spores per image. Assay repeated three times and data showed an average of three biological replicates. Error bars represent standard deviation. Student's t-test was conducted for the statistical analysis with significance at $p<0.05$.

5.4.5.3 Early Infection on Host

The same five *M. oryzae* fungal strains were also inoculated onto onion peels to capture the ability of germlings to penetrate and form early *in-planta* infective structures. All single and double mutant lines showed were able to successfully penetrate plant host surface and form invasive hypha within host cells. Red arrows from each panel (WT strain Guy11 and four mutant genotypes) showed developed thick invasive mycelium within the onion tissue, growing from melanised appressorium (Figure 5.21). These melanised appressoria are not clearly visible in the pictures shown (dark shadows), but were evident when the microscope was focused to another plane of view, showing collapsed spore and mature melanised appressoria on the surface of the peel, with invasive hypha at another, bottom plane of focus. From the images, it can be concluded that deletant strains are able to successfully penetrate and colonise host tissue, in a similar way to the WT.

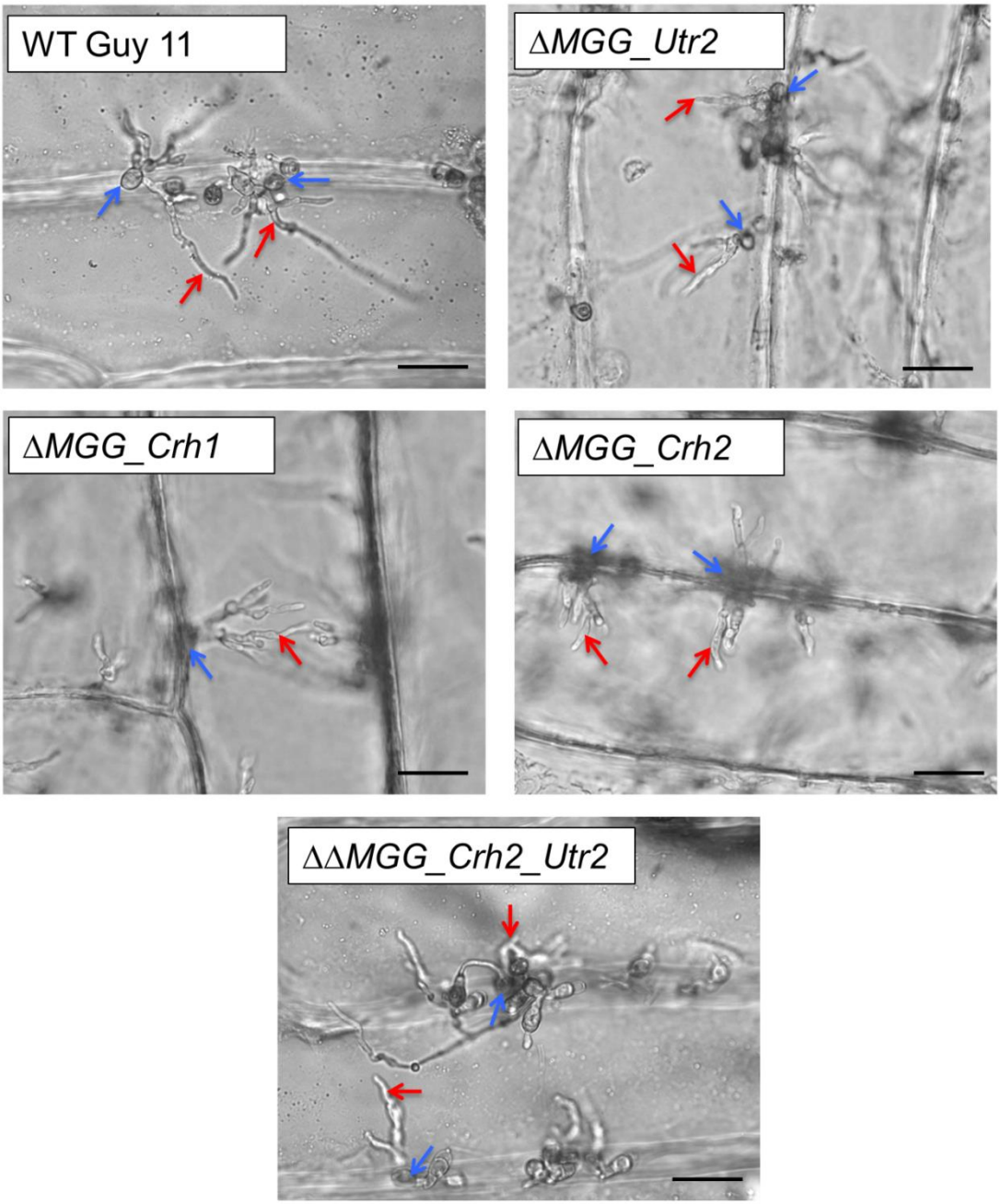

Figure 5.21. Germling Penetration Assay on Onion Sheath. Spore suspension for each mutant strain and control WT strain Guy11 were deposited onto onion sheaths respectively and incubated for 24 hpi under high humidity. Images show the development of melanised appressoria (dark circles or shadows) shown with blue arrows and invasive hypha grown within the single-celled layer of onion peel as indicated with red arrows. This is evident for all five genotypes at 24 hpi, indicating the ability of each mutant line to successfully penetrate a host plant. Each bar represents 40 µm.

5.4.5.4 Virulence Assay

Two deletant strains Δ*MGG_Crh1* Line 36 and ΔΔ*MGG_Crh2_Utr2* Line 25 with the control strain WT strain Guy11 were tested for pathogenicity against a non-specific host barley cut leaves (*Hordeum vulgare* cv Golden Promise) and specific susceptible host, rice cut leaves (*Oryza sativa* cv CO-39). The single deletant strains Δ*MGG_Utr2* and Δ*MGG_Crh2* were not included and only if a difference was seen in the double deletant strain was the assay to be repeated with these single deletant strains. Disease development in the form of lesions were evident in both mutant lines, similar to the WT and not present in the control leaf sprayed with only 0.2% gelatine, for both barley and rice leaves (Figure 5.22). Lesion count assay (Table 5.4) showed no significant differences ($p<0.05$) in lesion count per cm^2 between both mutants against WT, on both barley and rice cut leaves. Contrary to the orthologs in *C. albicans* (Pardini *et al.* 2006), it can be concluded from both pathogenicity assays that *M. oryzae Crh-like* mutants were fully pathogenic, even in the double deletant strain.

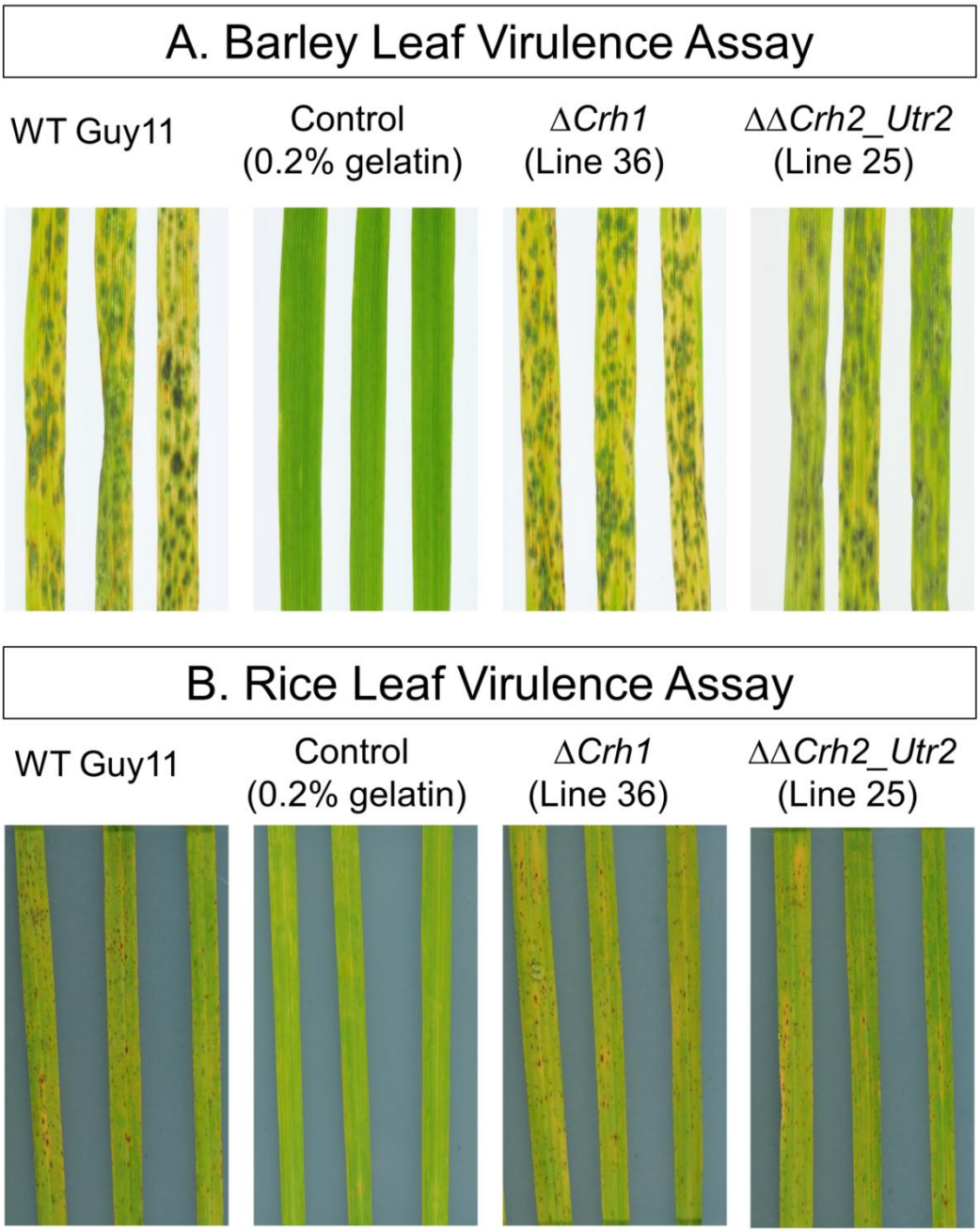

Figure 5.22. Mutant Strain Virulence Assay on Barley and Rice Cut Leaves. Spore suspension in 0.2% (w/v) gelatine for Δ*MGG_Crh1,* ΔΔ*Crh2_Utr2* and the control strain WT Guy11 were air sprayed onto seven day old barley and three weeks old rice cut leaves. Inoculated cut leaves were incubated as per routine *M. oryzae* growth conditions (Chapter 2 section 2.2.1) on 1% water agar for five days. **Panel A.** Inoculated barley leaves after five days of incubation. From left, WT (positive control), 0.2% (w/v) gelatine (negative control), Δ*MGG_Crh1* Line 36 and ΔΔ*Crh2_Utr2* Line 25. **Panel B.** Inoculated rice leaves after five days of incubation. From left, WT (positive control), 0.2% gelatine (negative control), Δ*MGG_Crh1* Line 36 and ΔΔ*Crh2_Utr2* Line 25. Both assays were repeated twice, each with three biological replicates.

Table 5.4. Average Number of Lesions per Unit Area. Cut leaf pathogenicity assay was prepared by spraying the leaves with the respective fungal strains. Five leaves per biological replicate, three biological replicates per genotype. Listed in the table below, the averaged number of lesion counter per unit are (cm^2) of the leaf, standard deviation in brackets. Students t-test analysis was conducted by comparing the number of lesions between WT strain Guy11 and each of the mutant lines Δ*MGG_Crh1* line 36 and ΔΔ*MGG_Crh2_Utr2* line 25.

Strain	**Mean number of Lesion/cm^2 (Standard Deviation)**	
	Oryzae sativa	*Hordeum vulgare L*
WT Strain Guy11	27 (7)	16 (3)
Δ*MGG_Crh1* Line 36	25 (10)	14 (3)
ΔΔ*MGG_Crh2_Utr2* Line 25	26 (9)	16 (2)

5.5 Chapter 5 Summary & Conclusions

It can be concluded from the growth assays that *M. oryzae Crh-like* genes *MGG_Utr2* and *MGG_Crh2* play an important role during the vegetative stage, especially under cell wall stress, and least important for germling development and pathogenicity. Despite the absence of morphological changes to the vegetative cell wall structure (CFW and TEM images), the apparent hypersensitivity when exposed to cell wall perturbants (plate assay and liquid biomass), suggests that the mutant strains may differ in the cell wall mechanical properties and composition. Given these findings, it is imperative that cell wall elasticity and composition of the mutant cell wall be explored and described in greater detail in the following Chapter 6.

Unexpectedly, phenotypic analysis of germling morphology and pathogenicity revealed viable germlings with full virulence in all mutants generated. This is in contrary to the hypothesis presented earlier. It is however, consistent with the gene expression analysis in Chapter 3, showing the down-regulation of these genes during germling morphogenesis, implicating that it is of lesser importance during this stage of the life cycle. It is also possible that the lack of mutant phenotype is attributable to the up-regulation of the remaining *Crh-like* homologous genes in the mutant lines. Chapter 7 will aim to explore this further.

In conclusion, while the absence of *Crh-like* genes, specifically *MGG_Crh2* and *MGG_Utr2* lead to a compromised well wall, it was insufficient to cause visual defects in the cell wall structure of vegetative hypha and germlings as well as affect fungal virulence

CHAPTER 6

Mutant Phenotyping – Cell Wall Elasticity, Topography,

&

Composition

6.1 Chapter Introduction

In previously described phenotyping work, the deletion of genes *MGG_Crh2* and *MGG_Utr2* resulted in hypersensitivity to cell wall perturbants. Furthermore, the observed phenotype for both single and double knockout mutants in Congo Red could be partially reverted by creating a hyperosmotic external environment. This suggests that there could be alterations to the cell wall rigidity in these mutant lines as a result of changes to the cell wall composition. Thus far, microscopic studies involving Transmission Electron Microscopy and cell wall staining by Calcofluor White have not shown any differences in the mutant cell wall relative to WT strain Guy11. It is possible that changes are minute or not visible, thereby requiring different methods of quantification or visualisation that the above methods are unable to provide.

To redress the above predicament, the Atomic Force Microscopy (AFM) technology was used to generate both nanoscale images of the cell surface as well as quantitative measurements of the cell wall elasticity in the knockout strain ΔΔ*MGG_Crh2_Utr2* line 25. This was followed by total cell wall carbohydrate and linkage analysis using Gas Chromatography/Electron Impact-Mass Spectrometry (GC/EI-MS).

6.1.1 Introduction to Atomic Force Microscopy

The AFM technology was first introduced in 1986 as a tool to visualise the surface topography of materials at the nanoscale level (Binnig *et al.* 1986). In the most basic form, the AFM technique is based on a sharp tip (probe) used to scan across the surface of a sample as shown in Figure 6.1. This physical contact, due to interatomic interactions between atoms in the tip apex and the surface, makes AFM fundamentally different from other microscopic techniques.

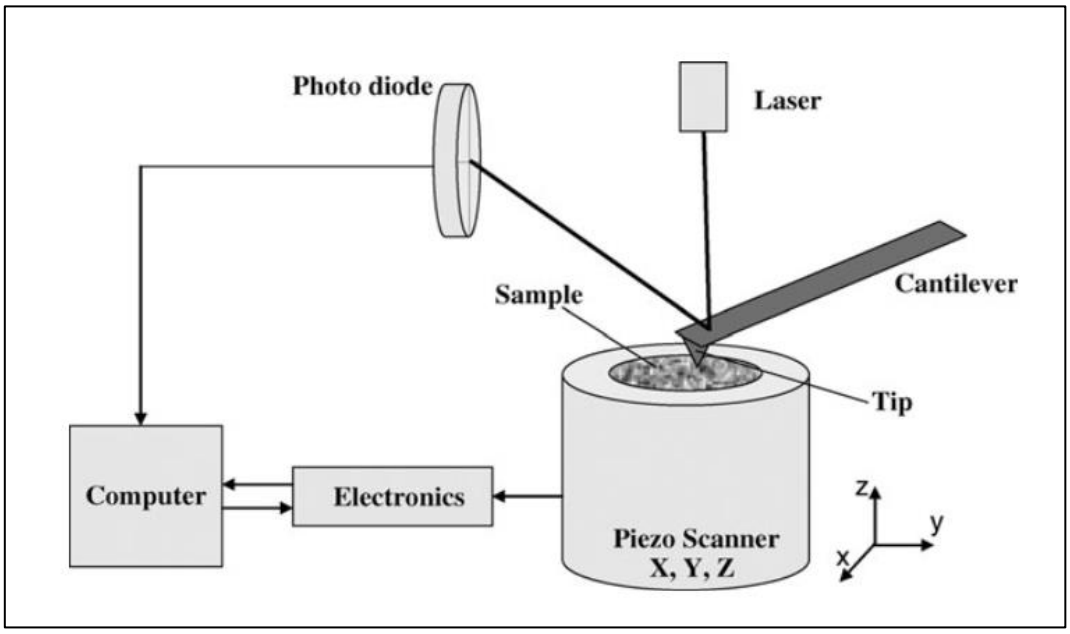

Figure 6.1. An Illustration of an AFM Apparatus. The probe (tip) is attached to a force-sensing/imposing lever (cantilever) with a laser directed onto the top surface of the cantilever. A sample is placed onto the piezoelectric scanner which can move the sample in three directions (x,y and z). The movement of the scanner will raster the sample with respect to the stationary probe, with the cantilever being deflected in response to the variable height of the specimen surface. This deflection changes the angle of reflection of the laser beam which is detected by the photo diode. Data is sent to the computer which will then generate a 3D-image of the surface topography based on these variations in laser beam deflection. Image and caption edited from (Barattin and Voyer 2008).

6.1.1.1 AFM Topographic Imaging

Topographic sample visualisation by AFM is imaged using two primary imaging modes: contact mode or tapping mode. In contact mode, the probe tip is constantly touching the surface of the sample (Dufrêne 2008). This imaging mode

is a useful and fast approach for anatomically flat surfaces involving small variations to cantilever deflections. However, in samples with large height variations such as in most biological tissues (e.g. *M. oryzae* germlings), large cantilever deflections can affect image quality as well as damage both sample and probe (Jalili and Laxminarayana 2004). Due to this, contact mode is not an appropriate approach for the study of fungal surface topography.

In the second imaging mode (tapping mode), the cantilever makes rapid intermittent contact to sample surface by stimulating the lever to oscillate at its characteristic resonance frequency (Giessibl 2003). This avoids problems associated with the contact mode, including issues with friction, adhesive forces due to Van der Waals forces and hydrophobic interactions. As a result, tapping mode often results in better quality images relative to contact mode (Möller *et al.* 1999, Song and Bhushan 2008), and has become the favoured imaging mode for soft biological materials. Additionally, the advantage of the tapping mode is a reduction in damage of samples and probe contamination. Small particles that are loosely attached to the substrate or surface could be dislodged and soft samples damaged with the sweeping movement of the probe in contact mode (Jalili and Laxminarayana 2004).

6.1.1.2 Force Spectroscopy (Elasticity)

The AFM technology has diversified and along with surface imaging, mechanical properties of biological samples can be explored; such as surface elasticity (Weisenhorn *et al.* 1993, Cappella *et al.* 1997). In force spectroscopy (by contact mode), the probe is not scanned across the sample but instead used to impose a force at a single point of contact on the sample and retracted (by stage movement in the z-direction), while changes to cantilever deflection are

continuously recorded. This procedure enabled the construction of a force versus distance (FD) curve as described in detail in Figure 6.2.

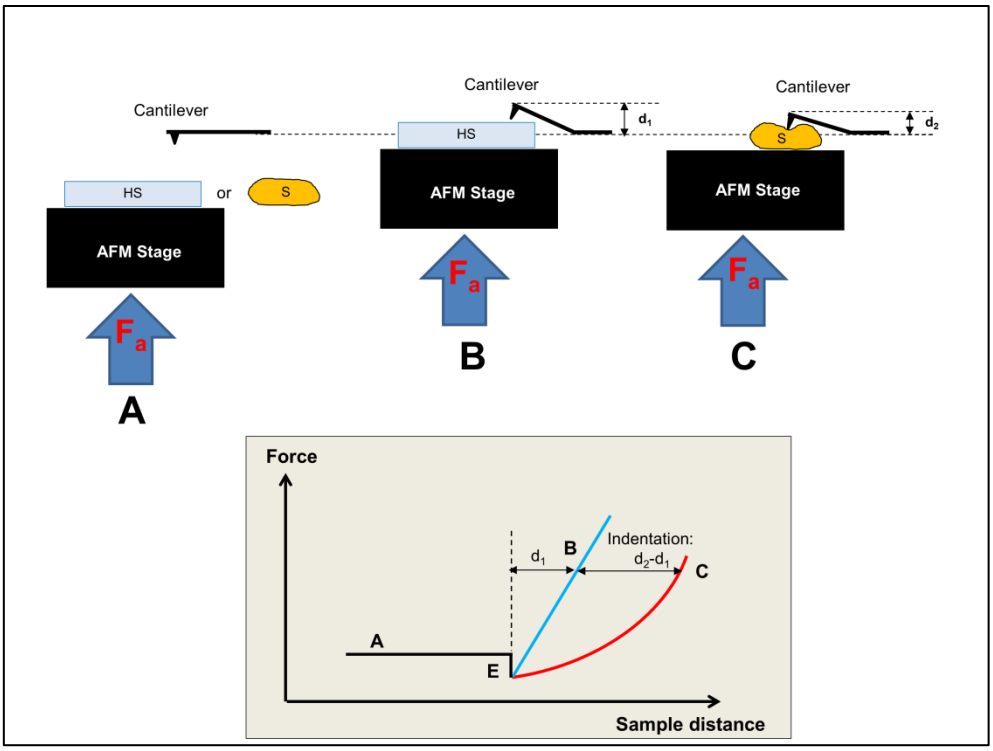

Figure 6.2. A Schematic Diagram Describing the Principles of Force Spectroscopy. Image A An incompressible hard surface (HS) or biological sample (S) is mounted onto a piezo scanner stage (AFM Stage), which is driven in the z direction, towards the cantilever. At this point, there is no change in lever deflection, as it is not in contact with the samples (Line A). As the samples approach the tip of the probe, the attractive van der Waals force pulls the tip quickly towards the sample, causing a sudden downward deflection from the graph (Line E). **Image B** Continued sample movement upward between HS and cantilever exerts a repulsive force that bends the lever at a distance of d_1. The HS results in a linear interaction (line B) between force exerted and distance moved by lever. **Image C** In a biological sample with the same upward repulsive force, less lever bending occurs, at a distance of d_2, as a softer surface will absorb some of the force by the probe by deformation of the sample surface. In this case, the system now consists of two compressible springs in series. This result is a non-linear interaction with the slope being less than the HS (Line C). The applied force (F_a) can be calculated using the reference calibrator (HS) according to Hooke's Law and the cantilever's known spring constant (k), where $F_a=k\Delta_{BE}$. Sample indentation distance is Δ_{CB}.

In reference to a typical FD curve, an incompressible hard surface such as a glass slide will result in a linear relationship while a soft biological sample will result in a non-linear curve. Consequently, this gives a less-steep slope in the force-distance (FD) curve of a biological sample compared with the hard surface. Additionally, another biological sample that is stiffer will exert more resistance, therefore theoretically, the slope will lie between the slope of the softer biological sample and the incompressible glass surface. This lead Blach *et al.* (2001) to conclude that a variation in the slope of the FD curves, therefore, indicates variations in the elastic properties of the sample surface. This logic is used for this work to determine the relative cell wall elasticity of mutants against the WT Guy11.

In several studies of fungal cell wall elasticity (Ma *et al.* 2005, Zhao *et al.* 2005, Dague *et al.* 2010), FD curves were used to further derive an elasticity value using the Young's Modulus formula based on the Hertz-Sneddon theory (Hertz 1881, Sneddon 1965, Timoshenko *et al.* 1970). However, given the extensive assumptions and variable experimental conditions, this calculation is deemed problematic (Emad *et al.* 1998) and does not generate reliable values for biological samples (Heinz and Hoh 1999, McElfresh *et al.* 2002). This is because the theory was developed for hard, non-biological materials and incorporates several assumptions such as the sample surface is smooth and flat, the material deforms in a linear manner (Hooke's law), and the sample is isotropic (uniform in all orientations). These assumptions do not apply to biological samples that are often of variable height and have a rough surface with a non-linear deformation (McElfresh *et al.* 2002). As aptly quoted by Vickier and Semenza (1998) "In fact, the absolute determination of Young's modulus of all

biological system, which is complex, is not always necessary." However, because of the relatively small number of studies utilising AFM in measuring the cell wall properties of fungal cell wall mutants, studies using the Young's Modulus approach are still discussed in the following section, albeit with caution.

6.1.1.3 Measuring Fungal Cell Wall Mechanical Properties by AFM

Cell wall robustness has been frequently and indirectly measured in mutant strains by assessing the ability of fungal cells to resist osmotic, cell wall or oxidative stress. This is seen in studies of *Crh-like* deletion mutants in both yeast and *C. albicans* (Rodriguez-Pena *et al.* 2000, Pardini *et al.* 2006, Cabib *et al.* 2007). However, given that the fungal cell wall is a dynamic structure with significant mechanical role, it is important to address these features directly and as a complement to genetic and biochemical studies.

Features of AFM that makes it relevant for fungal cell wall studies include the ability to visualise cell wall architecture at the nano-scale resolution, information on cell wall nano-mechanical properties, live imaging and manipulation of compounds at the single molecule level (Dufrêne 2008, Müller and Dufrêne 2011, Francois *et al.* 2013). For the purpose of this study, the latter is beyond the scope of this work and is not elaborated.

The AFM technique enabled living samples can be imaged in real time. Surfaces of living fungi have been successfully imaged such as in *S. cerevisiae* (Ahimou *et al.* 2003, Dupres *et al.* 2009), *Phanerochaete chrysosporium* (Dufrêne *et al.* 1999), *Aspergillus nidulans* (Zhao *et al.* 2005), and in the germinating spore of *Aspergillus fumigatus* (Dague *et al.* 2008). This means that data acquisition is

more realistic and in real-time, without the risk of sample fixing affecting the results.

Using AFM technology, it was discovered that the absence of several types of fungal cell wall proteins altered fungal surface topography and in some cases, cell wall elasticity. In *S. cerevisiae*, the absence of cell wall genes *Crh1, Crh2, Gas1* and *Chs* in yeast resulted in alterations to the surface topography when imaged by AFM, which increased in roughness relative to the wild type (Dague *et al.* 2010). Dague et al (2010) also measured and compared the cell wall elasticity (Young's Modulus) of mutants, with the deletion strain *crh1*Δ*crh2*Δ showing reduced elasticity compared with the wild type, although caution is given to accuracy of the calculated elasticity values.

To date, there is no available literature investigating the surface topography and elasticity of live *M. oryzae* vegetative hyphae by AFM. Other methods such as Scanning Electron Microscopy (SEM) and TEM involved profuse washing and sample fixing while live images of *M. oryzae* hyphae using light microscopy and confocal imaging cannot image down to the nano-scale level. There is also no knowledge on the effects of cell wall remodelling proteins on cell wall topography and elasticity. Due to this, AFM proved to be a suitable complementary tool to investigate the cell wall topography at the molecular scale and elasticity of *M. oryzae Crh-like* mutants. Given the sensitivity of *M. oryzae Crh-like* mutants to Congo Red (the tendency for hyphal tip swelling) and subsequent phenotype recovery by osmotic stress (prevention of tip swelling), it was hypothesised that the cell wall of mutant ΔΔ*MGG_Crh2_Utr2* has altered surface architecture and topography with compromised mechanical strength via reduced cell wall rigidity.

6.1.2 Introduction to Fungal Cell Wall Composition

Despite being unique to the fungal Kingdom, cell wall composition is diverse, varying across species and stages of the life cycle. Table 6.1 shows a comparative summary of cell wall components of four fungal species, illustrating the level of diversity and variation among species. These examples of diversity in cell wall composition emphasise the need to explore the cell wall composition of *M. oryzae*. It is hypothesised that while the cell wall composition of *M. oryzae* may be similar to the other filamentous fungi such as *A. fumigatus* and *N. crassa*, the phytopathogen may exhibit species-specific features that may provide valuable insights into using the fungal cell wall as an antifungal target.

Table 6.1. Comparative* Summary of Fungal Cell Wall Components n *S. cerevisiae, C. albicans*, *A. fumigatus* and *N. crassa*.

Cell Wall Component	*S. cerevisiae*	*C. albicans*	*A. fumigatus*	*N. crassa*
Chitin	1-2%	2-6%	7-15%	4%
β-1,3 Glucan	50-55%	30-39%	20-35%	87%
β-1,6 Glucan	10-15%	43-53%	No	No
Outer chain mannan	10-20%	38-40%	No	No
Galactomannan	No	No	20-25%	12%
Melanin	No	Yes-infective stage	Yes-conidia	Yes-ascospore and perithecia

*The cell wall components listed above were obtained from the following published work: *S. cerevisiae* (Lesage and Bussey 2006), *C. albicans* (Ruiz Herrera *et al.* 2006), *A. fumigatus* (Gastebois *et al.* 2009) and *N. crassa* (Maddi and Free 2010). Table was simplified from Free (2013).

The polysaccharide component of the cell wall can be up to 85-90% and plays a major role in providing mechanical strength (Nguyen *et al.* 1998). These polysaccharides are separated into two groups according to their solubility in hot alkali (Fontaine *et al.* 2000). It has been accepted that it is the linkage of the insoluble chitin to the soluble glucan polymers results in an alkaline insoluble

fraction. (Sietsma and Wessels 1979, Sietsma and Wessels 1981, Hartland *et al.* 1994, Kollár *et al.* 1997).

The cell wall remodelling proteins belonging to the Crh-like family, are enzymes responsible for catalysing the cross-links between chitin and glucan polymers. Therefore, lack of Crh enzymatic activity would then alter the proportion of glucan in the ASF/AIF of the fungal wall. In a study where this protein was first identified, cell wall composition analysis used chemical treatments (hot alkaline/acid) to produce glucan pellets derived from the Alkaline Soluble Fraction (ASF) and Alkaline Insoluble Fraction (AIF) which were then weighed and compared between strains. Rodriguez-Pena *et al.* (2000) showed that the ASF almost doubled in dry weight, and they reported a 39% reduction in the AIF relative to the WT strain FY1679.

Almost a decade later, acknowledging the need to specifically identify the function of Crhp, Cabib *et al* (2009) developed the chitosan method. In the study, Cabib *et al.* (2009) showed that chitin in the double knockout strain *utr2*Δ*crh1*Δ was almost 100% free, as opposed to 63% bound to glucan in the WT strain FY 001. A similar outcome was seen in *C. albicans* albeit with the use of more advanced cell wall composition analysis, involving chemical extraction, polymer acid hydrolysis and chromatography (Pardini *et al.* 2006). In this study they discovered that the triple mutant line *utr2*Δ*crh11*Δ*crh12* showed a 30% reduction in 1,3-glucan in the AIF. Also, there was a 70% increase in total chitin, and 30% reduction in total mannan (Pardini *et al.* 2006). While the reduction in mannan is puzzling and not explained by the authors, the increase in total chitin was accepted as a general indication of a mutant experiencing a compromised cell

wall, leading to the activation of the CWI pathway and subsequent chitin up-regulation. This compensatory mechanism is discussed in detail in Chapter 7.

Cell wall composition analysis has since developed and technology is now available to determine not only the various polysaccharide components but also to determine the type and quantity of linkages present. The basic principal of cell wall analysis first involves cell lysis and cell wall extraction, followed by a series of chemical treatments and washes to obtain the AIF and ASF components (Appendix D.1) and subsequent depolymerisation of the various polymers into monomers (Pérez and Ribas 2004). The monomers are then subjected to either traditional colorimetric analysis (Dubois *et al.* 1956, Aguilar-Uscanga and Francois 2003) for relative quantification of total glucose, or technologies involving Gas Chromatography (GC) or High Performance Liquid/Ionic Chromatography (HPLC/HPIC) (Ruiz and Date 1996, Dallies *et al.* 1998, François 2006) to identify and quantify the monomers eluted. Additionally, an extension of the GC tool coupled with Electron Impact-Mass Spectrometry (EI-MS), has enabled the determination of the various types and quantities of linkages present in each monomer, achieved using the polymer methylation-alditol acetate technique (Björndal *et al.* 1970). Due to this, the GC/EI-MS is considered a powerful tool in providing highly detailed and informative data that has significantly changed the field of cell wall composition analysis and has been applied in this study.

Given that little is known about the *M. oryzae* cell wall, and in an effort to better understand and control this phytopathogen, it is important to draw a definitive picture of the cell wall composition and various linkages present. Additionally, given the specific role of Crh-like proteins, it is imperative to observe changes to the cell wall composition of *Crh-like* knockout mutant lines. Given the various options available for cell wall composition analysis, the GC/EI-MS tool has proved most useful and informative for the purpose of this work.

It is hypothesised that *M. oryzae* cell wall composition is species-unique and that the absence of *M. oryzae Crh-like* genes changes the types of inter-polymer linkages present, with a reduction in chitin to glucan glycosidic bonds. It is expected, given the impairment in the cross-linking of chitin to glucan, that there will be an increase in the glucan component in the alkaline soluble fraction (ASF) compared with the amount of glucan found in the ASF of the WT cell wall. Additionally, given the compromised cell wall, compensatory mechanisms of other cell wall proteins could cause an increase in glucan branching (increase in 1,3,6 glycosidic linkages) and total chitin content (increase in 1,4-N-acetyglucosamine linkages).

6.2 Aims & Objectives

To determine any changes to surface topography and cell wall rigidity of the knockout line ΔΔ*MGG_Crh2_Utr2* relative to WT. To then subject these strains to a cell wall composition analysis to determine the type and quantity of carbohydrates in the cell wall and the glycosidic bonds linking the monomers of these carbohydrates. The above aims were achieved by the following experimental strategies:

Imaging and Quantification of Cell Wall Elasticity by AFM

1. To conduct topographical imaging of live vegetative hypha and germlings of fungal strains using tapping mode

2. To subject the vegetative hyphae in a series of force versus distance tests using the contact mode and compare between fungal strains

Cell Wall Composition Analysis by GC/EI-MS

1. To harvest mycelia of fungal strains, followed by cell wall extraction and a series of solubilisation treatments to obtain the alkaline soluble/alkaline insoluble fractions of the cell wall

2. Perform acid hydrolysis in the various fractions to hydrolyse polymers followed by monomer identification and quantification, measured in percentage molecule (% mol)

3. In a separate assay, to perform the polymer methylation-alditol acetate technique on the various fractions to determine the types and quantity of linkages found in the carbohydrates, measured in percentage molecule (% mol)

6.3 Materials & Methods

6.3.1 Cell Wall Topography & Elasticity

6.3.1.1 Tissue Preparation

6.3.1.1.1 Vegetative Hyphae

Two *M. oryzae* strains were used in this section: WT strain Guy11 and the double knockout *ΔΔMGG_Crh2_Utr2* line 25. Fungal mycelia overgrown on a small cover slip (0.5 cm x 0.5 cm) after 24 hours, was prepared as described in Chapter 2 (Section 2.2.1.6). The small cover slip was directly mounted onto a piezo scanner and viewed using the Park CP-II Autoprobe with a Multitask head and a 100 µm scanner. The AFM analysis was carried out at room temperature (20-22°C) with a relative humidity of 20-30%. The sample was replaced every hour to minimise imaging of desiccated fungal hyphae. The control WT was imaged with the mutant strain in each AFM session.

6.3.1.1.2 Germling

Germlings at 2 hpi and 24 hpi were prepared on an artificial surface as described in Chapter 2 (Section 2.2.1.3). The cover slip containing germlings were then mounted onto a piezo scanner and viewed as described for vegetative hyphae above. The sample was replaced every hour to minimise imaging of desiccated germlings.

6.3.1.1.3 AFM Analysis

A single probe, (Cantilever C by μMasch type NSC35/ALBS) was used for all AFM work presented in this section. The tip has a total opening cone angle of 40°, made from n-type silicon with aluminium as the reflective coating. It had a force constant (k) of 5.4 N/m, with a resonance frequency of approximately 150 kHz.

For topographical imaging, tapping mode by constant force (z-images) was used, with the size of image ranging from 1 μm x 1 μm up to 15 μm x 15 μm and a fast-scan rate of 0.5 Hz. Image processing was done with the 'VeecoDI SPMLab 6.0.2' (by Veeco Inc), a discontinued image analysis software, and the freely available software 'Gwyddion' version 2.4 (Gwyddion 2014). A minimum of two imaging session was performed for consistency and each session performed together the control WT.

To generate force-distance (FD) curves, the AFM was converted to contact mode. Mounted samples containing WT mycelium on a cover slip were first visualised using the in-build CCD optical camera (Nikon). Once a hypha was identified, a series of indentations, each 0.5 μm apart, were performed at the growing tip and the mature section as described in Figure 6.3 below. An indentation was never repeated on the same location more than once. Raw data from multiple indentations for each tip and mature regions were then averaged and a force versus distance curve constructed for each section. The procedure was repeated for the mycelium of the mutant *ΔΔMGG_Crh2_Utr2* line 25.

Force versus distance data acquisition and analysis involved two initial pilot runs. In the first assay (Pilot 1), indentations were conducted to compare the slope of

the FD curve between the growing tip and mature section of a WT, relative to the slope of a hard surface used to support the sample (cover slip). In a second pilot assay (Pilot 2), indentations were conducted to compare the slope of the FD curves from the mature section of a WT hypha to the mature section of *ΔΔMGG_Crh2_Utr2* line 25 hypha, relative to the control hard surface (cover slip). For both pilot studies, each sample type had a minimum of ten indentations, data were averaged and a force-distance curve was generated. From the pilot work, the decision was made to perform a total of 50 indentations at the mature section of multiple hyphae of each fungal strain and data averaged. The FD curves were then plotted onto one graph after shifting the curves by the addition of constant offsets (on both x and y axis) for ease of comparison. The slope of each FD curve was measured using the formula: Slope = $(y_2-y_1)/(x_2-x_1)$.

For each set of analyses, indentations on a hard surface (same cover slip used to mount the sample) were used as the reference control as described by Weisenhorn *et al.* (1993). Each analysis was performed on the same day, using the same laser beam positioning and force load (5 nN).

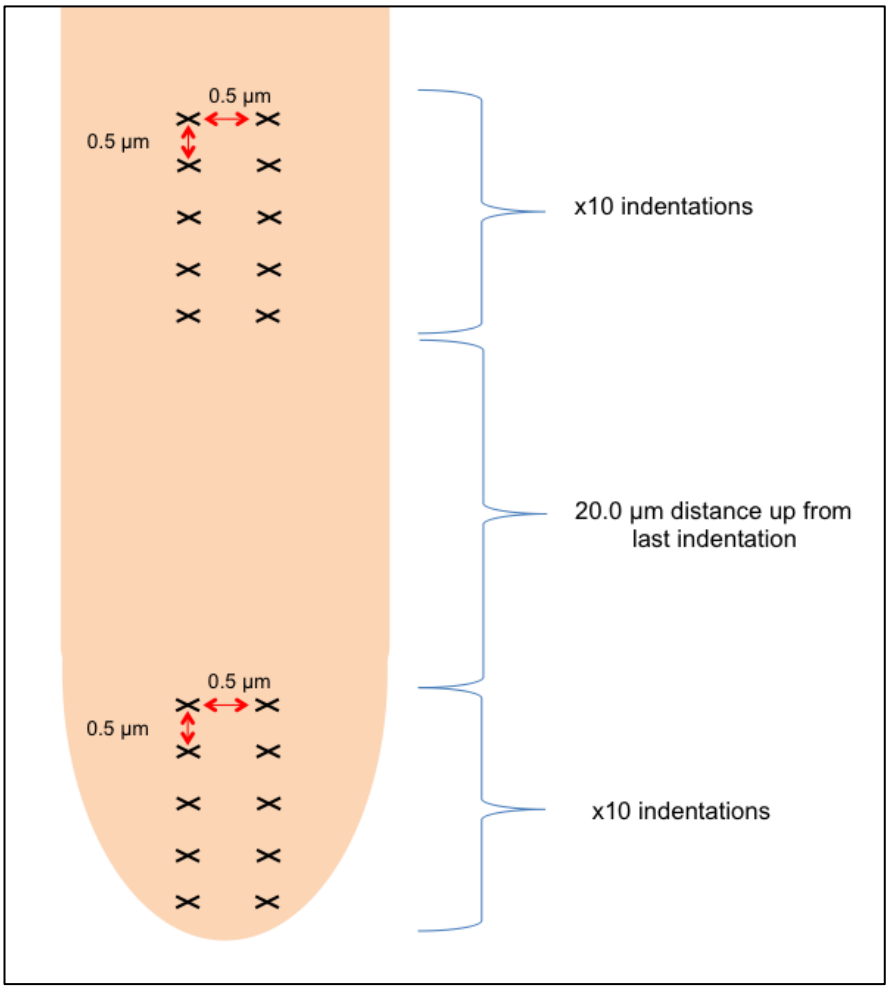

Figure 6.3. An Illustration for the Location of Indentations Made for The Force-Distance Curve Analysis on a Vegetative Hypha.

6.3.2 Cell Wall Analysis

6.3.2.1 Tissue Preparation

Vegetative mycelium for each strain was prepared in liquid CM (without yeast extract) and incubated as described in Chapter 2 (Section 2.2.1.5) using 100 µl of 30-40 x 10^4 spores/ml spore suspension. The 3-day-old mycelium was then harvested by pouring through a Buchner funnel and washed 3x with sterile MilliQ-H_2O. The fungal tissue was then freeze dried for two weeks and kept in -80^oC until ready for cell wall composition analysis.

Each genotype consisted of three samples from three independent biological replicates with WT strain Guy11 as the control sample. The single gene knockout *ΔMGG_Crh1* independent lines 36 and 43 and the double knockout *ΔΔMGG_Crh2_Utr2* lines 25 and 27 were used in this analysis. Data presented are averages from three biological replicates.

6.3.2.2 Cell Wall Preparation

Polysaccharides from the cell wall were extracted according to the method described in Mélida *et al.* (2013), with two modifications. Firstly, mechanical disruption of the fungal mycelia was conducted using a vibratory disc mill RS400 (Retsch) in two cycles of 30 minutes at 30 Hz/s. Secondly, the 'Alcohol Insoluble Residue' fraction was treated with α-amylase. This treatment was performed to remove any starch/glycogen-like carbohydrates found in this fraction and was conducted before the SDS-mercaptoethanol treatments.

6.3.2.3 Monosaccharide Analysis

Total sugar analysis was conducted as described by Blakeney *et al.* (1983) and hydrolytic conditions by Saeman (1981). The final stage monosaccharides were

then separated and analysed by GC/EI-MS as described in Mélida *et al.* (2013). In determining the type and amount (mol%) of glycosidic linkages, linkage analysis was performed using the CH_3I/NaOH methylation method described in (Ciucanu and Kerek 1984, Mélida *et al.* 2013). The partially methylated alditol acetates were then analysed by GC/EI-MS. Data presented are the average of three biological replicates each from three technical replicates.

6.4 Results & Discussion

6.4.1 Surface Topography & Elasticity

6.4.1.1 Surface Topography by Tapping Mode

Vegetative hyphae of WT and the double knockout strain ΔΔ*MGG_Crh2_Utr2* line 25 were imaged live in the tapping mode. This mode was chosen given that the sample is of biological origin, therefore to minimise sample damage, probe contamination and in addition to acquiring high-quality images, this mode was deemed the best approach. The resulting images were consistent and showed structures rarely seen with such clarity in a growing filamentous fungus. This was attributable to the high resolution of AFM imaging (nanoscale level) and realistic live imaging.

High magnification (1 µm x 1 µm) imaging of vegetative hyphae for both WT and the knockout strain ΔΔ*MGG_Crh2_Utr2* line 25 showed no obvious differences in surface topography (Figure 6.4 Panel A and Panel B). Through contour line analysis, the mature section of fungal hypha had an average height of 500-800 nm (Figure 6.5 Panel A). Consistently, lower magnification images (10-15 µm x 10-15 µm) for both WT and knockout strain ΔΔ*MGG_Crh2_Utr2* line 25 revealed the presence of a layer extruded from the vegetative mycelium, henceforth termed extracellular material (ECM) (Figure 6.5 and Figure 6.6). Images showed that the ECM has an average width of 2 to 5 µm on each side of the vegetative hyphae and growing tip. Line analysis of magnified ECM images (Figure 6.5 Panel A and Panel B) revealed that the ECM had an average thickness of 2 to 5 nm with randomly placed larger structures or globular ‘pebbles’ (Figure 6.6, red arrows in Panel B).

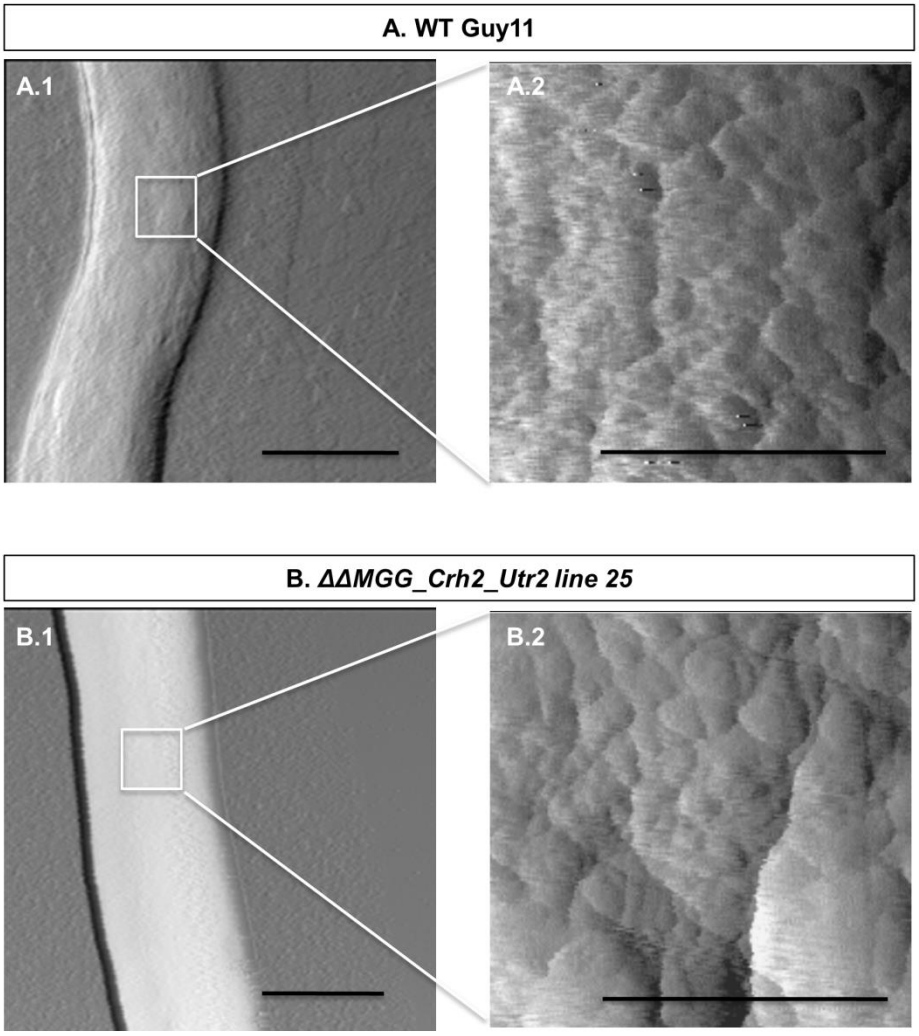

Figure 6.4. Magnified Imaging of the Surface Structures of Fungal Vegetative Mycelium. Panel A.1. A low magnification image of a WT vegetative hypha showing a typical site for high magnification imaging. **Panel A.2** A high magnification image (1µm x 1 µm) of the WT. **Panel B.1** A low magnification image of a mutant vegetative hypha showing a typical site for high magnification imaging. **Panel B.2** A high magnification image (1µm x 1 µm) of the mutant *MGG_Crh2_Utr2* line 25. Scale bar of low magnification images of hyphae (A.1 and B.1) represents 2.0 µm. Scale bar of high magnification imaged (A.2 and B.2) represents 0.5 µm. Images obtained by tapping mode using constant force with a scanning rate of 0.5 Hz and imaging repeated a minimum of twice for consistency.

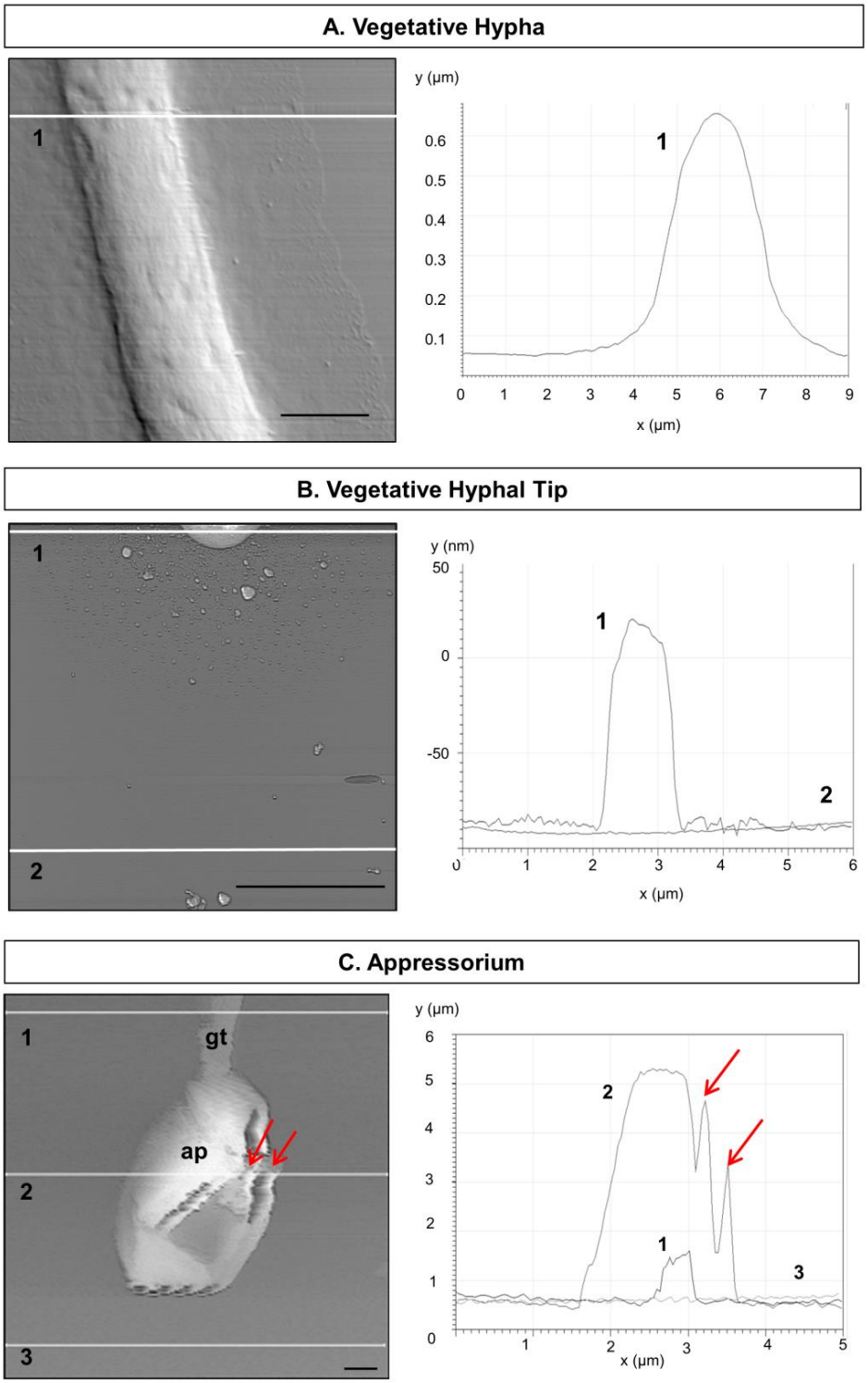

Figure 6.5. Contour Line Analysis on Strain Guy11 Fungal Structures. Panel A. Left: a mature section of a vegetative hypha with a profile line drawn across (1). Right: graph showing the height of the structures (µm) across the profile line (1). **Panel B** Left: a region around the growing tip of a vegetative hypha with profile lines (1) and (2). Right: graph showing the height of the structures (nm) across the profile line (1) and (2). **Panel C**. Image left show a partially collapsed appressorium of a germling at 24 hpi with three profile lines drawn across (1), (2) and (3). Graph on the right shows changes to height (µm) across the respective lines (1), (2) and (3). All images above were obtained by tapping mode using constant force with a scanning rate of 0.5 Hz.

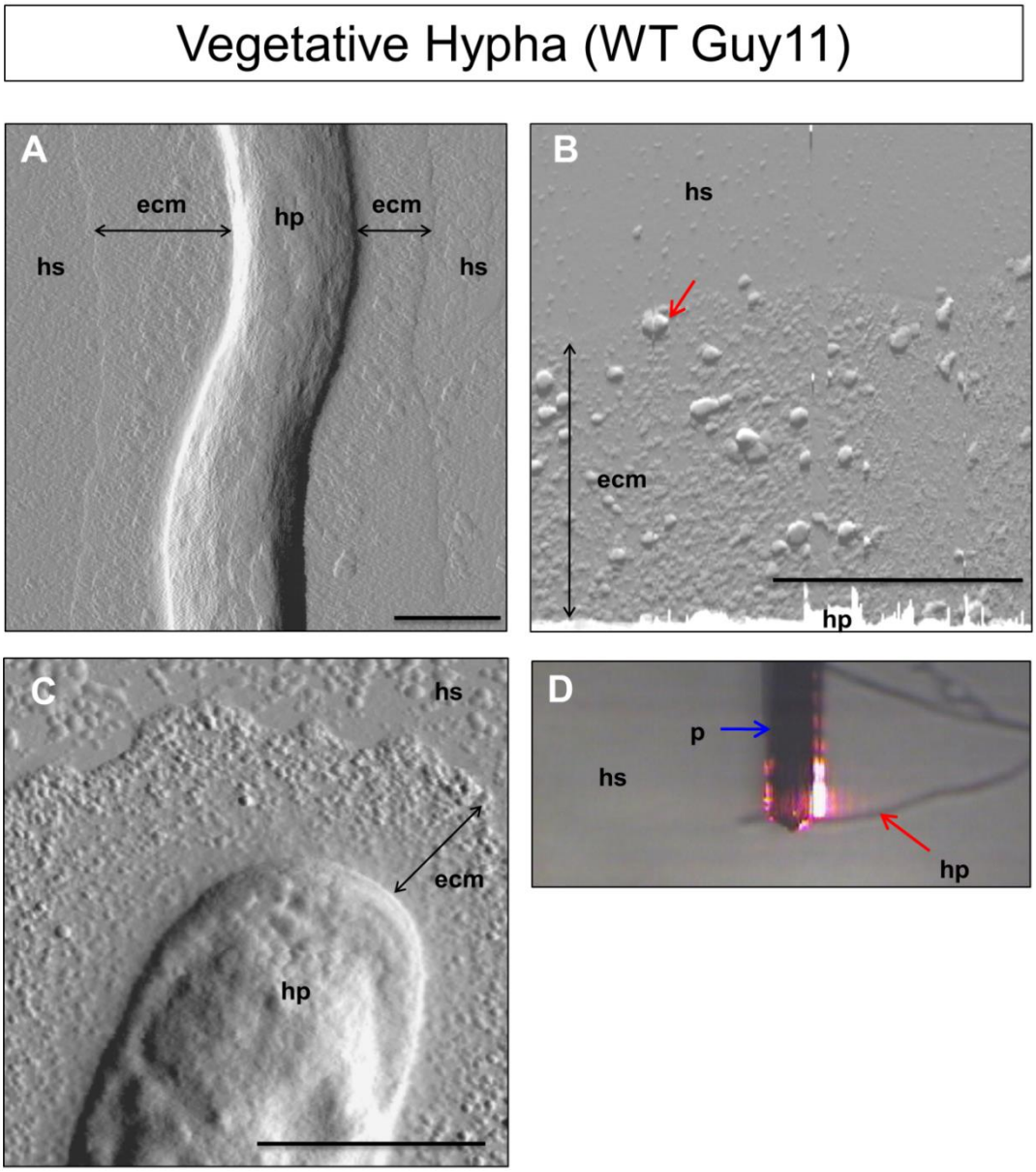

Figure 6.6. ***Magnaporthe oryzae*** **WT Vegetative Hypha Imaged by AFM.** Fungus cultured on CM agar with the edges of the colony allowed to grow over 1/10th of a cleaned cover slip (hard surface, hs) and imaged live. **Panel A** The middle section of a growing hypha (hp) with extracellular matrix (ECM) grown on the cover slip (hs).**Panel B** Area immediately beside a mature section of the hypha, amplifying the ECM region. **Panel C** Image of a growing tip with surrounding ECM. **Panel D** An optical image taken by the in-built CCD camera (Nikon) showing the probe (p) localised on a mature section of a hypha. Bar scale at 2.0 µm. Images obtained by tapping mode using constant force with a scanning rate of 0.5 Hz.

It is interesting to further observe that no ECM is seen surrounding the germ tube of germlings (Figure 6.7). In this representative image of a 2 hpi germling (Figure 6.7 Panel A), the germ tube is seen with early stages of tip swelling, without any ECM, although a small amount of unknown material is seen under the swelling germ tube tip (red arrow). Likewise, contrary to images of mature vegetative hypha (Figure 6.8), the germ tube connecting the spore to the melanised appressorium at 24 hpi showed no ECM (Figure 6.7 Panel B). To show that the absence of ECM is not due to poor quality images, Figure 6.7 (Panel B.3) shows an area immediately beside a 24 hpi germ tube with suspected polymers from Mira Cloth. Mira Cloth is a fabric used to harvest spores. This explains the reason for the absence of these fibres in vegetative samples. The ability of the AFM tapping mode to image single polymers of Mira Cloth, immediately beside the germ tube, but without ECM detected attests to the quality of the imaging used.

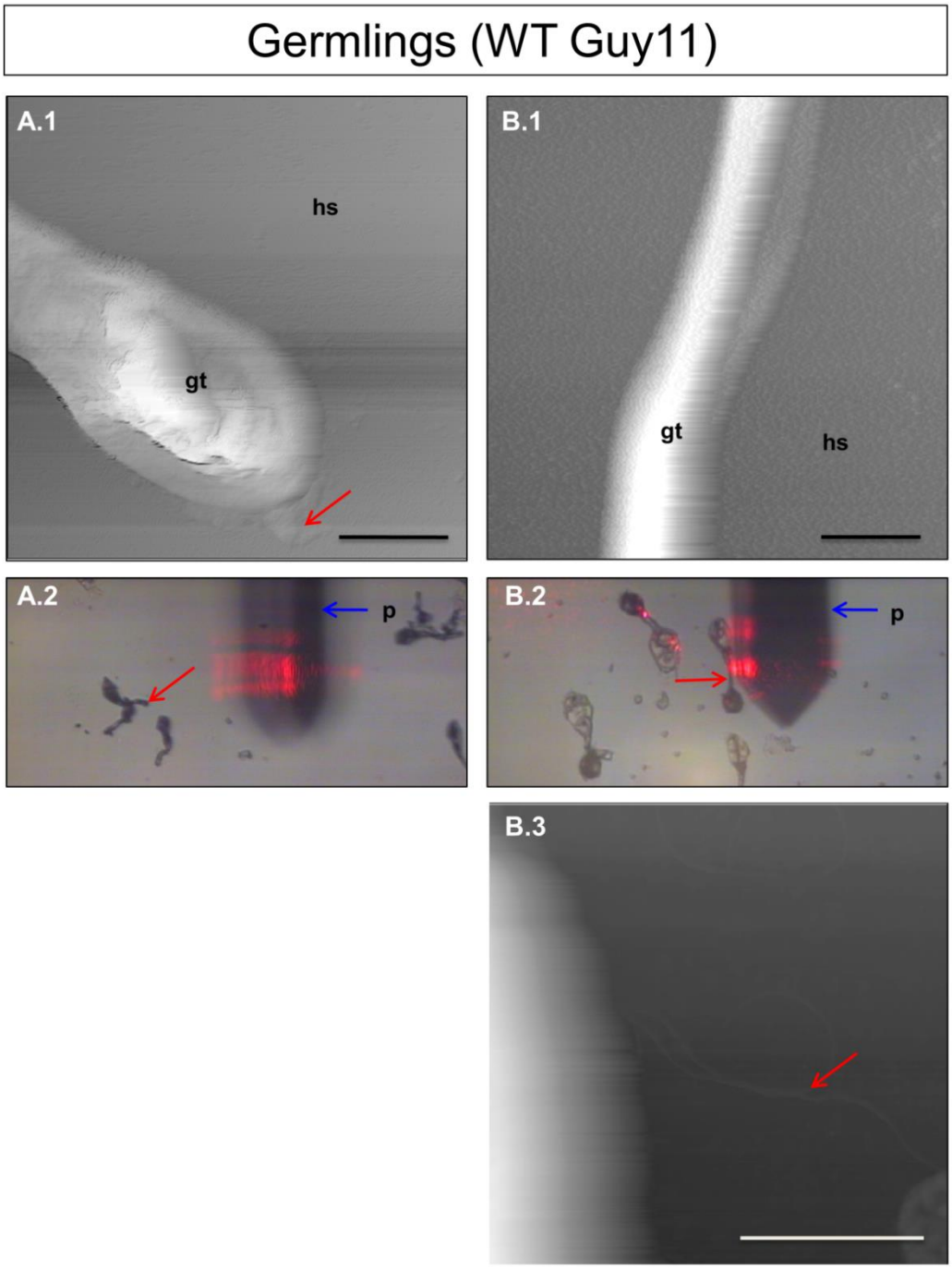

Figure 6.7. *Magnaporthe oryzae* WT Germlings Imaged by AFM. Spore suspension was inoculated for 2 hpi and 24 hpi on an artificial hydrophobic surface (Menzel slides) and kept under high humidity until ready for imaging. **Panel A** The germ tube of a 2 hpi germling (A1) with some ECM/mucilage (red arrow) and an optical image (A2) showing the location of the probe (blue arrow) and germling (red arrow). **Panel B** The germ tube of a melanised appressorium at 24 hpi (B1) and the corresponding optical image (B2) showing the location of the probe (blue arrow) and germling (red arrow). Additionally, an image showing an area beside a 24 hpi germ tube taken under high magnification (B3), with the presence of single-stranded fibres from the Mira Cloth (red arrow). Images for each stage of the germination were repeated twice for consistency. Bar scale at 2.0 µm. Images obtained by tapping mode using constant force with a scanning rate of 0.5 Hz.

An attempt was made to image melanised appressoria (24 hpi germling), thereby giving insights into the topography of a domed appressorium at the nanoscale level and evidence for any ECM surrounding the domed structure. Unfortunately, imaging of an appressorium by AFM was problematic due to the relatively large height of the appressorium dome, with an average of 6.0 µm in height (Skamnioti and Gurr 2009). The piezo scanner stage used has a maximum height extension of 7.0 µm. However, the practical working range is below 5.0 µm (Myhra S Pers.com 2014). Therefore, attempts to use the entire piezo scanner range gave poor images. Additionally, the steep increase in height between the hard surface and the dome made it impossible to image a section immediately beside the appressorium dome. This was due to the incomplete horizontal tracking by the probe top as it hits the vertical side of the dome, causing issues with the feedback loop. Several images of collapsed appressoria were successful due to the drop in height, as shown in Figure 6.5 (Panel C). In these images, the collapsed dome can be seen when a line profile was drawn across, giving irregular peaks (red arrows) corresponding to an irregularly deflated dome (Figure 6.7 Panel C). In this representative image, again no ECM is present. It is however, important to exercise caution when interpreting these images as germlings were by then, desiccated.

Topographical Imaging of Hyphae Revealed an Amorphous Layer

High-resolution imaging of the surface topography of *M. oryzae* WT vegetative hypha did not reveal any fibrillar or lattice-type arrangements of polymers (Figure 6.4). Instead, a 'carpet' layer covered the surface of the mycelium, which is presumed to be the cell wall's amorphous layer comprising the alkaline soluble fraction of the cell wall. In *A. fumigatus* real-time AFM imaging of cell wall remodelling, the rodlet pattern is seen on the conidia dramatically disappeared as the conidia germinated (Dague *et al.* 2008). Within 3 hours post inoculation, the hydrophobic rodlet layer was completely replaced by an amorphous layer. The occurrence of this layer or undulating surface is also seen in a mature hypha of *A. nidulans* (Ma *et al.* 2005) and is visually similar to those imaged in this study.

The ECM is an Extension of the Amorphous Layer

Perhaps the most exciting discovery of this AFM work is the appearance of a thin layer of unknown substance extruded during the vegetative stage of *M. oryzae.* It is likely that this structure, referred to in this work as extracellular matrix (ECM), was previously difficult to view via microscopic techniques probably due to it being water soluble or having an alkaline-soluble property. Consequently, the extensive washings in various solutions needed meant that this structure was un-intentionally removed during routine sample preparation for SEM and TEM type imaging. Furthermore, while confocal and light microscopy may be able to image living hyphal structures, these tools do not have the resolution to capture the thin, molecular nanoscale layer of the ECM. The only technique that can image ECM in fungi thus far is achieved by immuno-labelling work such as in the appressorium of *M. oryzae* (Inoue *et al.* 2007). However, the information is limited

to the specific type of antibody labelling used, and the literature has described only ECM associated with infective structures. This is the first time ECM is seen at high resolution, surrounding the vegetative stage hypha of *M. oryzae*.

Within the fungal literature, the extra cellular material (ECM) is a loose term and warrants clear definition to avoid confusion. In the human fungal pathogen *C. albicans*, it is synonymous to the biofilm produced by the pathogen (Hawser *et al.* 1998). In *M. oryzae,* it is often referred to as the spore tip mucilage (STM) related to plant surface adhesion (Inoue *et al.* 2007, Ikeda *et al.* 2012). In other literature, the ECM could also refer to the outer amorphous layer seen in Electron Micrographs as hair-like structures (Latgé 2010). For the purpose of this work, ECM refers to substances secreted outside the cell wall alkaline-insoluble layer, away from the cell membrane, into the surrounding area and is not limited to adhesion to host for infection.

The presence of ECM during vegetative growth is an exciting discovery worth further pursuit experimentally. Interestingly, the measured thickness of 2 to 5 nm suggests that this is a monolayer of molecules. Additionally, the thickness remains the same at both mature section of the hypha and at the growing tip region, suggesting that the matrix is extruded at the tip and the hypha likely grows over. It is postulated that the unidentified ECM secreted during vegetative growth is related to digestion of extracellular substances and provides anchorage of mycelium to the surface. In reference to ECM seen in Figures 6.7 and 6.8, it is likely that polysaccharides, sensory proteins as well as digestive enzymes were spread ahead of the growing tip. As the fungi grow over these regions, changes to the extruded components may already have taken place, allowing swift

response to phosphorylated sensory proteins (response to external stressors and chemotaxis) or absorption of organic material previously digested.

Several studies in fungal pathogen agree with the above theory of the possible components of ECM seen in vegetative *M. oryzae*. The ECM surrounding *B. cineria* mycelium were harvested and subjected to phenol, Lowry and gas chromatography, revealing about 20% carbohydrates (primarily glucose and to a smaller fraction, mannose), 28% proteins and 6% lipids from the total dry weight (Doss 1999). In the human fungal pathogen *C. albicans,* cell wall remodelling genes *Bgl2, Phr1* and *Xog1* were shown to play a role in trafficking and delivery of β-glucan from the site of synthesis (glucan synthase complex) to the extracellular biofilm matrix (Taff *et al.* 2012). Similarly, carbohydrates associated with the alkaline-soluble fraction were also identified in the extracellular hydrophobic matrix of aerial hypha of *A. fumigatus*, including galactomannan, α-1,3-glucans and proteins (Beauvais *et al.* 2007). From these studies, a probable conclusion is that the ECM found on vegetative *M. oryzae* shares similar components to the alkaline soluble fraction of the cell wall analysis performed in Section 6.4.2.1.2 and is a possible extension of the amorphous layer. In future, expanded experimental work is needed to determine the components and function of this vegetative ECM. This could be made possible by using the AFM biomolecular recognition tool by applying a receptor-ligand interaction which will provide both high-resolution images as well is surface component identification to a single-molecule level (Hinterdorfer and Dufrêne 2006).

Additionally, surface imaging of WT during germination at 2 hpi and 24 hpi obtained from the same sample preparation, showed an absence of ECM

surrounding the germ tube and only a small amount seen around the appressorium. The cellular organisation of a developing germling is for host recognition and subsequent penetration, with spore tip mucilage playing an important role in anchoring the spore in place (Wilson and Talbot 2009). As stated in Newtons' third laws of motion, the process of penetration by exerting high turgor pressure up to 8 Mpa (Wilson and Talbot 2009) must logically result in a strong resistance experienced by the appressorium to being dislodged from the host surface. Consequently, without a strong anchorage, (a 'glue'), the appressorium would have been pushed away from the leaf surface due to this counterforce (Ikeda *et al.* 2012). Attempts to image live fungal germling at 24 hpi proved problematic due to the tall structure of the melanised appressorium. Successful images were only obtained from deflated domes and in these images, a layer is seen just below the dome, although not as wide as the ECM seen in vegetative hyphae (Figure 6.7 Panel A.1). If there is a small amount of germling ECM, it is possibly concentrated underneath the appressorium for the purpose of anchorage as opposed to a dispersed feature of ECM meant for food searching and carbohydrate digestion seen in vegetative hyphae.

6.4.1.2 Surface Elasticity by Contact Mode

A total of 200 indentations were made to determine differences in elasticity between the cell wall surfaces of vegetative WT mycelium, double knockout strain ΔΔ*MGG_Crh2_Utr2* line *25* and the incompressible surface of a cover slip used to mount these fungal strains.

A pilot assay was first conducted to ensure that the AFM tool can successfully detect variations in elasticity in regions of the hypha known to have differences in elasticity: the growing tip and the mature section of the hyphae. Figure 6.8 (Assay 1) and Table 6.2 showed three averaged FD curves with the control having the steepest curve (14.80 µm/µN), and both WT mature section (WT_M) and growing tip (WT_Tip) having a non-linear, less steep curves (14.35 and 10.15 µm/µN respectively). The slope of the WT_Tip was calculated to be highly significantly less ($p<0.001$) than that of the slope of WT_M. Results from this pilot work suggest that AFM can indeed detect variations of elasticity on a living fungal hyphae under ambient temperatures. However, it was noted that due to the conical structure of the tip, it was relatively difficult to perform indentations as the probe easily fell off the small end of the tip, or erratic/ratty curves were obtained from raw data possibly due to the highly angled surface. Due to this, an attempt to measure differences in the elasticity of the hyphal tips of WT and mutant strains was discarded.

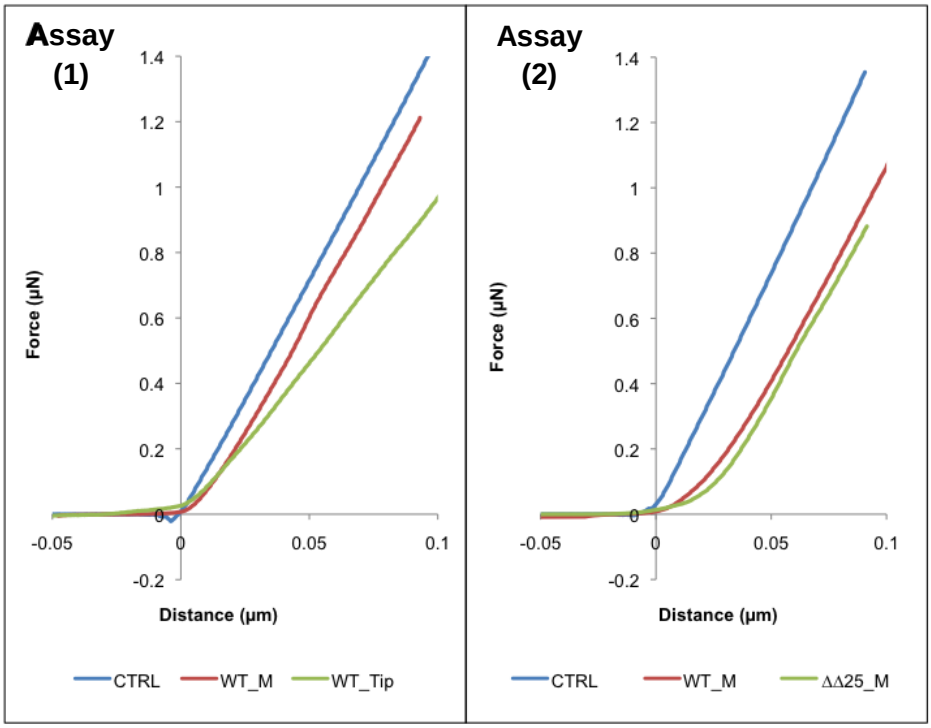

Figure 6.8. Pilot Force Versus Distance Curves of WT and Mutant Strain. The graphs above show two pilot assays using samples including the growing tip and mature section of the hypha of WT (WT_M, WT_Tip respectively), the deletion strain ΔΔ*MGG_Crh2_Utr2 line 25* (ΔΔ25_M) and the hard surface control (CTRL). **Assay (1)** A pilot assay to test for possible differences in surface rigidity between WT_M and WT_Tip. **Assay (2)** A pilot assay to test for possible changes to surface rigidity between WT_M and (ΔΔ25_M). Each curve was translated by a constant offset value to align all three curves at the origin of the FD plot. The slope of each curve above was measured from two points both located above 0.2 µN by the equation: slope=$(y_2-y_1)/(x_2-x_1)$.

In a second pilot assay, indentations were conducted on the mature section of the hyphae of two *M. oryzae* strains, with the incompressible cover slip supporting the sample mycelium, as the control. Continuous indentations leading to multiple force versus distance data were averaged per sample type as shown in Figure 6.8 (Assay 2) and statistically analysed by Student's t-test in Table 6.2. Here, as expected, the control, being the stiffest object, had the steepest gradient, followed by WT and mutant strain ΔΔ*MGG_Crh2_Utr2* line *25*. When repeated (Assay 3) on a different day, with larger numbers of indentations from multiple hyphae per strain, results were consistent with assay 2. In Figure 6.9, the FD curve for the control sample was the steepest, followed by WT and mutant

strain ΔΔ*MGG_Crh2_Utr2* line *25*. Statistical analysis by Student's t-test showed that the WT strain Guy11 is highly significantly ($p<0.001$) more rigid than the mutant line (Table 6.2), but still significantly ($p<0.01$) less rigid than the control.

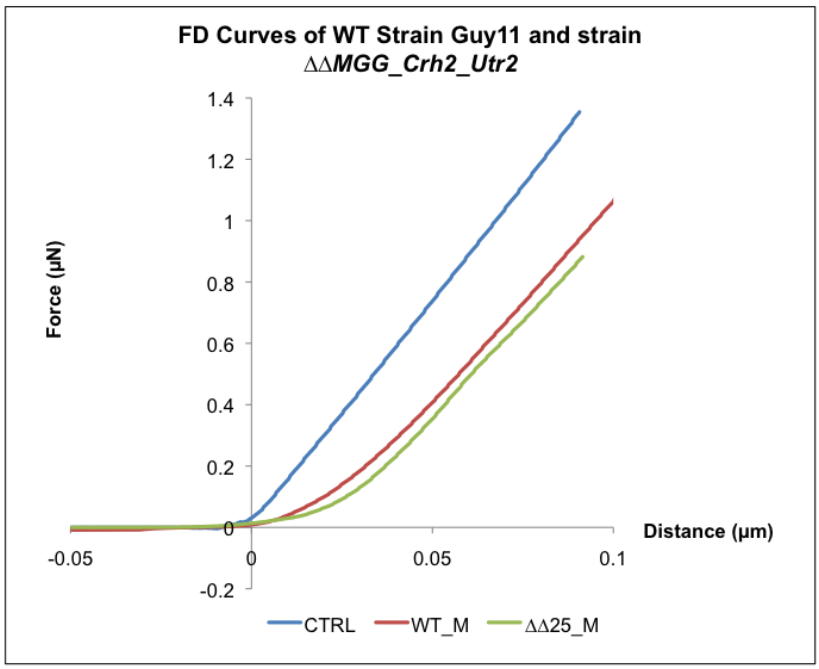

Figure 6.9. Force Versus Distance Curves of WT and Mutant Strain. Graph shows three averaged FD curves representing the mature section of the hyphae of WT (WT_M), the knockout strain ΔΔ*MGG_Crh2_Utr2 line 25* (ΔΔ25_M) and the hard surface control (CTRL). Each curve was translated by constant offset values to align all three curves at the origin of the FD plot. The slope of each curve were measured from two points both located above 0.2 µN by the equation: slope=$(y_2-y_1)/(X_2-X_1)$.

Table 6.2. Averaged Slopes of Force Versus Distance Curves in Three Assays. Assays compared hyphal indentation of various sample types: mature section of the hyphae of WT (WT_M), growing tip section of WT (WT_Tip), and mature section of the hypha of the double deletion strain ΔΔ*MGG_Crh2_Utr2 line 25* (ΔΔ25_M). The cover slip used to mount the sample was used as the incompressible control (CTRL). Student's t-tests were used to measure differences in slopes between samples and control.

Assay	Sample	Averaged slope[1] (μm/μN)	Number of Indentations (n)	St. Dev (μm/μN)
Assay (1)	CTRL	14.80	10	0.10
	WT_M	14.19[a*b**]	20	0.43
	WT_Tip	10.23[a**b**]	10	0.62
Assay (2)	CTRL	14.80	10	0.10
	ΔΔ25	12.57[a**b**]	20	1.02
	WT_M	14.19[a*b**]	20	0.43
Assay (3)	CTRL	15.06	10	0.12
	WT_M	13.14[a**b**]	50	0.21
	ΔΔ25	12.37[a**b**]	50	0.50

Key:

[1]Fungal sample is significantly different compared to hard surface control (CTRL)[a] or to WT strain[b]

* for p<0.01 and ** for p<0.001

Variations in Cell Wall Elasticity on a Fungal Structure

The aim of assay 1 was to show that sample preparation and measuring techniques used can provide reliable data about changes to surface elasticity. Variations in elasticity within a fungal structure have been shown in other studies. One of the earliest AFM studies of cell wall elasticity was performed by Touhami *et al.* (2003). Here, the authors showed that the living bud scar of a yeast cell is ten times more rigid than the surrounding region, measured in liquid buffer (Touhami *et al.* 2003). In another study more relevant to work in this section, *A. nidulans* by Ma *et al.* (2005) showed that in a sample-fixed (non-living) hypha, the apical tip is more elastic than the mature section of the wall (measured 20-40 μm from tip).

Differences in the elasticity of different parts of a fungal structure makes biological relevance. To achieve growth by elongation, the apical tip must be significantly more elastic than the remaining body of the hypha to allow internal hydrostatic pressure to push the elastic tip forward. It is, therefore, plausible to expect the growing tip of a vegetative hypha in *M. oryzae* to be relatively more elastic, (i.e., less stiff), than other regions of the hypha. Results from assay 1 showed these expected results whereby the incompressible surface (control) FD curve gave the steepest gradient, while the FD curve representing the growing tip, WT_Tip, had the least steep non-linear curve relative to WT_M and control. This means that for the same applied force, the extent of indentation by the probe tip on a hyphal tip was greater than on a mature section of the hypha.

Results from assay 1, and in combination with results from the literature, showed that live imaging of *M. oryzae* fungal samples, were sufficient to produce reliable and interpretable data. It can be concluded from this section that there is sufficient confidence in using the same techniques to measure differences in elasticity between WT and the mutant strain.

MGG_Utr2 and MGG_Crh2 is Important for Cell Wall Strength

Results from the assay 2 (Figure 6.8) and again when repeated in the main assay 3 (Figure 6.9) showed highly significant ($p<0.001$) differences in the slope of the FD curves between the WT and the knockout strain ΔΔ*MGG_Crh2_Utr2* line *25*. These AFM results indicate that the cell wall of the mutant strain is relatively less stiff than in WT. This is consistent with the increased sensitivity shown by the same mutant strain against Congo Red (100 µg/ml) when grown vegetatively (Chapter 5). It is theorised that a change in cell wall strength due to

the absence of MGG_Crh2p and/or MGG_Utr2p resulted in the inability to prevent hyphal tip swelling caused by Congo Red. This theory is further supported by the observation of partial phenotype recovery in an osmo-remedial assay (Chapter 5 section 5.4.1.3.1). Future work should explore the surface elasticity of the single knockout strains ∆*MGG_Crh2* and ∆*MGG_Utr2* to determine which Crh-like protein is more important for cell wall rigidity.

The important role of *Crh-like* protein family in maintaining cell wall mechanical properties was reflected in a yeast study (Dague *et al.* 2010). Here, the authors performed cell surface stiffness measurements by AFM on *S. cerevisiae* cell wall remodelling protein Crh1p and Crh2p (syn Utr2p). The knockout mutant *crh1*∆*crh2*∆ showed a difference in wall stiffness relative to WT. However, the elasticity data presented by Dague *et al.* (2010) was the opposite of those described here for *M. oryzae,* with mutant yeast *crh1*∆*crh2*∆ found to be more rigid than the WT strain. Some caution is required because data presented in Dague *et al.* (2010) can be questioned for two reasons: quantification of elasticity using the Young's modulus and Hertz models and no mention of the use of an incompressible calibrator. A carefully chosen control sample is important, as it is needed not only as a calibrator to calculate force versus indentation curves but also in providing a relative indication of stiffness by comparing FD slopes between samples. Also, as described in the introduction section, absolute quantification (Young's Modulus) of surface elasticity in biological samples is problematic and best avoided (Emad *et al.* 1998, Vinckier and Semenza 1998, Heinz and Hoh 1999, McElfresh *et al.* 2002, Kasas *et al.* 2013). This means that it is only sufficient to acknowledge that there were changes to surface stiffness in yeast *Crh1Crh2* mutants, but there is some doubt

as to the absolute value and relative stiffness of the WT strain in the work of Dague *et al.* (2010).

Furthermore, a steeper force versus indentation curve (obtained from force versus distance curve) is associated with a more rigid structure (Blach *et al.* 2001, Touhami *et al.* 2003). Thus, the use of two positive controls in the AFM work for this Chapter gave consistent results whereby the control sample had the steepest gradient, and the structure of least stiffness (hyphal tips) gave the least steep gradient. Therefore it can be confidently concluded that results in this Chapter warrant confidence and is a true reflection of changes in the physical properties of the cell wall of *M. oryzae Crh-like* knockout mutants.

6.4.2 Cell Wall Analysis

In this section, the vegetative mycelium of five *M. oryzae* strains were cultured under optimal conditions (CM) and prepared samples subjected to cell wall analysis by GC/EI-MS. This included the control strain WT, two independent lines of the single knockout strain *ΔMGG_Crh1* and two independent lines of the double knockout strain *ΔΔMGG_Crh2_Utr2.*

During sample preparation, unfortunately, there was a contamination in biological replicate 3 of *MGG_Crh1* line 36. As such for this genotype, only two instead of three biological replicates were used. Results showed that both independent lines 36 and 43 for *MGG_Crh1* were similar, confirming consistency of analysis. However, only one independent line, *MGG_Crh1* line 43 is presented and discussed in this section as it comprises three biological replicates, thereby providing reliable statistical analysis. It was also noted that sample preparation for genotype ΔΔ*MGG_Crh2_Utr2* line 27 was problematic. Post freeze drying, sample ΔΔ*MGG_Crh2_Utr2* line 27 biological replicate 2 gave an odd brown colour as opposed to a white powder like all other samples, resulting in suspicion of sample contamination for ΔΔ*MGG_Crh2_Utr2* line 27 biological replicate 2. Additionally, there were also doubts about the status of ΔΔ*MGG_Crh2_Utr2* line 27 biological replicate 3 with possible sample contamination. As such, data from this independent line was discarded, and only results from ΔΔ*MGG_Crh2_Utr2* line 25 with three biological replicates are described in this section.

Results for the cell wall composition analyses comprises four segments: fraction of ASF to AIF, total cell wall carbohydrates, total carbohydrate and

linkages in ASF as well as in AIF. The fraction of ASF to AIF per fungal strain was determined by weighing the pellets of each fraction after a series of solubilisation treatments, over the weight of the originally extracted cell wall. Total carbohydrate analyses were achieved by hydrolysing the sugar polymers (i.e. from the whole cell wall, AIF or ASF) into monomers by acid hydrolysis followed by GC/EI-MS for monomer identification and quantification. Linkage analyses were conducted to identify the types and quantities of glycosidic linkages found within AIF and ASF respectively. This was achieved by methylation of the polymers, followed by hydrolysis of monomers and subsequent derivation to permethylated alditol acetates (Appendix D.2). These permethylated alditol acetates were then separated and quantified using GC/EI-MS, enabling the determination of the type and quantity of linkages formed during the polymer stage.

6.4.2.1 Total Cell Wall Composition

The cell wall of WT Guy11 vegetative mycelium showed that 60% of the total cell wall comprised the Alkali Insoluble Fraction (AIF), with the remaining 40% as Alkali Soluble Fraction (ASF) (Figure 6.10). Surprisingly, there was no statistical difference (at 95% confidence interval) in the percentage of the ASF in the mutant lines, compared with the ASF in WT. Although the percentage mean ASF in the double mutant strain is indeed larger than in WT, the large standard deviation value made any changes non-significant. Indeed when AIF and ASF were analysed individually with statistical calculations, there were changes in the components between mutants and WT, as discussed in the upcoming sections.

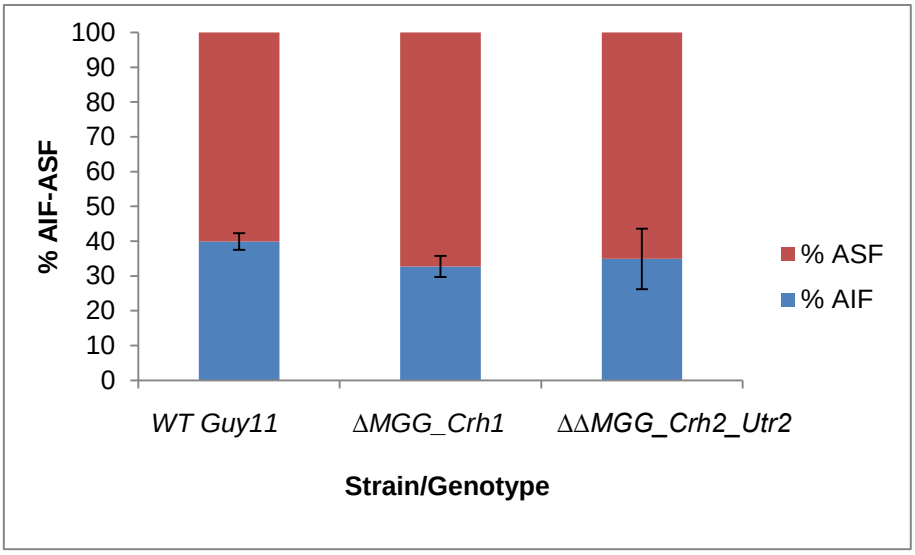

Figure 6.10. Contribution (% mol) of the Alkali Soluble/Insoluble Fractions to the Total Cell Wall in *Magnaporthe oryzae* Strains. Three strains were analysed, namely the control WT, single knockout strain *MGG_Crh1,* and the double knockout strain Δ*MGG_Crh2_Utr2*. Measurements were taken by comparing the weight of the total CW and the downstream weight of the AIF pellet after solubilisation treatments. Each data repeated in four replicates. Error bars represents Standard Deviations.

Total sugar analysis of the cell wall (Table 6.3) showed that the WT is made from 69.26% glucose (Glc), 22.25% mannose (Man), 4.12% chitin (GlcNAc), 3.93% galactose (Gal) and less than 0.5% of arabinose (Ara) and xylanose (Xyl). Statistical analysis showed that both mutant strains had significantly ($p<0.05$) higher percentage of chitin (18-20%) compared with the WT. In addition to this, the double mutant strain Δ*MGG_Crh2_Utr2* also showed a significant but slightly higher percentage of total glucose (3%) than the WT.

Table 6.3. *Magnaporthe oryzae* Total Cell Wall Carbohydrate Composition. The asterisks correspond to a significantly different percentage (% mol) at 95% confidence interval, calculated from the standard deviation (in brackets), relative to WT.

Percentage %	Ara	Xyl	Man	Gal	Glc	GlcNac
WT	0.37 (0.11)	0.07 (0.17)	22.25 (0.08)	3.93 (0.08)	69.26 (0.03)	4.12 (0.11)
Δ*MGG_Crh1*	0.25 (0.38)	0.11 (1.46)	21.75 (0.09)	3.69 (0.09)	69.32 (0.03)	4.87* (0.16)
Δ*MGG_Crh2_Utr2*	0.31 (0.20)	0.05 (0.39)	19.64* (0.05)	3.57 (0.06)	71.47* (0.02)	4.97* (0.17)

In the WT, the chitin content is notably higher than in the yeast *S. cerevisiae* (1-2%), the dimorphic pathogen *C. albicans* (2% to 6%) but similar to the closely related species of filamentous fungi, *N.* crassa at 4% (Maddi and Free 2010). The chitin content of *M. oryzae* is considered lower than that reported for several other species of filamentous fungi such as *A. fumigatus* (7% to 15%) (Gastebois *et al.* 2009) and *Fusarium oxysporum* (between 8% to 11%) (Schoffelmeer *et al.* 1999). More research will be needed to investigate the reason for these variations in chitin content across fungal species.

Statistical comparison of the carbohydrate components of the cell wall between mutant lines and WT showed changes characteristic of a compensatory response via the Cell Wall Integrity (CWI) pathway. The increase in chitin, glucan, and reduction in mannan, reflecting genes responding to the activation of the CWI pathway, is discussed in greater detail in the upcoming sections.

6.4.2.1.1 WT Alkaline Insoluble Fraction

Total sugar analysis of the AIF revealed that glucose is the main component, at 86.52%, followed by 7.45% chitin, 4.71 mannose and 1.32% galactose (Figure 6.11). These components can then be further analysed through linkage analysis to investigate the types of glycosidic bonds linking these monomers. Linkage analysis through the polymer methylation-alditol acetate technique revealed a total of eighteen different types of linkages identified and quantified (Figure 6.12). The most frequent type of glycosidic linkage in the AIF was (1-3)-glucan with 73.28% mol of 1,3-Glc*p,* followed by 8.14% mol t-Glc*p*, 7.45% mol 1,4-GlcNAc and to a lower fraction,1,3,6-Glc*p* (3.32% mol) and 1,4-Glc*p* (1.35% mol).

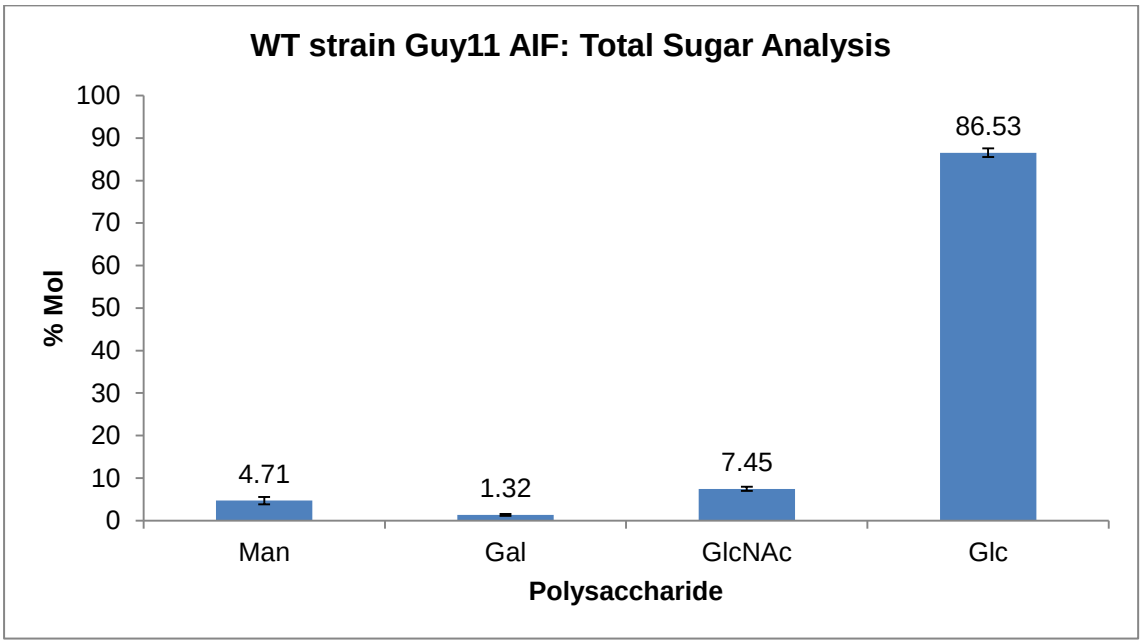

Figure 6.11. Total Sugar Composition of the Alkaline Insoluble Fraction of WT Cell Wall. Fungal vegetative mycelia were cultured for three days in liquid CM under optimal condition before sample preparation for cell wall analysis via a series of solubilisation treatments. Prepared cell walls were then hydrolysed and monomers identified and quantified by GC/EI-MS.The graph shows the percentage mol (% mol) of eighteen linkage types identified in this fraction.

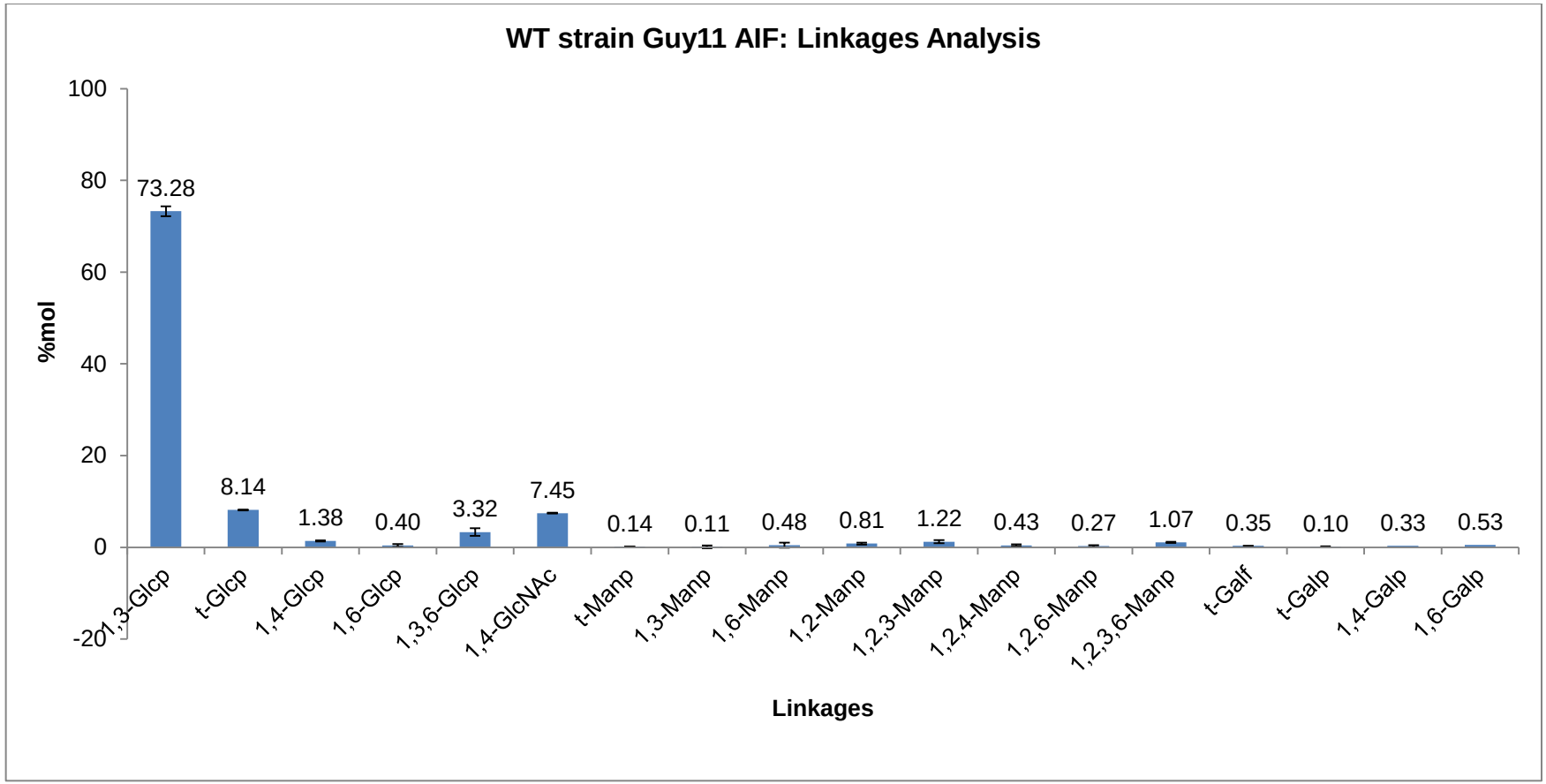

Figure 6.12. Linkage Composition of the Alkaline Insoluble Fraction of WT Cell Wall. Fungal vegetative mycelia were cultured for three days in liquid CM under optimal conditions. Mycelia were harvested and freeze dried prior to analysis. For linkage determination, the polymer methylation-alditol acetate technique was used and samples were analysed by GC/EI-MS. The graph shows the percentage mol (% mol) of eighteen linkage types identified in this fraction.

M. oryzae AIF Comprises Long Glucan and Chitin Polymers

Results from the AIF of the cell wall of WT showed that the largest carbohydrate component, glucose, is made of long polymers of 1,3-glucan chains with cross-links to other polymers. This is because of the low percentage of terminal glucose (t-Glc*p*), and a high percentage of internal glycosidic linkages (1,3-Glc*p*) and a low amount of 1,3,6-Glc*p* (3.32%) linkages, suggesting that there are many long 1,3-glucan polymers with only branching at position 6 of the glucose molecule to another polymer.

Literature shows that in the AIF of the yeast cell wall, the reducing end of chitin is linked to the non-reducing end of a glucan polymer by β(1,4) linkage (Kollár *et al.* 1995, Kollár *et al.* 1997). Therefore, this cell wall analysis should have generated 1,3,4-Glcp, indicating the branching of chitin to 1,3 glucan at carbon 4 of the glucose molecule. However, this linkage type was not detected in the analysis. The only branching type present on the long polymer of 1,3-glucan was branching at carbon 6 of the glucan molecule. A possible reason for this is that chitin is attached to a side glucan chain that branched from the main 1,3-glucan via linkage at carbon 6 of the glucose molecule. In addition to linking of chitin directly to 1,3-glucan polymers (Cabib 2009), the linking of chitin to a side chain of glucan polymers is also seen in the lateral walls of *S. cerevisiae.* In the lateral walls of yeat cells, chitin was found linked to a non-reducing end of 1,3-glucan side chains of a 1,6-glucan polymer (Kollár *et al.* 1997). However, irrespective of the location of chitin on the main polymer or glucan side branches, the absence of the glycosidic linkage between chitin and a glucose molecule is puzzling. It is possible that the percentage of this linkage is very low, as noted by Kollar *et al.* (1997), in yeast, where there is one chitin-glucan linkage for every

8000 glucose monomers. While there may be inter-species variation, it is a possibility that cross-linking in *M.* oryzae is also rare (but with significant impact), resulting in low signals and not possible for quantification via GC/EI-MS. This inability to detect linkages found in low amounts is seen in the chitin polymer.

In the AIF, chitin comprises 7.45% of the total carbohydrate, linked with 1,4-glycosidic bonds between N-acetyl glucosamine (1,4-GlcNac). The absence of a terminal chitin in the linkage analysis, and the presence of only 1,4-GlcNac at 7.45% mol, does not mean that the terminal chitin is not present (nearly impossible). Instead, Melida H. (Personal communication, January 2015) suggests that chitin in *M. oryzae* exists as very long polymers, resulting in low signal peaks in the GC/EI-MS for terminal N-acetylglucosamines, making quantification measurements difficult.

To summarise, the bulk of AIF in WT comprises long linear chains of 1,3-glucan, with occasional branching to other glucan polymers. It is hypothesised that chitin is attached to these side chains of glucan. There were very few or negligible linkages from mannose and galactose in the AIF of *M. oryzae*.

6.4.2.1.2 WT Alkaline Soluble Fraction

Total sugar analysis of the *Magnaporthe oryzae* cell wall ASF showed that glucose is the most abundant monosaccharide at 51.99% followed by mannose at 39.80% and galactose at about 6.53%. Almost no chitin, arabinose, and xylose was detected. Further linkage analysis suggests that most of the glucose chains are made of 1,3-linked glucosyl residues (20.68% mol) with a high amount of terminal glucose, at 26.20% mol and, 1,6-linked glucosyl residues in lower amount at 3.34% mol.

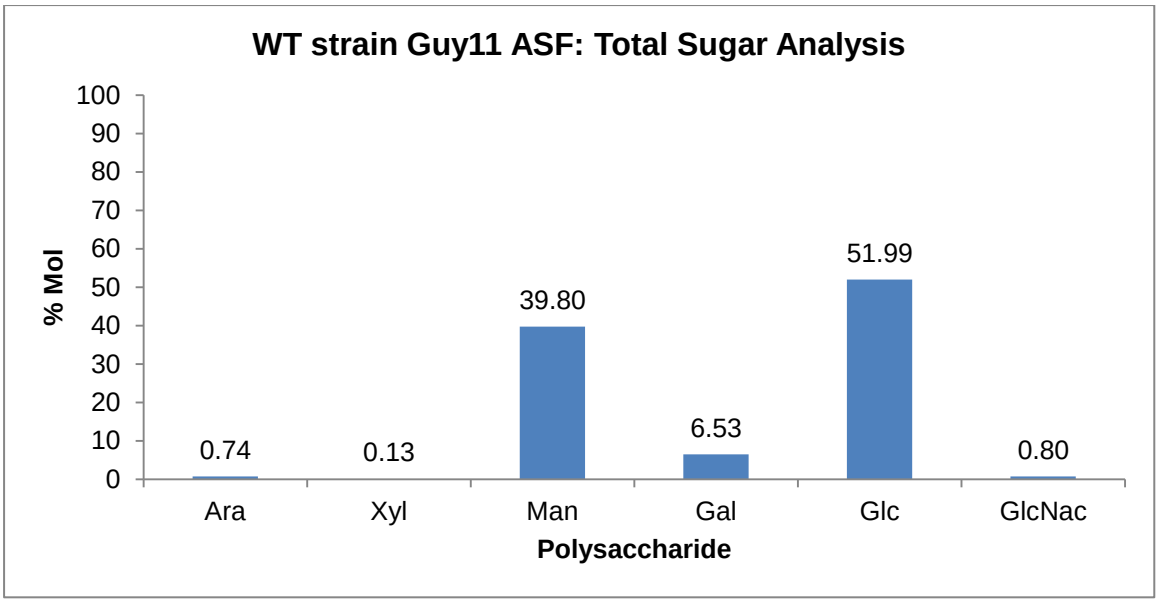

Figure 6.13. WT Guy11 Fungal Cell Wall Composition in the Alkaline Soluble Fraction. Fungal vegetative mycelia were cultured for three days in liquid CM under optimal conditions followed by harvesting and freeze drying of sample before analysis. The graph shows the percentage mol (% mol) of six carbohydrates identified in this fraction.

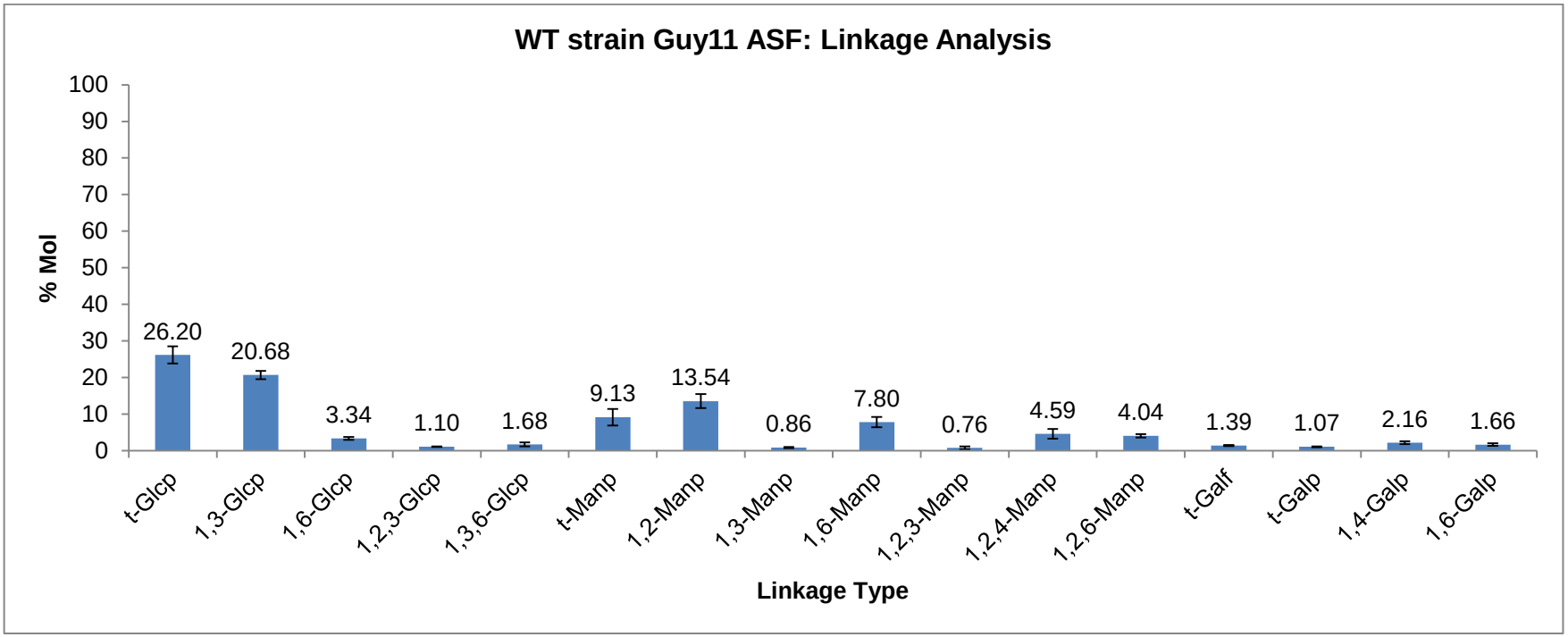

Figure 6.14. Linkage Composition of the Alkaline Soluble Fraction of WT Cell Wall. Fungal vegetative mycelia were cultured for three days in liquid CM under optimal conditions followed by mycelia harvesting and sample freeze dried prior to analysis. For linkage determination, polymer methylation-alditol acetate technique were used and analysed by GC/EI-MS. Graph show the percentage mol (% mol) of sixteen linkage types identified in this fraction.

M. oryzae ASF is Primarily Made of Short Glucan and Mannan Chains

Total sugar and linkage analysis of the ASF of the WT revealed a diversified composition. While glucose is still the largest component, the percentage is lower, at 51.99% and does not exist in long polymers. On the contrary, there was an almost similar % linkage type of terminal glucose to 1,3-linked glucosyl residues, indicating the presence of multiple short chains of 1,3-glucans with some branching at the carbon 6 position (1.68% mol of 1,3,6-Glc*p*). It can be theorised that these short 1,3-glucan chains are possibly newly synthesised chains, as glucan synthases are known to vectorially extrude between 60 to 80 glucose monomers (Shematek *et al.* 1980). These short chains remain in the ASF and cell wall remodelling enzymes such as the yeast Gas1p build long linear polymers, reaching up to 1500 glucose monomers (Bowman and Free 2006). It is when the addition of chitin branches by Crhp enzymes occurs (Cabib *et al.* 2007) that the chemical property of the linked polymer then changes to be alkaline insoluble (Hartland *et al.* 1994).

As opposed to the absence of 1,6-glucan in the AIF, there was about 3.34% mol of 1,6-Glc*p* in the ASF. The presence of 1,6-glucan linkages has not been reported in other filamentous fungi such as *N. crassa* (Borkovich *et al.* 2004) and *A. fumigatus* (Gastebois *et al.* 2009). Therefore it was a surprise to see this linkage present in *M. oryzae.* Also, there is an absence of 1,2-linked glucosyl residues. This is in agreement with the immuno-labelling work of Fujikawa *et al.* (2009) whereby α-1,2-glucans were found only during the infective stage at the outer region of the cell wall, ‘masking’ the pathogen from host detection.

For the mannan counterpart, the quantitatively most dominant type of linkage in the ASF after 1,3-Glcp, is 1,2-man*p* residue at 13% mol. This is an interesting observation because in model fungi such as yeast *S. cerevisiae* and filamentous fungi such as *A. fumigatus* the dominant linkage type is α-(1-6)-mannopyranosyl residue, with branching at position 2 giving a 1,2-man*p* residue (Gómez-Miranda *et al.* 2003, Bowman and Free 2006). In *M. oryzae,* there were more 1,2-man*p* residues than 1,6man*p* residues (13% and 7.8% respectively) with t-man*p* at 9.13% and further linkages at 1,2,4-man*p* and 1,2,6-man*p* residues (4.0% and 4.0% mol respectively). This suggests that the backbone consists of 1,2 mannan with frequent branching at carbon 3, 4 and 6 positions, via 1,2,3-man*p*, 1,2,4-man*p,* and 1,2,6-man*p* glycosidic linkages. Also, these mannose chains could also contain branching with galactose as about 1.7% mol of 1,6-gal*p* residues were found with an almost equal t-gal*p* residue at 1.4% mol, suggesting these galactose branches are short and few. These results are similar to those in the closely related species, *N. crassa*. In this fungus, the mannan backbone is made from alpha 1,2-mannans with branching from the backbone by 1,2 or 1,6 linkages (Nakajima *et al.* 1982).

Cell wall analyses of the WT described above have lead to a clear understanding of the cell wall composition of this fungus in vegetative mycelia. For the first time, a visual illustration of *M. oryzae* cell wall during the vegetative stage can be constructed (Figure 6.15). It is worth pursuing in the future, to explore variations in the cell wall composition during other stages of the life cycle, primarily in germlings and in sexual reproductive tissues. Apart from changes in α-glucan content as shown by Fujikawa *et al.* (2009), it would be exciting to see

if there are any other changes to the cell wall composition through the GC/EI-MS technology.

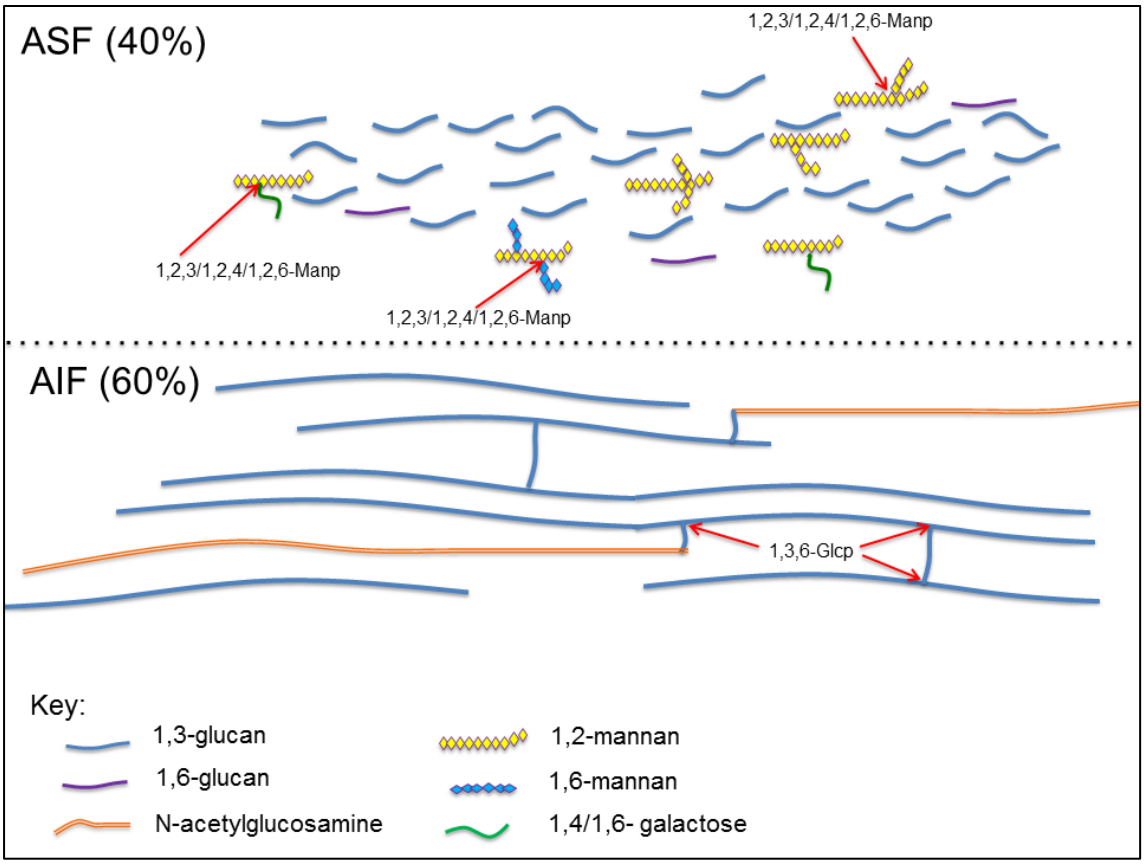

Figure 6.15. A Schematic Representation of *Magnaporthe oryzae* WT Cell Wall Composition in Vegetative Mycelium. The cell wall of the rice blast fungus can be categorised into two fractions: Alkaline Soluble Fraction (ASF) at 40% and Alkaline Insoluble Fraction (AIF) at 60%. In this fungus, the ASF comprises primarily, short chained 1,3-glucans (52%) and short mannan chains that are highly branched (40%). The AIF comprises long 1,3-glucan polymers (87%), followed by chitin (7%) and mannan (5%). These long glucan polymers are cross-linked at position 6 to other glucan polymers and chitin is possibly indirectly linked to these side-chain glucans.

6.4.2.2 Mutant Cell Wall Analysis

6.4.2.2.1 Single Gene Knockout Mutant *ΔMGG_Crh1*

Within the AIF, total sugar analysis showed a small yet significant ($p<0.05$) decrease in total glucan (1-3%), and a significant ($p<0.05$) increase in chitin content (17-20%) in ΔMGG_*Crh1* Line 43 relative to the WT (Figure 6.16). Alkaline Insoluble Fraction linkage analysis (Figure 6.17) showed no significant changes in the most abundant type of glucan linkage: 1,3-glc residue or any changes in 1,6-glc residue, relative to WT. However, a significant ($p<0.05$) decrease was seen in the percentage of terminal glucose residues (25-30% decrease) when compared with the WT. In agreement with the total sugar analysis, chitin linkages (1,4-GlcNac residue) showed a significant ($p<0.05$) increase of about 22% relative to the % mol of WT Guy11.

Total sugar analysis of the ASF showed no significant difference in the percentage of glucose, mannan and galactose relative the WT Guy11. As expected, almost no chitin monomers were detected in this fraction. Despite no changes in total monosaccharides, the contrary was seen for linkage type. Particularly there was a significant ($p<0.05$) reduction in terminal glucose residues (14-25%), suggesting that, in the Δ*MGG_Crh1* knockout mutant, there was an increase in glucan polymerisation or chain elongation. No significant ($p<0.05$) changes were observed in all other linkages.

6.4.2.2.2 Double Gene Deletion Mutant *ΔΔMGG_Crh2_Utr2*

Total sugar analysis of the AIF showed a significant ($p<0.05$) reduction by 40-50% in mannan and a significant ($p<0.05$) increase in chitin by 25-30% in the double knockout mutant in both independent lines with no changes to glucose or

galactose monomers. Linkage analysis of the AIF of the mutant *ΔΔMGG_Crh2_Utr2* cell wall showed changes to the percentage of certain types of linkages relative to WT. Here, a 4% reduction in 1,3-Glc linkage ($p<0.05$) compared with WT Guy11 is noted. Interestingly, there was also a 60% increase ($p<0.05$) in 1,3,6-Glc linkage, 27% increase ($p<0.05$) in 1,4-GlcNAc and 21% decrease ($p<0.05$) in 1,4-Glcp linkages.

Total sugar analysis of the ASF showed a slight yet significant increase in total glucan by 7-8% ($p<0.05$) and a significant reduction ($p<0.05$) in mannan by 8-9% relative to WT Guy11 for both independent lines of the double knockout mutant. No changes were observed in Galactose content. The linkage analysis of the ASF showed significant changes in glucan linkages relative to WT. Here, there was a significant ($p<0.05$) increase by 28% in 1,3-Glcp and 34% in 1,3,6-Glcp with a significant ($p<0.05$) decrease in 1,6-Glcp by 28%. Similar to AIF linkages, it is interesting that there seems to be more branching at molecule 6 of the glucan monomer, but no changes in the percentage of terminal glucose residue.

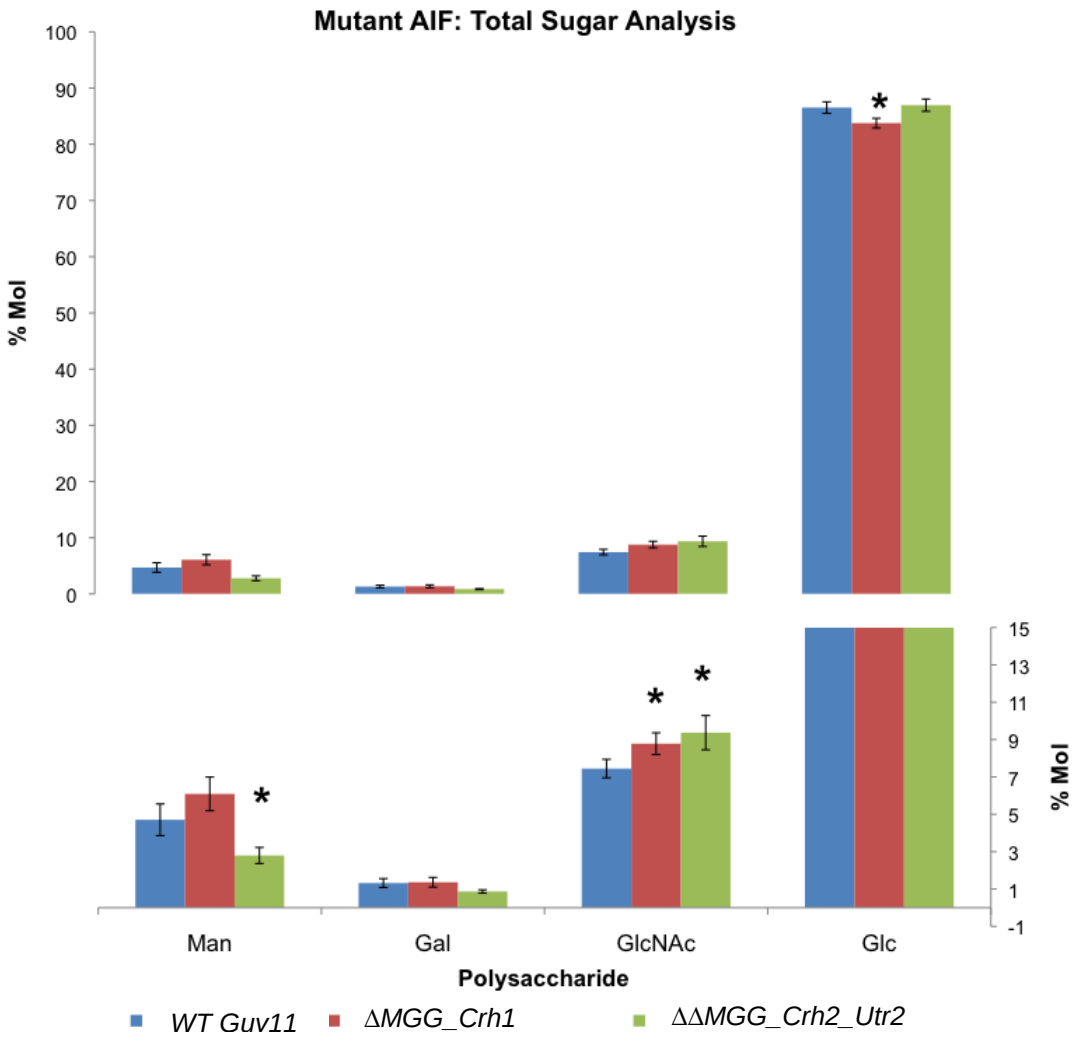

Figure 6.16. Sugar Composition of the Alkaline Insoluble Fraction of Mutant Cell Wall. Fungal vegetative mycelia were cultured for three days in liquid CM under optimal conditions followed by harvesting and sample freeze dried prior cell wall extraction and GC/EI-MS analysis. **Panel A**. Percentage molecule (% mol) of three carbohydrate monomers identified AIF: Mannose (Man), Galactose (Gal) and Chitin (GlcNAc). **Panel B**. Percentage molecule (% mol) of glucose monomers (Glc) in AIF. The asterisk indicates a highly significant difference ($p<0.05$) relative to WT.

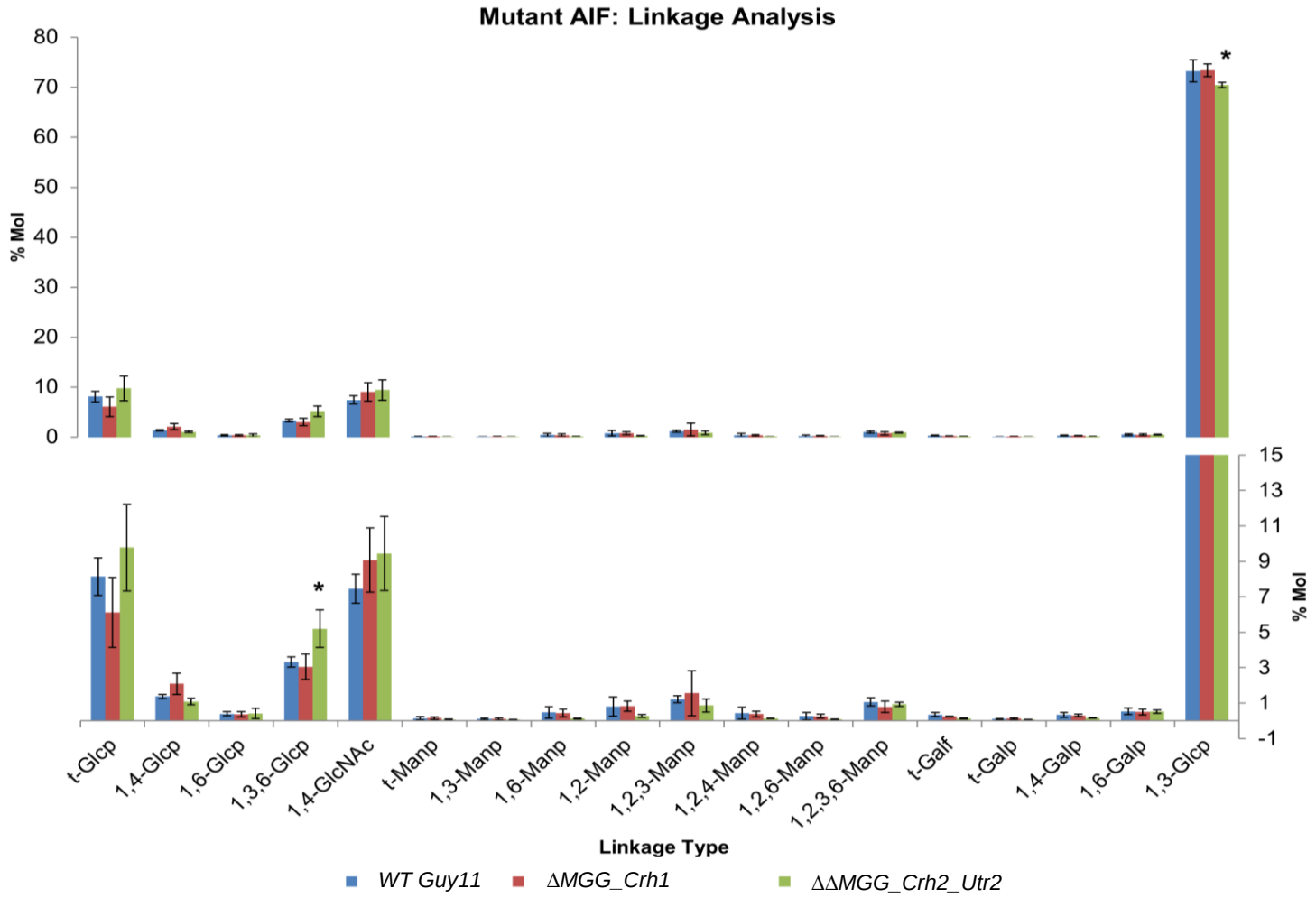

Figure 6.17. Linkage Composition of the Alkaline Insoluble Fraction of Mutant Cell Wall. Fungal vegetative mycelia were cultured for three days in liquid CM under optimal conditions followed by mycelia harvesting and freeze drying prior to cell wall extraction. For linkage determination, the polymer methylation-alditol acetate technique was used and samples were analysed by GC/EI-MS. The graph show the percentage molecule (% mol) of eighteen linkage types identified in this fraction. The asterisk indicates % mol to be significantly different at $p<0.05$ relative to WT.

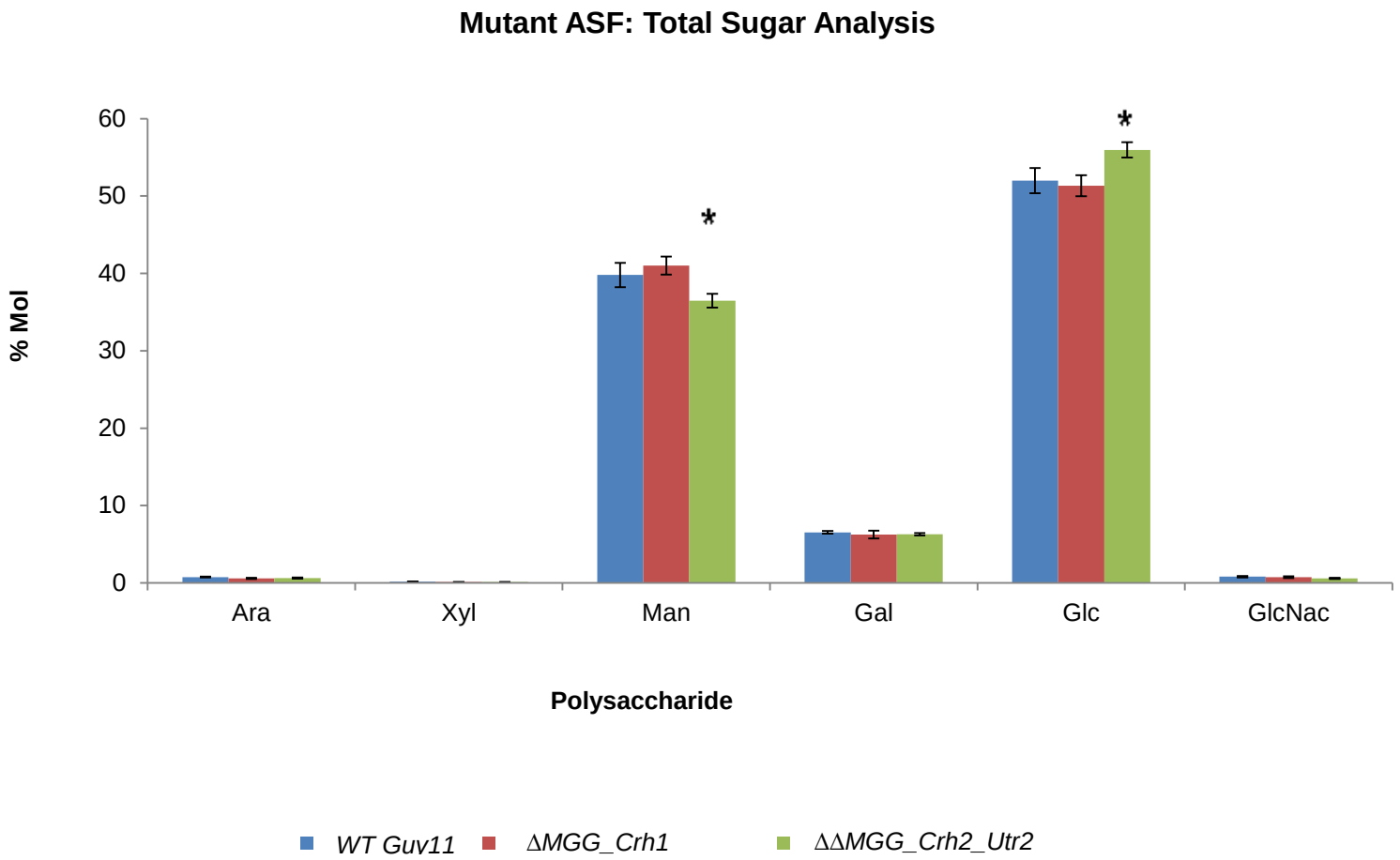

Figure 6.18. Alkaline Soluble Fraction of WT Guy11 Fungal Cell Wall Composition. Fungal vegetative mycelia were cultured for three days in liquid CM under optimal conditions followed by harvesting and freeze drying prior to cell wall extraction and GC/EI-MS analysis. The graph shows the percentage molecule (% mol) of six carbohydrates identified in this fraction. Asterisks indicate a significant difference at $p<0.05$ relative to WT.

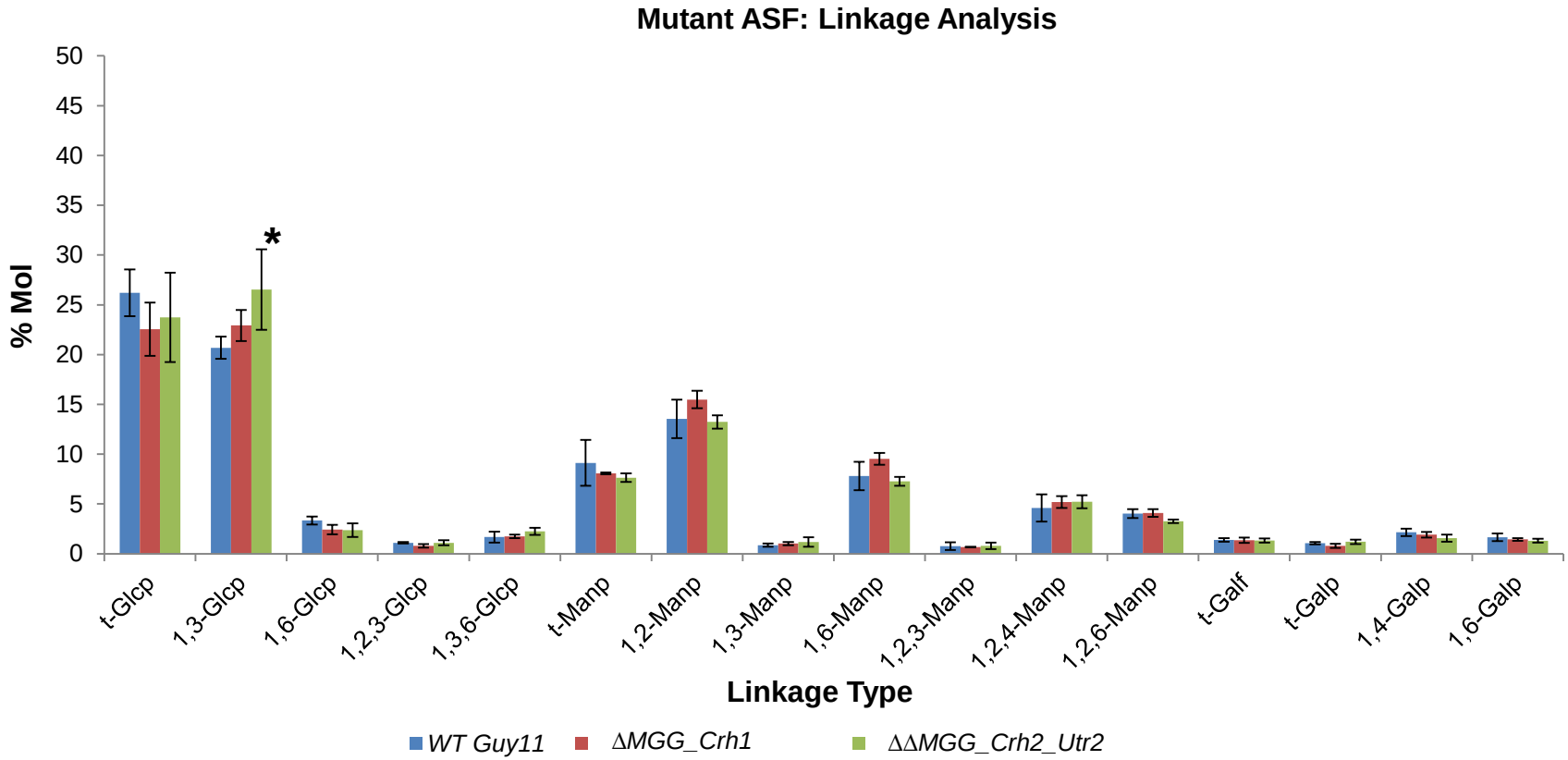

Figure 6.19. Linkage Composition of the Alkaline Soluble Fraction of Mutant Cell Wall. Fungal vegetative mycelia were cultured for three days in liquid CM under optimal conditions followed by harvesting and freeze drying prior to analysis. The graph shows above the percentage mol (% mol) of sixteen different linkage types identified through polymer methylation-alditol acetate technique and analysed by GC/EI-MS. The asterisk indicates % mol to be significantly different at $p<0.05$ relative to WT.

6.4.2.2.3 Discussion of Results for Mutant Cell Wall Analysis

Detailed cell wall composition and linkage analysis in both ASF and AIF of the cell wall of *M. oryzae Crh-like* mutants revealed significant differences from the WT. In particular, the double knockout strain ΔΔ*MGG_Crh2_Utr2* line 25 showed changes consistent with the triple knockout mutant Δ*Utr2*Δ*Crh11*Δ*Crh12* in *C. albicans* (Pardini *et al.* 2006). These include an increase in the amount of glucan in the ASF and reduction in AIF, increase in chitin content in AIF and a reduction in mannan.

The increase in total glucan in the ASF and decrease in AIF is a direct result of a reduction in Crhp activity. As mentioned earlier, the cross-linking of chitin to glucan polymers changes the chemical properties of the latter from alkaline soluble to alkaline insoluble. It is however, important to highlight the fact that since the AIF could still detect the presence of glucans (albeit reduced), this suggests that as opposed to a complete absence of Crhp activity, there is instead, a reduction in activity. This points to the possibility that other Crhp not deleted in the mutant genotype, could compensate for the absence of *MGG_Utr2* and *MGG_Crh2*. Chapter 7 will proceed to explore this possibility. Despite this apparent reduction as opposed to the absence in Crhp activity, the reduction was clearly sufficient to signal a cell wall compensatory response, evident in both the double knockout strain ΔΔ*MGG_Crh2_Utr2* line 25 as well as even the single Δ*MGG_Crh1* Line 43.

Both *Crh-like* knockout strains in *M. oryzae* showed a significant increase in chitin content in the AIF (Figure 6.16) and as such, is also reflected in the total cell wall carbohydrate composition (Table 6.3). Not only is this observation consistent with the *Crh-like* mutants in *C. albicans* (Pardini *et al.* 2006), it is also

observed in the knockout mutants of other cell wall proteins. These include genes associated with glucan synthesis, mannan and cell wall remodelling proteins such as Gas1p/Gelp in an apparent compensation for a compromised cell wall (Kapteyn *et al.* 1997, Popolo *et al.* 1997, Ram *et al.* 1998, Terashima *et al.* 2000, Carotti *et al.* 2002). The double knockout strain also exhibited changes relevant to an increase in Gas1p activity: more branching of glucan chains to another glucan, as indicated by the significant ($p<0.05$) increase in 1,3,6-Glc*p* (34%). Furthermore, total cell wall analysis (Table 6.3) also revealed the increase in glucan of the double knockout strain, relative to the control WT, suggesting an increase in glucan synthesis. These observations indicate that cell wall proteins such as those in the Chsp, Fksp and the Gas1p family in the double mutant line were upregulated due to a compromise in the cell wall as a result of the absence of *M. oryzae Crh-like* genes. This specific cell wall compensatory response is discussed in greater detail in Chapter 7 (Section 7.1.2).

Another unexpected outcome is the non-significant difference in ASF/AIF and the decline in total mannan of mutant lines, relative to WT. In reference to Figure 6.10, there is a reduction in the AIF fraction for both mutant lines, compared to WT. However, due to the large standard deviation values for both mutant lines, statistical analysis showed no difference. It is possible to argue that the method used here is relatively crude (weighing pellets) and could involve human errors or contaminations. On the contrary, the carbohydrate and linkage analyses were more accurate, being able to differentiate different types of carbohydrates and specific linkages. Thus in this section, indeed changes in the cell wall composition was obvious and statistically significant. The decline in total mannan is consistent with the observation in the *C. albicans* counterpart by

Pardini *et al.* (2006). It is probable that there was no change in the level of mannan expressed, but since the total carbohydrate composition changed due to the increase in chitin, this could have influenced the ratio measured.

For future work, it is imperative that this cell wall analysis by GC/EI-MS is repeated for both the single gene knockout strain Δ *MGG_Crh1* Line 36 mutant and the double gene knockout strain ΔΔ*MGG_Crh2_Utr2* Line 25 each with another independent line. Also, to include the single knockout mutants of Δ*MGG_Crh2* and Δ*MGG_Utr2* to determine which gene contributes more in the cross-linking of chitin to glucan during vegetative growth. It would also be informative to include cell wall composition analysis of these mutants in different types of tissues, such as in germlings and perithecia and under various external stressors, particularly when exposed to Congo Red. Another component that was unable to be tested in this study is the second component of the cell wall: the cell wall proteins. It is worth measuring identifying the various cell wall proteins and possible changes to cell wall protein quantity using the mass spectrometric analysis (Free 2013) or a through a transcriptomic approach as executed by Garcia *et al*. (2004).

6.5 Chapter Summary & Conclusion

Results from this AFM work showed the presence of vegetative ECM observed for the first time under high spatial resolution. Further work will need to be conducted to decisively identify the components of the ECM and its primary role. It was also shown that the double gene knockout strain had a cell wall that was relatively less stiff than the WT. Here it can be concluded that MGG_Crh2p and/or MGG_Utr2p is important for maintaining cell wall rigidity. Further AFM elasticity work on the corresponding single deletion strain will need to be conducted to determine which gene is more important for elasticity.

The cell wall composition analysis showed changes in the mutant lines. The cell wall of mutants is compromised and lead to the activation of cell wall compensatory mechanism evident through the significant ($p<0.05$) increase in chitin synthesis and the activity of other cell wall remodelling proteins. Importantly, while the exact linkage of chitin to glucan (i.e. 1,3,6-glc*p*) could not be quantified, changes in the glucan component of the ASF and AIF of the double knockout strains attests to the reduced activity of *M. oryzae* Crh-like proteins. This means that genes *MGG_Crh2* and *MGG_Utr2* indeed function in catalysing the cross- linking of chitin to glucan. Future work should be repeated on the single knockout strains Δ*MGG_Crh2* and Δ*MGG_Utr2* to determine which gene play a more important role in cell wall remodelling.

In summary, the AFM work correlates with the cell wall analysis results, whereby changes in cell wall elasticity is reflected in significant changes to the glucan components in the ASF/AIF of the cell wall in the same mutant strain.

CHAPTER 7

Gene Compensation

&

Protein Localisation

7.1 Chapter Introduction

In Chapters 5 and 6, phenotyping work with both single and double gene knockout strains suggested weak phenotypes with mutants being fully pathogenic. Five *M. oryzae Crh-like* genes identified in Chapter 3, suggest that these weak phenotypes (Chapter 5) and partial as opposed to complete absence of Crh-like function (Chapter 6), could be attributed to a compensatory mechanism by the remaining homologous *Crh-like* genes. As such, this chapter utilises qRT-PCR gene expression analysis to explore *M. oryzae Crh-like* gene compensation in these single and double gene deletion strains. This was achieved by comparing the expression of all five *M. oryzae Crh-like* genes in each of the knockout strains, relative to the WT.

Additionally, Chapter 4 described in detail the generation of revertant strains for the single knockout strains tagged with a fluorescent protein (eGFP/mCherry). The second aim of this Chapter was to then explore the fluorescence pattern and localisation of the tagged proteins under various stages of the life cycle in revertant strains, namely 13c_2ci_6 (eGFP tagged MGG_Crh2p) and #5_6_14 (mCherry tagged MGG_Utr2p).

7.1.1 Gene Redundancy & Compensation

According to Nowak *et al.* (1997), “Genetic redundancy means that two or more genes are performing the same function and that the inactivation of one of these genes has little or no effect on the biological phenotype”. Despite their ubiquitous occurrence in genomes, redundant genes seem to persist by natural selection, eluding random mutation (Wagner 1999). Based on this paradigm, three types of genetic redundancy models have been developed by Nowak *et al.*

(1997) to explain this persistence. The models described below assume that full fitness is one, no fitness is zero and that interaction is limited to two genes.

Model (1): True redundancy. An organism with the genotype AB is of equal fitness to one gene deleted, ie Ab or aB with the deletion of both genes (ab) resulting in a fitness of zero

Model (2): In this scenario, both genes A and B have functional redundancy but with variable efficiency. Assume A has an efficiency of one, and B a reduced efficiency of *h.* Deletion of gene B therefore, would cause no changes to phenotype, while deletion of gene A results in a small reduction in fitness.

Model (3): Pleiotropy and redundancy. In this model, genes have more than one specific function. This can be as simple as two genes sharing the same biological function, but with variation in their temporal and spatial expression.

In reference to results in Chapter 3, the five *Crh-like* genes in *M. oryzae* are likely to fit models 2 and 3. *In silico* analysis on *Crh-like* genes across various fungal species suggests that the more complex filamentous fungi, including *M. oryzae*, all share an expansion in the number of *S. cerevisiae Crh1* genes. In addition to this, studies found *S. cerevisiae Crh1* to be functionally redundant to *Utr2* with differences in enzyme efficiency and variations in its regulatory processes (Rodriguez-Pena *et al.* 2000, Blanco *et al.* 2014). Similarly, gene expression work (Chapter 3) showed that these genes are differentially regulated. *MGG_Crh2* is most highly and stably expressed (relative to internal reference genes), with an up-regulation under cell wall stress. The expression of the remaining *MGG_Crh1, MGG_Crh3* and *MGG_Crh4* is insignificant while *MGG_Utr2* responds to caffeine stress. This information, coupled with the weak

phenotype observed in *ΔMGG_Crh1, ΔMGG_Crh2, ΔMGG_Utr2,* and *ΔMGG_Crh2_Utr2*, supports the hypothesis that other *M. oryzae Crh-like* genes may share the same functionality but varying efficiencies (model 2), or are functionally redundant but vary in temporal or spatial expression (model 3).

Gene compensation through an up-regulation of expression by another gene/s has been observed in cell wall proteins. Fungal cell wall glucan and chitin synthases both have multi-copy genes that exhibit varying degrees of functional redundancy but varying efficacy, expression, and regulation. In *M. oryzae*, seven chitin synthases have been functionally characterised (Kong *et al.* 2012). Three were shown to be important for infection (*Chs1*, *Chs6,* and *Chs7*) and two are functionally redundant in response to external stressors (*Chs1* and *Chs3*). The generation of a double deletion mutant of *Chs5* and *Chs6* resulted in 2.6 and 2.4-fold increases in the expression of *Chs3* and *Chs4* respectively. Similarly, the *chs3* mutant caused an up-regulation of *Chs1*.

Collectively, these findings suggest the possibility that compensatory responses through gene up-regulation may occur between functionally redundant Crh-like proteins in mutant strains generated in this study. This could be the possible reason for the occurrence of a weak phenotype seen in Chapter 5 and reduced as opposed to complete absence of Crhp cross-linking role seen in Chapter 6. Due to this, it is important to investigate this further through the use of qRT-PCR to measure any changes in *M. oryzae Crh-like* gene expression between the WT and the mutant lines generated. It is hypothesised that the deletion of an *M. oryzae Crh-like* gene may have resulted in a weak phenotype as another functionally redundant *Crh-like* gene may compensate by an increased gene expression.

7.1.2 Protein Localisation

Protein localisation investigation provides useful information towards a better understanding of protein function, cellular signalling pathways and *in situ* spatial distribution (Stadler *et al.* 2013). Two of the most commonly used imaged based techniques are immunofluorescence (IF) and fluorescent protein (FP) tagging. Both were recently shown to be consistently co-localised (80% overlap) (Stadler *et al.* 2013), suggesting the reliability of both techniques. However, contrary to IF needing extensive sample fixing and preparation, FP enables real-time visualization of proteins in living cells and provides more room for downstream applications especially in temporal studies such as observing protein localisation during morphological changes or localisation when exposed to chemical stressors (Lorang *et al.* 2001). The above advantages of FP fit in well with the experimental aims of studying cell wall proteins in *M. oryzae*.

The use of FP in fungi is widespread and routine. Huh *et al.* (2003) managed to GFP tag and localise 97% of all *S. cerevisiae* proteins. Successful fluorescent tagging of *M. oryzae* proteins such as the chitin synthases, fungal hydrophobins and carnitine–acylcarnitine carrier proteins were achieved with informative results (Kershaw *et al.* 1998, Kong *et al.* 2012, Yang *et al.* 2012). However, one of the challenges with this technique is the risk of mis-localisation due to the erroneous engineering of the native protein if not carefully designed and addressed.

The presence of a signal-peptide at the N-terminus and a GPI-anchor site at the C-terminus, means that fluorophore tagging in fungal cell wall protein is not straight-forward. Despite this, the study of temporal and spatial localisation of Crh

proteins using fluorescently tagged GFP have been successful and informative. In *S. cerevisiae*, Rodriguez *et al.* (Rodriguez-Pena *et al.* 2000) developed Crh1-GFP and Utr2-GFP by taking advantage of a unique restriction enzyme cut site *Spe*I found in frame in both genes where a GFP fragment with the *Spe*I site at both ends were ligated to. This resulted in a fusion protein without any alterations to the N-terminus signal peptide or the GPI-anchorage site at the C-terminus. A different approach was taken by Pardini *et al.* (2006) to circumvent the N/C terminal problem in *C. albicans*. Here, through overlapping PCR and cloning work, the authors designed a transformation plasmid containing *C. albicans Utr2* coding gene with the GFP added internally before the GPI-anchor site at the C-terminus. Both approaches were able to express GFP and localisation of Crhp and Utr2p for both species were consistently found to be at the cell wall. In both studies, brighter fluorescence was observed at polarised growth sites such as at the mother-bud neck, septum, and hyphal tips, showing a spatial overlap with sites of chitin accumulation (Rodriguez-Pena *et al.* 2000, Pardini *et al.* 2006).

Given the protein localisation results obtained from studies in *S. cerevisiae* and *C. albicans,* it is hypothesised that *M. oryzae* Crhp and Utr2p localises to the cell wall, specifically at polarised growth sites. Currently, the literature is devoid of exploring *M. oryzae* Crh-like protein function through spatial and temporal localisation during infective germling progression and in the mycelia of the vegetative hypha.

7.2 Aims & Objectives

To first determine whether compensation of *M. oryzae Crh-like* genes occurs when one or more of the genes are deleted. Secondly, to explore the localisation of eGFP/mCherry-tagged *M. oryzae* Crh-like proteins in during germling development and in vegetative hyphae.

Gene Compensation Experimental Strategy:

1. Grow five *M. oryzae* genotypes vegetatively under optimal conditions in liquid Complete Medium (CM). These five genotypes are mutant strains *ΔMGG_Utr2, ΔMGG_Crh1, ΔMGG_Crh2, ΔΔMGG_Crh2_Utr2* and WT strain Guy11 as the control
2. Extract RNA and quantify relative expression levels of all five *Crh-like* query genes *MGG_Utr2, MGG_Crh1, MGG_Crh2, MGG_Crh3, MGG_Crh4* from each genotype using validated reference genes (Chapter 3) by quantitative real time polymerase chain reaction (qRT-PCR)
3. Repeat all the above when fungus is grown under cell wall stress induced by Congo Red (CR) and oxidative stress induced by Hydrogen Peroxide (H_2O_2)

Protein Localisation Experimental Strategy:

1. Prepare fungal tissues for protein visualisation comprising of vegetative mycelia, dormant spores, germlings at 2 hpi, 4 hpi and 24 hpi and *in-planta* growth

2. Visualise tissues using confocal microscopy with the appropriate lasers and settings

7.3 Materials & Methods

7.3.1 Gene Compensation Analysis

7.3.1.1 Tissue Preparation

Fungal mycelia from five *M. oryzae* genotypes (*ΔMGG_Utr2* line 2*, ΔMGG_Crh1* line 36*, ΔMGG_Crh2* line 39*, ΔΔMGG_Crh2_Utr2* line 25 and WT as the control) were harvested from liquid media as described below.

Fungal spores were harvested as described in Chapter 2 (Section 2.2.1.2). Inoculation, liquid culture growth under optimal conditions (CM) and mycelia harvest as described in Chapter 2 (Section 2.2.1.5). Harvested tissues were stored under -80°C until required. The procedure was repeated using spore suspension harvested from separate fungal colonies to obtain three biological replicates for each of the five genotypes mentioned. For the cell wall stress condition (CR), the procedure above was repeated for all five genotypes with the addition of filter sterilised 100 µg/ml Congo Red (Sigma-Aldrich) to the liquid media. For oxidative stress condition (H_2O_2), 2.5 mM of filter sterilised H_2O_2 (30% w/v) was added to each two day-old culture (spores germinated), prepared as above. It was observed that adding 2.5 mM H_2O_2 during inoculation prevented spore germination.

7.3.1.2 RNA Extraction, Quantity & Quality Assessment

Details of RNA extraction and determination of RNA quality and quantity as described in Chapter 2 (section 2.2.2.3).

Concentration adjustment of RNA samples to 500 ng/µl was conducted using a ‘NanoDrop® ND-1000’ spectrophotometer (Thermo Scientific).

7.3.1.3 Primer Quality Assessment

Primer pairs used for qRT-PCR analysis were those designed for Chapter 3 (Table 3.3 and Appendix A.6). These are primer pairs for *MGG_Utr2, MGG_Crh1, MGG_Crh2, MGG_Crh3, MGG_Crh4* and using the two validated reference genes for vegetative growth, *MGG_40S,* and *MGG_Ef1.* The quality of all primer stocks (100 µM) previously used in Chapter 3 were re-validated by conducting melt-curve analysis at the end of the qRT-PCR analysis, to show that the primers were still suitable for use in this analysis.

7.3.1.4 Complementary DNA Synthesis & qRT-PCR Analysis

Refer to Chapter 2 (Section 2.2.24) for routine cDNA synthesis, with the exception that a template concentration of 500 ng/µl was used instead. The synthesised cDNA (volume 20.0 µl) was diluted half by adding 20.0 µl RNAse-Free water (Qiagen) giving a new total cDNA reaction mix of 40.0 µl for each sample. This was followed by the use of 'Power SYBR® Green PCR Master Mix' assay (Applied Biosystems) for subsequent qRT-PCR reactions described in Chapter 2 (Section 2.2.2.1).

7.3.1.5 Data Analysis

The expression of five *M. oryzae Crh-like* genes in four knockout strains and WT was measured from mycelial fungi grown vegetatively under optimal conditions in liquid CM. The WT was used as the control sample, with each of the five *Crh-like M. oryzae* genes designated as the gene of interest (GOI), and both *MGG_40S* and *MGG_Ef1* used as the validated stably expressed internal reference genes. This means that the expression of each GOI in each knockout strain was measured relative to the same GOI in WT, normalised against two

internal reference genes. This is designated as Normalised Relative Quantities (NRQ_{GOI}), which were measured as per the formula shown below:

$$\text{Fold Change } (NRQ_{GOI}) = \frac{2^{\Delta ct\ GOI}}{\text{GEO MEAN}\ (2^{\Delta ct\ \text{reference gene1}}),(2^{\Delta ct\ \text{reference gene2}})}$$

Where:

Δct GOI = Mean ct GOI in control sample – Mean ct GOI in target sample

Δct reference gene = Mean ct Reference gene in control sample – Mean ct Reference gene in target sample.

Control sample is WT Guy11 genotype
Target sample is any one of the mutant lines

In each 96-well plate, sample maximisation was adhered to as recommended by Hellemans *et al.* (2007) to minimise technical variations between two or more 96-well plates. This means that all three biological replicates for the control sample (WT template cDNA) and up to two mutant line/s must be on the same 96-well plate. Each genotype analysed (WT and mutant), must have the reference genes *MGG_40S* and *MGG_Ef1* and the GOI included in each plate. This will allow complete analysis of the expression of each *Crh-like* gene in a mutant line relative to the expression in the WT line within one 96-well plate. See appendix E.1 for an example of a 96-well plate design.

Raw cycle threshold (ct) data was collected and averaged from two technical replicates. For each GOI, the Normalised Relative Quantities (NRQ_{GOI}) were calculated, logged, and NRQs from three biological replicates were averaged and presented as standard deviation. Standard Error of Mean was measured and statistical analysis analysed using a 95% confidence interval.

The qRT-PCR experimental design described above was repeated for tissues grown under cell wall stress (Congo Red) and oxidative stress (H_2O_2).

7.3.2 Protein Localisation

7.3.2.1 Protein Visualisation in Fungal Tissues

The germination stage used for this section included germlings on hydrophobic surfaces: dormant spores (0 hpi), germ tube (2 hpi), immature appressoria (4 hpi) and melanised appressoria (24 hpi). In addition, protein localisation for *in-planta* growth (onion peels) and vegetative mycelium were also analysed. Refer to Chapter 2 (Section 2.2.1.4 and 2.2.1.6) for the preparation of vegetative mycelium, germlings and *in-planta* (onion peels) fungal tissues for confocal imaging.

7.3.2.2 Sample Visualisation by Confocal Microscopy

A prepared glass slide as described above was placed onto the Zeiss LSM 510 Meta Microscope (Carl Zeiss Ltd., Welwyn Garden City, Herts, UK) stage and viewed using the C-Apochromat x40/1.2 water immersion lens. To capture eGFP fluorescence, Channel two (Ch2) containing an argon laser (excitation: 488 nm) and the filter LP 505 was used. For visualizing mCherry, Channel 3 (Ch3) with a diode laser (excitation 543 nm) with filter LP 585 was used. Images were collected as z-stacks, between a range of 8-18 optical slices for mycelial tissues, 15-25 for germlings and 60-70 optical slices for *in-planta* growth. All eGFP and mCherry images are displayed as a 3D Projection at 0° first angle. For optimal display purposes, each brightfield image shown is from a single optical z-stack. A minimum of two biological replicates was used per genotype, with WT strain as a control in each confocal session. A minimum of two confocal sessions was conducted for each tissue type, to ensure that images observed were replicable and consistent.

7.4 Results & Discussion

7.4.1 Gene Compensation Analysis

7.4.1.1 Sample and Primer Quality Assessment

Chapter 3 explained in detail the importance of consistency in template quality (High-quality RNA), primer performance (Efficiency and specificity) as well as the use of carefully selected internal reference genes. Thus, each extracted RNA sample was subjected to quality and quantity analysis. Since the same set of primers designed for Chapter 3 (Table 3.3 and Appendix A.6) were used again in this chapter, primer stocks were re-assessed for contamination or degradation by conducting primer efficiency and specificity checks (Melt-curve analysis).

In total, there were three treatments used to study changes in the expression of five *Crh-like* genes in the four *M. oryzae* mutant lines, relative to the WT. Each treatment (Optimal, cell wall stress, and oxidative stress) was analysed and data calculated independently of each other. Within each treatment, RNA was extracted from a total of 15 samples (Five genotypes, each with three biological replicates) and concentration of each sample normalised to 500 ng/µl. The integrity of each RNA sample (RIN) was determined using 'Agilent 2100 Bioanalyzer Instrument'. The presence of two sharp peaks corresponding to fungal 28S and 18S ribosomal subunits indicate that all mycelial RNAs were of very high quality with little to no degradation (Appendix E2 to E4). An RNA ladder was added for each Bioanalyzer 'Plant Nano Chip' run (12 samples maximum). Once RNA samples were normalised and quality checked, cDNA was synthesised on the same day. The presence of an additional small 'bump' at the precursor region, most evident in electropherograms for H_2O_2 samples, is due to

the low concentration of template RNA used. As a result, it amplified the negligible amount of contaminant (Appendix E.4) as opposed to an earlier set of CR and CM sample tissues where an excess of RNA was used. Similarly, in the manufacturer's protocol showed an example of an electropherogram (Appendix E.5) with high-quality RNA giving a similar pattern of a small peak in the precursor region (Mueller *et al.* 2004). If there was a small possibility of genomic DNA (gDNA) contamination, this was deemed to be of little concern as *M. oryzae Crh-like* gene primers were designed to be transcript-specific (Appendix A.6).

Also, primer specificity was validated by conducting a melt-curve analysis for each primer pair amplified to ensure that the primers were still specific and not contaminated as when used in Chapter 3. Each of the seven primer pairs used gave only one amplification product, indicating it was not contaminated (Appendix E.6). It can be concluded that these primers retained the same efficiency and specificity as indicated in Chapter 3.

7.4.1.2 Quantitative Real-Time PCR Results Analysis

The expression of five *M. oryzae Crh-like* genes were measured in each of the four knockout strains (generated in this study), relative to the WT. These are genes *MGG_Utr2, MGG_Crh1, MGG_Crh2, MGG_Crh3* and *MGG_Crh4* measured in the background of mutants Δ*MGG_Utr2* line 2, Δ*MGG_Crh1* line 36, Δ*MGG_Crh2* line 39 and ΔΔ*MGG_Crh2_Utr2* line 25. The expressions were measured in strains grown vegetatively in CM to validate possible compensation under optimal conditions. Chapter 3 showed that two *Crh-like* genes were significantly ($p<0.05$) up-regulated under cell wall stress induced by Congo Red (100 μg/ml). As such, homologous gene compensation in mutants under the same cell wall stress condition was also tested for. Additionally, Chapter 3

showed that oxidative stress induced by H_2O_2 (2.5 mM) caused significant ($p<0.05$) down-regulation in two *Crh-like* genes. Due to this, this stressor was added as an additional factor to analyse. Each treatment type was analysed independently. For this work, statistically, significant fold-change values above 2 fold were considered biologically meaningful as recommended by Karlen *et al.* (2007).

When the single knockout strain Δ*MGG_Utr2* was grown in CM, there were no significant ($p<0.05$) changes in the expression of the four other *M. oryzae Crh-like* genes when compared with the expression of these genes in the WT (Figure 7.1). A similar result is seen for all other knockout strains and the respective remaining *Crh-like* genes.

When the same set of fungal strains were grown in CR, knockout strains Δ*MGG_Utr2*, Δ*MGG_Crh1* and Δ*MGG_Crh2_Utr2* showed no changes to the expression of all five *Crh-like* genes relative to WT (Figure 7.2). However, a different pattern is seen in knockout strain Δ*MGG_Crh2* whereby gene *MGG_Utr2,* the second most highly expressed *Crh-like* gene (Chapter 3), was up-regulated 3-fold higher than the expression of the same gene, in WT. No changes to the expression level of the remaining genes *MGG_Crh1, MGG_Crh3* and *MGG_Crh4* were observed for this knockout strain.

Conversely and unexpectedly, when fungal strains were grown in H_2O_2, gene *MGG_Crh3* responded by a significant increase ($p<0.05$) of around 3-fold change in both single mutant lines Δ*MGG_Utr2* line 2, Δ*MGG_Crh2* line 39 as well as ΔΔ*MGG_Crh2_Utr2* line 25 relative to the expression of the same gene in WT (Figure 7.3). No changes were observed for the remaining four *M. oryzae Crh-like* genes in all four knockout strains relative to WT.

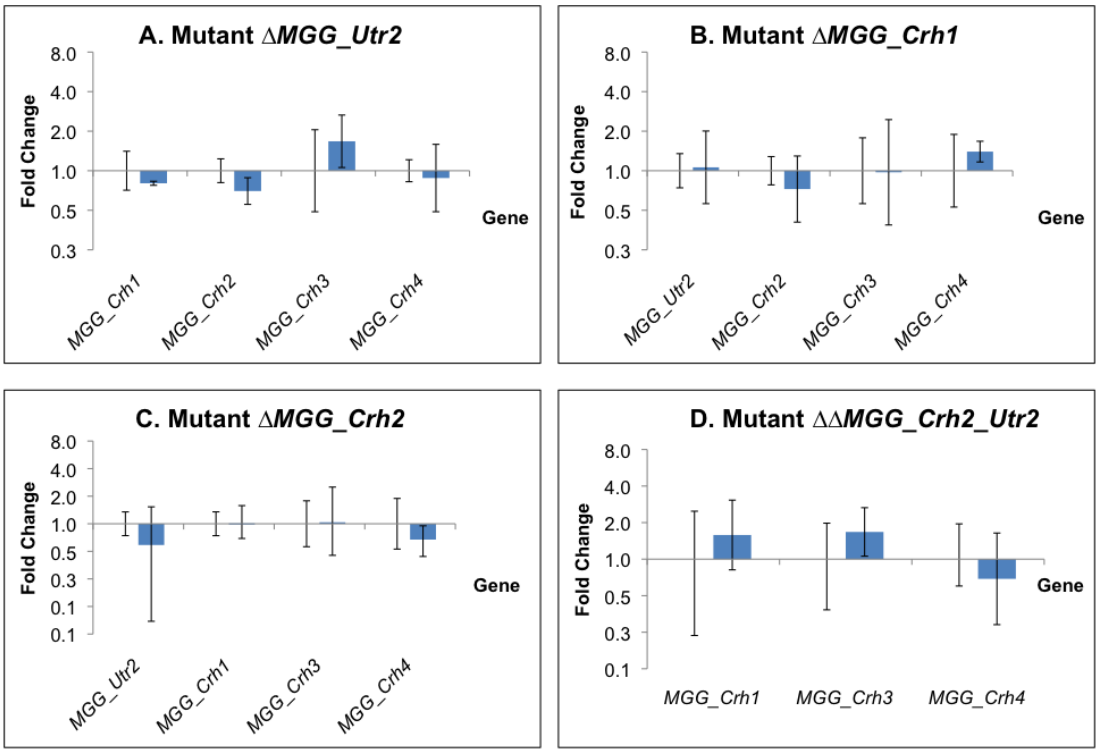

Figure 7.1. Expression of *Crh-like* Genes in Five *Magnaporthe oryzae* Genotypes Grown Under Optimal Conditions by qRT-PCR. RNA from five fungal genotypes was extracted from vegetative mycelia cultured in liquid CM for 3 days, respectively. **Panel A.** Expression of four *Crh-like* genes in Δ*MGG_Utr2* measured relative to WT (1.0-fold change). **Panel B** Expression of four *Crh-like* genes in mutant Δ*MGG_Crh1* relative to WT (1.0-fold change). **Panel C** Expression of four *Crh-like* genes in mutant Δ*MGG_Crh2* relative to WT (1.0-fold change). **Panel D** Expression of three *Crh-like* genes in mutant ΔΔ*MGG_Crh2_Utr2* relative to WT (1.0-fold change). The expression of these genes were normalised against *MGG_40s* and *MGG_Ef1* validated housekeeping genes. Data averaged from three independent biological replicates. Error bars represent 95% confidence interval.

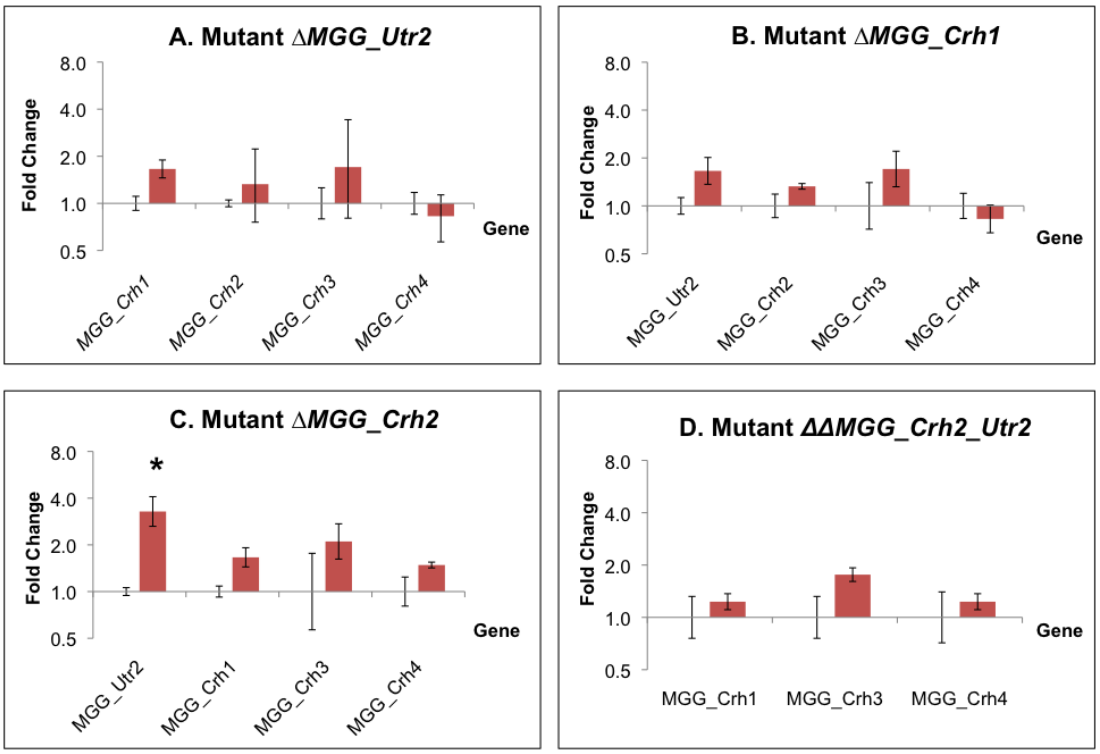

Figure 7.2. Expression of *Crh-like* Genes in Five *Magnaporthe oryzae* Genotypes Grown Under Cell Wall Stress by qRT-PCR. RNA from five fungal genotypes was extracted from vegetative mycelia cultured in liquid CM with 100 μg/ml Congo Red for three days, respectively. **Panel A** Expression of four *Crh-like* genes in Δ*MGG_Utr2* measured relative to WT (1.0-fold change). **Panel B** Expression of four Crh-like genes in mutant Δ*MGG_Crh1* relative to WT (1.0-fold change). **Panel C** Expression of four Crh-like genes in mutant ΔMGG_Crh2 relative to WT (1.0-fold change). **Panel D** Expression of three *Crh-like* genes in mutant ΔΔ*MGG_Crh2_Utr2* relative to WT (1.0-fold change). The expression of these genes were normalised against *MGG_40s* and *MGG_Ef1* validated housekeeping genes. Asterisk (*) indicate a significantly different (p>0.05) fold change relative to the same gene expressed in WT. Data averaged from three independent biological replicates. Error bars represent 95% confidence interval.

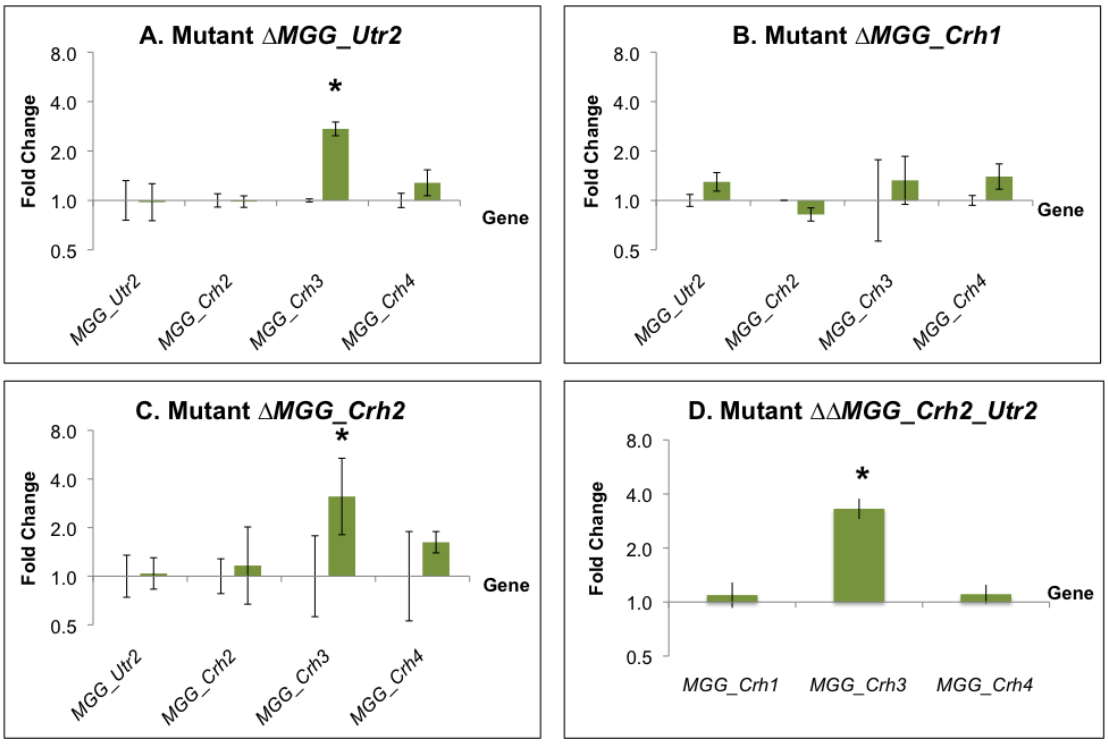

Figure 7.3. Expression of *Crh-like* Genes in Five *Magnaporthe oryzae* Genotypes Grown Under Oxidative Stress by qRT-PCR. RNA from five fungal genotypes was extracted from vegetative mycelia cultured in liquid CM with 2.5 mM H_2O_2 for 3 days, respectively**. Panel A.** Expression of four *Crh-like* genes in Δ*MGG_Utr2* measured relative to WT (1.0-fold change). **Panel B.** Expression of four *Crh-like* genes in mutant Δ*MGG_Crh1* relative to WT (1.0-fold change). **Panel C.** Expression of four *Crh-like* genes in mutant Δ*MGG_Crh2* relative to WT (1.0-fold change). **Panel D.** Expression of three *Crh-like* genes in mutant ΔΔ*MGG_Crh2_Utr2* relative to WT (1.0-fold change). The expression of these genes were normalised against *MGG_40s* and *MGG_Ef1* validated housekeeping genes. Asterisk (*) indicates a significantly different (p>0.05) fold change relative to the same gene expressed in WT. Data averaged from three independent biological replicates. Error bars represent 95% confidence interval.

Due to the unexpected increase in fold change of *MGG_Crh3* in the background of mutant lines under oxidative stress, the expression profile of *MGG_Crh3* and as an additional factor, gene *MGG_Crh4* in WT were measured under oxidative stress (H_2O_2) against growth in CM. The expression of both genes in WT was non-significantly different ($p<0.05$) relative to when the same fungal strain is grown in CM (Figure 7.4). It is possible that *MGG_Crh3* is indeed responding in a compensatory mechanism in the mutant lines. However, it should be noted that the raw ct values of *MGG_Crh3* detected are already very high as

shown in Table 7.1, reflecting very low expression level. As such, data reliability is questioned as these values are at the upper limit of qRT-PCR sensitivity (Chapter 3 paragraph 5). It is concluded that changes shown in the data calculation in Figure 7.3 may not be true transcriptional changes and pose little biological significance.

Table 7.1. Cycle Threshold Values for Gene *MGG_Crh3* Generated by qRT-PCR. Values of Gene *MGG_Crh3* Under Various background strain and growth conditions.

Background strain	Treatment	Mean (ct)	St. Dev
WT	Optimal Condition (CM)	28.68	0.34
WT	Oxidative Stress (H_2O_2)	29.79	0.23
Δ*MGG_Crh2_Utr2*	Optimal Condition (CM)	30.50	0.50
Δ*MGG_Crh2_Utr2*	Oxidative Stress (H_2O_2)	26.96	0.13

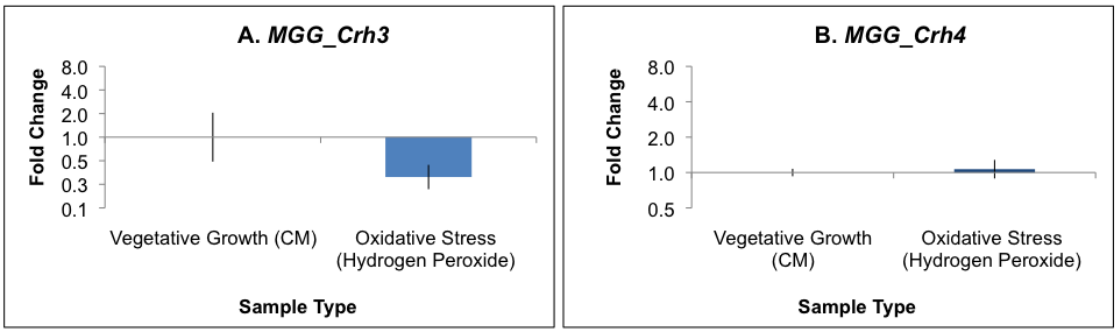

Figure 7.4. The Expression Profile of *MGG_Crh3* and *MGG_Crh4* Grown Under Oxidative Stress Relative to Growth Under Optimal Conditions by qRT-PCR. The WT strain was cultured vegetatively in CM liquid containing 5 mM H_2O_2, relative to the control sample containing CM liquid only. Data averaged from three biological replicates, with *MGG_Ef1* and *MGG_40s* as the internal reference gene. Error bars represent 95% confidence interval.

Gene MGG_Utr2 compensate under cell wall stress when MGG_Crh2 is absent

In summary, results concur with the hypothesis put forward. It can be concluded that under optimal conditions, the cell wall of mutant lines seemingly function without needing a compensatory response mechanism from other *M. oryzae Crh-like* genes. However, when these knockout strains were exposed to cell wall stress caused by Congo Red, a compensatory response was seen. Chapter 3 described in detail the expression profile of *M. oryzae Crh-like* genes, with *MGG_Crh2* being most highly expressed and up-regulated under cell wall stress, followed by *MGG_Utr2*. Therefore, when under cell wall stress, with the most highly expressed gene absent (*MGG_Crh2*), *MGG_Utr2* is seen to be up-regulated to compensate. On the contrary, when gene *MGG_Utr2* is absent in the Δ*MGG_Utr2* line 2 strain, the expression of *MGG_Crh2* is already sufficiently high to compensate for any loss in cell wall integrity without needing to up-regulate more than in the WT (which as shown in Chapter 3, is already up-regulated 2-fold under Congo Red, compared with WT in CM).

No Crh-like gene compensation in the double gene knockout strain

It is interesting to note that despite being under cell wall stress induced by Congo Red, the deletion of both genes in strain ΔΔ*MGG_Crh2_Utr2* did not result in changes in the expression of genes *MGG_Crh1, MGG_Crh3* or *MGG_Crh4*. Chapter 3 showed that these three genes are least expressed, with a suspicion that genes *MGG_Crh3* and *MGG_Crh4* are non-functional pseudogenes. Results in this section further support the suggestion that both *MGG_Crh3* and *MGG_Crh4* are least important in orchestrating *M. oryzae* cell wall remodelling. However, same cannot be said for *MGG_Crh1*. Cell wall analysis for mutant

∆*MGG_Crh1* (Chapter 6) showed 18% increase in total chitin content, which is an indication of the activation of cell wall compensatory response mechanism. It is possible that this protein has a role in cell wall remodelling. Perhaps *MGG_Crh1* was not up-regulated in the double knockout line as a separate regulatory system may govern it.

Having ruled out compensation by homologous genes in the double gene knockout strain, it is therefore concluded that the presence of a weak phenotype (Chapter 5) could be attributed to a compensatory mechanism by other cell wall proteins. The occurrence of a compensatory mechanism by other cell wall proteins is a frequently observed phenomenon. In a genome-wide analysis conducted by Lagorce *et al.* (2003), the global gene expression of cell wall mutant strains (∆*fks1,* ∆*knr4,* ∆*kre6,* ∆*gas1* and ∆mnn9) were compared and analysed. *In silico* clustering method identified a group of about 80 co-regulated genes all significantly up-regulated across all mutant strains analysed (Appendix E.7). In all the strains studied, cell wall compensatory genes comprising cell wall proteins such as *Crh1, Fks2* and *Chs3* were found to be up-regulated by 2 to 5 fold higher, relative to WT. Similarly in an earlier study, Terashima *et al.* (2000) showed that *Crh1* and *Chs3* in *S. cerevisiae* ∆*Fks1* knockout mutant was upregulated, with subsequent alterations to the cell wall composition (Kapteyn *et al.* 1997, Ram *et al.* 1998). Consistent with this, total chitin content in the cell wall of ∆∆*MGG_Crh2-_Utr2* increased by 18-20% and branching increased by 34% in the alkaline insoluble fraction, relative to WT. This further emphasises the suspicion that another CWP such as *Chs* and *Gel* was upregulated in a compensatory manner and future work should explore this possibility.

7.4.2 Protein Localisation

In complementation with *in silico* work, gene expression and phenotyping of mutant strains, protein localisation by fluorescent tagging were employed as a final tool used in this study to characterise the role *Crh-like* genes in *M. oryzae.* Specifically, based on results in Chapters 3-6, both genes *MGG_Utr2* and *MGG_Crh2* were found to be the most important genes from the five *M. oryzae Crh-like* genes predicted, and thus selected for complementation by fluorescent tagging. This is due to their high expression level in WT, phenotype seen on plate growth assays as well as the availability of single knockout strains which can be used to generate revertant strains tagged with either eGFP or mCherry.

7.4.2.1 Protein Localisation of eGFP tagged MGG_Crh2p

Linearised vector 13c_2ci containing the native promoter, the coding region for gene *MGG_Crh2* and the fluorescent protein eGFP were transformed into the background mutant line *ΔMGG_Crh2* Line 39, generating the revertant strain 13c_2ci_6. This strain was shown to complement the WT phenotype when grown for 10 days on CM agar containing Congo Red (Chapter 5 figure 5.10).

A total of six different living tissue types from various stages of the life cycle were analysed for eGFP-tagged MGG_Crh2p localisation. These include germlings on hydrophobic surfaces at various time points: dormant spore (0 hpi), germ tube (2 hpi), immature appressoria (4 hpi) and melanised appressorium (24 hpi). In addition to germination stage, included are fungal growth *in-planta* (24 hpi on onion peels) and vegetative mycelium all visualised in real-time.

It is important to note that a *M. oryzae* germling vary greatly in height and structure, making microscopic focus of the whole germling a challenge. For

example, data measurements using AFM (Chapter 6) showed that the averaged diameter of a germ tube is 1.0 µm, while an attached appressorium have an average height of 6 µm (Skamnioti and Gurr (2009). This large differences in height and angle between structures in a single germling resulted in brightfield image blurring when all z-stacks images were viewed together through 3D Projection at 0° first angle. Due to this, each brightfield image presented comprises of a single z-stack with the best compromise in image resolution of the various structures.

Additionally, it is important to highlight that reflective of the gene expression analysis in Chapter 3, eGFP fluorescence in mycelium is brightest (Figure 7.5 Panel B) relative to fluorescence in germlings. Therefore to obtain meaningful images, the detector gain for eGFP channel had to be lowered from 920 (used for capturing eGFP fluorescence in germlings) to 850 (Figure 7.5 Panel C). Confocal images of line 13c_2ci_6 were shown with a WT line prepared together as a control, to show that the fluorescence seen in line 2ci_6 is a true fluorescence due to MGG_Crh2p expression and not due to auto-fluorescence of the vacuole or other sources of contamination.

Confocal images of living vegetative mycelium showed that eGFP-tagged MGG_Crh2p is localised to the hyphal cell wall, with higher accumulation at hyphal tips and septae (Figure 7.5 Panel C and D).

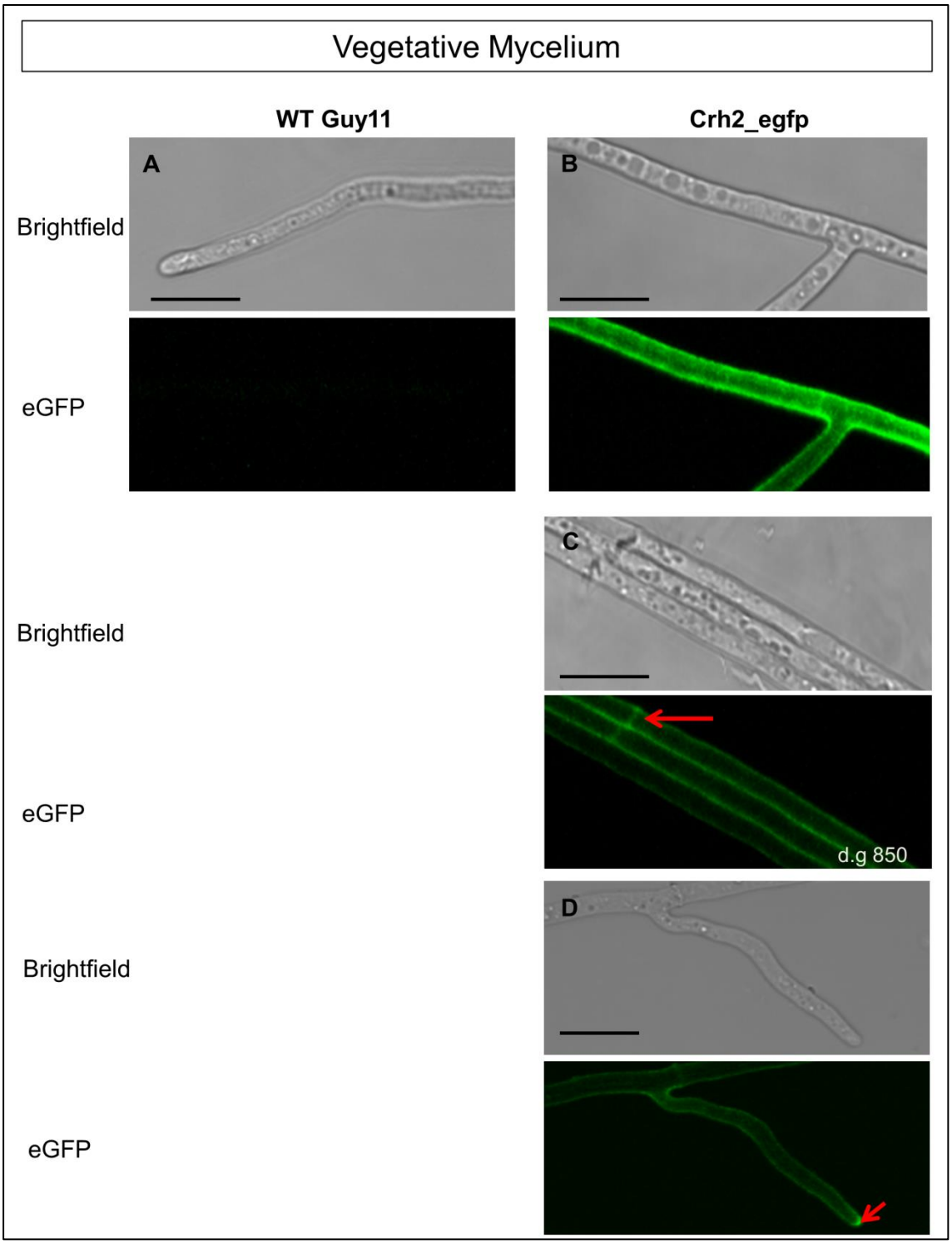

Figure 7.5. Visualisation of MGG_Crh2p Localisation in the Vegetative Structures of *Magnaporthe oryzae* Expressing eGFP. Fungal strains were inoculated onto CM agar and vegetative hypha imaged in real-time on cover slips. **Panel A** Hypha of control WT. **Panel B** Hypha of strain 13c_2ci_6 under Brightfield and eGFP at 920 detector gain (same detector gain level for all other germling images). **Panel C-D** Strain 13c_2ci_6 exposed to a lowered detector gain (850). Red arrows show the accumulation of eGFP fluorescence at septum and tip of hypha. Scale bar represents 10 µm. Image visualisation repeated twice with WT as control sample. Bright-field images presented as single-layer z-stacks while eGFP images presented as 3-D projections at 0° angle.

MGG_Crh2p can also be found in the cell wall of germlings. However, fluorescence found in germlings of strain 13c_2ci_6 were less bright relative to vegetative growth and localisation is temporal and spatially regulated. In dormant spores (Figure 7.6 Panel B), MGG_Crh2p can be seen localised throughout the spore cell wall with the brightest region at the spore tip and spore end. At 2 hours post inoculation, it is intriguing to note that no fluorescence is seen in the germ tube, but present at the spore wall (Figure 7.6 Panel D).

On the contrary to germling at 2 hpi, by 4 hpi, eGFP-tagged MGG_Crh2p can be seen localised to the cell walls of the germ tube and immature appressorium as well as still visible within the spore cell walls (Figure 7.7 Panel B). Howver, after 24 hpi, due to spore collapse, fluorescence was absent at the lysed section of the spore, and brightest at the section where germ tube protrude (Figure 7.7 Panel D). Fluorescence was no longer present in the melanised appressorium but accumulated at the cell wall of the germ tube.

The eGFP-tagged MGG_Crh2p can also be clearly viewed real-time *in-planta*. Here, 13c_2ci_6 spore suspension was inoculated on an onion peel and imaged after 24 hours. Consistent with 24 hpi on hydrophobic surface, no fluorescence was observed on melanised appressorium. Contrary, fluorescence is seen accumulated in young infective hyphae, mostly at the growing tips (Figure 7.8 Panel B).

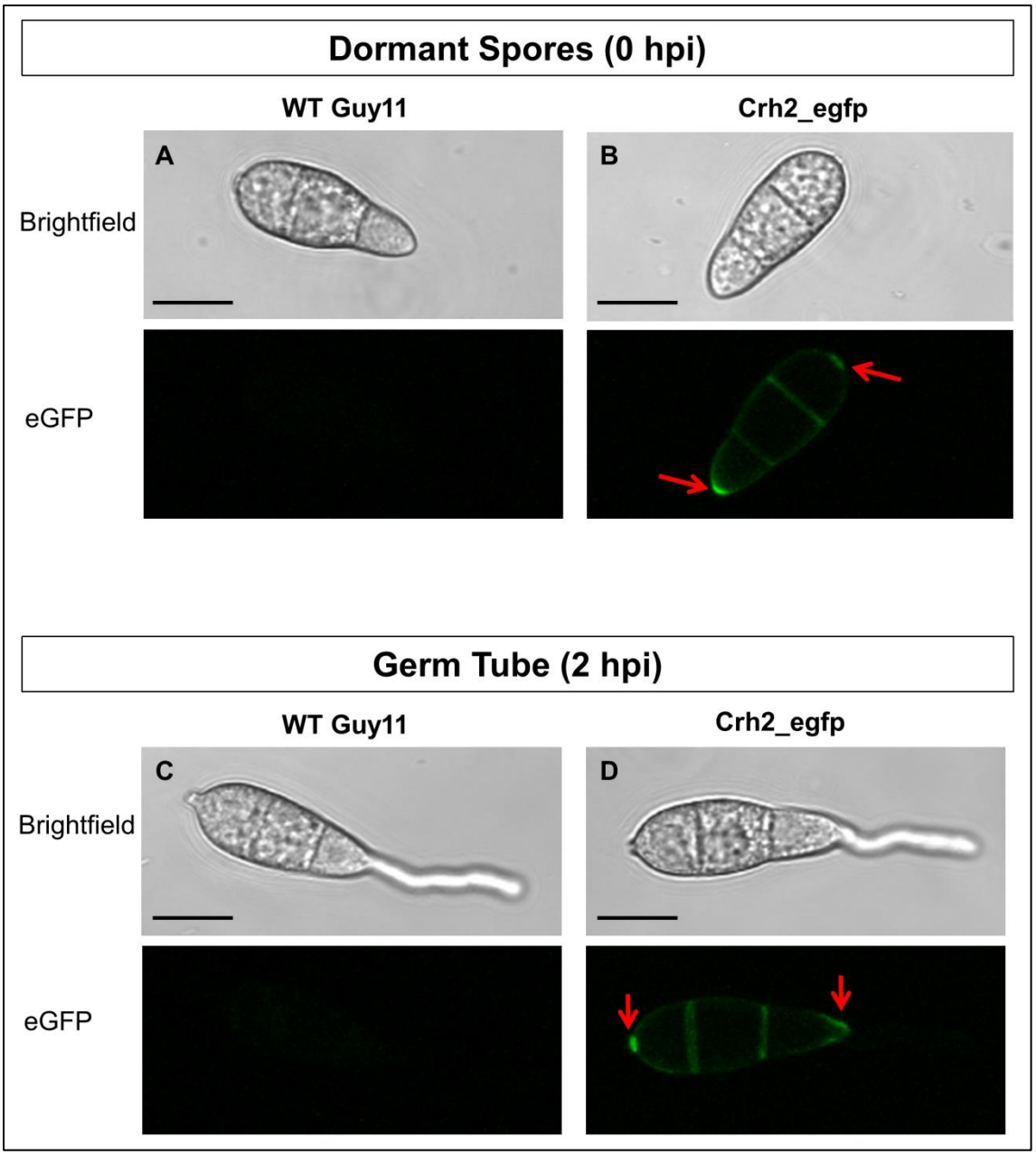

Figure 7.6. Visualisation of MGG_Crh2p Localisation in the Early Stage of Germling Development in *Magnaporthe oryzae* Expressing eGFP. Dormant spores for each strain were inoculated on a hydrophobic surface (Menzel slide) and incubated at the appropriate time frames in a high humidity chamber prior to imaging. **Panel A** WT dormant spore (0 hpi). **Panel B** Strain 13c_2ci_6 under the same conditions. Fluorescence can be seen localised to the spore wall with higher fluorescence at the spore ends. **Panel C** WT germling at 2 hpi. **Panel D** Strain 13c_2ci_6 under the same conditions. Here, eGFP is seen to localise to spore cell wall with higher fluorescence at both ends of the spore (red arrows). Scale bar represents 10 µm. Image visualisation repeated twice with WT as control sample. Bright-field images presented as single-layer z-stacks while eGFP images presented as 3-D projections at 0° angle.

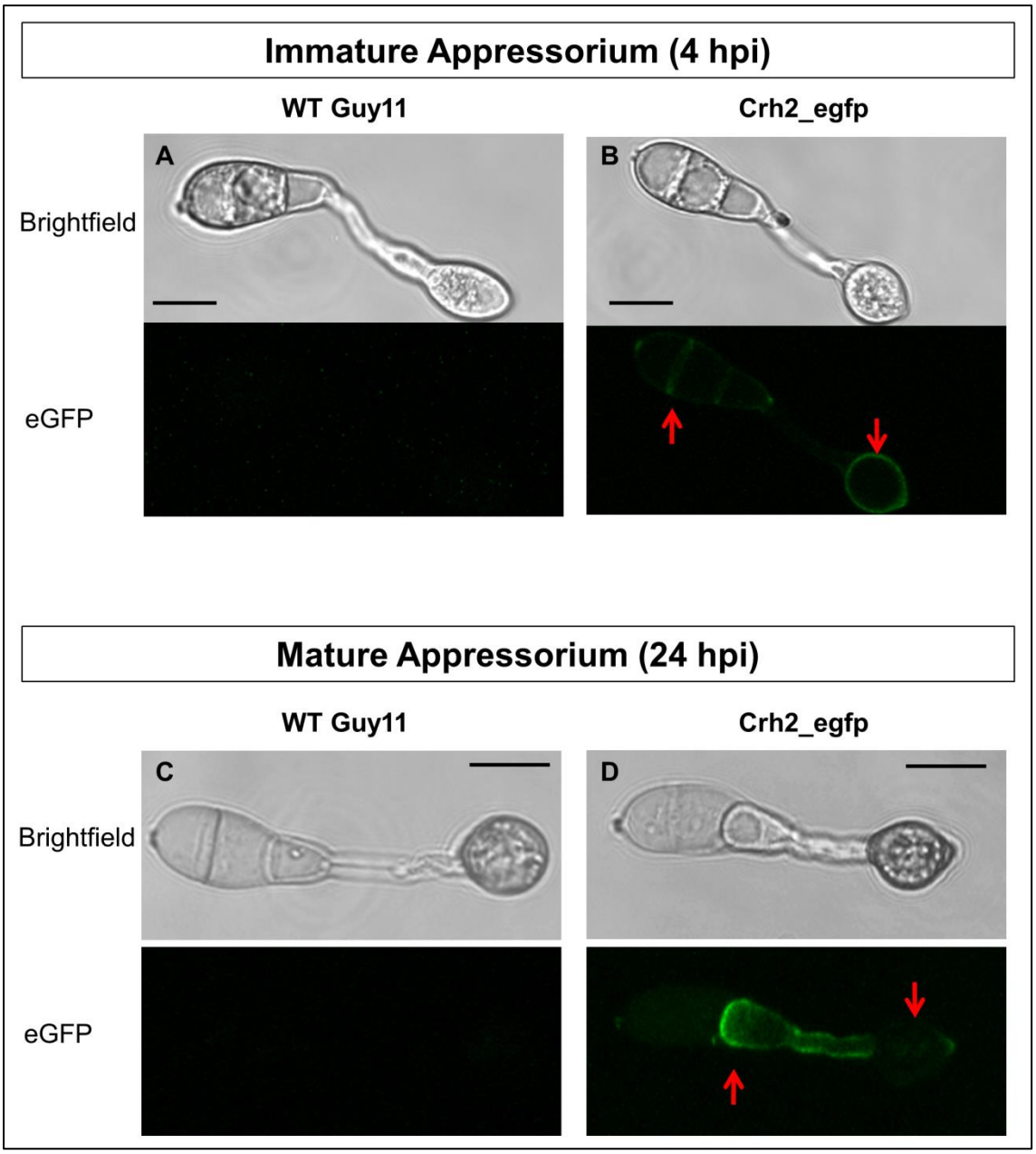

Figure 7.7. Visualisation of MGG_Crh2p Localisation in the Late Stage of Germling Development in *Magnaporthe oryzae* Expressing eGFP. Dormant spores for each strain were inoculated on a hydrophobic surface (Menzel slide) and incubated at the appropriate time frames in a high humidity chamber prior to imaging. **Panel A** WT germling at 4 hpi. **Panel B** Strain 13c_2ci_6 under the same conditions. Fluorescence seen localised to the spore wall as well as immature appressorium (red arrows). **Panel C** WT germling at 24 hpi. **Panel D** Strain 13c_2ci_6 under the same conditions. Here, eGFP is seen to localise to the germtube and the remaining living section of the spore (red arrows). Scale bar represents 10 µm. Image visualisation repeated twice with WT as control sample. Bright-field images presented as single-layer z-stacks while eGFP images presented as 3-D projections at 0° angle.

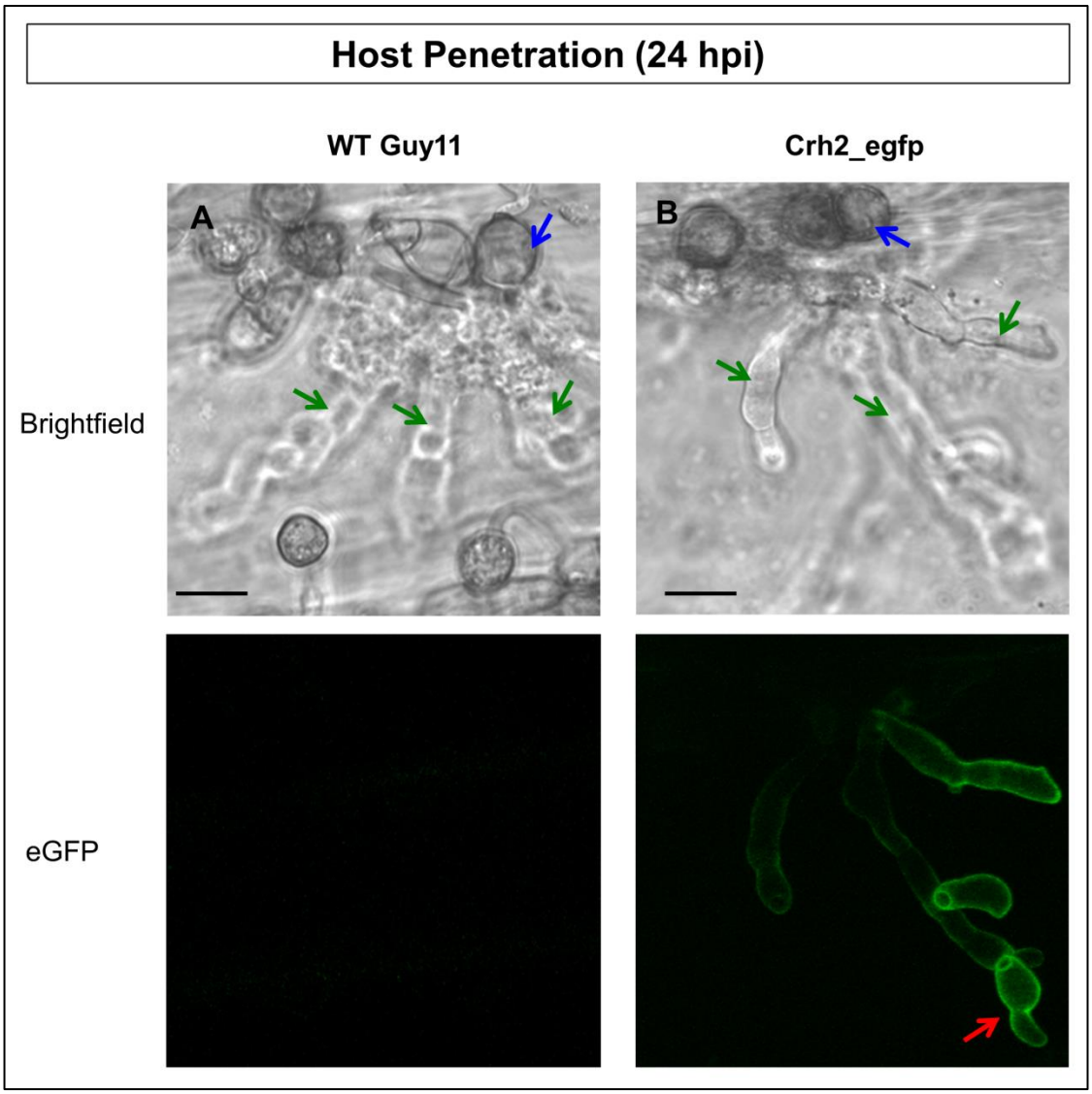

Figure 7.8. Visualisation of MGG_Crh2p Localisation *In Planta* in *Magnaporthe oryzae* Expressing eGFP. Dormant spores for each strain were inoculated on an onion peel and incubated for 24 hours in a high humidity chamber prior to imaging. **Panel A** WT infective structures at 24 hpi. **Panel B** Strain 13c_2ci_6 under the same conditions. Brightfield images of both WT and Line 13c_2ci_6 show the presence of melanised appressoria (blue arrows) and thick-bulbous infective hyphae (green arrows) spreading into the onion cell. Fluorescence in strain 13c_2ci_6 was strongly localised to the growing regions of the infective hyphae cell wall, absent on melanised appressoria and lower fluorescence at the old sections of the hyphae. Scale bar represents 10 µm. Image visualisation repeated twice with WT as control sample. Bright-field images presented as single-layer z-stacks while eGFP images presented as 3-D projections at 0° angle.

MGG_Crh2 is localised to the cell wall and at polarised growth sites

The localisation of MGG_Crh2 at the cell wall and polarised growth sites coincides with sites of chitin deposition. In Chapter 5, Calcofluor White (CFW) staining, known to for the specific affinity for fungal chitin (Elorza *et al.* 1983), showed the same pattern of fluorescence at the cell wall with brightest at tips and septum of the vegetative hypha. This is consistent with the co-localisation of eGFP tagged *S. cerevisiae* Utr2p and CFW staining (Pardini *et al.* 2006). The observed spatial overlap attests to the specific function of the *M. oryzae* Crh-like proteins in cross-linking chitin to glucan polymers.

The spatial localisation pattern of MGG_Crh2p is consistent with the localisation of Crh-like proteins in other fungal species. In *M. oryzae* strain 13c_2ci_6, MGG_Crh2p was found at the cell wall, with higher accumulation at the septum, hyphal tips, spore tip and spore attachment scar. Similarly, this cell wall localisation pattern is also seen in other fungal species such as *C. albicans* and *S. cerevisiae,* with higher accumulation at polarised growth sites, bud scars, and septum (Rodriguez-Peña et al. 2002, Pardini et al. 2006, Miller et al. 2010, Zelante et al. 2012). The accumulation at polarised growth sites in vegetative hypha and spore tip is expected, due to the need to cross-link newly synthesised chitin and glucan polymers actively produced at these ends. It, therefore, explains the lowered accumulation at mature sections of vegetative and infective hypha and absence in mature appressorium.

In an exception to the above, is the absence of any fluorescence in the developing germ tube at 2 hpi (Figure 7.6 Panel D). The only possible explanation is that at 2 hpi, MGG_Crh2p from the spore have yet to be trafficked to the tip of

the germ tube, and is still accumulated at the spore tip (red arrows, Figure 7.7 Panel B) to facilitate cross-linking in the newly synthesised cell wall polymers still actively protruding out. This is because by 4 hpi, accumulation of MGG_Crh2p at the swelling germ tube tip is seen, suggesting a role of MGG_Crh2p in forming the domed structure, and consistent with the theory of localisation at polarised growth sites.

Furthermore, it is noted that the intensity of the fluorescence (although not quantified), being highest in vegetative hypha and lowest in germlings, is in agreement with the expression profile of *MGG_Crh2* in Chapter 3, confirming the reliability of the gene expression tool employed and the realistic representation in the confocal images seen.

7.4.2.2 Protein Localisation: mCherry tagged MGG_Utr2p

An attempt was made to tag MGG_Utr2p with mCherry to fulfil a two-fold aim of MGG_Utr2p localisation information and downstream co-localisation with MGG_Crh2p strain 13c_2ci_6. Unfortunately, not only does the generated line #5_9a_14 not complement the *ΔMGG_Utr2* line 2 mutant phenotype, mCherry fluorescence was weak and difficult to capture (Figure 7.9). Despite initial screening using mycelial tissue where this gene is highly expressed (Chapter 3 Table 3.5), fluorescence is low and not localised to the cell wall but seem to be in vacuoles. Given that the brightness of mCherry is half less of eGFP under the same protein abundance (Shaner *et al.* 2005), coupled with a possible low expression of *MGG_Utr2,* this may lead to the extremely low fluorescence detected. However, this scenario is unlikely, given that *MGG_Utr2* expression data in Chapter 3 had cycle threshold values ranging from 13 to 18 (Chapter 3 Table 3.4 and 3.5). This is considered as within the range of a highly expressed

gene especially compared with the housekeeping gene *MGG_Ef1*. Thus it is unlikely to be due to the type of FP used.

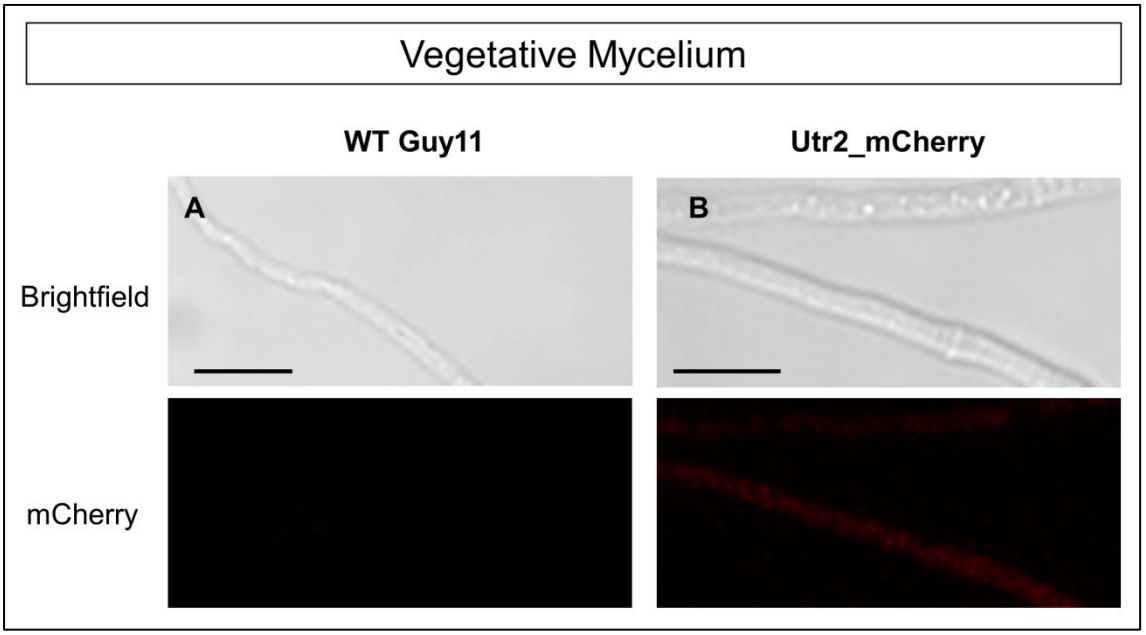

Figure 7.9. Visualisation of MGG_Utr2p Localisation *In Planta* in *Magnaporthe oryzae* Expressing mCherry. Fungal strains were inoculated onto CM agar and vegetative hypha imaged in real-time on cover slips. **Pane A.** WT Guy11 vegetative hypha. **Panel B.** Strain #5_9a_14 under the same conditions. Low fluorescence was observed within the cytoplasm of the hypha, most probably in the vacuolar structures. Scale bar represents 10 µm. Image visualisation repeated twice with WT as a control sample. Bright-field images presented as single-layer z-stacks while mCherry images presented as 3-D projections at 0° angle.

The second suspicion for the observed pattern of fluorescence in #5_9a_14 is that the addition of the FP may cause problems with protein folding. This was because no candidate lines complemented the phenotype of the knockout strain even though the un-tagged line #5_6 (same vector but without the addition of FP) did indeed complement the phenotype (Chapter 5). This is especially probable given the close proximity of the signal peptide cleavage site (Amino acid 21) to the predicted chitin binding domain (Amino acid 26-71) shown in Chapter 3 (Figure 3.8). So any addition of FP between amino acids 21 to 26 may have disrupted either the function of the signal peptide or the normal protein function.

For future work, it is recommended that an attempt is made to construct a FP similar to the one taken by Pardini *et al.* (2006), which is the addition of a GFP just prior to a GPI-anchor site. Here, *C. albicans* UTR2p-GFP were present at the cell surface for yeast and hyphal growth with variations in temporal and spatial accumulation. In the yeast phase, UTR2p-GFP strongly accumulated at the bud site and bud neck with an overlapping in spatial location when chitin was stained with Calcofluor White (CFW). Therefore, it is hypothesised that a functioning tagged MGG_Utr2p in *M. oryzae* should have similar fluorescence pattern as the one seen in the WT in CFW staining shown in Chapter 5 (Figure 5.15). This further justified the suspicion that line #5_9a did not produce a functional protein with problems in protein folding and subsequent trafficking to the cell wall.

7.5 Chapter Summary & Conclusion

The aim of the first section of this Chapter was to investigate any changes to the expression of *M. oryzae Crh-like* genes in the background of four knockout strains. Expression analysis showed that under optimal conditions, no observed changes in any of the five *Crh-like* genes in all four knockout strains, relative to WT. However, under cell wall stress, mutant Δ*MGG_Crh2* showed a three-fold up-regulation in the gene *MGG_Utr2.* No up-regulation of any *Crh-like* genes was seen in the remaining mutant lines. More importantly, is the absence of an up-regulation in the double gene knockout strain ΔΔ*MGG_Crh2_Utr2* shown to have a weak phenotype in Chapter 5.

In conclusion, compensation by other homologous *M. oryzae Crh-like* genes played a minor role in contributing towards a weak phenotype seen especially for the double gene knockout strain. Therefore, after ruling out compensation via homologous genes, it is worth exploring changes to gene expression of other cell wall proteins in future work.

Also, the role of two genes was further characterised by fluorescent tagging. From the localisation images obtained, it can be hypothesised that MGG_Crh2p may play a role in vegetative growth (brightest fluorescence under native promoter) as it is localised at sites of polarised growth in both vegetative hypha and germling development. Efforts to tag MGG_Utr2p with mCherry were unsuccessful possibly due to possible disruption of normal protein delivery and function. It is recommended for future work, to attempt fusion of FP at the C-terminus end, with careful consideration on the fusion site due to the presence of a GPI-anchor site at the C-terminus.

CHAPTER 8

Thesis Summary

8.1 Key Findings

Chapter 3: Bioinformatics & Gene Expression

- Four orthologues of *S. cerevisiae Crh1* and one *Utr2* were identified in *M.oryzae.*
- Gene *MGG_Crh2* was most highly expressed and was up-regulated under cell wall stress caused by Congo Red.
- *MGG_Utr2* was the second most highly expressed gene and was up-regulated under cell wall stress caused by Caffeine and Congo Red.

Chapter 4: Generation of Mutant & Revertant Strains

- Three single gene knockout mutants and a double gene knockout strain were generated
- Revertant strains for the single knockouts Δ*MGG_Crh2* and Δ*MGG_Utr2* were generated, with and without a fluorescent protein tag

Chapter 5: Mutant Phenotyping-Growth, Morphology & Pathogenicity

- Mutant Δ*MGG_Crh2* exhibited hypersensitivity to cell wall stress caused by Congo Red, with the phenotype reverted in the strains 13c_2 and 13c_2ci_6
- Mutant Δ*MGG_Utr2* exhibited hypersensitivity to cell wall stress caused by Caffeine (25 mM), with the phenotype reverted in complemented strain #5_6
- All mutant strains showed no phenotypic differences relative to WT during germling development and were equally pathogenic *in-planta*.

Chapter 6: Mutant Phenotyping- Cell Wall Elasticity, Topography & Composition

- Topography imaging by AFM showed similar cell wall surface in the vegetative hyphae of ΔΔ*MGG_Crh2_Utr2,* relative to WT
- Measurement of surface elasticity by AFM showed that ΔΔ*MGG_Crh2_Utr2* had reduced cell wall rigidity relative to WT
- Cell wall composition analysis by GC/EI-MS showed increased levels of total chitin in both Δ*MGG_Crh1* and ΔΔ*MGG_Crh2_Utr2* mutants relative to WT
- Mutant ΔΔ*MGG_Crh2_Utr2* showed reduced levels of 1,3-glucan in the AIF, with increased total glucan in the alkaline soluble fraction

Chapter 7: Gene Compensation & Localisation

- No change in the gene expression of five *Crh-like* genes in the background of all mutant lines when grown vegetatively under optimal conditions or oxidative stress
- Expression of *MGG_Utr2* was significantly upregulated three-fold in the Δ*MGG_Crh2* strain compared with that in WT. No changes in expression were seen in other genes in all other mutant lines
- MGG_Crh2 protein localisation by eGFP tagging revealed the strongest fluorescence in vegetative mycelium and protein is localised to the lateral cell wall and accumulates strongly in the septum and areas of polarised growth

8.2 Thesis Summary, Conclusion & Future Work

Recent years have seen growing interest in the fungal cell wall as a potential phylum-specific target for disease mitigation. In this regard, the aim is to describe the mechanisms which underpin wall construction and which endow it with sufficient plasticity to support expansion, growth and infection (Gow and Gadd 1995, Bowman and Free 2006, Klis *et al.* 2006). To achieve such plasticity, specialised groups of GPI-anchored glycosyltransferase (GST) proteins such as Gas1p/Gelp, (Mouyna *et al.* 2000), Crh1p (Pardini *et al.* 2006, Cabib *et al.* 2007), Dfg1p/Dcw5p (Kitagaki *et al.* 2002b) and Sps2p (Ecm33p) (Pardo *et al.* 2004) continuously remodel synthesised polysaccharides in response to changes in the external environment or with the developmental clock (Kitagaki *et al.* 2002a, Cabib *et al.* 2007, Hurtado-Guerrero *et al.* 2009, Calderon *et al.* 2010). Of the various GSTs, the *Crh*-like family became the focus of this thesis due to their importance in maintaining cell wall elasticity (Rodriguez-Pena *et al.* 2000, Dague *et al.* 2010) and their association with pathogen virulence (Pardini *et al.* 2006).

The first step, as described in Chapter 3, involved the identification of orthologous *Crh-like* genes in *M. oryzae* using sequences from *S. cerevisiae Crh1, Utr2,* and *Crr1*. Reciprocal Blast searches, multiple sequence alignment, promoter analysis, protein structure prediction as well as the construction of a maximum likelihood tree, revealed with confidence, five *M. oryzae Crh-like* genes. These genes are found in two clades, belonging to either the Crh1 Clade or the Crr1/Utr2 Clade, with the latter having a unique chitin binding domain. Three of the five genes (*MGG_Crh1, MGG_Crh2,* and *MGG_Utr2*) have the signatory cell

wall protein structures: GPI-anchor at the C-terminus, signal peptide cleavage site at the N-terminus and a Ser/Thr rich region.

Based on the *in silico* results in Chapter 3 and the literature reviewed in Chapter 1 showing the importance of *Crh* genes for cell wall integrity and virulence, the expression of these genes was measured by qRT-PCR in vegetative tissues grown under various stressors and at various stages of germling differentiation and infection. Expression was measured under cell wall stress imposed by two different types of compounds known to activate different routes of the CWI MAPK pathway (Caffeine and Congo Red). Additionally, as a comparison, expression in other growth conditions such as osmotic (Sorbitol), oxidative (H_2O_2), plasma membrane stress (SDS) and starvation tissues (MM) were also measured relative to growth in CM. Results revealed that *MGG_Crh2* and *MGG_Utr2,* from separate clades in the phylogenetic tree, had the highest levels of expression during vegetative growth, and were differentially upregulated under cell wall stress. *MGG_Crh1* expression was non-significantly regulated under any condition tested, while both *MGG_Crh3* and *MGG_Crh4* showed low transcript levels.

While *MGG_Crh2* only responded to cell wall stress imposed by Congo Red, *MGG_Utr2* responded to both Caffeine and Congo Red stress. Congo Red compound has been associated with the activation of the CWI via the Rlm1 pathway (Garcia et al. 2004), while Caffeine is associated with TOR1 (Reinke *et al.* 2006) and the cell-cycle regulator SBF complex (Swi4/Swi6) (Truman *et al.* 2009, Eriksson *et al.* 2011). Given that the SBF complex has been implicated as a cell-cycle regulator at the G1 phase (Koch *et al.* 1993, Breeden 2003), it is possible that *MGG_Utr2* may be more important for internal regulation than

MGG_Crh2. This variation in regulation begins to suggest the possibility of neo-functionalisation, especially since the unique chitin-binding domain in MGG_Utr2, not present in MGG_Crh2, has been shown in *S. cerevisiae* to have a specific function in forming disulphide bonds for protein folding and stability (Blanco et al. 2015).

An interesting discovery is that both *MGG_Utr2* and *MGG_Crh2* genes were significantly down-regulated ($p<0.05$) during infection and in vegetative mycelium grown under oxidative stress. The down-regulation of both tissue types may not be a co-incidence. Results shown in vegetative mycelium exposed to H_2O_2 stress suggests that the presence of host ROS may trigger the down-regulation of *M. oryzae Crh-like* genes. Studies have shown that Crh-like proteins in *C. albicans* and *A. fumigatus* are recognised by the host immune system as PAMPs (Stuehler *et al.* 2011a, Zelante *et al.* 2012, Jolink *et al.* 2013). It is possible that the fungus remodels the cell wall during infection by reducing the level of Crh proteins in *M. oryzae* to prevent host recognition, along with efforts of pathogen masking with α(1,2)-glucans as shown by Fujikawa *et al.* (2013). Therefore, albeit in contrary to initial hypothesis, it made logical sense to down-regulate these *M. oryzae Crh-like* genes. Gene expression results (Chapter 3) concur with the lack of phenotype seen in the corresponding knockout strains during germling development and the mutants being fully pathogenic.

Based on the *in silico* results and gene expression analyses in the above paragraphs, three genes were subsequently chosen for the generation of knockout strains by targeted homologous recombination. These are genes *MGG_Utr2, MGG_Crh1,* and *MGG_Crh2*, generating Δ*MGG_Crh1,* Δ*MGG_Crh2,* Δ*MGG_Utr2,* and the double knockout ΔΔ*MGG_Crh2_Utr2,* each

with two independent lines generated. Each mutant line was confirmed by PCR integration, Southern Blot as well as transcript absence by qRT-PCR. Additionally, revertant strains were generated in the background of Δ*MGG_Crh2* and Δ*MGG_Utr2*, using linearised plasmids containing the native promoter and coding regions, transformed by PEG-mediated ectopic insertion.

Outcome of the vegetative growth assays (plate and liquid biomass) were consistent with the qRT-PCR results in Chapter 3. Here, mutants with *MGG_Crh2* gene nulled exhibited hypersensitivity to Congo Red, while *MGG_Utr2* counterpart exhibited sensitivity to Caffeine. Both phenotypes were recovered in the revertant strains, 13c_2, and #5_6 respectively. Similarly, the *MGG_Crh1* expression profile showed no significant changes under any growth condition or at any stage of the life cycle, and this is reflected in the lack of phenotype seen in Δ*MGG_Crh1* in Chapter 5.

It was suspected that the phenotype seen when mutants were grown vegetatively under cell wall stress, could be attributed to changes in cell wall strength and rigidity. The cell wall perturbant Congo Red, shows a high affinity for glucan (Wood 1980), and thus competes with the cross-linking of chitin to glucan. As a result, Congo Red causes a reduction in cell wall rigidity and subsequent hyphal tip swelling due the inability of the weakened wall to withstand internal hydrostatic pressure (Pancaldi *et al.* 1984). A mutant with an already compromised cell wall would therefore, be more prone to tip swellings (i.e hypersensitivity). Therefore, an indication that a Congo Red hypersensitive mutant has altered cell wall rigidity is to test for phenotype recovery by osmo-remedial (prevention of hyphal tip swelling). This was the case for both Δ*MGG_Crh2* and ΔΔ*MGG_Crh2_Utr2* strains which showed hypersensitivity to

Congo Red with a significant ($p<0.05$) 30% reduction in growth that was partially reverted to WT by Sorbitol (1M). The hypothesis was further confirmed with the use of Atomic Force Microscopy (AFM) to measure surface elasticity in Chapter 6. Indeed, the double knockout strain ΔΔ*MGG_Crh2_Utr2* had significantly less rigid (softer) cell walls than WT. For future work, it would be worthwhile to test cell wall elasticity of the corresponding single knockout strains Δ*MGG_Crh2* and Δ*MGG_Utr2* to determine which gene is responsible for the change in wall elasticity.

It was speculated from results in Chapter 5 and Chapter 6 that this change in cell wall elasticity is attributed to the loss or reduction in cross-links between chitin and glucan chains. The specific glycosidic linkage involved in linking chitin to a (1,3)-glucan polymer would be 1,3,4-Glc*p*. Unfortunately, this linkage type is rare, occurring only once every 8000 glucan monomers in *S. cerevisiae* (Kollár *et al.* 1997). This means that the method of analysis, using gas chromatography with mass spectrometry (GC/EI-MS), could not effectively quantify the linkage type, and as shown in Chapter 6, this linkage was not detected even in the *M. oryzae* WT strain. However, it is possible to measure Crhp activity indirectly.

The function of Crhp can be assessed by measuring changes in the proportion of glucan in the ASF and AIF fraction of the mutant cell wall, relative to the WT. Glucan polymers, specifically 1,3-glucans, are water and alkaline soluble until they are cross-linked with chitin. When this happens, the chemical properties of the polymer change into an alkaline insoluble structure with added rigidity (Sietsma and Wessels 1981, Hartland *et al.* 1994). Therefore, when there is reduced cross-linking between chitin to glucan polymers, the proportion of glucan chains found in the ASF should be higher, with a reduction in the glucan

counterpart in AIF. This is appropriately seen in the cell wall composition of *Crh* mutants in both *S. cerevisiae* and *C. albicans* (Rodriguez-Pena *et al.* 2000, Pardini *et al.* 2006, Cabib *et al.* 2007). Using GC/EI-MS in combination with acid hydrolysis (total sugar) and polymer methylation-alditol acetate technique (linkage analysis) described in Chapter 6, it was revealed that significantly ($p<0.05$) more glucan was found in the ASF, with fewer 1,3-Glc*p* linkages in the AIF in the mutant ΔΔ*MGG_Crh2_Utr2*. This supports the hypothesis that changes in the elasticity of this mutant is due to a reduction on chitin-glucan cross links. This analysis should be repeated with both independent lines of ΔΔ*MGG_Crh2_Utr2* for consistency and the corresponding single knockout strains to show which genes contributed more in the cross-linking of polymers.

Another indication that *M. oryzae Crh-like* genes are important for cell wall integrity is the significant ($p<0.05$) up-regulation of total chitin in the cell wall of mutants by 20% relative to WT strain Guy11, shown in Chapter 6. An increase in chitin synthesis in wall-compromised mutants has also been observed in other fungal species and this is linked to a compensatory mechanism via activation of the CWI pathway (Popolo *et al.* 1997, Ram *et al.* 1998, Carotti *et al.* 2002). Importantly, the weak phenotype and full virulence seen even in the double knockout strain ΔΔ*MGG_Crh2_Utr2*, the increase in chitin synthesis and branching of (1,3)-glucan polymers at the Carbon 6 position, suggests a potential up-regulation of other cell wall proteins such as chitin synthases and Gelp in a compensatory manner. Chapter 7 attempted first to prioritise checking for gene compensation among the homologs of *Crh-like* genes. Given that results showed negative up-regulation of the homologs in the double knockout strain, it is suggested that future work should test for up-regulation in other cell wall proteins

and components of the CWI pathway, in the background of this mutant line. A transcriptomic approach such as RNA-seq, an approach successfully conducted in *M. oryzae* (Kawahara *et al.* 2012, Soanes *et al.* 2012, Gowda 2014), could be the appropriate strategy, followed with selecting a few key up-regulated genes for qRT-PCR analyses for a more accurate and reliable expression quantification.

Interestingly, an up-regulation of chitin content was not only seen in the double knockout strain, but also in the single knockout Δ*MGG_Crh1* strain. This is so despite the absence of a phenotype (Chapter 5) in the mutant strain Δ*MGG_Crh1* and the low expression of *MGG_Crh1* with no changes to the expression profile under various conditions or stages of the life cycle (Chapter3) in the WT strain. This suggests that *MGG_Crh1* does play a role in maintaining cell wall integrity perhaps under different regulatory factors not yet explored in this study, albeit of lowered importance relative to the homologue, *MGG_Crh2*. In the future, work should also include considerations of generating triple mutant lines comprising genes *MGG_Crh1, MGG_Crh2,* and *MGG_Utr2* deleted from the genome.

In agreement with the qRT-PCR results in Chapter 3, showing that the transcript levels of *Crh-like* genes were highest in vegetative tissues, protein localisation (Chapter 7) by tagging MGG_Crh2p with eGFP showed a similar outcome. The localisation of MGG_Crh2 to the lateral cell wall confirms the hypothesis made in Chapter 3 that this is indeed a cell wall protein. This study also showed that *M. oryzae* MGG_Crh2p accumulates to cell wall regions of polarised growth and to the septum, which overlaps with regions of high CFW staining shown in Chapter 5. Calcofluor White is a fluorescent dye with high affinity for chitin (Harrington and Hageage 2003). Therefore, the similarity in the

pattern of fluorescence seen suggests that MGG_Crhp co-localises to sites of chitin accumulation. This concurs with Crh-like protein localisation in other fungal species and further attests to the function of this enzyme in cross-linking of chitin to glucan.

Future work in protein localisation should include a co-localisation attempt between MGG_Crh2 and MGG_Utr2. This attempt was made in Chapter 4 using MGG_Utr2 tagged with mCherry. However, it was unsuccessful due to issues with the position of the chitin-binding domain in MGG_Utr2p located near the N-terminus. It is recommended in the future to try inserting the fluorescent protein at the C-terminus after the GH16 functional domain but before the predicted GPI-anchor site. More interestingly, perhaps it would be useful to co-localise MGG_Crh2p with another CWP, such as Gelp (syn Gas1p) and in various types of CWP mutant backgrounds. This could elucidate not only the localisation behaviour of Crh-like proteins but also the interaction with CWPs. Rolli *et al.* (2009) generated strains containing Gas1p-GFP in WT and in Δ*Crh1*Δ*Crh2* mutants and showed that Crh1p is responsible for immobilizing Gas1p to the chitin ring and bud scars.

Another area worth exploring in the future is to investigate the association between *M. oryzae* Crh-like proteins and the Crz1p/calcineurin pathway. Results from Chapter 3 promoter analysis of the *Crh-like* genes showed the presence of Crz1p DNA binding motif. This suggests that in a similar way to Crh-like proteins in yeast (Yoshimoto *et al.* 2002, Lagorce *et al.* 2003), orthologues in *M. oryzae* may be regulated by this transcription factor. In the model yeast *S. cerevisiae,* Ca^{2+}/calmodulin dependent phosphatase or calcineurin, mediate Ca^{2+} signalling and are important for cell viability through regulating responses to environmental

stress. Crucially, Lagorce *et al.* (2003) showed that the transcription factor motif for Crz1p frequently occurs in the cluster of genes associated with cell wall compensatory mechanisms, including *Crh1, Fks2, Chs3* and *Kre6* genes. As such, it would be interesting to investigate the regulatory response of *M. oryzae Crh-like* genes grown under Ca_{2+} stress in both WT and mutant lines.

The final suggestion towards expanding this work would be to generate double or triple deletion strains of different cell wall proteins in the *M. oryzae Crh-like* mutant strains. Work in this study showed the increase in the activity of chitin synthase and the cell wall remodelling protein Gelp, due to the increase in total chitin and glucan branching in the double knockout mutant. As such, it would be useful to conduct qRT-PCR gene expression analysis to identify which specific homologous *Chs* (seven in *M. oryzae*) and *Gel* (five in *M. oryzae*) that are upregulated in the mutant Δ*MGG_Crh2*. This could be followed by targeted homologous recombination of the respective *Chs* and *Gel* genes in the Δ*MGG_Crh2* background strain followed by phenotypic analysis and pathogenicity assay, thereby exploring the possibility of targeting multiple CWP in disease control.

The hypothesis developed at the beginning of this thesis was that the *Crh-like* genes in *M. oryzae,* the causal agent of Rice Blast disease, are important for cell wall integrity and pathogen virulence.

In conclusion, key findings from this thesis indicate that the *Crh-like* gene family in *M. oryzae* is indeed important for cell wall integrity and elasticity but dispensable for fungal pathogenicity. Unexpectedly, contrary to the counterpart in *C. albicans* (Pardini *et al.* 2006), this gene family proved not important for virulence and could be attributable to a compensatory mechanism by other cell wall proteins. Therefore, while targeting *Crh-like* gene family alone may prove ineffective in disease control, an antifungal compound that confers disease control by disrupting multiple components of the cell wall compensatory mechanism could prove useful and worth exploring in the future.

Reference List

Abascal, F., R. Zardoya and D. Posada (2005). "*ProtTest: selection of best-fit models of protein evolution*." Bioinformatics **21**(9): 2104-2105.

Aguilar-Uscanga, B. and J. Francois (2003). "*A study of the yeast cell wall composition and structure in response to growth conditions and mode of cultivation*." Letters in applied microbiology **37**(3): 268-274.

Ahimou, F., A. Touhami and Y. F. Dufrêne (2003). "*Real-time imaging of the surface topography of living yeast cells by atomic force microscopy*." Yeast **20**(1): 25-30.

Aimanianda, V., C. Clavaud, C. Simenel, T. Fontaine, M. Delepierre and J. P. LatgÈ (2009). "*Cell Wall Beta-(1, 6)-Glucan of Saccharomyces cerevisiae*." Journal of Biological Chemistry **284**(20): 13401.

Alberti-Segui, C., A. J. Morales, H. Xing, M. M. Kessler, D. A. Willins, K. G. Weinstock, G. Cottarel, K. Fechtel and B. Rogers (2004). "*Identification of potential cell surface proteins in Candida albicans and investigation of the role of a putative cell surface glycosidase in adhesion and virulence*." Yeast **21**(4): 285-302.

Alonso-Monge, R., F. Navarro-García, E. Román, A. Negredo, B. Eisman, C. Nombela and J. Pla (2003). "*The Hog1 mitogen-activated protein kinase is essential in the oxidative stress response and chlamydospore formation in Candida albicans*." Eukaryotic cell **2**(2): 351-361.

Alonso-Monge, R., E. Román, D. Arana, J. Pla and C. Nombela (2009). "*Fungi sensing environmental stress*." Clinical Microbiology and Infection **15**(s1): 17-19.

Altschul, S. F., W. Gish, W. Miller, E. W. Myers and D. J. Lipman (1990). "*Basic local alignment search tool*." Journal of molecular biology **215**(3): 403-410.

Apoga, D. and H.-B. Jansson (2000). "*Visualization and characterization of the extracellular matrix of Bipolaris sorokiniana*." Mycological Research **104**(05): 564-575.

Arana, D. M., C. Nombela, R. Alonso-Monge and J. Pla (2005). "*The Pbs2 MAP kinase kinase is essential for the oxidative-stress response in the fungal pathogen Candida albicans*." Microbiology **151**(4): 1033-1049.

Arbelet, D., P. Malfatti, E. SimondCote, T. Fontaine, L. Desquilbet, D. Expert, C. Kunz and M. C. Soulie (2010). "*Disruption of the Bcchs3a chitin synthase gene in Botrytis cinerea is responsible for altered adhesion and overstimulation of host plant immunity*." Molecular plant-microbe interactions **23**(10): 1324-1334.

Arroyo, J., J. Sarfati, M. T. Baixench, E. Ragni, M. Guillen, J. M. Rodriguez Pena, L. Popolo and J. P. Latge (2007). "*The GPI anchored Gas and Crh families are fungal antigens*." Yeast **24**(4): 289-296.

Aylon, Y. and M. Kupiec (2004). "*DSB repair: the yeast paradigm*." DNA repair **3**(8): 797-815.

Babujee, L. and S. Gnanamanickam (2000). "*Molecular tools for characterization of rice blast pathogen (Magnaporthe grisea) population and molecular marker-assisted breeding for disease resistance*." Current Science-Bangalore **78**(3): 248-257.

Baetz, K., J. Moffat, J. Haynes, M. Chang and B. Andrews (2001). "*Transcriptional coregulation by the cell integrity mitogen-activated protein kinase Slt2 and the cell cycle regulator Swi4*." Molecular and cellular biology **21**(19): 6515-6528.

Balhadere, P. V., A. J. Foster and N. J. Talbot (1999). "*Identification of pathogenicity mutants of the rice blast fungus Magnaporthe grisea by insertional mutagenesis*." Molecular plant-microbe interactions **12**(2): 129-142.

Barattin, R. and N. Voyer (2008). "*Chemical modifications of AFM tips for the study of molecular recognition events*." Chemical Communications(13): 1513-1532.

Barbeyron, T., A. Gerard, P. Potin, B. Henrissat and B. Kloareg (1998). "*The kappa-carrageenase of the marine bacterium Cytophaga drobachiensis. Structural and phylogenetic relationships within family-16 glycoside hydrolases*." Molecular biology and evolution **15**(5): 528.

Baumann, M. J., J. M. Eklöf, G. Michel, Å. M. Kallas, T. T. Teeri, M. Czjzek and H. Brumer (2007). "*Structural evidence for the evolution of xyloglucanase activity from xyloglucan endo-transglycosylases: biological implications for cell wall metabolism*." The Plant Cell Online **19**(6): 1947-1963.

Beauvais, A., C. Schmidt, S. Guadagnini, P. Roux, E. Perret, C. Henry, S. Paris, A. Mallet, M. C. Prévost and J. P. Latgé (2007). "*An extracellular matrix glues together the aerial-grown hyphae of Aspergillus fumigatus*." Cellular Microbiology **9**(6): 1588-1600.

Bernard, M. and J. P. Latgé (2001). "*Aspergillus fumigatus cell wall: composition and biosynthesis*." Medical Mycology **39**(1): 9-17.

Binnig, G., C. F. Quate and C. Gerber (1986). "*Atomic force microscope*." Physical review letters **56**(9): 930.

Björndal, H., C. G. Hellerqvist, B. Lindberg and S. Svensson (1970). "*Gas-Liquid Chromatography and Mass Spectrometry in Methylation Analysis of Polysaccharides*." Angewandte Chemie International Edition in English **9**(8): 610-619.

Blach, J., W. Loughlin, G. Watson and S. Myhra (2001). "*Surface characterization of human hair by atomic force microscopy in the imaging and F-d modes*." International journal of cosmetic science **23**(3): 165-174.

Blackwell, M. (2011). "*The Fungi: 1, 2, 3… 5.1 million species?*" American Journal of Botany **98**(3): 426-438.

Blakeney, A. B., P. J. Harris, R. J. Henry and B. A. Stone (1983). "*A simple and rapid preparation of alditol acetates for monosaccharide analysis*." Carbohydrate research **113**(2): 291-299.

Blanco, N., M. Reidy, J. Arroyo and E. Cabib (2012). "*Crosslinks in the cell wall of budding yeast control morphogenesis at the mother–bud neck*." Journal of cell science **125**(23): 5781-5789.

Blanco, N., A. B. Sanz, J. M. Rodríguez-P, C. Nombela, V. Farkaš, R. Hurtado-Guerrero and J. Arroyo (2014). "*Structural and Functional Analysis of yeast Crh1 and Crh2 Transglycosylases*." Febs Journal.

Blanco, N., A. B. Sanz, J. M. Rodríguez-Peña, C. Nombela, V. Farkaš, R. Hurtado-Guerrero and J. Arroyo (2015). "*Structural and functional analysis of yeast Crh1 and Crh2 transglycosylases*." Febs Journal.

Blobel, G. and B. Dobberstein (1975). "*Transfer of proteins across membranes. I. Presence of proteolytically processed and unprocessed nascent immunoglobulin light chains on membrane-bound ribosomes of murine myeloma*." The Journal of cell biology **67**(3): 835-851.

Boisramé, A., A. Cornu, G. Da Costa and M. L. Richard (2011). "*Unexpected role for a serine/threonine-rich domain in the Candida albicans Iff protein family*." Eukaryotic cell **10**(10): 1317-1330.

Bolton, M. D., J. A. Kolmer and D. F. Garvin (2008). "*Wheat leaf rust caused by Puccinia triticina*." Molecular plant pathology **9**(5): 563-575.

Boorsma, A., H. d. Nobel, B. t. Riet, B. Bargmann, S. Brul, K. J. Hellingwerf and F. M. Klis (2004). "*Characterization of the transcriptional response to cell wall stress in Saccharomyces cerevisiae*." Yeast **21**(5): 413-427.

Boraston, A., D. Bolam, H. Gilbert and G. Davies (2004). "*Carbohydrate-binding modules: fine-tuning polysaccharide recognition*." Biochem. J **382**: 769-781.

Borkovich, K. A., L. A. Alex, O. Yarden, M. Freitag, G. E. Turner, N. D. Read, S. Seiler, D. Bell-Pedersen, J. Paietta and N. Plesofsky (2004). "*Lessons from the genome sequence of Neurospora crassa: tracing the path from genomic blueprint to multicellular organism*." Microbiology and Molecular Biology Reviews **68**(1): 1-108.

Both, M., M. Csukai, M. P. H. Stumpf and P. D. Spanu (2005). "*Gene expression profiles of Blumeria graminis indicate dynamic changes to primary metabolism during development of an obligate biotrophic pathogen*." The Plant Cell Online **17**(7): 2107-2122.

Bowman, S. M. and S. J. Free (2006). "*The structure and synthesis of the fungal cell wall*." Bioessays **28**(8): 799-808.

Bowman, S. M., A. Piwowar, M. Al Dabbous, J. Vierula and S. J. Free (2006). "*Mutational analysis of the glycosylphosphatidylinositol (GPI) anchor pathway demonstrates that GPI-anchored proteins are required for cell wall biogenesis and normal hyphal growth in Neurospora crassa*." Eukaryotic cell **5**(3): 587.

Breeden, L. L. (2003). "*Periodic transcription: a cycle within a cycle*." Current Biology **13**(1): R31-R38.

Brinkman, H.-J., S. de Pee, I. Sanogo, L. Subran and M. W. Bloem (2010). "*High food prices and the global financial crisis have reduced access to nutritious food and worsened nutritional status and health*." The Journal of nutrition **140**(1): 153S-161S.

Broad Institute. "*Magnaporthe comparative sequencing project*." 2015, from http://www.broadinstitute.org/.

Broad Institute. (2009). "Fungal Orthogroups Repository." Search Orthogroups, 2014, from http://www.broadinstitute.org/regev/orthogroups/.

Broad Institute. (2015). "Fungal Genome Initiative." 2015, from http://www.broadinstitute.org.

Bustin, S. (2002). "*Quantification of mRNA using real-time reverse transcription PCR (RT-PCR): trends and problems*." Journal of molecular endocrinology **29**(1): 23-39.

Bustin, S. A., V. Benes, J. A. Garson, J. Hellemans, J. Huggett, M. Kubista, R. Mueller, T. Nolan, M. W. Pfaffl and G. L. Shipley (2009). "*The MIQE guidelines: minimum information for publication of quantitative real-time PCR experiments*." Clinical chemistry **55**(4): 611-622.

Bustin, S. A. and T. Nolan (2004). "*Pitfalls of quantitative real-time reverse-transcription polymerase chain reaction*." Journal of biomolecular techniques: JBT **15**(3): 155.

Cabib, E. (2009). "*Two Novel Techniques for Determination of Polysaccharide Cross-Links Show that Crh1p and Crh2p Attach Chitin to both Beta(1-6)-and Beta(1-3) Glucan in the Saccharomyces cerevisiae Cell Wall*." Eukaryotic cell **8**(11): 1626.

Cabib, E. and J. Arroyo (2013). "*How carbohydrates sculpt cells: chemical control of morphogenesis in the yeast cell wall*." Nature Reviews Microbiology **11**(9): 648-655.

Cabib, E., N. Blanco, C. Grau, J. M. Rodriguez Pena and J. Arroyo (2007). "*Crh1p and Crh2p are required for the cross linking of chitin to (1 6) glucan in the Saccharomyces cerevisiae cell wall*." Molecular microbiology **63**(3): 921-935.

Cabib, E., V. Farkas, O. KosÌk, N. Blanco, J. Arroyo and P. McPhie (2008). "*Assembly of the yeast cell wall*." Journal of Biological Chemistry **283**(44): 29859.

Cabib, E., D.-H. Roh, M. Schmidt, L. B. Crotti and A. Varma (2001). "*The yeast cell wall and septum as paradigms of cell growth and morphogenesis*." Journal of Biological Chemistry **276**(23): 19679-19682.

Calderon, J., M. Zavrel, E. Ragni, W. A. Fonzi, S. Rupp and L. Popolo (2010). "*PHR1, a pH-regulated gene of Candida albicans encoding a glucan-remodelling enzyme, is required for adhesion and invasion*." Microbiology **156**(8): 2484-2494.

Cantarel, B. L., P. M. Coutinho, C. Rancurel, T. Bernard, V. Lombard and B. Henrissat (2009). "*The Carbohydrate-Active EnZymes database (CAZy): an expert resource for glycogenomics*." Nucleic acids research **37**(suppl 1): D233-D238.

Cappella, B., P. Baschieri, C. Frediani, P. Miccoli and C. Ascoli (1997). "*Force-distance curves by AFM*." Engineering in Medicine and Biology Magazine, IEEE **16**(2): 58-65.

Cappellaro, C., V. Mrsa and W. Tanner (1998). "*New Potential Cell Wall Glucanases of Saccharomyces cerevisiae and Their Involvement in Mating*." Journal of Bacteriology **180**(19): 5030-5037.

Carbó, N. and J. Pérez-Martín (2010). "*Activation of the cell wall integrity pathway promotes escape from G2 in the fungus Ustilago maydis*." PLoS genetics **6**(7): e1001009.

Caro, L., H. Tettelin, J. H. Vossen, A. F. Ram, H. Van Den Ende and F. M. Klis (1997). "*In silicio identification of glycosyl-phosphatidylinositol-anchored plasma-membrane and cell wall proteins of Saccharomyces cerevisiae*." Yeast **13**: 1477-1489.

Carotti, C., L. Ferrario, C. Roncero, M. Valdivieso, A. Duran and L. Popolo (2002). "*Maintenance of cell integrity in the gas1 mutant of Saccharomyces cerevisiae requires the Chs3p-targeting and activation pathway and involves an unusual Chs3p localization*." Yeast **19**(13): 1113-1124.

Cartharius, K., K. Frech, K. Grote, B. Klocke, M. Haltmeier, A. Klingenhoff, M. Frisch, M. Bayerlein and T. Werner (2005). "*MatInspector and beyond: promoter analysis based on transcription factor binding sites*." Bioinformatics **21**(13): 2933-2942.

Cerqueira, G. C., M. B. Arnaud, D. O. Inglis, M. S. Skrzypek, G. Binkley, M. Simison, S. R. Miyasato, J. Binkley, J. Orvis and P. Shah (2013). "*The Aspergillus Genome Database: multispecies curation and incorporation of RNA-Seq data to improve structural gene annotations*." Nucleic acids research: gkt1029.

Chaffin, W. L. J. (2008). "*Candida albicans cell wall proteins*." Microbiology and Molecular Biology Reviews **72**(3): 495.

Chen, J., W. Zheng, S. Zheng, D. Zhang, W. Sang, X. Chen, G. Li, G. Lu and Z. Wang (2008). "*Rac1 is required for pathogenicity and Chm1-dependent conidiogenesis in rice fungal pathogen Magnaporthe grisea*." PLoS pathogens **4**(11): e1000202.

Cherry, J. M., E. L. Hong, C. Amundsen, R. Balakrishnan, G. Binkley, E. T. Chan, K. R. Christie, M. C. Costanzo, S. S. Dwight and S. R. Engel (2011). "*Saccharomyces Genome Database: the genomics resource of budding yeast*." Nucleic acids research: gkr1029.

Chesters, C. and A. Bull (1963). "*The enzymic degradation of laminarin. 2. The multicomponent nature of fungal laminarinases*." Biochemical Journal **86**(1): 31.

Choquer, M., M. Boccara, I. R. Goncalves, M. C. Soulie and A. Vidal-Cros (2004). "*Survey of the Botrytis cinerea chitin synthase multigenic family through the analysis of six euascomycetes genomes*." European Journal of Biochemistry **271**(11): 2153-2164.

Cinelli, R., A. Ferrari, V. Pellegrini, M. Tyagi, M. Giacca and F. Beltram (2000). "*The Enhanced Green Fluorescent Protein as a Tool for the Analysis of Protein Dynamics and Localization: Local Fluorescence Study at the Single-molecule Level*." Photochemistry and photobiology **71**(6): 771-776.

Ciucanu, I. and F. Kerek (1984). "*A simple and rapid method for the permethylation of carbohydrates*." Carbohydrate research **131**(2): 209-217.

Coronado, J. E., S. Mneimneh, S. L. Epstein, W. G. Qiu and P. N. Lipke (2007). "*Conserved processes and lineage-specific proteins in fungal cell wall evolution*." Eukaryotic cell **6**(12): 2269-2277.

Couch, B. C., I. Fudal, M. H. Lebrun, D. Tharreau, B. Valent, P. Van Kim, J. L. Notteghem and L. M. Kohn (2005). "*Origins of host-specific populations of the blast pathogen Magnaporthe oryzae in crop domestication with subsequent expansion of pandemic clones on rice and weeds of rice*." Genetics **170**(2): 613.

Couch, B. C. and L. M. Kohn (2002). "*A multilocus gene genealogy concordant with host preference indicates segregation of a new species, Magnaporthe oryzae, from M. grisea*." Mycologia **94**(4): 683-693.

Cuéllar-Cruz, M., M. Briones-Martin-del-Campo, I. Cañas-Villamar, J. Montalvo-Arredondo, L. Riego-Ruiz, I. Castaño and A. De Las Peñas (2008). "*High resistance to oxidative stress in the fungal pathogen Candida glabrata is mediated by a single catalase, Cta1p, and is controlled by the transcription factors Yap1p, Skn7p, Msn2p, and Msn4p*." Eukaryotic cell **7**(5): 814-825.

Cunningham, W. and D. Manners (1964). "*Studies on carbohydrate-metabolizing enzymes. 11. The hydrolysis of lichenin by enzyme preparations from malted barley and Rhizopus arrhizus*." Biochemical Journal **90**(3): 596.

Czechowski, T., R. P. Bari, M. Stitt, W. Ä. d. Scheible and M. K. Udvardi (2004). "*Real-time RT-PCR profiling of over 1400 Arabidopsis transcription factors: unprecedented sensitivity reveals novel root-and shoot-specific genes*." The Plant Journal **38**(2): 366-379.

Dague, E., D. Alsteens, J.-P. Latgé and Y. F. Dufrêne (2008). "*High-resolution cell surface dynamics of germinating Aspergillus fumigatus conidia*." Biophysical journal **94**(2): 656-660.

Dague, E., R. Bitar, H. Ranchon, F. Durand, H. M. Yken and J. M. Francois (2010). "*An atomic force microscopy analysis of yeast mutants defective in cell wall architecture*." Yeast **27**(8): 673-684.

Dallies, N., J. Francois and V. Paquet (1998). "*A new method for quantitative determination of polysaccharides in the yeast cell wall. Application to the cell wall defective mutants of Saccharomyces cerevisiae*." Yeast **14**(14): 1297-1306.

De Groot, P. W., A. F. Ram and F. M. Klis (2005). "*Features and functions of covalently linked proteins in fungal cell walls*." Fungal Genetics and Biology **42**(8): 657-675.

de Groot, P. W., C. Ruiz, C. R. Vázquez de Aldana, E. Dueñas, V. J. Cid, F. Del Rey, J. Rodríquez-Peña, P. Pérez, A. Andel and J. Caubín (2001a). "*A genomic approach for the identification and classification of genes involved in cell wall formation and its regulation in Saccharomyces cerevisiae*." Comparative and functional genomics **2**(3): 124-142.

de Groot, P. W., C. Ruiz, C. R. Vázquez de Aldana, E. Dueñas, V. J. Cid, F. Del Rey, J. M. Rodríquez-Peña, P. Pérez, A. Andel and J. Caubín (2001b). "*A genomic approach for the identification and classification of genes involved in cell wall formation and its regulation in Saccharomyces cerevisiae*." Comparative and functional genomics **2**(3): 124-142.

de Nobel, H., C. Ruiz, H. Martin, W. Morris, S. Brul, M. Molina and F. M. Klis (2000). "*Cell wall perturbation in yeast results in dual phosphorylation of the Slt2/Mpk1 MAP kinase and in an Slt2-mediated increase in FKS2–lacZ expression, glucanase resistance and thermotolerance*." Microbiology **146**(9): 2121-2132.

Dean, R., J. A. Van Kan, Z. A. Pretorius, K. E. Hammond-Kosack, A. Di Pietro, P. D. Spanu, J. J. Rudd, M. Dickman, R. Kahmann and J. Ellis (2012). "*The Top 10 fungal pathogens in molecular plant pathology*." Molecular plant pathology **13**(4): 414-430.

Dean, R. A., N. J. Talbot, D. J. Ebbole, M. L. Farman, T. K. Mitchell, M. J. Orbach, M. Thon, R. Kulkarni, J. R. Xu and H. Pan (2005). "*The genome sequence of the rice blast fungus Magnaporthe grisea*." Nature **434**(7036): 980-986.

Denning, D. W. (2003). "*Echinocandin antifungal drugs*." The Lancet **362**(9390): 1142-1151.

Dixon, K. P., J.-R. Xu, N. Smirnoff and N. J. Talbot (1999). "*Independent signaling pathways regulate cellular turgor during hyperosmotic stress and appressorium-mediated plant infection by Magnaporthe grisea*." The Plant Cell Online **11**(10): 2045-2058.

Doss, R. P. (1999). "*Composition and enzymatic activity of the extracellular matrix secreted by germlings of Botrytis cinerea*." Applied and environmental microbiology **65**(2): 404-408.

Douglas, C. (2001). "*Fungal fl (1, 3)-D-glucan synthesis*." Medical Mycology **39**(1): 55-66.

Dubois, M., K. A. Gilles, J. K. Hamilton, P. Rebers and F. Smith (1956). "*Colorimetric method for determination of sugars and related substances*." Analytical chemistry **28**(3): 350-356.

Dufrêne, Y. F. (2008). "*Towards nanomicrobiology using atomic force microscopy*." Nature Reviews Microbiology **6**(9): 674-680.

Dufrêne, Y. F., C. J. Boonaert, P. A. Gerin, M. Asther and P. G. Rouxhet (1999). "*Direct Probing of the Surface Ultrastructure and Molecular Interactions of Dormant and Germinating Spores of Phanerochaete chrysosporium*." Journal of Bacteriology **181**(17): 5350-5354.

Dupres, V., D. Alsteens, S. Wilk, B. Hansen, J. J. Heinisch and Y. F. Dufrêne (2009). "*The yeast Wsc1 cell surface sensor behaves like a nanospring in vivo*." Nature chemical biology **5**(11): 857-862.

Eisenhaber, B., G. Schneider, M. Wildpaner and F. Eisenhaber (2004). "*A Sensitive Predictor for Potential GPI Lipid Modification Sites in Fungal Protein Sequences and its Application to Genome-wide Studies for Aspergillus nidulans, Candida albicans Neurospora crassa, Saccharomyces cerevisiae and Schizosaccharomyces pombe*." Journal of molecular biology **337**(2): 243-253.

El Gueddari, N. E., U. Rauchhaus, B. M. Moerschbacher and H. B. Deising (2002). "*Developmentally regulated conversion of surface-exposed chitin to chitosan in cell walls of plant pathogenic fungi*." New Phytologist **156**(1): 103-112.

Elorza, M. V., H. Rico and R. Sentandrew (1983). "*Calcofluor white alters the assembly of chitin fibrils in Saccharomyces cerevisiae and Candida albicans cells*." Journal of general microbiology **129**(5): 1577-1582.

Emad, A., W. F. Heinz, M. D. Antonik, N. P. D'Costa, S. Nageswaran, C.-A. Schoenenberger and J. H. Hoh (1998). "*Relative microelastic mapping of living cells by atomic force microscopy*." Biophysical journal **74**(3): 1564-1578.

Engel, J., P. S. Schmalhorst and F. H. Routier (2012). "*Biosynthesis of the fungal cell wall polysaccharide galactomannan requires intraluminal GDP-mannose*." Journal of Biological Chemistry **287**(53): 44418-44424.

Eriksson, O. E. (2009). "*Ascomycota*." eLS.

Eriksson, P., D. Ganguli and D. J. Clark (2011). "*Spt10 and Swi4 control the timing of histone H2A/H2B gene activation in budding yeast*." Molecular and cellular biology **31**(3): 557-572.

Erni, R., M. D. Rossell, C. Kisielowski and U. Dahmen (2009). "*Atomic-resolution imaging with a sub-50-pm electron probe*." Physical review letters **102**(9): 096101.

Fankhauser, N. and P. Mäser (2005). "*Identification of GPI anchor attachment signals by a Kohonen self-organizing map*." Bioinformatics **21**(9): 1846-1852.

Fehser, S. and B. M. Moerschbacher (2011). "*Expression of green fluorescent protein in the obligately biotrophic fungal plant pathogen Puccinia graminis f. sp. tritici*." Journal for Plant Diseases and Plant Protection (JPDP) **6**(117): 258-260.

Fisher, M. C., D. A. Henk, C. J. Briggs, J. S. Brownstein, L. C. Madoff, S. L. McCraw and S. J. Gurr (2012). "*Emerging fungal threats to animal, plant and ecosystem health*." Nature **484**(7393): 186-194.

Fleet, G. H. (1985). *Composition and structure of yeast cell walls*. Current Topics in Medical Mycology, Springer**:** 24-56.

Fontaine, T., C. Simenel, G. Dubreucq, O. Adam, M. Delepierre, J. Lemoine, C. E. Vorgias, M. Diaquin and J.-P. Latgé (2000). "*Molecular organization of the alkali-insoluble fraction of Aspergillus fumigatus cell wall*." Journal of Biological Chemistry **275**(36): 27594-27607.

Fonzi, W. A. (1999). "*PHR1 and PHR2 of Candida albicans Encode Putative Glycosidases Required for Proper Cross-Linking of β-1, 3-and β-1, 6-Glucans*." Journal of Bacteriology **181**(22): 7070-7079.

François, J. M. (2006). "*A simple method for quantitative determination of polysaccharides in fungal cell walls*." Nature protocols **1**(6): 2995-3000.

Francois, J. M., C. Formosa, M. Schiavone, F. Pillet, H. Martin-Yken and E. Dague (2013). "*Use of atomic force microscopy (AFM) to explore cell wall properties and response to stress in the yeast Saccharomyces cerevisiae*." Current genetics **59**(4): 187-196.

Free, S. J. (2013). "*Fungal cell wall organization and biosynthesis*." Adv Genet **81**: 33-82.

Freitag, J., D. Lanver, C. Bohmer, K. O. Schink, M. Bolker and B. Sandrock (2011). "*Septation of Infectious Hyphae Is Critical for Appressoria Formation and Virulence in the Smut Fungus Ustilago Maydis*." PLoS pathogens **7**(5): e1002044.

Fuchs, B. B. and E. Mylonakis (2009). "*Our paths might cross: the role of the fungal cell wall integrity pathway in stress response and cross talk with other stress response pathways*." Eukaryotic cell **8**(11): 1616-1625.

Fujikawa, T., Y. Kuga, S. Yano, A. Yoshimi, T. Tachiki, K. Abe and M. Nishimura (2009). "*Dynamics of cell wall components of Magnaporthe grisea during infectious structure development*." Molecular microbiology **73**(4): 553-570.

Garcia, R., C. Bermejo, C. Grau, R. Perez, J. M. Rodriguez-Pena, J. Francois, C. s. Nombela and J. Arroyo (2004). "*The global transcriptional response to transient cell wall damage in Saccharomyces cerevisiae and its regulation by the cell integrity signaling pathway*." Journal of Biological Chemistry **279**(15): 15183-15195.

Gastebois, A., C. Clavaud, V. Aimanianda and J.-P. Latgé (2009). "*Aspergillus fumigatus: cell wall polysaccharides, their biosynthesis and organization*." Future microbiology **4**(5): 583-595.

Georgopapadakou, N. H. and J. S. Tkacz (1995). "*The fungal cell wall as a drug target*." Trends in microbiology **3**(3): 98-104.

Gerik, K. J., M. J. Donlin, C. E. Soto, A. M. Banks, I. R. Banks, M. A. Maligie, C. P. Selitrennikoff and J. K. Lodge (2005). "*Cell wall integrity is dependent on the PKC1 signal transduction pathway in Cryptococcus neoformans*." Molecular microbiology **58**(2): 393-408.

Gerland, P., A. E. Raftery, H. Ševčíková, N. Li, D. Gu, T. Spoorenberg, L. Alkema, B. K. Fosdick, J. Chunn and N. Lalic (2014). "*World population stabilization unlikely this century*." Science **346**(6206): 234-237.

Giessibl, F. J. (2003). "*Advances in atomic force microscopy*." Reviews of modern physics **75**(3): 949.

Goldman, R. C., P. A. Sullivan, D. Zakula and J. O. Capobianco (1995). "*Kinetics of β-1, 3 Glucan Interaction at the Donor and Acceptor Sites of the Fungal Glucosyltransferase Encoded by the BGL2 Gene*." European Journal of Biochemistry **227**(1-2): 372-378.

Gómez-Esquer, F., J. M. Rodríguez-Peña, G. Díaz, E. Rodriguez, P. Briza, C. Nombela and J. Arroyo (2004). "*CRR1, a gene encoding a putative transglycosidase, is required for proper spore wall assembly in Saccharomyces cerevisiae*." Microbiology **150**(10): 3269-3280.

Gómez-Miranda, B., A. Prieto, J. A. Leal, O. Ahrazem, J. Jiménez-Barbero and M. Bernabé (2003). "*Differences among the cell wall galactomannans from Aspergillus wentii and Chaetosartorya chrysella and that of Aspergillus fumigatus*." Glycoconjugate journal **20**(4): 239-246.

Gow, N. A. R. and G. M. Gadd (1995). *The growing fungus*, Springer.

Gowda, M. (2014). *Genome and Transcriptome Analyses of Indian Isolates of Rice Blast Fungus, Magnaporthe oryzae*. PAG Asia 2014, Plant and Animal Genome.

Guenin, S., M. Mauriat, J. Pelloux, O. Van Wuytswinkel, C. Bellini and L. Gutierrez (2009). "*Normalization of qRT-PCR data: the necessity of adopting a systematic, experimental conditions-specific, validation of references*." Journal of experimental botany **60**(2): 487-493.

Guerriero, G., L. Silvestrini, M. Obersriebnig, M. Salerno, D. Pum and J. Strauss (2013). "*Sensitivity of Aspergillus nidulans to the Cellulose Synthase Inhibitor Dichlobenil: Insights from Wall-Related Genes' Expression and Ultrastructural Hyphal Morphologies*." PloS one **8**(11): e80038.

Guo, M., Y. Chen, Y. Du, Y. Dong, W. Guo, S. Zhai, H. Zhang, S. Dong, Z. Zhang and Y. Wang (2011). "*The bZIP transcription factor MoAP1 mediates the*

oxidative stress response and is critical for pathogenicity of the rice blast fungus Magnaporthe oryzae." PLoS pathogens **7**(2): e1001302.

Gustin, M. C., J. Albertyn, M. Alexander and K. Davenport (1998). "*MAP Kinase Pathways in the Yeast Saccharomyces cerevisiae*." Microbiology and Molecular Biology Reviews **62**(4): 1264-1300.

Gutierrez, L., M. Mauriat, S. Guenin, J. Pelloux, J. F. Lefebvre, R. Louvet, C. Rusterucci, T. Moritz, F. Guerineau and C. Bellini (2008). "*The lack of a systematic validation of reference genes: a serious pitfall undervalued in reverse transcription-polymerase chain reaction (RT-PCR) analysis in plants*." Plant biotechnology journal **6**(6): 609-618.

Gwyddion. (2014). "Gwyddion-Free SPM (AFM, SNOM/NSOM, STM, MFM ...) data analysis software." 2014, from http://gwyddion.net/.

Haiyan, H., Z. Jieyun, Z. Kangle and L. Mingjiu (2012). "*Characterization of differentially expressed genes induced by virulent and avirulent Magnaporthe grisea strains in rice*." Plant Omics **5**(6): 542-546.

Hamada, K., S. Fukuchi, M. Arisawa, M. Baba and K. Kitada (1998). "*Screening for glycosylphosphatidylinositol (GPI)-dependent cell wall proteins in Saccharomyces cerevisiae*." Molecular and General Genetics MGG **258**(1-2): 53-59.

Hamel, L.-P., M.-C. Nicole, S. Duplessis and B. E. Ellis (2012). "*Mitogen-activated protein kinase signaling in plant-interacting fungi: distinct messages from conserved messengers*." The Plant Cell Online **24**(4): 1327-1351.

Hardison, S. E. and G. D. Brown (2012). "*C-type lectin receptors orchestrate antifungal immunity*." Nature immunology **13**(9): 817-822.

Harrington, B. J. and G. J. Hageage (2003). "*Calcofluor white: a review of its uses and applications in clinical mycology and parasitology*." Lab Medicine **34**(5): 361-367.

Hartland, R. P., C. A. Vermeulen, J. H. Sietsma, J. G. Wessels and F. M. Klis (1994). "*The linkage of (1–3)-β-glucan to chitin during cell wall assembly in Saccharomyces cerevisiae*." Yeast **10**(12): 1591-1599.

Hashimoto, H. (2006). "*Recent structural studies of carbohydrate-binding modules*." Cellular and Molecular Life Sciences CMLS **63**(24): 2954-2967.

Hawksworth, D. (2001). "*The magnitude of fungal diversity: the 1· 5 million species estimate revisited*." Mycological Research **105**(12): 1422-1432.

Hawksworth, D. L. (1991). "*The fungal dimension of biodiversity: magnitude, significance, and conservation*." Mycological Research **95**(6): 641-655.

Hawser, S., G. Baillie and L. J. Douglas (1998). "*Production of extracellular matrix by Candida albicans biofilms*." Journal of medical microbiology **47**(3): 253-256.

Heinz, W. F. and J. H. Hoh (1999). "*Spatially resolved force spectroscopy of biological surfaces using the atomic force microscope*." Trends in biotechnology **17**(4): 143-150.

Hellemans, J., G. Mortier, A. De Paepe, F. Speleman and J. Vandesompele (2007). "*qBase relative quantification framework and software for management and automated analysis of real-time quantitative PCR data*." Genome biology **8**(2): R19.

Hertz, H. (1881). "*On the contact of elastic solids*." J. reine angew. Math **92**(156-171): 110.

Hibbett, D. S., M. Binder, J. F. Bischoff, M. Blackwell, P. F. Cannon, O. E. Eriksson, S. Huhndorf, T. James, P. M. Kirk and R. Lucking (2007). "*A higher-level phylogenetic classification of the Fungi*." Mycological Research **111**(5): 509-547.

Hinterdorfer, P. and Y. F. Dufrêne (2006). "*Detection and localization of single molecular recognition events using atomic force microscopy*." Nature methods **3**(5): 347-355.

Hoch, H., C. Galvani, D. Szarowski and J. Turner (2005). "*Two new fluorescent dyes applicable for visualization of fungal cell walls*." Mycologia **97**(3): 580-588.

Hogan, L. H. and B. S. Klein (1994). "*Altered expression of surface alpha-1, 3-glucan in genetically related strains of Blastomyces dermatitidis that differ in virulence*." Infection and immunity **62**(8): 3543-3546.

Hohmann, S. (2002). "*Osmotic stress signaling and osmoadaptation in yeasts*." Microbiology and Molecular Biology Reviews **66**(2): 300-372.

Huh, W.-K., J. V. Falvo, L. C. Gerke, A. S. Carroll, R. W. Howson, J. S. Weissman and E. K. O'Shea (2003). "*Global analysis of protein localization in budding yeast*." Nature **425**(6959): 686-691.

Hurtado-Guerrero, R., A. W. Schüttelkopf, I. Mouyna, A. F. Ibrahim, S. Shepherd, T. Fontaine, J.-P. Latgé and D. M. van Aalten (2009). "*Molecular mechanisms of yeast cell wall glucan remodeling*." Journal of Biological Chemistry **284**(13): 8461-8469.

Hwang, J. S., D. H. Seo and J. Y. Kim (2006). "*Soluble forms of YlCrh1p and YlCrh2p, cell wall proteins of Yarrowia lipolytica, have beta-(1,3) glycosidase activity*." Yeast **23**(11): 803-812.

Igual, J., A. Johnson and L. Johnston (1996). "*Coordinated regulation of gene expression by the cell cycle transcription factor Swi4 and the protein kinase C MAP kinase pathway for yeast cell integrity*." The EMBO journal **15**(18): 5001.

Ikeda, K., H. Kitagawa, H. Meguro, K. Inoue, P. Park and S. Shimoi (2012). *The Role of the Extracellular Matrix (ECM) in Phytopathogenic Fungi: A Potential Target for Disease Control*, INTECH Open Access Publisher.

Inglis, D. O., M. B. Arnaud, J. Binkley, P. Shah, M. S. Skrzypek, F. Wymore, G. Binkley, S. R. Miyasato, M. Simison and G. Sherlock (2012). "*The Candida genome database incorporates multiple Candida species: multispecies search and analysis tools with curated gene and protein information for Candida albicans and Candida glabrata*." Nucleic acids research **40**(D1): D667-D674.

Inoue, K., T. Suzuki, K. Ikeda, S. Jiang, N. Hosogi, G.-S. Hyong, S. Hida, T. Yamada and P. Park (2007). "*Extracellular matrix of Magnaporthe oryzae may have a role in host adhesion during fungal penetration and is digested by matrix metalloproteinases*." Journal of General Plant Pathology **73**(6): 388-398.

Ishihara, S., A. Hirata, S. Nogami, A. Beauvais, J. P. Latgé and Y. Ohya (2007). "*Homologous subunits of 1, 3-beta-glucan synthase are important for spore wall assembly in Saccharomyces cerevisiae*." Eukaryotic cell **6**(2): 143-156.

Itoh, T., T. Tanaka, R. A. Barrero, C. Yamasaki, Y. Fujii, P. B. Hilton, B. A. Antonio, H. Aono, R. Apweiler and R. Bruskiewich (2007). "*Curated genome annotation of Oryza sativa ssp. japonica and comparative genome analysis with Arabidopsis thaliana*." Genome Research **17**(2): 175-183.

Jalili, N. and K. Laxminarayana (2004). "*A review of atomic force microscopy imaging systems: application to molecular metrology and biological sciences*." Mechatronics **14**(8): 907-945.

Jendretzki, A., J. Wittland, S. Wilk, A. Straede and J. J. Heinisch (2011). "*How do I begin? Sensing extracellular stress to maintain yeast cell wall integrity*." European journal of cell biology **90**(9): 740-744.

Jeon, J., J. Goh, S. Yoo, M.-H. Chi, J. Choi, H.-S. Rho, J. Park, S.-S. Han, B. R. Kim and S.-Y. Park (2008). "*A putative MAP kinase kinase kinase, MCK1, is required for cell wall integrity and pathogenicity of the rice blast fungus, Magnaporthe oryzae*." Molecular plant-microbe interactions **21**(5): 525-534.

Jolink, H., I. C. Meijssen, R. S. Hagedoorn, M. Arentshorst, J. W. Drijfhout, A. Mulder, F. H. Claas, J. T. van Dissel, J. F. Falkenburg and M. H. Heemskerk (2013). "*Characterization of the T-Cell–Mediated Immune Response Against the Aspergillus fumigatus Proteins Crf1 and Catalase 1 in Healthy Individuals*." Journal of Infectious Diseases **208**(5): 847-856.

Jones, M., I. Forn, C. Gadelha, M. J. Egan, D. Bass, R. Massana and T. A. Richards (2011). "*Discovery of novel intermediate forms redefines the fungal tree of life*." Nature **474**(7350): 200-203.

Kadotani, N., H. Nakayashiki, Y. Tosa and S. Mayama (2003). "*RNA silencing in the phytopathogenic fungus Magnaporthe oryzae*." Molecular plant-microbe interactions **16**(9): 769-776.

Kang, M. S. and E. Cabib (1986). "*Regulation of fungal cell wall growth: a guanine nucleotide-binding, proteinaceous component required for activity of (1-3)-beta-D-glucan synthase*." Proceedings of the National Academy of Sciences **83**(16): 5808-5812.

Kapteyn, J., A. Ram, E. Groos, R. Kollar, R. Montijn, H. Van Den Ende, A. Llobell, E. Cabib and F. Klis (1997). "*Altered extent of cross-linking of beta1, 6-glucosylated mannoproteins to chitin in Saccharomyces cerevisiae mutants with reduced cell wall beta1, 3-glucan content*." Journal of Bacteriology **179**(20): 6279-6284.

Kapteyn, J., P. Van Egmond, E. Sievi, H. Van Den Ende, M. Makarow and F. Klis (1999a). "*The contribution of the O-glycosylated protein Pir2p/Hsp150 to the construction of the yeast cell wall in wild-type cells and β1, 6-glucan-deficient mutants*." Molecular microbiology **31**(6): 1835-1844.

Kapteyn, J. C., H. Van Den Ende and F. M. Klis (1999b). "*The contribution of cell wall proteins to the organization of the yeast cell wall*." Biochimica et Biophysica Acta (BBA)-General Subjects **1426**(2): 373-383.

Karlen, Y., A. McNair, S. Perseguers, C. Mazza and N. Mermod (2007). "*Statistical significance of quantitative PCR*." BMC bioinformatics **8**(1): 131.

Kasas, S., G. Longo and G. Dietler (2013). "*Mechanical properties of biological specimens explored by atomic force microscopy*." Journal of Physics D: Applied Physics **46**(13): 133001.

Katoh, K., K.-i. Kuma, H. Toh and T. Miyata (2005). "*MAFFT version 5: improvement in accuracy of multiple sequence alignment*." Nucleic acids research **33**(2): 511-518.

Katoh, K. and D. M. Standley (2013). "*MAFFT multiple sequence alignment software version 7: improvements in performance and usability*." Molecular biology and evolution **30**(4): 772-780.

Kawahara, Y., Y. Oono, H. Kanamori, T. Matsumoto, T. Itoh and E. Minami (2012). "*Simultaneous RNA-seq analysis of a mixed transcriptome of rice and blast fungus interaction*." PloS one **7**(11): e49423.

Kershaw, M. J., G. Wakley and N. J. Talbot (1998). "*Complementation of the Mpg1 mutant phenotype in Magnaporthe grisea reveals functional relationships between fungal hydrophobins*." The EMBO journal **17**(14): 3838-3849.

Ketela, T., R. Green and H. Bussey (1999). "*Saccharomyces cerevisiae Mid2p Is a Potential Cell Wall Stress Sensor and Upstream Activator of thePKC1-MPK1 Cell Integrity Pathway*." Journal of Bacteriology **181**(11): 3330-3340.

Khush, G. S. (2005). "*What it will take to feed 5.0 billion rice consumers in 2030*." Plant Molecular Biology **59**(1): 1-6.

Kim, K.-Y. and D. E. Levin (2011). "*Mpk1 MAPK association with the Paf1 complex blocks Sen1-mediated premature transcription termination*." Cell **144**(5): 745-756.

Kim, K.-Y., A. W. Truman and D. E. Levin (2008). "*Yeast Mpk1 mitogen-activated protein kinase activates transcription through Swi4/Swi6 by a noncatalytic*

mechanism that requires upstream signal." Molecular and cellular biology **28**(8): 2579-2589.

Kitagaki, H., H. Wu, H. Shimoi and K. Ito (2002a). "*Two homologous genes, DCW1 (YKL046c) and DFG5, are essential for cell growth and encode glycosylphosphatidylinositol-(GPI)-anchored membrane proteins required for cell wall biogenesis in Saccharomyces cerevisiae*." Molecular microbiology **46**(4): 1011-1022.

Kitagaki, H., H. Wu, H. Shimoi and K. Ito (2002b). "*Two homologous genes, DCW1 (YKL046c) and DFG5, are essential for cell growth and encode glycosylphosphatidylinositol-(GPI)-anchored membrane proteins required for cell wall biogenesis in Saccharomycescerevisiae*." Molecular microbiology **46**(4): 1011-1022.

Kitagaki, H., H. Wu, H. Shimoi and K. Ito (2002c). "*Two homologous genes, DCW1 (YKL046c) and DFG5, are essential for cell growth and encode glycosylphosphatidylinositol (GPI)-anchored membrane proteins required for cell wall biogenesis in Saccharomyces cerevisiae*." Molecular microbiology **46**(4): 1011-1022.

Klimpel, K. R. and W. E. Goldman (1988). "*Cell walls from avirulent variants of Histoplasma capsulatum lack alpha-(1, 3)-glucan*." Infection and immunity **56**(11): 2997-3000.

Klis, F., A. Boorsma and P. De Groot (2006). "*Cell wall construction in Saccharomyces cerevisiae*." Yeast **23**(3): 185-240.

Klis, F., P. D. Groot and K. Hellingwerf (2001). "*Molecular organization of the cell wall of Candida albicans*." Medical Mycology **39**(1): 1-8.

Klis, F., G. J. Sosinska, W. De Groot and S. Brul (2009). "*Covalently linked cell wall proteins of Candida albicans and their role in fitness and virulence*." FEMS yeast research **9**(7): 1013-1028.

Koch, C., T. Moll, M. Neuberg, H. Ahorn and K. Nasmyth (1993). "*A role for the transcription factors Mbp1 and Swi4 in progression from G1 to S phase*." Science **261**(5128): 1551-1557.

Kollár, R., E. Petráková, G. Ashwell, P. W. Robbins and E. Cabib (1995). "*Architecture of the Yeast Cell Wall The Linkage between chitin and β (1,3)-glucan*." Journal of Biological Chemistry **270**(3): 1170-1178.

Kollár, R., B. B. Reinhold, E. Petráková, H. J. Yeh, G. Ashwell, J. Drgonová, J. C. Kapteyn, F. M. Klis and E. Cabib (1997). "*Architecture of the Yeast Cell Wall β (1→ 6)-glucan interconnects mannoprotein, β (1→ 3)-glucan, and chitin*." Journal of Biological Chemistry **272**(28): 17762-17775.

Kong, L. A., J. Yang, G. Li, L. L. Qi, Y. J. Zhang, C. F. Wang, W. S. Zhao, J. R. Xu and Y. L. Peng (2012). "*Different chitin synthase genes are required for various developmental and plant infection processes in the rice blast fungus Magnaporthe oryzae*." PLoS pathogens **8**(2): e1002526.

Kopecká, M. and M. Gabriel (1992). "*The influence of Congo red on the cell wall and (1→ 3)-β-d-glucan microfibril biogenesis in Saccharomyces cerevisiae*." Archives of microbiology **158**(2): 115-126.

Krantz, M., E. Becit and S. Hohmann (2006). "*Comparative genomics of the HOG-signalling system in fungi*." Current genetics **49**(3): 137-151.

Krappmann, S. (2007). "*Gene targeting in filamentous fungi: the benefits of impaired repair*." Fungal biology reviews **21**(1): 25-29.

Krupp, G. (2005). "*Stringent RNA quality control using the Agilent 2100 bioanalyzer*." Agilent Technologies Application Notes.

Kuge, S. and N. Jones (1994). "*YAP1 dependent activation of TRX2 is essential for the response of Saccharomyces cerevisiae to oxidative stress by hydroperoxides*." The EMBO journal **13**(3): 655.

Kültz, D. (1998). "*Phylogenetic and functional classification of mitogen-and stress-activated protein kinases*." Journal of molecular evolution **46**(5): 571-588.

Kuranda, K., V. Leberre, S. Sokol, G. Palamarczyk and J. François (2006). "*Investigating the caffeine effects in the yeast Saccharomyces cerevisiae brings new insights into the connection between TOR, PKC and Ras/cAMP signalling pathways*." Molecular microbiology **61**(5): 1147-1166.

Kurtz, M. and C. Douglas (1997). "*Lipopeptide inhibitors of fungal glucan synthase*." Medical Mycology **35**(2): 79-86.

Lacroix, B., T. Tzfira, A. Vainstein and V. Citovsky (2006). "*A case of promiscuity: Agrobacterium's endless hunt for new partners*." TRENDS in Genetics **22**(1): 29-37.

Lagorce, A., N. C. Hauser, D. Labourdette, C. Rodriguez, H. Martin-Yken, J. Arroyo, J. D. Hoheisel and J. Fran√ßois (2003). "*Genome-wide analysis of the response to cell wall mutations in the yeast Saccharomyces cerevisiae*." Journal of Biological Chemistry **278**(22): 20345-20357.

Larson, T. M., D. F. Kendra, M. Busman and D. W. Brown (2011). "*Fusarium verticillioides chitin synthases CHS5 and CHS7 are required for normal growth and pathogenicity*." Current genetics: 1-13.

Latgé, J.-P. and A. Beauvais (2014). "*Functional duality of the cell wall*." Current opinion in microbiology **20**: 111-117.

Latgé, J. P. (2007). "*The cell wall: a carbohydrate armour for the fungal cell*." Molecular microbiology **66**(2): 279-290.

Latgé, J. P. (2010). "*Tasting the fungal cell wall*." Cellular Microbiology **12**(7): 863-872.

Lee, F. N., R. Cartwright, Y. Jia and J. Correll (2009). "*Field resistance expressed when the PI-TA gene is compromised by Magnaporthe oryzae*." Advances in Genetics, Genomics and Control of Rice Blast Disease: 281-289.

Lee, Y.-H. and R. A. Dean (1993). "*cAMP regulates infection structure formation in the plant pathogenic fungus Magnaporthe grisea*." The Plant Cell Online **5**(6): 693-700.

Lesage, G. and H. Bussey (2006). "*Cell wall assembly in Saccharomyces cerevisiae*." Microbiology and Molecular Biology Reviews **70**(2): 317.

Lesage, G., A. M. Sdicu, P. Menard, J. Shapiro, S. Hussein and H. Bussey (2004). "*Analysis of {beta}-1, 3-Glucan Assembly in Saccharomyces cerevisiae Using a Synthetic Interaction Network and Altered Sensitivity to Caspofungin*." Genetics **167**(1): 35.

Levin, D. E. (2005). "*Cell wall integrity signaling in Saccharomyces cerevisiae*." Microbiology and Molecular Biology Reviews **69**(2): 262-291.

Levin, D. E. (2011). "*Regulation of cell wall biogenesis in Saccharomyces cerevisiae: the cell wall integrity signaling pathway*." Genetics **189**(4): 1145-1175.

Li, J., L. Li, Y. Tian, G. Niu and H. Tan (2011). "*Hybrid antibiotics with the nikkomycin nucleoside and polyoxin peptidyl moieties*." Metabolic Engineering.

Liu, Y.-W., S.-W. Lee and F.-J. S. Lee (2006). "*Arl1p is involved in transport of the GPI-anchored protein Gas1p from the late Golgi to the plasma membrane*." Journal of cell science **119**(18): 3845-3855.

Lommel, M., M. Bagnat and S. Strahl (2004). "*Aberrant processing of the WSC family and Mid2p cell surface sensors results in cell death of Saccharomyces cerevisiae O-mannosylation mutants*." Molecular and cellular biology **24**(1): 46-57.

Lorang, J., R. Tuori, J. Martinez, T. Sawyer, R. Redman, J. Rollins, T. Wolpert, K. Johnson, R. Rodriguez and M. Dickman (2001). "*Green fluorescent protein is lighting up fungal biology*." Applied and environmental microbiology **67**(5): 1987-1994.

Lynch, D. P. and D. K. Gibson (1987). "*The use of Calcofluor white in the histopathologic diagnosis of oral candidiasis*." Oral Surgery, Oral Medicine, Oral Pathology **63**(6): 698-703.

Ma, H., L. A. Snook, S. G. Kaminskyj and T. E. Dahms (2005). "*Surface ultrastructure and elasticity in growing tips and mature regions of Aspergillus hyphae describe wall maturation*." Microbiology **151**(11): 3679-3688.

Madden, K., Y.-J. Sheu, K. Baetz, B. Andrews and M. Snyder (1997). "*SBF cell cycle regulator as a target of the yeast PKC-MAP kinase pathway*." Science **275**(5307): 1781-1784.

Maddi, A. and S. J. Free (2010). "*α-1, 6-Mannosylation of N-linked oligosaccharide present on cell wall proteins is required for their incorporation into the cell wall in the filamentous fungus Neurospora crassa*." Eukaryotic cell **9**(11): 1766-1775.

Mantovani, M. S., M. F. Bellini, J. P. F. Angeli, R. J. Oliveira, A. F. Silva and L. R. Ribeiro (2008). "*[beta]-Glucans in promoting health: Prevention against mutation and cancer*." Mutation Research/Reviews in Mutation Research **658**(3): 154-161.

Marchler-Bauer, A. (2011). "*CDD: a Conserved Domain Database for the functional annotation of proteins*." Nucleic acids research **39(D)225-9**.

Marchler-Bauer, A., C. Zheng, F. Chitsaz, M. K. Derbyshire, L. Y. Geer, R. C. Geer, N. R. Gonzales, M. Gwadz, D. I. Hurwitz and C. J. Lanczycki (2012). "*CDD: conserved domains and protein three-dimensional structure*." Nucleic acids research: gks1243.

Marian, M., B. Noelia, K. Kristina, F. Zuzana, R. Pavel, F. Vladimir and A. Javier (2013). "*A novel fluorescence assay and catalytic properties of Crh1 and Crh2 yeast cell wall transglycosylases*." Biochemical Journal **455**(3): 307-318.

Martinez-Pastor, M., G. Marchler, C. Schüller, A. Marchler-Bauer, H. Ruis and F. Estruch (1996). "*The Saccharomyces cerevisiae zinc finger proteins Msn2p and Msn4p are required for transcriptional induction through the stress response element (STRE)*." The EMBO journal **15**(9): 2227.

Mathioni, S., A. Beló, C. J. Rizzo, R. A. Dean and N. M. Donofrio (2011). "*Transcriptome profiling of the rice blast fungus during invasive plant infection and in vitro stresses*." BMC genomics **12**(1): 49.

Matsuoka, H., H. C. Yang, T. Homma, Y. Nemoto, S. Yamada, O. Sumita, K. Takatori and H. Kurata (1995). "*Use of Congo red as a microscopic fluorescence indicator of hyphal growth*." Applied microbiology and biotechnology **43**(1): 102-108.

Maubon, D., S. Park, M. Tanguy, M. Huerre, C. Schmitt, M. Prevost, D. Perlin, J. Latge and A. Beauvais (2006). "*AGS3, an α (1–3) glucan synthase gene family member of Aspergillus fumigatus, modulates mycelium growth in the lung of experimentally infected mice*." Fungal Genetics and Biology **43**(5): 366-375.

McElfresh, M., E. Baesu, R. Balhorn, J. Belak, M. J. Allen and R. Rudd (2002). "*Combining constitutive materials modeling with atomic force microscopy to understand the mechanical properties of living cells*." Proceedings of the National Academy of Sciences **99**(suppl 2): 6493-6497.

Meaden, P., K. Hill, J. Wagner, D. Slipetz, S. Sommer and H. Bussey (1990). "*The yeast KRE5 gene encodes a probable endoplasmic reticulum protein required for (1----6)-beta-D-glucan synthesis and normal cell growth*." Molecular and cellular biology **10**(6): 3013-3019.

Mehrabi, R., S. Ding and J.-R. Xu (2008). "*MADS-box transcription factor Mig1 is required for infectious growth in Magnaporthe grisea*." Eukaryotic cell **7**(5): 791-799.

Mélida, H., J. V. Sandoval-Sierra, J. Diéguez-Uribeondo and V. Bulone (2013). "*Analyses of extracellular carbohydrates in oomycetes unveil the existence of three different cell wall types*." Eukaryotic cell **12**(2): 194-203.

Meyer, V. (2008). "*Genetic engineering of filamentous fungi--Progress, obstacles and future trends*." Biotechnology advances **26**(2): 177-185.

Michel, G., L. Chantalat, E. Duee, T. Barbeyron, B. Henrissat, B. Kloareg and O. Dideberg (2001). "*The κ-carrageenase of P. carrageenovora Features a Tunnel-Shaped Active Site: A Novel Insight in the Evolution of Clan-B Glycoside Hydrolases*." Structure **9**(6): 513-525.

Michels, C. A. (2002). *Genetic Techniques for Biological Research*. England, John Wiley & Sons, Ltd.

Miller, K. A., L. DiDone and D. J. Krysan (2010). "*Extracellular secretion of overexpressed glycosylphosphatidylinositol-linked cell wall protein Utr2/Crh2p as a novel protein quality control mechanism in Saccharomyces cerevisiae*." Eukaryotic cell **9**(11): 1669-1679.

Molina, J., M. Sikora, N. Garud, J. M. Flowers, S. Rubinstein, A. Reynolds, P. Huang, S. Jackson, B. A. Schaal and C. D. Bustamante (2011). "*Molecular evidence for a single evolutionary origin of domesticated rice*." Proceedings of the National Academy of Sciences **108**(20): 8351.

Molina, M., C. Gil, J. Pla, J. Arroyo and C. Nombela (2000). "*Protein localisation approaches for understanding yeast cell wall biogenesis*." Microscopy research and technique **51**(6): 601-612.

Möller, C., M. Allen, V. Elings, A. Engel and D. J. Müller (1999). "*Tapping-mode atomic force microscopy produces faithful high-resolution images of protein surfaces*." Biophysical journal **77**(2): 1150-1158.

Monheit, J., D. Cowan and D. Moore (1984). "*Rapid detection of fungi in tissues using calcofluor white and fluorescence microscopy*." Archives of pathology & laboratory medicine **108**(8): 616-618.

Moore, R. (1980). "*Taxonomic proposals for the classification of marine yeasts and other yeast-like fungi including the smuts*." Botanica marina.

Morgan, B. A., G. R. Banks, W. M. Toone, D. Raitt, S. Kuge and L. H. Johnston (1997). "*The Skn7 response regulator controls gene expression in the oxidative stress response of the budding yeast Saccharomyces cerevisiae*." The EMBO journal **16**(5): 1035-1044.

Mortensen, R. (2006). "*Overview of gene targeting by homologous recombination*."

Motoyama, T., N. Ochiai, M. Morita, Y. Iida, R. Usami and T. Kudo (2008). "*Involvement of putative response regulator genes of the rice blast fungus Magnaporthe oryzae in osmotic stress response, fungicide action, and pathogenicity*." Current genetics **54**(4): 185-195.

Mouyna, I., T. Fontaine, M. Vai, M. Monod, W. A. Fonzi, M. Diaquin, L. Popolo, R. P. Hartland and J.-P. Latgé (2000). "*Glycosylphosphatidylinositol-anchored glucanosyltransferases play an active role in the biosynthesis of the fungal cell wall*." Journal of Biological Chemistry **275**(20): 14882-14889.

Mrša, V. and W. Tanner (1999). "*Role of NaOH-extractable cell wall proteins Ccw5p, Ccw6p, Ccw7p and Ccw8p (members of the Pir protein family) in stability of the Saccharomyces cerevisiae cell wall*." Yeast **15**(10A): 813-820.

Mueller, O., S. Lightfoot and A. Schroeder (2004) "*RNA integrity number (RIN)–Standardization of RNA Quality Control*." Agilent Application Note, 1-8.

Müller, D. J. and Y. F. Dufrêne (2011). "*Atomic force microscopy: a nanoscopic window on the cell surface*." Trends in cell biology **21**(8): 461-469.

Myhra S Pers.com (2014). *M. oryzae* surface imaging and cell wall elasticity measurement by atomic force microscopy. . Department of Materials, University of Oxford, Personal communication.

Nakajima, T., C. Suzuki and K. Matsuda (1982). "*Extracellular galactomannan from Neurospora crassa*." Agricultural and Biological Chemistry **46**(4): 869-875.

Nakayashiki, H., S. Hanada, N. B. Quoc, N. Kadotani, Y. Tosa and S. Mayama (2005). "*RNA silencing as a tool for exploring gene function in ascomycete fungi*." Fungal Genetics and Biology **42**(4): 275-283.

Nandy, S., N. Mandal, P. Bhowmik, M. Khan and S. Basu (2010). "*8 Sustainable Management of Rice Blast (Magnaporthe grisea (Hebert) Barr): 50 Years of Research Progress in Molecular Biology*." Management of fungal plant pathogens: 92.

Navarro-García, F., B. Eisman, S. M. Fiuza, C. Nombela and J. Pla (2005). "*The MAP kinase Mkc1p is activated under different stress conditions in Candida albicans*." Microbiology **151**(8): 2737-2749.

Nguyen, T., G. Fleet and P. Rogers (1998). "*Composition of the cell walls of several yeast species*." Applied microbiology and biotechnology **50**(2): 206-212.

Nikolaou, E., I. Agrafioti, M. Stumpf, J. Quinn, I. Stansfield and A. J. Brown (2009). "*Phylogenetic diversity of stress signalling pathways in fungi*." BMC Evolutionary Biology **9**(1): 44.

Nishitani, K. (1997). "*The role of endoxyloglucan transferase in the organization of plant cell walls*." International review of cytology **173**: 157-206.

Nobel, H., H. Ende and F. M. Klis (2000). "*Cell wall maintenance in fungi*." Trends in microbiology **8**(8): 344-345.

Nuoffer, C., P. Jenö, A. Conzelmann and H. Riezman (1991). "*Determinants for glycophospholipid anchoring of the Saccharomyces cerevisiae GAS1 protein to the plasma membrane*." Molecular and cellular biology **11**(1): 27-37.

O'Brien, H. E., J. L. Parrent, J. A. Jackson, J.-M. Moncalvo and R. Vilgalys (2005). "*Fungal community analysis by large-scale sequencing of environmental samples*." Applied and environmental microbiology **71**(9): 5544-5550.

Odenbach, D., E. Thines, H. Anke and A. J. Foster (2009). "*The Magnaporthe grisea class VII chitin synthase is required for normal appressorial development and function*." Molecular plant pathology **10**(1): 81-94.

Oerke, E. C. and H. W. Dehne (2004). "*Safeguarding production--losses in major crops and the role of crop protection*." Crop Protection **23**(4): 275-285.

Oh, Y., N. Donofrio, H. Pan, S. Coughlan, D. E. Brown, S. Meng, T. Mitchell and R. A. Dean (2008). "*Transcriptome analysis reveals new insight into appressorium formation and function in the rice blast fungus Magnaporthe oryzae*." Genome Biol **9**(5): R85.

Okada, H., M. Abe, M. Asakawa-Minemura, A. Hirata, H. Qadota, K. Morishita, S. Ohnuki, S. Nogami and Y. Ohya (2010). "*Multiple Functional Domains of the Yeast l, 3-beta-Glucan Synthase Subunit Fks1p Revealed by Quantitative Phenotypic Analysis of Temperature-Sensitive Mutants*." Genetics **184**(4): 1013.

Orlean, P. (2012). "*Architecture and biosynthesis of the Saccharomyces cerevisiae cell wall*." Genetics **192**(3): 775-818.

Pancaldi, S., F. Poli, G. Dall'Olio and G. Vannini (1984). "*Morphological anomalies induced by Congo red in Aspergillus niger*." Archives of microbiology **137**(3): 185-187.

Pâques, F. and J. E. Haber (1999). "*Multiple pathways of recombination induced by double-strand breaks in Saccharomyces cerevisiae*." Microbiology and Molecular Biology Reviews **63**(2): 349-404.

Pardini, G., P. W. J. De Groot, A. T. Coste, M. Karababa, F. M. Klis, C. G. de Koster and D. Sanglard (2006). "*The CRH family coding for cell wall GPI proteins with a predicted transglycosidase domain affects cell wall organization and virulence of Candida albicans*." Journal of Biological Chemistry.

Pardo, M., L. Monteoliva, P. Vázquez, R. Martínez, G. Molero, C. Nombela and C. Gil (2004). "*PST1 and ECM33 encode two yeast cell surface GPI proteins important for cell wall integrity*." Microbiology **150**(12): 4157-4170.

Park, S.-Y., J. Choi, S.-E. Lim, G.-W. Lee, J. Park, Y. Kim, S. Kong, S. R. Kim, H.-S. Rho and J. Jeon (2013). "*Global Expression Profiling of Transcription Factor Genes Provides New Insights into Pathogenicity and Stress Responses in the Rice Blast Fungus*." PLoS pathogens **9**(6): e1003350.

Pastink, A., J. C. Eeken and P. H. Lohman (2001). "*Genomic integrity and the repair of double-strand DNA breaks*." Mutation Research/Fundamental and Molecular Mechanisms of Mutagenesis **480**: 37-50.

Pérez, P. and J. C. Ribas (2004). "*Cell wall analysis*." Methods **33**(3): 245-251.

Petersen, T. N., S. Brunak, G. von Heijne and H. Nielsen (2011). "*SignalP 4.0: discriminating signal peptides from transmembrane regions*." Nature methods **8**(10): 785-786.

Pfaffl, M. W. (2001). "*A new mathematical model for relative quantification in real-time RT-PCR*." Nucleic acids research **29**(9): e45.

Planta, R. J. and W. H. Mager (1998). "*The list of cytoplasmic ribosomal proteins of Saccharomyces cerevisiae*." Yeast **14**(5): 471-477.

Popolo, L., D. Gilardelli, P. Bonfante and M. Vai (1997). "*Increase in chitin as an essential response to defects in assembly of cell wall polymers in the ggp1delta mutant of Saccharomyces cerevisiae*." Journal of Bacteriology **179**(2): 463-469.

Popolo, L., T. Gualtieri and E. Ragni (2001). "*The yeast cell-wall salvage pathway*." Medical Mycology **39**(1): 111-121.

Popolo, L. and M. Vai (1999). "*The Gas1 glycoprotein, a putative wall polymer cross-linker*." Biochimica et Biophysica Acta (BBA)-General Subjects **1426**(2): 385-400.

Posas, F. and H. Saito (1997). "*Osmotic activation of the HOG MAPK pathway via Ste11p MAPKKK: scaffold role of Pbs2p MAPKK*." Science **276**(5319): 1702-1705.

Qi, Z., Q. Wang, X. Dou, W. Wang, Q. Zhao, R. Lv, H. Zhang, X. Zheng, P. Wang and Z. Zhang (2012). "*MoSwi6, an APSES family transcription factor, interacts with MoMps1 and is required for hyphal and conidial morphogenesis, appressorial function and pathogenicity of Magnaporthe oryzae*." Molecular plant pathology **13**(7): 677-689.

Quandt K, Frech K, Karas H, Wingender E and W. T (1995). "*MatInd and MatInspector: new fast and versatile tools for detection of consensus matches in nucleotide sequence data.*" Nucleic acids research **23**(23): 4878-4884.

Ram, A. F., J. C. Kapteyn, R. C. Montijn, L. H. P. Caro, J. E. Douwes, W. Baginsky, P. Mazur, H. van den Ende and F. M. Klis (1998). "*Loss of the Plasma Membrane-Bound Protein Gas1p in Saccharomyces cerevisiae Results in the Release of β1, 3-Glucan into the Medium and Induces a Compensation Mechanism To Ensure Cell Wall Integrity*." Journal of Bacteriology **180**(6): 1418-1424.

Ram, A. F. and F. M. Klis (2006). "*Identification of fungal cell wall mutants using susceptibility assays based on Calcofluor white and Congo red*." Nature protocols **1**(5): 2253-2256.

Rappleye, C. A., L. G. Eissenberg and W. E. Goldman (2007). "*Histoplasma capsulatum alpha-(1, 3)-glucan blocks innate immune recognition by the beta-glucan receptor*." Proceedings of the National Academy of Sciences **104**(4): 1366.

Rasconi, S., M. Jobard, L. Jouve and T. Sime-Ngando (2009). "*Use of calcofluor white for detection, identification, and quantification of phytoplanktonic fungal parasites*." Applied and environmental microbiology **75**(8): 2545-2553.

Reese, A. J., A. Yoneda, J. A. Breger, A. Beauvais, H. Liu, C. L. Griffith, I. Bose, M. J. Kim, C. Skau and S. Yang (2007). "*Loss of cell wall alpha (1-3) glucan affects Cryptococcus neoformans from ultrastructure to virulence*." Molecular microbiology **63**(5): 1385-1398.

Reinke, A., J. C.-Y. Chen, S. Aronova and T. Powers (2006). "*Caffeine targets TOR complex I and provides evidence for a regulatory link between the FRB and kinase domains of Tor1p*." Journal of Biological Chemistry **281**(42): 31616-31626.

Reynolds, R. C., P. O. B. Montgomery and D. H. Karney (1963). "*Nucleolar "caps"—a morphologic entity produced by the carcinogen 4-nitroquinoline N-oxide*." Cancer research **23**(4 Part 1): 535-538.

Rispail, N., D. M. Soanes, C. Ant, R. Czajkowski, A. Grünler, R. Huguet, E. Perez-Nadales, A. Poli, E. Sartorel and V. Valiante (2009). "*Comparative genomics of MAP kinase and calcium–calcineurin signalling components in plant and human pathogenic fungi*." Fungal Genetics and Biology **46**(4): 287-298.

Rodriguez-Pena, J. M., V. J. Cid, J. Arroyo and C. Nombela (2000). "*A novel family of cell wall-related proteins regulated differently during the yeast life cycle*." Molecular and cellular biology **20**(9): 3245.

Rodriguez-Peña, J. M., C. Rodriguez, A. Alvarez, C. Nombela and J. Arroyo (2002). "*Mechanisms for targeting of the Saccharomyces cerevisiae GPI-anchored cell wall protein Crh2p to polarised growth sites*." Journal of cell science **115**(12): 2549-2558.

Roelofsen, P. A. and I. Hoette (1951). "*Chitin in the cell wall of yeasts*." Antonie van Leeuwenhoek **17**(1): 297-313.

Roemer, T., G. Paravicini, M. A. Payton and H. Bussey (1994). "*Characterization of the yeast (1- 6)-beta-glucan biosynthetic components, Kre6p and Skn1p, and genetic interactions between the PKC1 pathway and extracellular matrix assembly*." The Journal of cell biology **127**(2): 567-579.

Rolli, E., E. Ragni, J. Calderon, S. Porello, U. Fascio and L. Popolo (2009). "*Immobilization of the glycosylphosphatidylinositol-anchored Gas1 protein into the chitin ring and septum is required for proper morphogenesis in yeast*." Molecular biology of the cell **20**(22): 4856-4870.

Roncero, C. and A. Duran (1985). "*Effect of Calcofluor white and Congo red on fungal cell wall morphogenesis: in vivo activation of chitin polymerization*." Journal of Bacteriology **163**(3): 1180-1185.

Ruiz Herrera, J., M. Victoria Elorza, E. ValentÌn and R. Sentandreu (2006). "*Molecular organization of the cell wall of Candida albicans and its relation to pathogenicity*." FEMS yeast research **6**(1): 14-29.

Ruiz, R. and T. E. Date (1996). *Determination of carbohydrates in biomass by high performance liquid chromatography*. Laboratory Analytical Procedure No. 002, National Renewable Research Laboratory, Citeseer.

Saeman, J. F. (1981). *Key factors in the hydrolysis of cellulose*. ACS Symp. Ser.;(United States), Forest Products Lab., Forest Service, USDA, PO Box 5130, Madison, WI 53705.

Sambrook, J. and D. W. Russell (2001). *Molecular Cloning: A Laboratory Manual* Cold Spring Harbor Laboratory Press, Cold Spring Harbor, New York.

Sandbaken, M. G. and M. R. Culbertson (1988). "*Mutations in elongation factor EF-1 alpha affect the frequency of frameshifting and amino acid misincorporation in Saccharomyces cerevisiae*." Genetics **120**(4): 923-934.

Sandula, J., E. Machova and V. Hribalova (1995). "*Mitogenic activity of particulate yeast [beta]-(1--> 3)-d-glucan and its water-soluble derivatives*." International journal of biological macromolecules **17**(6): 323-326.

Santos, B. and M. Snyder (2000). "*Sbe2p and sbe22p, two homologous Golgi proteins involved in yeast cell wall formation*." Molecular biology of the cell **11**(2): 435-452.

Sarthy, A. V., T. McGonigal, M. Coen, D. J. Frost, J. A. Meulbroek and R. C. Goldman (1997). "*Phenotype in Candida albicans of a disruption of the BGL2 gene encoding a 1, 3-β-glucosyltransferase*." Microbiology **143**(2): 367-376.

Schoffelmeer, E. A., F. M. Klis, J. H. Sietsma and B. J. Cornelissen (1999). "*The cell wall of Fusarium oxysporum*." Fungal Genetics and Biology **27**(2): 275-282.

Sernova, N. V. (2006). *Evalutation of programs for the prediction of GPI-anchor proteins*. Master Degree in Proteomics and Bioinformatics, Swiss Institute of Bioinformatics.

Shaner, N. C., R. E. Campbell, P. A. Steinbach, B. N. Giepmans, A. E. Palmer and R. Y. Tsien (2004). "*Improved monomeric red, orange and yellow fluorescent proteins derived from Discosoma sp. red fluorescent protein*." Nature biotechnology **22**(12): 1567-1572.

Shaner, N. C., P. A. Steinbach and R. Y. Tsien (2005). "*A guide to choosing fluorescent proteins*." Nature methods **2**(12): 905-909.

Shematek, E. M., J. Braatz and E. Cabib (1980). "*Biosynthesis of the yeast cell wall. Preparation and properties of beta-(1 leads to 3) glucan synthetase*." Journal of Biological Chemistry **255**(3): 888-894.

Sherman, D. J., T. Martin, M. Nikolski, C. Cayla, J.-L. Souciet and P. Durrens (2009). "*Genolevures: protein families and synteny among complete*

hemiascomycetous yeast proteomes and genomes." Nucleic acids research **37**(suppl 1): D550-D554.

Shetty, N. P., J. D. Jensen, A. Knudsen, C. Finnie, N. Geshi, A. Blennow, D. B. Collinge and H. J. L. Jorgensen (2009). "*Effects of beta-1, 3-glucan from Septoria tritici on structural defence responses in wheat*." Journal of experimental botany **60**(15): 4287.

Shinohara, A. and T. Ogawa (1995). "*Homologous recombination and the roles of double-strand breaks*." Trends in biochemical sciences **20**(10): 387-391.

Sietsma, J. and J. Wessels (1979). "*Evidence for covalent linkages between chitin and β-glucan in a fungal wall*." Journal of general microbiology **114**(1): 99-108.

Sietsma, J. and J. Wessels (1981). "*Solubility of (1-3)-β-D/(1-6)-β-D-glucan in fungal walls: Importance of presumed linkage between glucan and chitin*." Journal of general microbiology **125**(1): 209-212.

Singh, K. K. (2000). "*The Saccharomyces cerevisiae sln1p-ssk1p two-component system mediates response to oxidative stress and in an oxidant-specific fashion*." Free Radical Biology and Medicine **29**(10): 1043-1050.

Skamnioti, P. and S. J. Gurr (2007). "*Magnaporthe grisea cutinase2 mediates appressorium differentiation and host penetration and is required for full virulence*." The Plant Cell Online **19**(8): 2674.

Skamnioti, P. and S. J. Gurr (2009). "*Against the grain: safeguarding rice from rice blast disease*." Trends in biotechnology **27**(3): 141-150.

Smits, G. J., H. van den Ende and F. M. Klis (2001a). "*Differential regulation of cell wall biogenesis during growth and development in yeast*." Microbiology **147**(4): 781.

Smits, G. J., H. van den Ende and F. M. Klis (2001b). "*Differential regulation of cell wall biogenesis during growth and development in yeast*." Microbiology **147**(4): 781-794.

Snapp, E. (2005). "*Design and use of fluorescent fusion proteins in cell biology*." Current Protocols in Cell Biology: 21.24. 21-21.24. 13.

Sneddon, I. N. (1965). "*The relation between load and penetration in the axisymmetric Boussinesq problem for a punch of arbitrary profile*." International Journal of Engineering Science **3**(1): 47-57.

Soanes, D. M., A. Chakrabarti, K. H. Paszkiewicz, A. L. Dawe and N. J. Talbot (2012). "*Genome-wide transcriptional profiling of appressorium development by the rice blast fungus Magnaporthe oryzae*." PLoS pathogens **8**(2): e1002514.

Song, Y. and B. Bhushan (2008). "*Atomic force microscopy dynamic modes: modeling and applications*." Journal of Physics: Condensed Matter **20**(22): 225012.

Springer, M. L. (1993). "*Genetic control of fungal differentiation: the three sporulation pathways of Neurospora crassa*." Bioessays **15**(6): 365-374.

Stadler, C., E. Rexhepaj, V. R. Singan, R. F. Murphy, R. Pepperkok, M. Uhlén, J. C. Simpson and E. Lundberg (2013). "*Immunofluorescence and fluorescent-protein tagging show high correlation for protein localization in mammalian cells*." Nature methods **10**(4): 315-323.

Strohmeier, M., M. Hrmova, M. Fischer, A. J. Harvey, G. B. Fincher and J. Pleiss (2004). "*Molecular modeling of family GH16 glycoside hydrolases: Potential roles for xyloglucan transglucosylases/hydrolases in cell wall modification in the poaceae*." Protein Science **13**(12): 3200-3213.

Stuehler, C., N. Khanna, S. Bozza, T. Zelante, S. Moretti, M. Kruhm, S. Lurati, B. Conrad, E. Worschech and S. Stevanović (2011a). "*Cross-protective TH1 immunity against Aspergillus fumigatus and Candida albicans*." Blood **117**(22): 5881-5891.

Stuehler, C., N. Khanna, S. Bozza, T. Zelante, S. Moretti, M. Kruhm, S. Lurati, B. Conrad, E. Worschech and S. Stevanovi*ƒá* (2011b). "*Cross-protective TH1 immunity against Aspergillus fumigatus and Candida albicans*." Blood **117**(22): 5881.

Szostak, J. W., T. L. Orr-Weaver, R. J. Rothstein and F. W. Stahl (1983). "*The double-strand-break repair model for recombination*." Cell **33**(1): 25-35.

Taff, H. T., J. E. Nett, R. Zarnowski, K. M. Ross, H. Sanchez, M. T. Cain, J. Hamaker, A. P. Mitchell and D. R. Andes (2012). "*A Candida biofilm-induced pathway for matrix glucan delivery: implications for drug resistance*." PLoS pathogens **8**(8): e1002848.

Talbot, N. J. and A. J. Foster (2001). "*Genetics and genomics of the rice blast fungus Magnaporthe grisea: developing an experimental model for understanding fungal diseases of cereals*." Advances in Botanical Research **34**: 263-287.

Tamura, K., G. Stecher, D. Peterson, A. Filipski and S. Kumar (2013). "*MEGA6: molecular evolutionary genetics analysis version 6.0*." Molecular biology and evolution **30**(12): 2725-2729.

Terashima, H., N. Yabuki, M. Arisawa, K. Hamada and K. Kitada (2000). "*Up-regulation of genes encoding glycosylphosphatidylinositol (GPI)-attached proteins in response to cell wall damage caused by disruption of FKS1 in Saccharomyces cerevisiae*." Molecular and General Genetics MGG **264**(1-2): 64-74.

Thomas, S. W., S. W. Rasmussen, M. A. Glaring, J. A. Rouster, S. K. Christiansen and R. P. Oliver (2001). "*Gene identification in the obligate fungal pathogen Blumeria graminis by expressed sequence tag analysis*." Fungal Genetics and Biology **33**(3): 195-211.

Timoshenko, S., J. Goodier and H. Abramson (1970). "*Theory of elasticity*." Journal of Applied Mechanics **37**: 888.

Tirosh, I. and N. Barkai (2008). "*Evolution of gene sequence and gene expression are not correlated in yeast*." TRENDS in Genetics **24**(3): 109-113.

Touhami, A., B. Nysten and Y. F. Dufrêne (2003). "*Nanoscale mapping of the elasticity of microbial cells by atomic force microscopy*." Langmuir **19**(11): 4539-4543.

Treitschke, S., G. Doehlemann, M. Schuster and G. Steinberg (2010). "*The myosin motor domain of fungal chitin synthase V is dispensable for vesicle motility but required for virulence of the maize pathogen Ustilago maydis*." The Plant Cell Online **22**(7): 2476-2494.

Trouvelot, S., A. L. Varnier, M. Allegre, L. Mercier, F. Baillieul, C. Arnould, V. Gianinazzi-Pearson, O. Klarzynski, J. M. Joubert and A. Pugin (2008). "*A Beta-(1, 3) glucan sulfate induces resistance in grapevine against Plasmopara viticola through priming of defense responses, including HR-like cell death*." Molecular plant-microbe interactions **21**(2): 232-243.

Truman, A. W., K.-Y. Kim and D. E. Levin (2009). "*Mechanism of Mpk1 mitogen-activated protein kinase binding to the Swi4 transcription factor and its regulation by a novel caffeine-induced phosphorylation*." Molecular and cellular biology **29**(24): 6449-6461.

Ueno, K., Y. Namiki, H. Mitani, M. Yamaguchi and H. Chibana (2011). "*Differential cell wall remodeling of two chitin synthase deletants chs3A and chs3B in the pathogenic yeast Candida glabrata*." FEMS yeast research.

Vallone, P. M. and J. M. Butler (2004). "*AutoDimer: a screening tool for primer-dimer and hairpin structures*." Biotechniques **37**(2): 226-231.

Van Helden, J. (2003). "*Regulatory sequence analysis tools*." Nucleic acids research **31**(13): 3593-3596.

Vandesompele, J., K. De Preter, F. Pattyn, B. Poppe, N. Van Roy, A. De Paepe and F. Speleman (2002). "*Accurate normalization of real-time quantitative RT-PCR data by geometric averaging of multiple internal control genes*." Genome biology **3**(7): research0034.

Vasur, J., R. Kawai, E. Andersson, K. Igarashi, M. Sandgren, M. Samejima and J. Ståhlberg (2009). "*X-ray crystal structures of Phanerochaete chrysosporium Laminarinase 16A in complex with products from lichenin and laminarin hydrolysis*." Febs Journal **276**(14): 3858-3869.

Verna, J., A. Lodder, K. Lee, A. Vagts and R. Ballester (1997). "*A family of genes required for maintenance of cell wall integrity and for the stress response in Saccharomyces cerevisiae*." Proceedings of the National Academy of Sciences **94**(25): 13804-13809.

Vidal-Cros, A. and M. Boccara (1998). "*Identification of four chitin synthase genes in the rice blast disease agent Magnaporthe grisea*." FEMS microbiology letters **165**(1): 103-109.

Vilella, F., E. Herrero, J. Torres and M. A. de la Torre-Ruiz (2005). "*Pkc1 and the upstream elements of the cell integrity pathway in Saccharomyces cerevisiae, Rom2 and Mtl1, are required for cellular responses to oxidative stress*." Journal of Biological Chemistry **280**(10): 9149-9159.

Vinckier, A. and G. Semenza (1998). "*Measuring elasticity of biological materials by atomic force microscopy*." FEBS letters **430**(1): 12-16.

Wagner, A. (1999). "*Redundant gene functions and natural selection*." Journal of Evolutionary Biology **12**(1): 1-16.

Walker, S. S., Y. Xu, I. Triantafyllou, M. F. Waldman, C. Mendrick, N. Brown, P. Mann, A. Chau, R. Patel and N. Bauman (2011). "*Discovery of a novel class of orally active antifungal Beta-1, 3-D-glucan synthase inhibitors*." Antimicrobial Agents and Chemotherapy **55**(11): 5099-5106.

Wanke, V., E. Cameroni, A. Uotila, M. Piccolis, J. Urban, R. Loewith and C. De Virgilio (2008). "*Caffeine extends yeast lifespan by targeting TORC1*." Molecular microbiology **69**(1): 277-285.

Wapinski, I., A. Pfeffer, N. Friedman and A. Regev (2007). "*Natural history and evolutionary principles of gene duplication in fungi*." Nature **449**(7158): 54-61.

Watanabe, Y., G. Takaesu, M. Hagiwara, K. Irie and K. Matsumoto (1997). "*Characterization of a serum response factor-like protein in Saccharomyces cerevisiae, Rlm1, which has transcriptional activity regulated by the Mpk1 (Slt2) mitogen-activated protein kinase pathway*." Molecular and cellular biology **17**(5): 2615-2623.

Weisenhorn, A. L., M. Khorsandi, S. Kasas, V. Gotzos and H.-J. Butt (1993). "*Deformation and height anomaly of soft surfaces studied with an AFM*." Nanotechnology **4**(2): 106.

Weld, R. J., K. M. Plummer, M. A. Carpenter and H. J. Ridgway (2006). "*Approaches to functional genomics in filamentous fungi*." Cell research **16**(1): 31-44.

Willems, E., L. Leyns and J. Vandesompele (2008). "*Standardization of real-time PCR gene expression data from independent biological replicates*." Analytical biochemistry **379**(1): 127-129.

Wilson, R. A. and N. J. Talbot (2009). "*Under pressure: investigating the biology of plant infection by Magnaporthe oryzae*." Nature Reviews Microbiology **7**(3): 185-195.

Woese, C. R. and G. E. Fox (1977). "*Phylogenetic structure of the prokaryotic domain: the primary kingdoms*." Proceedings of the National Academy of Sciences **74**(11): 5088-5090.

Wood, P. J. (1980). "*Specificity in the interaction of direct dyes with polysaccharides*." Carbohydrate research **85**(2): 271-287.

Wood, V., M. A. Harris, M. D. McDowall, K. Rutherford, B. W. Vaughan, D. M. Staines, M. Aslett, A. Lock, J. Bähler and P. J. Kersey (2011). "*PomBase: a comprehensive online resource for fission yeast*." Nucleic acids research: gkr853.

Woodcock, D., P. Crowther, J. Doherty, S. Jefferson, E. DeCruz, M. Noyer-Weidner, S. Smith, M. Michael and M. Graham (1989). "*Quantitative evaluation of Escherichia coli host strains for tolerance to cytosine methylation in plasmid and phage recombinants*." Nucleic acids research **17**(9): 3469-3478.

Xie, X. and P. N. Lipke (2010). "*On the evolution of fungal and yeast cell walls*." Yeast **27**(8): 479-488.

Xu, J.-R. and J. E. Hamer (1996). "*MAP kinase and cAMP signaling regulate infection structure formation and pathogenic growth in the rice blast fungus Magnaporthe grisea*." Genes & development **10**(21): 2696-2706.

Xu, J.-R., C. J. Staiger and J. E. Hamer (1998). "*Inactivation of the mitogen-activated protein kinase Mps1 from the rice blast fungus prevents penetration of host cells but allows activation of plant defense responses*." Proceedings of the National Academy of Sciences **95**(21): 12713-12718.

Xu, Y. B., H. P. Li, J. B. Zhang, B. Song, F. F. Chen, X. J. Duan, H. Q. Xu and Y. C. Liao (2010). "*Disruption of the chitin synthase gene CHS1 from Fusarium asiaticum results in an altered structure of cell walls and reduced virulence*." Fungal Genetics and Biology **47**(3): 205-215.

Yang, J., L. Kong, X. Chen, D. Wang, L. Qi, W. Zhao, Y. Zhang, X. Liu and Y.-L. Peng (2012). "*A carnitine–acylcarnitine carrier protein, MoCrc1, is essential for pathogenicity in Magnaporthe oryzae*." Current genetics **58**(3): 139-148.

Yin, Q. Y., P. W. de Groot, H. L. Dekker, L. de Jong, F. M. Klis and C. G. de Koster (2005). "*Comprehensive proteomic analysis of Saccharomyces cerevisiae cell walls identification of proteins covalently attached via glycosylphosphatidylinositol remnants or mild alkali-sensitive linkages*." Journal of Biological Chemistry **280**(21): 20894-20901.

Yoshimoto, H., K. Saltsman, A. P. Gasch, H. X. Li, N. Ogawa, D. Botstein, P. O. Brown and M. S. Cyert (2002). "*Genome-wide analysis of gene expression regulated by the calcineurin/Crz1p signaling pathway in Saccharomyces cerevisiae*." Journal of Biological Chemistry **277**(34): 31079-31088.

Zeigler, R. and S. Savary (2010). *Plant Diseases and the World's Dependence on Rice*. The Role of Plant Pathology in Food Safety and Food Security, Springer**:** 3-9.

Zeigler, R. S. and A. Barclay (2008). "*The relevance of rice*." Rice **1**(1): 3-10.

Zelante, T., R. G. Iannitti, A. De Luca, J. Arroyo, N. Blanco, G. Servillo, D. Sanglard, U. Reichard, G. E. Palmer and J.-P. Latgè (2012). "*Sensing of*

mammalian IL-17A regulates fungal adaptation and virulence." Nature communications **3**: 683.

Zhang, H., K. Liu, X. Zhang, W. Song, Q. Zhao, Y. Dong, M. Guo, X. Zheng and Z. Zhang (2010). "*A two-component histidine kinase, MoSLN1, is required for cell wall integrity and pathogenicity of the rice blast fungus, Magnaporthe oryzae*." Current genetics **56**(6): 517-528.

Zhang, H., W. Tang, K. Liu, Q. Huang, X. Zhang, X. Yan, Y. Chen, J. Wang, Z. Qi and Z. Wang (2011). "*Eight RGS and RGS-like proteins orchestrate growth, differentiation, and pathogenicity of Magnaporthe oryzae*." PLoS pathogens **7**(12): e1002450.

Zhang, H., Q. Zhao, X. Guo, M. Guo, Z. Qi, W. Tang, Y. Dong, W. Ye, X. Zheng and P. Wang (2014). "*Pleiotropic function of the putative Zinc-finger protein MoMsn2 in Magnaporthe oryzae*." Molecular plant-microbe interactions **27**(5): 446-460.

Zhao, L., D. Schaefer, H. Xu, S. J. Modi, W. R. LaCourse and M. R. Marten (2005). "*Elastic properties of the cell wall of Aspergillus nidulans studied with atomic force microscopy*." Biotechnology progress **21**(1): 292-299.

Zhao, X., R. Mehrabi and J.-R. Xu (2007). "*Mitogen-activated protein kinase pathways and fungal pathogenesis*." Eukaryotic cell **6**(10): 1701-1714.

Zipfel, C. (2008). "*Pattern-recognition receptors in plant innate immunity*." Current opinion in immunology **20**(1): 10-16.

Abbreviations

Abbreviations	Meaning
AFM	Atomic Force Microscopy
Chs	Chitin synthase gene
CR	Congo Red. A cell wall perturbant compound
Crh	Congo Red Hypersensitivity gene
Crh-like genes	Referring to all three *S. cerevisiae Crh1, Utr2* and *Crr1* genes and the corresponding homologs in other species.
ct	Cycle threshold in relevance to qRT-PCR
CWI	MAPK Signal Transduction Cell Wall Integrity pathway
CWP	cell wall protein
Fks	Glucan synthase gene
Gas1	Glucan elongation enzyme. See *Gel*
Gel	Glucan Elongation enzyme, synonymous with *Gas1*. A GPI-anchored cell wall remodeling protein catalyzing the elongation and branching of glucan chains
GH16	Glycosyl Hydrolase 16 family of enzymes
GOI	Gene of Interest
GPI	Glycosylphosphatidylinositol
hpi	Hours post inoculation
Kre	(1,6)-Glucan syntase gene, a cell wall protein
PAMP	Pathogen Associated Molecular Pattern
Rlm1	Transcription factor for the CWI pathway
SBF Complex	Dimeric complex of two transcription factors, Swi4/Swi6
Swi4/Swi6	Transcription factors for the CWI pathway forming a dimeric complex (SBF complex)
TF	Transcription factor

Appendices

Appendix A. Figures and Tables for Chapter 3

A.1 *Saccharomyces cerevisiae* Crh-like Orthologues in *Magnaporthe oryzae*. Amino acid sequences from *S. cerevisiae* Crh1p, Crr1p and Utr2p were queried against *M. oryzae* 70-15 (Taxid: 242507) genome using the BLASTp search tool in NCBI.

***S. cerevisiae* gene**	**BLASTp results**	**E Value**	**Percentage Identity (%)**	**Reciprocal hit (*S. cerevisiae*)**
Crr1	*1. MGG_01134* (*MGG_Utr2*)*	$7e^{-68}$	35	*Utr2*
	2. MGG_09918 (*MGG_Crh1*)	$6e^{-30}$	33	*Crh1*
	3. MGG_00592 (*MGG_Crh2*)	$1e^{-29}$	39	*Crh1*
	4. MGG_10431 (*MGG_Crh3)*	$5e^{-29}$	34	*Crh1*
	5. MGG_12652 (*MGG_Crh4*)	$8e^{-26}$	32	*Crh1*
Utr2	1. *MGG_01134* (*MGG_Utr2*)*	$2e^{-104}$	*47*	*Utr2*
	2. *MGG_10431* (*MGG_Crh3*)	$2e^{-25}$	*32*	*Crh1*
	3. *MGG_12652* (*MGG_Crh4*)	*$1e^{-23}$*	*29*	*Crh1*
	4. *MGG_00592* (*MGG_Crh2*)	*$1e^{-21}$*	*30*	*Crh1*
	5. *MGG_09918* (*MGG_Crh1*)	$8e^{-19}$	*29*	*Crh1*
Crh1	1. *MGG_09918* (*MGG_Crh1)**	$2e^{-82}$	41	*Crh1*
	2. *MGG_00592* (*MGG_Crh2*)	$5e^{-62}$	38	*Crh1*
	3. *MGG_12652* (*MGG_Crh4*)	$2e^{-57}$	37	*Crh1*
	4. *MGG_10431*(*MGG_Crh3*)	$4e^{-51}$	32	*Crh1*
	5. *MGG_01134* (*MGG_Utr2*)	$1e^{-27}$	30	*Utr2*

* Best hit *M. oryzae* gene from the queried *S. cerevisiae* gene

A.2. Matinspector Transcription Factor DNA Binding Site Prediction. Two *S. cerevisiae* Crh-like genes *Crh1* and *Utr2* and the orthologues in *M. oryzae* were queried against the Matinspector database of matrix sequences (MatrixID) for transcription factor DNA-binding site prediction in the promoter region of each gene.

SC_Crh1	MGG_Crh1	MGG_Crh2	MGG_Crh3	MGG_Crh4	MGG_Utr2	Sc_Utr2	MatrixID
0	0	0	1	1	1	1	ABAA.01
0	0	0	0	0	0	1	ABF1.02
1	0	1	1	1	4	1	ABF1.03
0	1	0	0	1	1	0	ADR1.01
0	0	0	2	0	0	0	AFT1.01
0	0	1	0	0	0	0	AFT2.01
0	0	1	2	1	2	0	ARO80.01
0	1	0	0	0	0	0	ASG1.01
0	0	0	0	1	1	0	BAS1.01
0	1	2	0	1	1	0	CAT8.01
0	0	0	1	0	0	0	CBF1.01
2	1	1	1	3	1	0	CEP3.01
6	1	1	0	1	0	1	CIN5.01
0	1	1	0	1	0	0	CRZ1.01
3	2	0	0	0	0	0	CSRE.01
1	0	2	1	0	0	0	CST6.01
1	0	0	0	0	0	0	CUSE.01
1	3	0	0	2	0	0	DAL80.01
0	0	2	2	0	1	0	DAL82.01
2	0	0	0	1	0	1	ECM22_UPC2.01
0	0	1	0	2	0	0	FACBCA.01
0	0	0	2	2	0	1	FHL1.01
0	1	0	0	0	1	1	FKH1.01
0	1	0	0	0	0	0	FKH2.01
0	1	1	0	0	1	0	GAL4.02

0	1	0	0	0	1	2	GATA.01
0	1	0	1	0	0	1	GAT1.01
0	0	1	0	0	0	0	GAT3.01
4	0	1	0	0	0	3	GAT4.01
0	0	0	1	1	0	0	GCR1.01
0	0	2	0	0	0	0	GCR1.02
1	0	0	0	0	1	1	GCN4.02
0	0	0	0	0	1	1	GLN3.01
0	0	1	1	0	0	0	GZF3.01
0	0	0	1	0	0	0	HAC1.02
1	1	1	0	1	2	0	HAP1.01
1	1	0	0	2	0	1	HAP234.01
0	1	0	4	1	0	5	HSF1.01
0	0	0	0	1	0	1	HSF1.02
0	1	3	0	2	1	2	ICGG_N10.01
0	0	1	0	0	0	0	LAC9.01
0	0	0	0	0	0	2	LEU3.01
0	2	0	0	1	0	0	LEU3.02
1	0	0		0	0	2	LYS14.01
1	2	0	0	2	5	0	MAT1MC.01
0	0	0	0	0	0	1	MBP1.01
0	0	1	1	0	0	0	MCB.01
0	0	0	0	2	0	0	MCM1.02
2	0	0	0	1	1	0	MATA1.01
1	0	0	2	0	0	0	MATALPHA2.01
1	2	0	0	2	3	0	MATALPHA2.02
1	0	0	0	0	0	1	MAT1MC.01
2	4	0	0	0	1	1	MCB.01
2	0	1	0	0	1	2	MCM1.01
4	0	0	0	0	0	3	MCM1.02
1	0		0	0	1	0	MET31.01

3	1	1	0	2	0	1	MGA1.01
0	2	1	0	1	1	0	MIG1.01
0	0	0	0	1	0	0	MIG1.02
0	0	0	0	1	0	0	MIG2.01
1	0	0	0	0	0	0	MOT3.01
0	0	0	0	0	1	0	MSE.01
0	1	4	1	4	5	2	MSN2.01
0	3	0	3	1	3	0	NIT2.01
0	0	0	0	0	0	1	NRG1.01
3	3	1	0	2	3	1	OAF1.01
0	1	1	5	0	0	0	ORE.01
0	0	1	0	0	0	0	PACC.01
2	0	0	0	2	3	0	PDRE.01
0	1	0	0	0	0	1	PDR1.01
1	1	2	0	1	1	4	PHD1.01
0	0	0	1	0	0	0	PHD1.02
1	0	0	0	0	1	0	PHO2.01
0	1	0	0	0	0	0	PHO4.01
0	2	0	2	0	0	0	PPR1.01
0	1	1	2	1	0	0	QA1F.01
0	0	0	0	2	0	0	RAP1.02
0	5	2	1	0	2	0	RAP1.05
2	1	2	2	2	2	0	RDS1.01
0	0	0	0	0	5	1	RDS2.01
0	0	0	0	1	0	0	REB1.01
0	3	0	1	0	1	0	REB1.02
0	1	0	0	2	0	0	REPCAR1.01
2	1	1	5	2	1	0	RFX1.01
0	0	1	1	0	1	0	RIM101.01
2	0	1	2	0	0	1	RLM1.01
2	2	1	0	2	2	0	ROX1.01

2	1	0	1	0	0	1	RGT1.02
0	1	0	0	0	0	0	RPN4.01
0	0	0	0	1	0	0	RSC30.01
1	0	0	3	1	1	0	SIP4.01
0	0	2	0	0	0	0	SKN7.01
0	0	1	0	0	0	0	SMP1.01
1	0	0	0	0	1	0	SRD1.01
2	0	1	0	1	2	3	STB3.01
0	0	0	0	1	0	0	STE11.01
0	1	0	1	1	0	0	STE11.02
3	0	0	2	0	1	2	STE12.01
0	3	0	0	1	0	1	STP2.01
0	0	0	0	0	1	0	STP4.01
3	2	0	1	1	1	1	STUAP.01
0	0	0	0	1	1	0	SUM1.01
2	1	0	2	1	1	2	SWI4.01
1	0	0	0	0	0	0	SWI5.01
0	1	1	1	0	1	0	TBF1.01
1	0	0	0	0	0	1	TBF1.02
3	0	1	1	1	2	2	TEA1.01
0	0	0	2	1	0	1	TOS8.01
2	0	2	2	1	0	3	TEC1.01
0	0	1	2	1	0	2	UAY.01
1	0	1	0	0	1	0	UME6.01
0	3	0	2	4	0	2	XBP1.01
0	0	2	0	0	3	2	XBP1.02
1	2	2	0	1	1	1	YAP1.01
0	0	0	2	0	0	2	YAP1.02
0	0	0	0	0	3	0	YRR1.01
1	0	2	0	0	0	0	YOX1.01

5	1	0	0	2	0	7	YOX1.02
1	3	0	0	0	0	2	YRR1.01

A.3. Matinspector Matrix Information. Two *S. cerevisiae Crh-like* genes *Crh1* and *Utr2* and the orthologues in *M. oryzae* were queried against the Matinspector database of matrix sequences (Matrix ID) for transcription factor DNA binding site prediction in the promoter region of each gene. Listed below all matrixes identified in all genes querried, with a description of the motifs.

MatrixID	Detailed Matrix Information	Sequence
ABAA.01	Aspergillus spore/developmental regulator	tctcggCATTccaaaga
ABF1.02	ARS binding factor 1	gcataattacaaACGCgca
ABF1.03	ARS (autonomously replicating sequence)-binding factor I	ccatcacttaatACGGttt
ADR1.01	Alcohol Dehydrogenase Regulator, carbon source-responsive zinc-finger transcription factor	caCCCCaag
AFT1.01	Transcription factor involved in iron utilization and homeostasis (iron-sensing transcription factor AFT1)	cattttgCACCcgga
AFT2.01	Activator of Fe (iron) transcription 2, iron-regulated transcriptional activator	aggcaaaCACCcctg
ARO80.01	Aromatic amino acid requiring (activates transcription of aromatic amino acid catabolic genes in the presence of aromatic amino acids)	ggtcTCGGtacaagtct
ASG1.01	Fungal zinc cluster transcription factor Asg1	tCCGGtggctggacggt
BAS1.01	Transcription factor involved in the expression of genes encoding enzymes acting in histidine, purine, and pyrimidine biosynthetic pathways	tgtctcaGAGTcaacga
CAT8.01	Zinc cluster transcriptional activator binding to carbon source responsive elements (CSRE)	gccttgcgaCCGAat
CBF1.01	CBF1, bHLH protein binds centromeric CDE1 box and promoter regions of methionine biosynthesis genes	gtctCACAtgagttc
CEP3.01	Essential kinetochore protein, component of the CBF3 complex that binds the CDEIII region of the centromere	ggcgTCGGaaagaaaag
CIN5.01	bZIP transcriptional factor of the yAP-1 family that mediates pleiotropic drug resistance and salt tolerance	gagtctccatcactTAATacg
CRZ1.01	Calcineurin-responsive zinc finger 1	gtGGCTg
CSRE.01	Carbon source-responsive element (yeast)	caaatccgTCCGgcg

CST6.01	Chromosome stability, bZIP transcription factor of the ATF/CREB family (ACA2)	tactaactcgtACGTgattct
CUSE.01	Copper-signaling element, AMT1/ACE1 recognition sequence	ggtttttGCTGtat
DAL80.01	Degradation of allantoin, negative regulator of genes in multiple nitrogen degradation pathways	gagcGATAaaaaagc
DAL82.01	Transcriptional activator for allantoin catabolic genes	aatgTGCGa
ECM22_UPC2.01	Sterol regulatory element binding proteins Ecm22 and Upc2	tagTATAaaac
FACBCA.01	FACB, activator of acetate utilization genes with a GAL4-type Zn(II)2Cys6 zinc binuclear cluster	tcttctctctcgAGGAc
FHL1.01	Fork head transcription factor Fhl1	tggACGCaggaat
FKH1.01	Fork head transcription factor Fkh1	ccgagagTAAAgaacta
FKH2.01	Fork head transcription factor Fkh2	tggaaacTAAAcaaata
GAL4.02	GAL4 transcriptional activator in response to galactose induction	aggagggagccttgcgaCCGAataa
GATA.01	GATA binding factor (yeast)	aggaGATAacggtcg
GAT1.01	GATA-type Zn finger protein Gat1	tccagATAAaaattc
GAT3.01	GATA-type Zn finger protein Gat3	gaaaGATCcacccag
GAT4.01	GATA-type Zn finger protein Gat4	ggtgGATCtttccca
GCR1.01	GCR1 activates transcription of glycolytic enzymes, interaction with RAP1	ggCTTCctgcgcgtact
GCR1.02	GCR1 activates transcription of glycolytic enzymes, interaction with RAP1	tcCTTCctttcaccttg
GCN4.02	GCN4, dimerizing leucine zipper protein	gtgTGACttttgc
GLN3.01	Transcriptional regulator of nitrogen metabolism	gctgGATAaagggat
GZF3.01	GATA zinc finger protein Gzf3	gaatGATTagcgaaa
HAC1.02	bZIP transcription factor (ATF/CREB1 homolog) that regulates the unfolded protein response	cgttctcgacgGCGTttccaa
HAP1.01	HAP1, S. cerevisiae member of GAL family, regulates heme dependent cytochrome expression	aagcacatAACGcag
HAP234.01	Yeast factor complex HAP2/3/5, homolog to vertebrate NF-Y/CP1/CBF	ttgacCCAAttag
HSF1.01	Trimeric heat shock transcription factor	gagcgtttaaccacatGGAAataccttgagtg

HSF1.02	Trimeric heat shock transcription factor	aaagaaagaaaatcaggtaattaaccAGAAtca
ICGG_N10.01	Inverted CGG motifs separated by a spacer of 10 bp; Put3, Tea1 and Cha4 binding sites	gTGGAtctttcccaccgtctc
LAC9.01	LAC9 binding site, homologous to GAL4 of Saccharomyces cerevisiae	tccCGGAttcttcccatcagagcat
LEU3.01	LEU3, S. cerevisiae, zinc cluster protein	tagtcggtACCGaatag
LEU3.02	LEU3, S. cerevisiae, zinc cluster protein	cgtCCGGcgtggtcggg
LYS14.01	Transcriptional activator involved in regulation of genes of the lysine biosynthesis pathway	ttccgtGGAAtttccaa
MAT1MC.01	HMG-BOX protein interacts with M-box site, cooperativity with HMG-Box STE11 protein	ttgATTGtttt
MBP1.01	Transcription factor binding to the MluI cell cycle box (MCB)	cggaCTCGtcagg
MCB.01	Mlu I cell cycle box, activates G1/S-specific transcription (yeast)	actgCGCGtttgg
MCM1.02	Yeast factor MCM1 cooperating with MATalpha factors	tTTCCcctcttggaaag
MATA1.01	Homeodomain protein mating factor a1	gcgtGATGtgtga
MATALPHA2.01	Homeodomain protein mating factor alpha2	ggcacATGTcaat
MATALPHA2.02	Homeodomain transcriptional repressor Matalpha2	attgaTTGTtttt
MAT1MC.01	HMG-BOX protein interacts with M-box site, cooperativity with HMG-Box STE11 protein	ttgATTGtttt
MCB.01	Mlu I cell cycle box, activates G1/S-specific transcription (yeast)	cgccCGCGttacc
MCM1.01	Yeast factor MCM1 cooperating with MATalpha factors	tctCCCAaataagttga
MCM1.02	Yeast factor MCM1 cooperating with MATalpha factors	tTTCCcctcttggaaag
MET31.01	Zinc-finger DNA-binding protein, involved in transcriptional regulation of the methionine biosynthetic genes	gctttGTGGcgtgac
MGA1.01	Heat shock transcription factor Mga1	ttcgcttgtatgcgataGAATataaagttcttc
MIG1.01	MIG1, zinc finger protein mediates glucose repression	gaataaggagcGGGGtgga
MIG1.02	MIG1, zinc finger protein mediates glucose repression	gatgctgatgtGGGGggca
MIG2.01	MIG2, zinc finger protein mediates glucose repression	tgctgatgtggGGGGcaga
MOT3.01	Modifier of transcription 3, zinc finger transcription factor involved in repression of a subset of hypoxic genes	ggagtAGGCaattattgaaag
MSE.01	Middle sporulation element (MSE)	ttaatacaCAAAaaa

MSN2.01	Transcriptional activator for genes in multistress response	aggaccaGGGGtgtt
NIT2.01	Activator of nitrogen-regulated genes	TATCaag
NRG1.01	Transcriptional repressor Nrg1	aacAGGGtccaac
OAF1.01	Oleate-activated transcription factor, acts alone and as a heterodimer with Pip2p	ttcttttcttTCCGacgccagtccg
ORE.01	Oleate response element, binding motif of Oaf1 homodimers or Oaf1/Pip2 heterodimers	CGGGattgattgcctggctggctgt
PACC.01	pH-responsive regulator from Aspergillus	gccaGCCAggcaatcaa
PDRE.01	Pleiotropic drug resistance responsive element (yeast)	TCCAcggag
PDR1.01	Zinc cluster protein, master regulator involved in recruiting other zinc cluster proteins to pleiotropic drug response elements (PDREs)	gCCGCgaaa
PHD1.01	Transcription factor involved in regulation of filamentous growth	acctTGCAttgaa
PHD1.02	Transcription factor involved in regulation of filamentous growth	ggtcTGCGccagg
PHO2.01	Homeodomain protein Pho2	gtaTTAActtgatac
PHO4.01	PHO4 involved in regulation of phosphatase genes, repressed in presence of phosphate	agcgCACGtttgtgg
PPR1.01	Pyrimidine pathway regulator 1	gtaggacaattCCGAtg
QA1F.01	qa-1F, required for quinic acid induction of transcription in the qa gene cluster	ctggaaagaaaaTTATaatct
RAP1.02	RAP1 (TUF1), activator or repressor depending on context	gcctccacccgtcgtcCACCcgt
RAP1.05	RAP1 (TUF1), activator or repressor depending on context	gaccaagtcaccccTGCAgcttt
RDS1.01	Regulator of Drug Sensitivity 1, zinc cluster transcription factor involved in conferring resistance to cycloheximide	cgaCGGCcgactt
RDS2.01	Regulator of drug sensitivity 2, zinc cluster transcriptional activator involved in conferring resistance to ketoconazole	ctcgggaatCCGAac
REB1.01	REB1, S. cerevisiae	ctgttGCCCggcg
REB1.02	rDNA enhancer binding protein 1, termination factor for RNA polymerase I and transcription factor for RNA polymerase II	tcgTTACccaagt
REPCAR1.01	repressor of CAR1 expression	gtttcGCGGcttgca

RFX1.01	RFX1 (CRT1) is a DNA-binding protein that acts by recruiting Ssn6 and Tup1, general repressors to the promoters of damage-inducible genes	gcgcagtgGAAAcct
RIM101.01	Transcriptional repressor involved in response to pH and in cell wall construction	tcccGCCAagctctggc
RLM1.01	Yeast MADS-Box RLM1 transcription factor	gtttTCTAccattagtagc
ROX1.01	Heme-dependent transcriptional repressor of hypoxic genes	gcttTTGTtttcg
RGT1.02	Glucose-responsive transcription factor involved in regulation of glucose transporters	aaagaAGGAaaaaaaaa
RPN4.01	Transcriptional activator of proteasomal genes	caaCGCCactcaagg
RSC30.01	Component of the RSC chromatin remodeling complex	aaaagcgtcaCCCGcgtggta
SIP4.01	Zinc cluster transcriptional activator, binds to the carbon source-responsive element (CSRE) of gluconeogenic genes	tCCCTttatccagca
SKN7.01	SKN7, a transcription factor contributing to the oxidative stress response	TGGCtggacca
SMP1.01	Yeast MADS-Box SMP1 transcription factor	ggctaCTAAtggtagaaaa
SRD1.01	Protein involved in the processing of pre-rRNA to mature rRNA	cggaGATCcacatct
STB3.01	Ribosomal RNA processing element (RRPE)-binding protein	gcccgtttTTTCacagt
STE11.01	TR-boxes interacting with ubiquitous factor STE11	gattttCTTTcttttggat
STE11.02	M cell-specific TR-boxes, STE11 needs cooperative Mat1-Mc binding	aagcctATTTgtttagttt
STE12.01	Transcription factor activated by a MAP kinase signaling cascade, activates genes involved in mating or pseudohyphal/invasive growth pathways	aaatgcAACAagc
STP2.01	Proteolytically activated transcription factor	cgggcGCCGggcaac
STP4.01	Krueppel-type zinc finger protein	gatgAGCCgttcgaa
STUAP.01	Aspergillus Stunted protein, (bHLH)-like structure, regulates multicellular complexity during asexual reproduction	cgttCGCGactca
SUM1.01	Transcriptional repressor required for mitotic repression of middle sporulation-specific genes	tcacgcCACAaagca

SWI4.01	DNA binding component of the SBF(SCB binding factor) complex (Swi4p-Swi6p)	gagtcgCGAAcga
SWI5.01	SWI5, activates transcription of genes expressed at the M/G1 boundary and in G1 phase of the cell cycle	aaCCAGcaa
TBF1.01	TTAGGG repeat binding factor 1	ccatcCCTAacag
TBF1.02	TTAGGG repeat binding factor 1	tcAACCctagcca
TEA1.01	Ty1 enhancer activator, zinc cluster DNA-binding protein	ttctaaaTTAAatagcggtag
TOS8.01	Homeodomain-containing transcription factor	ctcttttGTCAaa
TEC1.01	Transposon enhancement control 1, required for full Ty1 epxression, Ty1-mediated gene activation, and haploid invasive and diploid pseudohyphal growth	gctaatcATTCcttctt
UAY.01	UAY (Aspergillus nidulans, involved in purine utilization)	ccCGGAttcttcccatc
UME6.01	UME6, key regulator of nitrogen repression and meiotic development	gcttgGCGGgaaatc
XBP1.01	*S.cerevisae* XhoI site-binding protein I, stress induced expression	aaacTCGAtgaaa
XBP1.02	Stress-induced transcriptional repressor	tctcTCGAggact
YAP1.01	Yeast activator protein of the basic leucine zipper (bZIP) family	aaaaccgtaTTAAgtgatgga
YAP1.02	Yeast activator protein of the basic leucine zipper (bZIP) family	atctcattgcttgGTAAcgcg
YRR1.01	Zinc cluster transcription factor, activates genes involved in multidrug resistance (PDR2)	gtccaCGGAgatccaca
YOX1.01	Yeast homeobox 1, homeodomain-containing transcriptional repressor	ttctaAATTaaatag
YOX1.02	Yeast homeobox 1, homeodomain-containing transcriptional repressor	gacccaATTAgaccg
YRR1.01	Monomeric Gal4-class motifs	cgcctCGGAcatgaaga

A.4. Glycophosphatidylinositol (GPI) Anchor Prediction in *Crh-like* Genes from Four Fungal Species. Amino acid sequences were queried against two prediction softwares, GPI-SOM (Fankhauser and Mäser 2005) and big-PI (Eisenhaber *et al.* 2004).

Species	Gene	a.a length	GPI-SOM (location)	big-PI (location)
S. cerevisiae	*Crr1*	422	No	No
	Crh1	507	Yes (475)	Yes (483)
	Utr2	467	Yes (444)	Yes (446)
M. oryzae	*MGG_Utr2*	439	Yes (423)	Yes (410)
	MGG_Crh1	357	Yes (330)	Yes (330)
	MGG_Crh2	367	Yes (347)	Yes (345)
	MGG_Crh3	739	No	No
	MGG_Crh4	499	No	No
N. crassa	*Nc_Utr2*	477	Yes (446)	Yes (445)
	Nc_crh1	375	Yes (343)	Yes (346)
	Nc_Crh2	364	Yes (353)	Yes (341)
	Nc_Crh3	320	No	No
	Nc_Crh4	510	No	No
C. albicans	*Ca_Utr2*	470	Yes (439)	Yes (440)
	Crh11	453	Yes (425)	Yes (430)
	Crh12	504	Yes (488)	Yes (478)

A.5. List of Genes Used for the Maximum Likelihood Phylogenetic Tree Construction

Conserved Domain Database (CDD)	Species	Given Gene Name (Systematic name)	NCBI Protein Accesion	Source*
GH16_fungal_CRH1_transglycosylase (cd02183)	*Saccharomyces cerevisiae*	Crh1 (YGR189C)	NP_011705	SGD
		Utr2 (YEL040W)	NP_010874	SGD
		Crr1 (YLR213C)	NP_013314	SGD
	Magnaporthe oryzae	MGG_Crh1 (MGG_09918)	XP_003710016	The Fungal Genomics
		MGG_Crh2 (MGG_00592)	XP_003718448	The Fungal Genomics
		MGG_Crh3 (MGG_10431)	XP_003719450	The Fungal Genomics
		MGG_Crh4 (MGG_12652)	XP_003721196	The Fungal Genomics
		MGG_Utr2 (MGG_01134)	XP_003717792	The Fungal Genomics
	Candida albicans	Ca_Utr2 (orf19.1671)	XP_721748	CGD via-Orthogroup
		Ca_Crh11 (orf19.2706)	XP_720457	CGD via-Orthogroup
		Ca_Crh12 *(orf19.3966)*	XP_722035	CGD via-Orthogroup
	Schizosaccharomyces pombe	Spombe (SPBC21B10.07)	NP_595680	PomBase via Orthogroup
	Neurospora crassa	NC_Utr2 (NCU05686)	XP_963048	AspGD via Orthogroup
		NC_Crh1 (NCU09117)	XP_958032	AspGD via Orthogroup
		NC_Crh2 (NCU05974)	XP_958627	AspGD via Orthogroup
		Nc_Crh3 (NCU09672)	XP_960762	AspGD via Orthogroup
		NC_Crh4 (NCU08072)	XP_965203	AspGD via Orthogroup
	Aspergillus nidulans	An_CrhB (AN4515)	XP_662119	Broad Fungal Genome Initiative
		An_CrhC (AN0933)	XP_658537	Broad Fungal Genome Initiative
		An_CrhA (AN3914)	XP_661518	Broad Fungal Genome Initiative
		An_CrhD (AN3053)	XP_660657	Broad Fungal Genome Initiative
	Yarrowia lipolytica	Yl_5510 (YALI0B15510g)	XP_500934	Orthogroup
		Yl_9680	XP_501652	Orthogroup

	(YALI0C09680g)		
	Yl_4673 (YALI0E24673g)	XP_504363	Orthogroup
Aspergillus fumigatus	Af_Crh1 (Afu6g08510)	Not available in NCBI	AspGD
	Af_Crh2 (Afu1g16190, syn Crf1	Not available in NCBI	AspGD
	Af_Crh3 (Afu6g03230)	Not available in NCBI	AspGD
	Af_Crh4 (Afu3g09250)	Not available in NCBI	AspGD
	Af_Utr2 (Afu2g03120)	Not available in NCBI	AspGD
Kluyveromyces lactis	Kl_Crh (KLLA0F22671g)	XP_456093	Genolevures via Orthogroup
	Kl_Utr2 (KLLA0F16907g)	XP_455839	Genolevures via Orthogroup
	Kl_Crr1 (KLLA0F04906g)	XP_455302	Genolevures via Orthogroup
Saccharomyces paradoxus	Spar_289 (spar289-g4.1)	Not available in NCBI	Broad Fungal Genome Initiative via Orthogroup
	Spar_355 (spar355-g8.1)	Not available in NCBI	Broad Fungal Genome Initiative via Orthogroup
	Spar_142 (spar142-g21.1)	Not available in NCBI	Broad Fungal Genome Initiative via Orthogroup
Saccharomyces mikatae	Smik_654 (smik654-g1.1)	Not available in NCBI	Broad Fungal Genome Initiative via Orthogroup
	Smik_281 smik281-g3.1	Not available in NCBI	Broad Fungal Genome Initiative via Orthogroup
	Smik_305 smik1305-g1.1	Not available in NCBI	Broad Fungal Genome Initiative via Orthogroup
Candida glabrata	Cg_Crh CAGL0G09449g	XP_446771	Genolevures via Orthogroup
	Cg_Utr2 CAGL0C02211g	XP_445272	Genolevures via Orthogroup
	Cg_Crr1 CAGL0J08910g	XP_448096	Genolevures via Orthogroup

	Fusarium graminearum	Fg_1 FGSG_06873	XP_387049	MIT Fusarium Comparative
		Fg_2 (FGSG_03017)	XP_383193	MIT Fusarium Comparative
	Ustilago maydis	UM_1 UM00891.1	XP_757038	MIT Ustilago maydis Database
		UM_2 UM00330.1	XP_756477	MIT Ustilago maydis Database
GH16_beta_agarase (cd02178) *beta agarase	*Pseudoalteromonas atlantica*	Pa_Bag	WP_011573732	NCBI
GH16_strep_laminarinase_like (cd02182)	*N. crassa*	Nc_Strep1	CAF06015	CDD via NCBI
		Nc_Strep2	XP_960049	CDD via NCBI
GH16_XET (cd02176)	*Asparagus officinalis*	Ao_XET	AAF80590	CDD via NCBI
	Festuca pratensis	Fp_XET	CAC40808	CDD via NCBI
GH16_lichenase (cd02175)	*Aliivibrio salmonicida*	As_Lic	YP_002264432	CDD via NCBI
	Bacillus circulans	Bc_Lic	AAG53947	CDD via NCBI
GH16_CCF (cd08024)	*Ciona intestinalis*	Ci_CCF	XP_002126690	CDD via NCBI
GH16_fungal_Kre6_glucanase (cd02180)	*S. cerevisiae*	Sc_KRE	NP_015485	CDD via NCBI
	Schizosaccharomyces pombe	Spombe (SPBC21B10.07)	NP_595680	PomBase via Orthogroup
GH16_beta_GRP (cd02179)	*Tenebrio molitor*	Tm_BetaGRP	Q76DI2	CDD via NCBI
GH16_kappa_carrageenase (cd02177)	*Zobellia galactanivorans*	Zg_Kcgase	AAC27890	CDD via NCBI
GH_16	*M. oryzae*	MGG_09861	XP_003720374	GH16 Pfam search tool in MIT Magnaporthe Comparative
		MGG_00374	XP_003718705	GH16 Pfam search tool in MIT Magnaporthe Comparative
		MGG_13777	XP_003710831	GH16 Pfam search tool in MIT Magnaporthe Comparative
		MGG_09733	XP_003717619	GH16 Pfam search tool in MIT Magnaporthe Comparative

		MGG_02573	XP_003721228	GH16 Pfam search tool in MIT Magnaporthe Comparative
GH7_CBH_EG (cdd:07999) outgroup	*A. nidulans*	GH7_An	XP_658098	CDD via NCBI

* *S. cerevisiae* amino acid sequences for Crh1p, Utr2p and Crr1p were obtained from Saccharomyces Genome Database (SGD) and used as queries in BLASTp search against other fungal genomes from databases mentioned

A.6. Primer Description and Efficiency. Primer sequences used, expected amplified product size, measured efficiency and source of reference.

Gene Symbol	Efficiency (E)	R^2 Value	Forward Primer*	Reverse Primer*	Size (bp)	Reference
Candidate Reference Genes						
MGG_β-Tubulin	1.95	0.9998	CTGCCATCTTCCGTGGAAAGG	GACGAAGTACGACGAGTTCTTG	86	Skamnioti et.al. 2007
MGG_Ef1	1.92	0.9995	CATCTTAACGTCGTCGTCATC	AGTGGCCGGTAGTCGTGG	62	This study
MGG_Actin	2.02	0.9975	ACAATGGTTCGGGTATGTGC	CGACAATGGACGGGAAGAC	76	This study
MGG_Ubiq	1.99	0.9996	ATCCTAATGTCTACCCGAG	GATGCGTGTTCGTAGTGG	85	This study
MGG_Gapdh	2.06	0.9988	CAAGTACGCCAAATACATGC	TTGCCGTTGACGACCAGG	96	This study
MGG_40S	1.95	0.9996	ACAAGCTCAAGACCCTCGTC	GGTGGTGATGGTGAAGCAG	80	This study
MGG_S8	1.90	0.9989	GCTCACTACCGCCAGAAGC	ACGGACGGTGTGAATGCG	87	This study
MGG_Fad	2.04	0.9984	ACCTTGTTGGCTGCGATG	TCCATCGAGTACACCCCAC	104	This study
MGG_Nuc	2.04	0.9978	AGTGCGGGTTATGGTCTCTTC	CTGCTCTCCAGGTCATCTGC	64	This study
Genes of Interest (GOI)						
MGG_Utr2	1.81	0.9932	CACCTTGCTGTGGTCTCTACG	TCGCAACCTCCAAGGCAG	63	This study
MGG_Crh1	1.92	0.9969	CATACGACAACATGCCCTGC	TTGACGGCTCCCTTGGTG	74	This study
MGG_Crh2	1.86	0.9908	GAGATCGACTGGGAGCACG	AGACGGTGTCATTACCCTTGG	79	This study
MGG_Crh3	2.11	0.9929	AATACAATTTTTGTGGAAACTCC	CTGACACCAAAGGTACCACC	94	This study
MGG_Crh4	1.92	0.99551	AAGATCGTTGAGGGTGAATCG	GTAGATACCGGTCCTTGCACC	118	This study

*underlined nucleotides represent second region of an exon in a primer that anneals to an exon/exon boundary

A.7. Nine *Magnaporthe oryzae* Candidate Reference Gene Primer Specificity Check by Melt Curve Analyses. PCR product dissociation curves for nine primer pairs used in this analysis using pooled cDNA of WT from all samples used. Melt curve data was obtained from the denaturation of amplified PCR product executed at the end of a qRT-PCR run, by temperature increment.

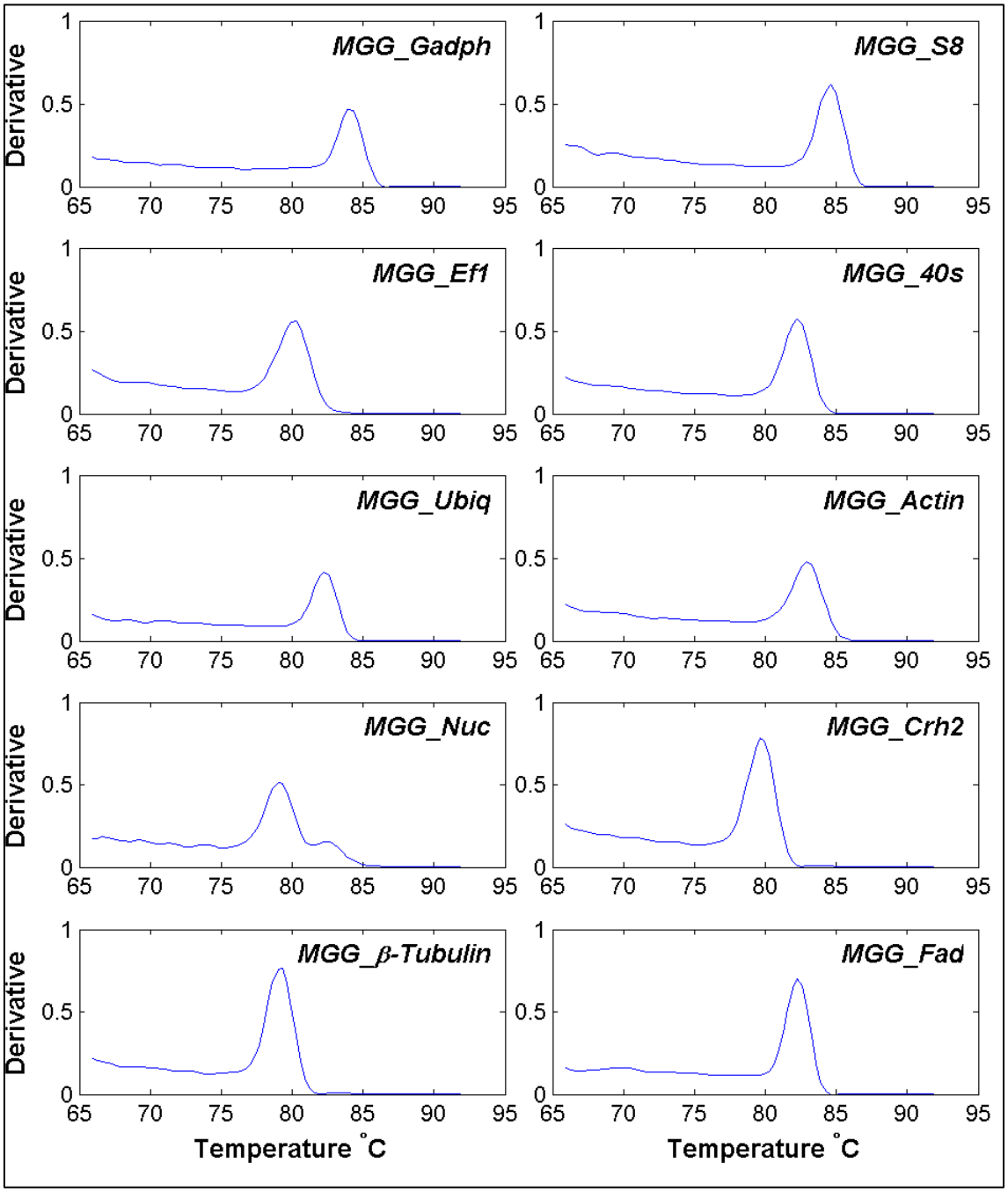

A.8. Five *Magnaporthe oryzae Crh-like* Gene Primer Specificity Check by Melt Curve Analyses. Graphs show PCR product dissociation curves for five primer pairs used in this analysis using pooled cDNA of WT from all samples used. These are primer pairs for genes: *MGG_Utr2, MGG_Crh1, MGG_Crh2, MGG_Crh3* and *MGG_Crh4*. Melt curve data was obtained from the denaturation of amplified PCR product executed at the end of a qRT-PCR run, by temperature increment.

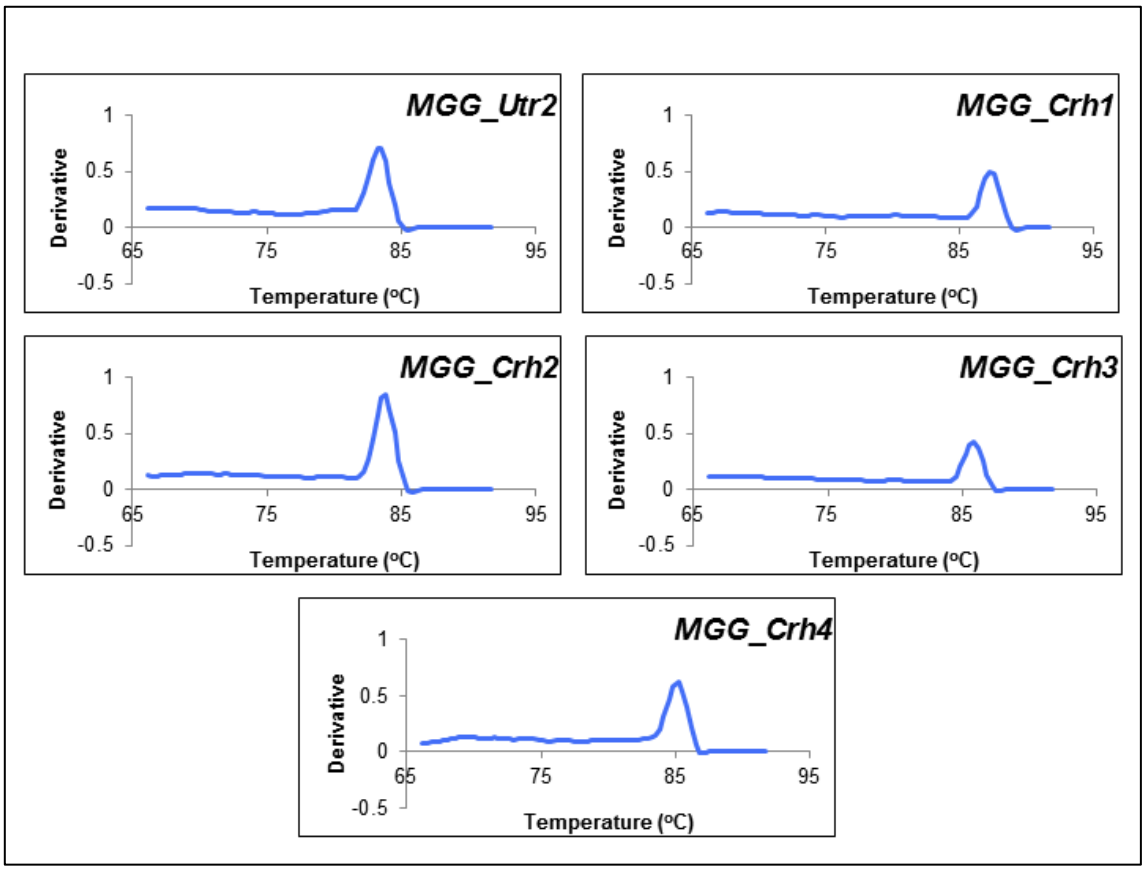

A.9. Nine *Magnaporthe oryzae* Candidate Reference Gene Primer Specificity Check by Gel Electrophoresis. GeneRuler™ Ultra Low Range DNA Ladder were used. Amplicons from each primer pair above were size separated on 2% Agarose gel at 60 volts.

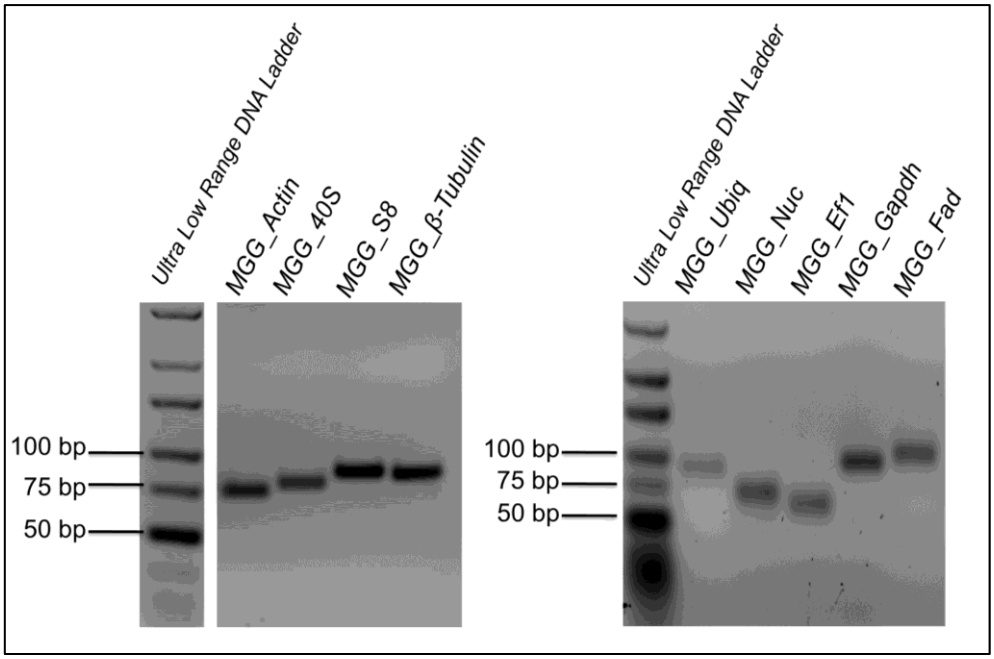

A.10. *Magnaporthe oryzae Crh-like* Gene Primer Specificity Check by Gel Electrophoresis. From left to right, DNA ladder used: GeneRuler™ Ultra Low Range DNA Ladder and GeneRuler™ 100 bp DNA Ladder. Amplicons from each primer pair above were size separated on 2% Agarose gel at 60 volts.

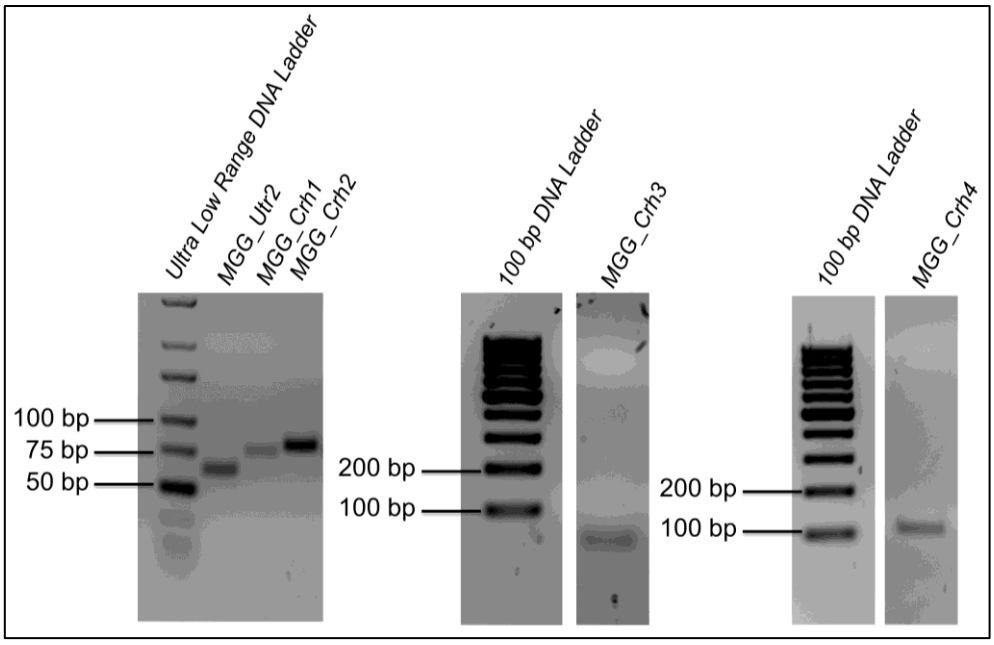

A.11. Regression Graphs of Nine Candidate Reference Genes. The cycle threshold (ct) of nine primer pairs for candidate reference genes plotted against a five-fold dilution of pooled cDNA from all samples analysed. These are primer pairs for genes: *MGG_Actin, MGG_40s, MGG_S8, MGG_β-Tubulin, MGG_Ubiq*, *MGG_Nuc*, *MGG_Ef1*, *MGG_Gapdh,* and *MGG_Fadh.* Each qRT-PCR reaction had two technical replicates, therefore the cycle threshold (ct) value above is an averaged data. All reactions conducted on the same 96-well plate. The slopes and r^2 values were calculated using a regression line across four-points.

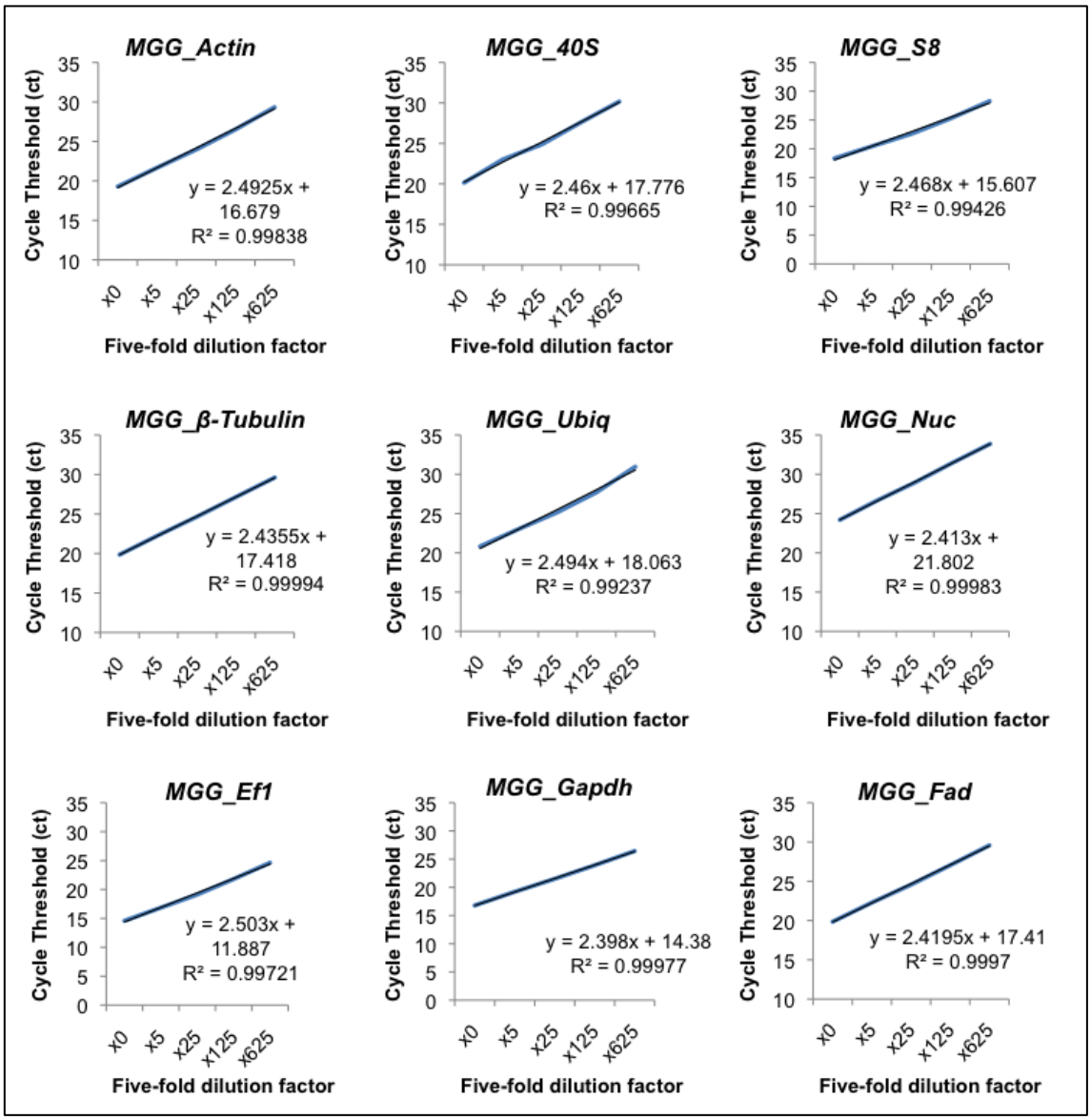

A.12. *Magnaporthe oryzae Crh-like* Gene Primer Regression Graphs. The cycle threshold (ct) of five primer pairs against a five-fold dilution of pooled cDNA from all samples analysed. These are primer pairs for genes: *MGG_Utr2, MGG_Crh1, MGG_Crh2, MGG_Crh3* and *MGG_Crh4*. Each qRT-PCR reaction had two technical replicates, therefore cycle threshold (ct) values given above are averaged data. All reactions were conducted on the same 96-well plate. The slopes and r^2 values were calculated using a regression line across four-points, in exception to qRT-PCR reaction with primer pair pairs amplifying *MGG_Crh3* transcript, whereby only three data points were used (red arrow).

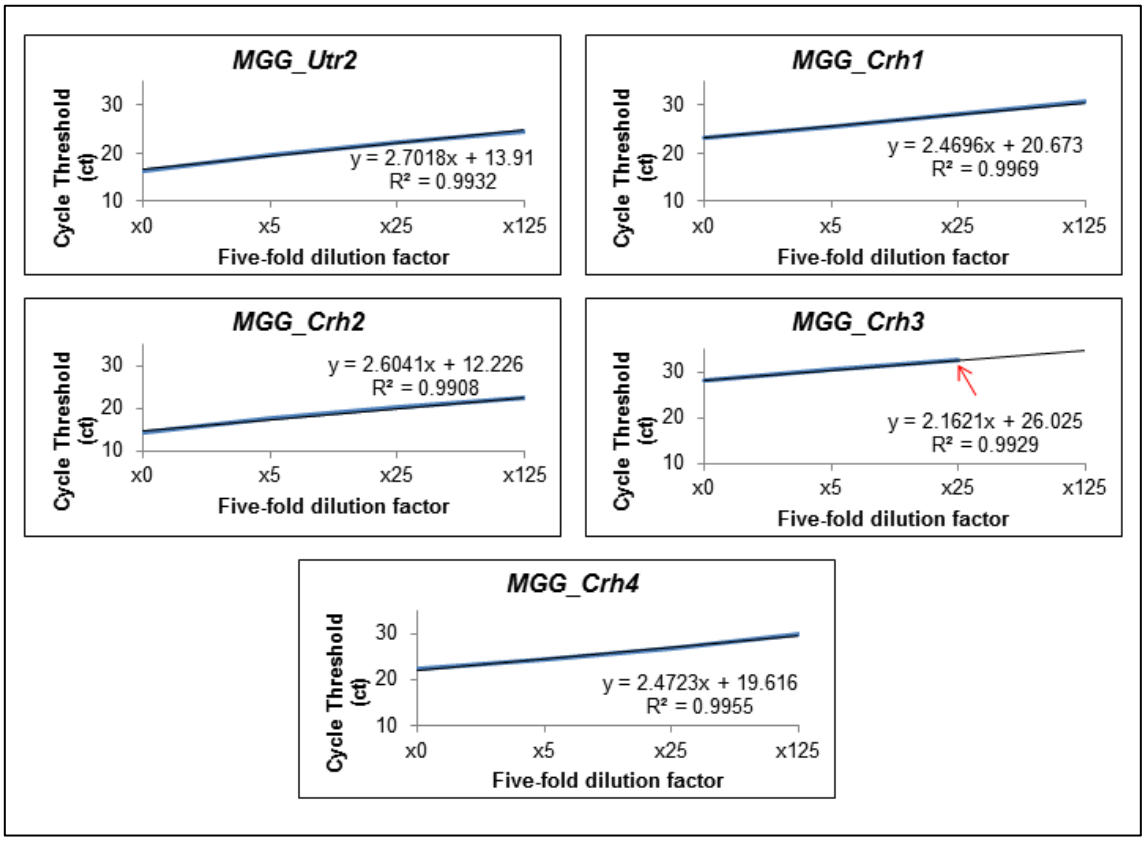

A.13. Fungal Tissue RNA Quality Check. Each electrophoregram comprise of RNA of fungal tissue grown vegetatively under various conditions, dormant spore (0 hpi) or perithecia. Each graph showed the presence of two sharp peaks, corresponding to two bands on the right side of each graph, indicating undegraded RNA.

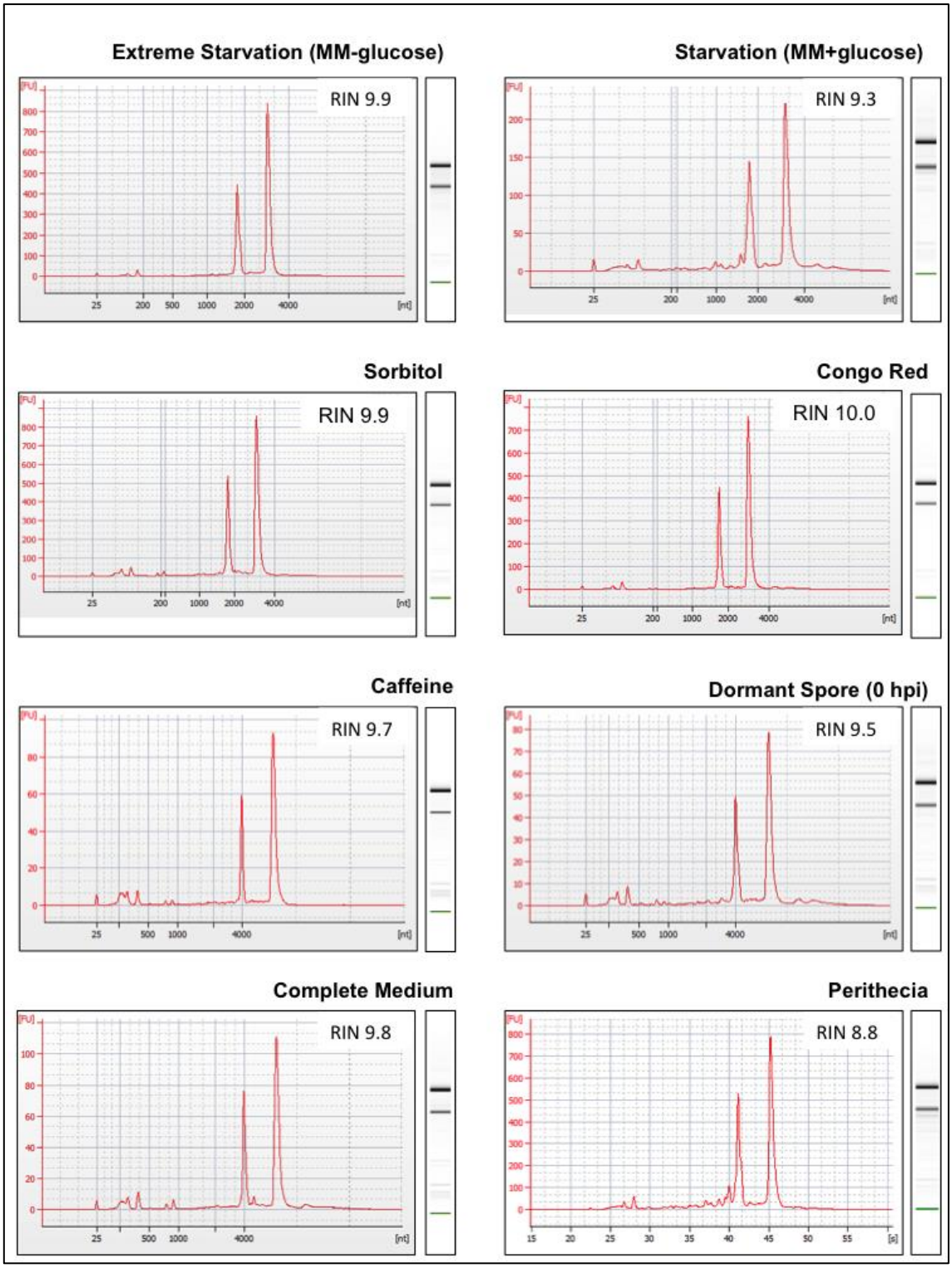

A.14. Infective Stage Sample RNA Quality Check. Each electrophoregram comprise of RNA taken from host leaf tissue inoculated with fungal spores (in 0.2% gelatine) at various hours post inoculation (hpi). Control leaf comprise of plant leaf sprayed with 0.2% gelatine. Each graph above showed the presence of two sharp peaks, corresponding to two bands on the right side of each graph, indicating undegraded RNA. Additional peaks correspond to chloroplastic ribosomes abundant in samples derived from host leaf tissues.

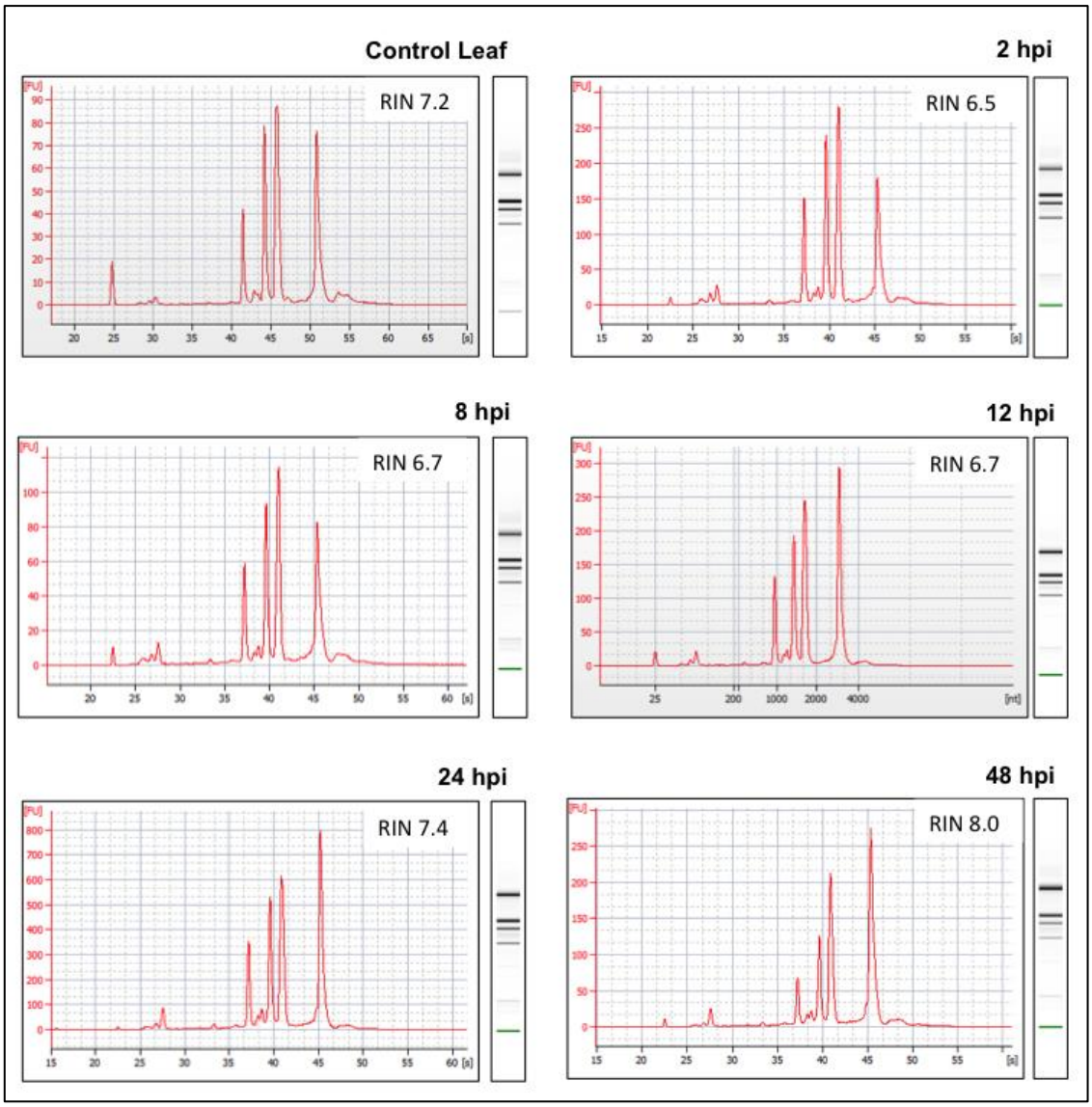

A.15. High Throughput-SuperSAGE Base Mean Data of Four *Magnaporthe oryzae Crh-like* Genes. Data were taken directly from the supplementary data Table S8 from the published work of Soanes *et al.* (2012).

Gene Symbol	Base Mean (Transcript abundance of gene/overall library)				
	Optimal Vegetative Growth (CM)	Starvation Vegetative Growth (MM)	Immature Appressorium (4 hpi)	Immature Appressorim (8 hpi)	Mature Appressoriu m (14 hpi)
MGG_Utr2	208.1	408.9	52.1	39.7	19.0
MGG_Crh1	0	0	0.5	0	0.4
MGG_Crh2	36,298.4	14,179.8	6,771.4	1,0131.9	7,814.1
MGG_Crh3	39.5	30.4	7.5	9.4	20.9
MGG_Crh4	n/a	n/a	n/a	n/a	n/a

Appendix B- Figures and Tables for Chapter 4

B.1. Example of a 96-Well Plate Designed for the Validation of Transcript Absence in Mutants. Shown are the types of qRT-PCR reactions required to be on the same 96-well plate for comparing the ct values of the gene of interest (GOI) in a mutant strain relative to WT. The tissue sample must comprise of the knockout strain (ΔSt) and control WT, each with three biological replicates (1), (2) and (3) and two technical replicates per reaction. A negative control gene *MGG_40s* (40s) for each sample type and a non-template control (NTC) for each gene must be included in each 96-well plate.

	1	2	3	4	5	6	7	8	9	10	11	12
A	WT (1) Gene: **GOI**	WT (1) Gene: **GOI**	WT (1) Gene: 40s	WT (1) Gene: 40s								
B	WT (2) Gene: **GOI**	WT (2) Gene: **GOI**	WT (2) Gene: 40s	WT (2) Gene: 40s								
C	WT (3) Gene: **GOI**	WT (3) Gene: **GOI**	WT (3) Gene: 40s	WT (3) Gene: 40s								
D	ΔSt(1) Gene: **GOI**	ΔSt (1) Gene: **GOI**	ΔSt (1) Gene: 40s	ΔSt (1) Gene: 40s								
E	ΔSt (2) Gene: **GOI**	ΔSt (2) Gene: **GOI**	ΔSt (2) Gene: 40s	ΔSt (2) Gene: 40s								
F	ΔSt (3) Gene: **GOI**	ΔSt (3) Gene: **GOI**	ΔSt (3) Gene: 40s	ΔSt (3) Gene: 40s								
G												
H	NTC **GOI**	NTC 40s										

B.2. A Description for the Construction of Crh1_Hyg Deletion Cassette by Overlapping PCR. **Panel A** The design of three PCR fragments (F1, F2 and F3) and the corresponding PCR product on gel electrophoresis. Note that fragment F2 not shown as it is the same Hygromycin fragment used to construct Utr2_Hyg. **Panel B** Overlapping PCR for fragments F4 and F5 using F1, F2 and F3 as the template, with amplified products shown on gel electrophoresis. **Panel C** An illustration for the amplification of the final product, F6 using fragments F4 and F5 as template, with final product shown on gel electrophoresis. GeneRuler™ 1 kb DNA Ladder was used as the molecular ladder (L) and all agarose gel prepared at 1%.

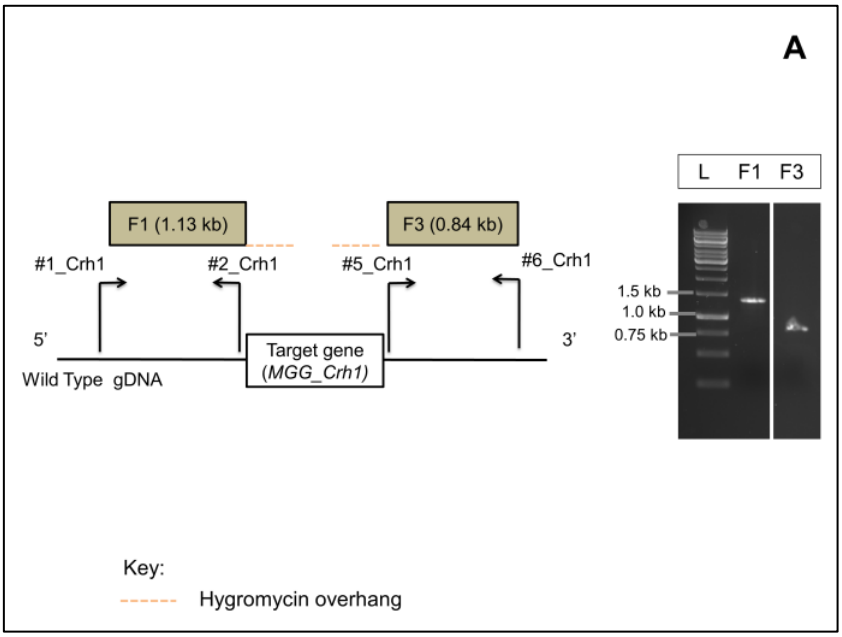

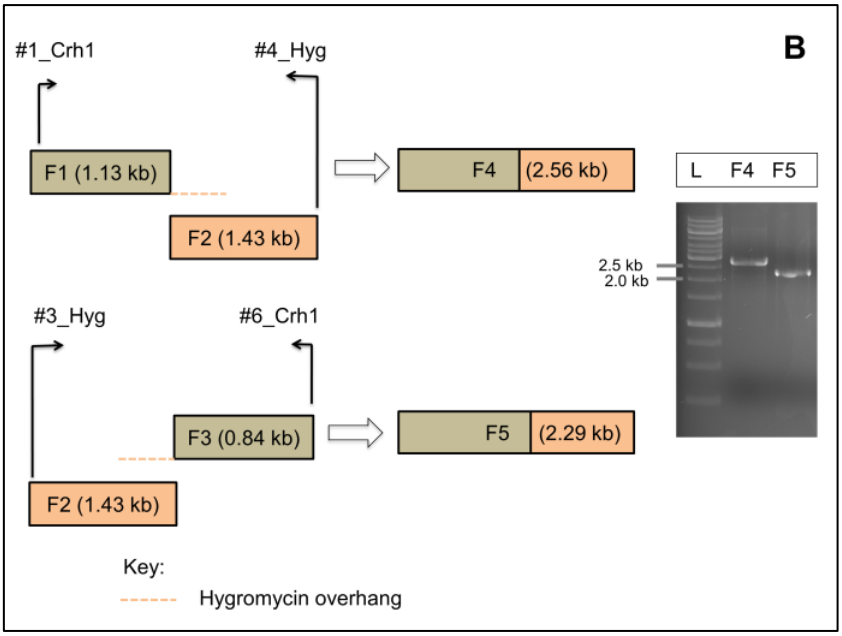
B
#1_Crh1
#4_Hyg
F1 (1.13 kb)
F2 (1.43 kb)
F4
(2.56 kb)
L F4 F5
2.5 kb
2.0 kb
#3_Hyg
#6_Crh1
F3 (0.84 kb)
F2 (1.43 kb)
F5
(2.29 kb)
Key:
Hygromycin overhang

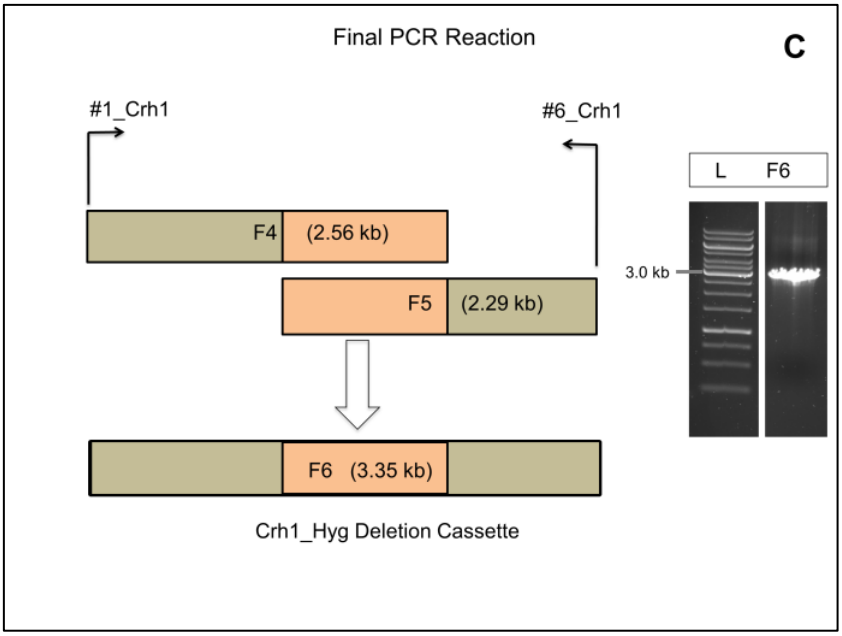
Final PCR Reaction
C
#1_Crh1
#6_Crh1
F4
(2.56 kb)
F5
(2.29 kb)
F6 (3.35 kb)
Crh1_Hyg Deletion Cassette
L F6
3.0 kb

B.3. A Description for the Construction of Crh2_Hyg Deletion Cassette by Overlapping PCR. Panel A The design of three PCR fragments (F1, F2 and F3) and the corresponding PCR product on gel electrophoresis. Note that fragment F2 not shown as it is the same Hygromycin fragment used to construct Utr2_Hyg. **Panel B** Overlapping PCR for fragments F4 and F5 using F1, F2 and F3 as the template, with amplified products shown on gel electrophoresis. **Panel C** An illustration for the amplification of the final product, F6 using fragments F4 and F5 as template, with final product shown on gel electrophoresis. GeneRuler™ 1 kb DNA Ladder was used as the molecular ladder (L) and all agarose gel prepared at 1%.

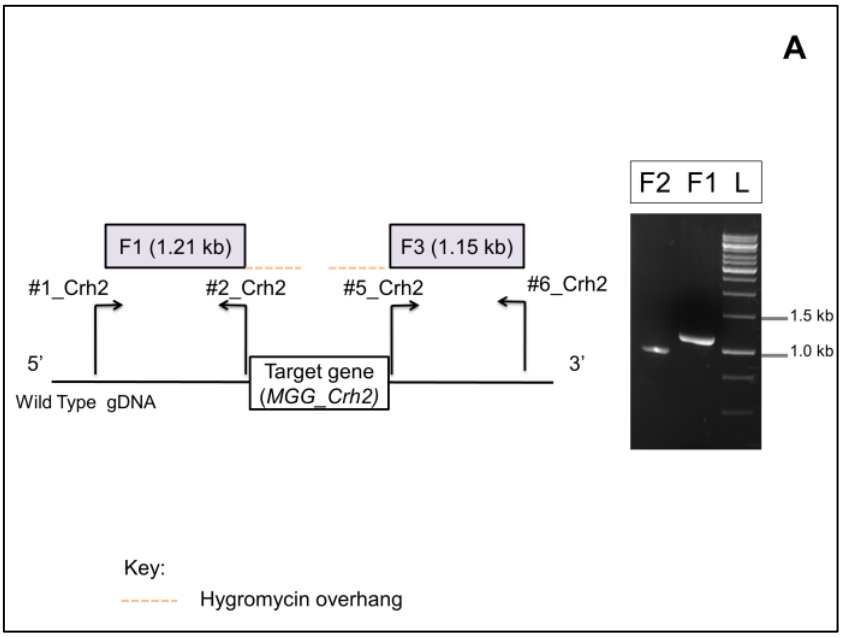

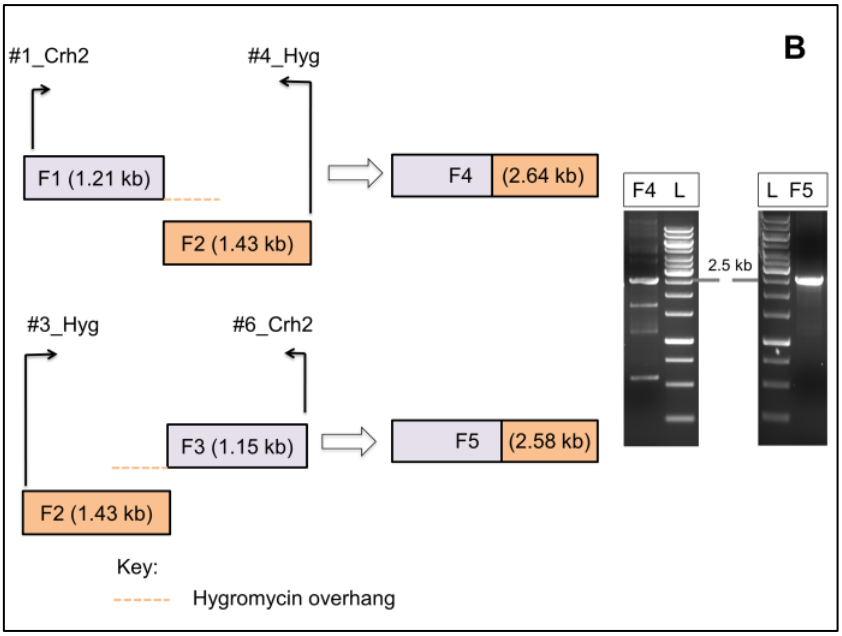
B
#1_Crh2
#4_Hyg
F1 (1.21 kb)
F2 (1.43 kb)
F4 (2.64 kb)
F4 L
L F5
2.5 kb
#3_Hyg
#6_Crh2
F3 (1.15 kb)
F2 (1.43 kb)
F5 (2.58 kb)
Key:
Hygromycin overhang

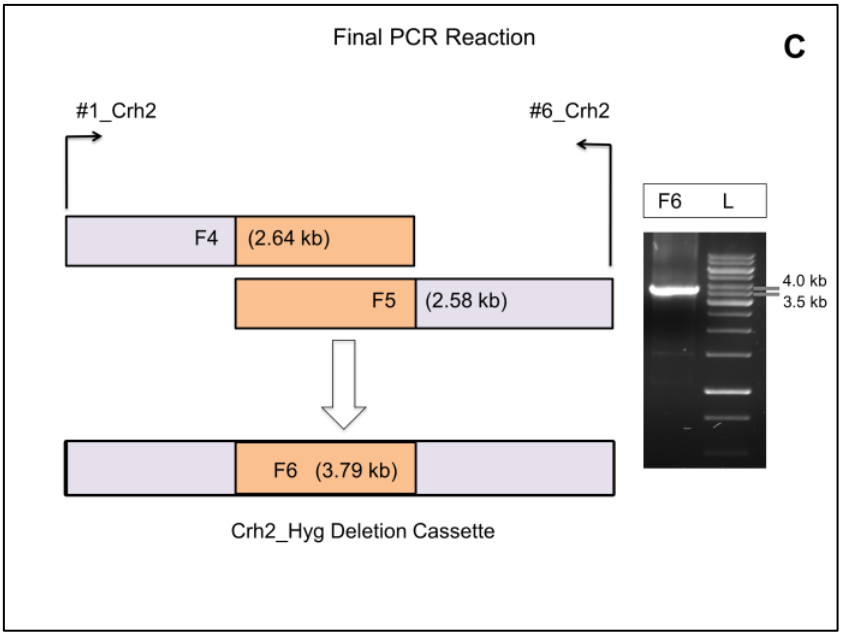
Final PCR Reaction
C
#1_Crh2
#6_Crh2
F4 (2.64 kb)
F5 (2.58 kb)
F6 (3.79 kb)
F6 L
4.0 kb
3.5 kb
Crh2_Hyg Deletion Cassette

B.4. A Description for the Construction of Utr2_BAR Deletion Cassette by Overlapping PCR. Panel A The design of three PCR fragments (F1, F2 and F3) and the corresponding PCR product on gel electrophoresis. **Panel B** Overlapping PCR for fragments F4 and F5 using F1, F2 and F3 as the template, with amplified products shown on gel electrophoresis. **Panel C** An illustration for the amplification of the final product, F6 using fragments F4 and F5 as template, with final product shown on gel electrophoresis. GeneRuler™ 1 kb DNA Ladder was used as the molecular ladder (L) and all agarose gel prepared at 1%.

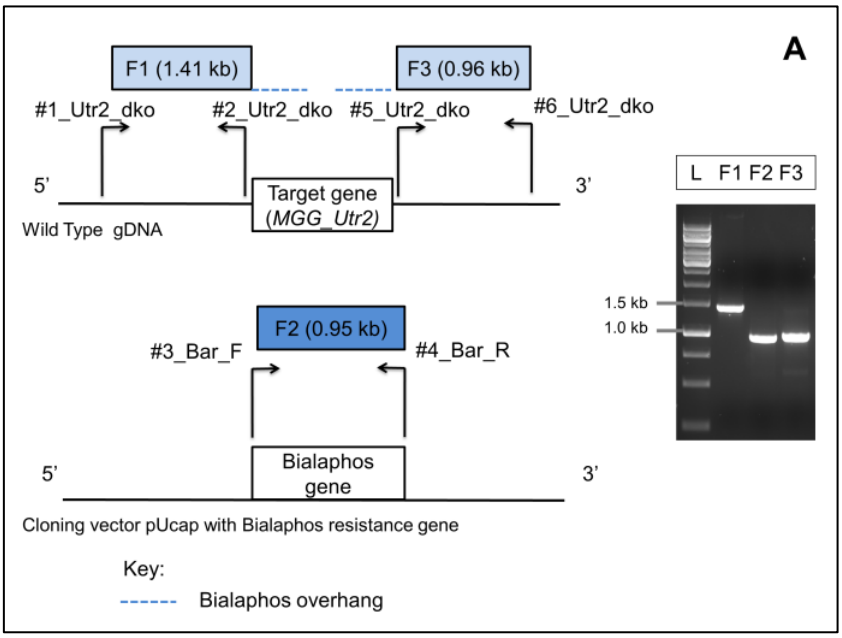

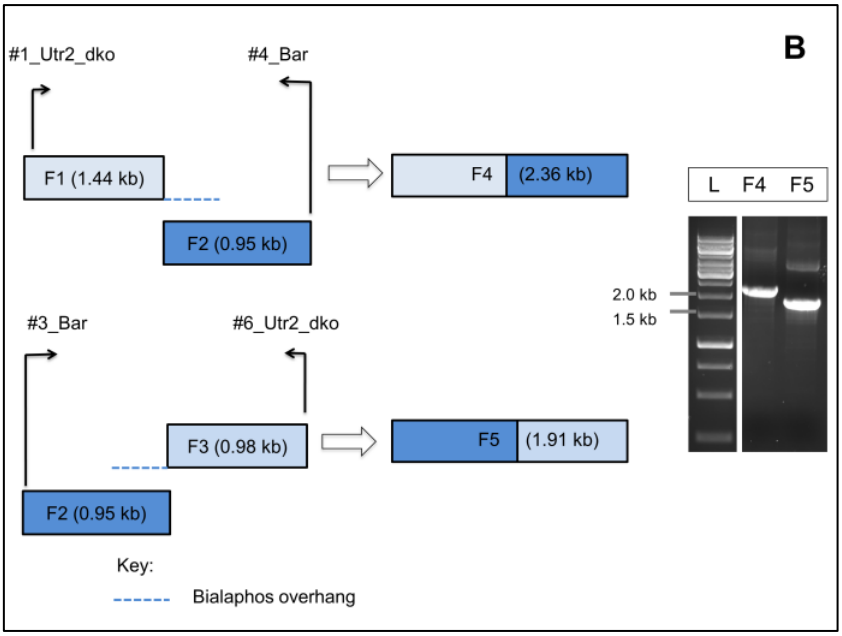
B
#1_Utr2_dko
#4_Bar
F1 (1.44 kb)
F2 (0.95 kb)
F4
(2.36 kb)
L F4 F5
2.0 kb
1.5 kb
#3_Bar
#6_Utr2_dko
F3 (0.98 kb)
F2 (0.95 kb)
F5
(1.91 kb)
Key:
Bialaphos overhang

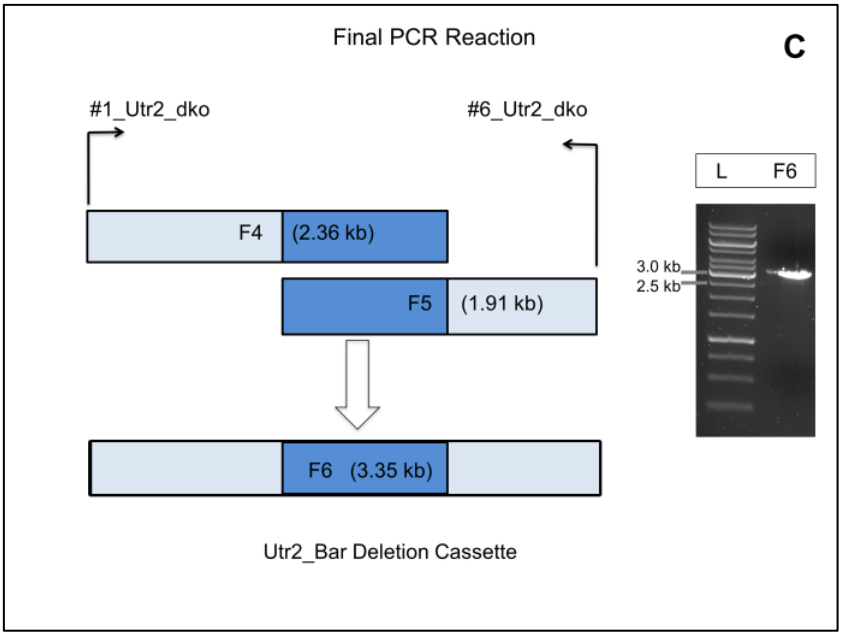
Final PCR Reaction
C
#1_Utr2_dko
#6_Utr2_dko
F4
(2.36 kb)
F5
(1.91 kb)
F6 (3.35 kb)
L F6
3.0 kb
2.5 kb
Utr2_Bar Deletion Cassette

B.5. Probe Purity Check by Gel Electrophoresis. Probes were amplified by PCR and cleaned (QIAquick PCR Purification Kit) and quality checked by running on 1% agarose gel. Lanes from left: GeneRuler™ 1 kb DNA Ladder (L), Hygromycin probe (Hyg) at 1.43 kb and Bialaphos probe (BAR) at 0.93 kb.

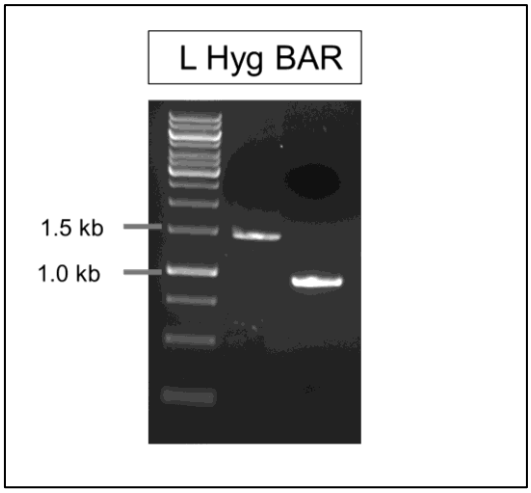

B.6. Appropriate Positioning of a Fluorescent Protein (FP) in a Fluorescent Fusion Protein Construct. Preferred sites of FP fusion in the primary sequence of the protein of interest are indicated by a 'tick', and domains to be avoided are indicated by 'crosses'. Each tertiary structure shows the folding of the sample construct with the FP (represented as a cylinder) fused at an optimal site. (**A**). A hypothetical globular protein expressed in the cytoplasm can have the FP fused at either the NH_2- or the COOH-terminus. Typically, one end of the protein of interest will contain a functional domain that may be sterically hindered by an FP, and so it is useful to make both of the possible constructs. (**B**) A hypothetical lumenal protein contains an NH_2-terminal signal sequence (SS), a mature domain, and a COOH-retention sequence (KDEL). An FP placed immediately after the SS or immediately before the retention sequence is less likely to interfere with the functioning of either sequence. (**C**) A single membrane–spanning protein has the additional constraint that the FP cannot be placed within or near the transmembrane domain (TMD), as this will disrupt the domain and cause problems with membrane integration. (**D**) A membrane multispanning protein has the same constraint as the example in panel C, but in multiple locations. The loops between the transmembrane domains are also poor choices, because the exact spacing between transmembrane domains is often important for protein folding, and because these loops often contain functional domains. Abbreviation: cyt, cytoplasm. Illustration and caption taken un-modified from a review publication by Snapp (2005).

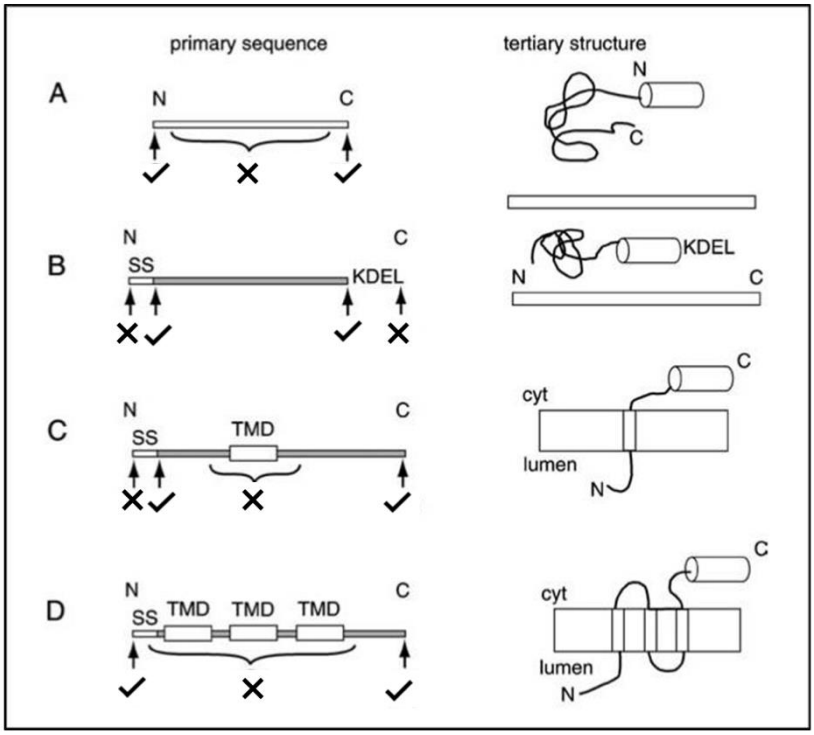

Appendix C- Figures and Tables for Chapter 5

C.1. List of Medium and Reagents Used For Plate Growth Assay.

Medium	Concentration	Preparation Method
Complete Medium (CM) Agar	n/a	Refer to Chapter 2 Table 2.1
CM agar buffered with Hepes (pH 7.0)	n/a	Complete medium (same as above) buffered with 50 mM Hepes, pH adjusted to 7.0 with NaOH (1M), 1.5% agar added and autoclaved.
CM (pH 7.0) with Congo Red (CR)	100 µg/ml Congo Red	The appropriate amount of 1% stock CR (Chapter 2 Table 2.1) was added to sterile molten CM agar buffered with Hepes (50 mM, pH 7.0). Plates prepared in flow hood without lights and used immediately.
Sorbitol	1 M	Complete medium prepared with 1 M Sorbitol (Sigma-Aldrich), 1.5% agar added and autoclaved.
Caffeine	2.5 mM	Complete medium prepared, 1.5% agar added and autoclaved. Filter sterilized stock caffeine (100 mM) added to sterile molten agar to give a final concentration of 2.5 mM Stock caffeine (100 mM): Caffeine prepared with hot Milliq_H_2O, mixed thoroughly to a concentration of 100 mM. Solution filter sterilized.
Sodium Dodecyl Sulphate (SDS)	0.005%	1% SDS (Sigma-Aldrich) diluted in Milliq_H_2O. Filter sterilized stock SDS (1%) then added to autoclaved CM to a final concentration of 0.005%.
Minimal Media	n/a	Refer to Chapter 2 Table 2.1
Congo Red with Sorbitol	100 µg/ml Congo Red and 1 M Sorbitol	The appropriate amount of 1% stock CR was added to sterile molten CM agar containing 1 M Sorbitol, buffered with Hepes (50 mM, pH 7.0).

C.2. Transmission Electron Micrographs of *Magnaporthe oryzae* Vegetative Mycelium Cultured in Congo Red. Samples were prepared by culturing fungal mycelium in CM liquid broth containing 100 µg/ml Congo Red. **Panel A.1-A.2** WT strain Guy11 fungal hypha. **Panel B.1-B.2** Double gene deletant mutant strain ΔΔ*MGG_Crh2*_Utr2 line 25 fungal hypha. Extracellular environment (em), cell wall (cw), septum (sp), plasma membrane (pm) and amorphous layer (am). Scale bars represents 200 nm.

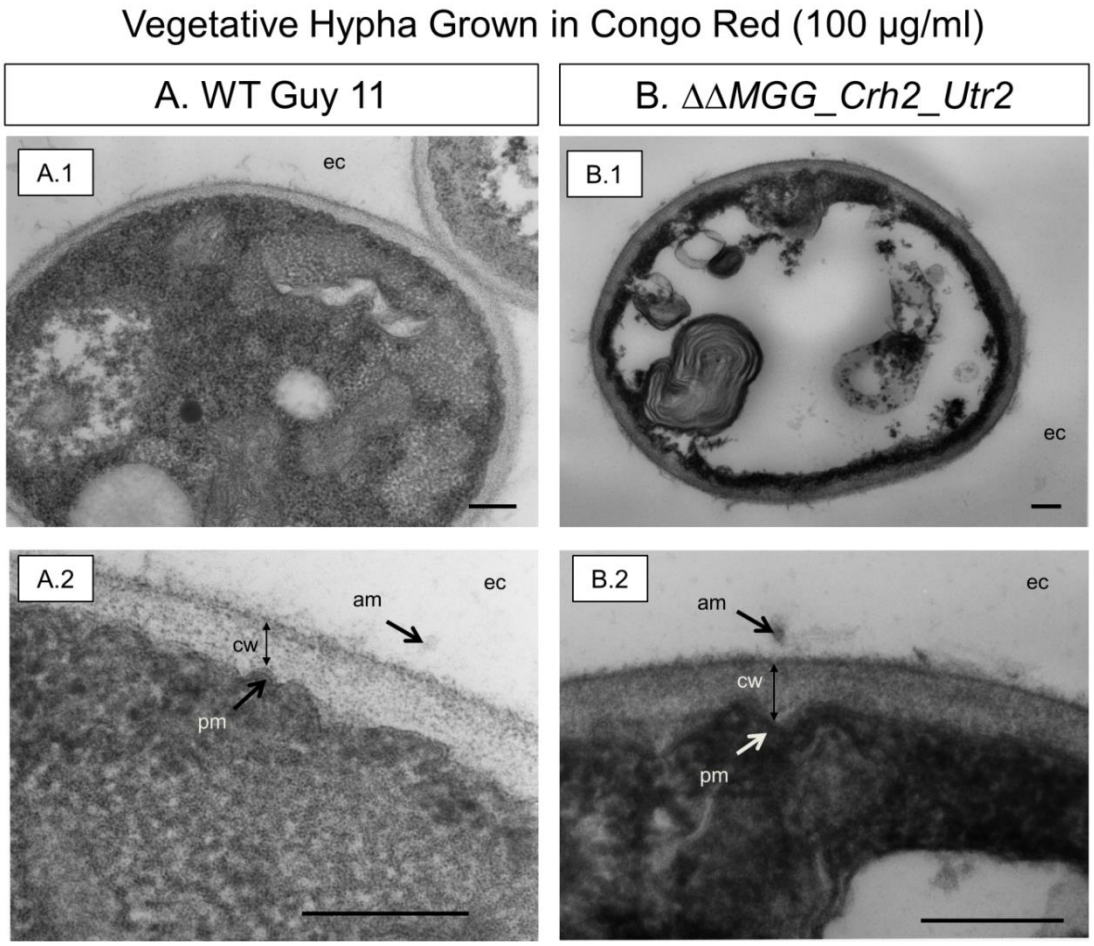

C.3. Transmission Electron Micrographs of *Magnaporthe oryzae* Dormant Spores Mycelium Cultured in Congo Red. Samples were prepared by harvesting spores from 10 day old fungal colonies grown respectively on CM agar containing 100 µg/ml Congo Red, followed by sample fixing. **Panels A.1-A.3. 2** Dormant spores of WT strain Guy11 **Panels B.1-B.3** Dormant spores of Double gene deletant mutant strain ΔΔ*MGG_Crh2*_Utr2 line 25. Extracellular environment (em), cell wall (cw), septum (sp), plasma membrane (pm) and melanin layer (m). Scale bars for Panels A1 and B1 represents 2 µm, scale bars for Panels A2, A3, B2 and B3 represents 200 nm.

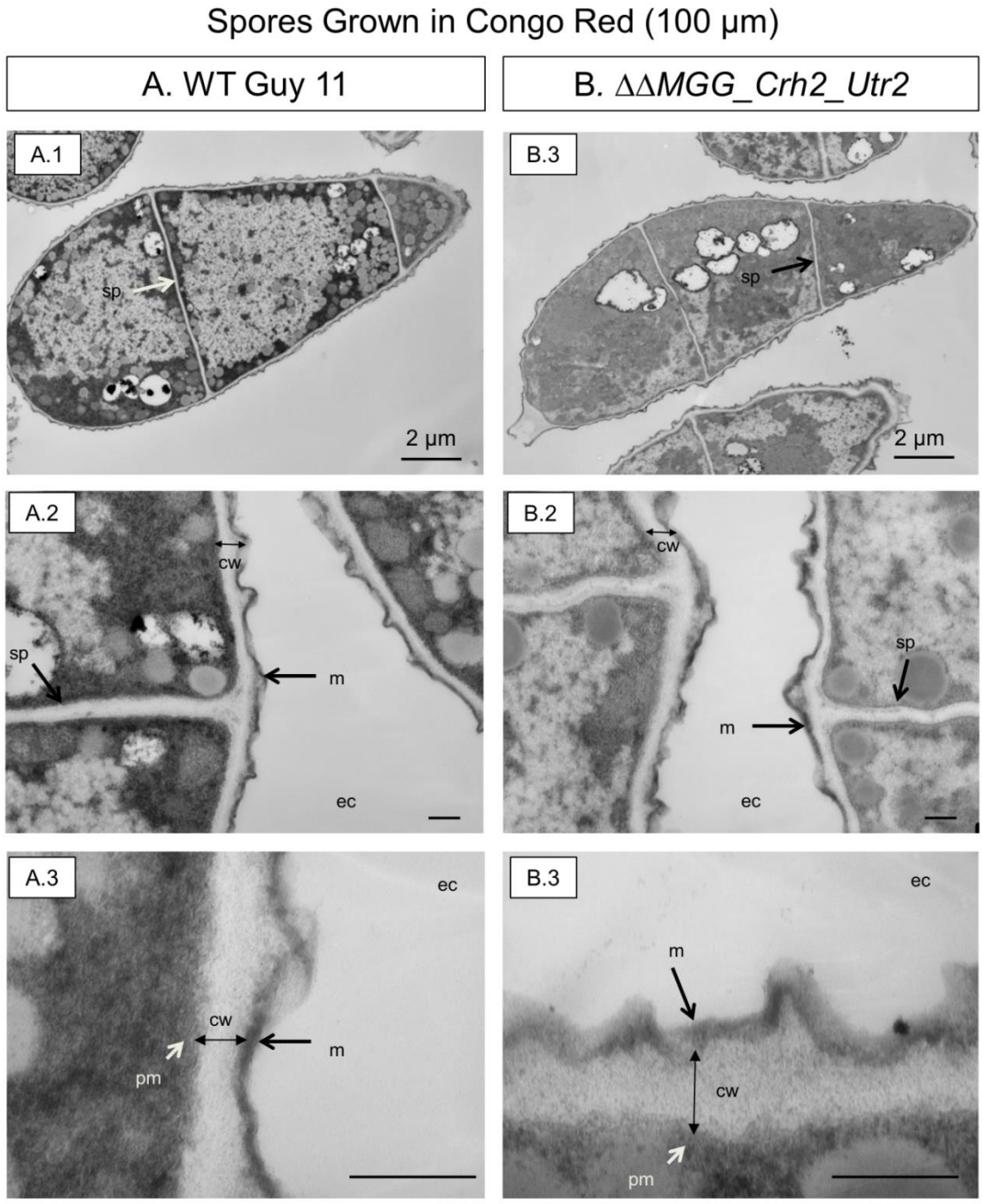

Appendix D- Figures and Tables for Chapter 6

D.1. Flow Chart for the Preparation and Fractionation of Cell Wall Carbohydrates. Shown above an example of a series of treatments and solubilisations to extract the ASF and AIF components of the cell wall. Diagram taken from, Mélida *et al.* (2013) and used for work in this thesis.

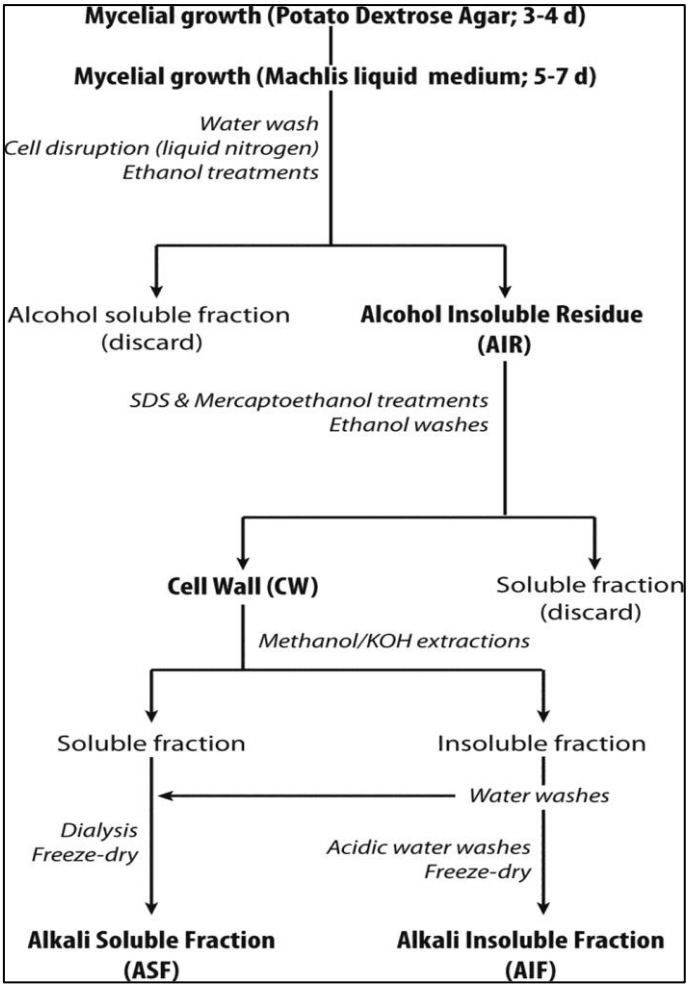

D.2. List of Linkages Identified in the Cell Wall of *Magnaporthe oryzae* WT Strain Guy11 from the Corresponding Permethylated Alditol Acetate Form.

Monosaccharide (used name)	Permethylatedalditol acetate	Deduced linkage
Glucopyranose (Glc)	1,5-Di-O-acetyl-2,3,4,6-tetra-O-methyl glucitol	t-Glc*p*
	1,3,5-Tri-O-acetyl-2,4,6-tri-O-methyl glucitol	1,3-Glc*p*
	1,5,6-Tri-O-acetyl-2,3,4-tri-O-methyl glucitol	1,6-Glc*p*
	1,4,5-Tri-O-acetyl-2,3,6-tri-O-methyl glucitol	1,4-Glc*p*
	1,3,4,5-Tetra-O-acetyl-2,6-di-O-methyl glucitol	1,3,4-Glc*p*
	1,3,5,6-Tetra-O-acetyl-2,4-di-O-methyl glucitol	1,3,6-Glc*p*
N-Acetylglucopyranose (GlcNAc)	1,4,5-Tri-O-acetyl-(2-deoxy,2-N-methylacetamido)-3,6-di-O-methyl glucitol	1,4-GlcNAc
Mannopyranose (Man)	1,5-Di-O-acetyl-2,3,4,6-tetra-O-methyl mannitol	t-Man*p*
	1,2,5-Tri-O-acetyl-3,4,6-tri-O-methyl mannitol	1,2-Man*p*
	1,3,5-Tri-O-acetyl-2,4,6-tri-O-methyl mannitol	1,3-Man*p*
	1,5,6-Tri-O-acetyl-2,3,4-tri-O-methyl mannitol	1,6-Man*p*
	1,2,3,5-Tetra-O-acetyl-4,6-di-O-methyl mannitol	1,2,3-Man*p*
	1,2,4,5-Tetra-O-acetyl-3,6-di-O-methyl mannitol	1,2,4-Man*p*
	1,2,4,5-Tetra-O-acetyl-3,6-di-O-methyl mannitol	1,2,6-Man*p*
Galactopyranose (Gal)	1,5-Di-O-acetyl-2,3,4,6-tri-O-methyl galactitol	t-Gal*p*
	1,3,5-Tri-O-acetyl-2,4,6-tri-O-methyl galactitol	1,3-Gal*p*
	1,5,6-Tri-O-acetyl-2,3,4-tri-O-methyl galacitol	1,6-Gal*p*
Galactofuranose (Galf)	1,4-Di-O-acetyl-2,3,5,6-tri-O-methyl galactitol	t-Gal*f*

Appendix E- Figures and Tables for Chapter 7

E.1. Example of a 96-Well Plate Designed to Measure the Expression of *MGG_Crh1* in the Mutant *ΔMGG_Utr2* Relative to WT. Each plate contains all three biological replicates (1), (2) and (3) for each tissue sample. The tissue sample is either *ΔMGG_Utr2* (**ΔUt**) or control WT (WT) grown under the same conditions. There are two technical replicates for each reaction: reference gene 1 (HKG1), reference gene 2 (HKG2) and *MGG_Crh1* (**Crh1**). Two types of controls, non-template control (NTC) and pooled no reverse transcriptase, (-RT) control were added for each gene on every 96-well plate. The –RT was pooled from –RT WT and –RT *ΔMGG_Utr2* as to do otherwise would be too costly and space consuming.

	1	2	3	4	5	6	7	8	9	10	11	12
A	WT (1) Gene: HKG1	WT (1) Gene: HKG1	WT (1) Gene: HKG2	WT (1) Gene: HKG2	WT (1) Gene: Crh1	WT (1) Gene: Crh1						
B	WT (2) Gene: HKG1	WT (2) Gene: HKG1	WT (2) Gene: HKG2	WT (2) Gene: HKG2	WT (2) Gene: Crh1	WT (2) Gene: Crh1						
C	WT (3) Gene: HKG1	WT (3) Gene: HKG1	WT (3) Gene: HKG2	WT (3) Gene: HKG2	WT (2) Gene: Crh1	WT (2) Gene: Crh1						
D	ΔUt (1) Gene: HKG1	ΔUt (1) Gene: HKG1	ΔUt (1) Gene: HKG2	ΔUt (1) Gene: HKG2	ΔUt (1) Gene: Crh1	ΔUt (1) Gene: Crh1						
E	ΔUt (2) Gene: HKG1	ΔUt (2) Gene: HKG1	ΔUt (2) Gene: HKG2	ΔUt (2) Gene: HKG2	ΔUt (2) Gene: Crh1	ΔUt (2) Gene: Crh1						
F	ΔUt (3) Gene: HKG1	ΔUt (3) Gene: HKG1	ΔUt (3) Gene: HKG2	ΔUt (3) Gene: HKG2	ΔUt (3) Gene: Crh1	ΔUt (3) Gene: Crh1						
G	Pool –RT HKG1	Pool –RT HKG2	Pool –RT Crh1									
H	NTC HKG1	NTC HKG2	NTC Crh1									

E.2. Electropherograms of RNA Samples from Mycelium of Five Fungal Strains Grown Under Optimal Conditions. Each electropherogram represents RNA from the mycelium of a mutant or WT, each grown in Complete Medium broth. These graphs were obtained from an analysis conducted using the 'Bioanalyzer 2100 Expert Software' by Agilent. The presence of two sharp peaks (rRNAs) corresponds to high quality, non-degraded RNA, yielding a high RIN value (>8.0).

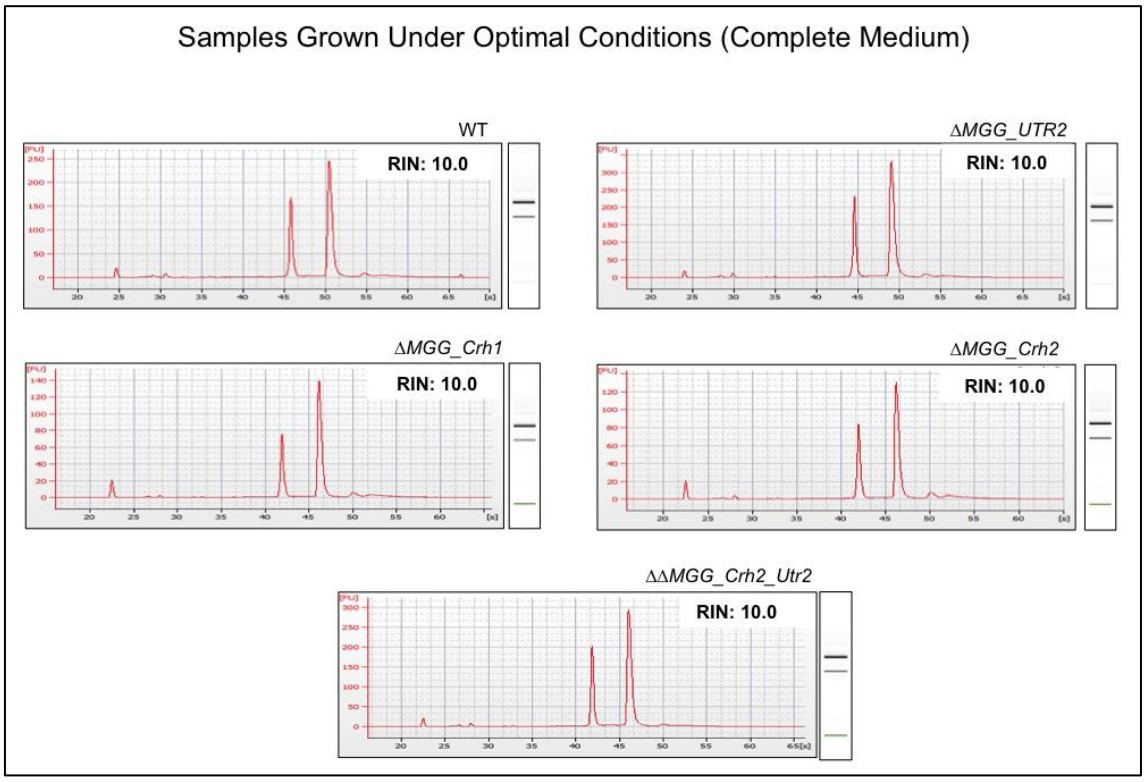

E.3. Electropherograms of RNA Samples from Mycelium of Five Fungal Strains Grown Under Cell Wall Stress. Each electropherogram represents RNA from the mycelium of a mutant or WT, each grown in Complete Medium broth containing Congo Red at 100 µg/ml. These graphs were obtained from an analysis conducted using the 'Bioanalyzer 2100 Expert Software' by Agilent. The presence of two sharp peaks (rRNAs) corresponds to high quality, non-degraded RNA, yielding a high RIN value (>8.0). Image on the bottom right is an example of a ladder run (positive control).

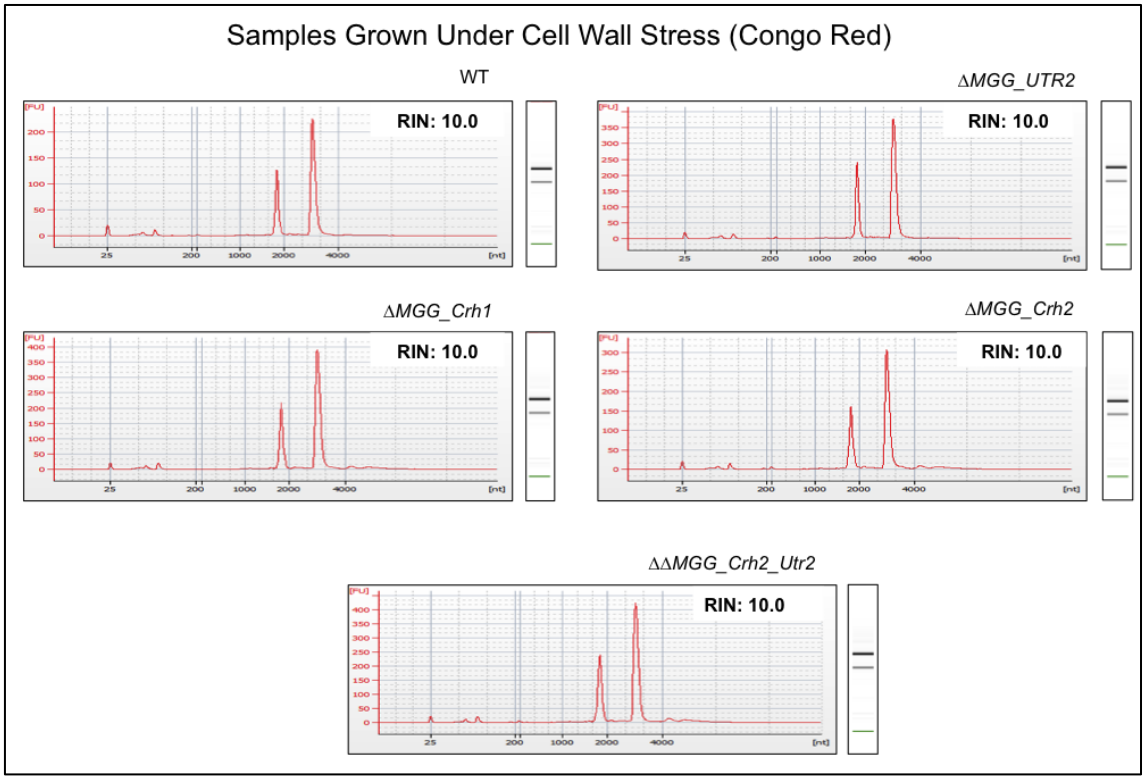

E.4. Electropherograms of RNA Samples from Mycelium of Five Fungal Strains Grown Under Oxidative Stress. Electropherograms of RNA samples extracted from mycelium of five genotypes grown under oxidative stress. Each electropherogram represents RNA from the mycelium of a mutant or WT, each grown in Complete Medium broth containing H_2O_2(2.5 mM). These graphs were obtained from an analysis conducted using the 'Bioanalyzer 2100 Expert Software' by Agilent. The presence of two sharp peaks (rRNAs) corresponds to high quality, non-degraded RNA, yielding a high RIN value (>8.0).

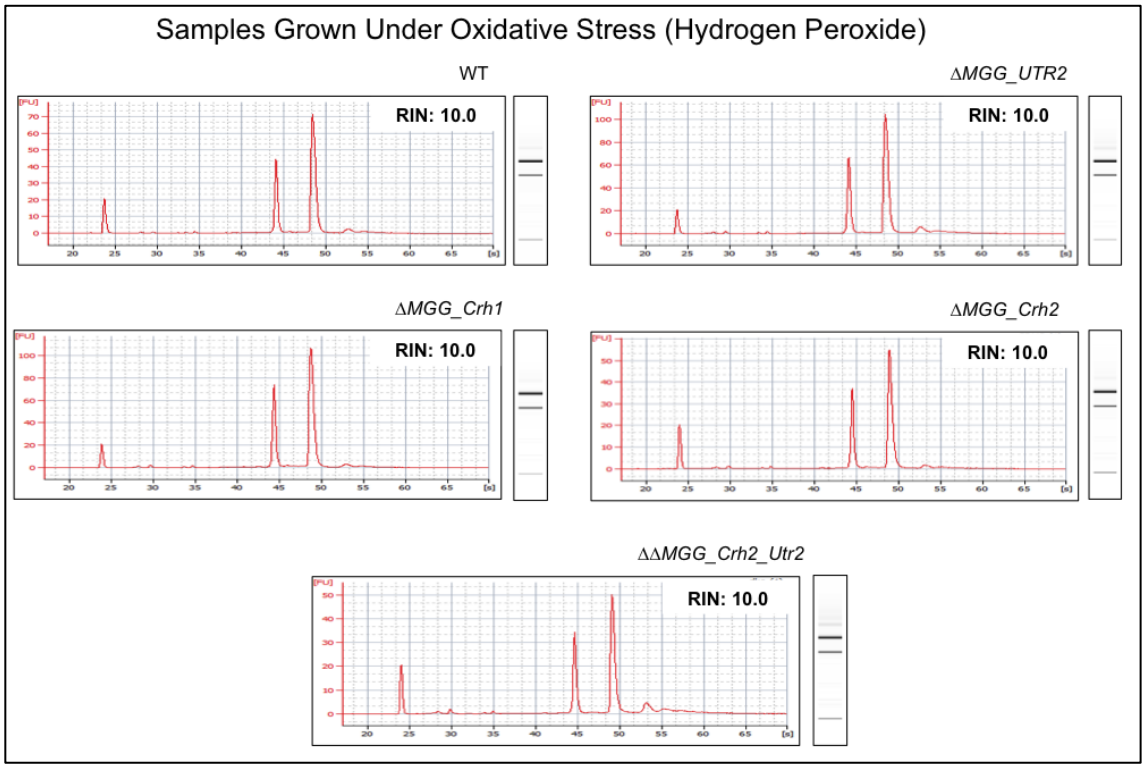

E.5. An Illustration of an Electrophoregram Detailing the Regions Indicative of RNA Quality. Diagram taken from Mueller *et al* (2004).

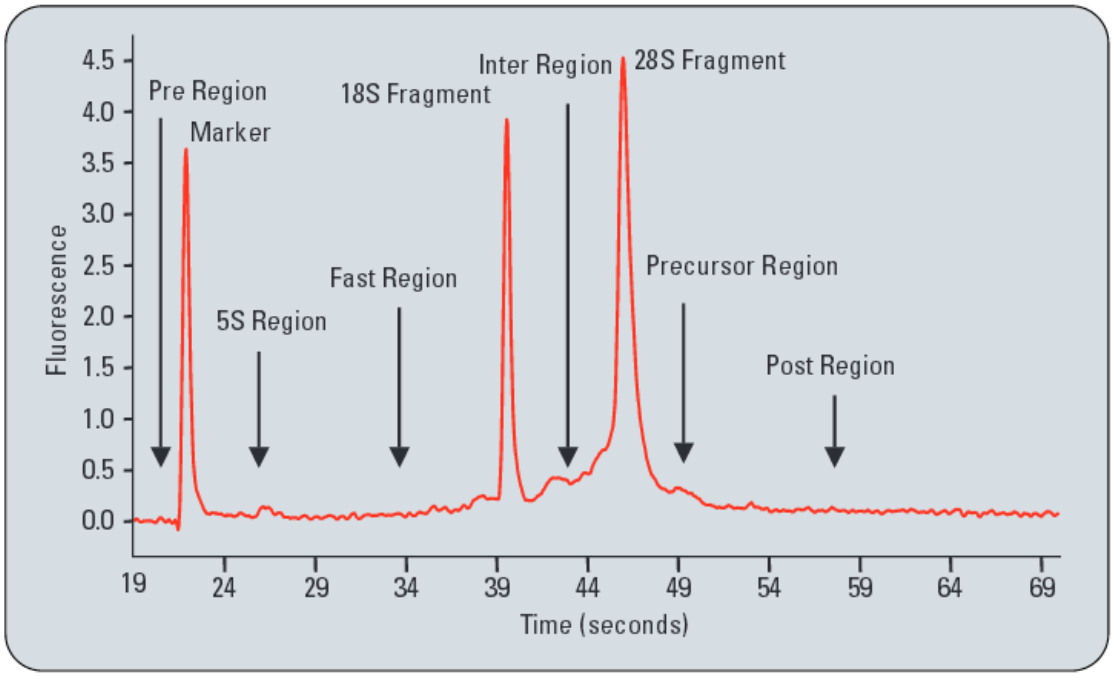

E.6. Primer Specificity by Melt-Curve Analysis. Graphs above show PCR product dissociation curves for seven primer pairs used in this analysis to amplify cDNA of seven genes of interest. The dissociation curve is the denaturation of amplified PCR product at the end of a qRT-PCR run, by temperature increment. The denaturation of a double-stranded DNA resulted in a change in fluorescence and this change in SYBR Green fluorescence is then measured against the standard reference dye, ROX, giving a derivative value that is then plotted against an increase in temperature. If more than one product is present, then the plotted dissociation graph will show multiple peaks as different products will have varying denaturing temperature.

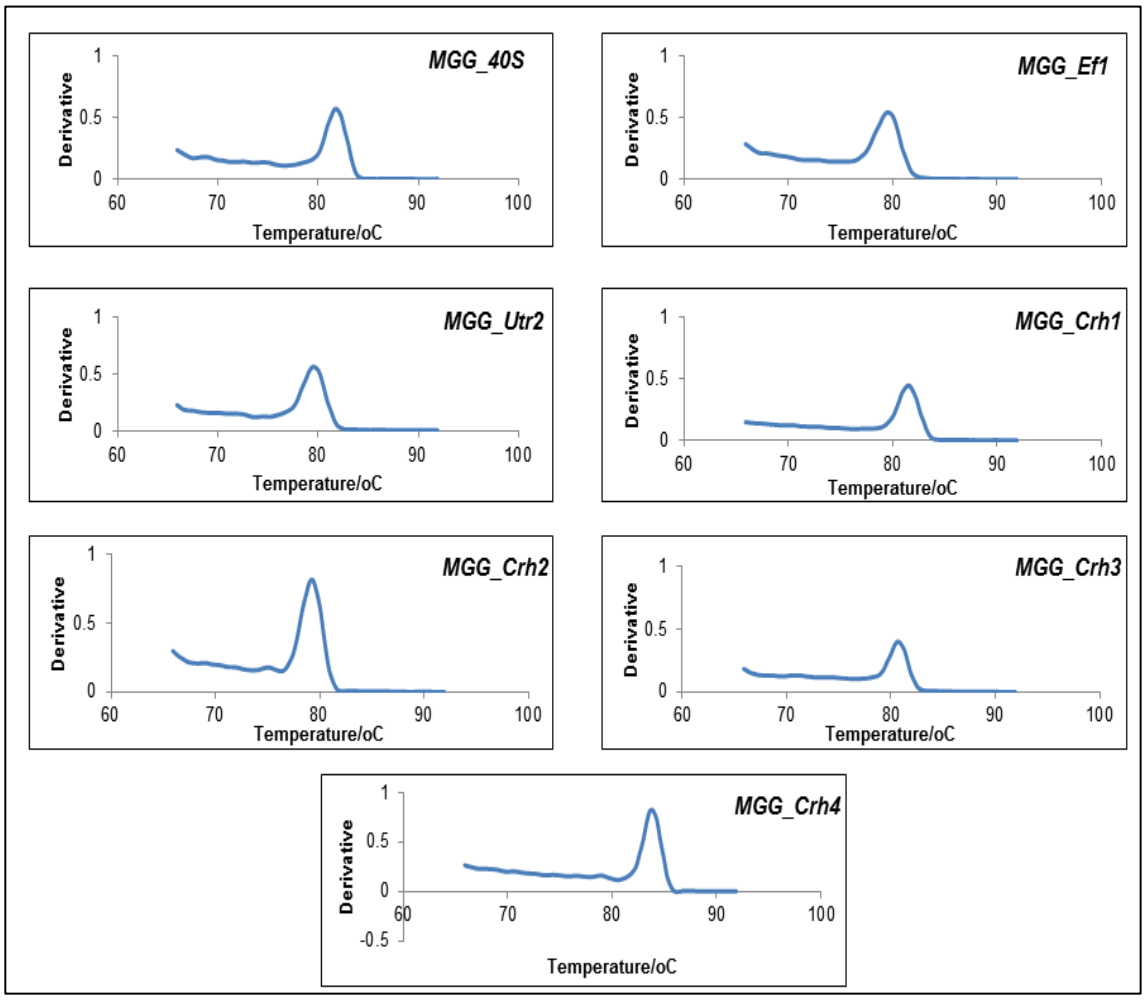

E.7. Hierarchical Clustering of Differentially Expressed Genes in the Five Cell Wall Mutants Versus the Isogenic Wild Type.The columns give the cell wall mutations (*gas1*, *mnn9*, *fks1*, *knr4*, and *kre6*). The red and green squares represent genes whose expression was statistically at least 2-fold higher or lower, respectively, than in the wild type strains, and the black squares indicate no significant change in expression. On the right is shown the cluster of genes that are up-regulated in all of the cell wall mutations, which were used for promoter analysis. Figure and caption taken un-modified from Lagorce *et al* (2003a).

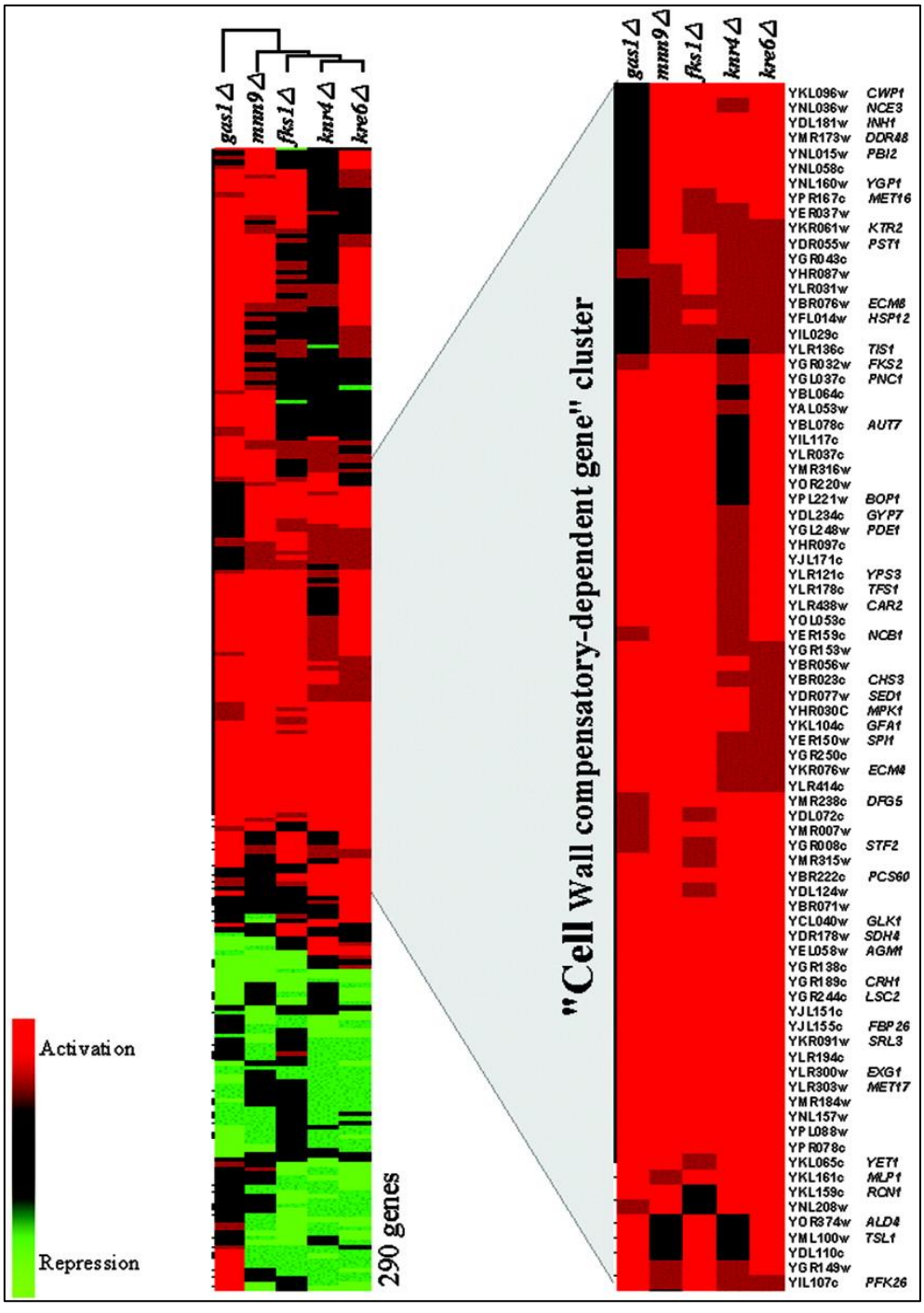

E.8. *Candida albicans* Utr2p and Chitin are Concentrated in Septal Regions. Localization of Utr2p-GFP and chitin in hyphae at different time points (from 30 to 90 min) after induction of hyphae formation in yeast nitrogen base (YNB) plus 10% fetal calf serum. Representative cells were chosen to show the location of the Utr2p-GFP fusion protein under the different conditions. *Bars* in each panel indicate a size of 10 µm. Black and white arrows indicate chitin-rich and Utr2p-GFP labelling, which co-localize especially at septum rings. Yellow arrowheads indicate the position of hyphal tips. Figure and captions edited from Pardini *et al.* (2006).

